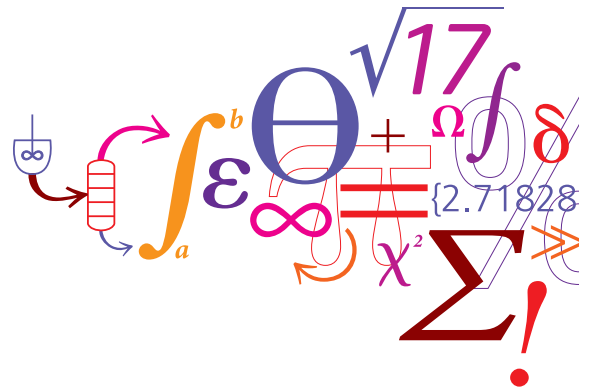# Development of an Electrolyte CPA Equation of state for Applications in the Petroleum and Chemical Industries

Bjørn Maribo-Mogensen
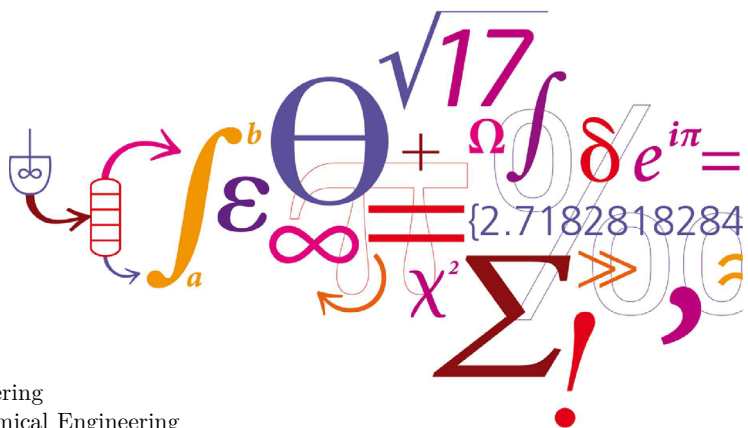Ph.D. Thesis
June 2014

Development of an Electrolyte CPA Equation of State for Applications in the Petroleum and Chemical Industries

Bjørn Maribo-Mogensen
June 23, 2014

Professor Georgios M. Kontogeorgis
Associate Professor Kaj Thomsen

Center for Energy Resources Engineering
Department of Chemical and Biochemical Engineering
Technical University of Denmark (DTU)
Kgs. Lyngby, Denmark

DTU Chemical Engineering
Department of Chemical and Biochemical Engineering

In loving memory of my father, Regner Maribo-Mogensen. 1957-2012

Preface

This thesis is submitted in partial fulfilment of the requirements for the Ph. D. degree at the Technical University of Denmark (DTU). The work was carried out at the Department of Chemical and Biochemiocal Engineering, DTU, from July 2010 to March 2014 under the supervision of Professor Georgios M. Kontogeorgis and Associate Professor Kaj Thomsen. The project was funded by the Joint Industry Project "Chemicals in Gas Processing" (CHIGP) (2/3) and DTU (1/3).

I wish to thank my supervisors for supporting me throughout the project and for the many hours we have spent discussing electrolyte solutions. They have throughout the project encouraged me to keep exploring my own ideas and to challenge the perceptions in the field. I am also grateful for the opportunities I have been given to attend several international conferences, at which I have had to chance to network and discuss with experts in the field. I will also thank my other colleagues and collaborators at DTU Chemical Engineering for their input and assistance.

I am grateful to Dr. Oliver Koch and Dr. Andreas Grenner for inviting me to stay with the ITP group at Linde Engineering (Munich) in September/October 2013, during which I investigated the role of standard state properties in relation to electrolyte solutions. I am thankful to Oliver and Andreas for taking their time to discuss the modeling of electrolyte solutions, and giving me an opportunity to learn about the industrial challenges related salt handling and chemical equilibrium. Finally, I will thank everyone in the ITP office for making me feel very welcome during my stay in Munich.

A three-months external stay with Professor Walter G. Chapman's group at Rice University from February 2013 was regrettably cancelled. Instead, thanks to a kind invitation from Walter I was able to visit Rice University during two weeks in November 2013. I sincerely appreciate the time taken by Walter and Professor Kenneth Cox to discuss the fundamentals of electrolyte equations of state. A special thanks goes to Essmaiil Djamali for giving me such a warm welcome in Houston and for the long discussions on standard state properties and the importance of the static permittivity. I will thank everyone else at the group for making my short stay in Houston memorable - I hope that our roads will cross in the future.

During the last three years, I have also fulfilled a part-time position as Software Manager, being responsible for dissemination of research results to industrial partners. This has given me with unique opportunity to combine my experience in software development with thermodynamic modeling and to provide engineers with access to the Cubic Plus Association (CPA) and Extended UNIQUAC models to solve specific process simulation tasks related to e.g. the production of natural gas, and CO_2 capture processes with novel solvents. Through discussions with industrial partners, I have gained an understanding of the industrial needs in advanced thermodynamic models, which has also been instrumental to the development of the electrolyte CPA framework. I will thank everyone that I have worked with in relation to thermodynamics

software over the past years, and especially Susan B. Little and Leslie W. Bolton from BP for hosting me during a short stay at the BP Research and Technology Center in Hull in November 2013. A special thanks also goes to Georgios Folas and Even Solbraa from Statoil and Michel Pons from CO-LaN for their assistance in relation to validation of the CAPE-OPEN implementation of the CPA equation of state.

Last, but certainly not least I will thank my wife Anush for her patience, support, and devotion throughout the project.

June 23, 2014
Bjørn Maribo-Mogensen

Abstract

This thesis extends the Cubic Plus Association (CPA) equation of state (EoS) to handle mixtures containing ions from fully dissociated salts. The CPA EoS has during the past 18 years been applied to thermodynamic modeling of a wide range of industrially important chemicals, mainly in relation to the oil- and gas sector. One of the strengths of the CPA EoS is that it reduces to the Soave Redlich Kwong (SRK) cubic EoS in the absence of associating compounds and is therefore compatible with existing tools for oil characterization. In a similar fasion, the electrolyte CPA (e-CPA) EoS reduces to the CPA EoS in the absence of electrolytes, making it possible to extend the applicability of the CPA EoS while retaining backwards compatibility and resuing the parameters for non-electrolyte systems .

There are many challenges related to thermodynamic modeling of mixtures containing electrolytes, and many different approaches to the development of an electrolyte EoS have been suggested by scientists in the field. However, most of these approaches are focusing on aqueous solutions and cannot easily be extended to handle mixed solvents. Furthermore, the approaches suggested in current literature have rarely been applied to all types of thermodynamic equilibrium calculations relevant to electrolyte solutions.

This project has aimed to determine the best recipe to deliver a complete thermodynamic model capable of handling electrolytes in mixed solvents and at a wide range of temperature and pressure. Different terms describing the electrostatic interactions have been compared and it was concluded that the differences between the Debye-Hückel and the "mean spherical approximation" models are negligible. A term accounting for the Gibbs energy of hydration (such as the Born term) must be included in order to provide sufficient driving forces for electrolytes towards the most polar phase.

The static permittivity of the mixture was found to be the most important property; yet it was shown that the empirical models suggested by literature could lead to unphysical behavior of the equation of state. A new theoretical model was developed to extend the framework for modeling of the static permittivity to hydrogen-bonding compounds and salts. The model relates the geometrical configuration of hydrogen-bonding dipolar molecules to the Kirkwood g-factor using the Wertheim association model that is included with modern EoS such as CPA or SAFT (Statistical Associating Fluid Theory). This new model was shown to give excellent predictions of the static permittivity of mixtures over wide ranges of temperature, pressure, and composition and thereby generalizes the handling of electrolytes in mixed solvents in an electrolyte EoS.

The CPA EoS was extended with a Debye-Hückel and a Born term to account for the electrostatics along with the new model for the static permittivity. This new e-CPA EoS was parameterized against osmotic coefficient, density, and mean ionic activity coefficient data of pure salts and validated against salt mixture data. The model was then applied to predict:

- the solubility of light gases, hydrocarbons, and aromatics in aqueous mixtures and mixed solvents
- solid-liquid equilibrium in aqueous salt mixtures and mixed solvents
- gas hydrate formation pressures of methane with salts in water+methanol
- liquid-liquid and liquid-liquid-liquid equilibrium with water-propan-1-ol-NaCl-octane solutions

It was demonstrated that the model has a good potential for applications in relation to e.g. flow assurance during the production of natural gas. The parameterization of electrolyte EoS is of high importance and more work is needed in order to obtain good ion-specific parameters that include interaction parameters with gases and relevant chemicals.

Resumé

I denne afhandling udvides Cubic Plus Association (CPA) tilstandsligningen til at håndtere blandinger med ioner fra fuldt dissocierede salte. CPA tilstandsligningen har gennem de sidste 18 år blevet anvendt til termodynamisk modellering af en række industrielt vigtige kemikalier, hovedsageligt i relation to olie- og gas produktion. Hvis en blanding ikke indeholder komponenter, der kan skabe hydrogen-bindinger vil CPA reducere til Soave-Redlich-Kwong (SRK) tilstandsligningen, hvilket muliggør at man kan anvende en række eksisterende værktøjer til eksempelvis oliekarakterisering. På samme hvis vil elektrolyt CPA (e-CPA) reducere til CPA tilstandsligningen når der ikke er ioner til stede, hvilket gør det muligt at udvide anvendelserne for CPA tilstandsligningen samtidig med at e-CPA er bagud kompatibel og kan anvende eksisterende parametre for klassiske systemer uden elektrolytter.

Der er mange udfordringer i forbindelse med den termodynamiske beskrivelse af blandinger med elektrolytter og forskere indenfor feltet har foreslået adskillige fremgangsmåder til udviklingen af en tilstandsligning for elektrolytter. Dog har de fleste grupper fokuseret på modellering af vandige opløsninger og deres fremgangsmåder kan ikke nemt blive udvidet til at håndtere blandede solventer. Ydermere er de publicerede fremgangsmåder ofte kun blevet afprøvet på få typer af termodynamiske ligevægtsberegninger med relevans saltopløsninger.

Dette projekt har søgt at klargøre den bedste opskrift på en komplet termodynamisk model, der kan håndtere elektrolytter i blandede solventer som funktion af temperatur og tryk. Der blev udført en sammenligning af forskellige modeller til beskrivelse de elektrostatiske interaktioner, og dette viste at der kun var ubetydelige forskelle mellem Debye-Hückel og "mean spherical approximation"modellerne. Derudover kræver en elektrolyt tilstandsligning et bidrag såsom Born modellen til beskrivelse af hydrationsenergien, da dette bidrag er ansvarlig for at give ionerne en tilstrækkelig drivkraft mod den mest polære fase.

Den vigtigste egenskab for beskrivelse af elektrostatiske interaktioner er den statiske permittivitet (eller dielektriske konstant) af blandingen. Dog kan de empiriske modeller, der foreslåes i litteraturen føre til ufysisk opførsel af tilstandsligningen. Det teoretiske grundlag til forudsigelsen af den statiske permittivitet blev med udviklingen af en ny model udvidet til at håndtere blandinger med tendens til at skabe hydrogen-bindinger samt blandinger indeholdende salte. Modellen relaterer den geometriske konfiguration af dipolære hydrogenbindinge molekyler til Kirkwood's g-factor ved brug af Wertheim's associations-model, der anvendes i mange moderne tilstandsligninger såsom CPA eller SAFT (Statistical Associating Fluid Theory). Den nye model giver gode forudsigelser af den statiske permittivitet i blandinger som funktion af temperatur, tryk, og sammensætning og generaliserer håndteringen af elektrolytter i blandede solventer med en elektrolyt tilstandsligning.

CPA tilstandsligningen blev dernæst udvidet til at tage højde for de elektrostatiske interaktioner ved brug af Debye-Hückel og Born modellerne samt den nye model for den statiske permittivitet. Denne nye e-CPA tilstandsligning blev parameteriseret ved brug af osmotiske koefficienter, densiteter samt middelionaktivitetskoefficienter for blandinger med enkelt-salte og valideret op imod data for blandede salte. Denne model blev dernæst anvendt til at forudsige:

- opløseligheden af gasser, alkaner, samt aromatiske stoffer i saltopløsninger i vand og blandede solventer
- opløseligheden af salte i vandige opløsninger og blandede solventer
- trykket for dannelse af methan's type I gashydrat i blandinger med vand, methanol, samt NaCl
- væske-væske og væske-væske-væske ligevægt for vand, propan-1-ol, NaCl med octane

Den nye model har udvist et godt potentiale for anvendelsen til modellering af blandinger relateret til produktion af naturgas. Parameteriseringen af tilstandsligningen spiller dog en stor rolle, og yderligere arbejde er nødvendigt for at kunne bestemme de optimale interaktionsparameter mellem ioner og vand, gasser, samt andre relevante kemikalier.

Contents

List of Figures

List of Tables

List of Physical Constants

$$
\begin{array}{rcllll}
k_B & = & 1.3806503 \cdot 10^{-23} & [\text{J/K}] & \text{Boltzmann constant} \\
N_A & = & 6.0221415 \cdot 10^{23} & [\text{mol}^{-1}] & \text{Avogadros constant} \\
R & = & k_B \cdot N_A = 8.314472 & \left[\dfrac{\text{Pa} \cdot \text{m}^3}{\text{mol} \cdot \text{K}}\right] & \text{Ideal gas constant} \\
e & = & 1.60217646 \cdot 10^{-19} & [\text{C}] & \text{Elementary charge} \\
F & = & e \cdot N_A = 96485.3365 & [\text{C/mol}] & \text{Faraday constant} \\
\mu_0 & = & 4\pi \cdot 10^{-7} & [\text{N/A}^2] & \text{Vacuum Permeability} \\
c & = & 299792458 & [\text{m/s}] & \text{Speed of light} \\
\epsilon_0 & = & \dfrac{1}{\mu_0 c^2} = 8.854187 \cdot 10^{-12} & [\text{F/m}] & \text{Vacuum Permittivity}
\end{array}
$$

List of Symbols

ΔU_{ij} Change in interaction energy between like and unlike interactions $\Delta U_{ij} = g_{ji} - g_{ii}$[J/mol]

Δ Included volume fraction in MSA , see Eq. (4.25)

$\Delta_{tr}^{1 \to 2}G$ Gibbs energy of transfer between phase 1 and 2   [J/mol]

$\Delta_f G^o$ Gibbs free energy of formation in the conventional aqueous standard state at 25°C, 1 bar   [J/mol]

$\Delta_f H^o$ Enthalpy of formation in the conventional aqueous standard state at 25°C, 1 bar[J/mol]

$\Delta_f G^{ig}$ Ideal gas Gibbs free energy of formation.   [J/mol]

$\Delta_f H^{ig}$ Ideal gas enthalpy of formation.   [J/mol]

$\Delta_{hyd}H$ Enthalpy of hydration.   [J/mol]

$\Delta_{hyd}C_p$ Change in heat capacity upon hydration   [J/mol]

$\Delta_{hyd}G$ Gibbs energy of hydration.   [J/mol]

$\Delta_{solvation}G$ Change in Gibbs energy upon ion solvation   [J/mol]

$\Delta_{A_i B_j}$ The association strength between site A on molecule i and site B on molecule j, calculated using (3.10).   [m^3/mol]

Γ MSA closure parameter. The distance $(2\Gamma)^{-1}$ is equivalent to the Debye length κ^{-1}[1/m]

Γ_i Reduced attractive energy parameter   [K]

Φ Osmotic Coefficient $\Phi = -\frac{x_w}{1-x_w} \ln x_w a_w$

Φ_i Debye-Hückel function , see Eq. (4.51)   [J/mol]

Π Osmotic pressure   [Pa]

Θ_i Fraction of molecule i that is not bound to any ions

Ξ_i Fraction of site i which is not bonded to any other sites

α_k Ion-specific constant for dielectric decrement   [L/mol]

$\alpha_{0,i}$ The molecular polarizability of molecule i [C^{2}m^2/J]

α_{ij} The NRTL non-randomness parameter

β Inverse temperature divided by Boltzmann constant $\beta = \dfrac{1}{k_B T}$ [1/J]

β_1 Fitting constant for static permittivity of water $\beta_1 = 3.1306$

$\epsilon_{A_iB_j}$	Association energy calculated using Eq. (3.13)	[J]
η	Packing factor, $\eta = b/4v$	
γ_0^{LR}	Activity coefficient of solvent in the Lewis-Randall framework	
γ_0^{MM}	Activity coefficient of solvent in the McMillan-Mayer framework	
$\gamma_\pm^m$	Mean molal activcity coefficient of salt based on the molality scale.	
γ_{ij}	The angle between the two dipole moments as shown in Figure 5.2	
κ^{-1}	Debye length , see Eq. (1.2)	[m]
λ	Wavelength of light	[m]
λ_{ij}	Ion-ion interaction as a function of the ionic strength	[m^3/mol]
$\mu'_{0,j}$	The dipole moment of molecules surrounding the central dipole	[C $\cdot$ m]
μ_i	Chemical potential of component i	[J/mol]
$\mu_{i,0}$	Dipole moment of component i in vacuum	[C $\cdot$ m]
$\mu_{w,0}$	Dipole moment of water in vacuum $\mu_{w,0} = 8.33 \cdot 10^{-30}$C $\cdot$ m	[C $\cdot$ m]
ν_i	The NRTL/Huron-Vidal volume parameter for component i at infinite pressure.	[m^3/mol]
ω	Angular frequency	[rev/s]
$\overline{V}_0$	Solvent molar volume	[m^3/mol]
ψ_i	Electrical potential around component i , see Eq. (4.4)	
ρ	Molar density	[mol/m^3]
ρ_c	Critical density	[mol/m^3]
ρ_i	Molar density of component i	[mol/m^3]
ρ_w	Density of water , see Eq. (4.41)	[g/cm^3]
σ	Direct current conductivity	[S/m]
σ_i	Hard-sphere diameter of component i	$\left[\text{Å}\right]$
τ	Characteristic dipole relaxation time	[s]
θ_{ij}	Rotation angle between hydrogen bonds in different shells. See Figure 5.3 p. 85.	
ε_r^w	Static permittivity of liquid water at saturation conditions	
ε_A	The Adelman static permittivity from statistical mechanics , see Eq. (4.85)	
ε_W	The Wertheim static permittivity from statistical mechanics , see Eq. (4.84)	
ε_∞	Permittivity at infinite frequency, typically replaced by square of the refractive index n^2	
ε_d^*	Complex permittivity (frequency dependent dielectric response)	
ε_r	Relative static permittivity (or dielectric constant)	

ε_s	Relative static permittivity of solvent in the presence of salts	
$\varepsilon_{s,0}$	Relative static permittivity of solvent in the absence of salts	
ε_{solute}	Relative static permittivity of a solute compound	
φ_i	Internal C-O-H angle. See Figure 5.2 p. 84.	
$g^{E,\infty}$	Excess Gibbs energy at infinite pressure.	[kJ/mol]
$a(T)$	Van der Waals attractive energy parameter of the mixture , see Eq. (3.4)	$\left[\dfrac{\text{Pa} \cdot \text{m}^6}{\text{mol}^2}\right]$
A	Debye-Hückel A coefficient , see Eq. (1.3)	$\left[(\text{kg/mol})^{1/2}\right]$
A^{assoc}	Total Helmholtz energy from association	[J/mol]
A^{hyd}	Helmholtz energy from hydrogen bonding	[J/mol]
A^{hyd}	Helmholtz energy from ion association	[J/mol]
A^e	Helmholtz free energy from electrostatics.	[J/mol]
A^r	Residual Helmholtz energy	[J/mol]
A^{dd}	Helmholtz energy of dipole-dipole interaction in the non-primitive MSA	[J/mol]
A^{DH}	Helmholtz energy from the Debye-Hückel model	[J/mol]
A^{id}	Helmholtz energy of ion-dipole interaction in the non-primitive MSA	[J/mol]
A^{ii}	Helmholtz energy of ion-ion interaction in the non-primitive MSA	[J/mol]
A^{MSA}	Helmholtz free energy from the mean spherical approximation (MSA)	[J/mol]
a_i	Activity of component i	
a_w	Water activity $x_w \gamma_w$.	
b_0	Co-volume parameter of the mixture , see Eq. (3.3)	[m³/mol]
Ba	Extended Debye-Hückel Ba coefficient , see Eq. (1.3)	$\left[(\text{kg/mol})^{1/2}\right]$
$c(r_{12})$	Direct correlation function between molecule 1 and 2	
C	Debye-Hückel C coefficient for the Hückel equation , see Eq. (1.3)	[kg/mol]
C_i	Concentration of component i in molality	[mol/L]
c_i	Charge density of component i	[C/m³]
C_p^o	Conventional aqueous standard state heat capacity	[J/mol/K]
c_{1i}	Pure component temperature dependence parameter for Soave's $\alpha(T)$-function	
d_0^2	Dipole density in non-primitive MSA , see Eq. (4.74)	
d_2^2	Charge density in non-primitive MSA , see Eq. (4.74)	
d_i	Min. distance of approach for component i	$\left[\text{Å}\right]$

$E(\mathbf{n}, V)$ Ion correction factor for static permittivity , see Eq. (4.40)

E^{MSA} Internal energy of the mean spherical approximation (MSA)   [J/mol]

EA Electron affinity   [eV]

F Reduced residual Helmholtz energy $F = A^r/RT$

$g(\rho)$ The radial distribution function at contact

$g(r_{12})$ Pair correlation function between molecule 1 and 2 $g(r_{12}) = 1 + h(r_{12})$

G^E Excess Gibbs free energy of a mixture   [J/mol]

G^{LR} Gibbs free energy from long-range interactions   [J/mol]

G^{MR} Gibbs free energy from middle-range interactions   [J/mol]

G^{SR} Gibbs free energy from short-range interactions   [J/mol]

g_i Kirkwood g-factor of component i

$h(r_{12})$ Indirect correlation function between molecule 1 and 2

I_m Molality-based ionic strength   [mol/kg]

IE Ionization energy   [eV]

k_i^S Setschenow salting out constant for component i for salt s   [L/mol]

K_B Bjerrum equilibrium constant for ion pairing , see Eq. (4.49)

K_E Ebeling equilibrium constant for ion pairing , see Eq. (4.50)

K_i Partition coefficient of molecule i between phase 1 and 2, $K_i = x_i^{(1)}/x_i^{(2)}$

l_B Characteristic Bjerrum length for ion pairing , see Eq. (4.45)   [m]

M_i Moles of the sites of type i [mol]

m_i Molality of component i [mol/kg]

m_S Molality of salt   [mol/kg]

n The refractive index

n_i Molar amount of component i [mol]

n_w Molar amount of water   [mol]

N_{ij} Number of molecules of type i around ion j

P Pressure   [Pa]

P^e Electrostatic pressure $P^e = -\left(\frac{\partial A^e}{\partial V}\right)_{T,\mathbf{n}}$

P_c Critical pressure   [Pa]

P_i Probability of first shell around central molecule i, $P_i = \sum\limits_{j \in S} P_{ij}$

P_i^k Probability of shell k around central molecule i

r_{Born}	Born radius.	[m]
r_{ij}	Distance between component i and j	[m]
r_{ion}	Ion radius (e.g. as observed from crystallography).	[m]
S_i^0	Solubility of component i in the salt-free solution	[mol/kg]
S^o	Conventional aqueous standard state entropy at 25°C, 1 bar	[J/mol]
S_i	Solubility of component i with salts	[mol/kg]
T	Temperature	[K]
T_0	Reference temperature $T_0 = 273.15K$	[K]
$T_{c,i}$	Critical temperature of component i	
V	Total volume	$[\text{m}^3]$
v	Molar volume	$[\text{m}^3/\text{mol}]$
v_e	Stoichiometric coefficient of the electrons in the half-cell reactions	
$v_{A_iB_j}$	Association volume calculated using Eq. (3.14) or Eq. (3.15)	$[\text{m}^3/\text{mol}]$
w_{ij}	Potential of average force exerted between molecule i and j	[J]
x_i	Mole fraction of molecule i	
x_i^{app}	Apparent mole fraction $x_i^{app} = e_i/e_T$	
x_w	Mole fraction of water in mixture	
X_{A_i}	Fraction of site A on component i not bonded to any other component	
z_i	Charge of component i	
z_{ij}	Coordination number of molecule j around a central molecule i	

Part I

Setting the Stage for the Development of an Electrolyte Equation of State

Chapter 1

Introduction to the Research Area

1.1 Industrial Needs and Challenges

Complex mixtures of non-polar, polar, ionic, and hydrogen-bonding components are fundamental to life, govern geochemical processes that occur over millions of years, and are encountered in most chemical processes such as acid gas cleaning, waste-water treatment, energy storage in batteries, desalination, fractional crystallization, extractive distillation, as well as bio-separations [1, 2]. Chemical engineers need knowledge of the physical properties of chemical compounds in mixtures and of the partition coefficients in multi-phase systems over wide ranges of temperatures and pressures in order to accurately design and optimize production of chemicals and energy [1–3]. This knowledge requires obtaining high-quality experimental data at different conditions, combined with accurate, predictive thermodynamic models that can represent the phase behavior and thermal properties of the fluid [1, 3–8].

In a recent study [3] by the Working Party of Thermodynamic and Transport Properties of the European Federation of Chemical Engineers (EFCE)), a questionnaire concerning the industrial needs within thermodynamics and transport properties was forwarded to and answered by key technical staff from 28 different companies from the oil and gas, chemical, and pharmaceutical/biotechnology sector. One key topic in the questionnaire was concerned about electrolyte solutions and the answers revealed that all industries recognized that:

> The predictive capabilities of thermodynamic models for electrolyte mixtures lag years behind their non-electrolyte counterparts and there is an industry-wide consensus that new predictive (rather than correlative) models are strongly needed. The models must be able to handle all types of phase behavior (VLE/LLE/SLE) and thermal properties of electrolytes in mixed solvents with hydrocarbons over extensive temperature and pressure ranges.

1.1.1 Electrolytes in the Oil and Gas Industry

In the oil and gas industry, the presence of salts will generally cause a salting out of hydrocarbons from the brine (thereby reducing the solubility compared to pure water), and furthermore, the presence of electrolytes may enhance the inhibitory effect of methanol and glycol on the formation of gas hydrates in natural gas pipelines [1]. It is well-known that the waterflood recovery can be affected by the chemistry of the injected brine and it has been argued that a low-salinity brine can enhance recovery of sandstone rocks [9]. Aggressive species (such as CO_2 and H_2S) may cause corrosion of tubing and lead to an environmental disaster with a potential for immense economic impact [10]. The situation becomes even more complex when corrosion processes occur under a layer of scale, wax, and asphaltene as shown in Figure 1.1. Salts also
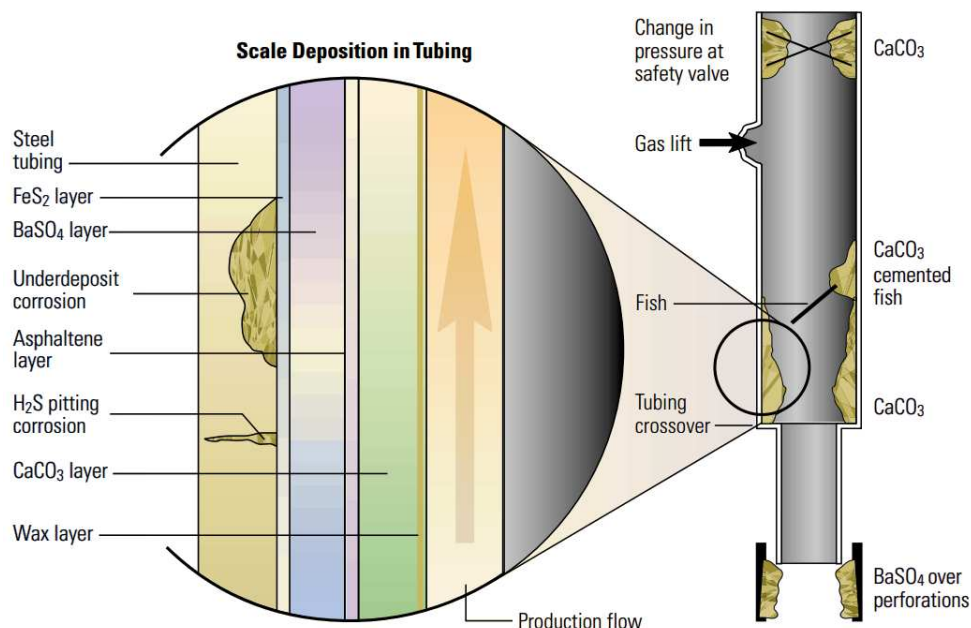
Figure 1.1: Typical production problems related to electrolytes - corrosion may occur under a layer of asphaltene, wax, and scale (adapted from Crabtree (1999) [11]).

become an economic and operational hazard when they precipitate inside the tubing, processing equipment or near the wellbore [11]. Salts are known to precipitate in the following situations [12]:

- When a water-flood brine containing sulfate is mixed with the formation water leads to precipitation of sulfate scales (typically $BaSO_4$, $CaSO_4$, $CaSO_4 \cdot 2\,H_2O$, or $SrSO_4$).

- When a sudden reduction in the pressure and/or increase in temperature causes deposition of carbonate salts (most commonly $CaCO_3$).

- When a dry gas stream is mixed with a brine stream causing evaporation of water it induces a super-saturation of salts and leads to the formation of e.g. solid NaCl.

The focus of the industry is therefore to plan ahead and select suitable strategies and materials that can assist in managing scale formation and corrosion from the reservoir e.g. by injecting a low-sulfate brine and by squeezing scale inhibitors in the reservoir to prevent scaling in the vicinity of the wellbore areas [11, 12].

As the oil exploration moves towards reservoirs with higher temperatures and pressures than before, the existing models become less reliable and experimental data increasingly scarse. A better fundamental understanding of electrolyte solutions is therefore crucial for predicting operation limits and putting in adequate safety measures in the harsh conditions offered by the new HPHT reservoirs.

The following sections will provide an introduction to the behavior of mixtures containing electrolytes and provide an overview of the current thermodynamic models for electrolyte solutions and their deficiencies. Finally, an overview of the scientific work performed in this PhD

to harmonize the modeling approaches for electrolyte equations of state is provided.

1.2   Behavior of Mixtures Containing Electrolytes

The complex behavior of mixtures containing electrolytes have caught the attention of scientists and engineers for hundreds of years and despite advances in our understanding of electrolyte solutions, there are still many unanswered questions in relation to thermodynamic models for electrolytes. Figure 1.2 and 1.3 shows some examples of the typical behaviour in mixtures containing salt.
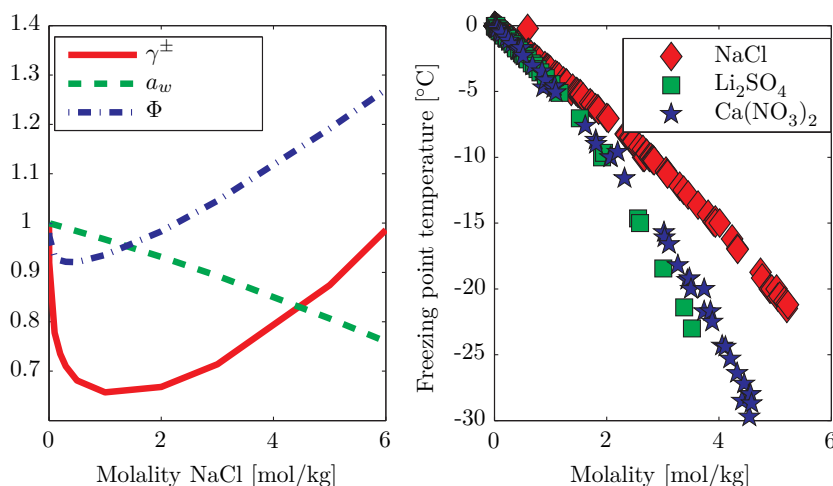
Figure 1.2: Effect of NaCl concentration at 25°C on mean ionic activity coefficient $\gamma_\pm^m$, water activity a_w, and osmotic coefficient Φ (left) [2]. Effect of different salts on the freezing point of water as a consequence of the reduced water activity (right) [13].

Salts will generally reduce the activity of water, causing e.g. a reduction in the freezing point and the vapor pressure. The apparent molar volume or heat capacity of the solution can be observed to either increase or decrease depending on the ions in the solution, due to the effect the ions have on the structure of the solvent (e.g. through the formation of solvation shells surrounding the ions). As demonstrated in Figure 1.4, the observed effect depends greatly on the solvent and temperature and shows far from trivial behavior in heat capacity near room temperature.

The maximum in the apparent molal heat capacity of salts near room temperature was explained by Cobble and Murray (1981) [19] by considering two different dominating effects at high and low temperatures and at infinite dilution:

$\left(\frac{\partial C_p^o}{\partial T}\right) > 0$ The fluid **structure** (especially the primary and secondary hydration shell of ions) dominates the properties at infinite dilution. The properties are affected by the structure of the solvent and explained by the unequal hydration of anions and cations, as well as structure-making (kosmotropic) and structure-breaking (chaotropic) ions.

$\left(\frac{\partial C_p^o}{\partial T}\right) < 0$ The region depends only on the electrical **field** around the ion and on the relative static permittivity ε_r (or dielectric constant) of the solvent. As ε_r is reduced, the electrical field
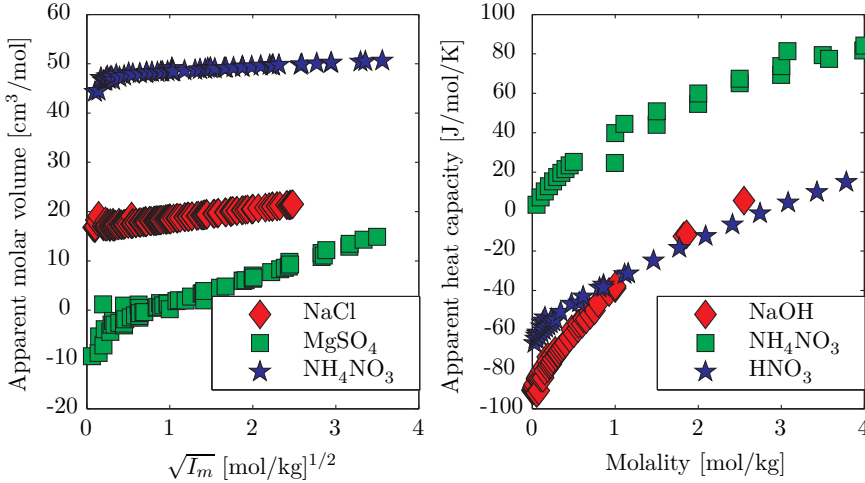
Figure 1.3: Apparent molar volume as a function of the square root of the ionic strength $I_m = 0.5 \sum_i m_i z_i^2$ (left) and heat capacity (right) of selected aqueous salt solutions [13].
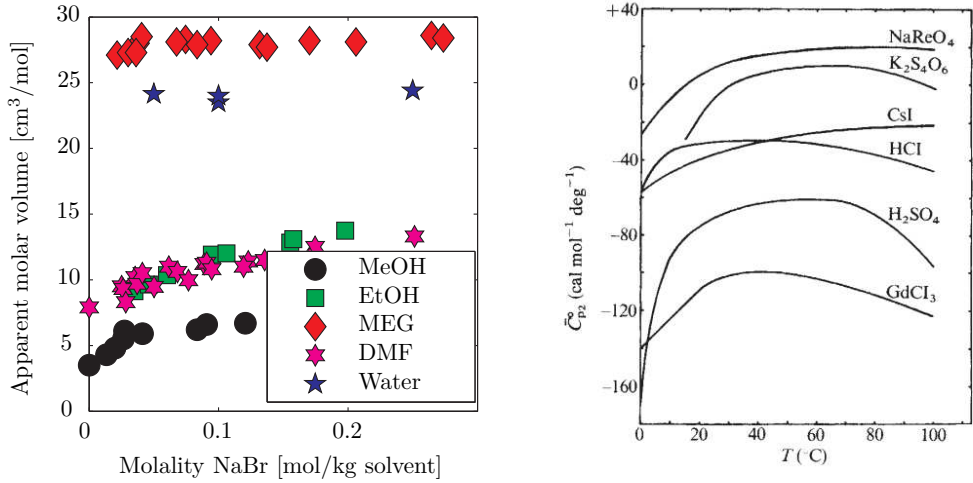
Figure 1.4: Apparent molal volume of NaBr at 25°C in methanol (MeOH), ethanol (EtOH), ethylene glycol (MEG), dimethylformamide (DMF), and water [13–18] (left). The temperature dependence of the heat capacity at infinite dilution of selected salts (right) (from [19]).

extends longer into the fluid. In this region, the fluid can be considered as a continuum of hydration surrounding the ions.

The concept of structure-making and structure-breaking ions has long been used to explain the Hofmeister effect [20, 21]. The effect was first observed by Hofmeister (1888) and Lewith (1888) who reported a great variation in the amount of salt that would cause precipitation of aqueous proteins. Depending on the combination of two ions, the solubility would either decrease (salting out) or increase (salting in) the protein solubility compared to pure water following the Hofmeister series shown in Figure 1.5.

$$F^- \approx SO_4^{2-} \quad > HPO_4^{2-} \quad > CH_3COO^- > Cl^- > Br^- > I^- \quad > CNS^-$$

Kosmotropic
(Salting out)

Chaotropic
(Salting in)

$$(CH_3)_4N^+ \quad (CH_3)_2NH_2^+ \quad > NH_4^+ > K^+ > Na^+ > Cs^+ > Li^+ > Mg^{2+} > Ca^{2+} > Ba^{2+}$$

Figure 1.5: The Hofmeister series of ions show how ions increase the solubility of proteins. The same series also affect other properties, such as the surface tension of water-salt and the viscosity.

In a comprehensive literature review of more than 1000 articles dealing with the ion-specific effects, Collins and Washabaugh (1985) [20] concluded that the Hofmeister effects are important above moderate ionic strength (>0.1M), that they are dominated by the anions, and that they are approximately additive. The Hofmeister sequence (or the reverse sequence) has a tendency to reappear in colloidal and interfacial science when investigating other properties such as the surface tension of aqueous solutions [22].

While the structural aspects are related to the short-range interactions of ions with the solvent [21], charged species will also interact over longer ranges through Coloumb's inverse-square root law given by Eq. (1.1):

$$F = \frac{e^2 z_i z_j}{4\pi \varepsilon_r \varepsilon_0 r_{ij}^2} \tag{1.1}$$

In Eq. (1.1), z_i is the charge of ion i and r_{ij} the distance between the two ions. The force between the ions increases as the relative static permittivity ε_r drops. Figure 1.6 shows some characteristic behavior of ε_r with temperature, solvent, and ion concentration.

Figure 1.6: Temperature and compositional dependence of the static permittivity for different solvents (left)[23] (MeOH = methanol, EtOH = ethanol, MEG = ethylene glycol). Reduction in the static permittivity at 25°C for different salts [24, 25].

1.3 Thermodynamic Modeling of Electrolytes

The theoretical foundation explaining the observed behavior of salts has been attributed to Debye and Hückel [26]. Debye and Hückel [26] derived a model for the excess chemical potential

due to electrostatic interactions by solving the linearized Poisson-Boltzmann equation. Whereas the electrical field $\psi_i(r)$ around a single ion is determined by Eq. (1.1) at infinite dilution, Figure 1.7 (left) shows how the presence of other ions affects the electrical field in the Debye-Hückel model depending on the characteristic Debye-length given by Eq. (1.2).

$$\kappa^{-1} = \sqrt{\frac{\varepsilon_r k_B T}{\sum\limits_i e^2 \rho_i z_j^2}} \tag{1.2}$$

Debye and Hückel [26, 27] derived an expression for the mean ionic activity coefficient which is often presented as shown in Eq. (1.3) [2]:

$$\ln \gamma_{\pm}^m = \ln x_w - |z_i z_j| \frac{A\sqrt{I_m}}{1 + Ba\sqrt{I_m}} + C I_m \tag{1.3}$$

In Eq. (1.3), the constants A, B, and C depend on the density, static permittivity, and temperature of the fluid and ^{m} indicates that it uses the molality concentration scale. A comparison of the mean ionic activity coefficient of HCl with different versions of the activity coefficient are shown in Figure 1.7 (right), in which the Debye-Hückel limiting law (DHL) has $Ba = C = 0$, and the Extended Debye-Hückel (DHE) has $C = 0$, whereas the Hückel equation also includes Ba and C.
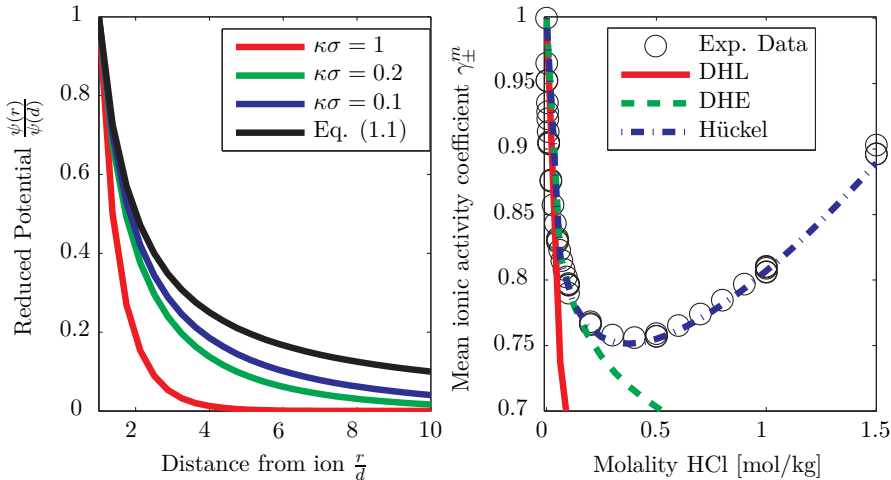
Figure 1.7: Debye screening of the Coulomb potential near ions with the inverse, reduced Debye length of an ion with diameter σ (left). Application of the Debye-Hückel activity coefficient models (Eq. (1.3)) to the activity coefficient of HCl [2]. DHL = Debye-Hückel limiting law, DHE = Extended Debye-Hückel law including the Ba parameter, and the Hückel model including the Ba and C parameter.

From Figure 1.7 it is evident that the limiting law can only represent the activity coefficients at low concentrations (<0.001M), and higher concentrations therefore requires the use of extended versions of the Debye-Hückel equation. Many researchers have since investigated how to represent activity coefficients of concentrated solutions. Bjerrum (1926) justified the use of the linearized Poisson-Boltzmann equation at even higher concentrations, as they will provide an explicit correction of the mean-field potential approximation used in the Debye-Hückel equation. Bjerrum (1926) [28] suggested to handle ions that are in close contact; separated by 0-2 solvent molecules ion pairs (see Figure 1.8).
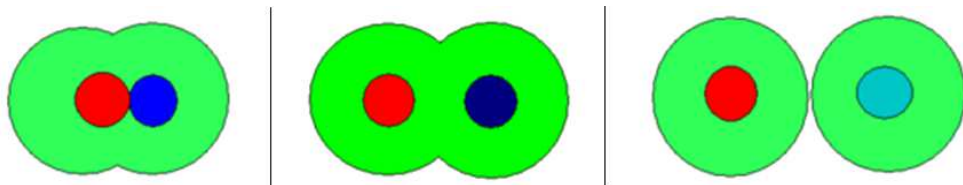
Figure 1.8: Different types of ion pairs; A contact ion pair (CIP) (left), A solvent-separated ion pair (SIP) (middle), and a fully solvated ion pair (SSIP) (right).

Ion pairs are neutral compounds that effectively reduce the ionic strength of the mixture, and they may be investigated through various experimental methods including the conductometry and dielectric relaxation spectroscopy [29–33].

Robinson and Stokes [34] presented a full version of the Debye-Hückel model useful for mixed solvents (DHF) and proposed that a proper treatment of electrolyte solutions would require a **civilised** model, that would account for the local structure; e.g. steric hindrances, ion-ion association, and the solvation of ions as shown in Figure 1.9.
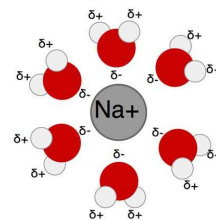
Figure 1.9: Ion hydration

Alternative empirical treatments of the activity coefficients of strong electrolyte solutions were introduced by Meissner [35, 36] and Bromley [37], while Pitzer [38] improved the Debye-Hückel equation in a form known as Pitzer-Debye-Hückel (PDH) and introduced a virial expression to account for specific (medium-range) ion-ion interactions not included in the Debye-Hückel term:

$$\frac{G^E_{virial}}{RT} = \frac{1}{n_w} \sum_i \sum_j n_i n_j \lambda_{ij}(I) \tag{1.4}$$

Where the virial coefficient B_{ij} is a function of the ionic strength containing possibly many temperature dependent parameters [39–42]. The functional form of the Pitzer model makes it very versatile and has ever since been a workhorse in correlation of the experimental data and applied to e.g. calculation of scaling in the oil and gas industry [43].

Figure 1.7 also shows another interesting aspect of models for electrolyte solutions. While normal compounds typically use the symmetrical activity coefficient $\gamma = 1$ in the pure liquid, the Debye-Hückel equation (and similar activity coefficient models) provide an unsymmetrical activity coefficient (where $\gamma^*_\pm = 1$ in infinite dilution). Electrolyte solutions are typically described using the unsymmetrical activity coefficient, which is adequate for describing chemical equilibrium and solid-liquid equilibrium from a single liquid phase (typically water). However, if the Debye-Hückel model is naïvely applied to predict the distribution of Na_2SO_4 between water and iso-propanol, the model falls short as it only accounts for the interaction energy between ions. Figure 1.10 shows how the introduction of the solubility of Na_2SO_4 is affected in a mixed solvent - at higher concentrations, the two liquid phases will split into two phases with $\varepsilon_r^{(1)} > \varepsilon_r^{(2)}$ and the ions show a significant preference for the most polar phase.

In order for a model to reproduce Fig. 1.10, the thermodynamic model must account for the interactions with the solvent. One approach suggested by Born [45] is a continuum model
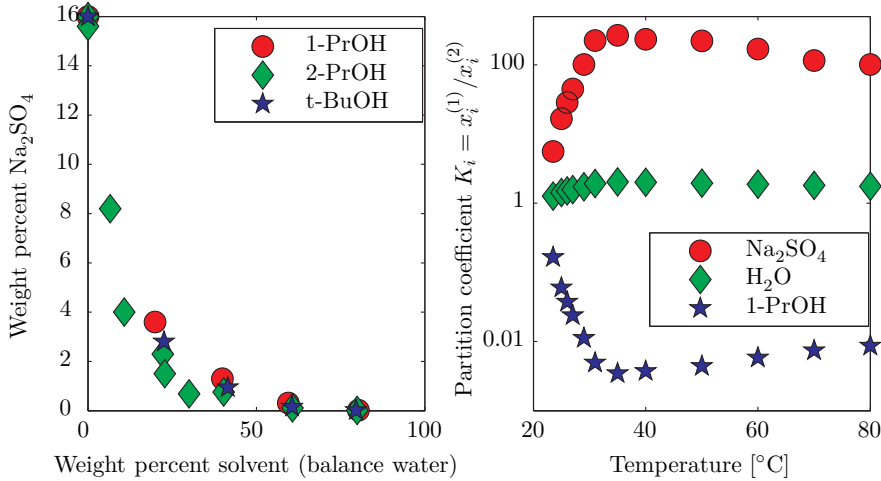
Figure 1.10: Solubility of salts in mixed solvents at 20 °C (left) (PrOH = propanol, BuOH = butanol) (left) and distribution of compounds in the Na_2SO_4-H_2O-1-propanol system at salt saturation (right). Data from [44].

for the Gibbs energy of solvation as a simple function of the static permittivity and an effective cavity diameter d_i. The Born equation can be used to estimate the Gibbs energy of transfer between solvent (1) and (2) using Eq. (1.5) [41, 45, 46]:

$$\Delta_{tr}^{1\rightarrow2}G = \frac{N_A e^2}{4\pi\varepsilon_0} \sum_i \frac{n_i z_i^2}{d_i} \left(\frac{1}{\varepsilon_r^{(2)}} - \frac{1}{\varepsilon_r^{(1)}} \right) \tag{1.5}$$

Where ε_0 is the vacuum permittivity, n_i is the number of moles of component i. By including the change in Gibbs energy of solvation, either through the Born-model or through other terms for the ion-solvent interactions, the thermodynamic models may also handle the distribution of salts between two polar phases [41].

1.3.1 Insights from Statistical Thermodynamics and Molecular Simulation

A significant effort has been made to understand the fundamentals of electrolyte mixtures through statistical thermodynamics, that provides a theoretical link between the macroscopic behavior of fluids with a microscopic description of intermolecular potentials via integral equation theory, requiring a solution of the Ornstein-Zernike (OZ) equation given by Eq. (1.6).

$$h(r_{12}) = c(r_{12}) + \rho \int d(\vec{r}_3)c(r_{13})(r_{23}) \tag{1.6}$$

The indirect correlation function $h(r_{12})$ is related to the radial distribution function $g(r_{12}) = 1 + h(r_{12})$, which descibes the ratio of the local density $g(r)\rho$ compared to the bulk density ρ. By relating the direct correlation function $c(r_{12}) = \beta\phi(r_{12})$ (where $\beta = (k_BT)^{-1}$) and through the use of a closure equation, Eq. (1.6) may be solved for a known intermolecular potenatial $\phi(r_{12})$.

Figure 1.11: Schematic of g(r).

Blum (1975) [47, 48] presented an analytical solution to mixtures containing electrolytes known

as the mean spherical approximation, which has since received considerable attention from the scientific community. For instance, the binding MSA [49–51] extends the MSA model to handle the formation of ion pairs, which will effectively reduce the ionic strength of the solution.

The hypernetted chain closure (HNC) for the Ornstein-Zernike equation enables a more detailed description of the interactions between solvents and ions than the MSA, but as it relies on heavy computations it is considered impractical as an engineering thermodynamic model for electrolytes [52]. Still the HNC or computer simulations using Monte Carlo (MC) or Molecular Dynamics (MD) have provided new insight in the structure of electrolytes solutions including the role of charge and size asymmetry as well as ion-ion and ion-solvent association [53–57] (see Figures 1.12-1.13).

One advantage of the modern approach is that computer simulations may e.g. be validated through comparison of the calculated correlation functions to neutron or X-ray scattering data [58]. Integral equation theories based on the same intermolecular potentials (such as the MSA) can then be compared to and validated against results from molecular simulation, creating the foundations for a systematic procedure to improve the models for electrostatic interactions [52]. This approach can also be used to validate first-principles models based on the solution of the Poisson-Boltzmann equation; Fisher and Levin [53] (1993) have shown that a model based on the full Debye-Hückel solution coupled with ion-pairing and an additional term for the (ion pair)-ion interactions yields good agreement with computer simulations (and in many cases better than MSA [54]). Boström (2005) [59] compared the numerical solution of the non-linear Poisson-Boltzmann equation to the HNC and Monte Carlo simulations to determine the radial distribution of ions near a protein (macro-ion) and showed that similar results were obtained from all three approaches.
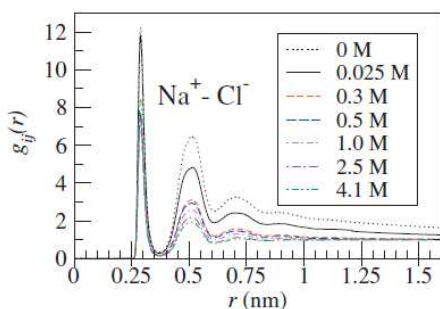
Figure 1.12: Radial distribution function of Cl^- around Na^+ indicating the presence of both contact ion pairs and solvent-separated ion pairs (for NaCl, there are two times more solvent-separated ion pairs than contact ion pairs) (adopted from [60])
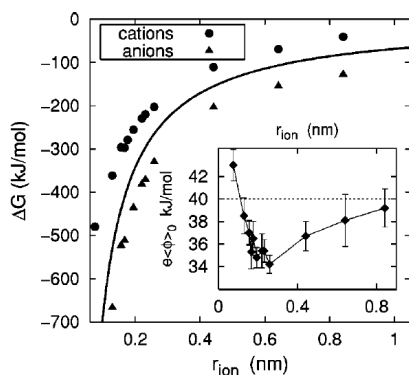
Figure 1.13: Gibbs free energy of hydration with the Born model and as calculated by molecular dynamics simulation with the SPC water with ions as Lennard-Jones spheres, showing an asymmetry in the hydration free energy of anions and cations [61].

The most noticeable development from the statistical mechanical treatment of electrolyte solutions has been the so-called **non-primitive** MSA model [62–64] that treats all dipole-dipole, dipole-ion, and ion-ion interactions explicitly through a perturbation theory. Where the Debye-

Hückel, Born and MSA are so-called **primitive** models that treat the solvent implicitly, thus requires knowledge of the static permittivity to obtain effective interaction potentials. The non-primitive model calculates this as an output from the model, making it a radically different approach from the primitive models. The non-primitive MSA is significantly more complicated than the primitive models, and must be solved numerically, but it provides an attractive approach to handling electrolyte mixtures, as it provides a self-consistent approach to calculating the electrostatic interactions as well as the static permittivity.

Liu (2002) [65] developed a low-density expansion of the non-primitive MSA and showed that when the Wertheim model [66] is used to determine the effective static permittivity, the ion-ion interaction energy from the non-primitive MSA is equivalent to the primitive MSA at low concentrations and that the ion-dipole interactions bears close resemblance of the Born-term. This insight enabled Liu (2005) [67] to develop a simpler model inspired by the non-primitive solution using the effective static permittivity of the fluid from the Wertheim equation. This builds on the work of Adelman (1976) [68, 69], who showed that the Ornstein-Zernike equation may be reformulated in terms of effective interaction potentials, requiring the formulation of an effective solvent+solute dependent static permittivity that is used to calculate the effective pair potentials $c_{ij}^{eff}(\mathbf{r}_{ij})$.

1.4 State-of the art: Activity Coefficient Models for Electrolyte Mixtures

While the previous section presented some of the fundamentals of electrolyte thermodynamics, this section focuses on the work-horse of the chemical industry in relation to thermodynamic models for electrolyte systems. These models are based on the concept of describing different contributions to the excess Gibbs energy, and typically consists of explicit terms to handle the short-range, intermediate-range and long-range interactions in the fluid given by Eq. (1.7):

$$G^E = G^{SR} + G^{MR} + G^{LR} \tag{1.7}$$

The most widely used activity coefficient models and their capabilities are presented in Table 1.1 [70].

Common to all activity coefficient models in Table 1.1 is that they are based on the extension of a local composition term (modified NRTL or UNIQUAC) with a model for the electrostatic energy. The models require a large amount of interaction parameters to be estimated against all known experimental data, and the parameters are generally not transferable outside the regime where they were estimated and have little physical significance [70].

To further complicate matters, the standard state properties of electrolytes are not well-established for many salts and intermediate species making it necessary to infer standard state properties from other experimental data (e.g. heat of dilution, speciation, or apparent molal heat capacity) [2].

Accurate thermodynamic models also require knowledge of the chemical speciation in the mixture. However, even for a seamingly simple compound as boric acid H_3BO_3(aq), Wang (2013) [42] defined no less than five ionic species ($B(OH)_4^-$, $B_2O(OH)_5^-$, $B_3O_3(OH)_4^-$, $B_4O_5(OH)_4^{2-}$, $B_5O_6(OH)_6^{3-}$) and two uncharged species (HBO_2(aq), B_2O_3(aq)) to succesfully represent the experimental data in aqeous mixtures with H^+, Li^+, Na^+, Ca^{2+}, Mg^{2+}, OH^-, requiring simultaneous or step-wise regression of more than 140 parameters (standard state, UNIQUAC, and interaction parameters) up to 300°C. Thomsen [78] modeled a similar system up to 200°C.

Model	Electrolyte NRTL [71, 72]	OLI Mixed Solvent Electrolyte [39–42, 73]	Extended UNIQUAC [2, 74, 75]
Non-electrostatic term	Modified NRTL [71]	UNIQUAC [76] + 2nd virial term [38]	UNIQUAC [76]
Electrostatic term	Modified Pitzer-Debye-Hückel [72, 77] and Born [45]	Modified Pitzer-Debye-Hückel [39, 77]	Extended Debye-Hückel [26]
Parameters	2-4 per binary (on ion pair basis)	3 per binary	4 per molecule, 2 per binary
Availability	Aspen Plus / Properties	Aspen Plus / HYSYS, Honeywell UniSim, gPROMS, Pro/II	Excel and Aspen Plus

Table 1.1: Overview of the most widely used models for electrolyte solutions and their applications. All models are capable of handling VLE, LLE, SLE, thermal properties, and combined physical and chemical equilibrium in mixed solvents allowing the application to a wide range of problems.

Thomsen [78] also included the SO_4^{2-} and K^+ ions but used a fewer number of borate-species (H_3BO_3 (aq), BO_2^-, $B_4O_7^{2-}$), which meant that only 75 parameters had to be determined. As different data were included in the two analyses, the two approaches are not directly comparable, but just shows that the speciation plays an important role in modeling of electrolyte systems.

In all cases, when sufficient experimental data is available to optimize the parameters for a given system of interest, the models represent an effective and important engineering tool for the design and optimization of processes. But the choice of intermediate species and fitted parameters is an expert task that requires thorough investigation of the experimental data and of the standard state properties available for these systems.

Lin et al. (2010) [70] compared the models in Table 1.1 by defining ten simple test systems; an aqueous mixture with up to three salts out of NaCl, Na_2SO_4, $MgCl_2$, KNO_3, K_2SO_4, $MgSO_4$, $MgNO_3$, and a mixed-solvent system with water, ethanol, and NaCl. Using the standard parameters (i.e. without refitting of the parameters to the sub-systems) Lin compared the model predictions of VLE and SLE against experimental data at temperatures from -22-110°C. While the models would generally give reasonable results for the boiling point pressure (VLE), the models would sometimes lead to precipitation of incorrect solid phases and result in wrong speciation. The Extended UNIQUAC performed best in the case of mixed solvent solutions even at high concentrations, despite that the electrostatic model (Extended Debye-Hückel) assumes that the solvent is pure water and does not use the Born term for the Gibbs energy of transfer, indicating that the interaction parameters of the UNIQUAC model can be used to compensate for the alternative representation of electrostatic interactions. It is questionable that these correlation models can give accurate predictions in regions with limited data, such as at high temperatures or pressures and the work by Lin et al. [70] justifies looking into the fundamentals of thermodynamic modeling of electrolyte solutions.

1.5 Towards the Electrolyte Equation of State

Over the past 30 years, great advances have been made in the development of thermodynamic models for hydrogen bonding mixtures through the Statistical Associating Fluid Theory (SAFT) [79], based on the Wertheim first order (TPT1) perturbation theory [80]. This has given rise to

a long list of SAFT-based models of which the most widely used [1] are the Perturbed Chain SAFT (PC-SAFT)[81] and the Cubic Plus Association (CPA)[82], that calculate contributions to the total residual Helmholtz energy of a fluid through a perturbation theory, that is based on a mathematical model for specific interactions in the fluid. Several groups have worked on introducing models for electrolyte mixtures in these equations of state in an attempt to develop a single framework for describing the thermodynamic properties of mixtures of non-polar, polar, associating, and ionic compounds or even polymers in the quest towards a universal thermodynamic model [1, 83]. Figure 1.14 shows how an equation of state would include some of the different complex phenomena occuring in electrolyte solutions, as described in the previous sections.
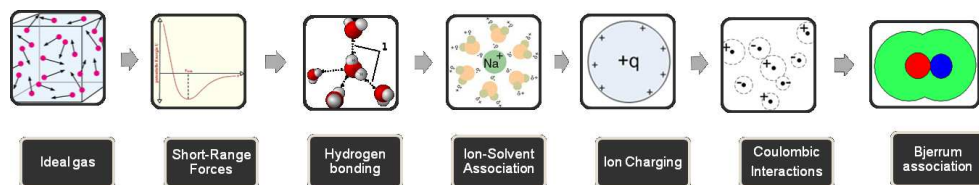
Figure 1.14: Contributions to an electrolyte Equation of State.

An overview of the electrolyte EoS published in literature are shown in Table 1.2 and an overview of the parameters, correlations, and predictions are shown in Table 1.3. Table 1.3 shows what properties are used in a correlation, and the ones that are predicted. G^E is a collection of mean ionic activity coefficients, $\gamma_{\pm}^{*m}$, osmotic coefficients Φ, water activity a_w, saturated vapor pressure P_{sat}, and water freezing point depression. $k_S = \lim_{c_s \to 0} \left[c_s^{-1} \log_{10} \frac{\hat{\phi}_{i,s}^{\infty}}{\hat{\phi}_{i,w}^{\infty}} \right]$ is the Setchenow constant that defines the salting out of a solute.

1.6 Critical Review of Literature on Electrolyte EoS

While all models in Table 1.2 have succesfully been able to correlate activity coefficients, so far none of the models have been applied to all possible types of experimental data. Each of the colored columns of Table 1.2 raises new questions that must be answered to harmonize the approach to development of electrolyte EoS.

How should electrostatic interactions be modeled?
The models for electrolyte mixtures can be categorized into three fundamental approaches:

- **Primitive models** assume that the static permittivity is equal to that of the solvent. A correlation of the static permittivity at the saturation line of water with temperature is typically applied in activity coefficient models [26, 38, 71, 73, 75, 147], and this approach has also been adopted in many cases of equation of state modeling [84–87, 89–95, 109, 110, 112, 114–118, 121, 128–131, 133, 139, 141] as well as in molecular simulation [148]. These models may also include empirical terms to take into account the effect of salts on the mixture permittivity.

- **Non-primitive models** use the coupling of all the electrostatic interactions (ion-ion, ion-dipole, dipole-dipole) and do not need to include models for the static permittivity [52, 67, 138].

Table 1.2: Overview of electrolyte EOS published in literature. BM-CS = Boublik-Mansoori extension of the Carnahan-Starling EOS, bMSA = Binding MSA, eMSA = explicit MSA, iMSA = implicit MSA, Hu = Lennard-Jones-based attractive term, LP = Ludecke and Prausnitz attractive term [142], npMSA = Non-primitive MSA (dipole-dipole, ion-dipole, and ion-ion), CSW = Cubic Square Well [143].

Source	Base model	Ion assoc. ion-solvent	Ion assoc. ion-ion	Ion-ion	With Born?	MM/LR	ε_r T	V	n	Ion	Pure	Binary	Max. Molal	T-range [°C]	# salt (mixed)	Other solutes
Raatschen et al. [84]	BM-CS+Hu+Virial	-	-	PDH	+	?	+	+	+	?	2	3	m_{sat}	-10-140	1 (0)	1
Copeman/Stein [85]	PY + LP	-	-	eMSA	?	?	+	?	+	?	1-2	-	m_{sat}	0-140	12 (0)	2
Jin/Donohue [86, 87]	PACT	-	-	npMSA	+	?	+	?	+	?	1	-	6	0-100	50 (0)	6
Jin/Donohue [88]	PACT	-	-	npMSA	+	?	+	?	?	?	1	-	6	25-90	29 (8)	-
Harvey et al. [89, 90]	BH	-	-	iMSA	?	?	+	?	?	-	-	1	6	25-170	8 (0)	6
Zuo/Guo [91]	PT	-	-	DHE	?	?	+	?	+	?	-	1	6	25-200	27 (0)	9
Simon et al. [92]	SRK	-	-	PDH	+	?	+	?	+	+	1	-	m_{sat}	0-80	2 (0)	1
Aasberg-Petersen [93]	ALS	-	-	DHF	?	?	+	?	?	?	-	1	4	25-120	2 (0)	3
Furst et al. [94, 95]	SRK+SR2	-	-	iMSA	-	?	+	+	+	+	-	1-3	6	-15-25	28 (30)	2
Gmehling et al. [96–108]	PSRK-LIQUAC	-	-	DHF	-	-	+	+	+	+	2	6	10	0-250	35 (4)	8
Wu/Prausnitz [109]	PR	+	-	iMSA	?	+	+	?	?	?	1-3	-	6	0-300	1 (0)	1
Galindo et al.[110–112]	SAFT-VR	-	-	eMSA	?	?	?	?	?	?	-	1	10	0-100	9 (1)	3
W. Liu et al. [113]	LJ-SAFT	-	-	npMSA	+	+	+	+	?	?	1	-	6	25	30 (13)	-
Myers/Sandler	PR	-	-	eMSA	+	+	+	+	+	+	3	-	6	25	138 (0)	-
Wood [114]		-	-		-	?	+	+	+	-	6	-	8	0-300	7 (2)	-
Sadowski et al. [115–120]	PC-SAFT	+	+	DHF	-	?	+	?	+	?	-	2-3	m_{sat}	0-100	115 (0)	5
Z. Liu et al. [65, 67]	LJ-SAFT	+	+	npMSA	+	-	+	+	+	+	2	-	6	25	15 (0)	-
Radosz et al. [121, 122]	SAFT1	-	-	eMSA	?	-	+	?	?	?	5 / 2	2	6	0-100	5 (6)	-
Radosz et al. [123–127]	SAFT2	-	-	eMSA	?	-	+[a]	?	?	?	5 / 2	2-3	6	25-200	26 (18)	-
Zhao et al. [52]	SAFT-VR	-	-	npMSA	+	-	Non-primitive				0-5	-	-	-	- (-)	-
Lin/Thomsen/	PR	-	-	eMSA	+	?	+	+	+	-	3	0-1	m_{sat}	25	5 (6)	-
de-Hemptinne [128]	PR	-	-	iMSA	+	?	+	+	+	-	3	0-1	m_{sat}	25	5 (6)	-
	SRK	-	-	DHE	+	?	+	?	?	?	2	1	m_{sat}	25	5 (6)	-
	CPA	-	-	iMSA	+	?	+	?	?	?	3	1	6	25	5 (6)	-
Inchekel et al. [129]	CPA+SR2	-	-	DHF	+	+	+	+	+	+	4	1	6	25	10 (0)	-
Haghighi et al. [130, 131]	CPA	+	-	MSA	?	?	?	?	?	?	5	-	6	-30-20	6 (4)	-
Y. Liu et al. [132]	FMSA	+	-	MSA	?	?	+	?	?	?	3	-	6	25-80	19 (18)	-
Lee and Kim [133]	PC-SAFT	-	-	MSA	+	?	?	?	?	?	4	-	m_{sat}	25	26 (22)	-
Pazuki et al. [134, 135]	SAFT	-	-	MSA	?	?	?	?	?	?	3	-	5	25	6 (0)	6
Haghtalab/	CSW	-	-	MSA	+	?	+	+	+	-	3	-	6	25	132 (0)	-
Mazloumi [136, 137]	CSW	-	-	MSA	+	-	+	+	+	-	9	-	10	0-100	8 (0)	-
Herzog/Gross/Arlt [138]	PC-SAFT	-	-	npMSA	+	?	+	?	?	-	3	-	6	25-140	12 (1)	3
Rozmus et al. [139]	PPC-SAFT	+	-	iMSA	+	?	+	+	+	+	1	0-1	m_{sat}	0-100	19 (0)	-
Zuber et al. [140, 141]	MTC	-	+	iMSA	+	?	+	+	+	+	1-2	-	6	25-300	20 (0)	-
		-	-	eMSA	+	?	+	?	?	+	2	-	m_{sat}	0-300	78 (20)	-

Legend: +Included in model · -Excluded from model · ?Not included, nor discussed · Non-primitive · Ion-specific · Salt-specific

---

[a][126] even introduced a pressure-dependent correlation, leading to an inconsistent EOS

Table 1.3: Overview of the parameters used in the published e-EoS and how they were estimated.

Source	Type (i)on (s)alt	Size σ/b_0	Energy ε/a_0	Binary Solvent	Binary Solute	Binary Ion	# of salts	Max. Molal	T-range °C	#Mixed salts	Other Solvents	G^E 25°C	G^E T	Vol. ρ	k_S@25°C	VLE	LLE	SLE	GH	CE
Raatschen et al. [84]	i	1	1	-	-	3	1	m_{sat}	-10-120	-	MeOH	+	+	+	-	+	-	-	-	-
Copeman/Stein [85]	s	1	1	1-2	1	-	12	m_{sat}	0-140	-	Aniline, MeOH	+	+	+	-	+	+	+	-	+
Jin/Donohue [86, 87]	s	1	1	1	-	-	50	6	0-100	-	MeOH	+	-	-	-	+	-	-	-	-
Jin/Donohue [88]	i	1	1	1	-	-	29	6	25-90	6	-	+	-	+	-	+	-	-	-	+
Harvey et al. [89, 90]	s	1	1	1	1	-	8	6	25-170	-	-	+	-	-	+	+	-	+	-	-
Zuo/Guo [91]	s	1	1	1	1	-	27	6	25-150	-	-	+	-	-	+	+	-	-	-	-
Simon et al. [92]	i	1	2	1	-	-	2	m_{sat}	0-80	-	MeOH, EtOH	+	-	-	-	+	-	+	-	+
Aasberg-Petersen [93]	s	-	-	1	1	-	2	4	25-120	-	-	+	-	-	-	-	-	-	-	-
Furst et al. [94, 95]	s	1	-	1	1	1-2	28	6	-15-25	30	MeOH	+	+	+	+	+	-	+	+	-
Gmehling et al. [96-108]	i	-	-	4-8	6	4-8	35	m_{sat}	0-250	4	MeOH-BuOH, acetone	+	+	+	-	+	+	+	-	-
Wu/Prausnitz [109]	i	1	1	1-3	1	-	1	6	0-300	-	-	+	-	-	-	+	-	-	-	-
Galindo et al. [110-112, 144]	i	1	1	1	-	-	9	10	0-170	1	-	+	-	+	-	+	+	+	+	-
W. Liu [113]	s	1	1	1	-	-	30	6	25	13	-	+	-	+	-	-	-	-	-	-
Myers/Sandler [114]	s	2	1	1	-	-	138	6	25	-	-	+	-	+	-	-	-	-	-	-
Wood [114]	s	3	2	1	-	-	7	8	5-300	2	-	+	+	+	-	-	-	-	-	-
Sadowski et al. [115-120]	i	1	1	-	-	-	115	m_{sat}	5-70	2	(Me-, Et-, Bu-)OH[a]	+	+	+	-	+	+	-	-	-
Z. Liu et al. [65, 67]	s	1	1	1	-	2[b]	15	6	25	-	-	+	+	-	-	+	-	-	-	-
Radosz et al. [121, 122]	i+s	3	2-3	-	-	3[b]+3	5	6	0-100	6	-	+	-	+	-	-	-	-	-	-
Radosz et al. [123-127]	i+s	3	2-6	-	-	-	26	6	25-200	18	-	+	+	+	-	+	+	-	-	-
Zhao et al. [52]	i	1	1	1	-	1	Molecular simulation			-	-	-	-	+	-	-	-	-	-	-
Lin et al. [128]	i	1-2	1	1	-	1	5	m_{sat}	25	6	-	+	-	+	-	-	-	+	-	-
Inchekel et al. [129]	i	-	1	1	-	-	10	6	25	-	-	+	-	+	-	-	-	-	-	-
Haghighi et al. [130, 131]	s	-	-	5	-	-	6	6	-30-125	6	-	+	+	-	-	-	-	-	+	-
Y. Liu et al. [132]	i	1	3	1	-	-	19	6	25-80	19	-	+	-	-	-	-	-	+	+	-
Lee and Kim [133]	i	1	3	1	-	-	26	m_{sat}	25	22	-	+	-	-	-	-	+	+	-	-
Pazuki et al. [134, 135, 145]	i	2	1	-	-	-	6	5	25	-	PEG, lysozyme	+	-	-	-	-	+	-	-	-
Haghtalab/	s	2	2	-	-	-	132	6	25	-	-	+	-	-	-	+	-	-	-	-
Mazloumi	s	3	6	2	-	1	8	10	0-100	-	-	+	-	+	-	-	-	-	-	-
[136, 137, 146]	i	2	2	2	2	-	12	10	0-140	-	-	+	-	+	-	-	-	-	-	+
Herzog et al. [138]	s	1	-	1	-	-	19	m_{sat}	0-100	2	MIDEA	+	+	-	-	+	-	-	+	-
Rozmus et al. [139]	i	[c]	1	-	-	-	20	5	20-300	-	-	+	+	+	-	+	-	-	-	+
Zuber et al. [140, 141]	i	1	-	1	-	1	78	m_{sat}	0-300	20	-	+	+	+	-	-	-	-	-	-

Legend: Adjusted parameter/data used in parameter estimation | Predicted parameter/data | - Not calculated or available.

[a] Sadowski et al. [118] also predicted the mean ionic activity coefficients in a mixture of water-methanol-ethanol from parameters fitted to binary solutions.
[b] Radosz et al. [121, 122] use a hydrated salt diameter, which is here categorized as an ion-ion parameter.
[c] Except for F$^-$ which is fitted

- **Civilized models** are non-primitive models that take into account steric effects, ion hydration and ion-ion association [34, 149]. They have not yet been used within an equation of state.

The difference between the primitive and non-primitive model is illustrated in Figure 1.15. The primitive models have the simplest functional form and seek to use interaction parameters and the static permittivity of the solvent to model the structural effects. The models become increasingly complex when going towards the civilized model where all electrostatic interactions (short and long-range) must be taken into account.

It is not uncommon to refer to the Debye-Hückel limiting law (DHL) which is only valid at infinite dilution [52, 85–89, 110–112, 114] as an argument for choosing the MSA model.
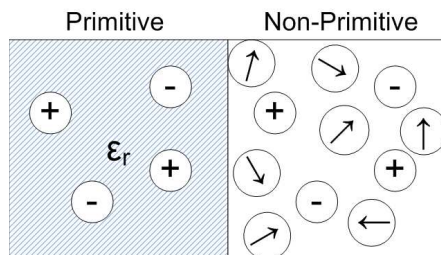
Figure 1.15: Sketch of the primitive and non-primitive approach to modeling of electrolytes. Primitive models include the effect of the solvent implicitly through the static permittivity ε_r.

It is arguably an unfair comparison to compare the infinite dilution limit of the Debye-Hückel against a full version of the MSA model. It should also be noted that the MSA model and the Debye-Hückel have the same limiting law behavior [85, 114].

Should activity coefficients be converted from the McMillan-Mayer to the Lewis-Randall framework?

Some groups state that since the primitive models developed with an assumption of an implicit solvent (in the McMillan-Mayer framework) and the physical part of the equation of state is developed by handling all species explicitly (the Lewis-Randall framework), it is necessary to make a conversion between the two frameworks [109, 114] and that this is not needed for non-primitive models [52, 67]. Most EOS developed from primitive models do not discuss the conversion between the frameworks, except for Radosz et al. [121–127] and Haghtalab et al. [136, 137] who state that the differences are negligible after parameterization.

What is the importance of ion-solvent association?

Some of the later work on e-EoS development have included ion-solvent and ion-ion association implemented using the Wertheim framework that was originally developed for highly directional forces (e.g. hydrogen bonds) [67, 109, 133, 138, 139]. The model allows specifying N association sites on a given molecule, and determines the fraction of site A on molecule i X_{A_i} that is not associated to any other molecule by solving Eq. (1.8):

$$\frac{1}{X_{A_i}} = 1 + \sum_j \rho_j \sum_{B_j} X_{B_j} \Delta_{A_i B_j}, \qquad \Delta_{A_i B_j} = \kappa_{A_i B_j} g_{ij}(\sigma_i j) \sigma_{ij}^3 \left(\exp(\epsilon_{A_i B_j}/k_B T) - 1 \right) \quad (1.8)$$

Where the cross-diameter $\sigma_{ij} = 0.5 (\sigma_i + \sigma_j)$ and $\Delta_{A_i B_j}$ is the association equilibrium constant between site A on molecule i and site B on molecule j. $\Delta_{A_i B_j}$ may be evaluated using the radial distribution function at contact $g_{ij}(\sigma_{ij})$ of the reference system (typically the hard sphere). In order to reduce the number of fitted parameters, authors define the association sites and association strength $\kappa_{A_i B_j}$ as shown in Table 1.4. However, as evident from Eq. (1.8), the balance between $\kappa_{A_i B_j}$ and $\epsilon_{A_i B_j}$ defines the temperature dependence. Most models are only investigated over a narrow range of temperatures, and only Rozmus et al. [139] attempted to correlate the temperature dependence over wide ranges of temperatures with a single parameter (but did not obtain a good correspondence with activity coefficients at higher temperatures).

Source	$\kappa_{A_iB_j}$	Number of association sites on ions						
		Li^+	Na^+	K^+	Cs^+	Cl^-	Br^-	I^-
Wu et al [109]	0.001	-	10	-	-	14	-	-
Lee and Kim [133]	0.001	8	8	8	-	7	7	7
Z. Liu et al. [67]	0.001	7	7	7	10	9	10	12
Y. Liu et al. [132]	0.03	8	8	8	-	6	6	6
Herzog et al. [138]	0.03	4	4	3	2	0	0	0
Rozmus et al. [139]	0.0356	7	7	7	7	6	6	6

Table 1.4: No. of association sites on selected ions as proposed by different authors and the fixed association strength proposed by the authors.

Wu and Prausnitz [109] used a 2nd order polynomial in temperature to correlate $\varepsilon_{A_iB_j}$ over wide temperature ranges and were in that case able to get reasonable correspondence with the activity coefficients even above 150°C. It remains an unsolved question whether including an association model is really an improvement, and does not only add new parameters.

What is the importance of ion-ion association?

Ion-ion association has been treated through essentially a mass-action approach (chemical equilibrium) by Sadowski et al. [117], and so it requires additional knowledge of the equilibrium constant; however, from statistical mechanics it is known that the equilibrium constant depends not only on temperature, but also on the static permittivity of the medium [53, 54, 56, 57]. So far, the approaches for ion-ion association developed for e-EoS have not been validated against molecular simulation or other experimental data (e.g. conductivity, Raman or dielectric spectroscopy). While Rozmus et al. (2013) [139] included the concept of ion-ion association, they did not account for the effect that ion pairs will have on the electrostatics (i.e. decreasing the ionic strength).

Should the model include an explicit term for the Gibbs energy of solvation?

Some researchers include a Born term or a non-primitive ion-dipole term to determine the Gibbs energy of solvation [52, 67, 84, 86–88, 92, 109, 113, 114, 128, 129, 138–141], but only Myers et al. [114] and Herzog et al. [138] have made comparisons to the Gibbs energy of solvation/Gibbs energy of transfer between solvents to validate the approach. Furthermore, none of these groups have presented speciation in a liquid-liquid equilibrium and only Simon (1991) [92] has attempted to model the solid-liquid equilibrium with a mixed solvent with an EoS that also includes the Born model. Inchekel [129] showed that when the model for the static permittivity takes into account the reduction caused by the presence of ions, the Born term provides an opposite contribution to the activity coefficient of NaCl; but due to the empirical nature of the model for the static permittivity it is not possible to say whether this should be considered to be an actual physical effect or purely mathematical consequence of the investigated model.

How should the static permittivity be modeled? And does it even matter?

The theoretical background of the static permittivity [150–155] suggests a dependence on temperature, volume, and composition, that will have the following general characteristical behavior:

- Increasing the volume will reduce ε_r

- Increasing the amount of polar compounds will increase ε_r

- Increasing the temperature will reduce ε_r

The non-primitive models [52, 67, 138] include the above physical behavior through the coupling of ion-ion, ion-dipole and dipole-dipole interactions and do not use the static permittivity; rather it can be obtained as an output from the model. Z. Liu et al. [65, 67] showed that the low-density expansion of the non-primitive MSA is similar to the MSA coupled with the dielectric calculated from the Wertheim (1971) theory [66], whereas Zhao et al. (2007) noted that the Adelman [68, 69, 156–158] static permittivity is needed when ions are present, and Adelman (1976) [68, 69] showed the similarity between replacing the explicit solvent-solute interactions with an effective static permittivity of the mixture that included contributions from both solvent and solutes in the case of electrolyte models.

In the case of primitive models, the choice of the model for the static permittivity should also be able to represent the basic physical behavior of ε_r to assure a correct physical behavior of the electrostatics. While some authors have attempted to model the static permittivity from a more fundamental perspective [84, 90, 92, 155], most have relied on empirical correlations without presenting evidence for how their choices affect the behavior of the model. Some have used empirical correlations that are functions of the density of water $\rho_w = n_w/V$ [114, 128, 129, 139] which should result in a correct physical behavior, but most have actually neglected the volumetric dependence by using a correlation of the static permittivity of water as a function of temperature at the saturation line. The compositional dependence is also often ignored unlesss the model is applied to mixed solvents. Besides a comparison of how well the activity coefficients of NaCl could be matched when using two empirical models for static permittivity performed by the Inchekel (2008) [129], little efforts have been made to show the importance of the static permittivity and determine what functional form would lead to a correct physical description of the electrostatic interactions.

Should the model use salt or ion-specific parameters?

The properties of aqueous solutions is heavily dominated by the anion and as evident from the Hofmeister series shown in Figure 1.5, fluorides and sulfates are expected to have significantly different behavior in comparison to chlorides, bromides and iodides. While the ion-specific effects are a well-established scientific fact, an ion-based parameterization of equations of state requires simultaneous regression of many salts to many different properties. While ion-specific parameters are generally most widely used a substantial number of researchers have decided to use salt-specific parameters and Radosz et al. have even used a combination of salt- and ion-specific parameters [121–127]. Many authors who derived ion-specific parameters have only looked at the behavior of halides with [138, 139] or without F⁻ [67, 84, 89, 90, 93, 109–112, 122, 129, 131, 134, 136] and not larger molecules such as sulfate or nitrate. Some authors have determined so-called ion-specific parameters (Raatschen et al. [84], Wu et al. [109]), despite only investigating a single salt, and Pazuki et al. [134] re-estimated ion-specific parameters for each salt (without considering the transferability). A simple degree of freedom analysis makes it doubtful that these ion-specific parameters can be used seamlessly with other salts. While the ion-specific approach is more fundamental, the salt-specific approach also has advantages in terms of making the parameterization significantly simpler, as each salt can be parameterized individually.

What data should be used in the regression of parameters?

The majority of models are fitted to data representing the excess Gibbs energy (G^E) based on activity coefficients of solvent or solute. The mean ionic activity coefficient, $\gamma_\pm^m$ can only be measured for certain species through specialized electrochemical cells (e.g. the Harned cell for HCl), that also provide a means to determine the standard state Gibbs energy of formation [2]. The vast majority of experimental data has therefore been obtained using indirect methods that determine the activity of the solvent, rather than of the ions. In aqueous solutions

containing non-volatile electrolyte the water activity is available through measurements of the freezing point depression, boiling point elevation, vapor pressures (either through a static or a dynamic method), or isopiestic measurements that measures the vapor pressure relative to a reference system with known water activity [2]. The mean ionic activity coefficients can then be related to the activity of water through the osmotic coefficient $\Phi = \frac{x_w}{1-x_w} \ln (x_w \gamma_w)$ and the Gibbs-Duhem equation [2]:

$$\ln \gamma_\pm^m = \Phi - 1 + \int_0^{m_i} \frac{\Phi - 1}{m} dm \tag{1.9}$$

Any (consistent) thermodynamic model that captures the osmotic coefficient will therefore also capture the mean ionic activity coefficient (and vice versa). Table 1.3 summarizes the methods used in literature to estimate parameters for electrolyte systems. While there is a large variation, most authors will use properties related to the mean ionic activity coefficient or the water activity (e.g. osmotic coefficient, water activity, freezing point depression, vapor pressure etc.). While the two properties are related through the Gibbs-Duhem equation, several authors [116, 121] note that the mean ionic activity coefficient is more sensitive to the parameters and should therefore be included in the regression.

How can the temperature dependence be captured by the model?

Prediction of the temperature dependence, or at least a proper behavior of the EoS is desirable. As shown in Figure 1.16, the activity coefficient data is only weakly temperature dependent in the region from 25-100°C, and validation in this region does not automatically mean that the EoS can be used to extrapolate beyond this interval. Furthermore, Figure 1.16 shows that the saturated vapor pressure is not a good indicator for the correspondence with the mean ionic activity coefficient (and especially not in a logarithmic plot). In order to validate the temperature-dependence of the model, it is preferable to compare the temperature dependence of the activity coefficients directly. Still, several groups have presented results for e.g. gas solubility, VLE, or LLE at higher temperatures without validating the activity coefficients [84–91, 93]. In order to describe the behavior at elevated temperatures, a large number of effective temperature-dependent parameters were correlated by Myers et al. [114], Radosz et al. [121–127], Haghighi et al. [130, 131] and Lee and Kim [133]. While this will improve the correlation of the experimental data, it does not provide insight into what fundamental changes must happen to the EoS to provide predictive powers. In terms of predictions, Herzog et al [138] and Sadowski et al. [116] both fitted the activity coefficients at 25°C and predicted the temperature dependence of the vapor pressure up to ca. 70°C. But the only models that attempt to predict or correlate the behavior at high temperatures (>100°C) without introducing empirical T-dependent parameters are Rozmus et al. [139], and Zuber et al. [140, 141], of which only Rozmus et al. actually present the results at high temperatures (see Figure 1.16).

Which parameters can be predicted?

Many groups have investigated how parameters may be predicted from physical knowledge of the system. Several groups [67, 85, 89, 91, 94, 109–112] have predicted the size of ions (σ) through data collections of the crystal radii (e.g. Pauling radii). Unfortunately, the size parameter is also of great importance to the calculation of the density/apparent molar volume of mixtures. While most groups do not report the correspondence of liquid densities, relatively poor correspondence was reported by Galindo et al. (1999) [110] and Rozmus et al. [139]. One exception to this rule is Liu et al. (2005) [67] who was able to get reasonable predictions of the density at 25°C as shown in Figure 1.17. The groups that include the ion diameter in the parameter fitting but do not include volumetric data in the regression generally fail to predict the apparent molar volume [86, 113, 114, 138].
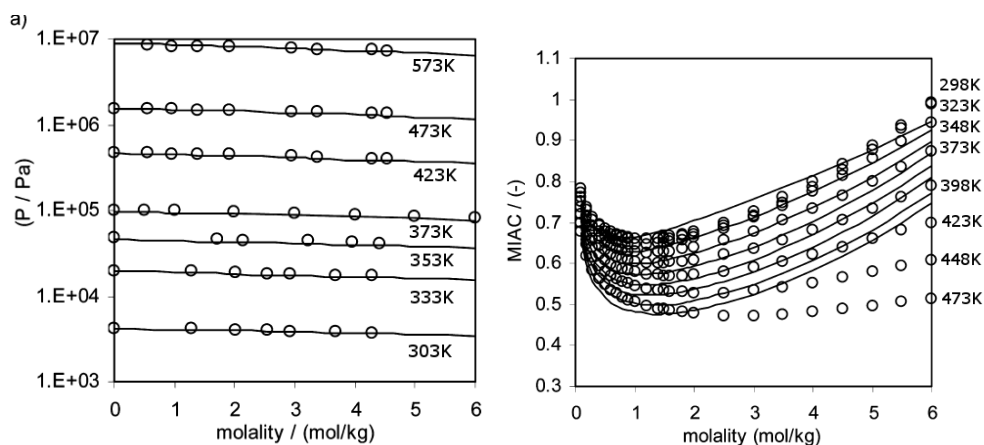
Figure 1.16: Temperature dependence of saturated vapor pressure P over aqueous KCl solutions (left) and mean ionic activity coefficients (MIAC) of NaCl (right). Both from Rozmus et al. [139].

.

Based on the results shown in literature, it is believed that using the crystal radii generally does not guarantee good correspondence with the liquid densities. The models that fit the ion diameter and include volumetric data in the parameter regression will typically obtain a reasonable agreement with both density and activity coefficients [115, 116, 118, 121–125, 128, 129, 132, 140, 141]. It is however problematic that most authors compare to the liquid densities rather than the apparent molar volume or the change in density relative to the pure fluid, since the main contribution originates from water and a comparison to the total density will therefore hide a large deviation in the apparent molar volume.

Whereas the molecular-based models typically use the diameter σ directly in the repusive/attractive terms, models that are based on cubic EoS will require calculation of the co-volume parameter b_0 which is related to the ion diameter using Eq. (1.10).

$$b_0 = \frac{2}{3} N_A \pi \sigma^3 \qquad (1.10)$$
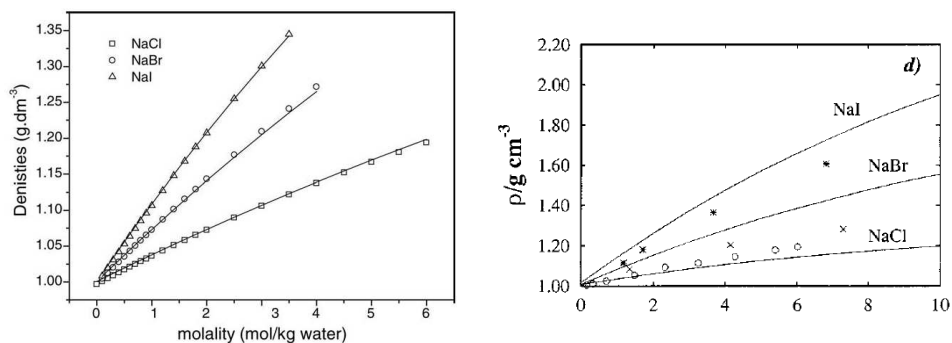
Figure 1.17: Predicted densities from Z. Liu et al. [67] (left) and Galindo et al. [110] (right)

Myers et al. (2002) [114] and Lin et al. (2007) [128] did not use the relationship between ion size and b_0 and both parameters independently, resulting in unphysical or undiscernible parameter trends.

Several groups [84, 86, 89, 90, 109, 110, 139] use Eq. (1.11) to determine the dispersive energy from the ion diameter σ, the polarizability α_0, and the number of electrons n_e, originating from dispersion theory by Mavroyannis and Stephen [159]:

$$\frac{\varepsilon_i}{k_B} = 386\sqrt{n_i^e}\left(\frac{\alpha_i}{4\pi\varepsilon_0}\right)^{1.5}\left(\frac{\sigma_i}{2}\right)^{-6} \tag{1.11}$$

Note that the dispersive energy of H^+ cannot be estimated using Eq. (1.11) equations as it does not possess any electrons; it is therefore fixed to 105K in the work by Jin/Donohue [86]. Zuo and Guo (1991) [91] related Eq. (1.11) to the attractive energy parameter a_0 of the cubic Patel-Teja EoS using Eq. (1.12) (with $f = 6$):

$$a_0 = 2.57012\pi\epsilon N_A^2\sigma^3 f \tag{1.12}$$

Simon et al. [92] proposed an alternative method for getting the cubic EoS parameters for the monatomic ions, by adopting the T_c, P_c, and ω parameters from the noble gas at the same period in the periodic table (e.g. Ne for Li^+), while for NH_4^+ he adopted the values of NH_3.

Wu et al. (1998) [109] noted that the London B-coefficient $B = 4\epsilon\sigma^6$ is independent of the volume of the ion and therefore only depends on the polarizability. Wu et al. (1998) [109] used a correlation of the critical volume ϵv_c against the London B-coefficient $B = 4\epsilon\sigma^6$ of different compounds to determine the critical volume of the ion, from which he estimated a_0 and b_0 for the Peng-Robinson EoS (but only for Na^+ and Cl^-). The effective diameter was then calculated from the co-volume parameter. In many cases the contributions from dispersion between ions has been defined as zero and only ion-solvent contributions are included.

Another approach to reduce the number of estimated parameters is used by Harvey et al. (1989) [89, 90], Zuo and Guo (1991) [91], and Aasberg-Petersen (1991), who obtained ion-solute interaction coefficients through Setschenow (salting-out) constants at 25°C and used them to (succesfully) calculate salting-out at elevated temperatures. Aasberg-Petersen (1991) furthermore fixed the ion-solvent interaction parameter is determined from the vapor pressure depression of a 1 molal solution at 100°C.

For engineering equations of state, it is desirable to have parameters that can be related to measurable properties that are available in data collections. This reduces the work-load on parameterization heavily, and thus the productivity of the engineers, if the model provides well-enough predictions. However, such experimental data only exists for salts and is therefore not easily applicable in the case of ion-specific approaches.

Mixed Solvents

Despite the many publications within e-EoS, only a surprisingly small fraction has been used to model electrolytes in mixed solvents. All models have used correlations to represent the static permittivity of the mixed solvent (see Figure 1.18 (left)), but only Simon et al. (1991) [92] have succesfully predicted the solubility of NaCl in water-ethanol mixtures without fitting additional parameters. Raatschen et al. (1987) [84] and Furst et al. (2002) [95] essentially obtained ternary parameters by fitting different ion-ion interaction parameters in water and methanol, and used volumetric mixing rules (based on salt-free mole fractions) to convert between the two. Sadowski et al. [118, 120] fitted the ion-solvent dispersion energy parameter for each ion-solvent pair and an effective (solvated) ion diameter of the ion (used in the electrostatic term)
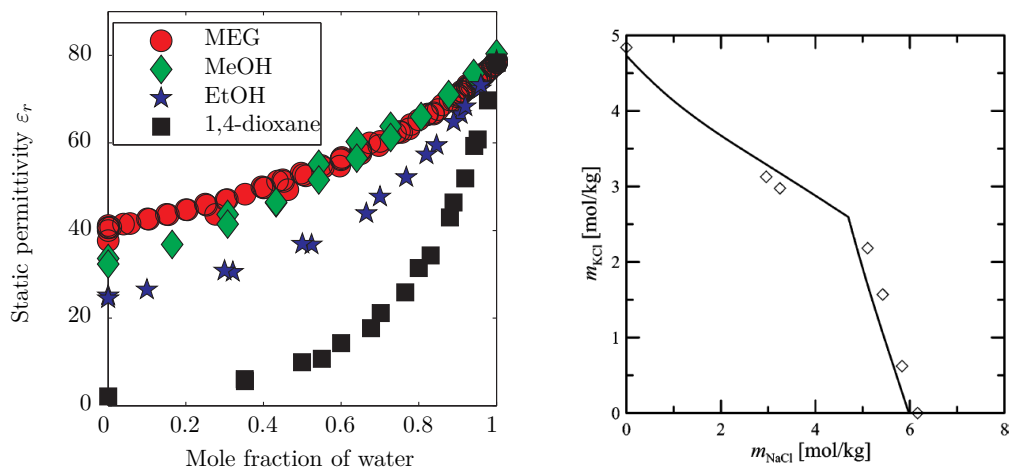
Figure 1.18: Static permittivity in mixed solvents at 25°C (MeOH at 20°C) (left) (data from [23]). Solubility and species in the mixed-salt system containing KCl and NaCl (taken from Radosz et al (2005) [122]).

to activity coefficients and liquid densities. For mixtures of water-alcohol, Sadowski et al. used a mixing rule based on the salt-free mole fraction to determine the ion size in a mixed solvent. The model by Gmehling et al. [96–108] has been used to correlate activity coefficients, and solubility of salts in other solvents (including mixtures). However, their approach rely on an excess Gibbs mixing rule with an activity coefficient model containing a series of temperature-dependent empirical interaction parameters, thus inheriting the advantages and disadvantages from the existing approaches to model electrolytes using the activity coefficient models shown in Table 1.1.

Mixed Salts
Various types of data is available for mixed salt solutions, and if the parameters have been obtained from e.g. activity coefficients of the pure salts, mixed salt data can serve as a platform for validation of the paramters. About half of the authors [88, 94, 110, 113, 114, 116, 121–125, 128, 130, 133, 160] predict either osmotic coefficients, vapor pressures, or solid-liquid equilibrium in solutions containing mixtures with 2-4 salts, indicating that most of approaches can be transferred to mixed salt solutions (see Figure 1.18).

1.7   Summary

Many different physical phenomena are occuring simultaneously in electrolyte mixtures, and the modeling of these effects is still challenging. The bottom line is that even today, engineers have limited choices of thermodynamic models that handle salts.

As ion-specific effects are ubiquitous in electrolyte solutions, it is important that thermodynamic models are based on ion-specific approaches. This is however inherently difficult, as the effect of a single ion cannot be studied individually due to the charge balance constraint, and the fact that the ions are derived from neutral salt compounds. A thermodynamic model should be able to predict the temperature dependence using a limited number of adjustable parameters.

There are many unanswered questions regarding how an equation of state should be developed to take into account the electrostatic interactions. Furthermore, since most studies have been concerned with the properties of aqueous solutions near room temperature, it still remains a challenge to develop a model that accurately predicts the properties and ion-specific effects in other solvents than water, and it often becomes a correlation exercise where additional parameters are included to counteract model deficiencies, such as the lack of an ion-solvent term to take into account Gibbs energy of solvation or the use of correlations for the static permittivity that does not include correct physical trends. The only model that has been able to predict salt solubility in a mixed solvent without fitting additional parameters is from Simon et al. (1991) [92]) and thus demonstrates that the feasibility of a more fundamental approach to modeling of the static permittivity (as opposed to correlative methods).

The critical review has also shown that there exists a variety of modeling approaches in the field of electrolyte EoS, suggesting a need to revisit the fundamentals of electrolyte thermodynamics during the course of the PhD to determine a fundamentally correct and practical approach to modeling of electrolyte mixtures with modern equations of state.

Chapter 2

Scope of this Research

While the thermodynamic modeling of mixtures containing electrolytes has received significant interest from many research groups worldwide, Table 1.2 and 1.3 illustrated that the research directions have not become harmonized. A systematic effort is needed to provide answers to the many question posed by the critical review of the current literature on electrolyte EoS shown in Section 1.6. Without such an understanding, it is doubtful that the field will become harmonized and be able to provide the industry with a new set of tools, capable of handling all types of phase behavior in electrolyte mixtures.

During this work, recommendations on how to deal with the questions posed in Section 1.6 will be provided. The columns in 1.2 therefore serves as a recipe for the initial investigations done towards developing a new equation of state based on the Cubic Plus Association EoS. In this work, the fundamentals of modeling of electrolyte systems will be investigated to shed light on the following key questions:

- How should electrostatic interactions be modeled?

- How should the static permittivity be modeled? And does it even matter?

- Should activity coefficients be converted from the McMillan-Mayer to the Lewis-Randall framework?

- Should the model include an explicit term for the Gibbs energy of solvation?

- What is the importance of ion-solvent and ion-ion association in an electrolyte EoS?

This knowledge will then be used to derive an extension to the Cubic Plus Association to describe mixtures of fully dissociated salts, and predict the solubility of light gases and hydrocarbons as well as the effect of salts on hydrate formation temperatures. This extension (herein known as e-CPA) will be developed as an engineering tool that can be integrated in commercial process simulators. We will provide recommendations on how this EoS should be further developed to tackle all types of experimental data shown in Table 1.2.

2.1   Thesis Structure

The structure of the thesis and the focus areas of different chapters is summarized below:

- **Chapter 3: The Cubic Plus Association Equation of State**
    - Introduction of the CPA model
    - Application of CPA to non-standard properties (apparent molar volume and heat capacity) for water and ethylene glycol

- **Chapter 4: Theory of Electrolyte Solutions**

  - Comparison of the Debye-Hückel and Mean Spherical Approximation Theories for Electrolyte Solutions (published in Ind. Eng. Chem. Res. (2012), 51, 5353-5363 [161]).

  - The role of the Gibbs energy of solvation in electrolyte EoS

  - Insights from molecular simulation in relation to ion-ion association and complex formation

  - Choice of the modeling framework - primitive, non-primitive, or civilized models and the conversion between McMillan-Mayer and Lewis-Randall frameworks

  - Perspectives on the role of standard states in the modeling of electrolyte solutions

- **Chapter 5: Modeling of the Static Permittivity of Complex Fluids**

  - The background for modeling of the static permittivity

  - The concept of the static permittivity in electrolyte EoS

  - Modeling of Dielectric Properties of Complex Fluids with an Equation of State (published in J. Phys. Chem. B. (2013), 117, 3389-3397) [162]

  - Modeling of Dielectric Properties of Aqueous Salt Solutions with an Equation of State (published in J. Phys. Chem. B. (2013), 117, 10523-10533) [163]

- **Chapter 6: Model Development**

  - Development of the electrolyte CPA model

  - Model structure and computational aspects

  - Parameterization and validation

- **Chapter 7: Results and Discussion**

  - Emphasis on **predictions** of the thermodynamic properties and phase equilibrium calculations, including:
    * Pressure and temperature dependence of mean ionic activity coefficients
    * SLE - Prediction of solid-liquid equilibrium in mixed salts and mixed solvents
    * VLE - Prediction of solubility of light gases, hydrocarbons, and aromatics in single salt aqueous solutions and mixed solvents
    * Gas hydrate formation pressure in single salt aqueous and mixed solvent mixtures
    * LLSE- Prediction of mutual solubilities in water-propan-1-ol-NaCl and solubility limit
    * LLLSE - Prediction of mutual solubilities in water-propan-1-ol-octane-NaCl system

  - Discussion and future work.

2.2   Overview of Research Activities

The study has been developed through four major phases:

- Investigations on the fundamentals of electrolyte thermodynamics (2010-2011) [161]

  - Comparison of the Debye-Hückel and MSA models

  - Investigation on the importance of the model for the static permittivity

- – Investigation on the role of the Born term

- Development of a predictive model for the static permittivity (2011-2013) [162, 163]

  - – Literature survey on the static permittivity of non-electrolyte mixtures
  - – Literature survey on the static permittivity containing electrolytes
  - – Model development and comparison to experimental data

- Revisiting fundamentals (2013-2014)

  - – Investigation on the role of standard state properties of electrolytes
  - – Investigation on volumetric properties for electrolytes
  - – Literature survey on ion-ion association
  - – Relationship to results from molecular simulation and statistical mechanics
  - – Harmonizing discourses and providing recommendations for future research directions

- Putting the pieces together - development of an engineering equation of state for electrolytes (2013-2014)

  - – Extension of Electrolyte Database at CERE [13] with static permittivity s of salts, new volumetric data, and performing quality assurance of existing thermal, SLE, VLE, and thermodynamic data.
  - – Implementation of thermodynamic models in FORTRAN code
  - – Model development and parameter estimation
  - – Application to VLE, LLE, and SLE

The project was supervised by Prof. G. M. Kontogeorgis and Asc. Prof. K. Thomsen at the Center for Energy Resources Engineering, Department of Chemical and Biochemical Engineering, Technical University of Denmark. Research results have continuously been presented and debated with researchers affiliated with the center, and with external collaborators from industry and academia.

The research topics have been investigated through a combination of literature surveys, data collection, and thermodynamic modeling. The results have been summarized in papers published in internationally recognized journals and presented at international conferences. A complete list of the attended conferences and publications is available in Appendix A.1-A.2. An external stay at Linde AG in September 2013 lead to additional insights in the industrial needs in electrolyte models, while a visit to Rice University in November 2013 the conclusions of the PhD study and it's implications for future theoretical research directions were discussed with other researchers in the field.

Throughout the PhD study, a dual position as Software Manager (25% of the time) has enabled a close collaboration with industrial partners and provided a unique opportunity to learn about applications of research in the field of chemical engineering thermodynamics. The main results from this work has been the:

- Development of CAPE-OPEN and Aspen Plus User Model for the Cubic Plus Association and Extended UNIQUAC models

- Development of generic library for exposing thermodynamic models and unit operations to process simulators through CAPE-OPEN

- Development of packages for performing thermodynamic modeling and parameterization using MATLAB

- Consultancy and short projects with industry (e.g. Linde AG, Gassnova, Shell, Statoil, BP, Chevron)

- Interactions with the CAPE-OPEN Laboratories Network (CO-LaN) e.g. through membership of the special interest group for thermodynamic models (ThermoSIG)

Finally, my time as the Chairman of the Society of Petroleum Engineers student chapter (2011-2012) has helped me to gain new insights on the multi-disciplinary approaches used in oil and gas industry to tackle industrial problems. A list of the courses followed during the PhD study are available in Appendix A.3 and a list of the teaching activities are available in Appendix A.4.

Part II

Thermodynamic Modeling of Electrolytes

Chapter 3

The Cubic Plus Association Equation of State

The cubic equations of state derived from the van der Waals equation of state have long been the workhorse of the oil- and gas industry [1] and many tools have been developed based on cubic EoS to e.g. describe the physical properties of mixtures of ill-defined oils and condensates. The most widely used formulations are the Soave-Redlich-Kwong (SRK) [164] and the Peng-Robinson (PR) [165] provide an excellent representation of the phase equilibrium properties of hydrocarbon mixtures. While the cubic EoS have been continuously improved through the introduction of advanced mixing rules based on the excess energy, their deficiencies are widely recognized when it comes to predicting mixtures containing both non-polar, polar and associating molecules [1].

During the past 30 years, significant advances have been made in the description of complex chemicals that display intermolecular association and hydrogen bonding. The statistical mechanical treatment of short-range directional forces (hydrogen bonding) was initially formulated in four papers by Wertheim (1984,1986) [80, 166–168] through the use of cluster expansions (graph theory). In the late 1980s, Chapman, Jackson, Radosz and Gubbins [79, 169–171] introduced a version of the Wertheim theory in the first formulation of the Statistical Associating Fluid Theory, and thereby showed how the statistical mechanical treatment by Wertheim could be readily used within the framework of thermodynamic models. In 1996, Kontogeorgis and co-workers [82] presented the first formulation of the Cubic Plus Association (CPA) EoS, which combines the cubic equations of state with the association theory from Wertheim. As the CPA EoS reduces to the SRK EoS in the absence of association, it is compatible with existing methods for e.g. characterization of oils and condensates and determine the EoS parameters from critical temperature T_c, pressure P_c, and acentric factor ω.

In this chapter the Cubic Plus Association (CPA) equation of state is introduced and an investigation on how it performs for phase equilibrium, volumetric properties, and thermal properties in mixtures of water with ethylene glycol is presented.

3.1 The Cubic Plus Association Equation of State

The CPA[1, 82, 172] equation of state (EoS) consists of the Soave-Redlich-Kwong (SRK)[164] cubic EoS with the Wertheim association theory[80] as formulated by the Statistically Associated Fluid Theory (SAFT)[79] to account for association of hydrogen bonding components. The model has been used to calculate phase equilibrium and liquid densities for many complex mixtures, especially in relation to the phase equilibrium of water, oil, natural gas and chemicals. The model was derived through perturbation of the residual Helmholtz energy of the SRK EoS

to also contain a contribution from association as shown in Eq. (3.1):

$$A^r_{\text{CPA}} = A^r_{\text{SRK}} + A^r_{\text{Association}} \tag{3.1}$$

The pressure equation of CPA is calculated from Eq. (3.2):

$$P\left(T, v, \mathbf{x}\right) = -\left(\frac{\partial A/RT}{\partial V}\right)_{T,\mathbf{n}} = \frac{RT}{v - b_0} - \frac{a\left(T\right)}{v\left(v + b_0\right)} - \frac{1}{2}\frac{RT}{v}\left(1 + \rho\frac{\partial \ln g}{\partial \rho}\right)\sum_i x_i \sum_{A_i}\left(1 - X_{A_i}\right) \tag{3.2}$$

P	[Pa]	Pressure
T	[K]	Temperature
b_0	[m^3/mol]	Co-volume parameter of the mixture , see Eq. (3.3)
$a(T)$	$\left[\dfrac{\text{Pa} \cdot \text{m}^6}{\text{mol}^2}\right]$	Van der Waals attractive energy parameter of the mixture , see Eq. (3.4)
x_i		Mole fraction of molecule i
v	[m^3/mol]	Molar volume
ρ	[mol/m^3]	Molar density
X_{A_i}		Fraction of site A on component i not bonded to any other component
$g(\rho)$		The radial distribution function at contact

The mixture co-volume is calculated from the van der Waals one fluid mixing rule[1] found in Eq. (3.3):

$$b = \sum_i \sum_j x_i x_j \left(\frac{b_i + b_j}{2}\right)\left(1 - l_{ij}\right) \tag{3.3}$$

In the case where $l_{ij} = 0$, Eq. (3.3) reduces to a simple linear mixing rule. The mixture attractive parameter $a(T)$ is normally calculated from the van der Waals one fluid mixing rules[1] shown in Eq. (3.4):

$$a\left(T\right) = \sum_i \sum_j x_i x_j \sqrt{a_i\left(T\right) a_j\left(T\right)}\left(1 - k_{ij}\right) \tag{3.4}$$

Where the pure component attractive parameter $a_i(T)$ is calculated from Eq. (3.5):

$$a_i\left(T\right) = \Gamma_i R_i b_i \left(1 + c_{1i}\left(1 - \sqrt{T_r}\right)\right)^2 \tag{3.5}$$

Γ_i	[K]	Reduced attractive energy parameter
c_{1i}		Pure component temperature dependence parameter for Soave's $\alpha(T)$-function
$T_{c,i}$		Critical temperature of component i

The k_{ij} parameter follows the temperature-dependence shown in Eq. (3.6). The temperature dependence can be used for correlation purposes over wide temperature ranges, but it is generally assumed T-independent.

$$k_{ij} = \alpha + \beta T + \gamma T^{-1} \tag{3.6}$$

The Cubic equations of state may also use excess Gibbs mixing rules for the attractive energy parameter. The Huron-Vidal/NRTL infinite pressure mixing rule has previously been applied to model mixtures with acetic acid [173], and offers an additional flexibility that helps to let the

CPA EoS accurately correlate binary interactions in complex mixtures. From the limit of the excess Gibbs energy at infinite pressure, Huron and Vidal [174] derived the mixing rule shown in Eq. (3.7) for the SRK EoS:

$$\frac{a}{b} = \sum_i x_i \frac{a_i}{b_i} - \frac{g^{E,\infty}}{\ln 2} \tag{3.7}$$

$g^{E,\infty}$ [kJ/mol]   Excess Gibbs energy at infinite pressure.

Huron and Vidal [174] introduced the modified form of the NRTL activity coefficient model shown in Eq. (3.8)

$$\frac{g^{E,\infty}}{RT} = \sum_i x_i \frac{\sum_j x_j \nu_j \exp\left(-\alpha_{ji}\frac{\Delta U_{ji}}{RT}\right)\frac{\Delta U_{ji}}{RT}}{\sum_j x_j \nu_j \exp\left(-\alpha_{ji}\frac{\Delta U_{ji}}{RT}\right)} \tag{3.8}$$

ν_i [m³/mol]   The NRTL/Huron-Vidal volume parameter for component i at infinite pressure.

α_{ij} The NRTL non-randomness parameter

ΔU_{ij} [J/mol]   Change in interaction energy between like and unlike interactions $\Delta U_{ij} = g_{ji} - g_{ii}$

In Eq. (3.8), $x_i \nu_i$ is the corrected volume fraction of molecule i at infinite pressure and this is different from the original NRTL formulation as it corrects the local volume fractions. ν_i is typically set to the co-volume parameter b_i from the EoS. Note that the Huron-Vidal/NRTL mixing rule reduces to the classical van der Waals one-fluid mixing rule when the following parameters are used:

$$\alpha_{ji} = 0 \qquad\qquad U_{ii} = \frac{a_i}{b_i}h(1) \qquad\qquad U_{ji} = \left(\frac{2a_i}{b_i} - \frac{a_{ji}}{b_j}\right)h(1)$$

$$\Delta U_{ji} = U_{ji} - U_{ii} = \left(\frac{a_i}{b_i} - \frac{a_{ji}}{b_j}\right)\ln 2 \qquad\qquad a_{ij} = \sqrt{a_i a_j}\left(1 - k_{ij}\right)$$

Generally, the CPA uses the parameters $\Gamma = a/Rb$, b, and c_1 for the physical part and the association strength β and association energy ϵ/k_B for hydrogen bonding. The site fractions are determined by solving Eq. (3.9) using the association strength $\Delta_{A_i B_j}$ between site A on molecule i and site B on molecule j.

$$\frac{1}{X_{A_i}} = 1 + \frac{1}{v}\sum_j x_j \sum_{B_j} X_{B_j} \Delta_{A_i B_j} \tag{3.9}$$

$$\Delta_{A_i B_j} = g(\rho)\, v_{A_i B_j}\left[\exp\left(\frac{\epsilon_{A_i B_j}}{k_B T}\right) - 1\right] \tag{3.10}$$

$\Delta_{A_i B_j}$ [m³/mol]   The association strength between site A on molecule i and site B on molecule j, calculated using (3.10).

$v_{A_i B_j}$ [m³/mol]   Association volume calculated using Eq. (3.14) or Eq. (3.15)

$\epsilon_{A_i B_j}$ [J]   Association energy calculated using Eq. (3.13)

The radial distribution function in CPA $g(\rho)$ is calculated from Eq. (3.11):

$$g(\rho) = (1 - 1.9\eta)^{-1} \tag{3.11}$$

In which the packing factor in CPA is give by $\eta = b/4v$. For a pure component, the site fractions X_A are related to the monomer fraction through Eq. (3.12):

$$X_1 = \prod_{A_i} X_{A_i} \tag{3.12}$$

In order to set up the association equilibrium constant $\Delta_{A_i B_j}$, Huang and Radosz [175] proposed to use association schemes based on the lone pairs of molecules as summarized in Table 3.1 for alcohols and water. The cross-association between associating molecules such as water and
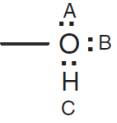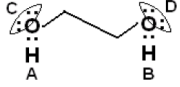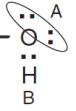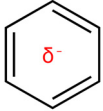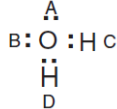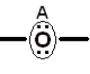
Species	Formula	Scheme	Species	Formula	Scheme
Alcohol		3B	Glycols		4C
Alcohol		2B	Benzene	One negative solvation site	
Water		4C	Ether		

Table 3.1: Examples of pure component association schemes.

ethylene glycol in CPA is modeled by using the near Elliott combining rule (Eq. (3.13) and Eq. (3.14))[1] or the CR-1 combining rule (Eq. (3.13) and Eq. (3.15)) for the cross-association energy and volume.

$$\epsilon_{A_i B_j} = \frac{\epsilon_{A_i} + \epsilon_{B_j}}{2} \tag{3.13}$$

$$v_{A_i B_j} = \sqrt{\beta_{A_i} \beta_{B_j} b_i b_j} \tag{3.14}$$

$$v_{A_i B_j} = \sqrt{\beta_{A_i} \beta_{B_j}} \left(\frac{b_i + b_j}{2} \right) (1 - l_{ij}) \tag{3.15}$$

The association constants between an associating compound i (e.g. water) a non-self-associating compound i, such as ethers or aromatic compounds and an associating compound such as water are obtained by fitting β_{ij} and determining $\epsilon_{ij} = \epsilon_i/2$ [1]. Both β_{ij} and ϵ_{ij} can be fitted to improve the temperature dependence of the cross-association (as is e.g. done for water-CO_2). However, it is generally preferred to use as few binary parameters as possible.

Given a pressure and a temperature, Eq. (3.2) is solved for the volume root V of the desired phase. Phase equilibrium is subsequently determined from the fugacity coefficients calculated using the EoS.

---

[1]The original Elliott combining rule is $\Delta_{A_i B_j} = \sqrt{\Delta_{A_i B_i} \Delta_{A_j B_j}}$ where $\Delta_{A_i B_i}$ is the association constant between two sites on the same molecule i calculated with Eq. (3.10).

In the case of non-associating compounds, the pure compound parameters Γ_i, b_i, c_{1i} are adjusted to match to vapour pressure and liquid density. For associating compounds, the first step is to decide on an association scheme and then include association energy ϵ/k_B and strength β in addition to the three other parameters in the fitting procedure. For certain classes of compounds (e.g. alcohols), the association parameters are reused. For aromatic compounds, it is also possible to reuse the solvation parameters from other aromatic compounds.

3.1.1 Applications Beyond Excess Properties and Phase Equilibrium

The binary parameters are correlated to vapor-liquid or liquid-liquid equilibrium data of binary mixtures, and these parameters are then used to predict the behavior of multi-component mixtures. The following section contains a case study on how well the CPA EoS predicts other properties, such as excess volume and excess enthalpy, as these properties are also important when developing an extensible framework for modeling of electrolyte mixtures with chemical equilibrium or solid-liquid equilibrium. While the main purpose of the EoS is to obtain good correspondence for the phase equilibrium properties, it must be realized that the activity coefficient models used for handling electrolyte systems are typically parameterized to all types of data. It is therefore interesting to determine how well the CPA equation of state reproduces the fluid properties, to evaluate whether the proiperties can be included in the parameterization of electrolyte systems.

3.1.1.1 Calculation of Excess Properties

The excess volume can be calculated from the total mixture volume v and pure component volumes v_i using Eq. (3.16), which are both calculated from the equation of state:

$$v^E = v - \sum_i x_i v_i \tag{3.16}$$

The thermal properties of pure compounds and mixtures with an equation of state can be calculated from Eq. (3.17):

$$H(T, P, \mathbf{n}) = H^{id} + H^r \tag{3.17}$$

The ideal gas enthalpy of the mixture is calculated from Eq. (3.18)

$$H^{id} = \sum_i x_i H_i^{id} \tag{3.18}$$

Where the ideal gas enthalpy of a pure compound is calculated from Eq. (3.19):

$$H_i^{id} = H_{i,ref}^{id} + \int_{T_{ref}}^{T} C_{p,i}^{id} dT \tag{3.19}$$

The residual contributions are obtained from the temperature fugacity coefficients given by Eq. (3.20):

$$\frac{H^r}{RT} = -T \sum_i x_i \left(\frac{\partial \ln \hat{\varphi}_i}{\partial T} \right)_{V,\mathbf{n}} \tag{3.20}$$

The heat capacity is calculated from Eq. (3.21)

$$C_p = \sum_i x_i C_{p,i}^{id} + C_p^r \tag{3.21}$$

The ideal gas heat capacity is obtained from the DIPPR correlation shown in Eq. (3.22):

$$C_{p,i}^i d = A_i + B_i \left(\frac{\frac{C_i}{T}}{\sinh \frac{C_i}{T}} \right) + D_i \left(\frac{\frac{E_i}{T}}{\sinh \frac{E_i}{T}} \right) \tag{3.22}$$

The residual heat capacity C_p^r can be obtained from the reduced residual Helmholtz energy $F = A^r/RT$ using Eq. (3.23):

$$\frac{C_p}{R} = -1 - \frac{1}{n_T} \left[T^2 \left(\frac{\partial^2 F}{\partial T^2} \right)_{V,\mathbf{n}} + 2T \left(\frac{\partial F}{\partial T} \right)_{V,\mathbf{n}} + \frac{T}{R} \left(\frac{\partial V}{\partial P} \right) \left(\frac{\partial P}{\partial T} \right)^2 \right] \tag{3.23}$$

The excess thermal properties are determined from the change relative to the pure components assuming an ideal mixture as shown in Eq. (3.24):

$$\begin{aligned} H^E(T, P, \mathbf{n}) &= H - \sum_i x_i H_i \\ &= -RT^2 \sum_i x_i \left[\left(\frac{\partial \ln \hat{\varphi}_i}{\partial T} \right)_{P,\mathbf{n}} - \left(\frac{\partial \ln \hat{\varphi}_i^o}{\partial T} \right)_{P,\mathbf{n}} \right] \\ &= -T \sum_i x_i \left(\frac{\partial \ln \gamma_i^o}{\partial T} \right)_{V,\mathbf{n}} \end{aligned} \tag{3.24}$$

Where the heat capacity is obtained from the temperature derivative of Eq. (3.24). The activity coefficients γ_i are calculated from the difference of the pure compont standard state fugacity coefficients $\hat{\phi}_i^o$ shown in Eq. (3.25):

$$\ln \gamma_i = \ln \hat{\varphi}_i - \ln \hat{\varphi}_i^o \tag{3.25}$$

In the case of regular compounds, such as water or ethylene glycol, the pure compound is used as the standard state. Ions, however, use the rational unsymmetrical standard state, i.e. at $\ln \hat{\varphi}_i^o$ denotes the standard state at infinite dilution in water.

3.1.1.2 Case Study: Water and Ethylene Glycol

The pure component parameters for water and ethylene glycol taken from previous work by Kontogeorgis et al. and summarized in Table 3.2:

	T_c [K]	P_c [bar]	ω	Γ [K]	b_0 [cm^3/mol]	c_1	Association scheme	$1000 \times \beta$	ϵ_{AB}/k_B [K]
H$_2$O	647.13	220.55	0.3449	1017.34	14.515	0.67359	4C	69.2	2003.25
MEG	720	77	0.4868	2531.71	51.4	0.6744	4C	14.1	2375.75

Table 3.2: Pure fluid parameters for water and ethylene glycol

The deviations from properties from freezing point and up to 200°C compared to the most recent correlations in the DIPPR database are presented in Table 3.3. Note that the heat of

RAD [%]	P_{sat}	ρ_{liq}	ΔH_{vap}	$C_{\text{p,liq}}$
H$_2$O	0.793	0.93	1.522	6.154
MEG	1.263	1.605	0.29	6.068

Table 3.3: Relative deviations from DIPPR correlations[176] from 0-200°C.

vaporization are related to the vapor pressures using Eq. (3.26):

$$\ln P^{sat} = -\frac{\Delta_{vap}H}{RT} + C \tag{3.26}$$

Where C is a constant of integration. The deviations in the heat of vaporization are therefore a different representation of the deviations in the vapor pressures and vice versa. While the deviations in the saturated vapor pressure, liquid density, and heat of vaporization are acceptable, the deviation in the heat capacity is not - and certainly not when the temperature-dependence of the deviations are as high as shown in Figure 3.1-3.2.
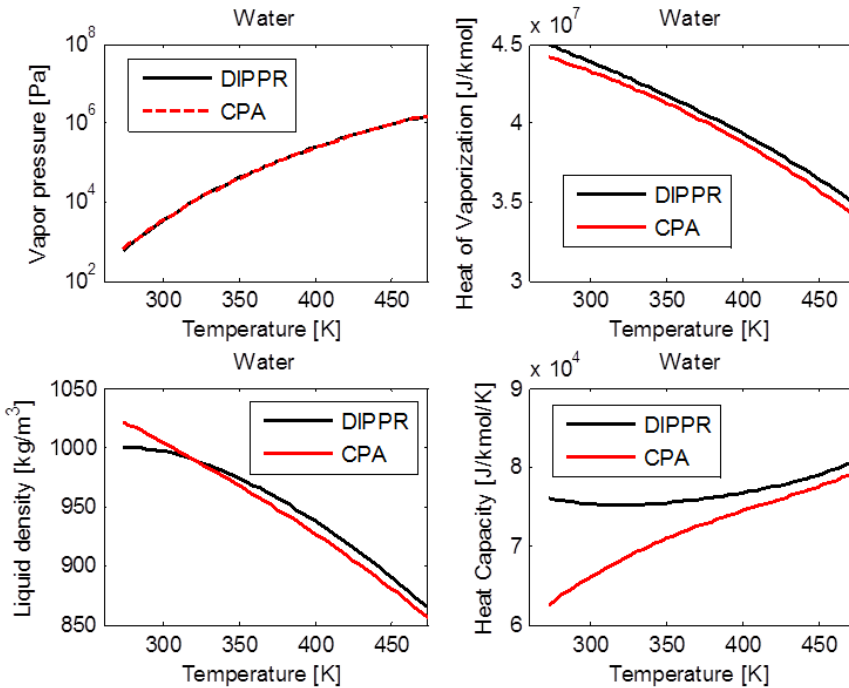
Figure 3.1: Pure component properties for water with CPA at the saturation line. The model was parameterized against the vapour pressure and liquid density, and the heat of vaporization and heat capacity was predicted.

It is considered infeasible to attempt correlating the heat capacity along with the EoS as the functional form of the CPA model is too simple to capture the non-monotonic behavior of complex chemicals. Since the CPA EoS does not predict the thermal properties of the liquid phase (especially water) to a high enough accuracy, a different approach must be used in order to include properties such as enthalpy of dilution and apparent molal heat capacity in parameterization. A separate model can then be used for the standard state properties and the EoS can be used to calculate the deviation from this standard state.

3.1.1.3 Case Study: Water-Ethylene Glycol Mixture

For the binary mixture of water-ethylene glycol, the CPA parameters were published in Derawi et al.[177]. The results obtained with the published parameters are defined as Case 1.
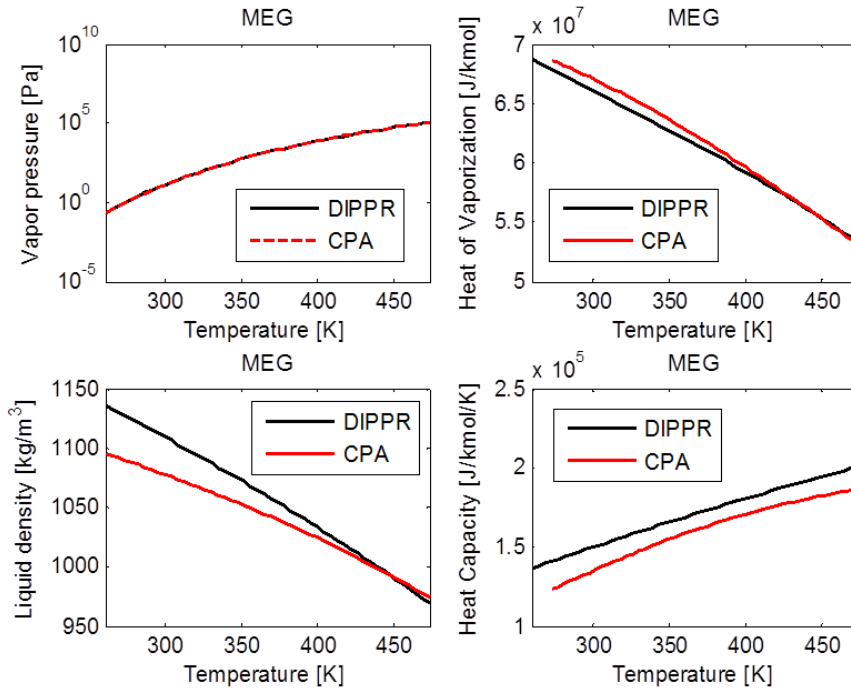
Figure 3.2: Pure component properties for ethylene glycol with CPA at the saturation line. The model was parameterized against the vapour pressure and liquid density, and the heat of vaporization and heat capacity was predicted.

A summary of the results for different cases is shown in Table 3.4. It was observed that the default parameters gave good correspondence with VLE and excess enthalpy, but that the correspondence with excess volume was less satisfactory and showed in fact the opposite trends (see Figure 3.3). While the excess volume is only a small part of the total volume (typically less than 1%), as it could be a sign of the current parameters giving a misrepresentation of the physical interactions in the system.

RAD[%]	kij	lij	Combining rule	$C_{p,liq}$	Excess $C_{p,liq}$	H_{liq}	Excess H_{liq}	V_{liq}	Excess V_{liq}	VLE
Case A	0	0	Elliott	12.70%	0.40%	0.23%	170%	1.60%	259%	Bad
Case B	0	0	CR-1	12.90%	0.50%	0.20%	145%	1.60%	255%	Bad
Case 1	-0.115	0	Elliott	12.60%	0.30%	0.05%	36%	1.20%	199%	Good
Case 2	-0.05	0.0368	Elliott	12.70%	0.40%	0.07%	49%	0.10%	28.50%	Good
Case 3	-0.05	0	CR-1	12.80%	0.40%	0.12%	87%	1.40%	220%	OK
Case 4	0	0.0368	CR-1	12.90%	0.60%	0.12%	84%	0.20%	41%	OK

Table 3.4: Results for water-ethylene glycol mixtures with CPA for different mixing rule parameters and combining rules (CR) for the cross-association from 0-200°C.

Figure 3.3 shows the correspondence of the CPA with the excess volume and a calculation of the free volume with and without fitting the l_{ij}. Note that the free volume decreases indi-

cating a less structured fluid in the mixtures of the two - this is well in line with the expected behavior. Figure 3.3 shows that with an l_{ij} it is possible to remedy some of the defects of the
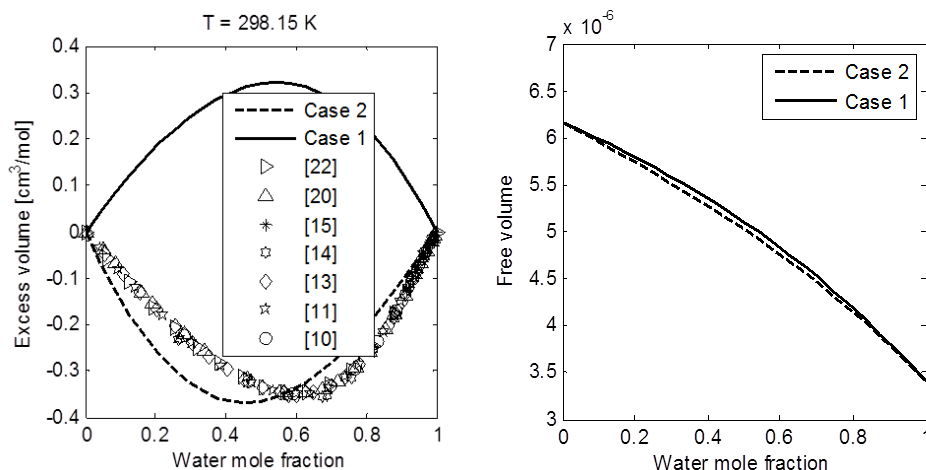
Figure 3.3: Excess molar volume (left) and free volume (V-b) calculated by the CPA EoS in Case 1 and Case 2 (see Table 3.4) at 25 °C and 1 atm.

model. Furthermore, the k_{ij} needed to correlate the VLE was significantly reduced (from -0.115 to -0.05, indicating improved predictions when the volume data and change in fluid structure was taken into account). The apparent molar volumes shown in Figure 3.4, shows that there are the structural changes occurring in the fluid that leads to a reduction in the volume required for a water molecule. This may be attributed to changes in the hydrogen bond network, but this effect is not included in the Case 1 (published) CPA parameters. Figure 3.4 shows that without using an $l_{ij} = 0$, CPA predicts the opposite trend in apparent molar volume. This can be remedied by using an l_{ij} obtained from the volumetric data. It was observed that the other binary parameter, k_{ij} and β_{ij}, cannot be adjusted to capture the excess volume satisfactorily without also losing other properties.

Table 3.4 also shows that the correspondence with excess enthalpy is slightly worse (but this only constitutes less than a half percent of the total enthalpy). Representative results for thermal properties and VLE are shown in Figures 3.5-3.7. Note that the CR-1 mixing rule (Case 3 and 4) does not perform so well for this mixture in terms of VLE as shown in Figure 3.8: Using an l_{ij} modifies both the volumetric properties and the combinatorial part of the activity coefficient, and has previously been shown to work well for highly unsymmetrical mixtures [179]. The dangers of using both an l_{ij} and a k_{ij} is that even with a cubic EoS the combination of these two interaction parameters can correlate many binary systems[180]; however, this success is not necessarily due to proper representation of the physics. Therefore, if an l_{ij} and k_{ij} is used to correlate a system, it is important to require considerable improvements over fitting only one of the parameters. When the l_{ij} that gives good correspondence with excess volumes is used for the water-MEG system, it reduced the absolute value of the binary interaction parameter k_{ij}, meaning that the predictions were improved. A more general investigation should be performed to see if the inclusion of an l_{ij} fitted to excess volume data would also improve predictions in other systems with considerable excess volume, such as mixtures of water with alcohols, ketones, and organic acids.
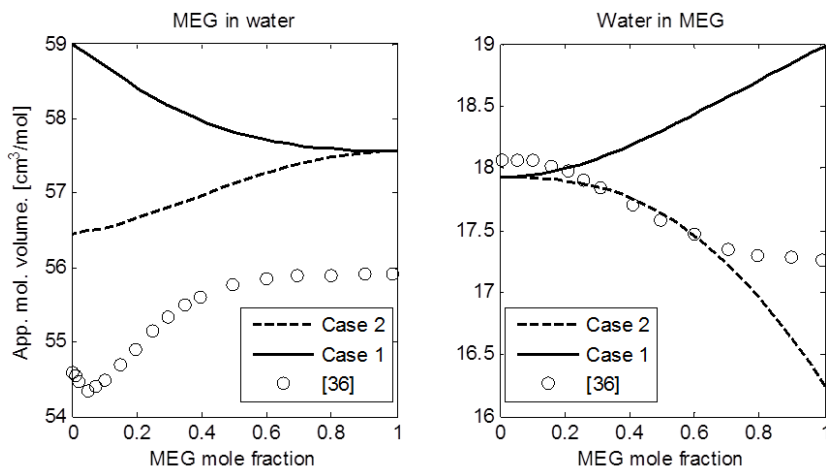
Figure 3.4: Apparent molar volume of water and ethylene glycol with CPA and comparison to experimental data[178] for Case 1 and 2 (see Table 3.4) at 25°C and 1 atm.
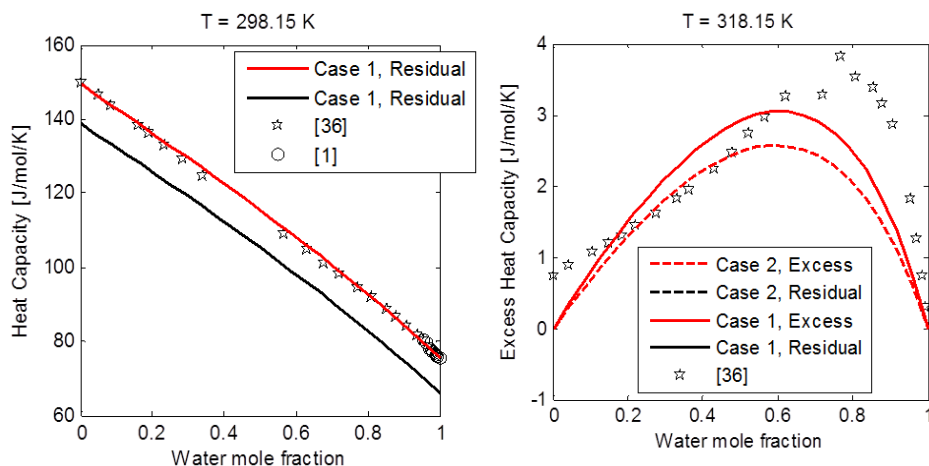
Figure 3.5: Total (left) and excess (right) heat capacities of the water-ethylene glycol mixture calculated by the CPA EoS in Case 1 and Case 2 (see Table 3.4) at 1 atm.

3.2 Summary

The Cubic Plus Association equation of state was presented in its complete form with the classical van der Waals one-fluid mixing rules and the Huron-Vidal/NRTL mixing rule. It was shown that the classical mixing rules are really a special case of the NRTL/Huron-Vidal mixing rules. The CPA EoS was applied to model mixtures of water and ethylene glycol to demonstrate the importance of selection of the combining rules for the association term. The investigation furthermore showed that while the EoS provides fair agreement with total volume and VLE, it does not accurately capture excess properties such as excess enthalpy, volume, or heat capacity. Furthermore, it was shown that the liquid heat capacities of pure water and ethylene glycol could not be accurately predicted from the ideal gas reference state, indicating that it is necessary to use the liquid standard state when precision is required for the thermal
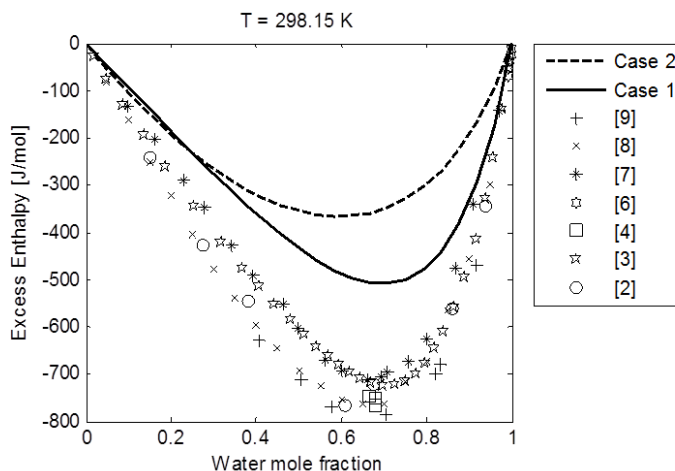
Figure 3.6: Excess enthalpy of water-ethylene glycol mixture at 25°C and 1 atm for Case 1 and 2 (see Table 3.4).
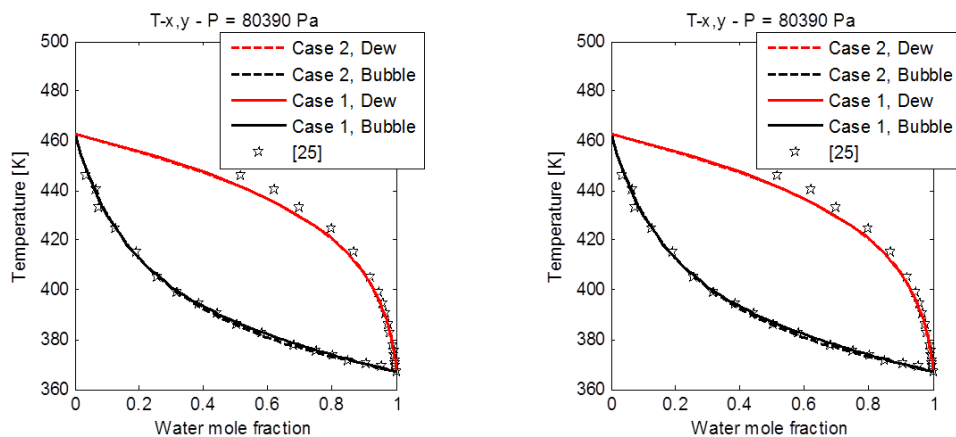
Figure 3.7: T-x,y (left) and P-x,y (right) diagrams for the vapor-liquid equilibrium of water and ethylene glycol for Case 1 and 2 (see Table 3.4).

properties (e.g. in relation to equipment design). Finally, it was shown how predictions of the VLE could be improved by fixing an l_{ij} to excess or apparent molar volumes for this particular system, but more work would be needed to show the generality of this approach.
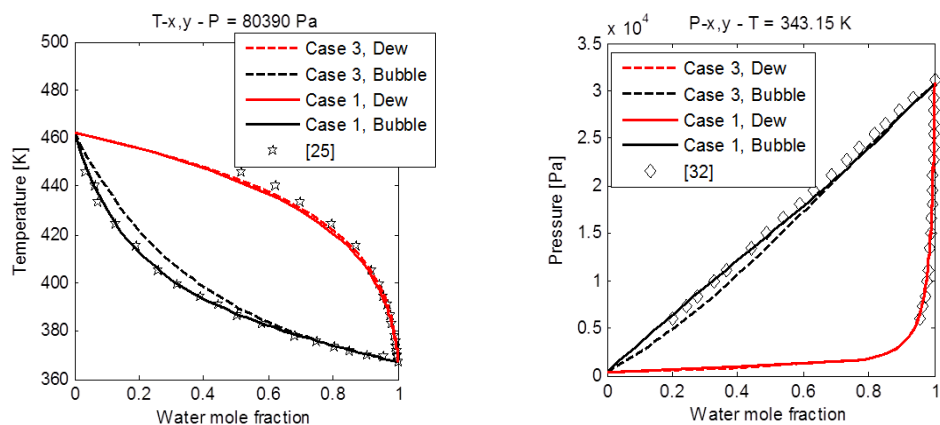
Figure 3.8: T-x,y (left) and P-x,y (right) diagram of the vapor-liquid equilibrium of water and ethylene glycol with Elliott (Case 1) or CR-1 (Case 3) (see Table 3.4).

Chapter 4

Theory of Electrolyte Solutions

From the literature review in the Chapter 1 it was demonstrated that there are several different interpretations of the background of electrolyte thermodynamics and conflicting opinions on how an electrolyte equation of state should be developed. A set of research questions were identified in order to harmonize the approach to developing electrolyte EoS. This chapter will systematically investigate the research questions and develop recommendations on how an engineering electrolyte EoS should be constructed.

The first sections deal with the primitive models for electrolyte mixtures. The Debye-Hückel equation and the mean spherical approximation are compared and the importance of the relative static permittivity ε_r (or dielectric constant) for the primitive models for electrolytes is highlighted. This work was published in Ind. Eng. Chem. Res. (2012), 51, 5353-5363 [161] and has been shortened to avoid repetition of the previous chapters. A short follow-up to the conclusions from this article is presented to demonstrate how the primitive models for electrolyte solutions could be improved by insights from molecular simulation and ion-ion association. Furthermore, the background for the Born model is investigated to show the importance of the Gibbs energy of hydration in electrolyte models. It will also be demonstrated how the Debye-Hückel and the Born equation can both be derived through a simple charging procedure. Additionally, it is suggested that the complete electrolyte equation of state offers new opportunities for modeling and prediction of the standard state properties based on the ideal gas state, which can help to simplify the treatment of systems with complex chemical speciation.

Following up on the discussion of primitive models, the relationship between the primitive and non-primitive models for electrolyte solutions is demonstrated. From a statistical mechanical perspective, these models are intrinsically linked through the static permittivity which must be calculated from a physically based model that takes into account interactions between all compounds in the mixture. Based on this evidence and a comparison with the non-primitive models, it is suggested that it becomes unnecessary to convert from the McMillan-Mayer to the Lewis-Randall framework in an electrolyte EoS when a physically realistic model is used for the static permittivity.

4.1 Modeling of Electrostatic Interactions

As illustrated in Chapter 3, equations of state may be formulated in terms of the residual Helmholtz energy using the perturbation theory where the total Helmholtz energy is written as the sum of different contributions. Eq. (4.1) shows how the electrostatic interactions can be included in CPA:

$$A^r = A^{\text{SRK}} + A^{\text{Association}} + A^{\text{Electrostatics}} \tag{4.1}$$

The derivative of each model for the Helmholtz energy will provide a contribution to the pressure/volume, chemical potential, and thermal properties of the mixture. Still, as illustrated in the introduction chapter, the literature on electrolyte equations of state do not agree on which term should be used for the electrostatic interactions. The most common primitive models for the electrolyte interactions are the Debye-Hückel model[26] and the electrostatic part of the mean spherical approximation (MSA)[47, 48]. Both models use Coulomb's law to describe the force between two charges z_i and z_j given by Eq. (4.2):

$$F\left(r\right) = \frac{e^2}{4\pi} \frac{1}{\varepsilon_r \varepsilon_0} \frac{z_i z_j}{r_{ij}^2} \tag{4.2}$$

The coulombic forces are lowered when the relative static permittivity of the medium increases (e.g. in water with $\varepsilon_r = 78$ at 25°C) which enables the dissociation of salts. Another fundamental equation is the electroneutrality condition, i.e. that the net charge of a system is zero:

$$\sum_i \rho_i q_i = 0 \tag{4.3}$$

ρ_i [mol/m^3]   Molar density of component i

The Debye-Hückel model[26] was first derived by Debye and Hückel (1923) from a linearization of the Poisson equation by treating all ions as point charges and assuming a minimum distance of d_i between the ions surrounding a central ion. The non-restricted primitive MSA model was developed by Blum[47, 48] from statistical mechanics, by treating ions as charged hard spheres of different diameters σ_i. In the original MSA model, the screening length Γ must be solved for numerically as it is done in this work, but several simplifications of the MSA theory making it into an explicit equation of the Helmholtz energy have been presented in literature[1, 110]. Figure 4.1 shows a visual interpretation of the assumptions of the two models.
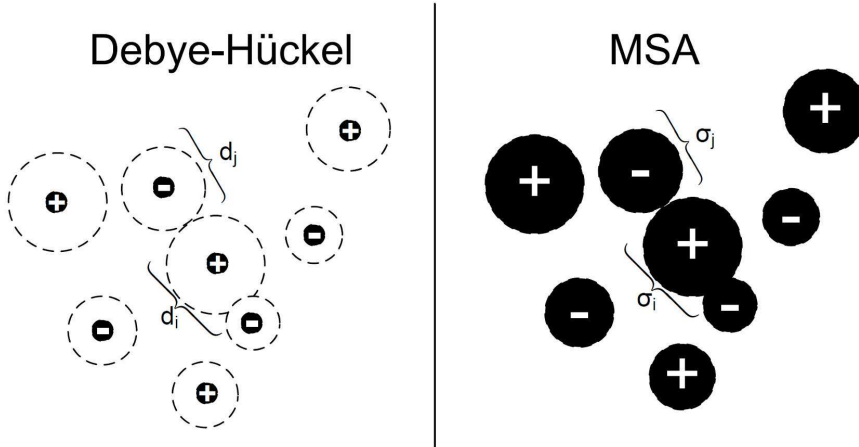
Figure 4.1: Illustration of assumptions used in the Debye-Hückel and in the MSA model. Debye-Hückel treats ions as point charges with a minimum separation distance, while MSA treats all ions as charged hard spheres.

Several authors have presented the differences between the Debye-Hückel and MSA models for use in an equation of state [52, 85–89, 110–112, 114]. Myers et al.[114] stated that MSA yields better results for the thermodynamic properties of electrolyte solutions at high concentrations. Along the same lines, Paricaud et al.[111] stated that since the simpler Debye-Hückel

theory treats ions as point charges it is only correct for infinitely dilute solutions and quickly breaks down at increasing electrolyte concentrations where the ion-ion and ion-solvent correlations become important. It has also been stated that the liquid densities are better described by MSA than Debye-Hückel[110, 112].

While the observations of these authors may be valid, it is important to realize that the liquid densities are obtained through an implicit function that includes volume and compositional derivatives from all contributions to the Helmholtz energy to solve for the bubble point pressure and vapor/liquid volumes. The results obtained from this procedure furthermore depend on the method used for parameter estimation and the experimental data that was used in the parameter estimation. Sadowski et al. [115–120] have succesfully developed an electrolyte extension of PC-SAFT based on Debye-Hückel, and Bostrom et al. [59] showed that similar results were obtained from numerical solution of the non-linear Poisson-Boltzmann equation to the HNC and Monte Carlo simulations to determine the radial distribution of ions near a protein (macro-ion), indicating that the Poisson-Boltzmann equation is not inferior to molecular simulation. Rather than comparing the complete EoS after parameterization, this investigation will perform a fair and un-biased comparison of MSA and Debye-Hückel by comparing the contributions to the residual Helmholtz energy from MSA and Debye-Hückel at constant temperature, volume and composition.

4.1.1 On the derivation of the Debye-Hückel theory

This section presents parts of the derivation of the Debye-Hückel theory to illustrate important concepts of electrolyte thermodynamics that are common to the Debye-Hückel and MSA theories for long-range electrostatic interactions. The derivation follows the approach presented by other authors[26, 181–183].

The Poisson equation relates the electrical potential ψ_i with the local charge density $c_i(r)$ of ion i. In spherical coordinates, the Poisson equation may be written as Eq. (4.4):

$$\nabla^2 \psi_i = -\frac{c_i(r)}{\varepsilon_0 \varepsilon_r} \tag{4.4}$$

ψ_i		Electrical potential around component i , see Eq. (4.4)
c_i	$[\text{C/m}^3]$	Charge density of component i

The local number density of the ions surrounding ion j may be written as Eq. (4.5):

$$c_j(r) = N_A e \sum_i^N z_i \rho_i g_{ij}(r) \tag{4.5}$$

Eq. (4.4) may only be solved when $g_{ij}(r)$ is a known function of the potential $\psi_i(r)$ [184]. To arrive at an expression for the pair correlation function, the potential of average force $w_{ij}(r)$ is first defined in Eq. (4.6):

$$g_{ij}(r) = \exp\left[-\frac{w_{ij}(r)}{k_B T}\right] \tag{4.6}$$

w_{ij}	$[\text{J}]$	Potential of average force exerted between molecule i and j

$w_{ij}(r)$ is then assumed to be proportional to the electrostatic potential as shown in Eq. (4.7):

$$w_{ij}(r) = e z_j \psi_i(r) \tag{4.7}$$

Inserting Eq. (4.7) into Eq. (4.6) gives an expression for the radial distribution function as shown in Eq. (4.8).

$$g_{ij}(r) = \exp\left[-\frac{ez_j\psi_i(r)}{k_BT}\right] \tag{4.8}$$

Onsager [185] showed that the assumption that the distribution of ions was given by Eq. (4.8) becomes inconsistent for charge-asymmetric electrolytes since the logical requirement that $\rho_j g_{ji}(r) = \rho_i g_{ij}(r)$ is not fulfilled, except for the linearized Poisson equation. Onsager [186] presented a procedure to remedy this discrepancy of the derivation by using higher order corrections of the Debye length, but this will not be investigated further here.

Using Eq. (4.8) the charge density of the Debye-Hückel theory can be determined from Eq. (4.9) and it follows that the Poisson-Boltzmann equation is given by Eq. (4.10):

$$c_i(r) = N_A e \sum_j^N z_j \rho_j \exp\left[-\frac{ez_j\psi_i(r)}{k_BT}\right] \tag{4.9}$$

$$\nabla^2\psi_i = -\frac{e}{\varepsilon_0\varepsilon_r}\sum_j^N z_j \rho_j \exp\left[-\frac{ez_j\psi_i(r)}{k_BT}\right] \tag{4.10}$$

Eq. (4.11) is obtained after linearizing Eq. (4.10):

$$\nabla^2\psi_i = -\sum_j^N ez_j\rho_j\left(1 - \frac{ez_j\psi_i(r)}{k_BT}\right) \tag{4.11}$$

The final expression for the linearized Poisson-Boltzmann equation (Eq. (4.13)) is obtained from Eq. (4.11) by inserting the electroneutrality condition from Eq. (4.3) and by defining the Debye length κ^{-1} from Eq. (4.12):

$$\kappa^2 = \frac{e^2}{k_BT}\frac{1}{\varepsilon_r\varepsilon_0}\sum_i^N \rho_i z_i^2 \tag{4.12}$$

$$\nabla^2\psi_i = \kappa^2\psi_i(r) \tag{4.13}$$

Thus, the electrical potential ψ_i may be deduced by the solution to Eq. 4.13 imposing the boundary conditions $\lim_{r\to\infty}\psi_i(r) = 0$ and Eq. (4.2) as presented in the derivation shown in e.g. McQuarrie[181] or Michelsen and Mollerup [182]. With both models, the electrostatic potential of a molecule with fractional charge λq_i may be calculated using Eq. (4.14):

$$\psi_i(r = d_i) = \frac{\lambda q_i}{4\pi\varepsilon_r\varepsilon_0}\frac{1}{d_{ij}}\frac{1}{1 + \lambda\kappa d_{ij}} \tag{4.14}$$

The total electrostatic potential at $r = d_{ij}$ may be related to the excess Helmholtz energy using the partial charging process [181, 182], where the ion with charge λq_i is charged from $\lambda = 0$ to 1, as presented in Eq. (4.15)-(4.16):

$$A^{DH} = \sum_i n_i ez_i \int_0^1 \psi_i(\lambda)\,d\lambda \tag{4.15}$$

$$A^{DH} = -\frac{k_BTV}{4\pi N_A \sum_i n_i z_i^2}\sum_i n_i z_i^2 \chi_i \tag{4.16}$$

A^{DH} [J/mol] Helmholtz energy from the Debye-Hückel model

Where the function χ_i is given by Eq. (4.17)

$$\chi_i = \frac{1}{d_i^3}\left[\ln\left(1 + \kappa d_i\right) - \kappa d_i + \frac{1}{2}(\kappa d_i)^2\right] \tag{4.17}$$

The complete derivatives of up to 2nd order are provided in the book by Michelsen and Mollerup[182].

Pitzer [38, 187] discussed how the hard-core contribution could be included in the Debye-Hückel theory using a statistical mechanical treatment of the osmotic pressure Π given by Eq. (4.18).

$$\Pi - \rho k_B T = -\frac{4\pi}{6}\sum_i\sum_j \rho_i\rho_j\int\limits_0^\infty\left(\frac{\partial u_{ij}}{\partial r}\right)g_{ij}\left(r\right)r^3 dr \tag{4.18}$$

Using a potential u_{ij} for the hard-core ions given by Eq. (4.19), Pitzer[38, 187] derived the expression shown in Eq. (4.20) by including the third order Taylor expansion of the radial distribution function g_{ij} from Eq. (4.8).

$$u_{ij} = \begin{cases} \infty & r < d_{ij} \\ \dfrac{z_i z_j e^2}{4\pi\varepsilon_r\varepsilon_0 r} & r >= d_{ij} \end{cases} \tag{4.19}$$

$$\frac{\Pi}{\rho k_B T} - 1 = -\frac{\kappa^3}{24\pi\rho\left(1 + \kappa d_i\right)} + \rho\left[\frac{2\pi d^3}{3} + \frac{1}{48\pi}\frac{\kappa^4 d_i}{\rho^2(1 + \kappa d_i)^2}\right] \tag{4.20}$$

As pointed out by Onsager[185], methods that use higher order terms of the radial distribution function will become inconsistent for unsymmetrical electrolytes as the logical requirement $\rho_j g_{ji}\left(r\right) = \rho_i g_{ij}\left(r\right)$ is not fulfilled. Pitzer notes that the method is consistent for symmetrical electrolytes, and that the inconsistency for unsymmetrical cases is small. Since the model by Pitzer includes the contribution from hard-core repulsions, it is not suited as a perturbation for the electrostatic forces in an EoS, as the EoS already contain terms that account for the short-range interactions. The Pitzer equation [38] is used to accurately correlate experimental data for osmotic coefficients and such correlations are e.g. used by the oil industry to evaluate scaling propensity using the ScaleSoftPitzer software from the Brine Chemistry Solutions [43].

4.1.2 On the derivation of the MSA theory

The fundamental difference between the derivations of the MSA and the Debye-Hückel theories is that MSA treats the ions as hard-core spherical molecules with diameter σ_i. This gives rise to an excluded volume that is inaccessible to other ions leading to different expressions for the Helmholtz energy and screening length compared to the Debye-Hückel theory. The lengthy derivation of MSA has been presented by Blum[47, 48] and will not be repeated here. The final expression for the excess internal energy is given by Eq. (4.21):

$$\Delta E^{\mathrm{MSA}} = -\frac{Ve^2}{4\pi\varepsilon_r\varepsilon_0}\sum_i^N \rho_i z_i\left[\frac{\Gamma z_i + \eta\sigma_i}{1 + \sigma_i\Gamma}\right] \tag{4.21}$$

In which Γ is given by the MSA closure equation from Eq.(4.22), and the function η is calculated from Eq. (4.23):

$$(2\Gamma)^2 = \frac{1}{k_B T}\frac{e^2}{\varepsilon_0\varepsilon_r}\sum_k \rho_k(z_k + N_k\sigma_k)^2 \tag{4.22}$$

$$\eta = \frac{1}{\Omega}\frac{\pi}{2\Delta}\sum_k \frac{\rho_k \sigma_k z_k}{1+\Gamma\sigma_k} = \frac{1}{\Omega}\frac{\pi}{2\Delta}\frac{N_A}{V}\sum_k \frac{n_k \sigma_k z_k}{1+\Gamma\sigma_k} \tag{4.23}$$

The distance $(2\Gamma)^{-1}$ is the MSA equivalent of the the screening length in the Debye-Hückel theory κ^{-1}, and the auxillary function Ω is calculated using Eq. (4.24):

$$\Omega = 1 + \frac{\pi}{2\Delta}\sum_k \frac{\rho_k \sigma_k^3}{1+\Gamma\sigma_k} = 1 + \frac{\pi}{2\Delta}\frac{N_A}{V}\sum_k \frac{n_k \sigma_k^3}{1+\Gamma\sigma_k} \tag{4.24}$$

Δ is a measure of the included volume fraction calculated using Eq. (4.25) and must be strictly positive and larger than ca. 1-0.74 (0.74 being the packing factor of the face-centered cubic lattice). Note that this term also includes the contribution from uncharged species in the mixture:

$$\Delta = 1 - \frac{\pi}{6}\sum_k \rho_k \sigma_k^3 = 1 - \frac{\pi}{6}\frac{N_A}{V}\sum_k n_k \sigma_k^3 \tag{4.25}$$

The Helmholtz energy may be calculated using the thermodynamic relation shown in Eq. (4.26):

$$\frac{\partial}{\partial(k_B T)^{-1}}\left(\frac{A^{\mathrm{MSA}}}{k_B T}\right) = \Delta E^{MSA} \tag{4.26}$$

The integration shown in Eq. (4.26) cannot be performed directly, but through the procedure by Höye and Stell[188], where the Helmholtz energy may be expressed from Eq. (4.27):

$$\frac{A^{\mathrm{MSA}}}{k_B T} = \frac{\Delta E^{\mathrm{MSA}}}{k_B T} - \int_0^\Gamma d\Gamma'\left(\frac{\partial}{\partial\Gamma'}\frac{\Delta E^{\mathrm{MSA}}}{kT}\right) \tag{4.27}$$

Note that taking the derivative of Eq. (4.27) wrt. Γ yields the identity in Eq. (4.28):

$$\frac{\partial}{\partial\Gamma}\left(\frac{A^{\mathrm{MSA}}}{k_B T}\right)_{T,V,n} = 0 \tag{4.28}$$

The solution to the integral in Eq. (4.27) gives the surprisingly simple result shown in Eq. (4.29):

$$\frac{A^{\mathrm{MSA}}}{k_B T} = \frac{V\Gamma^3}{3\pi} - \frac{1}{k_B T}\frac{Ve^2}{4\pi\varepsilon_r\varepsilon_0}\sum_i^N \rho_i z_i\left[\frac{\Gamma z_i + \eta\sigma_i}{1+\sigma_i\Gamma}\right] \tag{4.29}$$

Furthermore, another form of Eq. (4.22) as shown in Eq. (4.30) can be obtained by using Eq. (4.28):

$$(2\Gamma)^2 = \frac{1}{k_B T}\frac{e^2}{\varepsilon_r\varepsilon_0}\sum_i^N \rho_i z_i\frac{\partial}{\partial\Gamma}\left[\frac{\Gamma z_i + \eta\sigma_i}{1+\sigma_i\Gamma}\right] \tag{4.30}$$

The MSA theory has one internal variable Γ which is not known from explicit relations and must be obtained from numerical methods. An implicit function expressing the Helmholtz energy arises from the derivation of MSA. The equations may be solved using an iterative scheme of Eq. (4.22), but as Γ changes depending on temperature, pressure and composition, it becomes difficult and inefficient to obtain the second order derivatives of MSA explicitly using a successive substitution scheme. However, in this work a computationally more efficient approach based on an unconstrained minimization of the Helmholtz energy was used (see Appendix C.1).

4.1.3 The electrostatic moment conditions

Mixtures containing electrolytes should satisfy the so-called moment conditions [183]. The solutions to the four first moments are therefore interesting in terms of analyzing the importance of the assumptions done in the Debye-Hückel theory, i.e. that the radial distribution function is only a function of the long-range forces from the electrostatic interactions. From the Coulombic forces between ions (Eq. (4.2)) it is possible to derive a set of statistical mechanical moment conditions for electrolytes using the Ornstein-Zernike equation. A derivation of the moment conditions has been presented by e.g. Attard[183], and his results are summarized in this paper to illustrate that the Debye-Hückel theory cannot satisfy the fourth moment condition due to neglecting the short-range forces. The zeroth moment condition is shown in Eq. (4.31):

$$4\pi \sum_k \rho_k z_k \int_0^\infty r^2 h_{ik}(r)\, dr = -z_i \tag{4.31}$$

The left hand side of Eq. (4.31) represents integration over all ions in the vicinity of the central ion. The physical significance of Eq. (4.31) is that the total charge in the ion cloud surrounding the central ion i will be of same magnitude but opposite charge as the central ion i [48]. The zeroth moment is thus the microscopic equivalent of the electroneutrality condition from Eq. (4.3).

The Stillinger-Lovett second moment condition is given by Eq. (4.32):

$$\frac{4\pi e^2}{\varepsilon_0 \varepsilon_r k_B T} \sum_i \sum_j \rho_i \rho_j z_i z_j \int_0^\infty r^4 h_{ik}(r)\, dr = -6 \tag{4.32}$$

The physical significance of Stillinger-Lovett 2nd moment is that for finite size ions, a charge oscillation occurs in the ionic cloud[183]. Note that neither the 0th nor the 2nd moment depend on the short-range interactions (determined by the direct correlation function $c(r)$).

The fourth moment is presented in Eq. (4.33)[183]:

$$\frac{1}{120} \mathbf{Q} \mathbf{H}^{(4)} \mathbf{Q} = \left(\mathbf{H}^{(0)} - \mathbf{C}^{(0)} - \mathbf{H}^{(0)} \mathbf{C}^{(0)} \right) \left(\mathbf{I} - \mathbf{C}^{(0)} \right) \tag{4.33}$$

Where the matrix $\mathbf{Q}$ is given by Eq. (4.34), $\mathbf{H}^{(0)}$ from the first term of the linearization of the indirect correlation function $h_{ij}(r)$ in Eq. (4.35), and $\mathbf{C}^{(0)}$ from the first term of the linearization of the short-range part of the direct correlation function as given by Eq. (4.36)

$$\mathbf{Q}_{ij} = \frac{\sqrt{\rho_i \rho_j}}{k_B T} \frac{q_i q_j}{\varepsilon_0 \varepsilon_r} \tag{4.34}$$

$$\mathbf{H}_{ij}^0 = (\rho_i \rho_j)^{\frac{1}{2}} h_{ij}^0(\mathbf{r}) \tag{4.35}$$

$$\mathbf{C}_{ij}^0 = (\rho_i \rho_j)^{\frac{1}{2}} c_{ij}^0(\mathbf{r}) \tag{4.36}$$

It is evident that the fourth moment depends on the short-range interactions, represented by $\mathbf{C}^{(0)}$. The fourth moment condition has been related to the partial ionic structure factors and the isothermal compressibility of the electrolyte[189, 190]. The Debye-Hückel theory assumes that the short-range interactions are negligible, i.e. that $\mathbf{C}^{(0)} = 0$ but the MSA accounts for the short-range interactions by treating the ions as hard spheres. However, when the Debye-Hückel model is augmented by additional terms to account for the short-range interactions, as is done with electrolyte equations of state, one can argue that this deficiency is no longer problematic.

4.1.4 On the Relationship between EoS and Activity Coefficient Models

An EoS will include one of the terms for the Helmholtz energy from Debye-Hückel (Eq. (4.16)) or MSA (Eq. (4.26)) to account for the long-range electrostatic interactions, as a perturbation to reference EoS. Insofar, the efforts to form a working EoS for mixtures with electrolytes have not resulted in significant improvements over the activity coefficient (or excess Gibbs energy) models for electrolyte systems[1]. This section serves to present the relationship between the expressions for the long-range electrostatic forces developed for the Debye-Hückel and MSA theories, and the activity coefficient models that are widely used by the industry to predict thermodynamic properties of mixtures containing electrolytes. The chemical potential may be determined from the compositional derivative of either the Helmholtz or the Gibbs free energy:

$$\mu_i = \left(\frac{\partial A}{\partial n_i}\right)_{T,V,n_{j\neq i}} = \left(\frac{\partial G}{\partial n_i}\right)_{T,P,n_{j\neq i}} \tag{4.37}$$

The chemical potential may be split into two terms from the relation $\mu_i = \mu_i^i + \mu_i^E$, one term corresponding to the ideal mixture contribution μ_i^i, and one term corresponding to the excess chemical potential μ_i^E. The activity coefficient may then be obtained from the excess chemical potential using the well-known relation $\ln \gamma_i = \frac{\mu_i^E}{RT}$. The chemical potential may be calculated from either the rational (mole-fraction) or the molality scale, and may furthermore be given as the unsymmetrical activity coefficient, tending to 1 as the concentration goes to zero. Commonly, activity coefficient models for electrolyte mixtures use unsymmetrical activity coefficients using the molality scale for solutes, and the symmetrical rational activity coefficient for solvents.

Debye and Hückel[26] originally derived a model for the activity coefficient from the expression of the excess Helmholtz energy from Eq. (4.16) by replacing the molar volume and static permittivity by empirical correlations, and using the resulting equation as an expression for the excess Gibbs energy. This procedure has been used for activity coefficient models[38, 71, 75, 187], whereas electrolyte EoS determine the volume from the pressure equation given by Eq. (4.38).

$$P = -\left(\frac{\partial A}{\partial V}\right)_{T,\mathbf{n}} \tag{4.38}$$

Primitive electrolyte EoS[84, 94, 110–112, 114, 115, 121, 128, 129, 184] determine the static permittivity from (semi)-empirical solvent-specific correlations while non-primitive EoS[52, 67] determine the static permittivity from dipolar interactions. Common to both the electrolyte EoS and activity coefficient models, is that they include terms that account for the short-range interactions; activity coefficient models determine the short-range forces from local-composition models as UNIQUAC[75] or NRTL[71], or from Pitzer's modifications of the Debye-Hückel theory to include a hard-core repulsive term shown in Eq. (4.20).

4.1.5 Numerical Comparison of the Debye-Hückel and MSA Theories

The previous section introduced the Debye-Huckel and MSA models and showed the major differences between the assumptions of these two models. It is of interest to investigate the numerical differences in the excess Helmholtz energy to determine the differences between MSA and Debye-Hückel. It was decided to use the same numerical value of the ion diameter in MSA as in Debye-Hückel to provide a basis for comparing the two models, thus in this section, σ_i will be used as the symbol for the ion diameter and the distance of closest approach d_i. Typical Pauling radii are shown in Table 4.1:

To obtain the complete picture of the differences between the two models, it was decided to vary the ion diameter, ion charge, temperature, volume, and composition. Additionally, as has

Ion	Li^+	Na^+	Mg^{2+}	Ca^{2+}	Cl^-	SO_4^{2-}	NO_3^-
Radii [Å]	0.74	1.02	0.72	1.00	1.81	2.30	1.79
α [L/mol]	0.12	0.1062	0.1155	0.1097	0.1173	0.0022	0.1104

Table 4.1: Pauling radii for selected ions [191] and ion specific parameters for calculation of the static permittivity [182].

been shown by several authors[84, 92, 109, 114, 129, 182], the relative static permittivity ε_r is a function of temperature, volume, and composition, and that this dependence is of high importance to the performance of the electrolyte equation of state. To determine the influence of the static permittivity on the performance of the two models, the model presented by Michelsen and Mollerup[182] was implemented. According to this model, the relative static permittivity is calculated using the empirical expression shown in Eq. (4.39):

$$\varepsilon_r\left(T, V, \underline{n}\right) = \varepsilon_r^w\left(T\right) \times E\left(\mathbf{n}, V\right) \tag{4.39}$$

Where $E\left(\mathbf{n}, V\right)$ is an ion correction factor that effectively serves to reduce the relative static permittivity. ε_r^w is the relative static permittivity of water calculated as a function of temperature using Eq. (4.40):

$$\varepsilon_r^w\left(T\right) = \varepsilon_r^w(T_0)\left(1 + \frac{\beta_1}{2}\frac{N_A\mu_{w,0}^2}{k_B\varepsilon_0}\left(\frac{\rho_w\left(T\right)}{T} - \frac{\rho_w\left(T_0\right)}{T_0}\right)\right) \tag{4.40}$$

T_0	[K]	Reference temperature $T_0 = 273.15K$
ε_r^w		Static permittivity of liquid water at saturation conditions
$\mu_{w,0}$	[C $\cdot$ m]	Dipole moment of water in vacuum $\mu_{w,0} = 8.33 \cdot 10^{-30}$C $\cdot$ m
β_1		Fitting constant for static permittivity of water $\beta_1 = 3.1306$
ρ_w	[g/cm^3]	Density of water , see Eq. (4.41)

$$\rho_w\left(T\right) = 0.99984 + 1.51782 \times 10^{-4}\left(T - T_0\right) - 4.50573 \times 10^{-5}(T - T_0)^{1.55} \quad [g/cm^3] \tag{4.41}$$

The relative static permittivity and density of pure water are shown in Figure 4.2 and the E-factor is given by Eq. (4.42).

$$E\left(\mathbf{n}, V\right) = 1 + \sum_k^{ions}\left(0.010c_k - \frac{\alpha_k C_k}{1 + 0.160C_k}\right) \tag{4.42}$$

C_i	[mol/L]	Concentration of component i in molality
α_k	[L/mol]	Ion-specific constant for dielectric decrement

Selected values for α are shown in Table 4.1 and an example calculation for the static permittivity of NaCl and MgCl$_2$ are presented in Figure 4.3. The basis of the comparison utilizes a constant volume with the static permittivity of pure water, if not stated otherwise. This is done to more easily distinguish the effect of parameters on the models.

4.1.6 Comparison of Screening Length

Comparing Eq. (4.12) to Eq. (4.22) shows that the screening length in the Debye-Hückel theory is independent of diameter, while this is not true for MSA. Figure 4.4 compares the screening length of MSA and Debye-Hückel at 25°C, showing that the Debye-Hückel theory predicts an unphysical behavior where increasing the ion size does not increase the screening length. The difference between the screening length in MSA and Debye-Hückel depends on the molality and the ion diameter. When the volume and static permittivity are kept constant, the screening length of the Debye-Hückel and MSA display a linear dependence on temperature, i.e. the higher
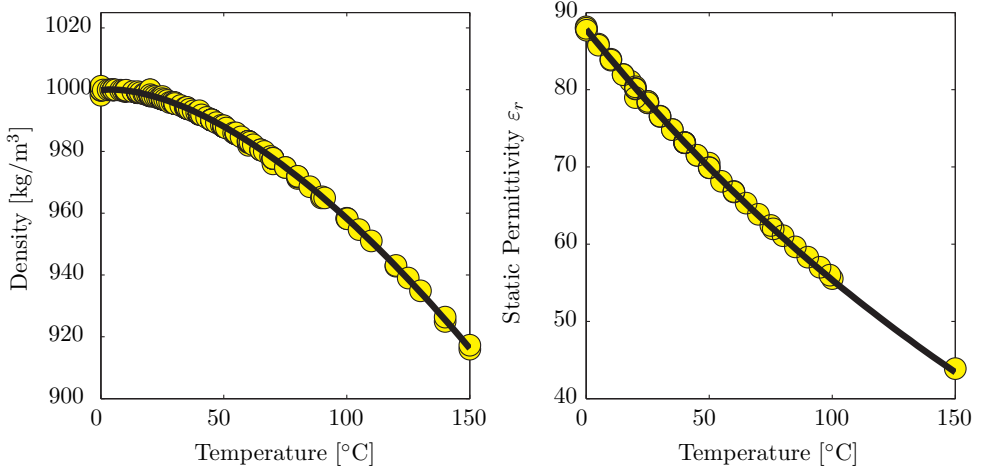
Figure 4.2: Temperature dependence of liquid density and relative static permittivity for water using Eqs. (4.40)-(4.41). Experimental data indicated by black dots are from the Landolt Börnstein database [23]
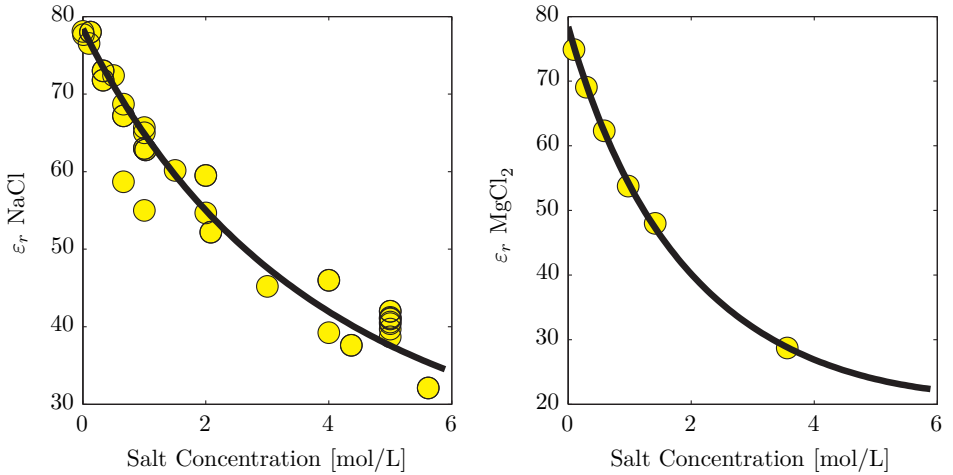
Figure 4.3: Effect of salt concentration on relative static permittivity of NaCl and MgCl$_2$ using Eq. (4.42). Experimental data indicated by black dots are taken from the collections of Akhadov[24] and Barthel et al. [25].

the temperature, the higher the screening length. A similar and weak temperature dependence of the screening length at 3 molal and constant volume is observed from Figure 4.5. Note that the volume change due to the presence of electrolytes was not included in either Figure 4.4 or Figure 4.5, as the comparisons have been carried out at constant volume and not constant pressure. Figure 4.7 illustrates illustrates that the volume dependence of the screening length in the two models is rather weak but proportional to the volume.
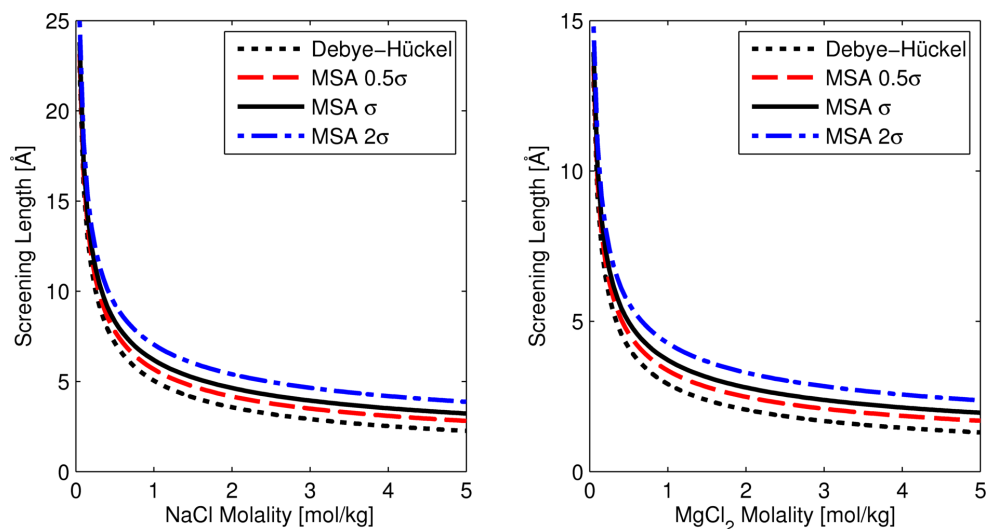
Figure 4.4: Comparison of screening lengths at 25°C, a 2.8L volume, and constant relative static permittivity $\varepsilon_r = 78$.

Finally, Figure 4.6 shows that both models display similar dependence of the screening length on the relative static permittivity. A decrease in the static permittivity caused by the compositional changes or due to an increase in the temperature will yield a decrease in the screening length. Due to its typical range of values in aqueous electrolytes presented in Figure 4.3, the static permittivity has a larger influence on the screening lengths than temperature and volume alone. To summarize, the two models display the same trends for the screening length when changing the temperature, volume, ion charges, composition and static permittivity. However, only MSA predicts an increase in the screening length with increasing ion diameters. MSA can therefore be considered a better choice in cases where the absolute value/magnitude of the screening length is important (e.g. for interfacial phenomena).
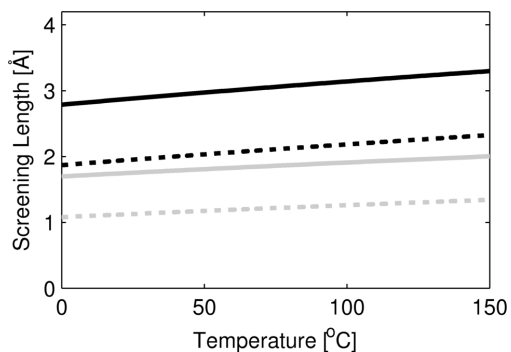
Figure 4.5: Effect of temperature on the screening lengths calculated with MSA (solid) and Debye-Hückel (dashed) for NaCl (black) and $MgCl_2$ (gray) at 25°C, 3 molal, 1.2L volume with relative static permittivity $\varepsilon_r = 78$.

4.1.7 Comparison of Helmholtz Energy

The Helmholtz energy and its derivatives are of great importance for equations of state that incorporate either MSA or Debye-Hückel to account for the ion-ion interactions. It is therefore of interest to compare the trends and values obtained from using the two models.
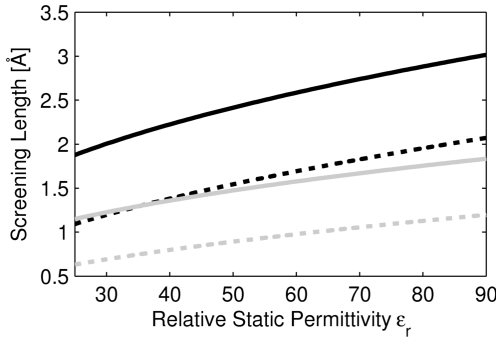
Figure 4.6: Effect of static permittivity on the screening lengths calculated by MSA(solid) and Debye-Hückel (dashed) for NaCl(black) and MgCl$_2$ (gray) at 3 molal, constant volume at 1L, and constant temperature at 25°C.
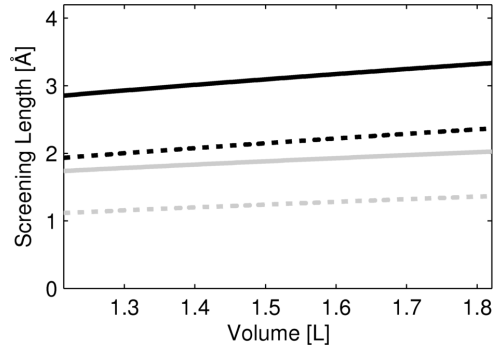
Figure 4.7: Effet of volume on the screening length calculated by MSA (solid) and Debye-Hückel (dashed) for NaCl (black) and MgCl$_2$ (gray) at 25°C, 3 molal, and relative static permittivity ε_r=78.

4.1.8 Influence of Ion Diameter

Although the ion diameter does not influence the screening length in the Debye-Hückel theory, it is important for the calculation of the Helmholtz energy. Figure 4.8 compares the reduced Helmholtz energy $\frac{A^r}{RT}$ using the Debye-Hückel and MSA models for different ion diameters. Figure 4.8 together with Figure 4.4 show that an increase in the ion size leads to an increase
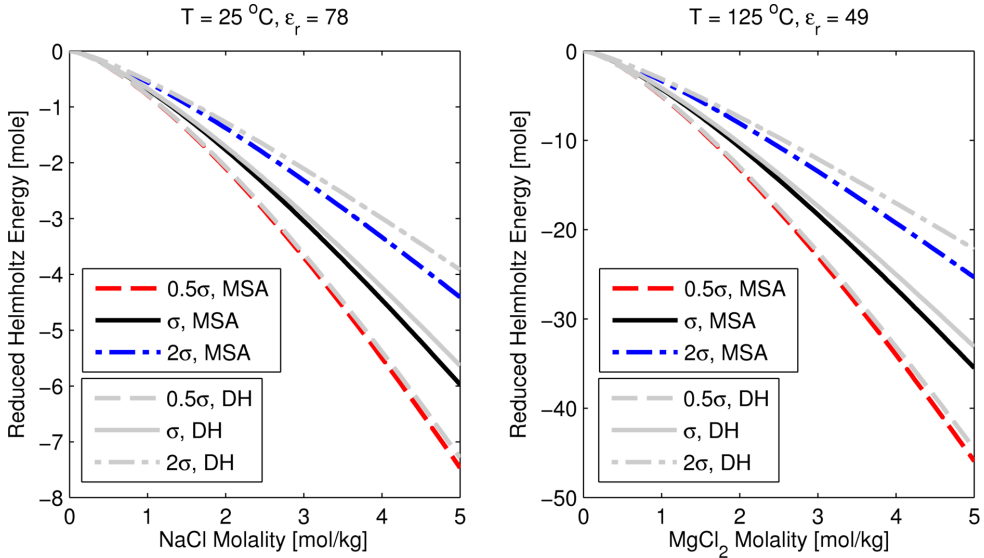
Figure 4.8: Effect of diameter on the electrostatic Helmholtz energy with relative static permittivity equal to that of water (shown above the figures). MSA is black/colored, Debye-Hückel is gray. Volume is fixed at 2.8L.

in the separation distance between the ions in both models, thereby reducing the interaction energy and thus the Helmholtz energy. In all cases MSA yields lower energies at the same

concentration. The larger excluded volume at higher concentrations contributes to lowering the Helmholtz energy in the case of MSA, whereas the Debye-Hückel theory does not account for this effect. Since the Helmholtz energy from the Debye-Hückel theory is always slightly larger than the Helmholtz energy calculated using MSA, it is possible to make an empirical modification of the ion diameter in the Debye-Hückel and MSA theories as shown in Eq. (4.43), in order to obtain nearly identical results from the two models:

$$d_i = \omega \sigma_i \qquad (4.43)$$

Interestingly, when choosing $\omega = \frac{5}{6}$, the values of the Helmholtz energies and their derivatives from both models become similar (within 5%) for different ion sizes, ion charges, and temperatures up to 5 molal. The largest deviations are observed in the volume derivative for large ions. It was furthermore found that the size of the solvent does not change the optimal ω factor significantly, but it does have an effect on the value of the volume derivative. Since the MSA theory accounts for the excluded volume explicitly and Debye-Hückel does not, the physical significance of the ω factor is to account for the effect of the excluded volume by reducing the separation distance of the ions. From this analysis, it may be concluded that if the ion size is fitted during pure component parameter estimation, the two models can perform similarly.

When the static permittivity is calculated from the composition using the empirical model given by Eq. (4.39), the reduced Helmholtz energy changes by 50-100% as evidenced by Figure (4.9): Figure 4.9 shows that the static permittivity has a profound effect on the reduced
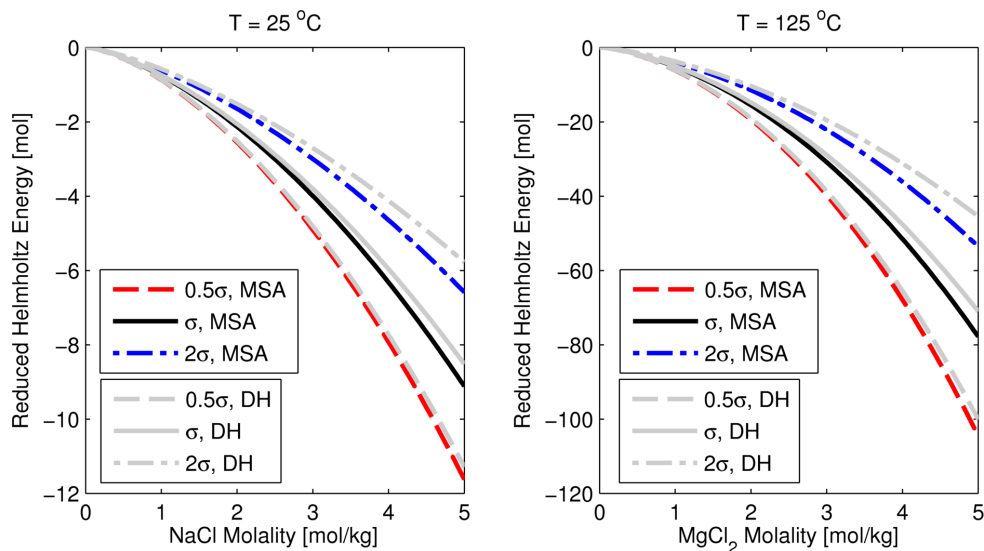
Figure 4.9: Effect of Diameter on the electrostatic Helmholtz energy with composition dependent static permittivity. MSA is black/colored, Debye-Hückel is gray. Volume is fixed at 2.8L.

Helmholtz energy, and in the following sections the influence of using the empirical model on the derivatives of the residual Helmholtz energy is investigated.

4.1.9 Comparison of Volume Derivative

Figure 4.10 shows that the volume derivative of Helmholtz energy increases with increasing ion concentration and temperature. Figure 4.10 does not include the effect of volume on the static permittivity, as this is not included in the empirical model for the static permittivity of pure

water given by Eq. (4.40). However, Figure 4.11 shows that the volume derivatives are affected if the static permittivity is modeled using Eq. (4.39). As the volume derivative is inversely
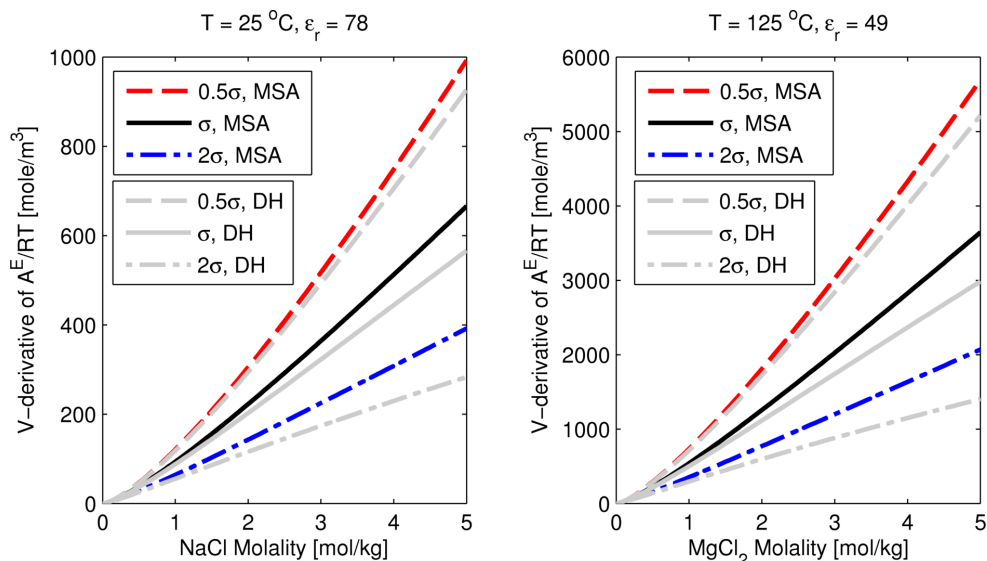
Figure 4.10: Comparison of the volume derivative of Helmholtz energy at different diameters at constant temperature and relative static permittivity (shown above the figure). MSA is black/colored, Debye-Hückel is gray. Volume is fixed at 2.8L.

dependent on the static permittivity, the reduction of ε_r due to the presence of salts contribute to increase the volume derivative. Additionally a volume dependency is introduced through the $E(\mathbf{n}, V)$ correction function given by Eq. (4.42). Figure 4.11 illustrates that accounting for the effect of salts has a substantial effect on the volume derivative. However, the result shown in Figure 4.11 is not necessarily the correct physical behavior, but rather a result of fitting the empirical model parameters to concentration data (see Eq. (4.42)). If the correction factor was depending on molality or mole fractions rather than concentrations, the volume dependency would become zero, which would influence the behavior shown in Figure 4.11. Utmost vigilance should be exercised when using empirical correlations for the static permittivity, as they may end up including a non-physical behavior of the Helmholtz energy expression of the electrostatic models. It is considered of high importance to have a model for the permittivity that not only fits the data, but actually resembles the correct physical dependence on temperature, volume and composition.

4.1.10 Comparison of Temperature Derivative

The influence of temperature, ion charge, and ion size on the temperature derivative is presented in Figure 4.12: The same trend is observed for both MSA and Debye-Hückel in Figure 4.12 where the absolute value of the temperature derivative increases with increasing ion size and temperature for both models. Figure 4.13 shows that when the temperature derivative of the static permittivity is included together with the empirical correlation for the static permittivity, the temperature derivative changes sign, but is of the same order of magnitude.
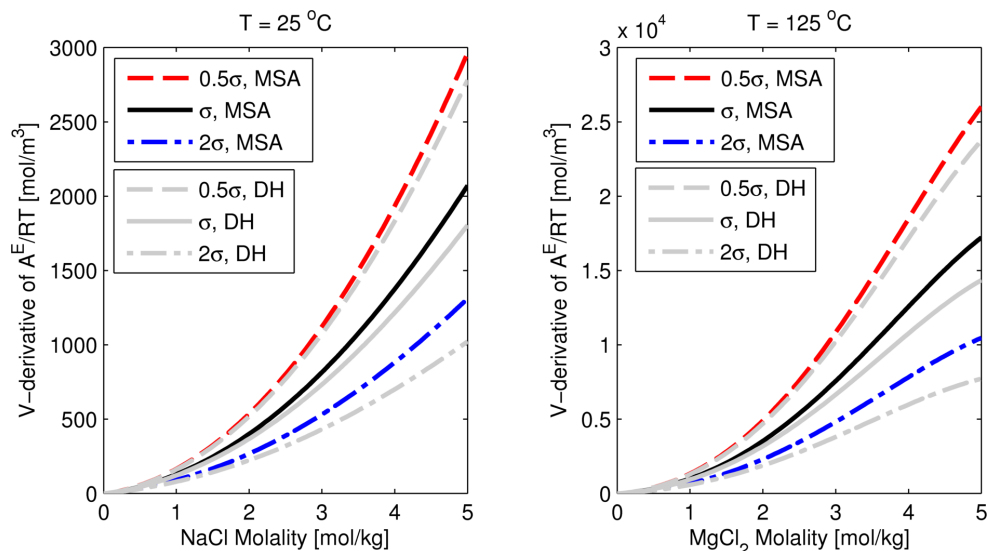
Figure 4.11: Comparison of the volume derivative of Helmholtz energy when Eq. (4.39) is used to model the relative static permittivity. MSA is black/colored, Debye-Hückel is gray. Volume is fixed at 2.8L.

4.1.11 Comparison of Compositional Derivatives

As shown in Eq. 4.37, the fugacity coefficient depends on the compositional derivatives of the Helmholtz energy. The fugacity coefficients are used in the calculation of the thermodynamic equilibrium properties at constant temperature and pressure. In an EoS, the fugacity coefficients at constant pressure are determined by first solving for the volume root from the pressure specified in Eq. (4.38) and then inserting this volume into Eq. (4.37). In Figure 4.14 compares the contribution to the Helmholtz energy from MSA and Debye-Hückel at constant volume (e.g. same volume in MSA and Debye-Hückel), but as evidenced by Figure 4.8 and Figure 4.10, the difference in the volume derivative may lead to a slightly different volume root and thus somewhat different results for the activity coefficients at constant temperature and pressure, depending on the parameters and the other terms in the EoS. Figure 4.14 shows that the compositional dependence of the static permittivity (see Figure 4.3) may completely change the behavior of the compositional derivatives at higher concentrations, and thus is important to the calculation of activity coefficients. While Figure 4.10 showed that careful considerations must be used to select the model that is used for the static permittivity, Figure 4.14 shows that it is of great importance to include the compositional dependence of the static permittivity. The importance of the relative static permittivity on the compositional derivatives was also noted by other authors [84, 92, 109, 114, 129, 182]. As the empirical model of the static permittivity does not depend on the concentration of uncharged molecules, only the MSA model provides a small contribution to the compositional derivative of the Helmholtz energy for water, but this contribution is very small compared to the contribution of the ions. If the effect of increasing solvent concentration was included in the model for the static permittivity, both models would yield a larger contribution to the compositional derivative of the Helmholtz energy for water.

4.1.12 Conclusions from work on Debye-Hückel vs. MSA

The long-range columbic forces may be described by either the Debye-Hückel or the MSA theories. The MSA model was derived based on statistical mechanics and includes the effect of an
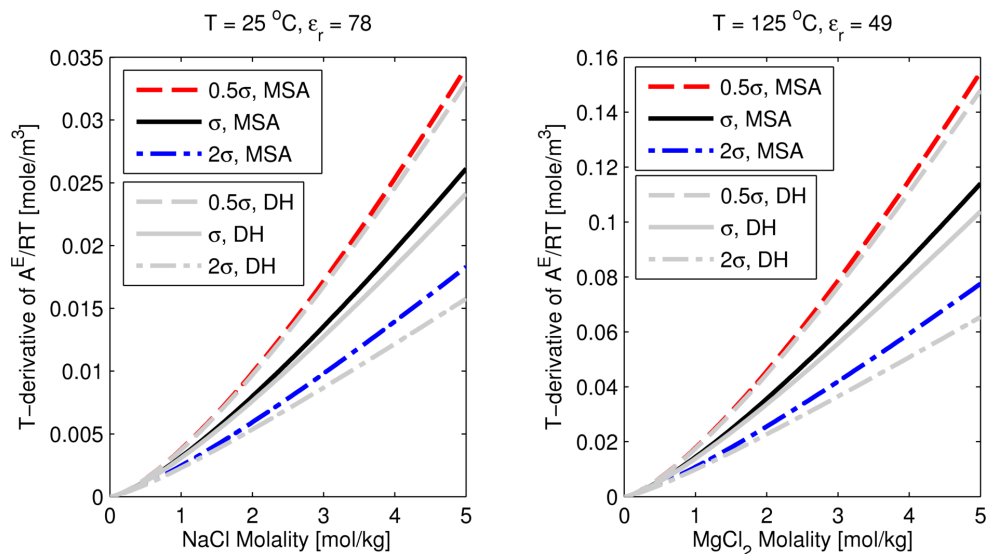
Figure 4.12: Comparison of temperature derivative of Helmholtz energy at different ion diameters. The temperature derivative of the static permittivity of pure water was set to zero to observe the behavior of the model without including the temperature dependence of the static permittivity. MSA is black/colored, Debye-Hückel is gray. Volume is fixed at 2.8L.

excluded volume on the electrostatic interactions. The two models were compared numerically in terms of the screening length, the contribution to the residual Helmholtz energy and the first order derivatives of the Helmholtz energy. Both models predict similar trends with regards to temperature, volume and compositional dependence of the Helmholtz energy, while only MSA correctly predicts an increase in the screening length when the ion diameter is increased. Nearly identical quantitative results of the two theories are obtained if the distance of closest approach d_i of the Debye-Hückel theory is taken as $\frac{5}{6}$ of the hard sphere diameter σ used in the MSA model. It is thus concluded that the two theories will perform similarly if the ion diameter is included as a fitted parameter in the parameter estimation. The static permittivity was found to be a key parameter and the effect of temperature, volume and composition on the static permittivity will affect the predicted behavior of ions in the solution. The current models for the static permittivity are empirical and this makes it difficult to obtain trustworthy results for multicomponent solutions using the current equations of state for electrolytes.
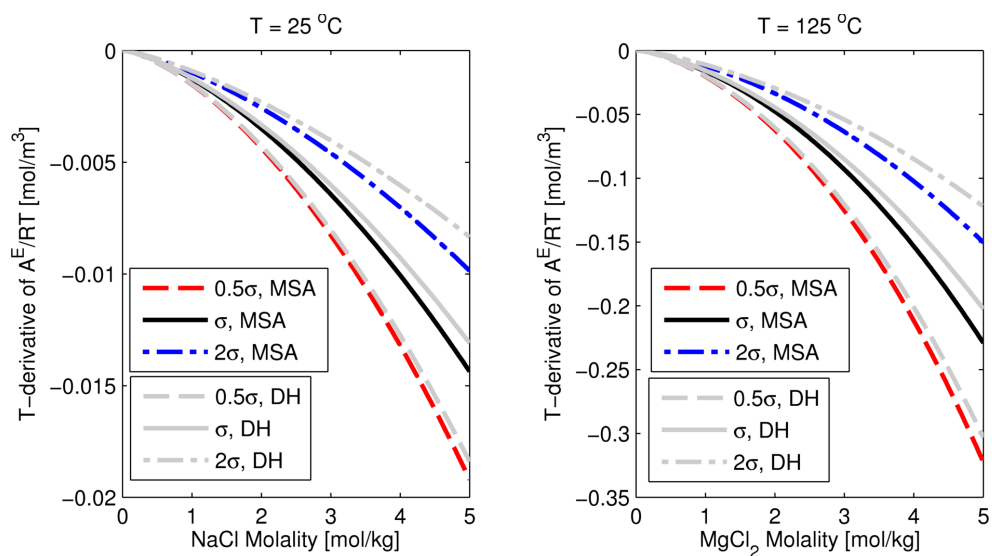
Figure 4.13: Comparison of temperature derivative of Helmholtz energy at different ion diameters using the empirical correlation for the relative static permittivity shown in Eq. (4.39). MSA is black/colored, Debye-Hückel is gray. Volume is fixed at 2.8L.
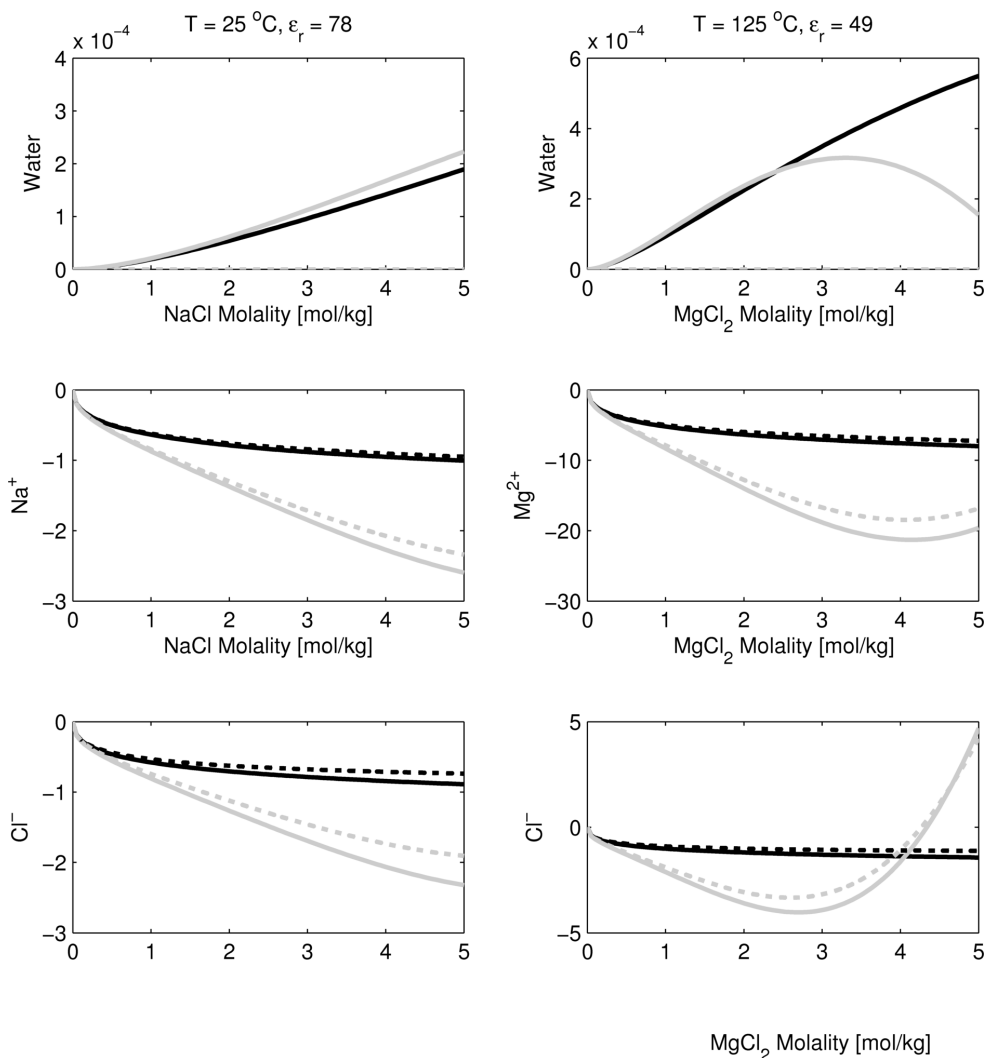
Figure 4.14: Comparison of the compositional derivative of the Helmholtz energy calculated by MSA (solid) and Debye-Hückel (dashed) at constant temperature using a constant static permittivity (black lines) (shown above the top figure) and the empirical correlation from Eq. (4.39) (gray lines). Results are obtained using a constant volume V = 1.3L.

4.2 Insights from Molecular Simulation

The previous section illustrated that the full Debye-Hückel model provides a similar representation of the contributions from ion-ion interactions to the Helmholtz energy as the mean spherical approximation model. The consequence is that if it is possible to improve the simpler Debye-Hückel model with additional terms, it may be possible to derive a more complete description of the total electrostatic interactions. The most important assumption in the derivation of the Debye-Hückel model is related to the linearization of the Poisson-Boltzmann equation in Eq. (4.13). As demonstrated by Kirkwood [192], the linearization is only strictly valid provided that the exponent is close to zero. when inserting the shortest separation distance (the distance of closest approach d_i), this becomes Eq. (4.44):

$$\frac{e^2}{k_B T} \frac{z_i z_j}{4\pi\varepsilon_r\varepsilon_0} \frac{1}{d_i} << 1 \tag{4.44}$$

It is evident that the criterion will be valid at small charges, high temperatures, and high static permittivity. Bjerrum [28] suggested that ions that are in close contact would be treaeted as seperate species, and defined the Bjerrum length l_B as the value where the left hand side of Eq. (4.44) of a 1:1 electrolyte is unity:

$$l_B = \frac{1}{k_B T} \frac{e^2}{4\pi\varepsilon_r\varepsilon_0} \tag{4.45}$$

All ions that are separated by a shorter distance will be treated as ion pairs, effectively reducing the ionic strength of the solution. While there are advanced models that incorporate the mass-action law in the mean spherical approximation (such as the binding MSA (BIMSA) [49–51, 56, 193]), it is also possible to account for this effect in the simple Debye-Hückel framework through a chemical equilibrium shown in Eq. (4.46):

$$\text{A}^+ + \text{B}^- \rightleftharpoons [\text{A}^+\text{B}-] \tag{4.46}$$

The total density may then be calculated from Eq. (4.47):

$$\rho = \rho_A + \rho_B + 2\rho_{AB} \tag{4.47}$$

The density ρ_{AB} is then calculated from Eq. (4.48) where γ_i denotes the activity coefficient of the species [54]:

$$\frac{\rho_{AB}}{\rho_A\rho_B} = K(T)\frac{\gamma_A\gamma_B}{\gamma_{AB}} \tag{4.48}$$

Bjerrum suggested that the equilibrium constant for reaction Eq. (4.46) should be calculated from K_B in Eq. (4.49). The functional form for the equilibrium constant $K(T)$ has however been debated for a long time [56, 194]. Today, the most common form is that of Ebeling K_E [54, 56, 194], as it guarantees an exact representation of the restricted primitive model's second virial coefficient. Still, the choice may be different when non-electrostatic contributions are included in the equation of state (or the model for the activity coefficient γ).

$$K_B(T) = K(T, q = l_B) = 4\pi \int_{\sigma/2}^{q} r^2 \exp\left(2l_B/r\right) dr \tag{4.49}$$

$$K_E(T) = 4\pi \int_{\sigma/2}^{\infty} r^2 \left[\exp\left(\frac{2l_B}{r}\right) + \exp\left(-\frac{2l_B}{r}\right) - 2 - \left(\frac{2l_B}{r}\right)^2\right] \tag{4.50}$$

The Onsager book-keeping principle [194, 195] states that in a complete theory of electrostatics including a chemical model for ion pairing, the results will be insensitive to the finer details in

the definition of an ion pair and small changes in the equilibrium constant. In Onsager's own words from a conference in Montpellier (1968) [194, 195]):

> *The distinction between free ions and associated pairs depend on an arbitrary convention. Bjerrum's choice is good, but we could vary it within reason. In a complete theory this would not matter; what we remove from one page of the ledger would be entered elsewhere with the same effect.*   L. Onsager (1968)

Based on the Onsager book-keeping principle Ebeling et al. [194] made a thorough analysis of the different definitions for ion pairs and choices for mass-action rules. They showed that a consistent model based on the Bjerrum equilibrium constant would require a redefinition of the Debye-Hückel diameter into one that depends on temperature, whereas the Ebeling equilibrium constant was consistent with the Debye-Hückel model without further modifications. Ebeling et al. [194] defined an ion pair as any two ions that are within a distance $\sigma < r < q$, where the distance q is calculated by equating the Ebeling with the Bjerrum equilibrium constant.

Several authors have compared the various electrostatic models against molecular simulation data [53, 54, 56, 196–198]. The phase behavior and critical behavior of a pure ionic fluid has been of particular interest as molecular simulations of a known potential can help to validate the analytical theories. Primitive models may be simulated based on the reduced temperature and density as shown in Table 4.2. Simulations of hard spheres with the long-range Coulombic potential requires special methods (e.g. the Ewald summation technique) to obtain a description of the system, and there is therefore some deviations between simulations from different authors. While the critical temperature for Debye-Hückel model is quite close to the molecular simulation results, the density is quite far off. If the concept of ion-ion association is included using the Ebeling equilibrium constant it improves the critical density while retaining the critical temperature [54]. However, as pointed out by Fisher and Levin ([53]), while the Debye-Hückel theory coupled with the Bjerrum theory improves the description of the critical point, it deteriorates the vapor-liquid coexistence curve unless the interactions between the ion-pair (a strong dipole) and the ions are included through the Kirkwood equation [199] or the improved version by Fisher and Levin [53]. The pure restricted primitive MSA has similar deviations but may be improved through the same means as shown by Jiang et al. [56].

Model	Reduced critical temperature $T_c^* = k_B T_c \dfrac{4\pi\varepsilon_r\varepsilon_0 d_i}{e^2 z_i^2}$	Reduced critical density $\rho_c^* = N_A d^3 \rho_c$
Molecular simulation [53, 54, 56, 196, 200]	0.048-0.058	0.030-0.080
Debye-Hückel [26]	$1/16 = 0.0625$	$1/64/\pi = 0.005$
Debye-Hückel + Bjerrum [53]	$1/16 = 0.0625$	0.045
Debye-Hückel + Bjerrum + Ion-Dipole [53]	0.057	0.028
MSA [47, 48]	0.0786	0.0144

Table 4.2: Critical temperature and density for ionic fluids from simulations and models.

The results from molecular simulation indicate that a complete theory for electrostatics should include a concept for ion pairing as well as it should include the interactions between ions and ion pairs. Still, the vague definition of an ion pair used in primitive electrolyte models does not provide a molecular picture of ion-ion association. On a molecular basis, ion pairs are observed as three distinct types in close contact; separated by 0-2 solvent molecules ion pairs (see Figure 4.15). When the ions are present in a dipolar solvent, solvation shells will be formed surrounding the molecules, requiring a treatment of ion-solvent association. Such effects cannot
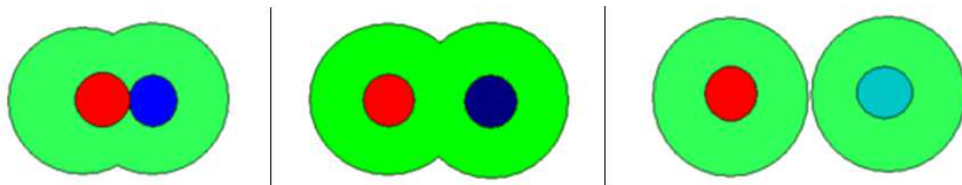
Figure 4.15: Different types of ion pairs; A contact ion pair (CIP) (left), A solvent-separated ion pair (SIP) (middle), and a fully solvated ion pair (SSIP) (right).

be described by molecular simulations based on primitive electrolyte models with an implicit solvent and require a more fundamental (and computationally expensive) treatment with an explicit solvent. Figures 4.16-4.17 show the ion pairs observed in a recent molecular dynamics study by Kalcher et al. [60, 201] as distinct peaks in the pair distribution function $g_{ij}(r)$. From Figure 4.17 it is evident that the ion-ion and ion-solvent association are also intrinsically linked since there are more solvent-separated ion pairs for NaCl and LiCl than for KCl or CsCl due to the size assymmetry and preference for the solvent. This indicates that a complete description of association in electrolyte systems will not only require modeling of ion-ion association, but also ion-solvent association and the interdependence of the two. More work is needed to determine the appropriate modeling approach in an electrolyte EoS.
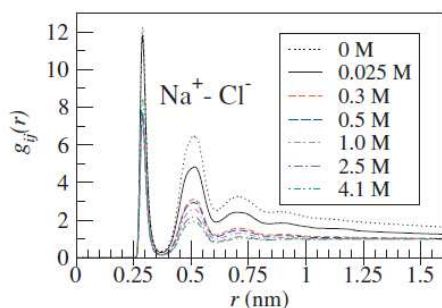
Figure 4.16: Radial distribution function of Cl⁻ around Na⁺ indicating the presence of both contact ion pairs and solvent-separated ion pairs (for NaCl, there are two times more solvent-separated ion pairs than contact ion pairs) (adopted from [60])
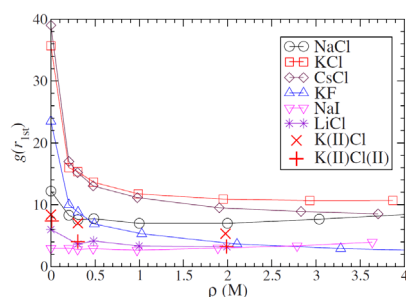
Figure 4.17: Height of the first peak in the radial distribution function from the molecular dynamics simulations of Kalcher [60].

4.3 Importance of the Born Term

In the previous section, the Debye-Hückel model was found to give a similar representation of the Helmholtz energy as the mean spherical approximation. These models both provide a description of the excess energy due to ion-ion interactions. Still it is not the only contribution to the total Gibbs energy; another part is the so-called self-potential, which was first introduced by Born (1920) [45]. In Chapter 1 it was shown that more than half of the electrolyte EoS models presented in literature include a Born term, but still many prominent research groups within thermodynamics (e.g. Gmehling at University of Oldenburg [96–108], Radosz at University of Wyoming [121–127], Galindo at Imperial College [110–112], and Sadowski at TU Dortmund [115–120]) have omitted the Born term from their electrolyte equation of state. The most com-

monly quoted reason for the omission is that the Born model does not provide a contribution to the excess chemical potential, and only serves to let the ions stay in the polar phase [109]. If ions are artificially constrained to the liquid phase it will provide the same effect [89]. This is a typical assumption used by researchers when performing calculations with a single liquid polar phase or calculations of the excess properties of liquid phases.

The Born potential is derived from the energy of charging a sphere in a medium with static permittivity ε_r. In fact, the Born model may be derived from the same framework as Debye-Hückel, provided that the integration limit is changed from the surface of the ion to the center of the ion, as illustrated by Figure 4.19. The Helmholtz free energy may be obtained through the charging process assuming that each molecule has the partial charge λq [182]:

$$A^e = N_A \sum n_i \int_0^{q_i} \psi_i dq = N_A \sum n_i q_i \int_0^1 \psi_i d\lambda$$

$$= N_A \sum n_i \int_0^1 \left[\psi_0 \left(\tfrac{1}{2} d_i \right) - \psi_{0,i} \left(0 \right) + \psi_1 \left(d_i \right) - \psi_1 \left(\tfrac{1}{2} d_i \right) - \psi_2 \left(d_i \right) \right] d\lambda$$

The contributions are summarized in Table 4.3. A slightly more concise form of the Debye-Huckel including the self-potential as shown in Eq. (4.51) is obtained by summing up the different terms.

$$A^e = -\frac{N_A e^2}{4\pi\varepsilon_r\varepsilon_0} \sum_i^N \frac{n_i z_i^2}{d_i} \left[\Phi_i - \beta \right] \qquad \Phi_i = \frac{\ln\left(1 + \kappa d_i\right) - \kappa d_i}{\left(\kappa d_i\right)^2} + \frac{1}{2} \qquad (4.51)$$

The original Debye-Hückel model is recovered when $\beta = 0$, whereas $\beta = 1$ gives Debye-Huckel with a self potential. It should be realized that in order to avoid numerical errors at low concentrations in the actual implementation of Eq. (4.51) must use the infinite dilution limit of $\Phi_i = 1/3\kappa\sigma$ at low concentrations as seen in Figure 4.18. It will lead to other values for β if
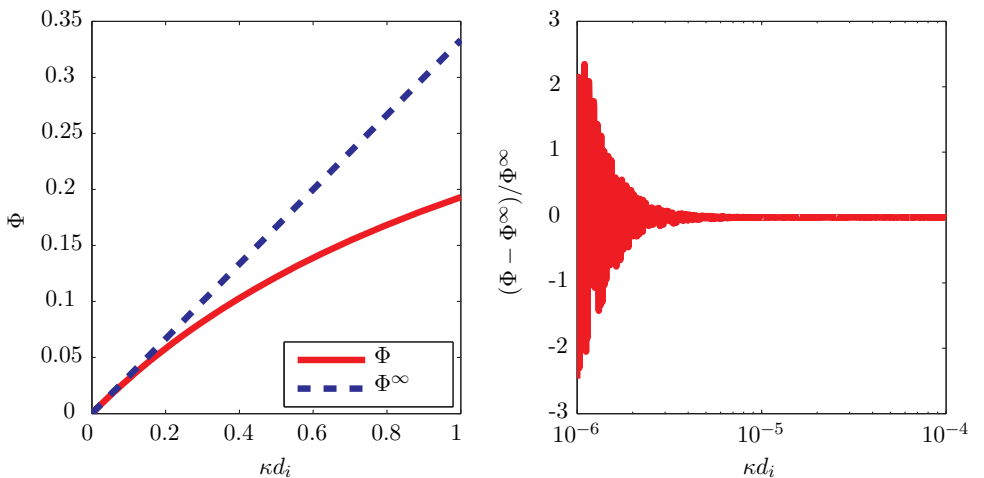
Figure 4.18: Numerical errors in Φ function defined in Eq. (4.51) at infinite dilution in comparison with the limiting law $\Phi = 1/3\kappa d_i$

different terms are used for the electrical field used in ψ_0', but this will not affect the other term of the function, which originates from the Debye-Hückel model. For instance, if the spheres are

assumed to have a uniform charge distribution, the electrical field and contribution to Helmholtz energy can be written as Eq. (4.52) leading to $\beta = 0.5$.

$$\psi'_0 = \frac{q}{4\pi\varepsilon_0\varepsilon_r}\frac{r}{\left(\frac{d}{2}\right)^3} \qquad \psi_0\left(\tfrac{1}{2}d_i\right) - \psi_{0,i}(0) = \frac{1}{4\pi\varepsilon_0\varepsilon_r}\frac{q_i}{d_i} \tag{4.52}$$

Figure 4.19: Electrical field in the vicinity of an ion with diameter d_i.

Description	Electrical Field ψ'
Conductive sphere	$\psi'_0 = 0$
Continuum model	$\psi'_1 = -\dfrac{1}{4\pi\varepsilon_r\varepsilon_0}\dfrac{q}{r^2}$
Debye-Hückel	$\psi'_2 = \dfrac{\exp\kappa\left(d-r\right)}{4\pi\varepsilon_r\varepsilon_0}\dfrac{q}{r}\dfrac{1+\kappa r}{1+\kappa d}$
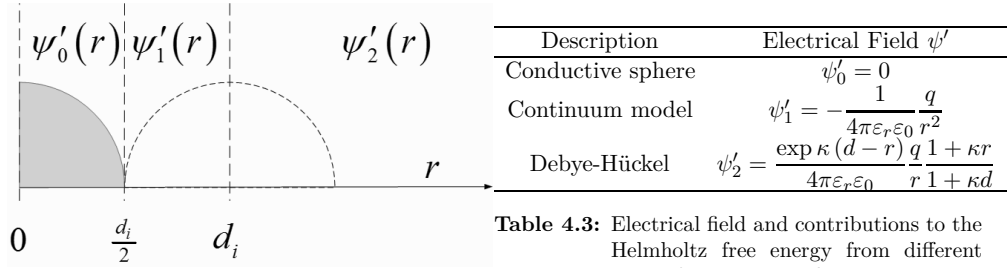
Table 4.3: Electrical field and contributions to the Helmholtz free energy from different parts of the electrical field shown in Figure 4.19.

The chemical potential at constant volume of Eq. (4.51) is given by Eq. (4.53):

$$\mu_i^e = \left(\frac{\partial A^e}{\partial n_i}\right) = \left(\frac{\partial A^e}{\partial n_i}\right)_{\varepsilon_r} + \left(\frac{\partial \varepsilon_r}{\partial n_i}\right)\left(\frac{\partial A^e}{\partial \varepsilon_r}\right) \tag{4.53}$$

The limit of the chemical potential at infinite dilution Eq. (4.53) can be written as Eq. (4.54)

$$\lim_{n_i\to 0}\mu_i^e = \beta\frac{N_Ae^2}{4\pi\varepsilon_r\varepsilon_0}\frac{z_i^2}{d_i} \tag{4.54}$$

It is noted that the Gibbs free energy of hydration in the Born model is calculated from Eq. (4.55) [45]:

$$\Delta_{hyd}G = \frac{N_Ae^2}{4\pi\varepsilon_0}\frac{z_i^2}{d_i}\left(\frac{1}{\varepsilon_r} - 1\right) \tag{4.55}$$

The chemical potential of transferring one molecule from an ideal gas phase with $\varepsilon_r = 1$ to a liquid may be calculated from Eq. (4.54) as shown in Eq. (4.56)

$$\lim_{n_i\to 0}\mu_i^{(2)} - \mu_i^{(1)} = \beta\frac{N_Ae^2}{4\pi\varepsilon_0}\frac{z_i^2}{d_i}\left(\frac{1}{\varepsilon_r} - 1\right) \tag{4.56}$$

The correct driving forces and the Gibbs energy of hydration are recovered when this potential is used. β corrects the Debye-Hückel diameter for the near-ion field, which supports the idea of fitting a Born radius or diameter to Gibbs energy of hydration data. To illustrate the importance of including the Born term in an equation of state for electrolytes, Figure 4.20 shows an approximation of the contributions from different terms of an electrolyte CPA equation to the chemical potential of NaCl at infinite dilution in liquid water with $\varepsilon_r = 78$, liquid decane with $\varepsilon_r = 2$, and a vapor phase with $\varepsilon_r = 1$. It is evident that the Born term provides the main contribution to the fugacity coefficient at infinite dilution.

The closer the values of ε_r between two phases, the less important becomes the Born term and other terms may therefore be used to calculate the Gibbs energy of transfer. The Gibbs
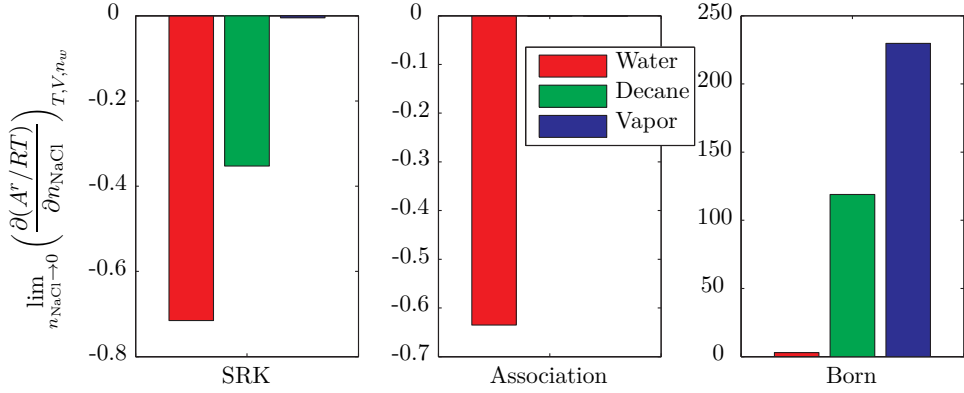
Figure 4.20: EOS contributions to the chemical potential of NaCl at infinite dilution. NaCl was modeled using critical parameters suggested by Simon et al [92] and the Pauling diameters shown in Table 4.1 p. 49, whereas water and decane were modeled with standard CPA parameters [82, 177, 202].

energy of transfer may also be written in terms of the fugacity coefficients at infinite dilution as shown in Eq. (4.57):

$$\Delta_{hyd}G = RT \left(\ln \hat{\phi}_{i,\infty}^{(2)} - \ln \hat{\phi}_{i,\infty}^{(1)} \right) \tag{4.57}$$

The typical thermodynamic cycle used to include the Born term in an equation of state involves discharging of the ions in the gas phase as shown in Figure 4.21, whereas Eq. (4.51) assumes that ions are initially uncharged. The difference between Eq. (4.51) and "regular" Born term is therefore just the reference state, and the original Born term can be recovered from Eq. (4.53) by setting $\beta = 1$ and subtraction of $\frac{N_A e^2}{4\pi\varepsilon_0} \frac{z_i^2}{d_i}$. As it is a consequence of the reference state, this difference does not change the distribution of ions between phases, as this is determined by the difference in the inverse static permittivity of the two phases.

4.3.1 Relationship to the Standard State Properties of Electrolyte Models

While most equation of state modeling is focusing on vapor-liquid, and liquid-liquid equilibrium, the electrolyte models have become specialized in handling of chemical equilibrium and solid-liquid equilibrium. It is therefore important that an electrolyte EoS can be developed to handle these properties in order to provide an alternative to the current approaches for modeling of electrolyte solutions. The standard state properties of electrolyte solutions are required in order to make any calculations of the thermal properties, solid-liquid equilibrium, and chemical equilibrium (weak electrolytes). This section will illustrate the different options for determining the standard state properties of the e-CPA EoS.

Electrolyte mixtures typically make use of the aqueous unsymmetrical molal standard state for electrolytes and other neutral solutes and the symmetrical standard state for the solvent[203]. The aqueous standard state may be described through the thermodynamic pathways presented in Figure 4.22, which shows that the path from the idael gas state to the liquid state involves the energy of ion hydration (where the main contribution originates from the Born term [203–205]):

The standard state formation Gibbs energies can be measured using voltaic or galvanic cells. The electromotive force $\mathcal{E}$ may be measured at different concentrations and this may be related
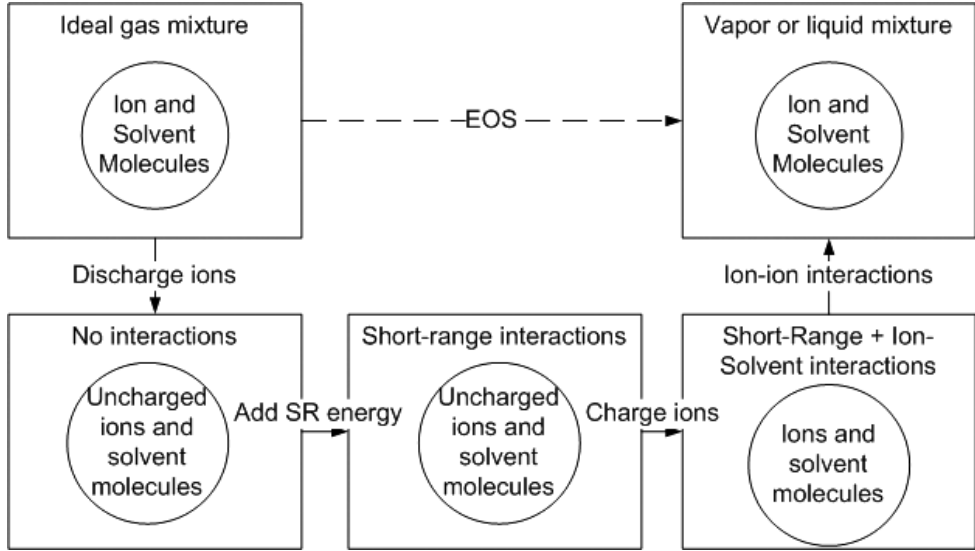
Figure 4.21: Typical thermodynamic cycle for deriving equations of state including the Born term. Inspired by Myers et al. (2002) [114].
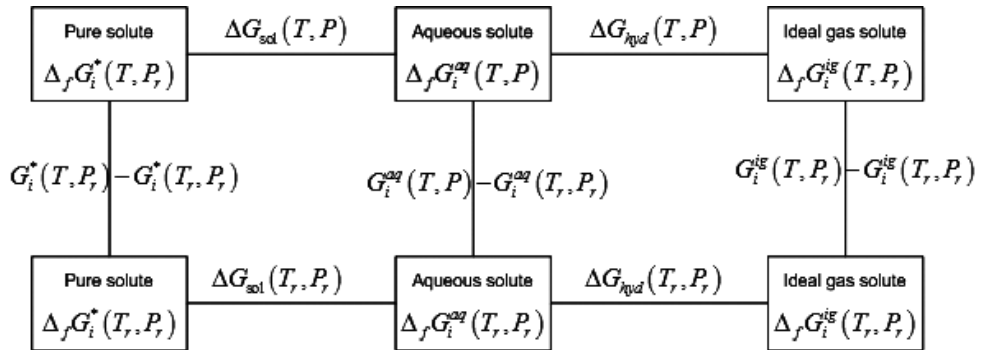
Figure 4.22: Thermodynamic relationship between different phases and their respective Gibbs energy.

to the standard state $\mathcal{E}_0$ by extrapolation to 0 molal as shown in Eq. 4.58:

$$\mathcal{E} = \mathcal{E}_0 - \frac{RT}{v_e F} \ln \left(\prod_i a_i^{v_i} \right) \tag{4.58}$$

v_e Stoichiometric coefficient of the electrons in the half-cell reactions
a_i Activity of component i

By using the standard hydrogen cell electrode H/H^+ as the anode or cathode, the Gibbs energy of formation can be calculated directly from $\Delta_f G = -v_e F \mathcal{E}_0$. Care must be taken in the extrapolation towards 0 molal, as the activity coefficients are very non-linear [2]. The conventional standard state provides the following relationship between the "true" aqueous properties (indicated by superscript aq) of the ion M^z carrying charge z, and the properties relative to hydrogen as shown in Eq. (4.59) and Eq. (4.60), where the superscript $\bullet$ indicates the related

neutral species of the ion.

$$\Delta_f X^o_{M^z}(conv) = \left(X^{aq}_{M^z} - \frac{1}{v}X^{\bullet}_{M_v}\right) - z\left(X^{aq}_{H^+} - \frac{1}{2}X^{\bullet}_{H_2}\right) \qquad X = G, H, A \qquad (4.59)$$

$$X^o_{M^z}(conv) = X^{aq}_{M^z} - zX^{aq}_{H^+} \qquad X = S, C_p, V \qquad (4.60)$$

Standard state properties for the enthalpy of formation and the aqueous standard state entropy is available online in the CO-DATA collection [206], the CRC Handbook of Physics and Chemistry [207], or Wagman et al. (1982) [208]. The standard state properties of selected ions are summarized in Table 4.4.

	$\Delta_f G^o$ [2] [kJ/mol]	$\Delta_f H^o$ [2] [kJ/mol]	S^o [206] [J/mol/K]	C_p^o [2] [J/mol/K]	C_p^o [207] [J/mol/K]
H^+	0	0	0	0	0
Li^+	-293.31	-278.49	13.4	68.6	68.6
Na^+	-261.91	-240.12	59	35.767	46.4
K^+	-283.27	-252.38	102.5	6.1055	21.8
Mg^{++}	-454.8	-466.85	-138.1	-18.635	-
Ca^{++}	-553.58	-542.83	-53.1	-32.809	-
F^-	-278.49	-333.05	-13.8	-102.95	-106.7
Cl^-	-131.23	-167.16	56.5	-126.17	-136.4
Br^-	-103.96	-121.5	82.55	-177.8	-141.8
SO_4^{2-}	-744.53	-909.27	20.1	-267.76	-293.0
NO_3^-	-111.25	-207.36	146.4	-60.97	-86.6

Table 4.4: Aqueous standard state properties of selected ions at 25°C from different sources. While the different sources agree on the formation energy/entropy, some discrepancies are observed in the heat capacity.

While the IUPAC recommended standard state is at a reference pressure of 1 bar, the description of aqueous electrolytes typically requires a pressure-dependent standard state to accurately describe solid-liquid equilibria of electrolyte systems over a wide range of conditions [203]. The geochemical community has developed several models available for the standard state properties of ions at wide ranges of temperature and pressure. Most famous is the Helgeson-Kirkham-Flowers, HKF [203]. The HKF package is implemented in the software SUPCRT92 [209] or the SOCW [210]. Common to these models are that they are build on correlations of measured apparent molar volume and heat capacities. The HKF and SOCW model both have the limitation that they cannot be used at temperatures below -30 degrees due to a divergence of the heat capacity correlation. Another disadvantage is that these approaches require determination of a large number of parameters and thus require a large amount of high-quality data.

The Extended UNIQUAC activity coefficient model by K. Thomsen [75] or the Electrolyte NRTL model [71] use the IUPAC aqueous standard state at 1 bar where parameters have been fitted to low temperature, low pressure data (ca. -30-110°C, 1 bar). To handle the pressure dependence of e.g. solubility, a 2nd order pressure-correction has been introduced for the standard state properties of certain salts with Extended UNIQUAC [211, 212], whereas Aspentech have recently introduced the possibility of using a linear pressure dependency in the equilibrium constants [213].

For the standard state heat capacity (i.e. the temperature dependence of the standard state properties), the data is less reliable. Marcus (1997) [214] e.g. cites ideal gas heat capacities for Mg^{++} and Ca^{++} and the values by K. Thomsen[2] differ for several of the other ions. However, the temperature dependence is of high importance and it is therefore needed to determine the optimal way of establishing this. The approach used e.g. by K. Thomsen [2] in Extended UNIQUAC is to evaluate the aqueous heat capacity relative to the hydrogen ion, which is assigned $C_{p,i} = 0$, whereas all other compounds are correlated using Eq. (4.61). This results in the non-monotonic behaviour for different valency salts as shown in Figure 4.23:
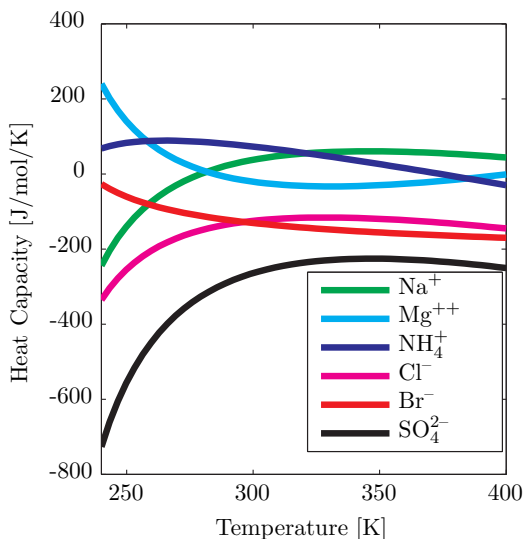
Figure 4.23: Standard state heat capacities as calculated with Eq. (4.61).

$$C_p^o = A + BT + \frac{C}{T - 200} \quad (4.61)$$

Note that the due to the standard state convention where H^+ has zero heat capacity, Eq. (4.61) includes the true heat capacity of the hydrogen ion as shown in Eq. (4.62). The T-dependent correlation shown in Eq. (4.61) must therefore capture the temperature and pressure dependence from the heat of hydration of the ion and that of H^+ as shown in Eq. (4.62):

$$C_{p,M^z}^{aq}(T) \approx C_{p,M^z}^{ig}(T, P_r) + \Delta_{\text{hyd}}C_{p,M^z}(T, P) - z \times \left(C_{p,H^+}^{ig}(T, P_r) + \Delta_{\text{hyd}}C_{p,H^+}(T, P)\right) \quad (4.62)$$

A pressure-dependent standard state is however necessary in order to correctly represent the heat capacity and apparent molar volume of the electrolytes over wider temperature and pressure ranges. Alternatively, it is possible to use the ideal gas standard state with an EoS capable of representing the hydration free energy. While the approach in e.g. Extended UNIQUAC and Electrolyte NRTL may be used to correlate the data, they are of an empirical nature as it is the hydration free energy and properties of the electrolyte solution that depend on pressure, rather than the properties of the salt [203–205].

Born (1920) estimated the solvation radius R_i by setting the work required to charge the ion in vacuum equal to the ionization energy or electron affinity of a range of molecules using Eq. (4.55), neglecting the effect on entropy. Table 4.5 presents the radii calculated from Eq. (4.55) using the ionization energy (IE) and electron affinity (EA) from the NIST JANAF tables [215].

The differences between the measured ion diameters and the calculated Born radius is often interpreted as being due to the inclusion of the solvation shell surrounding the molecules [216]. There are also experimental sources available for the enthalpy of hydration. Marcus (1987) [217] reviewed different sources for the enthalpy of solvation of various ions, and showed that the enthalpy and entropy of hydration of the H^+ ion was given by:

$$\Delta_{hyd}H = \begin{cases} -1098 \pm 5 \\ -1091 \pm 10 \\ -1104 \pm 17 \\ -1103 \pm 7 \end{cases} \left[\frac{\text{kJ}}{\text{mol}}\right] \quad \Delta_{hyd}S^o \approx -131 \pm 1 \frac{\text{J}}{\text{mol}\times\text{K}}$$

	IE / EA [eV]	Ion	r_{Born} [Å]	r_{ion} [Å]	$r_{\text{Born}}/r_{\text{ion}}$	$r_{\text{Born}} - r_{\text{ion}}$ [Å]
H	13.6	H^+	0.53	-	-	-
Li	5.392	Li^+	1.34	0.69	1.93	0.64
Na	5.139	Na^+	1.4	1.02	1.37	0.38
K	4.341	K^+	1.65	1.38	1.2	0.28
Mg	Mg=>Mg$^+$: 7.646	Mg^{++}	1.27	0.71	1.79	0.56
	Mg$^+$=>Mg^{++}: 15.04					
Ca	Ca=>Ca$^+$: 6.113	Ca^{++}	1.6	1	1.6	0.6
	Ca$^+$=>Ca^{++}: 11.87					
F	3.401	F^-	2.11	1.33	1.59	0.78
Cl	3.613	Cl^-	1.99	1.81	1.1	0.18
SO$_4$	5.1±0.1	SO_4^-	1.41	-	-	-
	5.1-1.69	SO_4^{2-}	8.44	2.3	3.67	6.14
NO$_3$	3.937	NO_3^-	1.83	1.79	1.02	0.04

Table 4.5: Ionic radii as calculated from Eq. (4.55) and measured ion diameters Marcus (1997)[214].

The relatively similar standard hydration enthalpies were determined from extrapolation methods, measured via electrode potentials and from the so-called TATB extrathermodynamic assumption, where the enthalpy of hydration of three molecules of similar size and charge are defined as equal, enabling determination of other ions from the lattice enthalpy and heats of solution of salts with tetraphenyl ions and suitable counterions [217]. The correction shown in Eq. (4.63) must be applied in order to convert between the aqueous standard state (where the Gibbs energy of formation of the H^+ ion is fixed to 0 at 25°C) and the ideal gas standard state (where z is the charge of the ion). A similar conversion can be made for enthalpy, entropy, and heat capacity.

$$\underbrace{\Delta_f H_{M^z}^{ig}}_{\text{Ideal gas}} + \underbrace{\Delta_{hyd} H_{M^z}^{aq}}_{\text{True hyd. energy}} = \underbrace{\Delta_f H_{M^z}^{aq}}_{\substack{\text{Conventional} \\ \text{Aqueous S.S.}}} + z \times \underbrace{\Delta_f H_{H^+}^{aq}}_{\substack{\text{True formation} \\ \text{enthalpy of } H^+}} \tag{4.63}$$

The conventional standard state formation properties can be calculated when the true hydration energy is available. The ideal gas and aqueous standard states are related through standard thermodynamic routes and so the ideal gas Gibbs energy may be transformed into the aqueous state using the following steps (shown for H^+):

$$\tfrac{1}{2}H_2(g) \rightleftharpoons H(g) \qquad \Delta G = \Delta_f G^{ig}$$

$$H(g) \rightleftharpoons H^+(g) + e^- \qquad \Delta G = IE$$

$$H^+(g) \rightleftharpoons H^+(aq) \qquad \Delta G = \Delta_{\text{solvation}} G$$
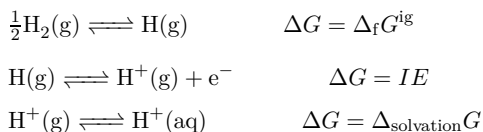
As shown in Table 4.6 good agreement with the values presented by K. Thomsen [13] for all ions but sulphate are obtained using this approach. In the calculation, the ideal gas enthalpy of formation from the NIST Computational Chemistry Comparison and Benchmark Database [218] and the NIST Gas-Phase Ion Thermochemistry database [219] were utilized. If the 2nd ionization energy is back-calculated from the conventional standard state, EA $\left(SO_4^- \rightarrow SO_4^{--}\right) = -0.1$eV, which is significantly less than -1.6eV obtained from quantum chemical calculations [220]. By using this value, $r_{Born} = 5.76$Å is obtained, which is closer to the crystallographic radius. The decision on the standard state is crucial to the development of the equation of state for thermal properties and solid-liquid equilibria, as chemical accuracy (<1kcal/mol) is required in order to get useful results for speciation and solid-liquid equilibrium. Figure 4.22 indicates two practical approaches for calculating the total chemical potential:

Ion	$\Delta_f H^{\text{ig}}$ [kJ/mol]	$\Delta_{hyd} H^{\text{ig}}$ [kJ/mol]	$\Delta_f H^{\text{aq}}$ [kJ/mol]	$\Delta_f H^{\text{aq,conv}}$ (calc) [kJ/mol]	$\Delta_f H^{\text{aq,conv}}$ [206] [kJ/mol]
H^+	1530.1	-1103	427.05	0	
Li^+	679.55	-531	148.55	-278.5	-278.49
Na^+	603.34	-416	187.34	-239.71	-240.12
K^+	507.85	-334	173.84	-253.21	-252.38
Mg^{++}	2336	-1949	386.97	-467.13	-466.85
Ca^{++}	1912.9	-1602	310.9	-543.2	-542.83
F^-	-248.87	-510	-758.77	-331.72	-333.05
Cl^-	-227.29	-367	-594.3	-167.24	-167.16
SO_4^-	-737.8±12				
SO_4^{2-}	-574.7±18	-1035	-1609.7	-755.64	-909.27
NO_3^-	-306.16	-325	-631.17	-204.11	-207.36

Table 4.6: Calculation of conventional standard state aqueous formation enthalpy from the ideal gas enthalpy and the heat of hydration. Ideal gas formation enthalpies were taken from Table 4.5. Hydration energies were taken from Marcus [214]

- Use the aqueous solute standard state

- Use the ideal gas standard state

So far, all known work on electrolyte systems has used the aqueous reference state. This is mainly due to two reasons:

- The thermodynamic models employed have mainly been based on activity coefficients

- Using the ideal gas reference state requires accounting for the Gibbs energy of solvation

However, none of the above points are show-stoppers for using the ideal gas as the reference state in e-CPA, if the residual properties can be represented to a reasonable accuracy. From a scientific point of view, the choice of the ideal gas as the reference state is the most desirable since that is the most fundamental choice for equations of state. If the equation of state could provide accurate description of the Gibbs energy of hydration over wide ranges of temperature and pressure, it will become possible to use standard state properties predicted by ab initio methods (e.g. statistical thermodynamics or quantum chemical methods), which will improve the predictions of intermediate or reactive species. However, as shown in Chapter 3, the Cubic Plus Association EoS does not provide an accurate description of thermal properties when the ideal gas standard state is used, due to inaccuracies in the residual Helmholtz energy and must use the pure liquid reference state to improve the accuracy on thermal properties. Still, the pressure-dependent standard states currently employed in activity coefficient-based models could potentially be eliminated by EoS models that include a term for the Gibbs energy of hydration (e.g. the Born term), as the pressure dependence would be handled by the EoS.

4.4 Insights from Non-Primitive Models and Statistical Thermodynamics

In 1901, van't Hoff received the Nobel prize for his work on establishing the thermodynamics of osmotic pressure and chemical equilibrium [221, 222]. van't Hoff showed that when a solution containing e.g. water and sugar is seperated by a semi-permeable membrane that allows transport of water molecules, the solution side will have a greater pressure than the pure water. The pressure difference is known as the osmotic pressure Π and by equating the chemical potentials

on each side of the membrane it is then possible to write the thermodynamic equilibrium using Eq. (4.64).

$$\mu_s(T, P) = \mu_s(T, P + \Pi) + RT \ln \gamma_s x_s \qquad \Pi = cRT \left(1 + Bc + Cc^2 ...\right) \qquad (4.64)$$

The osmotic pressure can be modeled through a virial equation of state in the solute concentration, and thus rather than considering all molecules in the solution the osmotic equation of state reduces the thermodynamic treatment of solutes to effective solute-solute potentials in a background medium, measuring only the effect of solutes on the solvent properties (e.g. vapor pressure). In 1945, McMillan and Mayer [223] presented the first formal statistical mechanical treatment of multicomponent solutions, by transforming the Grand canonical partition function into an effective form involving only solute species where the effect of the solvent enters through the calculation of effective solute potentials. In 1976, Adelman [68, 69, 156] derived an Ornstein-Zernike equivalent for solutes by transforming the multi-component Ornstein-Zernike equation with the indirect and direct correlation functions (H_{ij} and C_{ij}) between component i and j (Eq. (4.65)) into a form that only included solute species shown in Eq. (4.66) and effective direct correlation functions c_{ij}^{eff}:

$$h_{ij}(\mathbf{X_1}, \mathbf{X_2}) = c_{ij}(\vec{X}_1, \mathbf{X_2}) + \Omega^{-1} \sum_{k}^{n} \int c_{ik}(\mathbf{X_1}, \mathbf{X_3}) \rho_k h_{kj}(\mathbf{X_3}, \mathbf{X_2}) d\mathbf{X_3} \qquad (4.65)$$

$$h_{\alpha\beta}(\mathbf{X_1}, \mathbf{X_2}) = c_{\alpha\beta}^{eff}(\vec{X}_1, \mathbf{X_2}) + \Omega^{-1} \sum_{\gamma}^{p} \int c_{\alpha\gamma}(\mathbf{X_1}, \mathbf{X_3}) \rho_\gamma h_{\gamma\beta}(\mathbf{X_3}, \mathbf{X_2}) d\mathbf{X_3} \qquad (4.66)$$

Where $\mathbf{X_i}$ is a vector property containing the position and orientation of molecule i, and Ω is the angular phase space volume (equal to 4π for linear molecules and $(8\pi)^2$ for non-linear molecules [69]). The effective Ornstein-Zernike in Eq. (4.66) is as general as the original Ornstein-Zernike equation, but only includes a summation over the solute compounds and furthermore the properties that may be derived from Eq. (4.66) are related to the osmotic properties - for instance, the compressibility equation can be written as Eq. (4.67), which is identical to that of the Ornstein-Zernike equation, with the exception that it uses the osmotic pressure and effective direct correlation function rather than the total pressure and the true direct correlation function.

$$\beta \frac{\partial \Pi}{\partial \rho_\alpha} = 1 - \Omega^{-1} \sum_{\gamma}^{p} \int c_{\alpha\gamma}^{eff}(\mathbf{X_1}, \mathbf{X_3}) d\mathbf{X_3} \qquad (4.67)$$

When the actual direct and indirect correlation functions are known, Adelman [69] showed that the effective direct correlation function can be calculated from Eq. (4.68) in which the subscripts p indicate polar and q indicate charged compounds:

$$\begin{aligned}
c_{pp}^{eff}(\mathbf{X_1}, \mathbf{X_2}) = \quad & \mathbf{c_{pp}}(\mathbf{X_1}, \mathbf{X_2}) + \int \mathbf{c_{pq}}(\mathbf{X_1}, \mathbf{X_3}) \rho_q c_{qp}(\mathbf{X_3}, \mathbf{X_2}) d\mathbf{X_3} \\
& + \int \int \mathbf{c_{pq}}(\mathbf{X_1}, \mathbf{X_4}) \rho_q h_{qq}(\mathbf{X_4}, \mathbf{X_5}) \rho_q c_{qp}(\mathbf{X_5}, \mathbf{X_2}) d\mathbf{X_4} d\mathbf{X_5})
\end{aligned} \qquad (4.68)$$

Adelman derived the effective direct correlation function in the case of polar-ionic solutions where the true direct and indirect correlation functions were derived from electrostatic ion-ion, ion-dipole, and dipole-dipole interactions using the procedure by Blum [47]. He showed that it was possible to relate the pure ion-ion interaction given by the Coulomb potential to an effective Coulomb potential (shown in terms of the Fourier transform of the direct correlation function in Eq. (4.69)) where ion-ion interactions are shielded by an effective static permittivity ε_r. The

effective static permittivity of the fluid was calculated from in Eq. (4.70) for a pure dipolar solvent (indicated by the subscript s) with ions of charge ± 1:

$$(2\pi)^{3/2} c_{ion-ion}^{eff}(k) = -\frac{\beta e^2}{\varepsilon_r \varepsilon_0 k^2} \tag{4.69}$$

$$\varepsilon_r = \frac{q^+}{q^-} \qquad q^+ = 1 - (2\pi)^{3/2}\rho_s c_{ss}(k=0) \qquad q^- = 1 + (2\pi)^{3/2}\rho_q c_{ss}^{(1)}(k=0) \tag{4.70}$$

That is, q^+ and q^- are functions of the dipole-dipole interactions that lead to an effective shielding of the electrostatic interactions. In the limit of infinite dilution, Eq. (4.70) becomes equal to the static permittivity of the pure solvent and thus equal to the Wertheim theory [66]. Furthermore, Adelman showed that in the limit of infinite dilution, the molecular model gives the exact same results for the Debye inverse shielding length and the radial distribution function of Debye-Hückel. Adelman thus showed an equivalence between the molecular model and the continuum model, provided that the static permittivity is calculated from a molecular model of the solvent + solutes.

4.4.1 Relationship to Non-Primitive Electrolyte EoS

The equations for the full non-primitive MSA equation of state which explicitly treats the ion-ion, ion-dipole, and dipole-dipole interactions were initially presented by Blum et al. [62–64]. The first attempts for non-primitive modeling of electrolytes with an electrolyte EoS were made by Jin and Donohue [86–88] and later by W. Liu et al. [113], who included explicit terms for the ion-ion, ion-dipole, and dipole-dipole interactions. These attempts were unsuccesful as they required the static permittivity ε_r of the solvent as an additional input to accurately model the excess properties. Z. Liu et al [65, 67], Zhao et al. [52], and Herzog et al. [138] all presented equations of state based on the non-primitive MSA, but only Herzog et al. [138] showed applications to actual experimental data. The equations from Herzog et al. [138] are repeated below for the restricted primitive case where the ion diameter σ_i is equivalent to the dipole diameter σ_d. In the non-primitive MSA, the electrostatic contributions to the Helmholtz free energy depend on balancing of the ion-ion, ion-dipole, and dipole-dipole interactions, which is in practice done by solving the closure equations in Eq. (4.71)-(4.73) for the parameters:

$$0 = a_1^2 + a_2^2 + d_0^2 \tag{4.71}$$

$$0 = a_1 k_{10} - a_2(1 - k_{11}) - d_0 d_2 \tag{4.72}$$

$$0 = k_{10}^2 + (1 - k_{11})^2 - y_1^2 - d_2^2 \tag{4.73}$$

The two parameters d_0^2 and d_2^2 represent the charge and dipole density, respectively, and are calculated from Eq. (4.74):

$$d_0^2 = 4\pi\beta e^2\sigma \sum_j^{ions} \rho_j z_j^2 \qquad d_2^2 = 4/3\pi\beta\mu_s^2\rho_s \tag{4.74}$$

The remaining constants used to calculate Eq. (4.71)-(4.73) are repeated below:

$$\beta_3 = 1 + b_2/3 \qquad \beta_6 = 1 - b_2/6 \qquad \beta_{12} = 1 + b_2/12 \tag{4.75}$$

$$\lambda = \beta_3/\beta_6 \qquad \Delta = b_1^2/4 + \beta_6^2 \qquad y_1 = \beta_6/\beta_1 2^2 \tag{4.76}$$

$$D_F = 1/2 \left(\beta_6 \left[1 + b_0 \right] - b_1^2/12 \right) \qquad a_1 = \left(2D_F^2 \right)^{-1} \left(\Delta - 2\beta_6 D_F \right) \tag{4.77}$$

$$a_2 = -b_1/\beta_6 \left(2D_F^2 \right)^{-1} \left(\Delta/2 + D_F\beta_3 \right) \qquad \Lambda = 1/2 \left(1 + b_0 \right) + \beta_6/6 \tag{4.78}$$

$$k_{10} = b_1/(2\Delta)(1 + a_1\Lambda) \qquad k_{11} = 1 - 1/\Delta(\beta_3 - a_2 b_1 \Lambda) \tag{4.79}$$

Eq. (4.71)-(4.73) are then solved for b_0, b_1, and b_3 using the initial estimates shown below:

$$b_0 = -2d_0(1+d_0)F_H^{1/2}/(4 + 8d_0 + 3d_0^2), \qquad b_1 = -b_0(2b_2)^{1/2} \qquad b_2 = 3d_2^2 F_H/(2 + d_2^2 \tag{4.80}$$

Where $F_H = 1 - 3/2 x_{ion} x_s \xi_3^{1/2}$ and ξ_3 is the packing fraction $\pi/6\rho\sigma^3$. The ion-ion, ion-dipole, and dipole-dipole energy may then be calculated from Eq. (4.81)-(4.83):

$$\beta A^{ii} = V \frac{2d_0^2 b_0 - Q_{ii}^2}{12\pi\sigma^3} \qquad Q_{ii} = -a_1 - 2 + \beta_6/D_F \tag{4.81}$$

$$\beta A^{id} = \frac{V}{12\pi\sigma^3} \left(-2d_0 d_2 b_1 - 2Q_{id}^2 \right) \qquad Q_{id} = \frac{b_1}{\beta_6^2 D} \left(\beta_3 + a_1 \left[3\Lambda - 2D_F \right] \right) \tag{4.82}$$

$$\beta A^{dd} = \frac{-V}{12\pi\sigma^3} \left(Q_{dd}^2 + 2 \left[b_2/\beta_{12}^2 \left(1 - b_2/24 \right) \right]^2 \right) \qquad Q_{dd} = \frac{1}{\Delta} \left(2\beta_3^2 - b_1 a_2 \left[3\Lambda - 2D_F \right] \right) - 2 \tag{4.83}$$

The non-primitive MSA model was implemented in order to investigate the differences between the non-primitive contributions to the Helmholtz energy/chemical potentials as well as the calculated static permittivity. Z. Liu et al. [65, 67] derived a low-density expansion of the non-primitive MSA and showed that this is equivalent to the primitive MSA with an effective static permittivity as discussed by Adelman. Z. Liu et al. [65] then derived an electrolyte EoS based on the result from the primitive MSA equation, but using the static permittivity of the fluid as calculated from the Wertheim model [66] given by Eq. (4.84) and also compared the solution to the non-primitive MSA.

$$\varepsilon_W = \frac{1}{16}\lambda^2 \left(1 + \lambda \right)^4 \qquad \left(\lambda + 2 \right)^2 \left(\lambda^2 - \frac{16}{(1+\lambda)^4} \right) = 12\pi\beta\rho_d\mu_d^2 \tag{4.84}$$

Zhao [52] noted that the expression for the effective static permittivity is modified in the presence of electrolytes and should be calculated from Eq. (4.85).

$$\varepsilon_A = 1 + \frac{\rho_d \alpha_2^2 \beta_6^2 (1+\lambda)^4}{16} \tag{4.85}$$

When using $\sigma = 2.75$Å and the dipole moment of water $\mu = 1.85$D, the predicted static permittivity of the pure solvent at 25°C is only 45.2, as opposed to the experimental value of 78.2. By adjusting $\mu = 2.22$D, it is possible to match the static permittivity of water at 25°C. Figure 4.24 shows the static permittivity as calculated by either model, when the total volume is calculated as the density of NaCl. It is evident that the non-primitive modeling approach also includes a decrease of the static permittivity with the concentration of electrolytes, but that this decrease is more pronounced than evidenced from the experimental data. Furthermore, Figure 4.24 compares the ion-ion and ion-dipole interactions as calculated by the npMSA model with the Debye-Hückel and Born models using the static permittivity as calculated by Eq. (4.84) and Eq. (4.85). There exists a noticeable disagreement between the primitive and non-primitive

models.

To extend the investigation to derivative properties, the derivatives of the models were calculated through numerical differentiation. Figure 4.25 it may be observed that the volume derivatives differs by a factor 5-10 from that of the Debye-Hückel and Born models at higher concentrations. The npMSA furthermore has a minimum in the volume derivative, which could introduce additional volume roots. The temperature dependence shown in Figure 4.26 is observed to display the same trends - the agreement is better when using the Wertheim static permittivity from Eq. (4.84). The chemical potentials from ion-ion interactions of the two models shown in Figure 4.27 are in better agreement, whereas the chemical potential from the ion-dipole interactions shown in Figure 4.28 display a significant difference as the ion concentration increases. However - this does not imply that it is the Born model that is wrong; Herzog et al. [138] compared the solvation free energy calculated with the semirestricted non-primitive MSA but did not obtain proper correspondence with the hydration free energy of the salts even when the ion diameter was adjusted, whereas the Born model has succesfully been applied to modeling of the Gibbs energy of hydration over wide ranges of temperature and pressure[204, 205, 224, 225].

While not shown in this investigation, the non-primitive MSA term also includs dipole-dipole interactions, that provides an additional contribution to the overall Helmholtz free energy, and the delicate balancing of ion-ion, ion-dipole, and dipole-dipole energetics requires further investigation in order to conclusively validate the non-primitive modeling approach for e.g. mixtures of polar and hydrogen bonding compounds. Models that include the dipole-dipole interactions actually have to turn off the dipolar interactions for hydrogen-bonding compounds to describe e.g. water over wide ranges of temperature and pressure [226], as the interaction between association and polarity is not well accounted for with the present models.

All in all, it may be concluded that even when using the dielectric constant from the npMSA model as calculated by Eq. (4.85), the Debye-Hückel and Born models do differ from the npMSA, but that the trends are generally in good agreement. More importantly, the chemical potential calculated from the npMSA and the Debye-Hückel model show comparable trends; and it is important to notice that the models provide a significant contribution to the chemical potential of the solvent, due to the dependence of the dielectric constant on the solvent density. Such a significant contribution to the chemical potential was not observed in Figure 4.14 p. 58 where an empirical model is used for the static permittivity in the Debye-Hückel model. This shows that the Debye-Hückel and Born models coupled with the npMSA dielectric constant captures a different physical effect; namely that when the dipole density increase, the static permittivity will increase. This contribution is ignored when using an empirical correlation for the dielectric constant that is independent ofthe solvent density. Still, the investigatoin shows that npMSA could have several problems; for instance must the dipole moment be adjusted to match the static permittivity of the solvent - but perhaps more problematically, it overestimates the decrease in the static permittivity as the salt concentration increases. This error cannot be easily solved by adjusting ion-specific parameters may imply a problem with the coupling of the ion-ion, ion-dipole and dipole-dipole interactions in the npMSA model; however, it would require a more detailed investigation including a comparison to molecular simulation to determine whether this is indeed the case.

4.4.2 On the conversion from the McMillan-Mayer framework

The introduction chapter highlighted the confuson in literature on whether the primitive models need to be converted from the McMillan-Mayer (MM) to the Lewis-Randall (LR) framework. As mentioned in Section 4.4, the McMillan-Mayer framework enables a statistical mechanical
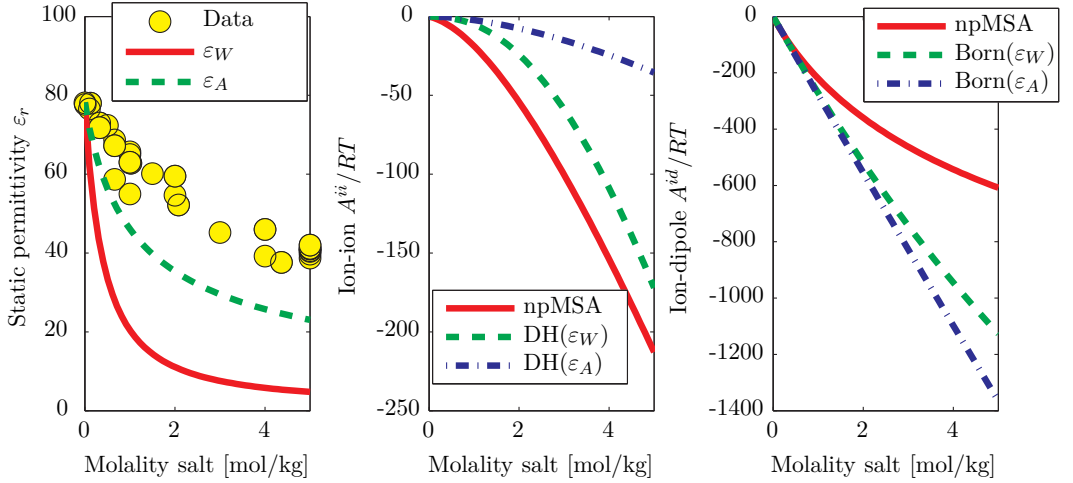
Figure 4.24: Dielectric Constant from Non-primitive MSA and Helmholtz Energy. DH(ε_X) or Born(ε_X) indicates whether the Wertheim static permittivity ϵ_W from Eq. (4.84) or the Adelman A from Eq. (4.85) was used in the model.
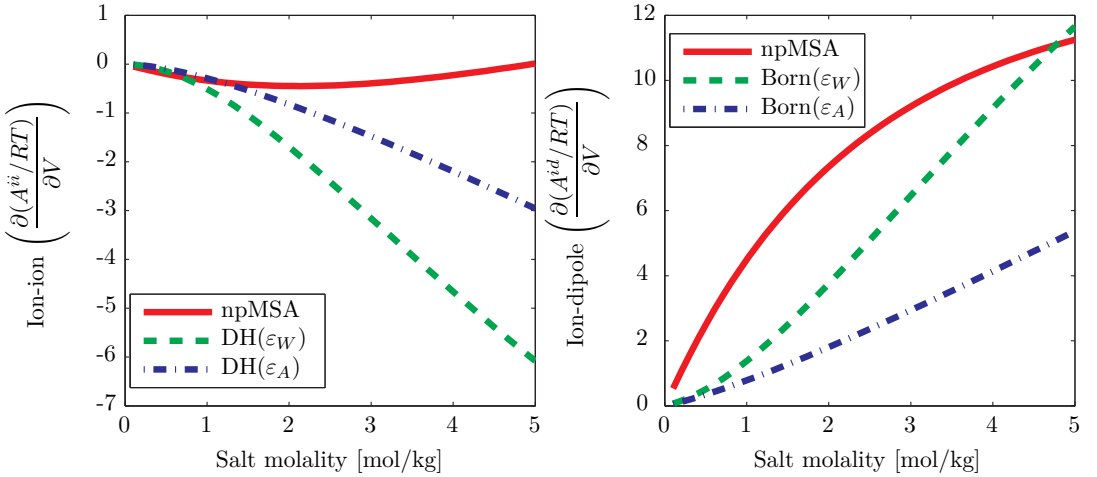
Figure 4.25: Volumetric derivatives of the Helmholtz free energy from Non-primitive MSA and Debye-Huckel/Born. DH(ε_X) or Born(ε_X) indicates whether the Wertheim static permittivity ϵ_W from Eq. (4.84) or the Adelman A from Eq. (4.85) was used in the model.

treatment of solute molecules immersed in a solvent through effective solute-solute potentials. The LR framework does not distinguish between solvent and solute molecules, and is based on the state variables T, P, and $\mathbf{n}$, whereas the MM framework depends on the concentration of solute compounds, $\mathbf{c}$, T, and the pressure of the pure solvent P_0. In order to convert between activity coefficients calculated with the two frameworks, the following conversion is needed:

$$\ln \gamma_0^{LR}(T, P, \mathbf{n}) - \ln \gamma_0^{MM}(T, P, \mathbf{n}) = -\frac{\overline{V}_0 P^e}{RT} \tag{4.86}$$
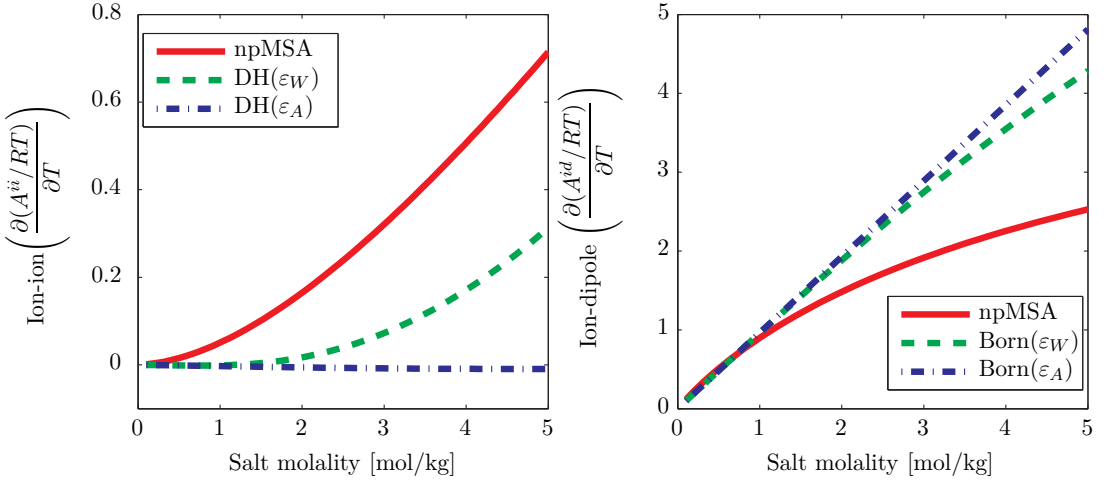
Figure 4.26: Temperature derivative of the Helmholtz free energy from Non-primitive MSA and Debye-Huckel/Born. DH(ε_X) or Born(ε_X) indicates whether the Wertheim static permittivity ϵ_W from Eq. (4.84) or the Adelman A from Eq. (4.85) was used in the model.
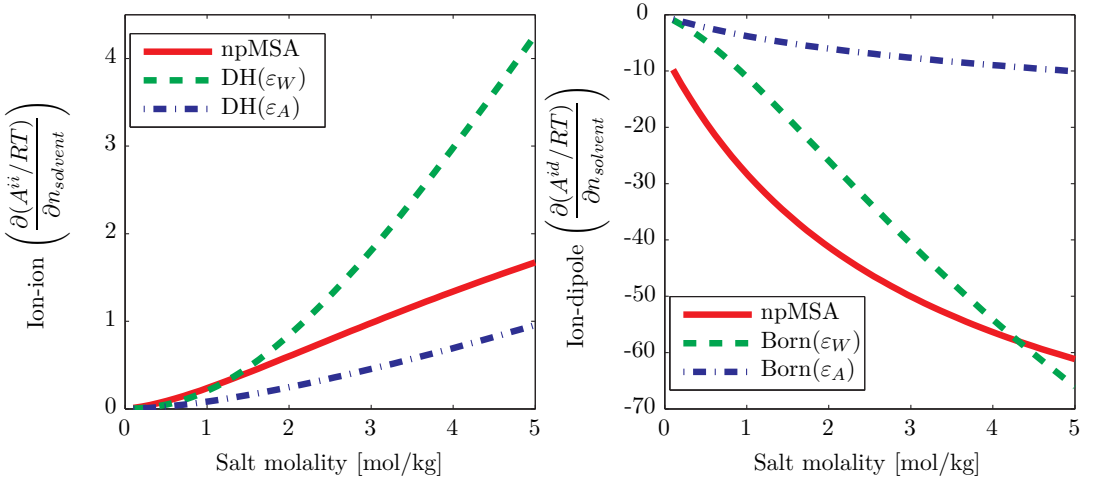
Figure 4.27: Chemical potential of salt and solvent from Non-primitive MSA and Debye-Huckel. DH(ε_X) or Born(ε_X) indicates whether the Wertheim static permittivity ϵ_W from Eq. (4.84) or the Adelman A from Eq. (4.85) was used in the model.

In which $\overline{V}_0$ is the partial molar volume of solvent and the electrostatic pressure $P^e = -\left(\frac{\partial A^e}{\partial V}\right)_{T,\mathbf{n}}$. From Table 1.2 in the introduction chapter (p. 14) it was shown how most authors do not mention the discrepancy on the conversion between the frameworks. Wu and Prausnitz [109] stated that since the primitive MSA model was developed from a MM framework, one should not include derivatives of the static permittivity on the Helmholtz energy; but it is the opinion of this author, that this statement cannot be true - if the derivatives of a function used to calculate the Helmholtz energy are neglected it will lead to an inconsistent thermodynamic model.
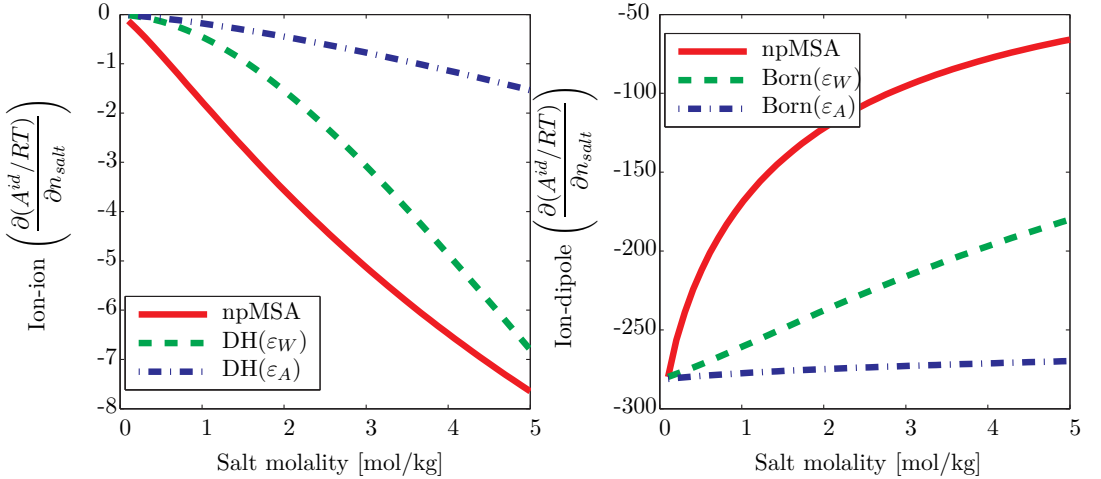
Figure 4.28: Chemical potential of salt and solvent from Non-primitive MSA and Born. DH(ε_X) or Born(ε_X) indicates whether the Wertheim static permittivity ϵ_W from Eq. (4.84) or the Adelman A from Eq. (4.85) was used in the model.

Myers et al. [114] perform the conversion between the frameworks to calculate the corrected activity coefficient of the solvent, while Radosz et al. [121–127] and Haghtalab et al. [136, 137] state that the correction is insignificant and will be hidden by the parameters. Advocates of the non-primitive models for electrolyte mixtures argue that since the non-primitive models are developed from the T, V, **n** state variables, they do not require any conversion between the frameworks [52, 138], making the non-primitive model a more suitable choice for electrolyte equations of state.

In an attempt to clarify the situation on conversion from the McMillan-Mayer framework, Breil and Mollerup (2006) [227] stated that the electrostatic contribution to the chemical potential of the solvent at constant volume must be zero, since the solvent is not involved in the charging process. They showed that when the T, V, **n** state variables were used, the conversion between the two frameworks was superfluous and argued that it is unnecessary to perform a conversion from the McMillan-Mayer framework in electrolyte equations of state when the Helmholtz energy from the original Debye-Hückel is used. This contrasts Herzog et al. [138] who state that the primitive MSA must be converted, irrespective of whether it is used as an activity coefficient model or in an equation of state [228], which has also been done by e.g. Simonin et al. [50, 51].

Despite several attempts, the recent literature on electrolyte EoS do not provide a completely satisfactory explanation on the necessity of conversion between the McMillan-Mayer and Lewis-Randall frameworks. It is the oppinion of this author that a different interpretation is needed in order to rectify the situation. As discussed in Section 4.4, Adelman [68, 69, 156] developed a generalization of the Ornstein-Zernike relations for effective solute-solute potentials and showed that the electrostatic interactions may be calculated from the shielded Coulomb potential (Eq. (4.69)), where the static permittivity of the solute ε_r is calculated from the direct and indirect correlation functions of the entire mixture. Friedman (1982) [158] investigated the Adelman approach further and showed the similarity between the McMillan-Mayer theory and the effective direct correlation functions from Adelman, which on the other hand do not require conversion between the frameworks as it is simply an alternative transformation of the Ornstein-Zernike

equations. This provides an alternative view on the static permittivity, as a description of the dipole-dipole and ion-dipole interactions in the mixture, and therefore **requires** differentiation with regards to all of the molecules in the mixture. Whereas Adelman [69] developed the statistical mechanical framework for describing the effective correlation functions, it is suggested to use the reverse scheme as an alternative approach that will allow the use of primitive models, such as the Debye-Hückel model to model the effective ion-ion interactions in the mixture, provided that the static permittivity is modeled using a physically correct approach. This is an indirect approach to model the direct correlation functions between all molecules in the actual mixture.

4.5 Summary and Conclusions

This chapter investigated the fundamentals of thermodynamic modeling of electrolyte systems and in the process provided answers and guidelines for several of the research questions:

- How should electrostatic interactions be modeled?

- Should activity coefficients be converted from the McMillan-Mayer to the Lewis-Randall framework?

- How should the static permittivity be modeled? And does it even matter?

- Should the model include an explicit term for the Gibbs energy of solvation?

- What is the importance of ion-solvent and ion-ion association in an electrolyte EoS?

The residual Helmholtz free energy of the Debye-Hückel model was compared to the implicit non-restricted primitive mean spherical approximation model ([161] Ind. Eng. Chem. Res. (2012), 51 (14), 5353-5363) and it was shown that the models provide quite similar results for the energy and its derivatives with regards to temperature, volume and composition. It was concluded that either model could be used to represent the contribution to residual Helmholtz energy from electrostatic interactions, and that the choice of model for the static permittivity would have a much larger effect than the differences between the two models.

Molecular simulation has provided insight in the behavior of electrolyte mixtures and has shown that ion pairs are a natural consequence of the short-range interactions between ions. Their appearance of ion pairs is ubiquitous and necessary in order to get agreement with molecular simulation - furthermore, associated ions have been investigated through various experimental means such as conductometry and dielectric spectroscopy. While it is common to consider salts such as NaCl as fully dissociated in water at room temperature, it may become important to include such a model, when treating mixed solvents as ion pairs will be more prevalent in low-permittivity solvents where the Bjerrum length l_B is large. A real mixture of e.g. water and ions will display several ion-specific traits as a consequence of the ion-solvent and ion-ion interactions, and Kalcher et al. [60, 201] showed that the ion-solvent association and ion-ion association are linked and that ions that have strong interactions with the solvent will have a greater tendency to form solvent-separated ion pairs, leading to an increased complexity of the system.

The Born model was shown to be of great importance to the fugacity coefficient at infinite dilution, and therefore the main contributor to the driving force of ions towards the most polar phase. If the model has a good description of the Gibbs energy of hydration, it was furthermore shown that it would become possible to use the ideal gas standard state for standard state properties. This would in itself lead to new possibilities for predicting e.g. the chemical speciation

and reduce the need for fitting unknown standard state properties. It was concluded that the EoS must have a term that accounts for the Gibbs energy of hydration, in a manner that takes into account the dipole-ion interactions; either through the Born model or an improved model.

The ion-ion and ion-dipole contributions to the non-primitive MSA was compared to the Debye-Hückel and Born models using the static permittivity calculated from the non-primitive model. It was shown that while there are differences in the derivatives wrt. temperature and volume, a reasonable agreement was observed between the chemical potential for the Debye-Hückel model and the npMSA. The contributions to the chemical potential of the Born model differed significantly at higher salt concentrations, but gave a nearly identical contribution at infinite dilution. While the non-primitive approach is of great interest to the development of electrolyte EoS, the non-primitive model also includes an explicit dipole-dipole interaction term, which makes it impossible to include as an extension to the CPA model without refitting parameters for all polar compounds. Since the goal of this study is to extend the existing model to handle electrolytes while maintaining backwards compatibility with the existing model, the model will be based on the Debye-Hückel and Born.

The confusion in literature concerning conversion from the McMillan-Mayer to the Lewis-Randall framework was also addressed. Following the work by Adelman [69], a new interpretation of the problem was proposed, in which the static permittivity is viewed in terms of its shielding effect on the Coulomb potential in electrolyte solutions. The comparison of the primitive and non-primitive electrolyte models furthermore indicated that new physical behavior of the primitive electrostatic models is incorporated when the static permittivity is calculated from a physically based model. The development of a physically correct model to describe the static permittivity of complex mixtures will be the main topic of the next chapter.

Chapter 5

Modeling of the Static Permittivity of Complex Fluids

The previous chapter demonstrated that the static permittivity ε_r is a key property for describing the electrostatic interactions and the Gibbs energy of hydration for primitive electrolyte models. The non-primitive MSA (npMSA) elminates the need of using a static permittivity by directly determining the ion-ion, ion-dipole, and dipole-dipole interactions. Adelman [69] derived a solute-based Ornstein-Zernike equation and demonstrated the relationship to the effective Coulomb potential in a medium with a static permittivity arising from the interactions between all molecules in the mixture:

$$\psi_{ij}^{eff} = \frac{e^2 z_i z_j}{4\pi\varepsilon_r\varepsilon_0 r_{ij}^2}$$

In Section 4.4.1 it was demonstrated that the static permittivity predicted by the npMSA model is 40% lower than its experimental value when using the vacuum dipole moment of water. While it is possible to adjust the dipole moment manually to obtain better agreement with the liquid static permittivity, there are other problems remaining; for instance is theoi dipole-dipole interaction energy turned off for hydrogen-bonding compounds in dipolar SAFT-type as it leads to incorrect representation of the phase equilibrium in mixtures with polar compounds [226]. Additionally, the dipole-dipole interaction energy is incompatible with the existing CPA formulation making it impossible to use the npMSA as the basis for an electrolyte extension to CPA.

It was shown that the chemical potential of the solvent at constant volume was affected by the concentration of ions in the case of the non-primitive MSA since the static permittivity depends on the density of the solvent. As shown in Chapter 4, this behavior is not observed when an empirical correlation that is independent of the solvent density is used for the static permittivity in the Debye-Hückel model . It was therefore argued that rather than using a non-primitive model to determine all interactions between ion-ion, ion-solvent, and solvent-solvent, it may be more feasible to develop a physically realistic model of the static permittivity and thereby indirectly provide a measure of the balance between ion-ion, ion-dipole, and dipole-dipole interactions. This model for the static permittivity can then be used within primitive electrolyte models such as Debye-Hückel and Born to calculate the effective charge-charge interaction potential and in the process avoid the need to convert from the McMillan-Mayer framework.

In this chapter, the efforts to develop a new model for predicting the static permittivity of complex mixtures containing non-polar, polar, and hydrogen-bonding compounds are presented. This work was published in two articles in J. Phys. Chem. B in 2013:

- Modeling of Dielectric Properties of Complex Fluids with an Equation of State (published in J. Phys. Chem. B. (2013), 117, 3389-3397) [162]

- Modeling of Dielectric Properties of Aqueous Salt Solutions with an Equation of State (published in J. Phys. Chem. B. (2013), 117, 10523-10533) [163]

5.1   Introduction

The static permittivity is a key property for describing solutions containing polar and hydrogen bonding compounds. However, the precise relationship between the molecular and dielectric properties is not well-established. Here it is shown that the relative permittivity at zero frequency (static permittivity) can be modeled simultaneously with thermodynamic properties. The static permittivity is calculated from an extension of the framework developed by Onsager, Kirkwood, and Fröhlich to associating mixtures. The thermodynamic properties are calculated from the Cubic-Plus-Association (CPA) equation of state that includes the Wertheim association model as formulated in the Statistical Associating Fluid Theory (SAFT) to account for hydrogen bonding molecules. It is shown that by using a simple description of the geometry of the association, the Kirkwood g-factor can be calculated as a function of the probability of hydrogen bond formation. The results show that it is possible to predict the static permittivity of complex mixtures over wide temperature and pressure ranges from simple extensions of well-established theories simultaneously with the calculation of thermodynamic properties.

5.2   Literature Survey

5.2.1   Measurement of Static Permittivity of Complex Fluids

The static permittivity of polar non-conducting fluids may be measured directly from the real part of the permittivity from the frequency range 0.1-1MHz, but for conducting fluids (e.g. in mixtures containing electrolytes), it is required to assess the dielectric losses through dielectric relaxation spectroscopy (DRS) to determine the static permittivity[32, 229]. When analyzing the equilibrium dielectric properties of conducting mixtures, the measured permittivity ε^* must be corrected for the direct-current conductivity σ causing ion drift at low frequencies using Eq.(5.1) [32, 230–234]

$$\varepsilon_d^* = \varepsilon^* + i\frac{\sigma}{\omega\varepsilon_0} \tag{5.1}$$

ω	[rev/s]	Angular frequency
σ	[S/m]	Direct current conductivity
ε_d^*		Complex permittivity (frequency dependent dielectric response)

Note that the real part of the frequency-dependent dielectric response ε_d will tend towards the static permittivity of the solution in the limit of zero frequency. DRS provides insight in the relaxation processes in the mixture, and has e.g. been used to derive information on the dynamics of solvation of pure components and mixtures. The frequency-dependent behavior may be determined using a model, such as the first-order Debye relaxation model[235] as shown in Eq. (5.2)[32, 230, 236–238]:

$$\varepsilon_d^* = \varepsilon_\infty + \frac{\varepsilon_r - \varepsilon_\infty}{1 + i\omega\tau} \tag{5.2}$$

τ	[s]	Characteristic dipole relaxation time

Note that τ is a measure of the time it takes for dipoles to become randomly arranged after removal of the electrical field. In practice, several relaxation processes may be involved in analyzing the frequency-response of the permittivity, and therefore permittivity data is often analyzed using a number of relaxation models, each of which are fitted to the more generic form given by Eq. (5.3) where $0 \leq \alpha_j, \beta_j \leq 1$:

$$\varepsilon_d^* = \sum_{j=1}^{N} \frac{S_j}{\left[1 + (i\omega\tau_j)^{1-\alpha_j}\right]^{\beta_j}} + \varepsilon_\infty \qquad (5.3)$$

The dielectric response of pure water at $20°C$ is shown in Figure 5.1, where the characteristic relaxation time τ_c corresponds to the cooperative relaxation of the hydrogen-bond network and τ_f the free water and memory of dielectric friction [33].

Additionally, the imaginary part of the permittivity shows four intermolecular vibrations; v_{50} for bending, v_{180} for stretching, and v_{400}/v_{700} for libration of hydrogen bonds [33]. Typical relaxation schemes following Eq. (5.3) are shown in Table 5.1 to the right. After data acquisition the data must be corrected for the dielectric responses arising from the measurement equipment, and then analyzed by a relaxation model such as Eq. (5.3)[32, 239].
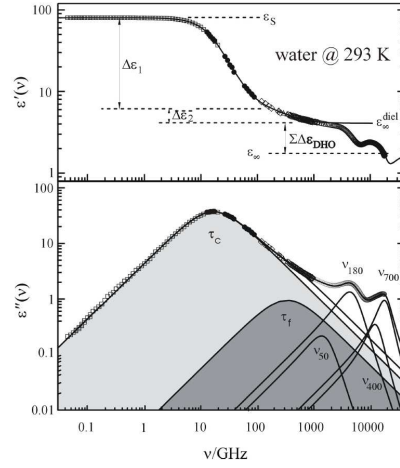
Figure 5.1: Dielectric profile of water at 20 °C [33]

	α_j	β_j
Debye	0	1
Cole-Davidson	0	Fitted
Cole-Cole	Fitted	1

Table 5.1: Typical relaxation models and parameters for Eq. (5.3)[32, 239]

5.2.2 Theory of the Static Permittivity

Dielectric spectroscopy is widely used to gain insight in molecular properties of fluids[24, 154, 240, 241]. The dielectric properties of fluids are characterized from the complex permittivity $\varepsilon' + i\varepsilon''$, which can be measured from the response of the fluid to an external electrical field[24, 154, 240, 241]. The electrical response ultimately depends on many factors, including transport and thermodynamic properties (density, viscosity, etc.), molecular properties (dipole moment, molecular polarizability, etc.), and also the fluid structure (e.g. due to hydrogen bonding) [24, 150–152, 154, 240–243]. The zero-frequency limit of the relative permittivity of a material, also known as the static relative permittivity is a measure of the ratio of capacitance of a medium relative to the capacitance of vacuum[24, 240, 243]. The static permittivity is required as input to primitive models for the electrostatic interactions between ions in a polar medium[161], such as the Debye-Hückel[26] theory and the Born[45] model of the solvation free energy.

The static permittivity has also been used to correlate solubility and speciation of neutral compounds and pharmaceuticals[30] and to predict the scaling propensity of produced water containing gas hydrate inhibitors[224]. Online measurements of the permittivity are used for non-destructive sensing of moisture content of soils and food[154, 244]. It also serves as a valuable resource for assessment of water saturation in geological formations and determination

of the hydrocarbon content in the presence of fresh formation water or water with unknown salinity[245].

The theoretical background for predicting the static permittivity (ε_r) of polar compounds from molecular properties relies on the famous papers by Onsager[150] and Kirkwood[151]. Fröhlich[152] introduced the Kirkwood g-factor accounting for the local structure in Onsager's relations and Hasted[154] extended the formulation to mixtures as shown in Eq. (5.4). A derivation of Eq. (5.4) is available in Appendix C.2.

$$\frac{(2\varepsilon_r + \varepsilon_\infty)(\varepsilon_r - \varepsilon_\infty)}{\varepsilon_r(\varepsilon_\infty + 2)^2} = \frac{N_A}{9\varepsilon_0 k_B T v} \sum_i x_i g_i \mu_{i,0}^2 \tag{5.4}$$

ε_∞		Permittivity at infinite frequency, typically replaced by square of the refractive index n^2
$\mu_{i,0}$	$[\mathrm{C} \cdot \mathrm{m}]$	Dipole moment of component i in vacuum
g_i		Kirkwood g-factor of component i

When the polarizability is included, the Onsager equations provides a good description of the static permittivity of real liquids [157]. Stell et al. [157] attributes this to the quadrupolar interactions and anisotropic interactions, which effectively counterbalances the contribution to the g-factor that is ignored by the Onsager theory. While the Onsager theory is inaccurate for describing results from molecular simulation of simple dipolar models it is actually a good approximation for real liquids that have multipolar moments leading to error cancellations [157].

Eq. (5.4) can be derived using the procedure by Buckingham[153] and by assuming the same infinite frequency permittivity ε_∞ for all spherical enclosures (see Appendix C.2). ε_∞ is calculated from the Clausius-Mossotti[24, 240] equation for mixtures shown in Eq. (5.5):

$$\frac{\varepsilon_\infty - 1}{\varepsilon_\infty + 2} = \frac{1}{3\varepsilon_0} \frac{N_A}{v} \sum_i x_i \alpha_{0,i} \tag{5.5}$$

$\alpha_{0,i}$	$[\mathrm{C}^2\mathrm{m}^2/\mathrm{J}]$	The molecular polarizability of molecule i

Oster and Kirkwood[242] derived a model for the pure component g-factor for water and alcohols using Eq.(5.6) with a coordination number $z = 4$ for water and using the statistical mechanical average angle γ of the projected dipole moment of surrounding molecules onto the central molecule:

$$g = 1 + z \langle \cos \gamma \rangle \tag{5.6}$$

Haggis et al.[241] used the "broken-down ice" structure of water, to accurately predict the static permittivity of water over wider temperature ranges by accounting for a reduction in the degree of hydrogen bonding. Suresh and Naik[246, 247] presented a model for predicting the static permittivity of binary mixtures of methanol, water, and acetone by calculating $\cos \gamma$ from molecular geometry and the probability of association determined by a chemical model for hydrogen bonding. Suresh improved the model for mixtures[248] and used the model to analyze two proposed schemes for the cross-association between water and dimethyl sulfoxide.

5.2.3 Refractive Index

The infinite frequency polarizability ϵ_∞ is often approximated by the square of the refractive index, which has been measured for many compounds (especially at 589 nm). The refractive index is a measure of the relative speed of electromagnetic waves in a given material compared

to vacuum. As a light wave with wavelength λ propagates from one transparent medium with refractive index n_1 to another with refractive index n_2, part of the light will be reflected at the interface, while another part of the beam will appear to bend according to Snell's law given by Eq. (5.7) [249]:

$$\frac{\sin \theta_1}{\sin \theta_2} = \frac{n_2}{n_1} \tag{5.7}$$

This process is known as refraction and is due to the change in relative speed of the light in the different media. The refractive index defined by Eq. (5.8) as a measure of the relative speed of the light wave in a medium compared to the speed of light in vacuum [249, 250]:

$$n = \frac{c}{v} \tag{5.8}$$

In Eq. (5.8), c is the speed of light in vacuum and v is the velocity of light in the material. As the speed of light cannot be higher than the speed of light in vacuum, $|n| \geq 1$. The refractive index is a characteristic function of both the type of medium and conditions (temperature, pressure, volume), as well as the wavelength of the incipient light λ. The dependence of refractive index of solids on the wavelength is known as dispersion, and will e.g. cause the separation of sun light into it's color spectrum as a beam enters a prism [249]. The dispersion contributions to the refractive index can be related to the wavelength of the incipient light through the Cauchy polynomial given by Eq. (5.9) [249, 250], whereas a more advanced form is needed to take into account absorption lines.

$$n = a + \frac{b}{\lambda^2} + \frac{c}{\lambda^4} + \frac{d}{\lambda^6}... \tag{5.9}$$

The refractive index can also be derived from the Maxwell equations [250]. This yield the expression shown in Eq. (5.10):

$$n^2 = \varepsilon_\lambda \mu_r \tag{5.10}$$

Where μ_r is the relative magnetic permeability of the material and ε_λ the relative permittivity of the medium at the wavelength λ. For non-ferromagnetic materials, the magnetic permeability becomes approximately unity, and for non-polar substances the dependence of relative static permittivity on the wavelength becomes negligible and it is sufficient to use the relative static permittivity.

The refractive index depends on the conditions and the given medium. The refractive index in a gas is close to unity, as the concentration of molecules in the gas is small and thereby the light maintains most of its momentum. In a liquid, the refractive index increases due to the increased molecular density and the interaction between the molecules. Examples of the refractive index of different medium are shown in Table 5.2.

Medium	Temperature [°C]	Refractive Index
Air (g)	0	1.000293
Water (l)	20	1.333
Acetic Acid (l)	20	1.3716
Ethanol (l)	20	1.3614
NaCl (s)	26.85	1.544

Table 5.2: Refractive indices at 589nm at 1atm in various media [207].

In general, the refractive index depends on temperature, pressure and composition. Refractrometry uses the composition dependence to determine the concentration of a solute in a solvent from known empirical relationships between concentration and refractive index at a given temperature and pressure.

Refractometry has e.g. been used to correlate and measure the concentration of sucrose in an aqueous medium [251] or to determine the relative ratio of refrigerant and refrigerant oil

under pressurized condition[252]. Breil and Mollerup used the refractive index calculated by the Clausius-Mossotti equation along with an activity coefficient model to calculate the turbidity and scattering ratio of a mixture of sucrose and lysozyme [253]. The refractive index has also been used as a method to correlate other physical properties. Escobedo and Mansoori [254] proposed a corresponding states expression for calculation of the Parachor parameter for a corresponding states approach to calculation of the surface tension of a liquid mixture. Riazi and Roomi [255] utilized the refractive index to correlate thermodynamic and physical properties such as heat capacity and viscosity as well as parameters for the cubic EoS, and showed that this gives better correspondence with the liquid density of heavier compounds. Riazi and Roomi [255] also present a characterization scheme using the refractive index for petroleum pseudocomponents.

In this work, the refractive index or infinite frequency permittivity will be calculated from the molecular polarizability and the Clausius-Mossotti equation from Eq. (5.5) to provide an estimate of the polarizability of the medium.

5.3 Extension of the Theory of the Static Permittivity to Handle Hydrogen-Bonding Compounds

5.3.1 Derivation of a Geometrical Model for Calculation of the Kirkwood g-factor

The following section summarizes the development of a new model for the static permittivity of mixtures containing hydrogen-bonding compounds. It extends the model for mixtures shown in Eq. (5.4), in which the g-factor can be calculated from Eq. (5.11) (see derivation in Appendix C.2):

$$g_i = 1 + \frac{1}{\mu_{0,i}^2} \left\langle \sum_{j \neq i} \mu_{0,i} \cdot \mu'_{0,j} \right\rangle \tag{5.11}$$

$\mu'_{0,j}$ $[\mathrm{C \cdot m}]$ The dipole moment of molecules surrounding the central dipole

Eq. (5.11) is approximated from the projected dipole moments of all molecules that are hydrogen bonded to a fixed central molecule C. A sketch of the innermost neighbor is shown in Figure 5.2 to the right. It is evident that the angle between the two dipole moments, γ, can be calculated from the projection of the dipole moment of a de-central molecule μ_D onto the central molecule μ_C using Eq. (5.12):

$$\langle \cos \gamma \rangle = \frac{\langle \mu_C \cdot \mu_D \rangle}{\mu_C \mu_D} \tag{5.12}$$

By assuming free rotation around the hydrogen bond, Eq. (5.12) can be rewritten in terms of the dipole moment in the direction of the hydrogen-bond μ_H towards the other molecule as shown in (5.13):

$$\langle \cos \gamma \rangle = \frac{\mu_H \cdot \mu_D}{\mu_C \mu_D} \tag{5.13}$$
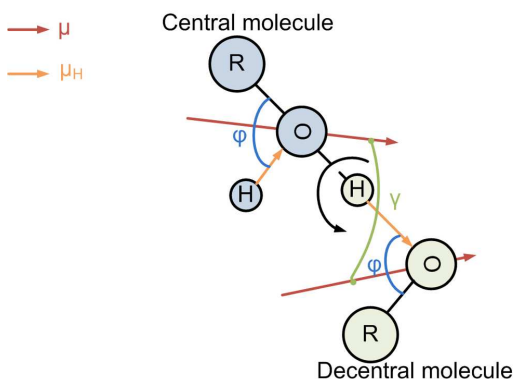
Figure 5.2: Sketch of bonding angles and dipole moments with the innermost neighbor

Eq. (5.13) is transformed using simple trigonometric relationships into Eq. (5.14) for tetrahedral, and Eq. (5.15) for planar networks (see Appendix C.3).

$$\langle \cos \gamma \rangle = -\frac{\mu_{OH} + \mu_{OR} \cos \varphi}{\mu_C \mu_D} \left(\mu_{OH} \cos \theta + \mu_{OR} \left(\cos \theta \cos \varphi - \frac{1}{2} \sin \theta \sin \varphi \right) \right) \tag{5.14}$$

$$\langle \cos \gamma \rangle = -\frac{\mu_{OH} + \mu_{OR} \cos \varphi}{\mu_C \mu_D} \left(\mu_{OH} \cos \theta + \mu_{OR} \left(\cos \theta \cos \varphi - \sin \theta \sin \varphi \right) \right) \tag{5.15}$$

In Eq. (5.14) and Eq. (5.15), μ_{OH} and μ_{OR} are the constituents to the dipole moment in the O-H and O-R directions, respectively. Eq. (5.14) and Eq. (5.15) may be used for pure components and mixtures to determine angles between proton donors and proton acceptors and vice versa. $\theta = 109.47°$ is used for the predictions with the tetrahedral network and $\theta = 120°$ is used for the planar network. Assuming that the central molecule C can form up to z_{CD} hydrogen bonds with molecule D in the first shell the contribution to the scalar product of the dipole moments of the first z_{ij} neighbors can be calculated from Eq. (5.16):

$$\langle \mu_C \cdot \mu_D \rangle^{(1)} = z_{CD} \mu_C \mu_D \langle \cos \gamma \rangle \tag{5.16}$$

The simplified picture of the hydrogen bonding network shown in Figure 5.3 (to the right) is constructed in order to determine the projected dipole moment from all neighbors to the central molecule including hydrogen-bonded molecules from the first, second, and nth shell. If the molecules can form more than 2 hydrogen bonds, each shell will contain more molecules than the first. As shown by Suresh and Naik[246] the geometrical configurations in the tetrahedrally coordinated shells result in that the dipole moments of all but z_{CD} molecules will be cancelled out. It is therefore assumed that there are only z_{CD} molecules in each shell that give a net contribution to the central dipole moment.

Figure 5.3: Sketch of color-coded important dipole moments and angles in a hydrogen-bonding system.

The projected dipole moment from the k$^{\text{th}}$ shell onto the first shell may then be calculated from the rotation angle θ which is multiplied onto the projected dipole moment of the first shell using Eq. (5.17):

$$\langle \mu_C \cdot \mu_D \rangle^{(k)} = \langle \mu_C \cdot \mu_D \rangle^{(1)} \cos^{k-1} (\pi - \theta), \qquad k = 2..\infty \tag{5.17}$$

The statistical mechanical average in Eq. (5.11) for mixtures of associating compounds is then approximated by a summation over the surrounding shells for all molecules given by Eq. (5.18):

$$\left\langle \sum_{j \neq i} \mu_{0,i} \cdot \mu'_{0,j} \right\rangle = \left\langle \sum_{k}^{shells} \sum_{j}^{components} \left\langle \mu_{0,i} \cdot \mu'_{0,j} \right\rangle \right\rangle \tag{5.18}$$

The statistical mechanical average $\left\langle \mu_{0,i} \cdot \mu'_{0,j} \right\rangle$ depends on the probability of molecule i and j being associated (P_{ij}) and on the projection of the dipole moment onto the central molecule. The statistical mechanical average of the projection of the dipole moments from the first hydration shell onto the central molecule can be calculated from Eq. (5.19) (obtained by using Eq. (5.16)), in which we have dropped the bracket notation $\langle \rangle$ for the statistical mechanical average angle:

$$\sum_{j} \left\langle \mu_{0,i} \cdot \mu'_{0,j} \right\rangle = \mu_{0,i} \sum_{j} z_{ij} P_{ij} \mu_{0,j} \cos \gamma_{ij} \tag{5.19}$$

z_{ij}	Coordination number of molecule j around a central molecule i
γ_{ij}	The angle between the two dipole moments as shown in Figure 5.2

The contributions from the 2nd, 3rd and the kth shell are calculated using Eq. (5.17). The probability of the kth shell to exist is equal to P_i^k, where $P_i = \sum\limits_{j \in S} P_{ij}$ is the probability of the molecule i to be bonded to any of the molecules in the set S. The contribution from the kth shell to Eq. (5.18) is then given by Eq. (5.20):

$$\sum_j \left\langle \mu_{0,i} \cdot \mu'_{0,j} \right\rangle^{(k)} = \mu_{0,i} \sum_j z_{ij} P_{ij} \mu_{0,j} \cos \gamma_{ij} [P_i \cos (\pi - \theta_{ij})]^k \qquad (5.20)$$

It is then possible to calculate the sum of the contributions over all shells as shown in Eq. (5.21):

$$\left\langle \sum_k^{shells} \sum_j^{components} \left\langle \mu_{0,i} \cdot \mu_{0,j} \right\rangle \right\rangle = \mu_{0,i} \sum_j \frac{z_{ij} P_{ij} \mu_{0,j} \cos \gamma_{ij}}{P_i \cos \theta_{ij} + 1} \qquad (5.21)$$

By inserting Eq. (5.21) in Eq. (5.11), the explicit expression shown in Eq. (5.22) for the g-factor in mixtures of associating compounds is obtained.

$$g_i = 1 + \sum_j \frac{z_{ij} P_{ij} \cos \gamma_{ij}}{P_i \cos \theta_{ij} + 1} \frac{\mu_{0,j}}{\mu_{0,i}} \qquad (5.22)$$

Note that Eq. (5.22) does not account for closed (e.g. ring-like) structures. Furthermore, the parameters for Eq. (5.22) cannot easily be deduced for components with multiple conformers and must be fitted to experimental data. Note also that if $\cos \gamma_{ij}$ is negative (corresponding to the dipoles being aligned antiparallelly) Eq. (5.22) may result in $g < 1$.

5.3.1.1   Examples

Applying Eq. (5.14) in the case of water ($\mu_0 = 1.855D$, $\varphi = 104.5°$, $\theta = 109.5°$) results in $\gamma = 69.4°$. By assuming that the bond length of the $O - H$ bond does not change significantly in water compared to alcohols, and by using the value $\mu_{OH} = 1.52D$ from water for methanol the angle for methanol $\gamma = 57.8°$ is calculated for a planar configuration and $\mu_0 = 1.7D$ using (5.15).

5.3.1.2   Selection of Hydrogen Bonding Network

Before any calculations of the static permittivity can be performed, it is necessary to determine the hydrogen bonding network. The Kirkwood g-factor can be obtained from experimental data by rearranging Eq. (5.4) to form Eq. (5.23):

$$g_i = \frac{1}{\mu_i^2} \frac{(2\varepsilon_r + \varepsilon_\infty)(\varepsilon_r - \varepsilon_\infty)}{\varepsilon_r(\varepsilon_\infty + 2)^2} \frac{9\varepsilon_0 k_B T v}{N_A} \qquad (5.23)$$

The g-factor calculated near the freezing point temperature (i.e. at high degree of association), serves as a good indicator for the choice of the hydrogen bonding network. It may be compared to the maximum g-factor that is calculated from the model by inserting $P_{ij} = 1$ into Eq. (5.22) for a pure component:

$$g_{\max} = 1 + \frac{z_{ij} \cos \gamma_{ij}}{\cos \theta_{ij} + 1} \qquad (5.24)$$

To illustrate how the choice of hydrogen network affects the calculated g-factors, the experimental g-factor for methanol is calculated to be in the range of 3.25-3.5 at 163-183K. If methanol

was in a tetrahedral configuration ($\theta = 109.47°$) with a maximum of three hydrogen bonds (from the two lone pairs on oxygen and the one hydrogen bond), the maximum g-factor calculated using Eq. (5.24) and Eq. (5.14) is 2.76, and thus, a tetrahedral hydrogen bonding configuration cannot reproduce the experimental data. If a planar configuration ($\theta = 120°$) with two hydrogen bonds is used instead, the maximum g-factor calculated using Eq. (5.24) and Eq. (5.15) is 3.67, which is in much better accordance with the observed values.

5.3.1.3 Handling of Different Conformations

The nature of the problem changes in the case of multi-functional molecules and molecules with internal degrees of freedom as these conformational changes may affect the overall magnitude and direction of the dipole moment. In such situations, the total mixture may contain different conformers of the molecules and essentially requires us to perform calculation of the distribution of conformers, and then perform calculations for each geometrical configuration. In practice, this becomes a difficult task and would require additional information about e.g. intramolecular association. Instead it is proposed that the model parameters are used as effective parameters, where e.g. μ_{OH}, $zcos\gamma$, or θ is fitted to the static permittivity at a known temperature - this makes it possible to get reasonable predictions of the static permittivity over wide ranges of temperature for many molecules.

5.3.2 Correlation of Pure Component Parameters

The thermodynamic model was described in Section 3. The model parameters fitted to thermodynamic properties are adopted as shown in Table 5.3. In connection with prediction of the static permittivity, CPA is used to calculate the volume and the probability of association, which are already calculated by in terms of the unbonded site fractions X_{A_i} obtained from solving Eq. (3.9) p. 31 within the equation of state. The probability of two sites to be hydrogen bonded is calculated from Eq. (5.25):

$$P_{A_i B_j} = \rho x_j \Delta_{A_i B_j} X_{A_i} X_{B_j} \tag{5.25}$$

For a pure component, the probability of two molecules to be bonded may be obtained using Eq. (5.26):

$$P_{ij} = \sum_{B_j} P_{A_i B_j} = 1 - X_{A_i} \tag{5.26}$$

Eq. (5.25) is then used to determine the Kirkwood g-factor from Eq. (5.22).

The static permittivity has been calculated for pure compounds using the densities calculated from correlations available in the DIPPR database[176], and the probability of association calculated from solving Eq. (5.25) using the parameters from Table 5.3. The results are summarized in Table 5.4 and have been slightly modified in comparison to the published paper, as it was decided to base the parameter estimation on the angle γ rather than θ. Note that it is also possible to obtain a good correspondence with experimental data (within 5% RAD for most fluids) by only fitting the parameter γ to ε_r at 20°C. Note that AAD is the absolute average deviation $\text{AAD} = \frac{1}{N} \sum_i^N |x(calc) - x(experimental)|$ and RAD is the relative average deviation $\text{AAD} = \frac{1}{N} \sum_i^N \left| \frac{x(calc) - x(experimental)}{x(experimental)} \right|$.

The model generally shows excellent agreement with the experimental data for static permittivity of the pure compounds that are hydrogen bonding. The largest deviation is observed for hydrogen sulfide for which Eq. (5.4) reduces to the Onsager equation. For hexane and n-decane,

Component	T_c	b	$\Gamma = \dfrac{a_0}{Rb}$	c_1	$1000 \cdot \beta_{A_i,B_j}$	$\dfrac{\varepsilon_{A_i,B_j}}{k_B}$	Association scheme
Unit	[K]	[cm^3/mol]	[K]			K	
Water	647.13	14.52	1017.3	0.6736	69.2	2003.25	4C
Methanol	512.64	30.98	1573.7	0.431	16.1	2957.78	2B
Ethanol	513.92	49.11	2123.8	0.7369	8	2589.85	2B
Propan-1-ol	536.78	64.11	2234.5	0.9171	8.1	2525.86	2B
Butan-1-ol	563.05	79.7	2368.6	0.9784	8.2	2525.86	2B
Pentan-1-ol	586.15	97.46	2808.8	0.9358	3.6	2525.86	2B
Hexan-1-ol	611.35	110.8	2950.2	0.9805	3.3	2525.86	2B
Octan-1-ol	652.5	148.5	3368	1.1486	0.14	3218.55	2B
Ethylene glycol	719.7	51.4	2531.7	0.6744	14.1	2375.75	4C
Diethyl ether	466.7	92.36	2302.7	0.5946	-	-	-
Hydrogen sulfide	373.53	28.5	1878.2	0.6027	-	-	-
1,4-dioxane	587.0	73.58	3004.7	0.8417	-	-	-
Hexane	507.6	107.9	2640	0.8313	-	-	-
Decane	617.7	178.7	3190.5	1.1324	-	-	-

Table 5.3: CPA parameters, association strengths and reduced energy for selected components[1, 82, 172]

the static permittivity ε_r becomes equal to the infinite frequency permittivity ε_∞ calculated from the Clausius-Mossotti-equation, Eq. (5.5).

Component	$\alpha_0 \times 10^{40}$	μ_0	ε_r at $20°C$		γ	φ	θ	z	AAD	RAD
Unit	$\left[\frac{C^2 m^2}{J}\right]$	$[D]$	Calc.	Exp.	$[°]$	$[°]$	$[°]$			$[\%]$
Water	1.613	1.855	78.8	80.1	69.3*	104.5	109.47	4 (T)	0.8	3.1
Methanol	3.661	1.7	34	33	54.4*	109.47	120.0	2 (P)	0.8	1.9
Ethanol	6.019	1.69	25.2	25.3	51.9*	109.47	120.0	2 (P)	1.0	4.7
Propan-1-ol	7.499	1.68	20.8	20.8	43.6*	109.47	120.0	2 (P)	0.5	2.2
Butan-1-ol	9.88	1.66	18.5	17.8	38.3*	109.47	120.0	2 (P)	0.4	4.0
Pentan-1-ol	11.8	1.7	15.4	15.1	41.6*	109.47	120.0	2 (P)	0.3	3.2
Hexan-1-ol	13.84	1.65	12.8	13	37.7*	109.47	120.0	2 (P)	0.3	3.3
Octan-1-ol	17.92	1.76	10.6	10.3	48.6*	109.47	120.0	2 (P)	0.1	1.5
Ethylene Glycol	6.342	2.36	43.4	41.4	74.7*	109.47	109.47	4 (T)	0.4	1.0
Diethylether	11.35	1.3	4.39	4.27	-	-	-	-	0.3	4.7
		1.43*							0.1	2
Hydrogen Sulfide	4.395	0.978	5.17	5.93	-	-	-	-	0.6	12.8
1,4-dioxane	9.553	-	2.22	2.22	-	-	-	-	0	0.3
Hexane	13.24	-	1.89	1.89	-	-	-	-	0	0.4
Decane	21.25	-	1.99	1.99	-	-	-	-	0	0.3

Table 5.4: Pure component properties for calculating the static permittivity using densities from DIPPR correlations and the deviation from experimental data.

Unless stated otherwise, the values for polarizability, dipole moment, and static permittivity are from CRC Handbook of Chemistry and Physics[207] and the DIPPR database[176]. The experimental data was from the Landolt-Börnstein database[23]. * indicates fitted value. (T) indicates tetrahedral configuration (i.e. using Eq. (5.14)), (P) indicates planar (i.e. using Eq. (5.15)).

However, one of the difficulties arising for accurate calculation of the static permittivity is the scatter in the experimental data reported in literature for the vacuum dipole moment (see Figure 5.4 for the case of 1-alcohols as a function of chain length). Still the dipole moment recommended by the DIPPR database[176] is used by default. The results indicate that the model is suitable for calculation of static permittivity of pure components - however, in general the main interest is in the prediction of static permittivity for multi-component systems over wide ranges of temperature and pressure. To enable calculation for multicomponent systems, the model is coupled with the CPA EoS using the calculation procedure shown below:

Figure 5.4: Scatter of reported dipole moments for alcohols available in the DIPPR 801 database[176].

- Specification of temperature, pressure, composition

- Solve numerically for liquid volume (Eq. (3.2))

- Solve association equations numerically (Eq. (3.9) p. 31)

- Calculate static permittivity (Eq. (5.4) and Eq. (5.22))

While the CPA parameters are fitted to vapor pressure and liquid density, the CPA EoS does not always yield perfect agreement with DIPPR densities. This affects the calculation of the static permittivity in accordance with Eq. (5.4), and it is therefore necessary to adjust the parameters slightly to match the experimental data. Table 5.5 shows the results and parameters when densities are calculated using CPA.

Component	ε_r at 20°		γ	θ	AAD	RAD
Unit	Calc.	Exp.	[°]	[°]		[%]
Water	80.2	80.1	63.5*	95.80*	0.7	4.0
Methanol	34.3	33	54.6*	120.0	0.8	1.8
Ethanol	24.8	25.3	49.1*	120.0	0.8	3.1
1-propanol	20.7	20.8	39.2*	120.0	0.5	2.7
1-butanol	18.4	17.8	50.13	128.6*	0.6	4.4
	18.4	17.8	34.1*	120.0	0.9	7.9
1-pentanol	14.9	15.1	37.3*	120.0	0.4	4.1
1-hexanol	12.9	13	38.1*	120.0	0.4	4.5
1-octanol	10	10.3	42.2*	120.0	0.2	1.8
Ethylene Glycol	41.6	41.4	73.3*	109.47	0.5	1.3

Table 5.5: Refitted pure component properties for calculation of static permittivity using densities calculated by CPA and deviation from experimental data from the Landolt Börnstein database[23]. * indicates a fitted parameter.

Figure 5.5 shows the predicted water permittivity with DIPPR and CPA densities using the predicted bonding angles from assuming a tetrahedral geometry (see Section 5.3.1.1). The results with CPA are evidently poorer than when using the DIPPR densities, since the liquid density is not accurately represented with CPA (see Figure 5.6). This discrepancy made it necessary to fit both angles (θ and γ) to obtain a satisfactory fit with RAD<5%. For the other compounds it was only necessary to adjust the angles γ or θ. A comparison of the static permittivity of pure water calculated from DIPPR and CPA densities with fitted parameters are shown in Figure 5.7.

Figure 5.5: Comparison of experimental data[256–261] for the static permittivity of water the predictions using the bonding angles calculated by assuming a tetrahedral configuration of the hydrogen bond network ($\theta = 109.47°$).

Figure 5.8-5.9 shows that the model displays good correspondence with the experimental data for methanol and ethylene glycol.

5.3.3 Relationship to Monomer and Free OH Fraction

Another method to evaluate the performance of the new model would be to use it to calculate the monomer fraction $X_A = 1 - P_{ii}$ based on the assumed network. A tetrahedral hydrogen bond
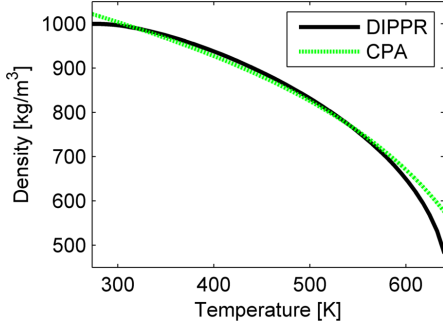
Figure 5.6: Comparison of calculated liquid density of water using CPA and DIPPR [176].
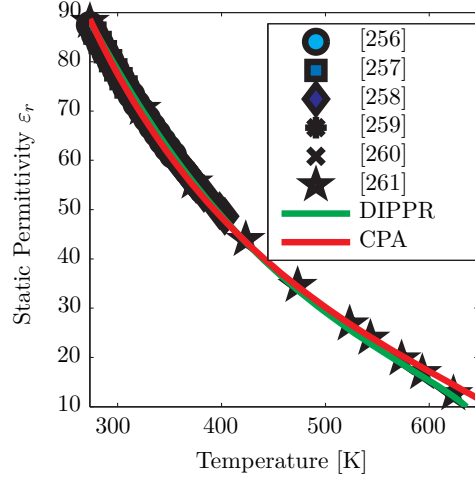
Figure 5.7: Calculated static permittivity of water using DIPPR and CPA densities and comparison to experimental data [256–261].
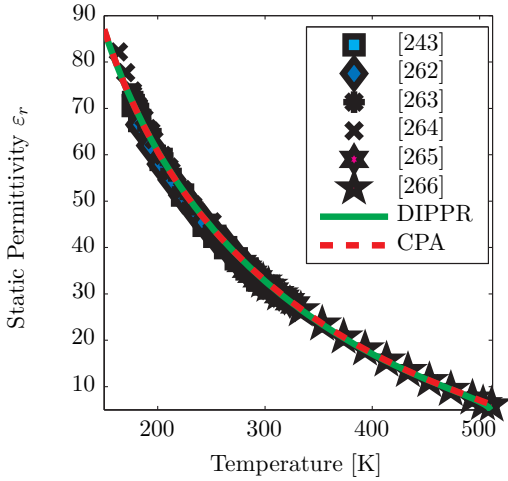
Figure 5.8: Calculated static permittivity of methanol using DIPPR and CPA densities and comparison to experimental data.
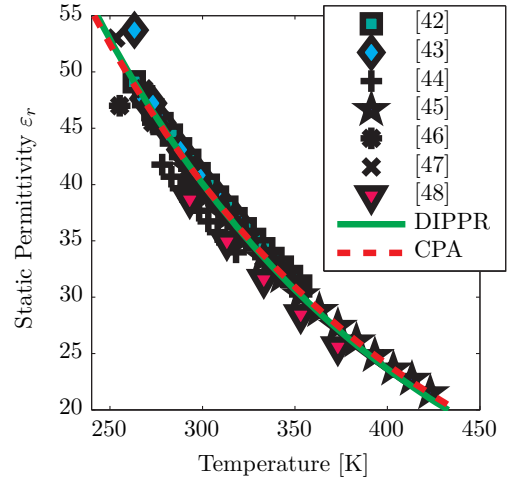
Figure 5.9: Calculated static permittivity of MEG using DIPPR and CPA densities and comparison to experimental data [267–273].

network with 4 neighbors and the theoretical angles calculated in Section 5.3.1.1 is assumed in the case of water. Figure 5.10 shows a comparison of the degree of hydrogen bonding as calculated with the present theory in comparison to experimental data measured with vibrational spectroscopy[274] or NMR [275, 276] and the monomer fractions calculated with the original CPA parameters. The data from NMR was recalculated from the hydrogen bonding fraction η using the relation $\eta = 2(1 - X_A)/1.73$[276]. It is evident from Figure 5.10, that the results from monomer fraction predicted by this theory disagree with experimental data at higher temper-
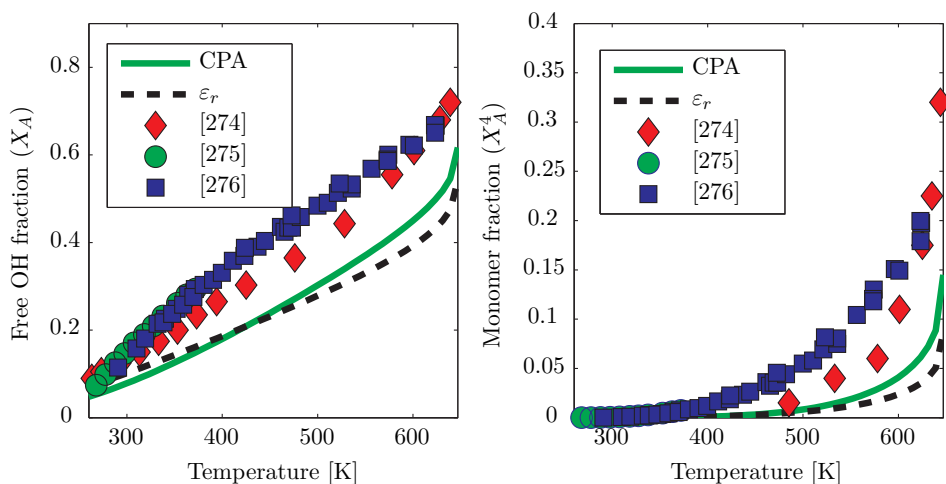
Figure 5.10: Fraction of monomer and the free OH fraction of water as calculated by the CPA and from static permittivity data, in comparison to measurements performed using vibrational spectroscopy [274] and NMR[275, 276]

atures. Von Solms[172] showed that the site fractions calculated from association models such as CPA, are not always in good agreement with experimental results for monomer fractions. Still, as there is significant discrepancy between data from different sources and methods used to determine the monomer fraction more high-quality data is needed [1].

Highly polar compounds, such as acetone, may exhibit behavior that can be treated as self-association [277, 278]. The lowest energy configuration in a system consiting of two "associated" acetone molecules is shown in Figure 5.11[277]. Such anti-parallel arrangements will reduce the effective dipole density of the liquid and therefore the static permittivity (shown in Figure 5.12).

Figure 5.12 shows the two larger sets of experimental data is available. The data from Cole (1941) [279] was measured at 1 bar, while the data from Teutenberg et al. (2009) [280] was measured at 100 bar. Using the vacuum dipole moment of acetone (2.88D)[176], the refractive index calculated from Eq. (5.5) using the acetone molecular polarizability ($7.121 \cdot 10^{-40} \mathrm{C}^2 \mathrm{m}^2/\mathrm{J}$)[176], and the density of acetone from the DIPPR correlation[176], the g-factor is calculated using Eq. (5.23) as shown in Figure 5.13.
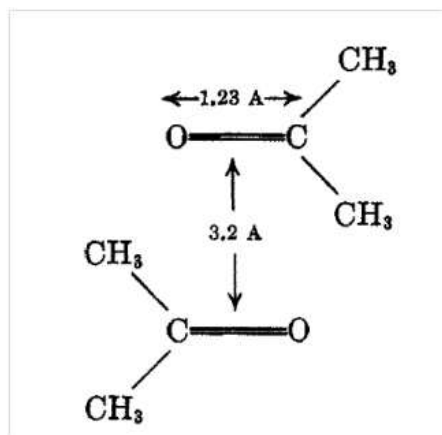
Figure 5.11: The anti-parallel configuration of acetone (figure from [277])

Figure 5.12: Static permittivity of of acetone and comparison to experimental data from Cole (1941) [279] and Teutenberg (2009) [280]

The data set by Cole [279] shows the trend for acetone at low temperatures, and does indeed display an increasing trend for the g-factor as could be expected from an anti-parallel configuration (where the degree of association will decrease with increasing temperature). The fact that the g-factor is above 1 could be modified by increasing the dipole moment slightly. However, the more recent data by Teutenberg et al. [280] shows the opposite trend with regards to the Kirkwood g-factor. The contradictory results obtained from analysis of data from the two sets of experimental data, indicates that more low-temperature data (where the polar forces are larger) is needed to say whether such antiparallel configurations are present at sufficient concentrations to affect the static permittivity. In either case, the new model may be parameterized to match these patterns, but more reliable experimental data is needed.

Figure 5.13: Calculated g-factor of acetone using (5.23) using experimental data for the static permittivity (see Figure 5.12 and DIPPR density [176].

5.3.4 Calculation of the Static Permittivity of Mixtures

In the case of mixtures, bonding angles, coordination numbers, and the type of hydrogen bonding network must be determined. While the parameters can be fitted to experimental data they may also be predicted, once the hydrogen bonding network is known. In the original paper [162], the hydrogen bonding network was fixed from chemical knowledge/considerations, but in order to further simplify the scheme and improve the predictions it was decided to fix the hy-

drogen bond network based on the association scheme of the central molecule; e.g. a 2B central molecule is assumed to coordinate two molecules with a planar configuration and therefore use Eq. (5.15) to calculate γ, whereas a 4C molecule is assumed to coordinate four molecules and use Eq. (5.14). The near-Elliott combining rule[1] shown in Eq. (3.14) and Eq. (3.13) p. 32 is used to determine cross-association energies and volumes between positive and negative sites on the molecules.

Since no parameters are fitted to the experimental data, the results shown in this section are predictions from the pure component parameters. Figure 5.14 compares the predicted static permittivity of mixtures of water and methanol with the experimental data as a function of temperature and composition. To ease the comparison, it also shows the excess static permittivity defined by (5.27):

$$\epsilon_r^E = \epsilon_r(mixture) - \sum_i^N x_i \epsilon_{r,i} \tag{5.27}$$

Figure 5.14 reveals good agreement with the experimental data, except for the sudden jump in static permittivity at low methanol mole fractions observed in the data from Travers and Douzou[263], which is attributed to experimental error. Fig. 5.15 shows good correspondence with the predicted permittivity of water + ethanol and Figure 5.16 that also the binary mixture of methanol and ethanol is well predicted.
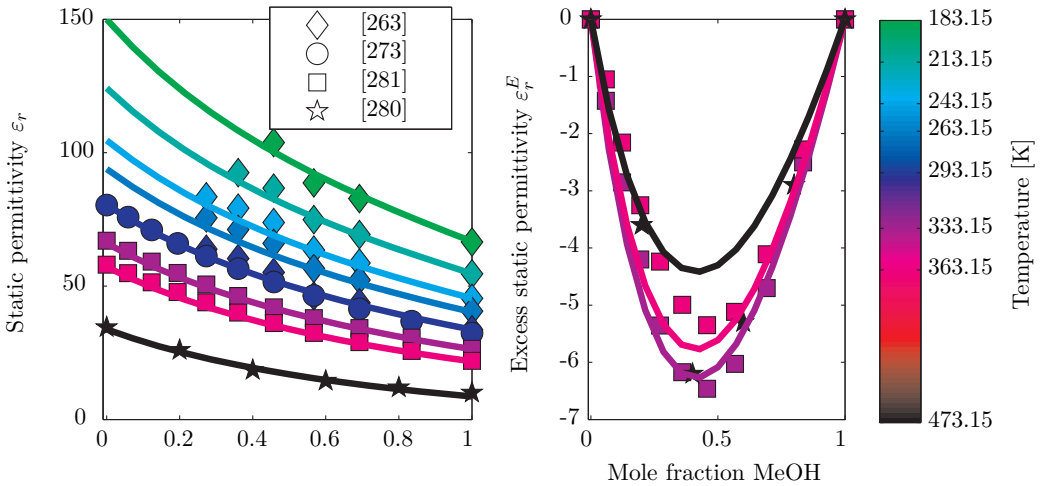
Figure 5.14: Static permittivity of water-methanol mixture at different temperatures. The data at 473.15K from Teutenberg et al.[280] is measured at 100 bar, the remaining at 1 bar or the saturation pressure.

Figure 5.17 shows results for the temperature-dependence of the static permittivity in the binary water-ethylene glycol system. Since molecular simulation has revealed that the coordination numbers of water around ethylene glycol can be larger than five [285, 286], it is assumed that ethylene glycol coordinates up to six water molecules, which also gives the best agreement with the mixture data. Note that the data from Akerlöf[273] are consistently under-estimating the static permittivity of ethylene glycol rich mixtures. This deviation is attributed to experimental error, as the data for pure component ethylene glycol from Akerlöf[273] shown in Figure 5.9 is significantly lower than data from other sources. Figure 5.18 shows the static permittivity of water-ethylene glycol mixtures at 25°C illustrating that the new model also captures
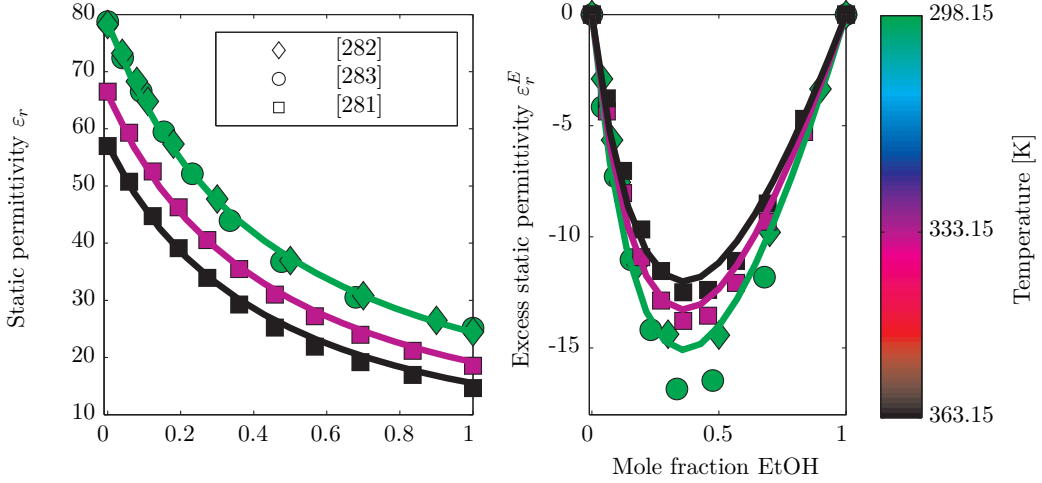
Figure 5.15: Static permittivity of water-ethanol mixture at different temperatures. Pressure is 1 bar.
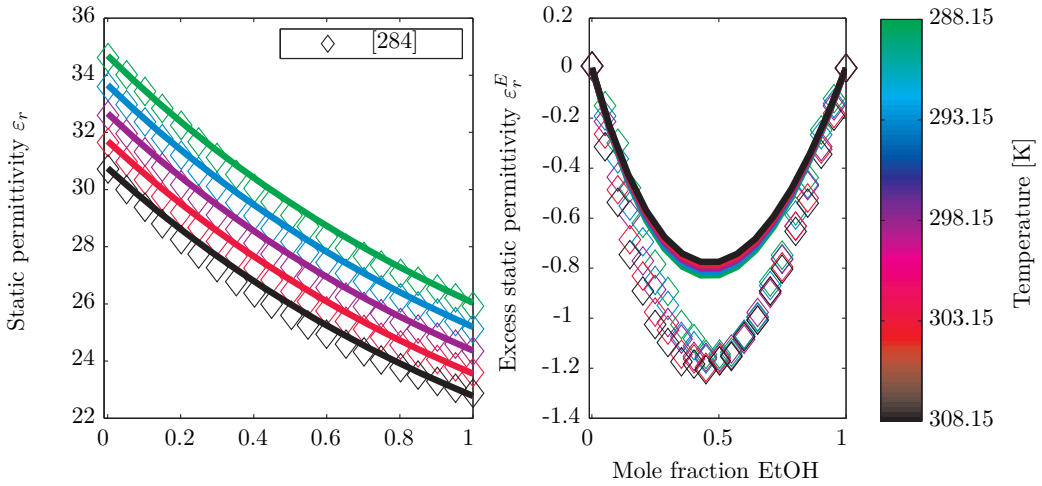
Figure 5.16: Static permittivity of methanol-ethanol mixture at different temperatures. The excess permittivity is smaller than in the case of e.g. water-alcohol or water-glycol mixtures.

the pressure dependence up to high pressures (2500 bar). Figure 5.19 shows that the model gives excellent predictions that are possibly better than the experimental data for the system ethanol-ethylene glycol.

The binary system water-1,4-dioxane was also investigated in order to further validate the modeling approach for systems with a large difference in structure and dipole moments. 1,4-dioxane is a non-polar cyclic ether that is fully miscible in water, due to the lone pairs on its ether bonds, which was modeled with four negative sites. The cross-association energy ϵ_{ij}/k_B and strength β was fitted to match the vapor-liquid equilibrium data from 283-430K, with representative results shown in Figure 5.20 using a $k_{ij} = 0$. The system exhibits a large negative excess static permittivity due to the large differences between the molecules, and this is reflected
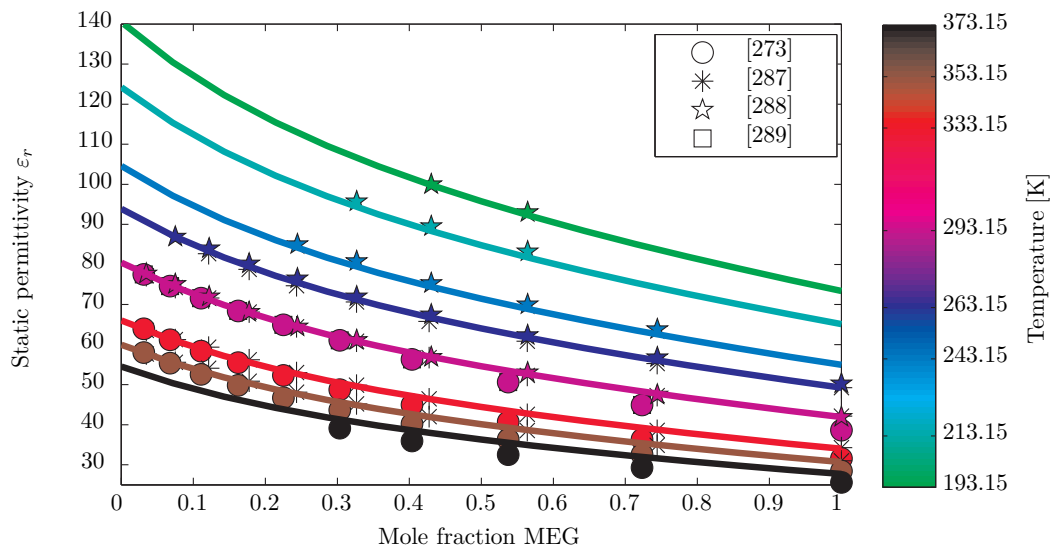
Figure 5.17: Static permittivity of water-ethylene glycol mixture[273, 287–289]. Data by Akerlöf[273] systematically display a lower static permittivity in ethylene-glycol rich mixtures, which is attributed to experimental error.

by the experimental and modeling results shown in Figure 5.21. The model shows excellent predictions of the static permittivity even in this highly asymmetric system.

Finally, Figure 5.22 validates the modeling approach for prediction of the static permittivity of ternary mixtures containing water/methanol/ethylene glycol as well as water/methanol/ethanol as a function of temperature. As demonstrated by Figures 5.14-5.22, the static permittivity of binary and ternary mixtures of associating compounds is well predicted by the present model. No new parameters were fitted to the binary or ternary systems; instead the model parameters were calculated directly from Eq. (5.14), and thus the presented results are true predictions from the model.

5.3.5 Summary

A new model was proposed to calculate the static permittivity for complex mixtures containing polar, non-polar, and associating compounds. The model extends the framework by Onsager, Kirkwood, and Fröhlich and enables modern EoS using a term to take into account hydrogen-bonding/association to predict the static permittivity of multicomponent mixtures. By adjusting one or two parameters, the model succesfully correlates the pure component static permittivity typically within 1-4% relative deviation over wide ranges of temperature and pressure. Using a simple geometrical model for the hydrogen bond network to determine the bonding angles in a mixture, the model succesfully predicts the static permittivity of binary and ternary mixtures over wide ranges of temperature and pressure. The new model will become the basis for calculation of the static permittivity in the electrolyte CPA EoS.
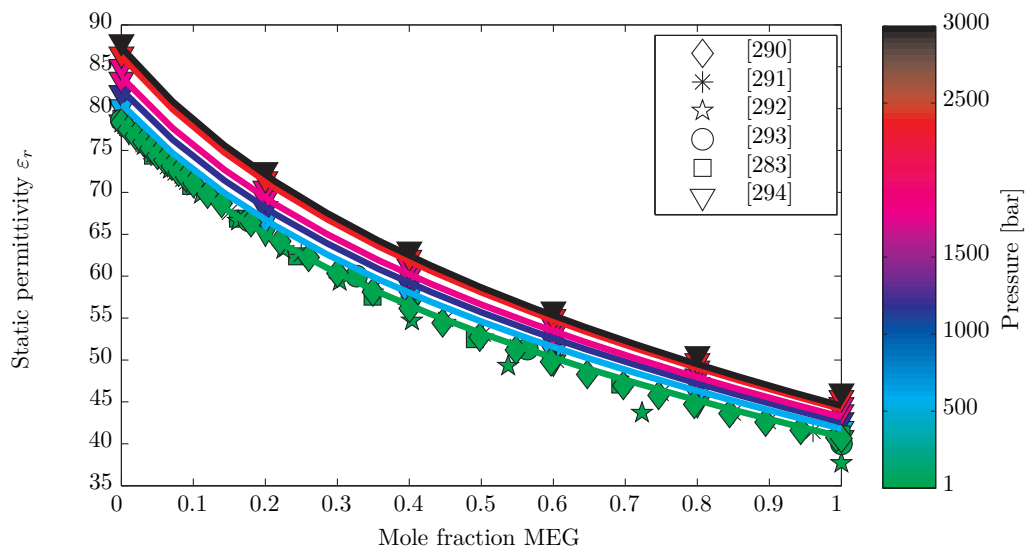
Figure 5.18: Pressure dependence of static permittivity of water-ethylene glycol mixture at 25°C [283, 290–294].
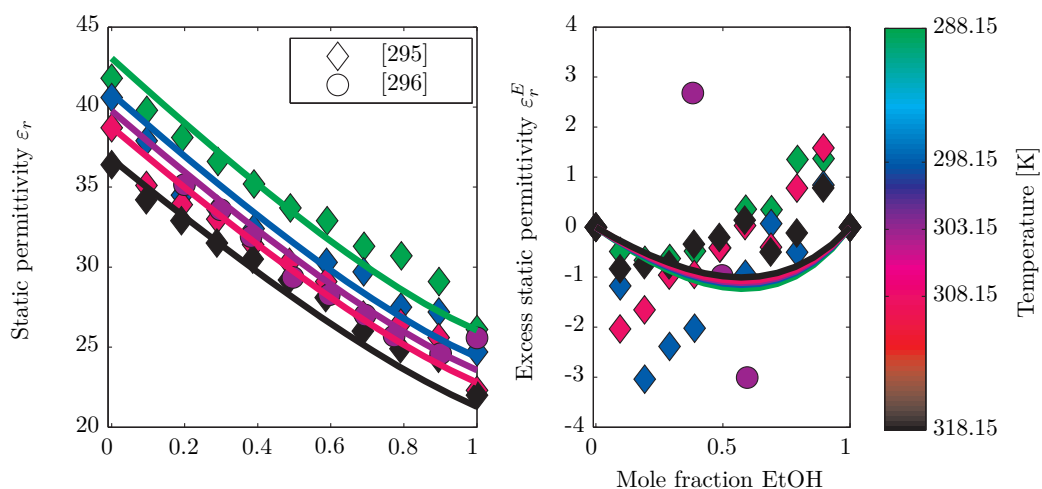
Figure 5.19: Static permittivity of water-ethylene glycol mixture. The experimental data for this system is scattered and most likely errorneous, but model predictions appear reasonable.
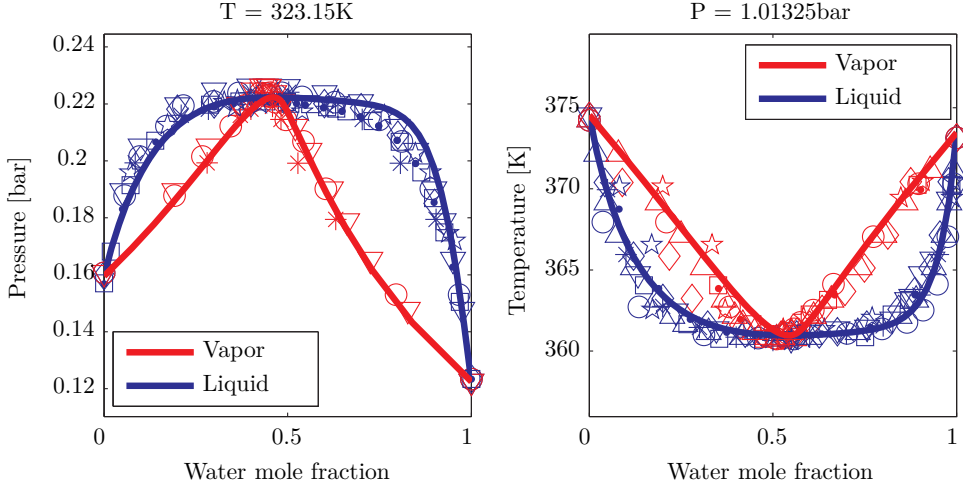
Figure 5.20: P-x,y and T-x,y of the water-1,4-dioxane mixture. Experimental data from the Landolt-Bornstein database [23]. The modeling results were obtained by fitting cross-association parameters $\beta_{ij} = 14.88 \cdot 10^{-3}$ and $\epsilon_{ij}/k_B = 1775$K using four negative sites on 1,4-dioxane.
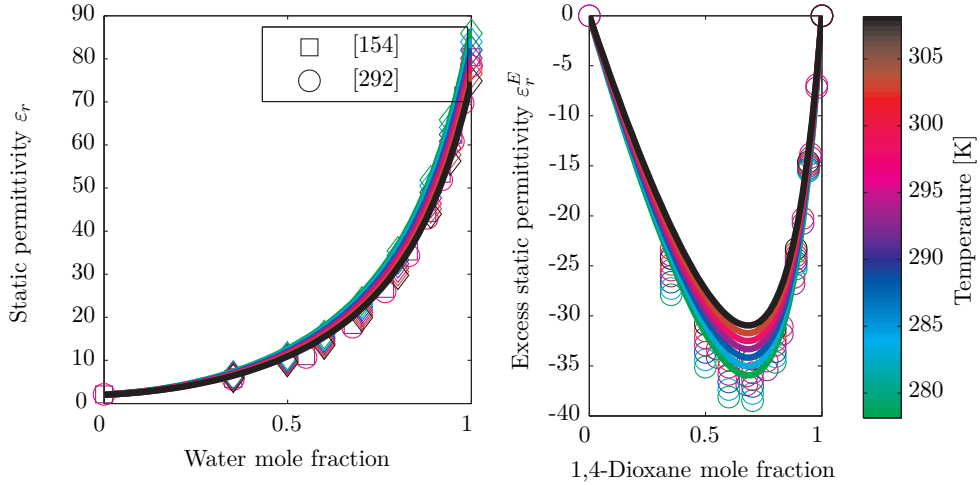
Figure 5.21: Static permittivity of water-1,4-dioxane mixture. The model displays excellent predictions of the order of magnitude and temperature trends in the excess permittivity. No parameters were adjusted to obtain the static permittivity and it is therefore a pure prediction using the binary interaction parameters from the VLE shown in Figure 5.20.
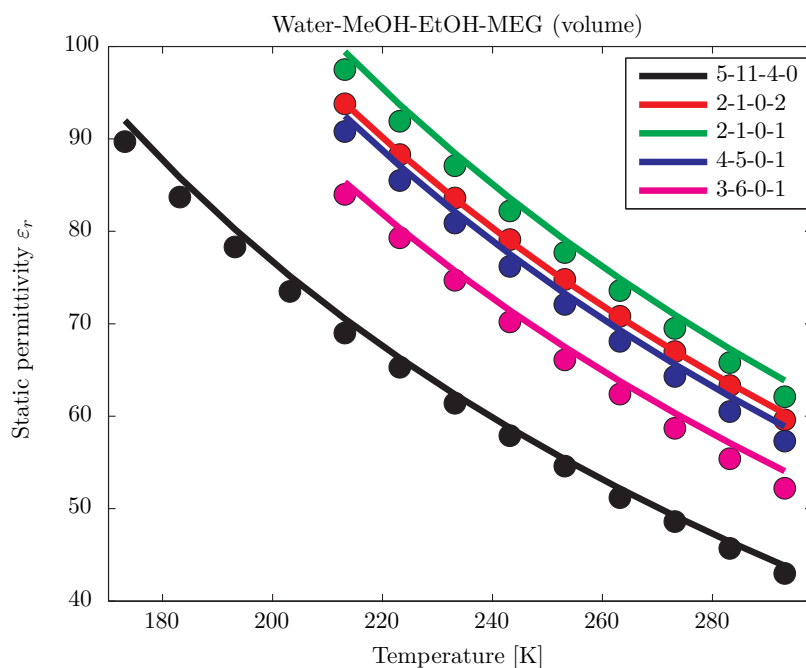
Figure 5.22: Static permittivity of mixtures of different volume fractions (prepared at 20°C) of wa-
ter:methanol:ethanol:ethylene glycol, as a function of temperature. Data from Travers et
al. [263, 297]

5.4 Extension of the Theory of Static Permittivity to Mixtures Containing Salts

The model presented in the previous section was shown to provide an excellent description of the static permittivity of pure compounds and mixtures with a limited number of adjusted parameters. In the following sections the model is extended to handle salts. This work was published in J. Phys. Chem. B. (2013), 117, 10523-10533) [163]. It will present a literature study on microscopic models for the effect of kinetic depolarization and dielectric saturation and this insight will then be used to develop continuum models through mixing rules and ion-solvent association. A literature survey on methods used to calculate the static permittivity of aqueous salt solutions (including phenomenological models) is presented. Finally a new methodology for obtaining the static permittivity over wide ranges of temperatures, pressures, and composition for the use within an equation of state for mixed solvents containing salts is presented. The static permittivity is calculated from a new extension of the framework developed by Onsager, Kirkwood, and Fröhlich to associating mixtures. The Wertheim association model as formulated in the Statistical Associating Fluid Theory is used to account for hydrogen bonding molecules and ion-solvent association. Finally, the effect of the new model for the static permittivity is illustrated through a comparison of the Helmholtz energy and first order derivatives obtained using the Debye-Hückel Helmholtz energy obtained using the new model and an empirical model given by Eq. (4.39).

5.4.1 Effect of Salts on the Static Permittivity

The static permittivity is the most important physical property for thermodynamic models that account for the electrostatic interactions between ions. The measured static permittivity in mixtures containing electrolytes is reduced due to kinetic depolarization and reorientation of the dipoles in the electrical field surrounding ions. Kinetic depolarization may explain 25-75% of the observed decrease in the permittivity of solutions containing salts, but since this is a dynamic property, this effect should not be included in thermodynamic modeling of electrolytes. Kinetic depolarization has, however, been ignored in relation to thermodynamic modeling, and authors have either neglected the effect of salts on permittivity or used empirical correlations fitted to the measured static permittivity, leading to an over-estimation of the reduction in the thermodynamic static permittivity.

The static permittivity, ε_r, is required as input to models for the Coulombic interactions between ions in a polar medium[84, 92, 109, 114, 128, 129, 161, 182], such as the Debye-Hückel[26] theory and the Born[45] model of the solvation free energy. Accurate modeling of the static permittivity and its derivatives is therefore important for representing chemical and phase equilibrium in mixed-solvent electrolyte solutions[298], but unfortunately, the empirical models applied in the context of thermodynamic models may introduce unphysical behavior[161]. Despite the importance of the static permittivity there is no consensus on what expressions to use in relation to modeling of electrolyte systems. Researchers have used either ε_r of the pure or mixed solvent[85, 86, 89, 91, 93, 109, 110, 112, 114, 115, 128], some have accounted for the effect of ions through empirical models where the calculated solvent permittivity is reduced by a factor[51, 92, 94, 95, 129, 139]. Others use non-primitive models where the static permittivity is calculated implicitly within the equation of state itself from dipole-dipole, ion-dipole, and ion-ion interactions[52, 67].

The presence of salts will reduce the static permittivity of the mixture through kinetic depolarization and formation of solvation shells around the ions, where water becomes irrotationally

bounded effectively removing their contribution to the dielectric relaxation of the solvent[32, 241, 299, 300]. A monovalent cation is expected to coordinate 6-8 water molecules[241], while anions are expected to coordinate slightly less. The coordination number is typically estimated from hydrated molar volumes and ion diameters[241, 301].

Kinetic depolarization gives rise to a systematic error in analysis of the measured zero-frequency permittivity, since it is caused by the flow of current and is therefore not a thermodynamic effect[157, 230]. Following the treatment by Hubbard and Onsager[231–234], the measured real part of the permittivity at zero frequency of conducting mixtures may be separated into a static (equilibrium) contribution, ε_r, affected by dielectric saturation, and a dynamic contribution $\Delta\varepsilon_D$ caused by kinetic depolarization as shown in Eq. (5.28) [231–234, 302]:

$$\lim_{\omega \to 0}\varepsilon_d^* = \varepsilon_m = \varepsilon_r + \Delta\varepsilon_D \tag{5.28}$$

In Eq. (5.28) ε_r is the static permittivity and $\Delta\varepsilon_D$ is the kinetic depolarization, calculated from Eq. (5.29)[231–234], when assuming a no-slip condition, and $\frac{2}{3}$ of Eq. (5.29) when assuming perfect slip.

$$\Delta\varepsilon_D = -\left(1 - \frac{\varepsilon_\infty}{\varepsilon_r}\right)\frac{\tau\sigma}{\varepsilon_0} \tag{5.29}$$

The magnitude of $\Delta\varepsilon_D$ was shown to account for 25-75% of the observed decrease in the static permittivity[231–234, 302, 303], yet it has been ignored by groups working with thermodynamic properties of electrolytes in analysis of the experimental data for the static permittivity. Figure 5.23 shows the effect of kinetic depolarization calculated from Eq. (5.29) for NaCl at 25°C compared with the empirical model from Eq. (4.39) p. 49[182]. The kinetic depolarization effect is calculated from Eq. (5.29) using experimental conductivities[207] and $\tau = 8.7$ps as the relaxation time for pure water at 20°C[304].
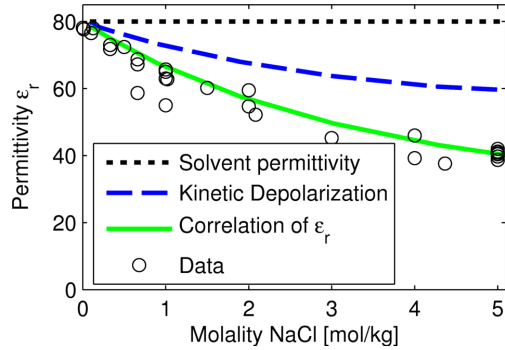
Figure 5.23: Effect of kinetic depolarization on measured static permittivity of NaCl. The correlation to the experimental data[24, 25] is calculated from the empirical correlation by Mollerup (Eq. (4.39) p. 49) [182].

Figure 5.23 shows that while the empirical model matches the experimental data for the observed static permittivity, it actually over-estimates the reduction of the static permittivity ε_r since 50% of the observed reduction is due to a dynamic effect from the kinetic depolarization. This has a profound effect on the thermodynamic properties. Unfortunately, Eq. (5.29) does not give an exact contribution from kinetic depolarization, making it essentially impossible to determine the true static permittivity that should be used in connection with thermodynamic models from measurements of the permittivity. The scatter in the experimental data observed in Figure 5.23 is generally observed for all salts and the data from different groups are in some cases inconsistent[299].

5.4.2 Modeling of Dielectric Saturation

The effect of dielectric saturation is caused by the strong interactions between dipoles and the electrical field surrounding the ions[27, 32, 241, 305]. This effect was modeled by Booth[305],

who derived a relationship between the electrical field, the dipole moment of the solvent molecules, and the radial dependence of the dielectric saturation as shown in Eq. (5.30):

$$\varepsilon_r = n^2 + \alpha \pi N_0 \left(n^2 + 2\right) \mu_v E^{-1} L \left(\frac{\beta \mu_v \left(n^2 + 2\right) E}{k_B T} \right) \tag{5.30}$$

Where the parameters $\alpha = 4/3$ and $\beta = 1/2$, when using the Onsager definition of the local field, while it is $\alpha = \frac{28}{3}\sqrt{73}$ and $\beta = \frac{1}{6}\sqrt{73}$ using the Kirkwood definition. Booth[306] made detailed calculations of the electrical field to verify the assumptions used in deriving Eq. (5.30) and obtained a new corrected equation where $\alpha = 3.3$ and $\beta = 0.55$, obtained by increasing the Onsager field by 10%, as indicated by the calculations. In order to match the static permittivity of the solvent at distances far from the ion, it is noted that this is equivalent to take the limit at zero field strength from Eq. (5.30).

$$\lim_{r \to \infty} \varepsilon\left(r\right) - n^2 = \lim_{E(r) \to 0} \varepsilon\left(r\right) - n^2 = \varepsilon_r - n^2 \tag{5.31}$$

By combining Eq. (5.31) and Eq. (5.30), it is straightforward to derive the relationship shown in Eq. (5.32):

$$\frac{\varepsilon\left(r\right) - n^2}{\varepsilon_r - n^2} = \frac{3}{x} \left(\coth x - \frac{1}{x} \right) \qquad x = \frac{\beta \mu_v \left(n^2 + 2\right) E}{k_B T} \tag{5.32}$$

The value of β depends on the assumption of the local field. $E\left(r\right)$ is the electrical field from the ion with charge q given by $q\left[4\pi\varepsilon_r\left(r\right)\varepsilon_0 r^2\right]^{-1}$. Figure 5.24 presents the dielectric saturation profiles calculated from Eq. (5.32) for the case of ions with charges from 1 to 4 in water at 25°C assuming $\varepsilon_\infty = 2$, and using $\beta = 0.55$[306]. It is evident from Figure 5.24 that the dielectric saturation depends largely on the ion charge. It should be noted that the effect of dielectric saturation may be represented as a type of ion solvation, where larger ion valencies lead to higher coordination numbers as the dipoles in the ion hydration shell are assumed to be aligned with the electrical field of the ion and thus do not contribute to the dipolar fluctuations and static permittivity [229, 230].
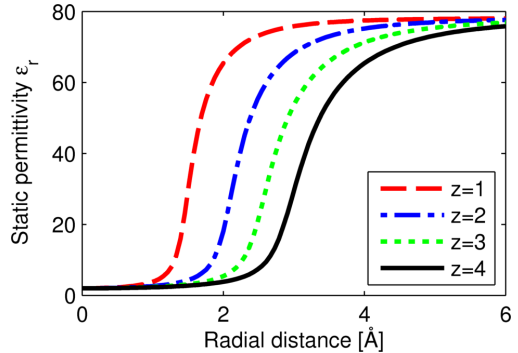
Figure 5.24: Dielectric saturation profile for different ion valencies in water using the Booth model (Eq. (5.32)).

The Booth model neglects the discrete nature of the solvent structure around the ions, and only provides qualitative insight in the influence of the electrical field from the ions. To describe the effect of ions on the discrete solvent structure, ions are commonly characterized in two groups[300]; **kosmotrophic ions** such as Li$^+$ that cause an increasing order in the solvent structure (associated with a large negative entropy change) and **chaotrophic ions** like Cs$^+$ that break down the solvent structure (resulting in a large positive entropy change). Dill et al. [300] showed that the solvation entropy is related to the distance between the dipole moment of water and the charge through the Mercedes-Benz model of water; see Figure 5.25. Lenart et al.[307] performed grand canonical Monte Carlo simulations of 1:1 electrolyte solutions using the effect of dielectric saturation to determine the radial dependence of static permittivity, combined with a model for the first hydration layer around ions giving good correspondence with the observed activity coefficient of LiCl, NaCl, and KCl. Lenart et al.[307] note that using
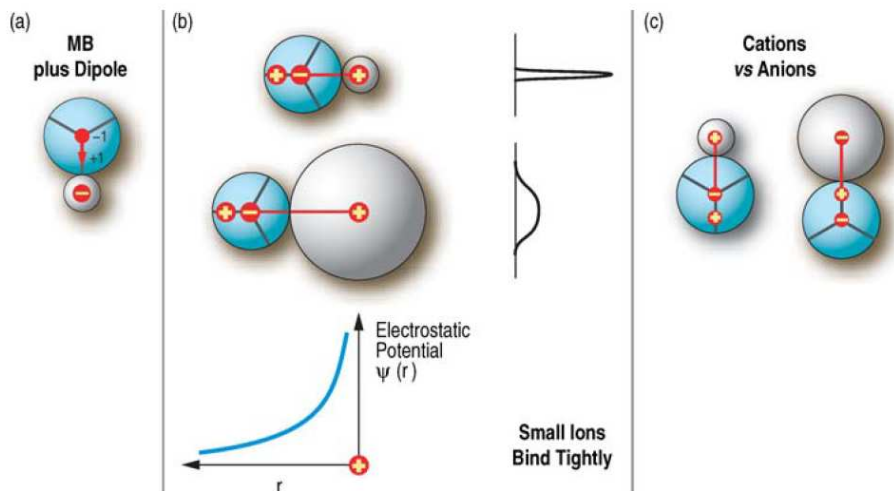
Figure 5.25: a) The Mercedes-Benz (MB) + dipole model of water. b) As the distance between the water dipole and the charge is shorter the electrostatic interactions are higher for smaller ions. c) Cations will interact more strongly with water as the distance is shorter. Figure from Dill et al. [300].

an overall concentration-dependent static permittivity is a measure of the macroscopic effect of dielectric saturation and that the effect of dielectric saturation in simulations directly provides more detailed knowledge of the hydration structure and effect on activity coefficients.

The effect of dielectric saturation may be represented as a type of ion solvation, where the molecules in the ion hydration shell are assumed not to contribute to the dipolar fluctuations as the dipoles become aligned with the electrical field of the ion[229]. This effect has been included through mixing rules assuming that each ion removes N molecules of water from the solution forming spheres with a lower static permittivity [27, 229, 241, 308, 309].

5.4.3 Ion Solvation Models

The effect of dielectric screening may be represented as a type of ion solvation, where the molecules in the ion hydration shell do not contribute to the dipolar field as the dipoles are aligned with the electrical field of the ion[229]. The first of such solvation models was presented by Hückel[27], who determined the reduction in the static permittivity using the linear model shown in Eq. (5.33), and showed how it improves the correlation of the activity coefficient at high concentrations, c:

$$\varepsilon_r = \varepsilon_w - 2\delta c \tag{5.33}$$

Hückel found that if δ was determined from the predicted reduction in the static permittivity obtained from a different model and measurements of the refractive index, it was larger than the value obtained from fitting δ to the activity coefficient. In a recent review, Marcus [310] provided an overview of the dielectric decrement of many different salts with ion-specific parameters for the linear decrement. Haggis et al.[241] used the linear model for the reduction of the static permittivity, and fit the constant δ to experimental data. Haggis et al.[241] also related the parameter δ to the hydration number n_c, the molar volume v and the molar volume of water

v_w starting from the correlation by Fricke[311] shown in Eq. (5.34):

$$\varepsilon_r - \varepsilon_w = \frac{\beta\rho}{1-\rho}\left(\varepsilon_{solute} - \varepsilon_r\right) \tag{5.34}$$

In which ε_r is the static permittivity of the mixture, ε_{solute} the static permittivity of the solute (taken as 2), β is a function of the particle axial ratio, and ρ the volume fraction of particles. Eq. (5.34) reduces to Eq. (5.35) at low solute concentrations

$$\varepsilon_r = \varepsilon_w - \beta\rho\left(\varepsilon_w - \varepsilon_{solute}\right) \tag{5.35}$$

Finally, Haggis et al.[241] presented the expression shown in Eq. (5.36) that enables calculation of δ from the coordination number of water, n_c:

$$\delta = 1.5\left(v\left(\varepsilon_w - \varepsilon_{\infty,s}\right) + v_w\left(\varepsilon_w - \varepsilon_{\infty,w}\right) \times n_c\right) \tag{5.36}$$

Giese et al.[308] proposed a scheme where spherical enclosures with a static permittivity of $\varepsilon_\theta \approx 2$ were submersed in water with the static permittivity $\varepsilon_w = 78.2$. The relationship between the static permittivity of the solvent ε_s and the fraction of spheres f, is calculated from the mixing formula shown in Eq. (5.37):

$$f = \frac{2\varepsilon_w + \varepsilon_\theta}{\varepsilon_w - \varepsilon_\theta}\frac{\varepsilon_w - \varepsilon_s}{2\varepsilon_w + \varepsilon_s} \tag{5.37}$$

For alkali halide solutions it was found that the static permittivity ε_s could only be related to f if it was assumed that each ion was removing z_f moles of water from the solution. Thereby Giese et al. [308] showed that the fraction of the water molecules that was irrotationally bounded by the ions did not contribute to the overall dipolar contributions to the polarizability.

Ruff[309] approximated the effect of dielectric saturation using the Booth equation by an exponential function and determined the volume average static permittivity by a volume integral of the dielectric saturation effect, leading to the average static permittivity being represented by Eq. (5.38):

$$\varepsilon_r = \varepsilon_s\left(1 - g\exp\left(-hf_a r_0\right)\right) \tag{5.38}$$

Where ε_s is the static permittivity of the solvent, g and h are solvent-dependent parameters determined from approximation of the Booth function, f_a is a function of the anion and cation concentration and volumes, and r_0 a measure of the interionic separation.

5.4.4 Ion Screening

A different approach was presented by Weiss and Schröer[312], who considered the mixture of equisized spherical ions and dipolar ion pairs in the restricted primitive model. By equating the energy from ion-dipole and dipole-ion interaction energy, they obtained the expression for the static permittivity as a function of ionic concentration shown in Eq. (5.39):

$$\frac{(\varepsilon_r - \varepsilon_\infty)\left[(2\varepsilon_r + \varepsilon_\infty)(1 + \kappa\sigma) + \varepsilon_r(\kappa\sigma)^2\right]}{\varepsilon_r(1 + \kappa\sigma)} = \frac{\mu^2\rho_d}{\varepsilon_0 k_B T} \tag{5.39}$$

Where ρ_d is the density of dipoles from the association of ions, κ is the inverse Debye length and σ is the ion/dipole diameter. Weiss and Schröer[312] applied their model to determine the static permittivity used for modeling of the phase behavior of a pure ionic fluid, where Eq. (5.39) lead to a significant reduction of the static permittivity due to shielding compared to the Onsager model.

5.4.5 Field-Theory Approach

Using field-theoretical methods Levy et al.[313] calculated the effect of ions on the static permittivity from a self-consistent solution of the Poisson-Boltzmann equation, using Eq. (5.40) to describe the radial dependence of the static permittivity of a solvent with bulk permittivity ε_s:

$$\varepsilon_r\left(r\right) = \frac{\varepsilon_s}{3h^2\left(l_h/r\right) + 1} \tag{5.40}$$

In Eq. (5.40), l_h is a characteristic hydration length scale that depends on the dipole size and Bjerrum length and where the function $h\left(x\right)$ gives rise to a similar behavior as the Booth function shown in Figure 5.24. By solving correction to the Gibbs free energy due to the hydration behavior, Levy et al. [313] shows that the static permittivity of water with salts can be calculated using Eq. (5.41):

$$\varepsilon_r = \varepsilon_w + \frac{\left(\varepsilon_w - 1\right)^2}{\varepsilon_w}\frac{4\pi}{3c_d a^3} - \frac{\left(\varepsilon_w - 1\right)^2}{\varepsilon_w}\frac{\kappa^2}{\pi c_d a}\left(1 - \frac{\kappa a}{2\pi}\tan^{-1}\frac{2\pi}{\kappa a}\right) \tag{5.41}$$

In Eq. (5.41), c_d is the dipole density and ε_w is the permittivity of water. Levy et al.[313] fits the dipole moment and the ion size and obtains good correspondence with the static permittivity of different salts in water.

5.4.6 Phenomenological Models

A range of phenomenological models have been presented in literature. Helgeson et al.[299] presented an empirical relationship between the static permittivity of water ε_w and the static permittivity of the solvent as shown in Eq. (5.42):

$$\varepsilon_r^{-1} - \varepsilon_w^{-1} = \sum_k b_k \psi_k m_k \tag{5.42}$$

In which m_k is the molality of the salt, $b_k\psi_k$ is a salt specific constant fitted to the measured reduction of static permittivity. The authors observed a linear relationship between the Gibbs energy of solvation and the reduction of static permittivity.

Pottel (1973) [314] developed the following model based on packing considerations:

$$\epsilon_r - 1 = \left(\epsilon_s - 1\right)\frac{1 - \xi_3}{1 + 0.5\xi_3} \qquad \xi_3 = \frac{N_A\pi}{6V}\sum_i n_i\sigma_i^3 \tag{5.43}$$

Simonin (1996) [315] simplified the Pottel equation to take only a single parameter α to determine the decrease as a function of the ion concentration, and Inchekel (2008) [129] found that it was easier to fit the experimental data of osmotic coefficients when using the simpler model based on mole fractions rather than concentrations:

$$\epsilon_r^{\text{Simonin}} = \frac{\epsilon_s}{1 + \alpha\sum\limits_i^{\text{ions}} C_i} \qquad\qquad \epsilon_r^{\text{Inchekel}} = \frac{\epsilon_s}{1 + \alpha\sum\limits_i^{\text{ions}} x_i} \tag{5.44}$$

In which α is an adjustable parameter.

Wang and Anderko[298] modeled the effect of salts using the empirical equation shown in Eq. (5.45):

$$\varepsilon_s = \frac{\varepsilon_{s,0}}{1 + \sum\limits_i^{ions} A_i x_i \ln\left(1 + B_i\sqrt{I_X}\right)} \tag{5.45}$$

In which $\varepsilon_{s,0}$ is the static permittivity calculated for the pure solvent and ε_s is the static permittivity of the medium including salts. A_i and B_i are ion-specific parameters, and I_X is the ionic strength based on the mole fraction scale, as presented in Eq. (5.46):

$$I_X = \frac{1}{2} \sum_i^{ions} x_i z_i^2 \tag{5.46}$$

Michelsen and Mollerup[182] presented a different empirical model given by in Eq. (4.39) p. 49, with results shown in Figure 4.3 p. 50.

While the empirical correlations given by Eqs. (4.39), (5.42)-(5.45) give reasonably good correspondence with the experimental data, the derivatives with regards to temperature, volume, and composition may be very different. Additionally, these models do not account for the significant contribution from kinetic depolarization, and this omission gives rise to a systematic error. This may result in unphysical behavior for the model of the static permittivity, and thus affect the derivatives from the electrostatic contributions to Helmholtz energy[161].

5.5 Extension of Model to Mixtures Containing Salts

In Section 5.3.1 and publication [162] the derivation of a new model for the static permittivity based on a geometrical model for the dipolar correlations for calculation of Kirkwood's g-factor (Eq. 5.22) coupled with Wertheim's association theory[80] within the Cubic-Plus-Association (CPA) equation of state[82] was presented. The model succesfully correlates the static permittivity over wide ranges of temperature and pressure for pure compounds and through assumptions on the hydrogen bond network in mixtures the model enables excellent predictions of the static permittivity of mixed solvents. In this section the model is extended to handle mixtures containing electrolytes by accounting for the effect of dielectric saturation through a ion-hydration model.

5.5.1 Extension of Model to Salts

Molecules that are located in the solvation shell around ions become oriented in the strong symmetrical electrical field around ions. This effect may be observed by a reduction in the static permittivity due to cancellation of the oppositely directed dipole moments as illustrated in Figure 5.26. Following the concepts used in models for the static permittivity incorporating ion solvation, it is assumed that the molecules in the first hydration shell surrounding an ion will not contribute to the projected dipole moment. This is the case since the symmetrical electrical field will cause cancellation of dipoles that are aligned in the electrical field, as illustrated by Figure 5.26 to the right.
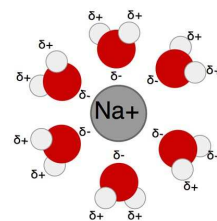
Figure 5.26: Canceling out of dipole moments due to alignment in the electrical field surrounding an ion.

By assuming cancellation of the dipole moments of molecules in the first hydration shell and therefore a Kirkwood g-factor of 1, Eq. (5.4) can be rewritten into the form shown in Eq. (5.47):

$$\frac{(2\varepsilon_r + \varepsilon_\infty)(\varepsilon_r - \varepsilon_\infty)}{\varepsilon_r} = \left(\frac{\varepsilon_\infty + 2}{3}\right)^2 \frac{N_A}{\varepsilon_0 k_B T v} \sum_i x_i \Theta_i g_i \mu_{i,0}^2 \tag{5.47}$$

In which Θ_i is the fraction of component i that is not bound to an ion and is calculated using Eq. (5.48):

$$\Theta_i = 1 - \sum_{j}^{ions} P_{ij} \tag{5.48}$$

The charged ions are assumed to associate with polar molecules, forming a solvation shell containing N_{ij} molecules of type i around ion j as shown in Figure 5.26.

5.5.2   Treatment of Ion-Solvent Association

In order to separate the ion-ion, ion-solvent, and solvent-solvent interactions, the contribution to the total Helmholtz energy from association is calculated from Eq. (5.49):

$$A^{\mathrm{assoc}} = A^{\mathrm{hyd}} + A^{\mathrm{ion}} \tag{5.49}$$

In which A^{hyd} is the contribution from hydrogen bonds, while A^{ion} is the contribution from ion-dipole and ion-ion association due to electrostatic forces. The probability of association is calculated from the site fractions, which are related using Eq. (3.9) p. 31.

The interaction energy between a point dipole and the electrical field from an ion may be calculated using Eq. (5.50)[316]:

$$w\left(r,\theta\right) = -\frac{\mu q}{4\pi\varepsilon_r\varepsilon_0}\frac{\cos\theta}{r^2} \tag{5.50}$$

In Eq. (5.50) $\cos\theta$ denotes the angle between the dipole moment and the electrical field. Quantitatively Eq. (5.50) results in very strong interaction energies that are decreasing with the distance squared, i.e. the forces felt by the second solvation shell will be significantly smaller than in the first solvation shell. Ion solvation will therefore be modeled as a short-range interaction using the association framework by Wertheim[80]. The static permittivity for the short-range interaction is lower than the solvent permittivity as evidenced by the dielectric saturation curves shown in Figure 5.24, and it is assumed that the local interaction energy in Eq. (5.50) is independent of the static permittivity of the bulk solvent.

Eqs. (5.51)-(5.53) show how Eq. (3.9) for the ion-solvent association is written for a mixture containing n_i moles of the polar molecule i, and a salt with molality m_{salt} containing the ions j and k of opposite charge and the stoichiometric factors v_j and v_k. The fraction of molecule i that is not bound to any other molecules is then given by Θ_i. The polar molecule has a single site representing the dipole moment, while the ions have N_j and N_k identical sites, respectively.

$$\frac{1}{\Theta_i} = 1 + \frac{m_{salt}}{V}\left(v_j N_j \Theta_j \Delta_{ij} + v_k N_k \Theta_k \Delta_{ik}\right) \tag{5.51}$$

$$\frac{1}{\Theta_j} = 1 + \frac{n_i}{V}\Theta_i \Delta_{ij} + \frac{m_{salt}}{V}v_k N_k \Theta_k \Delta_{jk} \tag{5.52}$$

$$\frac{1}{\Theta_k} = 1 + \frac{n_i}{V}\Theta_i \Delta_{ik} + \frac{m_{salt}}{V}v_j N_j \Theta_j \Delta_{jk} \tag{5.53}$$

At infinite dilution, it is found that the sensitivity of Θ_i to a change in salt concentration is calculated from Eq. (5.54), which has been generalized for salts containing more than two ions:

$$\left(\frac{\partial\Theta_i}{\partial m_{salt}}\right)_{m_{salt}=0} = -\frac{1}{V}\sum_{j}^{ions}\frac{N_j v_j \Delta_{ij}}{1 + \frac{1}{V}n_i \Delta_{ij}} \tag{5.54}$$

At large association strengths Δ_{ij}, Eq. (5.54) may be written as Eq. (5.55):

$$\lim_{\Delta_{wi} \to \infty} \left(\frac{\partial \Theta_i}{\partial m_{salt}} \right)_{m_{salt}=0} = -\frac{1}{n_i} \sum_j N_j v_j \tag{5.55}$$

Eq. (5.54) and Eq. (5.55) can then be used to determine the relationship between the site numbers in the Wertheim association framework and the observed coordination numbers around water. If the probability that an ion j is associated with N_{ij} numbers of molecule i at infinite dilution is 100%, the probability Θ_i can be calculated using Eq. (5.56), which is valid at low concentrations:

$$\Theta_i = 1 - \frac{m_{salt}}{n_i} \sum_j^{ions} N_{ij} v_j \tag{5.56}$$

A comparison of Eq. (5.54) and Eq. (5.56) reveals the relationship between the apparent coordination number N_{ij} from Eq. (5.56) and the site numbers and association strengths from Eq. (5.57):

$$N_{ij} = \frac{n_i}{V} \frac{N_j \Delta_{ij}}{1 + \frac{1}{V} n_i \Delta_{ij}} \tag{5.57}$$

Eq. (5.57) can then be used to determine the association strength Δ_{ij} as shown in Eq. (5.58):

$$\Delta_{ij} = \frac{1}{\rho_i} \left(\frac{N_{ij}}{N_j - N_{ij}} \right) \tag{5.58}$$

Where ρ_i is the pure compound molar density of component i. By using water as the reference, it is possible to define $N_j = 2N_{wj}$ and obtain the association strength at infinite dilution $\Delta_{wj} = \rho_w^{-1}$. For all other solvents the association strength is calculated from Eq. (5.58) using Eq. (5.59):

$$\Delta_{ij} = \frac{1}{\rho_i} \left(\frac{N_{ij}}{2N_{wj} - N_{ij}} \right) \tag{5.59}$$

The temperature dependence of the association strength Δ_{ij} calculated from Eq. (5.59) is determined from the saturated liquid density of the pure compound, and the coordination number, which is assumed to be independent of temperature in this work.

At higher salt concentrations, there are competing mechanisms that will either increase (reduction in static permittivity) or decrease (ion screening) the association strength Δ. Accounting for the concentration dependence of the association constant is beyond the scope of this article, and in the following it is simply assumed that the local static permittivity for calculation of the forces between dipolar molecules and the central ion is independent of the bulk static permittivity. Interested readers are referred to the work by Hubbard et al.[234] for a discussion on how the concentration dependence may be included through modification of the radial distribution function.

5.5.3 Dielectric Properties for an Electrolyte Equation of State

The new model for the static permittivity enables a self-consistent manner to take into account the effect of dielectric saturation on the static permittivity as the ion-solvent association does not only lead to a reduction in the static permittivity due to dielectric saturation - in itself the ion-solvent association provides a contribution to the Helmholtz energy through Eq. (5.49). The physical coupling of ion-solvent association to the (thermodynamic) static permittivity through

Eq. (5.47) makes it possible to avoid the problems related to quantification of the dynamic part of the measured static permittivity, by including the coordination number in parameterization against thermodynamic data. After parameterization, the static permittivity can be calculated using the new model and it may then be compared to the measured static permittivity (incl. kinetic depolarization), to determine whether the model gets reasonable agreement with the experimental data.

The following section focuses on fitting upper bounds for the coordination numbers of individual ions based on the measured static permittivity and subsequently it is analyzed how this new model affects the derivatives of the Debye-Hückel equation in comparison with using a static permittivity obtained from the empirical expression by Mollerup [182] shown in Eq. (4.39) p. 49.

This section compares the static permittivity and its derivatives using the following four models:

A) Temperature dependent correlation for static permittivity of water[182]

B) Empirical model from Eq. (4.39) used to calculate static permittivity[182]

C) New model without ion association (Eq. (5.4))

D) New model with ion association (Eq. (5.47)) with hydration numbers from Table 5.6.

Ion	Na^+	K^+	Ca^{2+}	Cl^-	Br^-	I^-	NO_3^-	SO_4^{2-}
Molecular Polarizability $\alpha_0 \times 10^{40} \left[\frac{C^2 m^2}{J}\right]$	2.221	3.166	5.138	3.557	5.256	8.151	4.4	5.775
Hydration number	6	6	8	5	5	5	5	5

Table 5.6: Parameters for modeling of static permittivity and refractive index of salts.

5.5.4 Modeling of Static Permittivity

The density of the liquid phase is determined through correlations as a function of salt concentration and temperature [317–319]. The squared refractive index $n^2 = \varepsilon_\infty$ is modeled using Eq. (5.5), using the polarizabilities shown in Table 5.6. Reasonable agreement with the experimental data for the refractive indices is obtained from this model as evidenced by Figure 5.27. The hydration number is assigned to 6 in the case of monovalent cations and 8 in the case of divalent cations, whereas the hydration number of anions is set to 5. These hydration numbers were in reasonable agreement typical hydration numbers seen in literature and also had a trend of lower hydration numbers for anions in comparison to cations. The static permittivity of NaCl from 0 to 60 degrees is shown in Figure 5.28, showing that the new model gives similar agreement with the experimental data compared to the empirical correlation from Eq (4.39).

Figure 5.27: Refractive index of selected salts at 20°C modeled using the Clausius-Mossotti equation (Eq. (5.5)) and polarizabilities shown in Table 5.6 compared with experimental data[207].

The new model yields good agreement with the pressure dependence of the static permittivity, as evidenced by Figure 5.29.

Figure 5.28: Static permittivity of NaCl at 0, 25, 40, and 60°C (from top to bottom) using Model B and D with coordination numbers from Table 5.6. See model descriptions on p. 107. Experimental data is taken from data collections[24, 25].
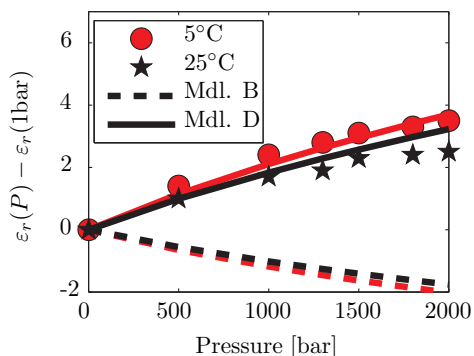
Figure 5.29: Change in static permittivity as a function of pressure at 5°C and 25°C. See model descriptions on p. 107. Experimental data from Pottel et al.[320].

Figure 5.29 shows that the empirical model does not give the right trend in terms of the pressure dependence of the static permittivity. The model based on ion solvation is in much better agreement with the experimental data. Figure 5.30 shows the calculated vs. the measured static permittivity for different salts at 25°C. The model displays a reasonable agreement considering the scatter of the experimental data.

Figure 5.30: Comparison of the calculated vs. experimental values of selected salts at 25°C. Data from [24, 25].

5.5.5   Contributions to Helmholtz Energy

In this section a comparison using the four different models for the static permittivity is made to determine the effects of the model on the contributions to derivatives of Helmholtz energy using the full Debye-Hückel theory (Eq. (4.16) p. 44). As previously shown, the full Debye-Hückel theory has similar dependence on the static permittivity as the mean spherical approximation (MSA)[161], and the observations are therefore also applicable to equations of state based on the MSA. Models A-D (see model descriptions on p. 107.) are compared at densities calculated from empirical correlations. The results for the static permittivity of NaCl using these models are compared in Figure 5.31.
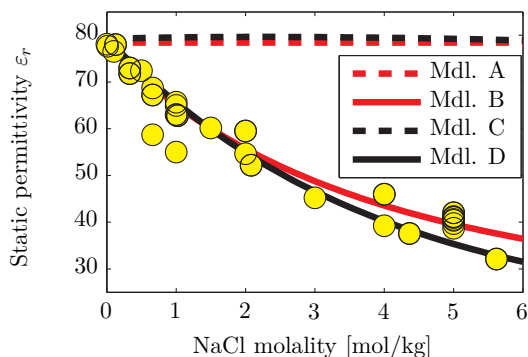
Figure 5.31: Static permittivity of NaCl calculated by models A-D. See model descriptions on p. 107. Experimental data from data collections [24, 25]

The contributions to the Helmholtz energy from electrostatic interactions may be calculated using the Debye-Huckel equation shown in Eq. (4.16) p. 4.16 [26, 161, 182]. A comparison of the volume, temperature, and compositional derivatives of the Helmholtz energy from the Debye-Hückel given by Eq. (4.16) is presented.

This analysis provides us with the individual contributions of ion-ion interactions to residual pressure, enthalpy, and fugacity coefficients[161].

The volume, temperature, and compositional derivatives are shown in Figures 5.32-5.35. It is evident that the new model significantly affects the calculations of the temperature-, volume- and compositional derivatives. Since the empirical model from Eq. 4.39 depends on the volume of the mixture, it gives rise to a volume derivative. However, the sign is opposite of the theoretical model from Eq. (5.47), and the peak in volume may furthermore give rise to two additional volume roots (one of which is unstable). The compositional derivatives of the new model are monotonically decreasing, whereas the empirical model displays an increasing trend at higher concentrations.
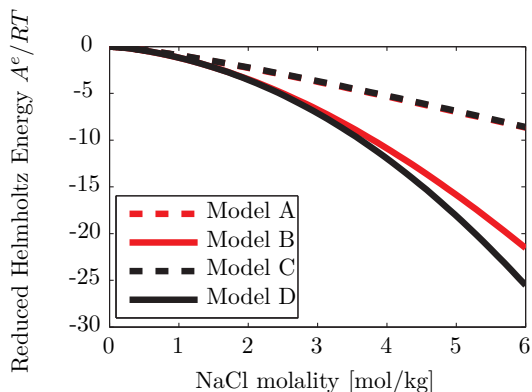
Figure 5.32: Reduced Helmholtz energy from Eq. (4.16) for the different models of static permittivity. Model A and Model C coincide. See model descriptions on p. 107.
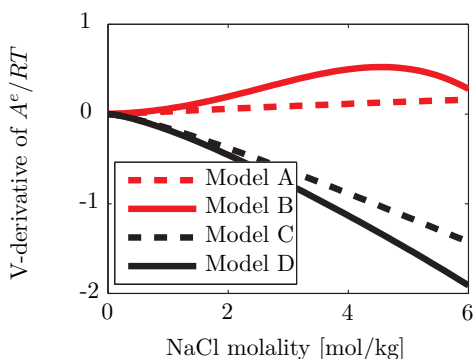
Figure 5.33: Volume derivative of reduced Helmholtz energy from Eq. (4.16) for the different models of static permittivity. See model descriptions on p. 107.
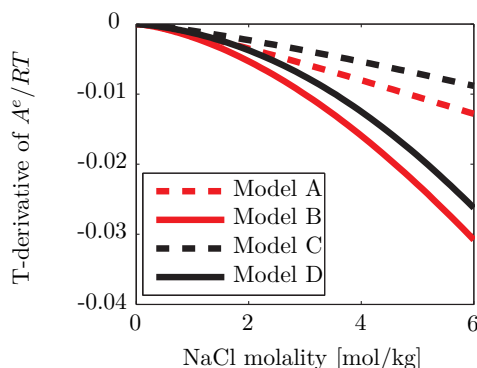
Figure 5.34: Temperature derivative of reduced Helmholtz energy from Eq. (4.16) for the different models of static permittivity. See model descriptions on p. 107.

Furthermore, the new model predicts a significant contribution to the water activity through the effect of water on the static permittivity. Increasing the water concentration will increase the static permittivity as the total dipole density of the fluid will increase, giving a positive contribution to the Helmholtz energy even when ion solvation is ignored. These results can then be used to set up guidelines for what functional form the static permittivity should provide in order to give a reasonable contribution and trends in the Helmholtz energy from Debye-Hückel or MSA:

- Increasing the volume or temperature will reduce the energy (negative $\partial A/\partial V$ as the static permittivity decreases.
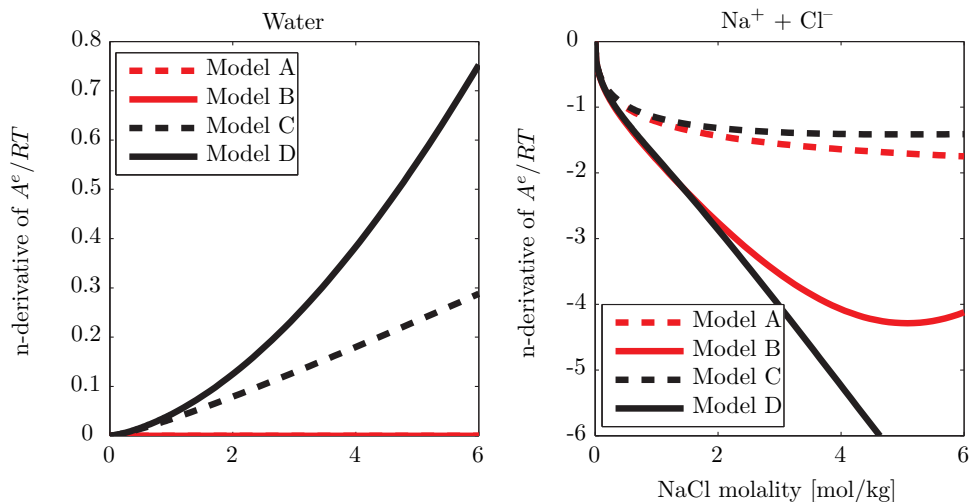
Figure 5.35: Compositional derivative of Helmholtz energy from Eq. (4.16) for the different models of static permittivity. See model descriptions on p. 107.

- Increasing the concentration of a polar molecule should increase the energy (positive $\partial A/\partial V$ as the static permittivity at constant volume increases.

5.6 Conclusion on Modeling of the Static Permittivity

In the previous sections, the framework for calculating the static permittivity was extended to associating compounds using an equation of state based on the Wertheim association theory. A model for the geometrical arrangements in hydrogen-bonding systems has been derived, and it was shown how this model allows for prediction of the static permittivity of pure compounds and mixtures over wide ranges of temperature and pressure when used within an equation of state using the association term by Wertheim[80]. The model does not account for ring-type structures, or multiple conformers, but the general experience is that the model parameters can be fine-tuned to match experimental data. Fitting one parameter to the static permittivity at 20°C is sufficient for most compounds, provided that the density is accurately reproduced by the equation of state. The static permittivity of mixtures may be predicted solely from parameters calculated by a model of the geometrical configuration of the hydrogen-bonding structure involving the binary compounds.

The static permittivity of aqueous salt solutions decreases due to the effect of dielectric saturation. However, the experimental data should be corrected for dynamic contributions caused by the kinetic depolarization in order to obtain the static permittivity to use in calculations of thermodynamic properties. A new model for the prediction of the static permittivity of aqueous salt mixtures has been presented. The new model uses the Wertheim association framework to account for the effect of dielectric saturation, and has been shown to give a good representation of the temperature-, pressure-, and salt concentration dependence of the static permittivity of several aqueous salt solutions. It is shown that empirical models for the static permittivity may introduce unphysical behavior in the derivatives of the electrostatic Helmholtz energy from the full Debye-Hückel equation. The new model improves the physical description of the effect of solvents and solutes on the static permittivity and electrostatic energy, and provides similar trends as observed in the analysis of the non-primitive model in Chapter 4.

Part III

The Electrolyte CPA Equation of State

Chapter 6

Model Development

During the preceding chapters the fundamentals of modeling of electrolyte solutions were investigated. In Chapter 4, the similarity between the non-primitive and primitive electrolyte models was investigated, and it was proposed that an electrolyte EoS could be based on the primitive electrolyte models provided that the static permittivity was calculated through a model based on the physics of dipolar mixtures. The similarity between the Debye-Hückel and the more complex mean spherical approximation was illustrated, and it was furthermore shown that the electrolyte EoS must include a term accounting for the Gibbs energy of hydration, such as the Born model. In Chapter 5, a new model for predicting the static permittivity of complex mixtures containing non-polar, polar, associating compounds and salts was developed. This chapter describes the electrolyte CPA equation of state and the tools developed during the PhD work. Secondly, it will present how the experimental data has been treated and finally show how the e-CPA model can been parameterized for ion- and salt-specific parameters in a systematic manner.

6.1 Description of the Thermodynamic Model

As illustrated by the preceding chapters, a complete electrolyte equation of state should include various contributions to the Helmholtz free energy. Primitive electrolyte models should furthermore include a good physical model for the static permittivity. As the electrolyte CPA is developed from the CPA EoS and should be compatible with existing parameter sets, it was decided to extend the e-CPA model by including the Debye-Hückel and Born terms for electrostatics. The electrolyte CPA equation of state has the following contributions:

$$A^r = A^{\text{SRK}} + A^{\text{Association}} + A^{\text{Debye−Hückel}} + A^{\text{Born}} \tag{6.1}$$

Furthermore, the static permittivity is calculated using the model described in Chapter 5 and [162, 163]. The fugacity coefficients are calculated using the procedure shown in Figure 6.1, where the largest difference in comparison to the CPA is that the static permittivity and its derivatives must be calculated from the site fractions obtained from the solver for the association equations. The task of the volume root solver is to determine a volume, where the pressure calculated from the equation of state equals the specified pressure (cf. Eq. (6.2)):

$$Q_1 = P(V) - P_{spec} = 0 \tag{6.2}$$

A Newton-Raphson scheme may be utilized to find the root (cf. Eq.(6.3)):

$$V^{(k+1)} = V^{(k)} - Q_1/Q'_1 \tag{6.3}$$

Once Eq. (6.2) is satisfied and the relative change is sufficiently small, it is possible to calculate the compressibility factor and the fugacity coefficients. In practice, it was found that more

rapid convergence was possible by transforming the independent variable into $X = B/V$ and the objective into $Q_2 = (1 - X)Q_1 = 0$. A more comprehensive discussion on the volume root solver is presented in Appendix C.4. Appendix C.6 shows how the generalized Cubic EoS was implemented with the NRTL/Huron-Vidal mixing rule. The site fractions are solved using the procedure by Michelsen and Hendriks [321, 322], which is described in Appendix C.7 along with a discussion of the implementation details related to the association term. The static permittivity is calculated from the new theory presented in Chapter 5 and is implemented using the procedure summarized in Appendix C.8.
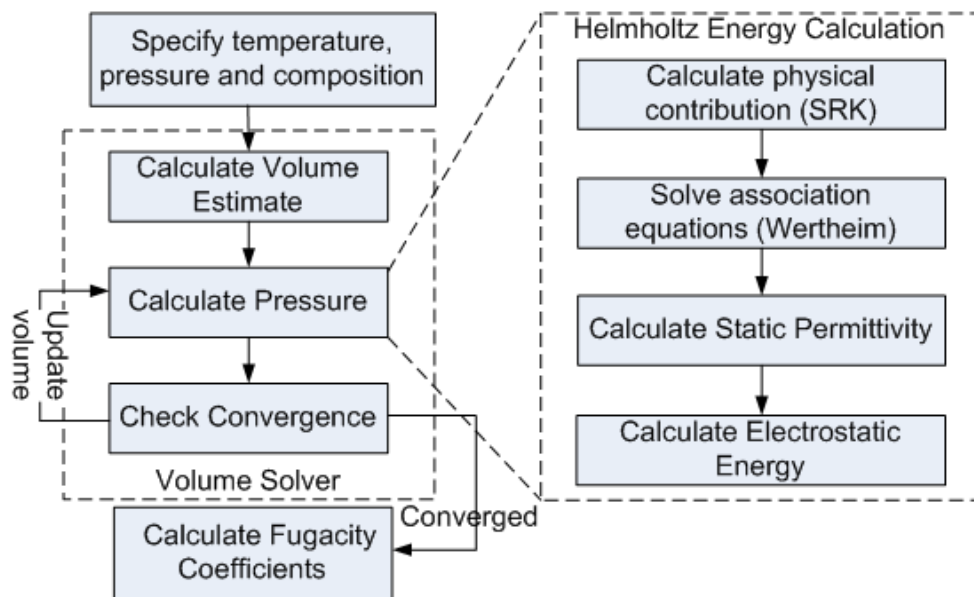
Figure 6.1: Procedure for calculation of the fugacity coefficient in electrolyte CPA.

In addition to making the procedure for calculating fugacity coefficients slightly more complex, the presence of ions leads to further complications that affect existing phase equilibrium algorithms as the charge balance imposes a further requirement for phase equilibrium. Rather than modifying existing algorithms, it was decided that this problem could be circumvented by introducing neutral salts as apparent components, and returning only fugacity coefficients based on these apparent components. This step requires a recalculation of the fugacity coefficients using Eq. (6.4):

$$\ln \hat{\varphi}_i^{\text{app}} = -\ln \frac{x_i^{\text{app}} P}{P_0} + \sum_j v_{ij} \ln \frac{x_j \hat{\varphi}_j P}{P_0} \tag{6.4}$$

A more detailed discussion on the use of the apparent compounds in an electrolyte EoS is presented in Appendix C.5. All elements of the e-CPA EoS was implemented (from scratch) in FORTRAN and subsequently linked to MATLAB through the MEX interface, so that all modeling and figures can performed using MATLAB.

6.2 Parameterization and Data Treatment

The electrolyte CPA equation of state must be parameterized against experimental data in order to be applied to modeling of thermodynamic properties of complex mixtures. This chapter

presents the approach taken to select and evaluate the experimental data used in the parameter estimation and provides an overview of the methods used to regress ion parameters. As the FORTRAN implementation of e-CPA was interfaced to MATLAB, the complete optimization toolbox of MATLAB is available. While different approaches have been attempted, this chapter presents the final parameterization procedure and shows how salts and ions can be gradually parameterized to obtain physically realizable parameters. The goal is to present a traceable and reproducible approach to the parameter estimation with electrolytes. All parameters were optimized using the *lsqnonlin* method in MATLAB. The *lsqnonlin* is a trust-region gradient-search method, it provides reproducible results given the same initial estimates. The initial estimates are selected so that they display a physical significance.

6.3 Experimental Data

The experimental data can be categorized in four different types [2]:

- Water activity $(x_w \gamma_w)$

  - Vapor pressure $(y_w P = x_w \gamma_w P_{sat}))$
  - Boiling point temperature $(RT \ln(x_w \gamma_w) = \Delta_f G^o_{steam}(T, P) - \Delta_f G^o_w)$
  - Freezing point depression $(RT \ln(x_w \gamma_w) = \Delta_f G^o_{ice}(T, P) - \Delta_f G^o_w)$
  - Isopiestic measurements that measures the vapor pressure relative to a reference system with well-known water activity (e.g. $MgCl_2$ or NaCl). At concentrations above 0.1 molal this provides a reliable source for osmotic coefficients ($\Phi = -\dfrac{x_w}{1 - x_w} \ln x_w \gamma_w$)

- Salt activity $(m_\pm \gamma_\pm^m)$

  - Direct measurements of mean ionic activity coefficients through specialized cells (e.g. the Harned cell for HCl) [2]
  - Salt solubility ($\sum\limits_{i \in j} v_i \ln(m_i \gamma_i^m) = \ln K_j$, where K_j is the equilibrium constant of salt j)

- Volumetric (V_0^ϕ, ρ)

  - Direct measurements of liquid density ρ or the density relative to a reference $\rho - \rho_w$.

- Thermal $(\Delta H / C_p)$

  - Apparent molar heat capacity
  - Differential/integral enthalpy changes when e.g. diluting the mixture.
  - Heat of solution

All of these thermodynamic properties are closely related and a complete electrolyte equation of state must be able to obtain reasonable agreement for all properties. The parameter estimation will focus on the excess properties that can be provided directly from the equation of state and later use data that requires standard state properties (or equilibrium constants) as a means of validating the parameters. As shown in section 3, the CPA equation of state does not always provide reasonable results for thermal properties, and it was therefore decided to estimate parameters against water activity data recalculated as osmotic coefficients, mean molal activity coefficients, as well as volumetric data. The electrolyte database developed and maintained by K. Thomsen [13] at the Center for Energy Resources Engineering (CERE) contains many types of data for a large number of systems. An overview of the data available in the database for

the different ions of interest in this study are presented in Figure 6.2-6.4. For salts where no volume data was available, a suitable correlation for the liquid density was used to determine the apparent molar volume using Eq. (6.5)

$$V_0^\phi = \frac{1}{m}\left(\frac{1}{\rho} - \frac{1}{\rho_w}\right) + \frac{M_{salt}}{\rho} \tag{6.5}$$

Several sources for correlations of the liquid density of aqueous salts solutions have been evaluated and compared to available experimental data. It was found that correlations by Lalibertè [317, 318] or Novotnỳ and Söhnel [319] were generally reliable.

All data has been visually inspected and outliers have been removed. Additionally, certain datapoints have been excluded from the parameter estimation by transforming freezing point data and activity coefficient data into osmotic coefficient data.
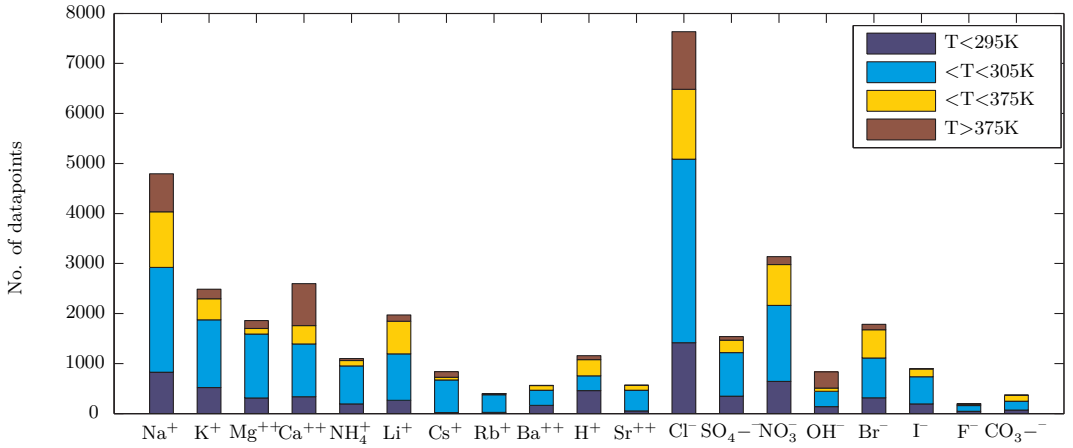
Figure 6.2: Overview of water activity data (vapor pressure, freezing point depression, and osmotic coefficient) for different species. Data from the CERE Electrolyte Database [13].
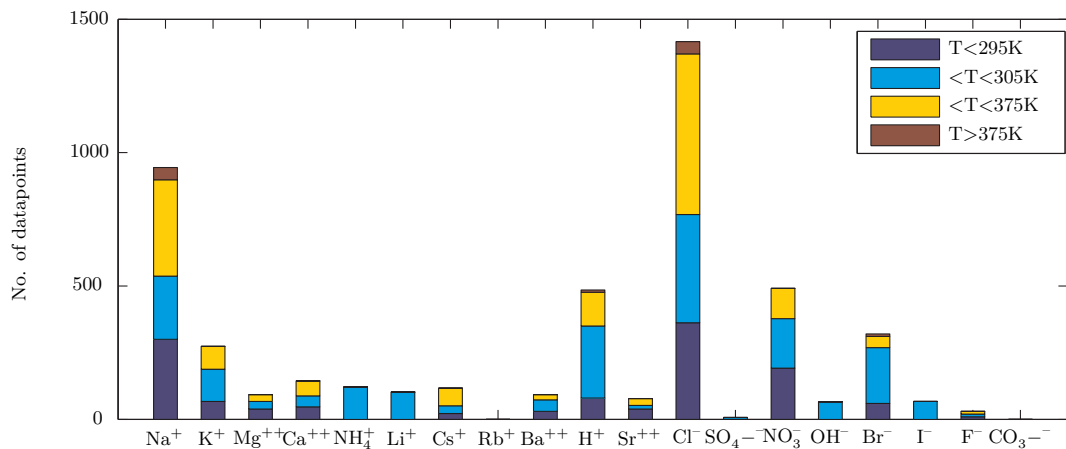
Figure 6.3: Overview of mean ionic activity coefficients $\gamma_\pm^m$ for different species. Data from the CERE Electrolyte Database [13].
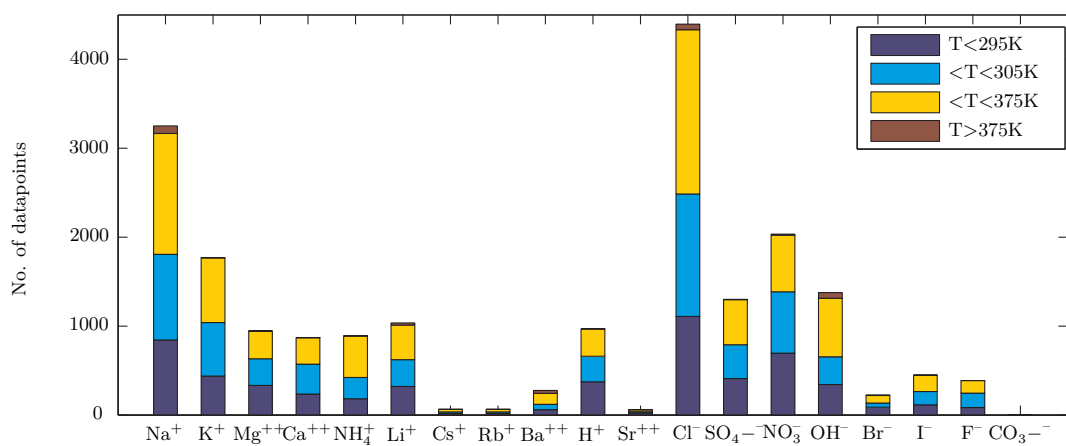
Figure 6.4: Overview of apparent molar volume data for different species. Data from the CERE Electrolyte Database [13].
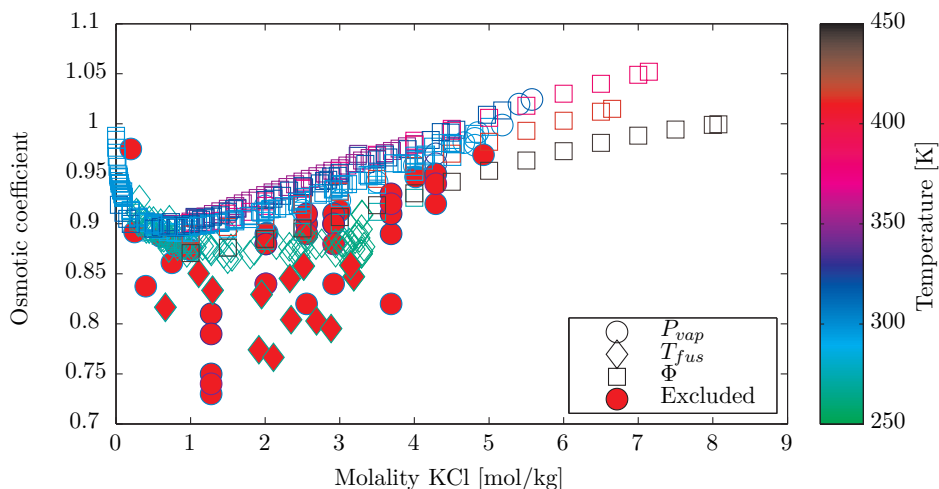
Figure 6.5: Overview of included and excluded water activity data recalculated as osmotic coefficients for KCl. Data from the CERE Electrolyte Database [13].
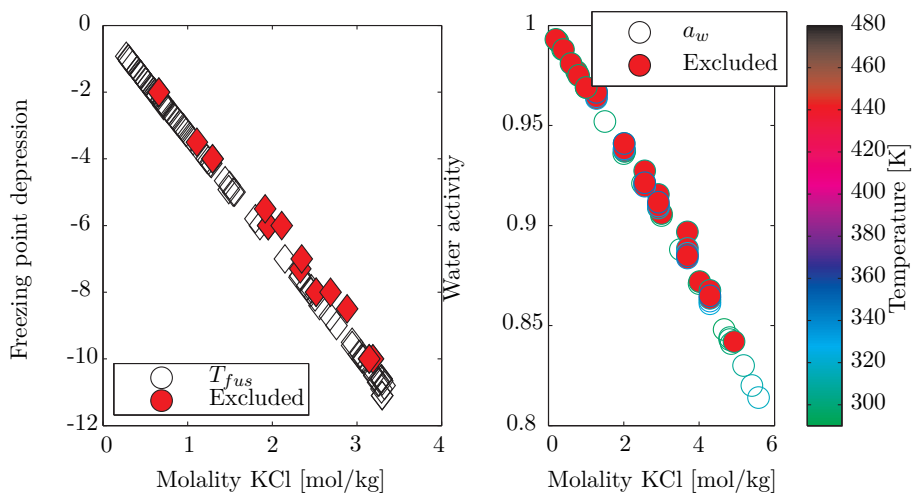
Figure 6.6: Overview of water activity and freezing point depression data for KCl. Data was excluded after comparison to the osmotic coefficient data as shown in Figure 6.5. Data from the CERE Electrolyte Database [13].

6.4   Prediction of Parameters

The e-CPA equation of state has many possibilities for defining adjustable parameters. In order to reduce the number of adjustable parameters, it is important to use prior knowledge about e.g. ion sizes to reduce the parameter space. This section highlights how some parameters in the e-CPA model are defined from other sources. Furthermore, the importance of different parameters in the model will be illustrated in order to define the adjustable parameters.

6.4.1   Free Energy of Hydration

The hydration free energy, enthalpy, and entropy are related to the difference between the ideal gas reference state to the aqueous standard state given by Eq. (6.6):

$$\Delta_{hyd}G = \Delta_f G^{aq} - \Delta_f G^{ig} \qquad \Delta_{hyd}H = \Delta_f H^{aq} - \Delta_f H^{ig} \qquad \Delta_{hyd}S = \frac{\Delta_{hyd}H - \Delta_{hyd}G}{T} \quad (6.6)$$

The hydration energy and entropy are therefore related to the fugacity coefficients at infinite dilution using Eq. (6.7)

$$\Delta_{hyd}G_i = \lim_{n_i \to 0} RT \ln \hat{\phi}_i \qquad \Delta_{hyd}H_i = \lim_{n_i \to 0} -RT^2 \left(\frac{\partial \ln \hat{\phi}_i}{\partial T} \right)_{P,\mathbf{n}} \tag{6.7}$$

To reduce the number of parameters, the Born radius is defined from the hydration free energy of the ion at 25°C. The Born radius will depend on the other parameters used in the EoS (e.g. the co-volume parameter b_0 and the ion-solvent interaction energy). When the hydration free energy is unknown, it may be estimated using Eq. (6.8), which provides an empirical relationship between the ion diameter σ and the Born radius first proposed by Latimer et al. [323] and later supported by e.g. molecular simulation [61].

$$R_{Born}^{anion} = 0.5\sigma + 0.85\text{Å} \qquad R_{Born}^{cation} = 0.5\sigma + 0.1\text{Å} \tag{6.8}$$

6.4.2   Prediction of co-volume parameters

As simple monatomic ions such as Na^+ and Cl^- can be assumed to be completely spherical, it is expected that the co-volume parameter can be predicted to fair accuracy using Eq. (6.9). Table 6.1 shows the predicted co-volume parameters for selected monatomic ions. When b_0 is used in the parameter estimation, its value should be close to the predicted values shown in Table 6.1.

$$b_0 = 2/3\pi N_A \sigma^3 \tag{6.9}$$

Linear mixing rules are used for obtaining the mixture co-volume in the EoS using Eq. (6.10).

	Li^+	Na^+	K^+	Rb^+	Cs^+	Mg^{++}	Ca^{++}	Sr^{++}	Ba^{++}	F^-	Cl^-	Br^-	I^-
σ	2.08	2.36	2.80	2.89	3.14	2.09	2.42	2.64	3.00	2.63	3.19	3.37	3.65
b_0	11.35	16.49	27.63	30.44	39.01	11.51	17.92	23.21	34.05	22.94	40.83	48.40	61.18
V_0^ϕ	-0.88	-1.21	9.02	14.07	21.34	-21.17	-17.85	-18.16	-12.47	-1.16	17.83	24.71	36.22

Table 6.1: Predicted co-volume parameters for ions. Diameters in [Å], b_0 and V_0^ϕ in [cm^3/mol]. The standard partial molar volume V_0^ϕ of the ions were taken from [21] (based on defining $V_0^\phi = 0$ for H^+).

Since cations and anions are always present in ratios that obey the charge balance, this adds an extra degree of freedom which may affect the parameter estimation.

$$b_{mix} = \sum_i x_i b_i = \sum_i x_i \tilde{b}_i + c \sum_i x_i z_i \tag{6.10}$$
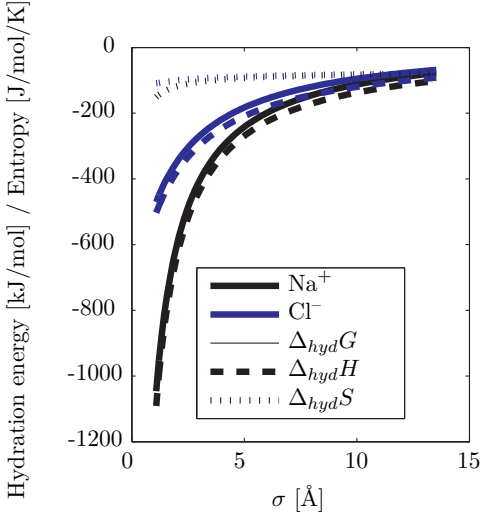
Figure 6.7: Effect of ion diameter on hydration free energy, enthalpy, and entropy of NaCl. The Born radius is calculated from Eq. (6.8)

Ion	$\Delta_{hyd}G$ [kJ/mol]	r_{Born} [Å]	r_{ion} Size	r_{Born}^{calc} Eq. (6.8)
H^+	-1050	0.64	0.30	1.15
Li^+	-475	1.38	0.69	1.53
Na^+	-365	1.77	1.02	1.87
K^+	-295	2.16	1.38	2.23
Rb^+	-275	2.31	1.49	2.34
Cs^+	-250	2.52	1.70	2.55
Mg^{2+}	-1830	1.48	0.72	1.57
Ca^{2+}	-1505	1.79	1.00	1.85
Sr^{2+}	-1380	1.95	1.13	1.98
Ba^{2+}	-1270	2.15	1.36	2.21
F^-	-465	1.41	1.33	1.43
Cl^-	-340	1.89	1.81	1.91
Br^-	-315	2.03	1.96	2.06
I^-	-275	2.31	2.20	2.30
SO_4^{2-}	-1080	2.49	2.30	2.40
NO_3^-	-300	2.13	1.79	1.89

Table 6.2: Hydration free energy from Marcus (1991) [216] and the calculated Born radius using the CPA EoS and the specified hydration energy. Comparison to the measured ion diameters collected by Marcus (1991) [216] and the calculated radius from Eq. (6.8)

If b_i is the true co-volume parameter, the charge balance means that any ion co-volume parameter obtained from the parameter regression could in fact be $b_i = \tilde{b}_i + c$, where c is a free parameter. This extra degree of freedom requires us to define the parameters of one compound, and estimate all remaining parameters based on this component. While such a choice of a reference component is not obvious it was decided to build on the experience from the development of the Extended UNIQUAC model by K. Thomsen [75] where the parameters of the hydrogen (H^+) ion have been fixed.

6.5 Parameter Estimation

6.5.1 Parameterization of HCl

HCl was selected as a good starting point, since the co-volume and energy parameters of H^+ could be fixed as 0.0. It was attempted to adjust the vdW attractive energy parameter $\Gamma_i = a_i/R/b_i$ of Cl^- to match the experimental data of HCl, but it was found that a more effective method was to fit the NRTL/Huron-Vidal water-ion interaction parameter $\Delta U_{iw}/R = \Delta U_{wi}/R = u_{iw}^0$, while setting the ion-ion interaction parameter u_{ij} to zero as a first approximation, reducing the number of adjustable parameters to one per ion. This failure of the Γ parameter to effectively correlate the data could be that it provides contributions to the dispersive interactions for not just ion-solvent but also for ion-ion; setting $u_{ij}^0 = 0$ between ions is equivalent to neglecting the ion-ion dispersive energy, which has also been done in several SAFT-based electrolyte EoS (e.g. Herzog (2010) [138] and Galindo (1999) [110]). As u_{iw}^0 for H^+ was defined as zero in it only remains to estimate the H^+ diameter σ_{H+}. Figure 6.9 shows how the optimal Cl^- parameters depend on the H^+ diameter fitted against the experimental

data up to 6 mol/kg by minimizing the objective function shown in Eq. (6.11).

$$F = \sum \left[\frac{\gamma_{\pm}^m(calc) - \gamma_{\pm}^m(exp)}{\gamma_{\pm}^m(exp)} \right]^2 + \sum \left[\frac{\Phi(calc) - \Phi(exp)}{\Phi(exp)} \right]^2 \tag{6.11}$$

From Figure 6.9 it is evident that the H^+ diameter should be selected in the range from 2-4Å. The average value of 3Å is selected as it is close the molecular diameter of H_2O, which is reasonable considering that H^+ will be mainly present as H_3O^+ and larger clusters. The parameters in Fig. 6.9 were estimated without using the volumetric data, which results in a large overestimation of the apparent molar volume as shown in Table 6.3. In order to obtain better correspondence with the liquid volume it would be necessary to include a term that would reduce the apparent molar volume. Figure 6.8 shows that only the Born term and the ion-solvent association term (using the ion-water association equilibrium constant as determined from Chapter 5) provide negative contributions to the apparent molar volume at infinite dilution.

Figure 6.8: Effect of hydration number and Born radius on the apparent molar volume of HCl at infinite dilution.

Since the Born term was already fixed to the hydration free energy, there remains only three
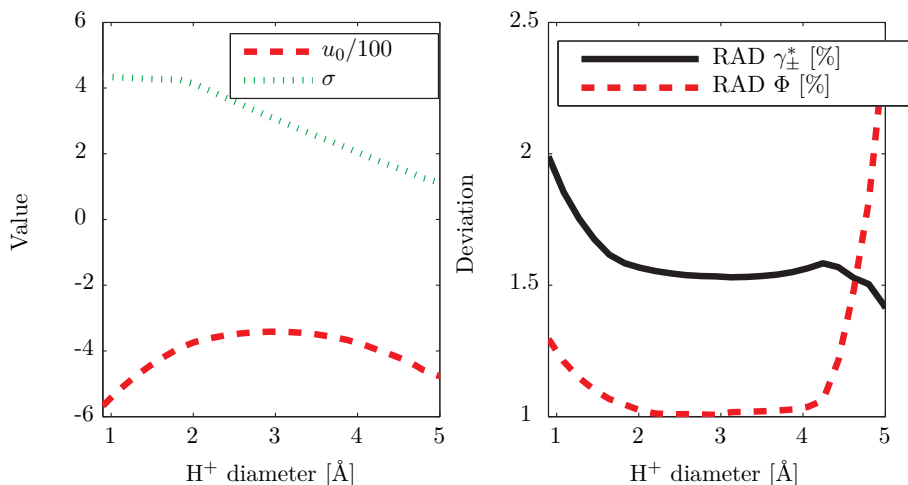
Figure 6.9: Optimized Cl^- parameters as a function of the H^+ diameter. Parameters were optimized against experimental activity and osmotic coefficients $\gamma_{\pm}^m$ and Φ. b_0 parameter was taken from Table 6.1.

possibilities for remedying the errorneous apparent molar volume:

Option 1 Adopt co-volume parameters from Table 6.1 and fit a Peneloux volume translation term to correct the volume from the EoS: $V = V(EoS) + \sum_i x_i c_i$.

Option 2 Include co-volume parameters in regression

Option 3 Include ion-solvent association

Table 6.3 shows the results of the parameter estimation for option 1 and 2 and Figure 6.10 shows a comparison of the two methods with different number of adjustable parameters.

	σ_{H+}	b_0	u^0	σ_{Cl^-}	c_i	RAD $\gamma_\pm^*$	RAD Φ	AAD V_0^ϕ
		[cm^3/mol]	[K]	[Å]	[cm^3/mol]	[%]	[%]	[cm^3/mol]
Case 0		40.83	-332.35*	3.19	0	1.53	1.02	28.68
Case 1		40.83	-341.67*	3.05*	0	1.53	1.01	28.65
Case 2		40.83	-341.67*	3.05*	-26.86*	1.53	1.01	1.92
Case 3		20.26*	-2153*	3.19	0	1.76	1.12	2.10
Case 4		20.21*	-2118*	3.53*	0	1.82	1.16	2.05

Table 6.3: Overview of parameters for Cl$^-$ estimated through different approaches against activity and osmotic coefficient data up to 6 molal at 25°C. * indicates a fitted parameter.

While option 2 would seem as a good practical work-around it has the limitation that the co-volume parameter cannot become negative and as many of the cations have large negative apparent molar volumes, the inclusion of this parameter drives the co-volume towards zero. It was furthermore illustrated in Chapter 5, that the effect of ion-solvent association is important to model the decrease in the static permittivity with salt concentration. Still, as illustrated by Figure 6.11, option 1 actually provides an alternative method to represent the decrease of the static permittivity as a function of the salt concentration due to the over-estimation of the apparent molar volume with b_0 from Table 6.1.
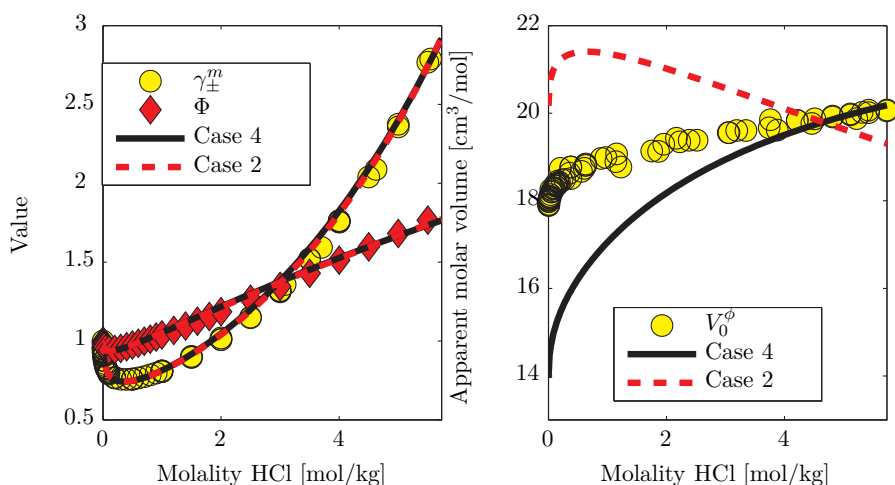
Figure 6.10: Activity/osmotic coefficients and apparent molar volume of HCl in H$_2$O for Case 2 and 4 at 25°C (see Table 6.3).

By correcting the apparent molar volume subsequently, the model can still obtain good correspondence with liquid volumes. This approach also has the advantage that all parameters but $u_{iw}^0 = \Delta U_{iw}/R = \Delta U_{wi}/R$ can be predicted from other sources. While it is possible and more
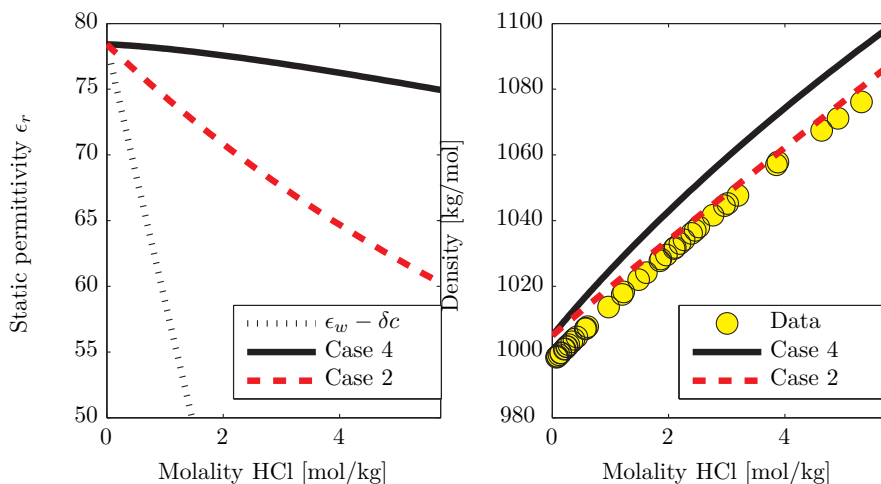
Figure 6.11: Static Permittivity and Density of HCl for Case 2 and 4 at 25°C (see Table 6.3). Linear decrease is taken from the recommended correlation by Marcus (2013) [310].

physically correct to explicitly account for ion-solvent association, this requires the introduction of additional parameters and increases the computational requirements. Furthermore, as indicated by Table 6.3, a good agreement with experimental data for activity coefficients and osmotic coefficients is possible from fitting only u_{iw}^0. It was therefore decided to parameterize a simplified electrolyte CPA that does not include ion-solvent association, as a first approximation. By setting up a simplified reference model, it will become easier to quantify the advantage of adding additional physics and parameters to the model at a later stage.

6.5.2 Parameter Estimation for Other Ions

After the parameterization of the interaction parameter of Cl⁻ with water from HCl, it is possible to sequentially obtain parameters for other salts by fixing the parameters for the other ions. Table 6.4 summarizes the parameters fitted at 25°C. It is then possible to use these parameters to provide predictions for other salts as shown in Table 6.5.

From Table 6.4 it is evident that a single parameter u^0 may be used to fit parameters and obtain good correspondence with the osmotic coefficients and activity coefficients up to a certain concentration for different salts. Table 6.5 shows that when these parameters are used to predict properties of other salts, the results are somewhat mixed - in some cases, predictions are excellent, while the predictions in other cases are fairly poor, except for the density which works very satisfactorily in all cases. This could be seen as a sign that additional binary interaction parameters or additional physics is required in order to obtain proper predictions with the simplified model. The introduction of binary interaction parameters will lead to a large increase in the number of parameters, and will also require the inclusion of a large amount of additional data for salt mixtures in order to define the parameters. The simultaneous parameter regression is one of the largest hurdles to modeling of mixtures containing salts, and is also prevalent in the case of activity coefficient models such as Extended UNIQUAC and Electrolyte NRTL. The parameter estimation makes it difficult for engineers to apply electrolyte models effectively in their work.

Inspired by the good results with ion-specific parameters shown in Table 6.4 it is suggested

Ion	Salt	σ	b_0	u^0	c_i	RAD $\gamma_\pm^*$	RAD Φ	AAD V_0^ϕ
		Å	[cm^3/mol]	[K]	[cm^3/mol]	[%]	[%]	[cm^3/mol]
F$^-$	KF	2.63	22.94	-648.8*	-15.82*	1.33	1.04	2.5
Cl$^-$	HCl	3.19	40.83	-335.3*	-26.84*	1.66	1.15	1.9
Br$^-$	KBr	3.37	48.40	-346.2*	-29.56*	4.62	3.24	5.5
I$^-$	KI	3.65	61.18	-360.1*	-30.98*	0.53	0.88	6
NO$_3^-$	KNO$_3$	3.16	39.80	-12.68*	-14.01*	0.24	0.67	0.4
SO$_4^{--}$	Na$_2$SO$_4$	3.82	70.03	163.3*	-46.45*	-	1.12	7.0
Li$^+$	LiCl	2.08	11.35	-663.2*	-22.50*	3.34	2.50	6.0
Na$^+$	NaCl	2.36	16.49	-34.23*	-31.36*	1.73	1.67	5.9
K$^+$	KCl	2.78	27.62	131.8*	-36.96*	0.37	0.39	5
Rb$^+$	RbCl	2.89	30.4	95.12*	-36.10*	1.14	0.93	5.5
Cs$^+$	CsCl	3.14	39.01	111.5 *	-39.48*	3.64	1.76	6.0
Mg^{++}	MgCl$_2$	2.09	11.51	-1500*	-37.30*	7.32	6.80	3.9
Ca^{++}	CaCl$_2$	2.42	17.92	-685.2*	-44.97*	5.76	5.31	4.0
Sr^{++}	SrCl$_2$	2.64	23.20	-370.1*	-54.93 *	5.08	5.66	3.8
Ba^{++}	BaCl$_2$	3.00	34.05	198.8*	-66.54*	3.94	1.47	1.8
Average						2.864	2.33	4.36

Table 6.4: Parameters fitted to data up to 6 mol/kg for monovalent salts, and up to 4 molal for divalent salts at 25°C. * indicates a fitted parameter.

that the model could be fitted for salt-specific parameters, which will work in case that there are not too many/too different ions present. The contribution from salts to the NRTL/Huron-Vidal mixing rule (Eq. (3.8) (p. 31) may in the case of salts with a non-randomness factor $\alpha = 0$ and the ion-ion interactions $u_{ij} = 0$ be rewritten as Eq. (6.12):

$$\frac{g^{E,\infty}}{RT} = \left(n_T^2 \sum ß x_i \nu_i \right)^2 \left(n_w n_a \left(\nu_w + \nu_a \right) \frac{\Delta U_{aw}}{RT} + n_w n_c \left(\nu_w + \nu_c \right) \frac{\Delta U_{cw}}{RT} \right) \tag{6.12}$$

Eq. (6.12) may be rewritten into Eq. (6.13) using that $n_a = v_a m_{salt}$ and $n_c = v_c m_{salt}$:

$$\frac{g^{E,\infty}}{RT} = \left(n_T^2 \sum ß x_i \nu_i \right)^2 \left(n_w m_{salt} \left([v_c + v_a] \nu_w + v_a \nu_a + v_c \nu_c \right) \frac{\Delta U_{sw}}{RT} \right) \tag{6.13}$$

In which ΔU_{sw} is the salt-water interaction parameter, which can be calculated from Eq. (6.14):

$$\frac{\Delta U_{sw}}{RT} = \frac{v_a \left(b_w + \nu_a \right)}{(v_a + v_c) b_w + v_c \nu_c + v_a \nu_a} \frac{\Delta U_{aw}}{RT} + \frac{v_c \left(b_w + \nu_c \right)}{(v_a + v_c) b_w + v_c \nu_c + v_a \nu_a} \frac{\Delta U_{cw}}{RT} \tag{6.14}$$

In order to determine the salt-specific parameters, it is possible to set $\Delta U_{aw}/R = \Delta U_{cw}/R = u_{sw}^0$ for a given salt, and subsequently calculate ΔU_{sw} from Eq. (6.14). Similarly, the ion-specific parameters can be calculated from the salts requested by a user. Examples:

- The engineer wants to calculate a system containing NaCl-MgCl$_2$-CsCl. This system contains four ions and three salts. As the system only has one anion, it is not possible to include additional salts to fix the last degree of freedom. But if the anion ΔU_{iw} is fixed from HCl, it is possible to obtain an optimal ΔU_{iw} and thereby uniquely determine the parameters for all ions.

- The engineer wants to calculate a system containing NaCl-CaSO$_4$. This system contains four ions and two salts. By including the parameters for Na$_2$SO$_4$ and CaCl$_2$, the degree of freedom is zero, and it is possible to uniquely determine ΔU_{iw} for all ions.

Salt	RAD $\gamma_\pm^*$ [%]	RAD Φ [%]	AAD V_0^ϕ [cm^3/mol]	Salt	RAD $\gamma_\pm^*$ [%]	RAD Φ [%]	AAD V_0^ϕ [%] [cm^3/mol]
LiBr	5.75	4.16	0.2	CsNO$_3$	1.25	1.84	-
LiI	4.24	3.13	1.4	Cs$_2$SO$_4$	15.12	35.4	-
LiNO$_3$	16.5	9.55	1.5	MgBr$_2$	13.05	4.3	2.8
Li$_2$SO$_4$	13.2	12.0	6.3	MgI$_2$	11.01	7.75	2.5
NaF	5.35	5.48	0.7	Mg(NO$_3$)$_2$	9.35	16.1	4.5
NaBr	2.48	3.63	0.5	MgSO$_4$	-	49.5	7.5
NaI	0.81	2.27	0.3	CaBr$_2$	9.85	5.66	3.3
NaNO$_3$	7.08	4.80	1.2	CaI$_2$	5.89	3.41	1.4
K$_2$SO$_4$	2.5	9.02	5.0	Ca(NO$_3$)$_2$	6.71	3.61	4.0
RbF	5.08	2.23	1.0	CaSO$_4$	14.0	-	6.5
RbBr	11.4	5.66	0.2	SrBr$_2$	3.96	3.00	1.9
RbI	11.7	5.67	0.2	SrI$_2$	4.49	3.32	1.4
RbNO$_3$	0.94	1.28	0.5	Sr(NO$_3$)$_2$	4.86	10.8	4.5
Rb$_2$SO$_4$	11.2	25.9	2.3	BaBr$_2$	10.5	4.35	0.5
CsF	9.0	5.08	0.8	BaI$_2$	17.8	10.8	1.1
CsBr	7.34	3.05	-	Ba(NO$_3$)$_2$	2.18	4.08	1.5
CsI	12.63	7.45	-	Average	8.04	8.57	2.3

Table 6.5: Predictions using the parameters determined from the sequential parameter estimation using other salts in Table 6.4 at 25°C. These salts were not used in the parameter estimation and the results are therefore predictions.

- The engineer wants to calculate a system containing Na$_2$SO$_4$-K$_2$CO$_3$-Mg(NO$_3$)$_3$. This system contains 6 ions and three salts. It is possible to include parameters for three additional salts to fix the degree of freedom - but still, the system will be under-specified, as the system of ions forms up to 9 (anhydrous) salts. Different results may be obtained depending on which salts are selected as reference salts.

The last case shows the true limitation of a salt-specific approach - that there are many more salts than there are ions. The more combinations of anions and cations that are possible, the less accurate will the predictions from the salt-specific parameters become, whereas a perfect equation of state based on the ion-specific approach can be expected to perform better. However, that would most likely require a much stronger representation of the physics by e.g. including ion-ion and ion-solvent association or by fitting ion-ion interaction energies ΔU_{ii}. Fitting of ion-ion interaction energies fitted to aqueous solutions may however be problematic when they are used in mixed solvents, and has previously lead researchers to introduce solvent-dependent ion-ion interactions [95, 118, 120] (effectively ternary parameters). Table 6.6 shows the salt-specific parameters when u^0 and the Peneloux volume correction are fitted, whereas Table 6.7 shows the results when the volume parameter ν_i in Eq. (6.12) is included in the parameter regression. By including ν_0 for the salt, it is possible to extend the applicability range up to the solubility limit for most salts.

Salt	u_{sw}^0 [K]	c_i [cm^3/mol]	RAD $\gamma_\pm^*$ [%]	RAD Φ [%]	AAD V_0^ϕ [cm^3/mol]	Max. molality
NaF	-158.7*	-52.93*	1.87	1.10	0.8	1.0
KF	-222.2*	-54.38*	0.62	0.61	1.6	3.8
RbF	-286.4*	-55.55*	1.98	1.30	1.0	3.5
CsF	-285.6*	-55.92*	0.86	0.74	0.8	3.5
HCl	-252.9*	-26.89*	1.12	0.97	2.0	6.0
LiCl	-447.1*	-45.79*	3.95	2.70	0.8	6.0
NaCl	-227.3*	-54.70*	1.74	1.68	1.2	6.0
KCl	-133.5*	-60.31*	0.363	0.39	0.8	5.0
RbCl	-142.3*	-59.45*	1.14	0.93	0.3	5.5
CsCl	-114.5*	-62.84*	2.88	1.81	0.6	6.0
MgCl$_2$	-557.1*	-83.98*	7.32	6.79	3.6	3.9
CaCl$_2$	-414.8*	-91.66*	5.74	5.33	4.0	4.0
SrCl$_2$	-344.1*	-104.6*	5.08	5.66	1.4	3.8
BaCl$_2$	-166.3*	-113.3*	4.44	1.85	3.1	1.8
HBr	-356.0*	-29.69*	3.20	2.82	0.9	5.5
LiBr	-430.1*	-49.13*	4.79	4.07	0.2	5.5
NaBr	-262.3*	-57.80*	2.45	2.77	0.5	5.9
KBr	-154.5*	-62.69*	0.70	0.71	0.5	5.8
RbBr	-142.7*	-62.04*	1.27	1.01	0.3	5.0
CsBr	-117.1*	-38.48*	2.90	2.23	76.6	5.0
MgBr$_2$	-594.0*	-85.90*	12.83	6.49	2.6	3.8
CaBr$_2$	-479.8*	-94.11*	9.33	7.37	3.1	3.9
SrBr$_2$	-352.7*	-104.2*	3.96	3.06	1.9	2.1
BaBr$_2$	-244.2*	-113.4*	2.40	2.47	0.6	2.4
HI	-339.8*	-33.67*	3.40	2.45	0.7	5.5
LiI	-404.9*	-70.91*	1.85	1.94	1.4	3.2
NaI	-284.3*	-62.56*	1.85	2.68	0.3	5.5
KI	-184.2*	-67.95*	0.54	0.88	0.4	5.5
RbI	-156.0*	-67.16*	2.58	1.99	0.3	5.0
CsI	-117.4*	-38.48*	1.93	1.35	92.3	3.0
MgI$_2$	-581.7*	-99.04*	15.48	10.63	2.2	4.0
CaI$_2$	-412.5*	-112.3*	5.76	3.24	1.4	2.0
SrI$_2$	-370.5*	-116.9*	4.30	3.71	1.4	2.0
BaI$_2$	-318.4*	-123.3*	3.40	3.13	0.9	2.0
LiNO$_3$	-381.6*	-34.91*	1.21	0.79	1.3	5.7
NaNO$_3$	-56.88*	-44.35*	2.51	1.16	1.2	5.8
KNO$_3$	49.53*	-50.97*	0.27	0.65	0.4	3.8
RbNO$_3$	30.10*	-49.63*	1.15	0.78	0.4	4.5
CsNO$_3$	27.96*	-53.44*	0.84	0.79	0.0	1.5
Mg(NO$_3$)$_2$	-481.3*	-61.35*	7.44	3.16	2.7	4.0
Ca(NO$_3$)$_2$	-161.5*	-75.92*	6.88	3.21	3.2	3.5
Sr(NO$_3$)$_2$	-30.21*	-76.29*	5.89	4.53	4.2	3.5
Ba(NO$_3$)$_2$	112.9*	-95.00*	3.12	0.67	1.5	0.4
Li$_2$SO$_4$	-48.40*	-90.78*	1.74	1.24	6.6	3.2
Na$_2$SO$_4$	79.25*	-109.2*	1.25	1.11	7.0	3.8
K$_2$SO$_4$	51.91*	-124.0*	2.94	0.67	5.0	0.7
Rb$_2$SO$_4$	-17.92*	-113.2*	1.64	0.84	2.3	1.8
Cs$_2$SO$_4$	-40.63*	-120.4*	1.98	0.93	1.9	1.8
MgSO$_4$	64.65*	-85.03*	-	5.31	8.7	3.6
CaSO$_4$	27.73*	-105.0*	13.82	0	6.5	0.015
Average			3.6	2.5	5.3	

Table 6.6: Salt-specific parameters at 25°C. Using ion-specific co-volume parameters and ion diameters from Table 6.4. * indicates a fitted parameter.

Salt	u_{sw}^0 [K]	ν_0 [cm^3/mol]	c_i [cm^3/mol]	RAD $\gamma_\pm^*$ [%]	RAD Φ [%]	AAD V_0^ϕ [cm^3/mol]	Max. molality
NaF	-549.4*	19.50*	-30.37*	2.01	1.20	0.8	1.0
KF	-2302*	10.17*	-9.855*	2.36	1.44	1.8	17.5
RbF	-1050*	21.41*	-14.22*	3.29	2.15	0.8	3.5
CsF	-1246*	21.60*	-3.119*	2.40	1.29	0.5	3.5
HCl	-226.5*	49.01*	-23.41*	3.72	2.01	3.9	16.5
LiCl	-1900*	20.51*	-25.76*	8.63	4.33	0.4	20.1
NaCl	-888.4*	19.89*	-30.49*	1.50	1.05	1.5	6.2
KCl	-348.1*	29.54*	-24.63*	0.64	0.46	1.0	5.0
RbCl	-677.2*	18.05*	-17.48*	0.31	0.29	1.2	7.8
CsCl	-554.6*	18.68*	-10.60*	2.92	1.75	1.5	11.4
MgCl$_2$	-5014*	23.28*	-55.45*	9.76	4.61	7.6	6.0
CaCl$_2$	-1157*	58.08*	-61.61*	12.0	9.64	4.6	10.5
SrCl$_2$	-2118*	30.44*	-63.37*	4.78	2.74	0.6	4.0
BaCl$_2$	-113.8*	167.4*	-72.65*	3.23	1.90	2.4	1.8
HBr	-2644*	13.41*	-23.96*	2.57	1.85	0.7	11
LiBr	-3525*	16.32*	-26.36*	14.3	5.26	1.4	20
KBr	-401.8*	32.41*	-26.84*	0.83	0.51	0.5	5.8
RbBr	-549.8*	23.02*	-21.38*	0.17	0.14	0.5	5.0
CsBr	-427.0*	23.40*	-64.93*	2.16	1.79	0.5	5.0
MgBr$_2$	-4848*	27.87*	-57.29*	13.60	5.14	2.0	5.6
CaBr$_2$	-4356*	29.27*	-55.32*	16.08	7.66	1.0	9.3
SrBr$_2$	-526.4*	93.98*	-74.50*	4.18	3.12	1.5	2.1
BaBr$_2$	-414.3*	94.14*	-70.61*	2.77	2.54	1.1	2.4
HI	-2874*	14.83*	-27.28*	3.69	1.59	1.2	10.0
LiI	-745.1*	47.37*	-54.66*	2.15	1.73	1.4	3.2
NaI	-2113*	17.42*	-31.88*	2.27	1.18	1.0	12.3
KI	-326.1*	50.01*	-32.44*	1.38	0.37	0.8	8.6
RbI	-553.6*	28.41*	-26.18*	0.31	0.31	0.6	5.0
CsI	-355.6*	29.93*	-81.19*	1.00	0.75	0.5	3.0
MgI$_2$	-5678*	29.84*	-67.95*	10.93	5.32	3.8	5.0
CaI$_2$	-579.6*	112.8*	-88.96*	5.81	2.99	1.1	2.0
SrI$_2$	-619.0*	103.7*	-86.13*	4.42	3.29	1.0	2.0
BaI$_2$	-547.7*	108.0*	-79.46*	3.61	2.76	0.4	2.0
LiNO$_3$	-544.3*	40.94*	-18.18*	2.59	1.47	2.4	24.0
NaNO$_3$	-37.42*	79.75*	-22.67*	1.22	0.40	2.1	10.8
KNO$_3$	151.5*	38.83*	-17.25*	1.31	1.09	0.5	3.8
RbNO$_3$	139.8*	34.85*	-12.45*	2.91	2.05	0.5	4.5
CsNO$_3$	207.2*	39.80*	-6.332*	0.88	0.92	0.1	1.5
Mg(NO$_3$)$_2$	-1420*	44.39*	-41.20*	7.91	3.20	2.0	5.1
Ca(NO$_3$)$_2$	-227.2*	88.69*	-52.30*	6.80	2.72	3.3	7.8
Ba(NO$_3$)$_2$	184.8*	79.60*	-53.56*	3.37	0.43	1.4	0.4
Sr(NO$_3$)$_2$	-16.30*	318.39*	-47.82*	4.79	1.74	3.9	4.0
Li$_2$SO$_4$	-303.0*	35.88*	-61.41*	1.96	1.62	5.9	3.2
Na$_2$SO$_4$	80.69*	70.03*	-68.53*	2.93	3.67	6.5	4.4
K$_2$SO$_4$	126.9*	70.37*	-56.30*	2.94	0.72	5.0	0.7
Rb$_2$SO$_4$	-17.17*	62.54*	-38.06*	1.47	1.40	2.1	1.8
Cs$_2$SO$_4$	-142.7*	33.82*	-23.18*	1.70	1.18	1.7	1.8
MgSO$_4$	4.340*	72.37*	-71.04*	-	6.15	7.8	3.6
CaSO$_4$	14.65*	70.03*	-82.51*	13.69	-	6.5	0.0153
Average				4.3	2.3	2.1	

Table 6.7: Salt-specific parameters at 25°C when ν is included in the parameter estimation. Using ion-specific co-volume parameters and ion diameters from Table 6.4. * indicates a fitted parameter.

The salt-specific parameters also enables an examination of the optimal temperature dependence of the interaction parameter ΔU_{iw}. When data is available at elevated temperatures, it was found that the form in Eq. (6.15) would give reasonable fits to the experimental data:

$$\Delta U_{iw}/R = u_{iw}^0 + u_{iw}^{(1)}T + u_{iw}^{(2)}\ln T \tag{6.15}$$

Figure 6.12 shows the correspondence of the fitted temperature dependence of NaCl with $\nu = 52.90$ $u_{iw} = -250.8$K, $u_{iw}^{(1)} = 12.52$, and $u_{iw}^{(2)} = -4294$. It is believed that the T-dependence can be improved either by improving the physics of the model, or by setting up more advanced correlations of the parameters, but this would require the inclusion of SLE-data as many salts do not contain osmotic/activity coefficient data beyond 25°C.
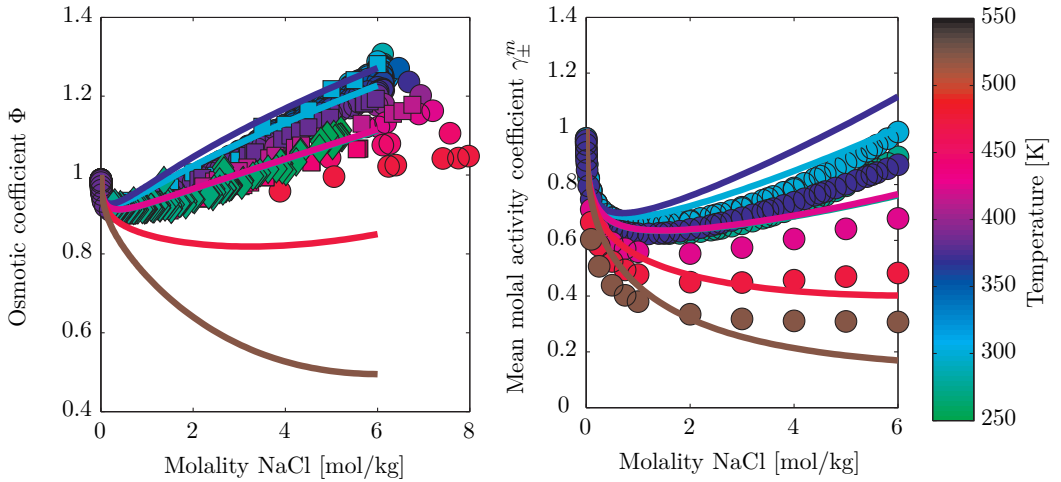
Figure 6.12: T-dependence of Osmotic Coefficient and Activity Coefficients of NaCl with Salt-Specific Parameters. The colored lines are correlations from the e-CPA EoS at different temperatures.

6.5.3 Improving the Ion-Specific Parameters

During the parameterization of salt-specific parameters it was shown that it was possible to extend the applicability range of the model up to the solubility limit by including the volume used in the NRTL/Huron-Vidal mixing rule. The next step is to fit ion-specific parameters ν and u^0 by first performing a sequential procedure used in Section 6.5.2 (with results shown in Appendix D.1) and then performing a global optimization including all salts. Before the ion-specific parameters parameters can be optimized through a gradient-based scheme, it is advantageous to normalize the parameters. It is noted that while the ion-specific parameters are not unique due to the linear mixing rules in Eq. (6.10) and Eq. (6.12) giving rise to the following combinations of solutions:

$$\nu_i = \tilde{\nu}_i + z_i c_v \tag{6.16}$$

$$\left(\nu_w + \nu_i\right) u_{iw}^0 = \left(\nu_w + \tilde{\nu}_i\right) \tilde{u}_{iw}^0 + z_i c_U \tag{6.17}$$

Normalized parameters $\tilde{\nu}$ and $\tilde{u}_{iw}^0$ can be obtained by finding the coefficients c_v and c_U and subtracting them from the original parameters. Figure 6.13 shows how the parameters depends
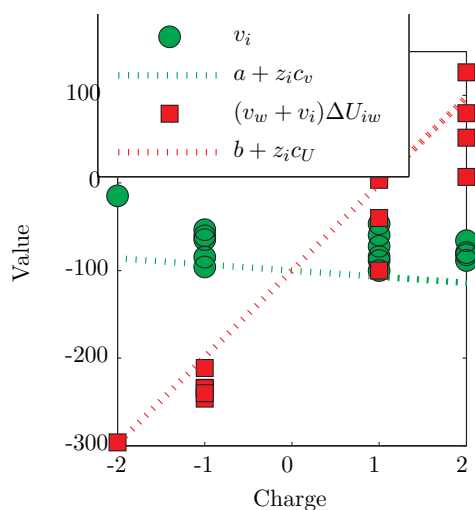
Figure 6.13: Parameter trend with ionic charge used for obtaining the normalized ion-specific parameters in Table 6.8.

Ion	$\tilde{\nu}_i$ [cm^3/mol]	$\tilde{u}_{iw}$ [K]	$\tilde{c}_i$ [cm^3/mol]
H$^+$	6.99	-251.10	37.5
Li$^+$	18.34	-1245.4	-13.7
Na$^+$	22.66	71.54	-26.7
K$^+$	34.62	309.0	-33.5
Rb$^+$	47.33	265.9	-32.2
Cs$^+$	60.40	268.4	-35.4
Mg^{++}	25.50	-2373	-23.2
Ca^{++}	31.91	-1081	-29.2
Sr^{++}	34.40	-452.4	-47.7
Ba^{++}	48.12	391.7	-59.4
F$^-$	-3.04	-3958	-14.5
Cl$^-$	8.29	-1443	-25.8
Br$^-$	28.38	-779.6	-28.7
I$^-$	39.50	-726.4	-33.1
NO$_3^-$	32.64	-220.5	-17.5
SO$_4{}^{--}$	71.24	64.84	-55.7

Table 6.8: Normalized ion-specific parameters for the different ions. Note that the parameters have a reasonable trend in terms of volume and energy and that all new Peneloux parameters are negative, as they account for ion-solvent association.

on the ionic charge, and Table 6.8 shows the normalized parameters.

In the following sections, the $\tilde{\nu}$ notation for the normalized parameters is omitted as all parameters have been normalized. After normalization it is possible to further improve the parameters by performing a simultaneous regression of all salts. The parameter regression is performed using the volume parameter v_i and the combined energy parameter $(v_w + v_i)u_{iw}$ as independent variables. Furthermore, the Newton step is modified in order to remove any trend with ionic charge:

$$\Delta x^{(k)} = \Delta \tilde{x}^{(k)} + z_i c_x^{(k)} \tag{6.18}$$

In practice, this is done by modifying MATLAB's *snls* function, which determines the step of the *lsqnonlin* method. Parameters are summarized in Table 6.9 and the results are shown in Table 6.12.

In order to further improve the correspondence with the experimental data, it was attempted to include the ion diameter in the simultaneous parameter regression (see Appendix D.3. This would generally reduce the deviation from the experimental data, but as it was noted that this procedure could lead to unphysical trends in the ion sizes, it was decided not to use this approach in the final parameterization. The unphysical ion diameters were shown to have a negative impact on predictions in multicomponent mixtures. The discussion of using the ion diameter in the parameterization is presented in Appendix D.3. Furthermore, it was decided to limit the range of data used in the parameter regression to up to 6 mol/kg, in order to get the best performance for the desired applications to gas solubility and gas hydrate formation in brines, and to make the modeling results more easily comparable with literature on e-EoS, that most often are only concerned with concentrations up to 6 mol/kg. The suggested parameter estimation scheme for e-CPA is shown in Figure 6.14.

Ion	σ [Å]	b_0 [cm^3/mol]	$\tilde{v}_i$ [cm^3/mol]	u_{iw}^0 [K]	c_i [cm^3/mol]
H$^+$	3	0.0	9.809*	836.3*	0.7
Li$^+$	2.08	11.35	7.732*	-2314*	-14.7
Na$^+$	2.356	16.49	1.891*	-1512*	-20.3
K$^+$	2.798	27.63	1.071*	-496.7*	-24.2
Rb$^+$	2.89	30.44	-0.09152*	-851.9*	-23.0
Cs$^+$	3.139	39.01	-0.9733*	-743.4*	-23.8
Mg^{++}	2.09	11.51	13.36*	-4183*	-24.1
Ca^{++}	2.422	17.92	15.08*	-2156*	-26.0
Sr^{++}	2.64	23.21	13.50*	-1407*	-39.0
Ba^{++}	3	34.05	10.87*	-334.4*	-46.8
F$^-$	2.63	22.94	24.57*	-674.4*	-21.0
Cl$^-$	3.187	40.83	8.783*	-2269*	-22.6
Br$^-$	3.373	48.40	8.076*	-4416*	-23.4
I$^-$	3.647	61.18	11.34*	-4079*	-27.3
NO$_3^-$	3.16	39.80	29.35*	401.9*	-14.7
SO$_4{}^{--}$	3.815	70.03	-10.08*	-2006*	-47.2

Table 6.9: e-CPA parameters for different ions when all parameters were optimized simultaneously to osmotic and activity coefficient data at 25°C. Results are summarized in Table 6.12. * indicates a fitted parameter.
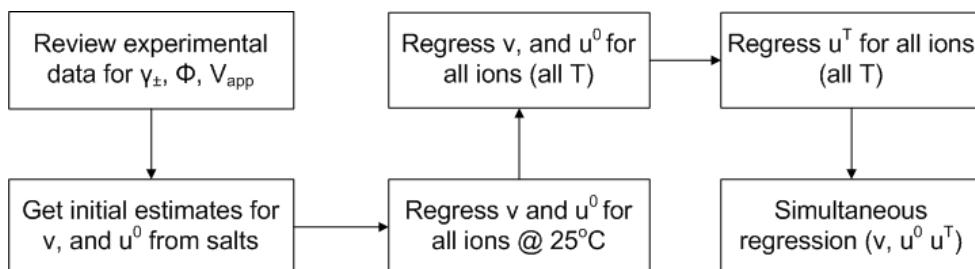
Figure 6.14: Procedure for estimating ion-specific parameters.

6.5.4 Temperature Dependence

It is possible to introduce temperature-dependent parameters for the water-ion interaction to improve the correspondence at other temperatures. It is suggested to use a linear T-dependence of the water-ion interaction parameters $\Delta U_{iw} = \Delta U_{wi} = u_{iw}^0 + u_{iw}^T(T - 298.15)$. The parameters are shown in in Table 6.11 and the results are summarized in 6.12. The parameters were improved by fitting the temperature-dependent parameters u_{iw}^T independently initially and then let all parameters (ν, u_{iw}^0 and u_{iw}^T) be optimized simultaneously leading to the final parameters shown in Table 6.11. Results for the prediction and correlation are summarized in Table 6.12. Figures of the T-dependency for all salts are presented in Appendix D.2, while the results at 25°C for different anions are shown in Figures 6.15-6.20, while the freezing point depression results are shown in Figure 6.21. The freezing point temperature at a given salt concentration is calculated from the water activity and the change in Gibbs energy was determined from Eq.

(6.19):

$$\ln a_w(T, m_{salt}) = \frac{\Delta_{fus}}{RT_{fus}} \left(1 - \frac{T_{fus}}{T} \right) + \frac{\Delta_{fus}C_p^0}{R} \left(\frac{T_{fus}}{T} - \ln \frac{T_{fus}}{T} - 1 \right)$$
$$+ \frac{\Delta C_p^T T_{fus}}{R} \left(\frac{T}{T_{fus}} - \frac{T_{fus}}{T} + 2 \ln \frac{T_{fus}}{T} \right) \tag{6.19}$$

Where the enthalpy of fusion at $T_{fus} = 273.15K$ is $\Delta_{fus}H = 6001.4$ J/mol with the change in heat capacity at $\Delta_{fus}C_p = \Delta_{fus}C_p^0 + \Delta_{fus}C_p^T (T - T_{fus})$, in which the change in heat capacity at T_{fus} is $\Delta_{fus}C_p^{T_{fus}} = 38.03$ J/mol/K with a small T-dependence $\Delta_{fus}C_p^T = -0.146$ J/mol/K^2 [176].

6.6 Summary

This chapter explored the development of a practical engineering electrolyte CPA equation of state based on the theoretical background from the previous chapters. It was shown that the electrolyte CPA EoS can be parameterized using either salt or ion-specific parameters with good agreement with experimental data for osmotic and activity coefficients. An overview of the results is presented in Table 6.10.

$\Delta U_{iw}/R$	ν_{iw}	Type	Parameters	Results	T-range [K]	m-range [mol/kg]
Fitted u_{iw}^0	Predicted	Ion	Table 6.4	Table 6.5	298.15	0-6
Fitted u_{iw}^0	Predicted	Salt	Table 6.6	Table 6.6	298.15	0-6
Fitted u_{iw}^0	Fitted	Salt	Table 6.7	Table 6.7	298.15	0-Solubility
Fitted u_{iw}^0	Fitted	Ion	Table 6.9	Table 6.12	298.15	0-6
Fitted $u_{iw}^0 + u_{iw}^T$	Fitted	Ion	Table 6.11	Table 6.12	240-473.15	0-Solubility

Table 6.10: Summary of parameter estimation results.

It was shown that it would be necessary to account for ion-solvent association to obtain good correspondence with the apparent molar volume V_0^ϕ. In this work it was decided to fit a Peneloux volume-correction to experimental data for the density in order to develop a simplified electrolyte EoS, that can be used as a reference to assess the impact of including other physical interactions or parameters. The final ion-specific EoS shown in Table 6.11 includes four adjustable parameters:

- The NRTL/Huron-Vidal volume ν

- Two parameters for the T-dependent interaction energy between water and salt $\Delta U_{iw}/R = u_{iw}^0 + u_{iw}^T(T - 298.15)$

- A Peneloux volume correction term c

The first three parameters are adjusted to water and salt activity data, whereas the Peneloux volume correction can be fixed from the density of the salt at the solubiity limit. The ion diameter and co-volume is obtained from crystallographic ion radii shown in Table 6.1 and furthermore the Born radius is adjusted to match the hydration free energy at 25°C shown in Table 6.2.

Ion	σ	b_0	ν	u_{iw}^0	u_{iw}^T	c_i
	[Å]	[cm^3/mol]	[cm^3/mol]	[K]	[-]	[cm^3/mol]
H$^+$	3	0.0	-5.345*	-5496*	33.44	1.4
Li$^+$	2.08	11.35	0.7758*	-3848*	-0.6412	-15.5
Na$^+$	2.356	16.49	2.848*	241.5*	-12.62	-25.1
K$^+$	2.798	27.63	2.006*	1247*	-7.387	-32.5
Rb$^+$	2.89	30.44	-1.840*	860.0*	-37.13	-28.8
Cs$^+$	3.139	39.01	-5.566*	-1323*	-64.62	-24.6
Mg^{++}	2.09	11.51	-2.029*	-11991*	-33.72	-22.6
Ca^{++}	2.422	17.92	16.55*	-157.5*	8.353	-30.0
Sr^{++}	2.64	23.21	19.10*	377.0*	1.864	-46.8
Ba^{++}	3	34.05	54.76*	1044*	1.162	-61.3
F$^-$	2.63	22.94	27.38*	-1121*	2.181	-13.1
Cl$^-$	3.187	40.83	13.94*	-1911*	4.489	-22.2
Br$^-$	3.373	48.40	17.00*	-2113*	-2.086	-25.2
I$^-$	3.647	61.18	19.50*	-2352*	-7.080	-28.5
NO$_3^-$	3.16	39.80	15.51*	-314.4*	0.4739	-12.6
SO$_4{}^{--}$	3.815	70.03	-0.03378*	6041*	-15.25	-53.9

Table 6.11: e-CPA parameters for different ions when all parameters were optimized simultaneously with all water activity data recalculated as osmotic coefficients. Results are summarized in Table 6.12. * indicates a fitted parameter.

Salt	RAD [%] $\gamma_\pm^*$		Np.	RAD [%] Φ		Np.	RAD [%] a_w		Np.	m-range	T-range
Table	6.9	6.11	$\gamma_\pm^*$	6.9	6.11		6.9	6.11			
NaF	6.83	6.27	47	8.39	7.91	24	0.29	0.24	8	1.0	269-308
KF	2.61	2.00	28	2.82	0.93	49	0.48	0.44	6	6	251-357
RbF	5.54	6.07	24	2.44	2.64	17	-	-	-	3.5	298.15
CsF	11.5	4.01	24	6.53	1.16	17	-	-	-	3.5	298.15
HCl	7.71	2.66	180	1.69	0.87	42	1.39	1.11	44	6	246-353
LiCl	3.83	2.08	47	2.95	3.41	270	3.69	0.27	76	6	243-473
NaCl	7.70	4.70	704	2.31	1.99	862	0.68	0.74	177	6	253-473
KCl	1.68	2.14	216	2.88	3.49	282	0.31	0.19	103	6	262-445
RbCl	5.76	6.44	28	3.57	4.09	84	0.52	0.33	34	6	263-343
CsCl	2.12	1.06	145	5.74	3.06	198	0.62	0.38	26	6	264-473
MgCl$_2$	8.94	13.59	49	7.14	5.40	305	1.69	1.18	130	6	240-473
CaCl$_2$	10.22	10.95	97	15.7	7.85	666	18.9	4.78	192	6	222-473
SrCl$_2$	4.47	4.18	38	3.99	3.52	90	0.45	0.69	41	4.03	267-444
BaCl$_2$	3.93	4.64	19	6.93	3.78	161	0.19	0.26	30	3.02	268-444
HBr	3.51	3.37	72	2.92	0.97	22	-	-	-	6	298-398
LiBr	6.66	4.43	38	4.05	2.91	102	0.96	0.09	19	6	243-373
NaBr	7.43	2.53	149	4.43	1.75	135	0.83	0.39	70	6	252-374
KBr	4.03	3.08	32	4.27	3.36	63	0.53	0.29	64	6	261-343
RbBr	4.14	2.01	27	2.58	1.86	53	-	-	-	5.0	298.15
CsBr	4.80	2.02	27	3.28	1.93	53	-	-	-	5.0	298.15
MgBr$_2$	12.95	12.15	60	6.47	5.98	61	2.96	1.77	13	5.8	230-323
CaBr$_2$	10.38	14.23	61	11.03	7.45	173	2.64	1.72	67	6	221-473
SrBr$_2$	6.64	5.17	40	4.86	4.44	28	0.49	0.61	41	3.3	251-343
BaBr$_2$	6.33	3.85	55	5.27	4.10	30	1.16	0.44	48	3.4	254-343
HI	4.57	4.73	28	2.24	1.64	37	-	-	-	6	298.15
LiI	4.07	3.90	23	3.28	2.47	84	3.29	0.38	10	6	248-343
NaI	8.55	5.27	32	3.76	2.12	51	1.57	0.37	51	6	250-362
KI	5.89	5.47	33	3.62	2.78	54	2.84	0.80	31	4.9	257-298
RbI	3.30	2.38	27	3.41	2.63	53	-	-	-	5.0	298.15
CsI	2.11	1.49	23	1.73	1.58	-	-	-	-	3.0	298.15
MgI$_2$	9.17	8.14	41	4.81	4.32	52	5.14	3.31	5	5.0	226-298
CaI$_2$	8.27	7.67	38	5.55	3.09	38	7.13	3.65	44	6	208-343
SrI$_2$	9.57	7.56	38	3.09	2.47	28	1.00	0.65	44	4.2	264-343
BaI$_2$	15.37	8.18	38	5.53	1.48	28	2.32	0.58	19	3.3	240-298
LiNO$_3$	9.28	8.83	28	4.94	3.56	144	3.72	0.40	42	6	273-378
NaNO$_3$	4.54	7.07	31	2.75	4.25	154	1.74	0.49	33	6	255-373
KNO$_3$	0.70	1.49	24	4.62	1.66	156	12.8	0.77	13	6	270-422
RbNO$_3$	1.53	5.51	26	0.97	4.24	50	-	-	-	4.5	298.15
CsNO$_3$	0.84	7.04	19	0.92	5.76	29	-	-	-	1.5	298.15
Mg(NO$_3$)$_2$	7.94	9.40	78	4.56	3.20	174	2.22	2.56	75	6	241-413
Ca(NO$_3$)$_2$	8.26	10.13	78	26.11	6.46	71	8.80	3.63	92	6	243-413
Sr(NO$_3$)$_2$	7.63	7.57	78	5.16	5.27	18	0.12	0.18	9	4.0	266-318
Ba(NO$_3$)$_2$	4.23	6.70	60	0.80	8.90	6	0.01	0.08	4	0.4	273-318
Li$_2$SO$_4$	4.78	6.73	36	1.60	5.00	57	0.40	0.23	55	3.08	263-298
Na$_2$SO$_4$	5.76	0.90	31	7.72	4.74	163	0.32	0.10	35	4.44	272-398
K$_2$SO$_4$	4.66	1.94	24	3.50	3.28	80	0.076	0.04	13	0.96	272-373
Rb$_2$SO$_4$	2.70	3.09	31	7.00	7.69	13	-	-	-	1.80	298.15
Cs$_2$SO$_4$	5.43	2.53	31	12.07	4.62	13	-	-	-	1.80	298.15
MgSO$_4$	-	-	-	10.47	7.38	131	0.18	0.20	26	5.0	268-448
CaSO$_4$	13.73	13.68	7	-	-	-	-	-	-	0.015	298.15
Average	6.17	6.01	3268	5.14	3.74	6293	2.51	2.78 (2.17)	2.16	2025	

Table 6.12: Deviations from experimental data with parameters from Table D.3 and the number of points Np.

Figure 6.15: Correlated osmotic coefficients, water activities, activity coefficients and apparent molar volumes of flourides.

Figure 6.16: Correlated osmotic coefficients, water activities, activity coefficients and apparent molar volumes of chlorides.
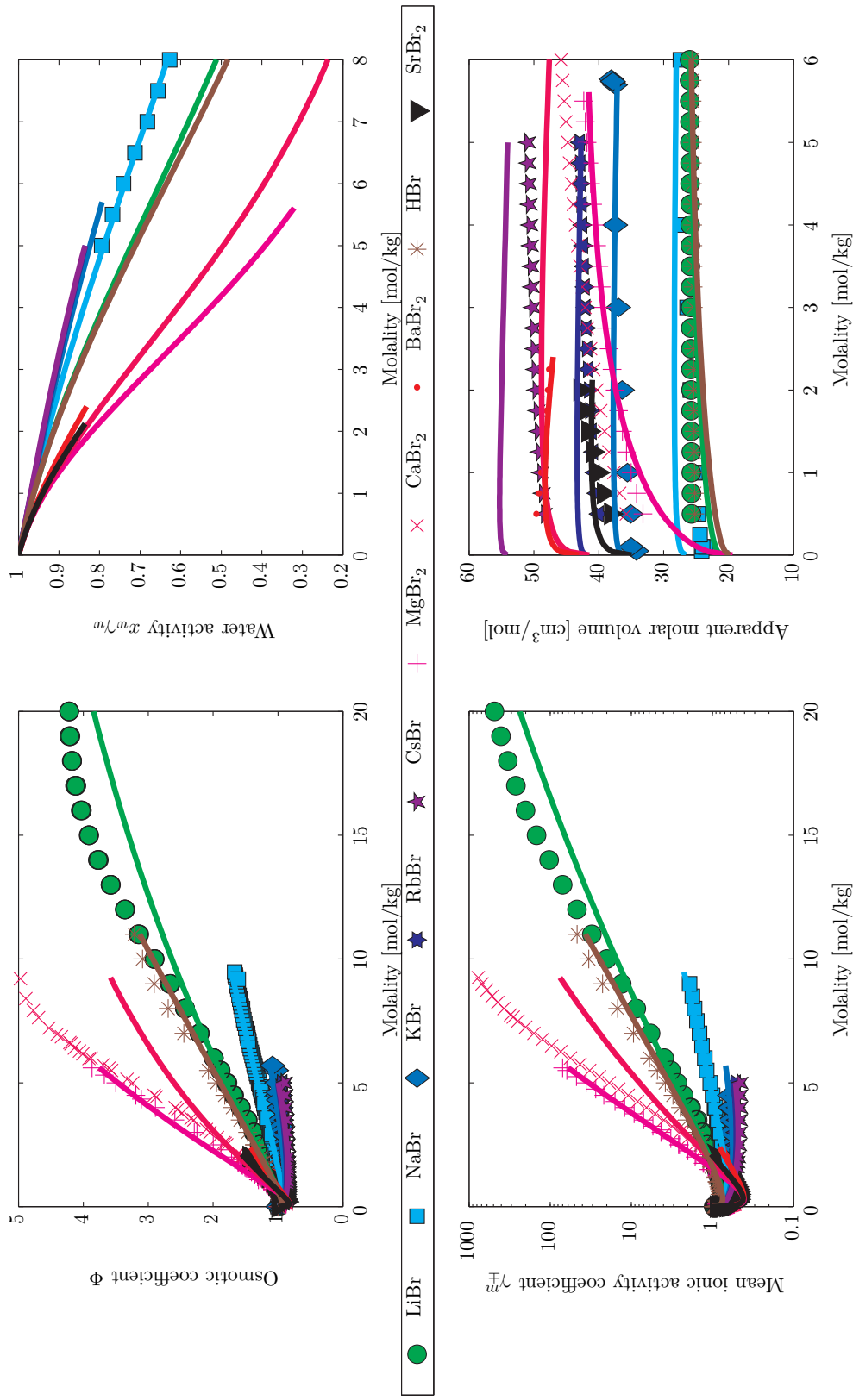
Figure 6.17: Correlated osmotic coefficients, water activities, activity coefficients and apparent molar volumes of bromides.
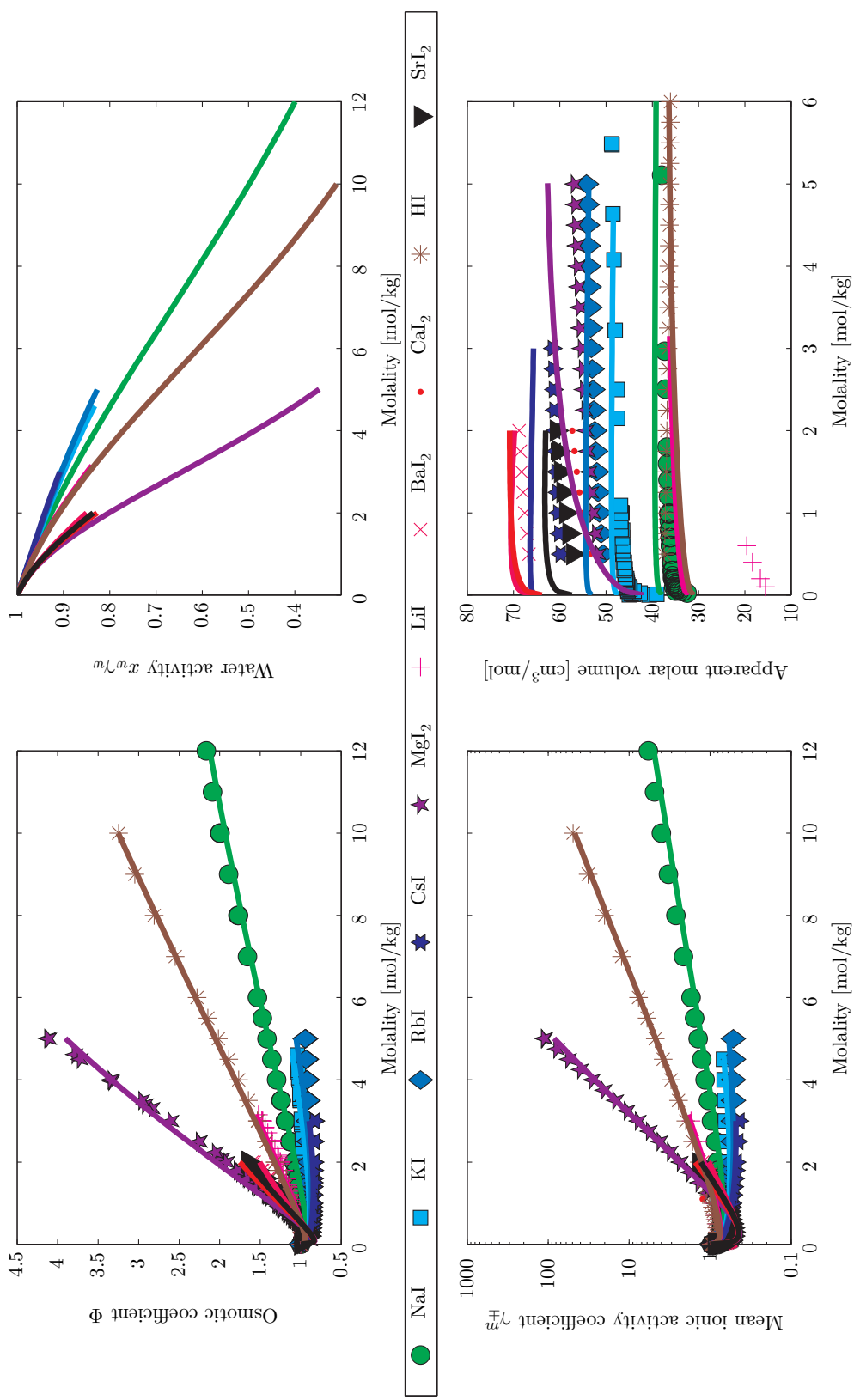
Figure 6.18: Correlated osmotic coefficients, water activities, activity coefficients and apparent molar volumes of iodides.
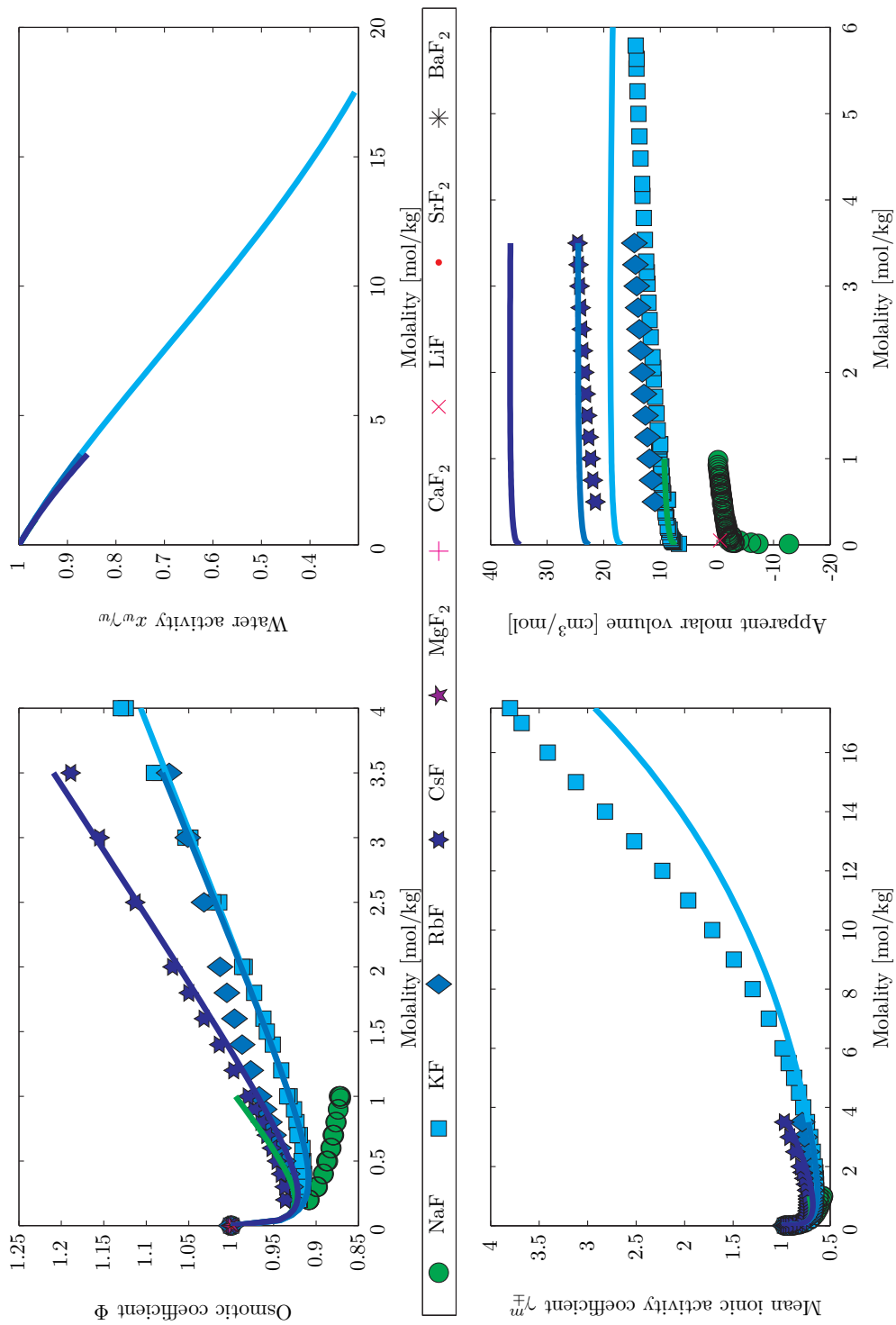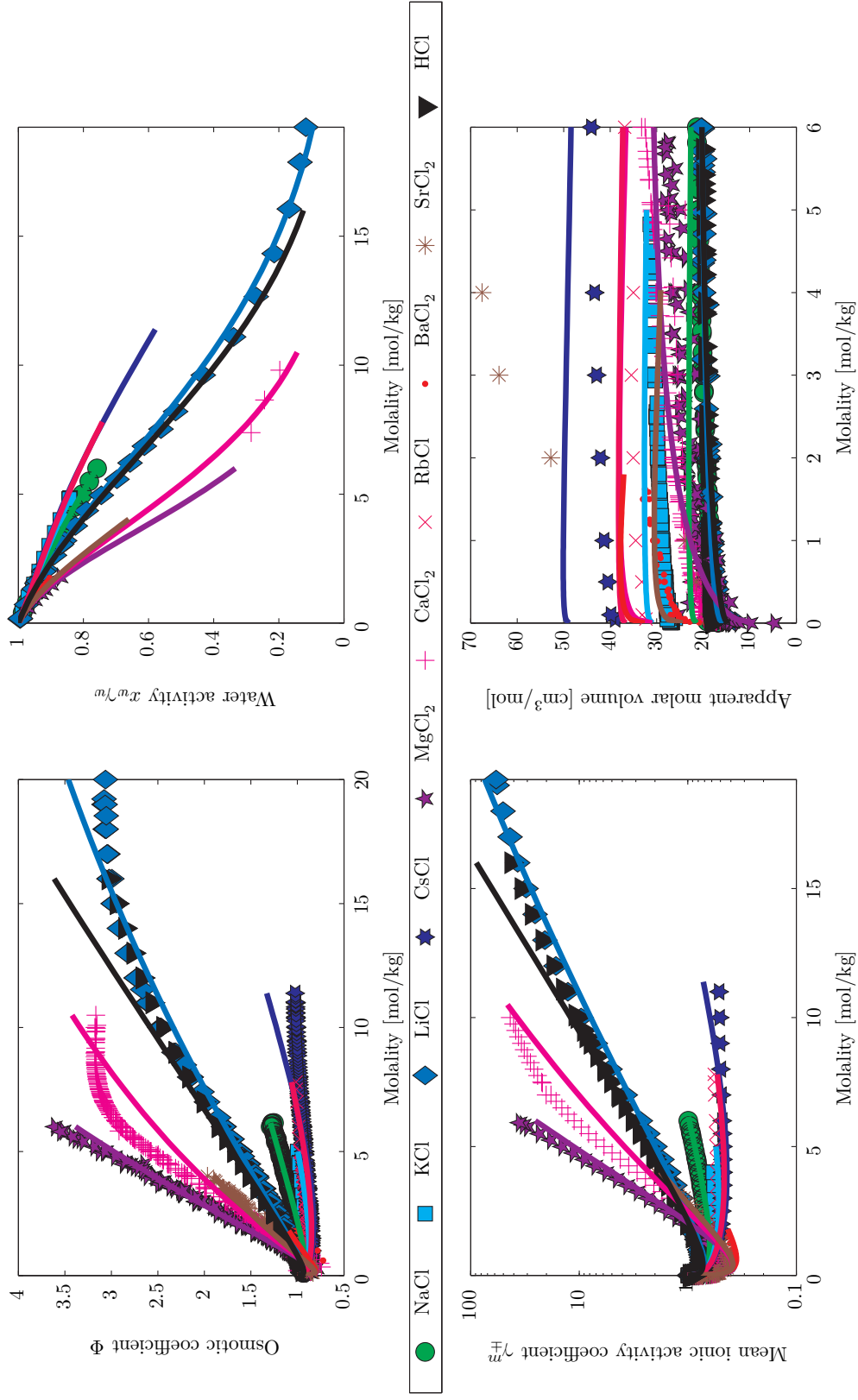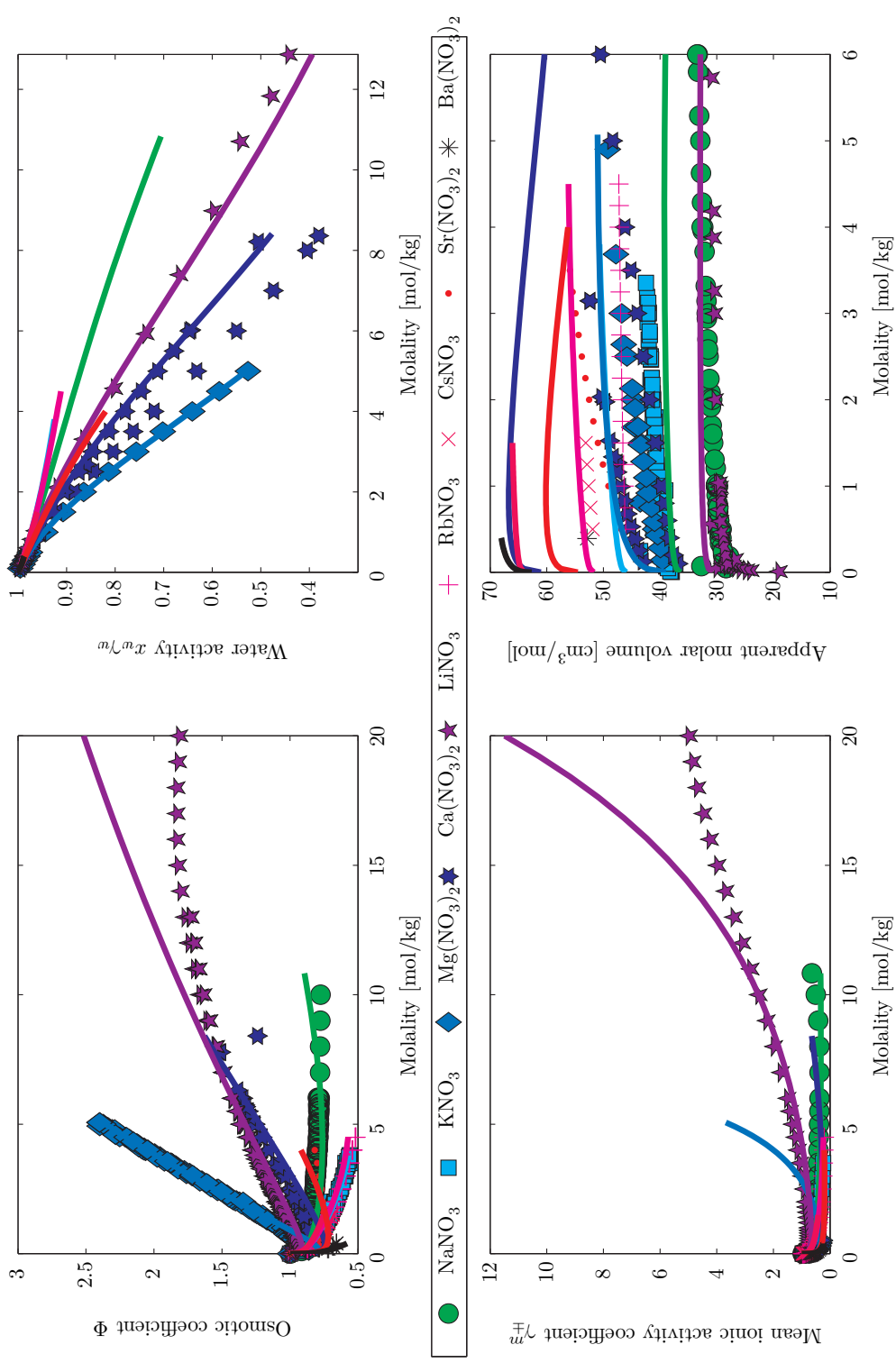
Figure 6.19: Correlated osmotic coefficients, water activities, activity coefficients and apparent molar volumes of nitrates.
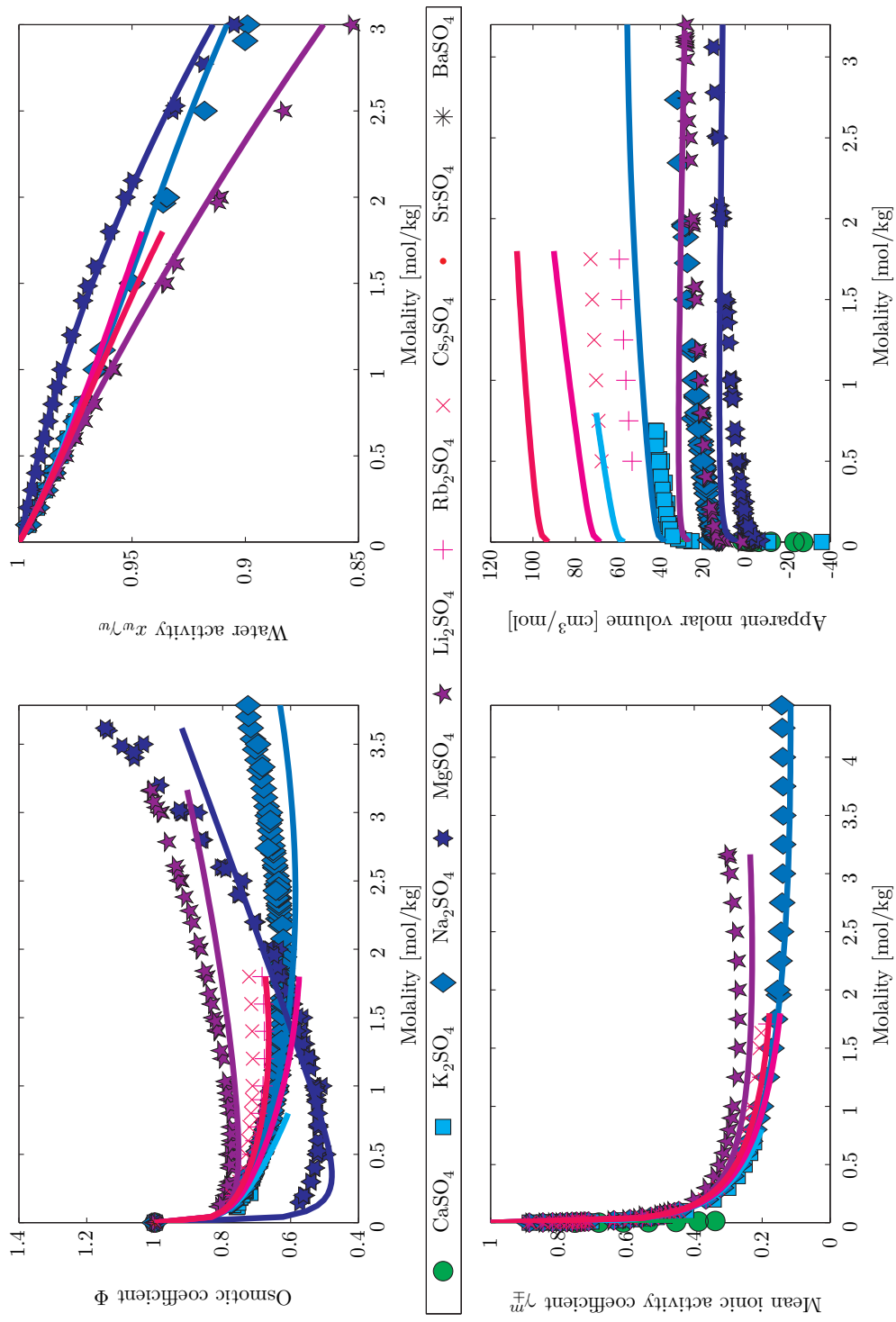
Figure 6.20: Correlated osmotic coefficients, water activities, activity coefficients and apparent molar volumes of sulfates.
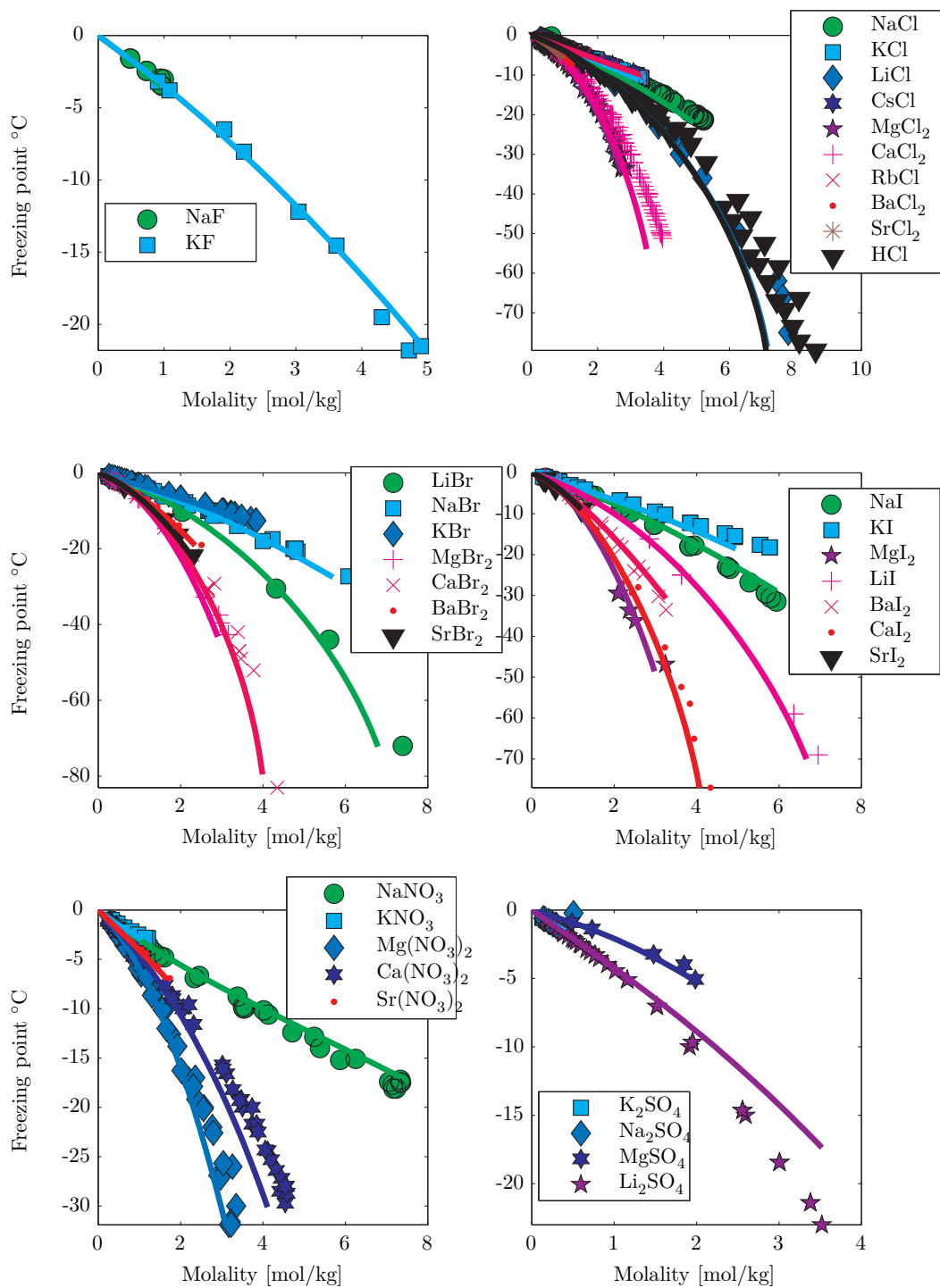
Figure 6.21: Predicted freezing point temperatures.

Chapter 7

Results and Discussion

Chapter 6 explored different options for parameterizing the electrolyte CPA (e-CPA) EoS. It was demonstrated that it is possible to determine parameters for ions or for each salts. The salt-specific parameters will provide the highest accuracy if only a single salt is going to be studied, but may also be used in salt mixtures. The ion-specific parameters can also be estimated simultaneously to all salts, in which case the results inevitably become "best on average" and may have deviations for individual salts. It was furthermore decided that while the ion diameter could be adjusted to obtain better correlations with experimental data, this would introduce inconsistencies in the parameter trends, which could lead to worse predictive behavior. The final model uses the Huron-Vidal/NRTL volume parameter ν_i as well as a linear temperature dependence in the ion-water interaction $\Delta U_{iw}/R = u_{iw}^0 + u_{iw}^T(T - 298.15)$ for each ion.

This chapter the predictive capabilities of the e-CPA EoS is investigated by using the final ion-specific parameters shown in Table 6.11 p. 133 are used to predict data that was not included in the parameter estimation. The investigation will include only a limited selection of salts (and salt mixtures) in order to apply the model to a diverse set of applications including vapor-liquid, liquid-liquid, liquid-solid, liquid-liquid-solid, and even three-liquid-solid equilibrium in mixed solvents.

7.1 Temperature and Pressure Dependence of SLE, Volume, and Excess Properties

Solid-liquid equilibrium provides the best source for temperature-dependent data for a wide range of salts. It is therefore of interest to see how well e-CPA performs when it is applied to prediction of solid-liquid equilibrium. Figure 7.1 shows that the e-CPA model has a good correspondence with the experimental data, and also illustrates that it may be possible to use the ideal gas reference state even for solid-liquid equilibrium. The failure to obtain the solubility at higher/lower temperatures is ascribed to problems in the representation of the activity coefficient at higher temperatures and salt concentrations, indicating that the current representation of $\Delta U/R$ with a linear T-dependence is not sufficient to provide a correlation over wider ranges of temperature. This problem requires further attention and possibly extension of the model in order to be able to use the solid-liquid equilibrium data as a reliable data source.

Pitzer et al. (1984) [324] developed a reference model for sodium chloride as a function of temperature and pressure. Figure 7.2 shows the temperature and pressure dependence of the excess enthalpy of NaCl, which increases the confidence in the temperature dependence, at least at high temperatures and low molalities. Figure 7.3 shows that the e-CPA model has excellent representations of the trends from the reference model. The model extrapolates well to high
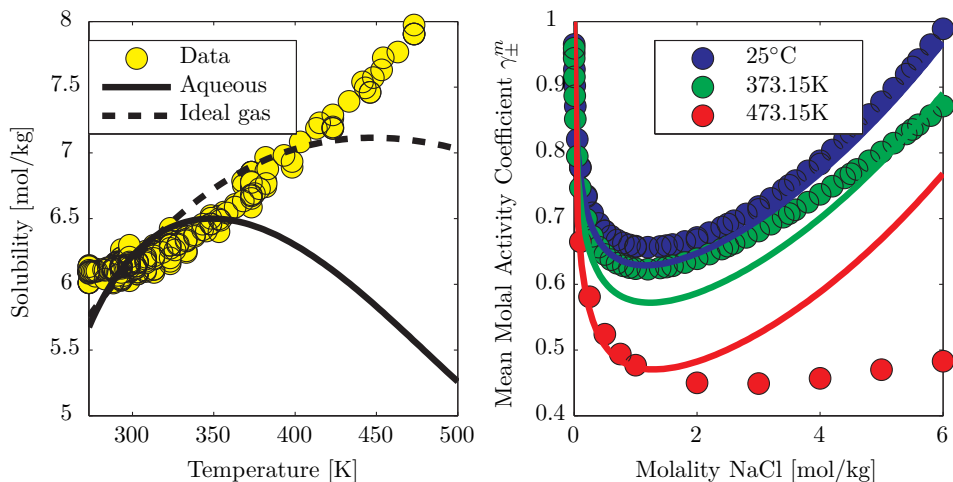
Figure 7.1: Temperature dependence of NaCl solubility using the aqueous standard state adopted from Extended UNIQUAC by K. Thomsen [13] and the ideal gas reference state. The aqueous standard state parameters for ions were taken from Table 4.4. The ideal gas formation energies were taken from Table B.7-B.9 in Appendix B. The solid NaCl uses $\Delta_f G^o = -384.14$kJ/mol, $\Delta_f H^o = -411.15$ kJ/mol and $C_p = 50.5$ J/mol/K.

temperatures whereas the structure-dominated region at low temperatures are described with less accuracy using e-CPA. The temperature and pressure dependence of the apparent molar volume is illustrated in Figure 7.4, from which it is evident that while the simple representation with a Peneloux volume translation does provide the correct trends, the simplification fails at high temperatures. It is suggested that e-CPA model will have to be extended with ion-solvent association to handle the low-temperature regime. This could also improve the correspondence with the apparent molar volume at high temperatures, as the model for ion-solvent association will also affect the concentration-dependence of the static permittivity, which may in turn correct the deficiencies at high temperatures and concentrations.
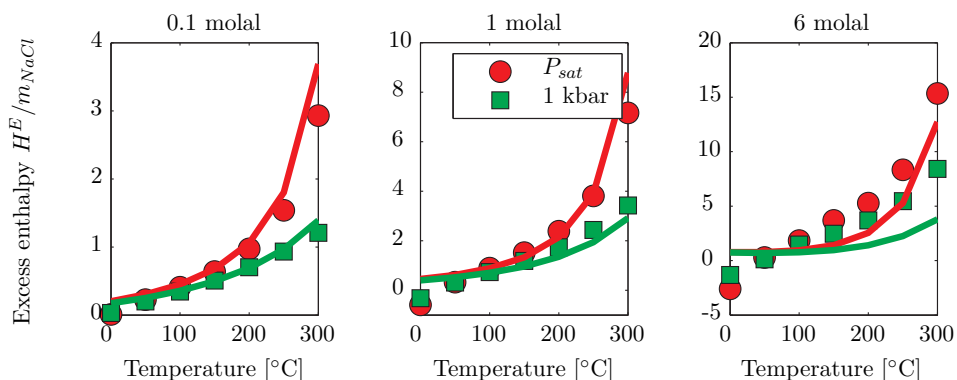
Figure 7.2: Pressure and temperature dependencence of excess enthalpy of NaCl in water at 0.1, 1, and 6 molal. Legend applies to all figures.
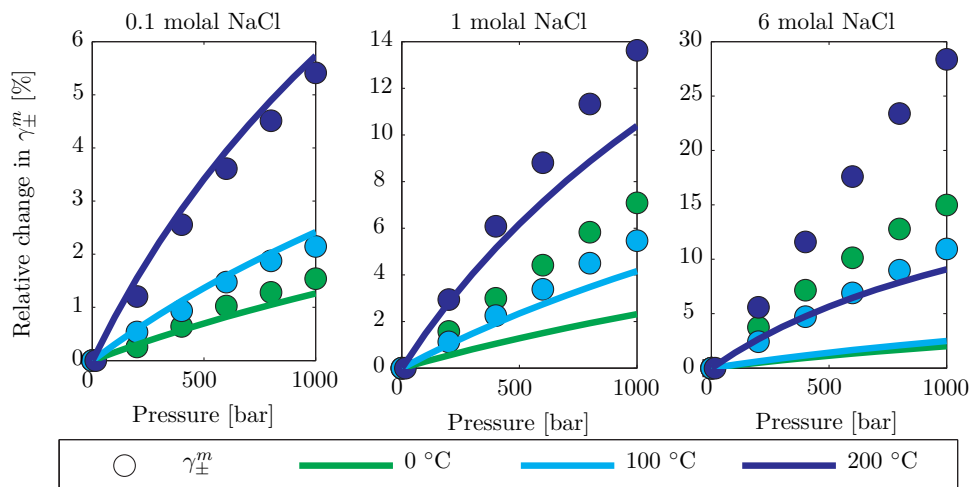
Figure 7.3: Effect of pressure on mean ionic activity coefficients of NaCl in water at 0.1, 1, and 6 molal. Figure shows relative change compared to the solution at the vapor pressure of water (or 1 bar below 100°C).
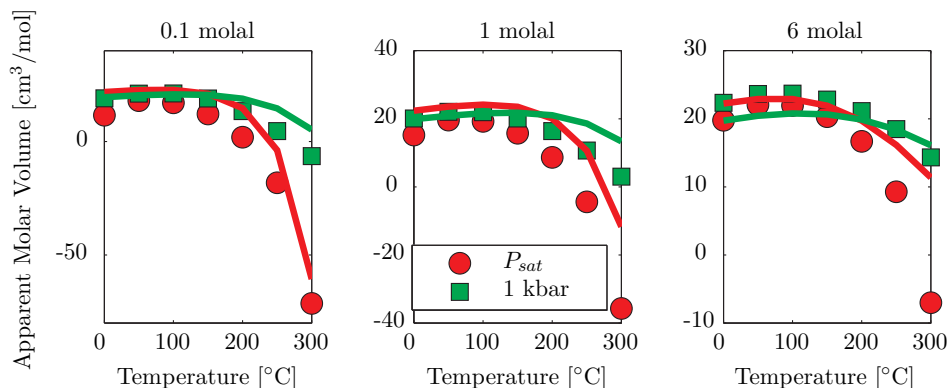
Figure 7.4: Pressure and temperature dependencence of apparent molar volume of NaCl in water at 0.1, 1, and 6 molal.

7.2 Mixed Salt Solid-Liquid Equilibrium and Osmotic Coefficients

As the parameters were obtained by fitting only to pure salt data, it is important to validate how well these parameters work in the case of mixed salts. Figure 7.5 shows the activity coefficients of mixed chloride salts, indicating that the mixed salt solutions are reasonably well described with the ion-specific parameters.
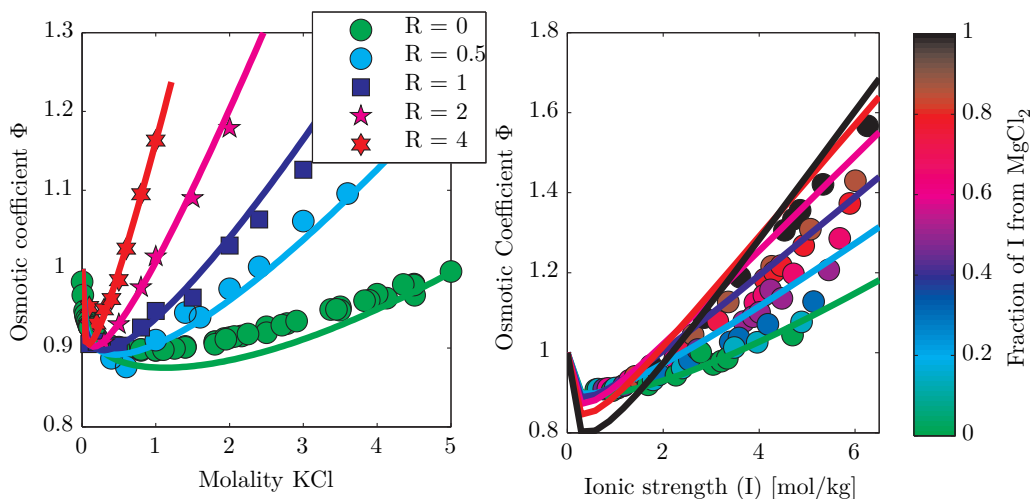
Figure 7.5: Osmotic coefficients in aqueous solution of KCl+NaCl (left) with $R = m_{\text{NaCl}}/m_{\text{KCl}}$ and KCl+NaCl+MgCl$_2$ (right) of mixtures of Water+KCl+NaCl+MgCl at 25°C and R = 0.752. Data from [325].

Figure 7.6 shows the solubility of NaCl as a function of the HCl concentration, as well as the density of the saturated solution. The solubility and density of NaCl are slightly over-estimated, but display reasonable trends and are overall satisfactory.

Figure 7.7 shows the osmotic coefficient of pure NaCl and Na$_2$SO$_4$ calculated from the ion-specific parameters shown in Table 6.11 within a reasonable accuracy. However, a good representation of the pure compounds with ion-specific parameters does **not** guarantee that the mixture is modeled correctly, as evidenced by Figure 7.8 showing the SLE diagram and osmotic coefficients of mixtures of Na$_2$SO$_4$ and NaCl. The salt-specific parameters were determined by setting the size parameter ν_i equal to the co-volume parameter b_i and the salt-water interaction parameter was adjusted to match the solubility of NaCl and Na$_2$SO$_4 \cdot 10$ H$_2$O. The water-ion interaction parameter for Na$^+$ was defined as zero whereas $\Delta U_{iw} = -453.3K$ and $\Delta U_{iw} = 179.9K$ for Cl$^-$ and SO$_4^{2-}$, respectively. This resulted in an excellent representation of the salt mixture, indicating that the model should be capable of handling this.

It is evident from Figure 7.8 that the ion-specific parameters from Table 6.11 fall short and cannot predict the salt mixture. This problem is somewhat surprising, as the ion-specific parameters displayed an excellent performance in the case of the pure salts (see Figure 7.7) and from these results the conclusion must be that pure salt data for osmotic coefficients and activity coefficients are insufficient for the parameterization of ion-specific (or even salt-specific) parameters. It was found that this was especially true when the NRTL/Huron-Vidal volume
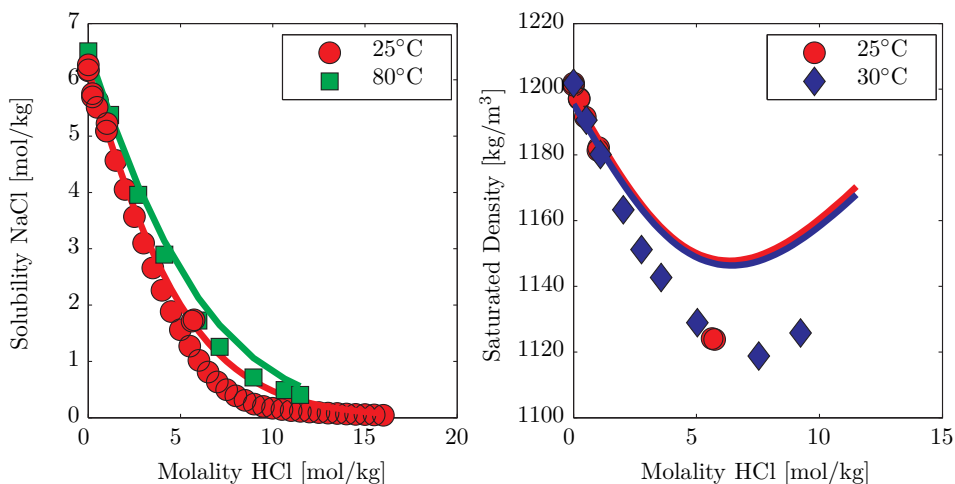
Figure 7.6: Solubility and Density of Saturated Salt Mixtures of NaCl+HCl (Data from [326–328]). Aqueous standard state parameters were as in Figure 7.1.

parameter ν_i was included in the parameter estimation, and while it may improve the correspondence with the osmotic and activity coefficients for the pure salt, it can introduce an unphysical mixing behavior unless mixed salt data is included in the parameter estimation. Therefore, it is recommended that mixed salt and SLE-data should be included in the parameter estimation in the future.

Nevertheless in all following sections the ion-specific parameters from Table 6.11 will be applied, in order to show how the model handles different calculations for single-salt mixtures.

7.3 Salting out of Light Gases and Non-electrolytes

The Cubic Plus Association has been applied to modeling of aqueous and mixed solvent systems with emphasis on hydrocarbons and light gases, such as CO_2, H_2S, and N_2 [1, 82, 83, 172, 202]. Since 2003 the CPA equation of state has been developed in the Joint Industry Project "Chemicals in Gas Processing" (CHIGP) [330] project in terms of modeling, parameterization, and experimental investigation related to vapor-liquid-liquid equilibrium and gas hydrate formation in complex mixtures containing water, oil, natural gas, alcohol, glycols, acid gases, and other chemicals. The parameters obtained in the CHIGP project can be adopted directly for use with the e-CPA model and Table 7.1 summarizes the binary interaction parameters used in this study.

Salts will typically decrease the solubility of gases in water and the magnitude of this decrease is often characterized using the Setschenow constant k_{is}^S of component i in salt s, as defined by Eq. (7.1):

$$k_{is}^S = \lim_{m_S \to 0} \frac{1}{m_S} \log \frac{S_i^0}{S_i} \tag{7.1}$$

The Setschenow constants in different salts have been determined and collected by various authors (see e.g. [331–334]). They are generally tabulated as salt-specific parameters and are
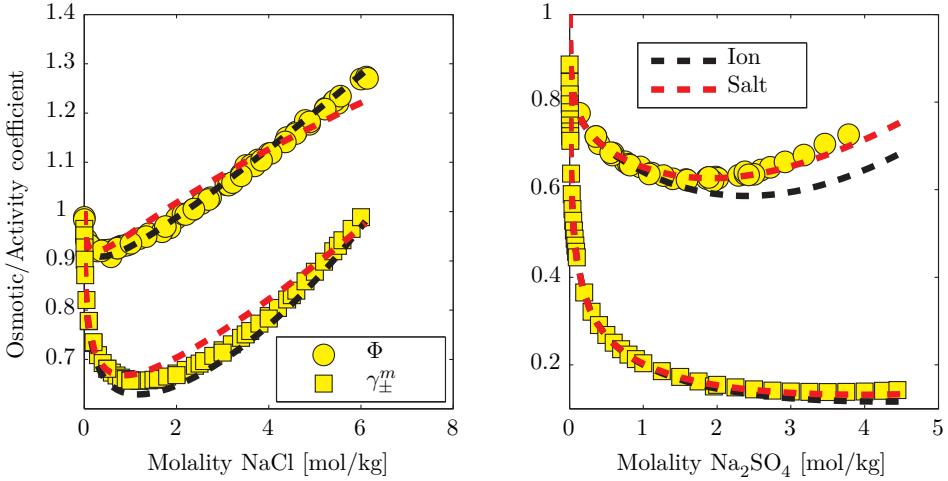
Figure 7.7: Osmotic coefficients of NaCl and Na$_2$SO$_4$ at 25°C. Data from the CERE Electrolyte Database [13]. Legends and ordinate axis apply to both figures. Ion indicates that ion-specific parameters from Table 6.11 were used, whereas Salt indicates that the $\gamma_\pm^m$ parameter was fitted to solubility data for the pure salt in water.

Binary	Binary interaction	Solvation
Water-N$_2$	$k_{ij} = 1.0741 - 368.3/T$	None
Water-CH$_4$	$k_{ij} = 0.7988 - 236.5/T$	None
Water-CO$_2$	$k_{ij} = 0.0046 + 0.331 \cdot 10^{-3}T$	One negative site on CO$_2$
		$\beta_{ij} = 16.4 \cdot 10^{-3}$. $\epsilon_{ij}/k_B = 1707.9$K.
Water-Pentane	$k_{ij} = 0.0615$	None
Water-Octane	$k_{ij} = -0.0165$	None
Water-Benzene	$k_{ij} = 0.0355$	One negative site on Benzene.
		$\beta_{ij} = 79 \cdot 10^{-3}$. m-CR1.
Water-Methanol	$k_{ij} = -0.09$	Elliott combining rule
Water-Ethanol	$k_{ij} = -0.11$	Elliott combing rule
Water-Propan-1-ol	$k_{ij} = -0.08$	Elliott combining rule
Methanol-CO$_2$	$k_{ij} = 0.0479$	One negative site on Benzene.
		$\beta_{ij} = 19.6 \cdot 10^{-3}$. $\epsilon_{ij}/k_B = 1489$K.
Methanol-CH$_4$	$k_{ij} = 0.0528$	None

Table 7.1: CPA binary interaction parameters used in this report. T in K.

therefore not directly applicable to an equation of state based on ion-specific parameters. Nevertheless, Aasberg-Peterson et al. [93] used Setschenow constants at low temperature to develop a predictive scheme for salt-solute interaction coefficients for an electrolyte equation of state.

Perez-Tejeda et al. (1990) attempted to determine ion-specific Setschenow constants [335], which could be used to provide prediction of ion-specific interaction parameters. As this exrcise generally requires knowledge of the solubility in a large number of salts it is beyond the scope of this model validation. As shown in Chapter 6, the binary interaction may (as a first approximation) be defined from salt-specific parameters. This is also possible for salt-solute interactions. While the ion-gas interaction parameters may be improved by including experimental data for different salts, this flexibility of the e-CPA EoS makes it possible to obtain effective ion-specific
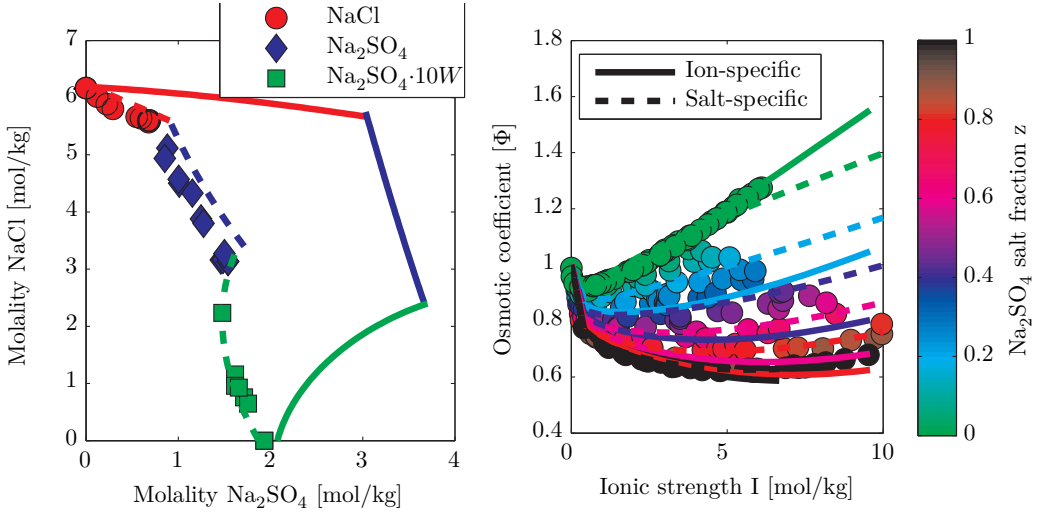
Figure 7.8: Solubility of NaCl, Na$_2$SO$_4$, and Na$_2$SO$_4 \cdot 10\,$H$_2$O and osmotic coefficient of mixtures of NaCl and Na$_2$SO$_4$ at 25°C. Data from the CERE Electrolyte Databank [13] Rard et al. (2003)[329]. The aqueous standard state parameters for ions were taken from Table 4.4. The solid NaCl uses $\Delta_f G^o = -384.14$kJ/mol, $\Delta_f H^o = -411.15$ kJ/mol and $C_p = 50.5$ J/mol/K, solid Na$_2$SO$_4$ uses $\Delta_f G^o = -1270.2$kJ/mol, $\Delta_f H^o = -1387.1$ kJ/mol and $C_p = 128.2$ J/mol/K, and finally the Glauber salt Na$_2$SO$_4 \cdot 10\,$H$_2$O uses $\Delta_f G^o = -3646.9$kJ/mol, $\Delta_f H^o = -4327.3$ kJ/mol and $C_p = 492.2$ J/mol/K. Ion indicates that ion-specific parameters from Table 6.11 were used, whereas Salt indicates that the ΔU_{iw} parameter was fitted to solubility data for the pure salt in water.

parameters from the salt-specific parameters using Eq. (7.2):

$$\frac{\Delta U_{sg}}{RT} = \frac{v_a\,(b_g + \nu_a)}{(v_a + v_c)\,b_g + v_c\nu_c + v_a\nu_a}\frac{\Delta U_{ag}}{RT} + \frac{v_c\,(b_g + \nu_c)}{(v_a + v_c)\,b_g + v_c\nu_c + v_a\nu_a}\frac{\Delta U_{cg}}{RT} \tag{7.2}$$

Salting out constants used in this study are summarized in Table 7.2, and Figure 7.9 shows the linear correlation between $\Delta U_{sg}/R = u_{sg}^0$ and the Setschenow coefficient.
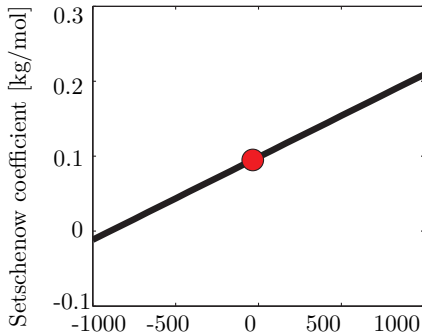
Figure 7.9: The effect of ΔU_{SG} (solid line) on k_S for CO$_2$ in NaCl and exp. $k_s = 0.095$ kg/mol.

Solute	k_{is}^S @ 25°C [kg/mol]	$\Delta U_{sg}/R$ [K]
	NaCl	
N$_2$	0.134	453.4
CH$_4$	0.139	376.6
CO$_2$	0.095	-34.30
Pentane	0.221	-240.9
Benzene	0.195	-203.8
Toluene	0.235	-243.2
	CaCl$_2$	
CO$_2$	0.375	305.3

Table 7.2: Salting out constants for selected salts and solutes [332, 333, 335, 336]

By matching the Setschenow coefficient of CO_2 in NaCl and $CaCl_2$, the e-CPA EoS shows excellent predictions of the solubility at elevated temperatures and pressures as shown in Figure 7.10-7.11. It is evident that the solubility is systematically underestimated and the degree of under-estimation increases with the salt concentration, indicating that adjusting the salt-gas interaction coefficient could improve the results. The same procedure was used to calculate the solubility of N_2 and CH_4 in water+NaCl (see Figure 7.13). Figure 7.12 shows that this method can also be used for hydrocarbons and aromatics. Overall, it may be concluded that the e-CPA provides satisfactory predictions. The results may in all cases be improved by fitting the interaction parameters to experimental data (including e.g. a temperature dependence).
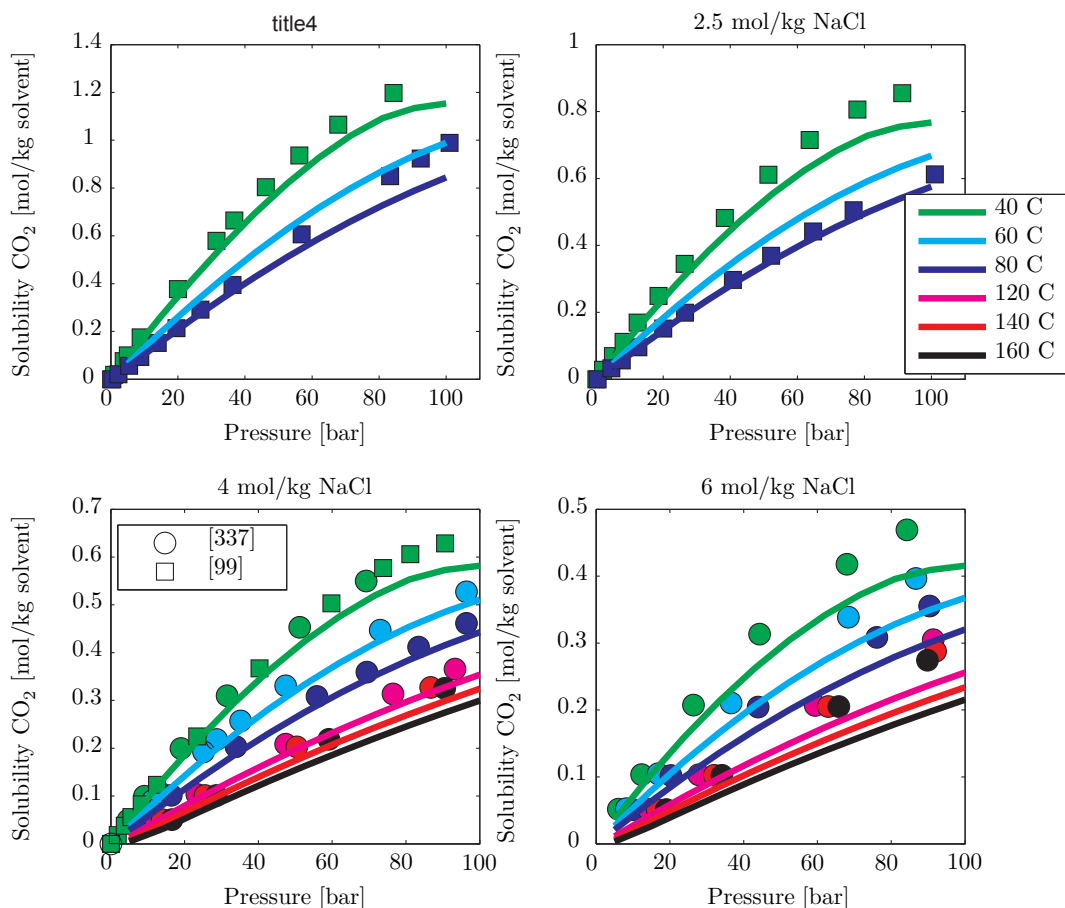
Figure 7.10: Solubility of CO_2 in Water with 0.5, 2.5, 4, or 6 mol/kg NaCl from 40-160°C. Data from Rumpf et al. [337] and Kiepe et al. (2002) [99]. The deviations are significantly larger at high salt concentrations, indicating that the salt-water interaction coefficient may be improved. Legends apply to all figures.
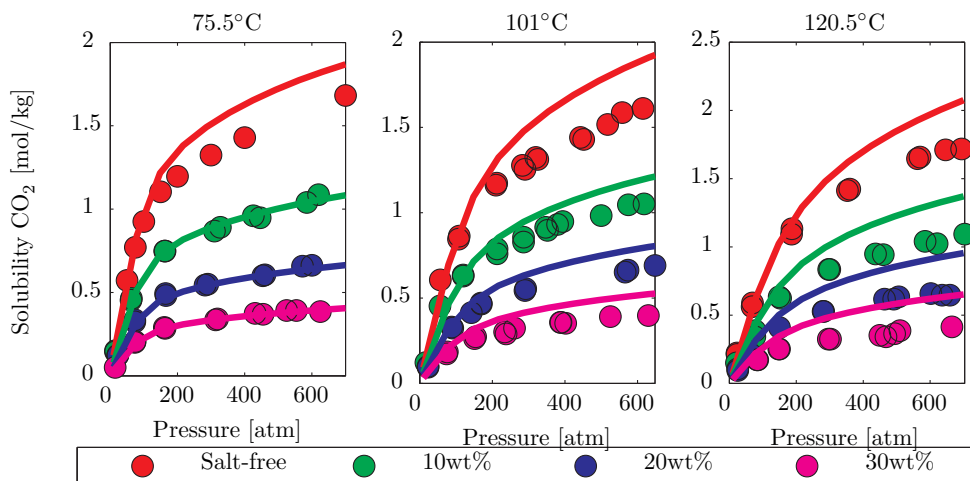
Figure 7.11: Predicted solubility of CO_2 in Water+$CaCl_2$. Data from Prutton and Savage (1945) [338] and Wiebe and Gaddy (1940) [339].
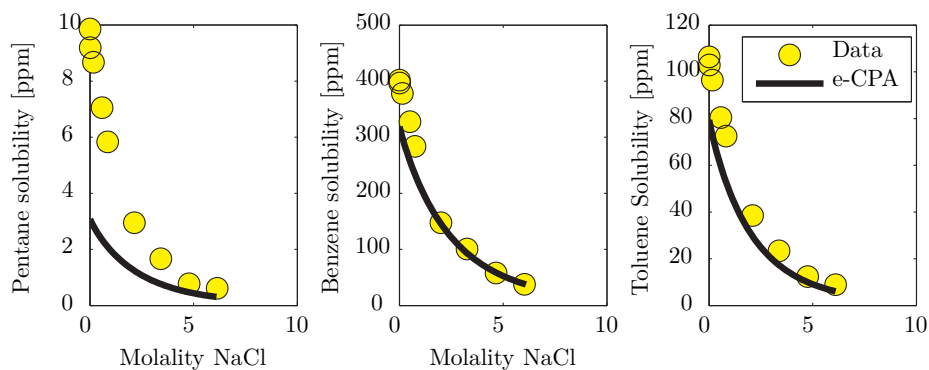
Figure 7.12: Solubility of pentane, benzene, and toluene in Water+NaCl at 25°C. Data from Price (1976) [340].
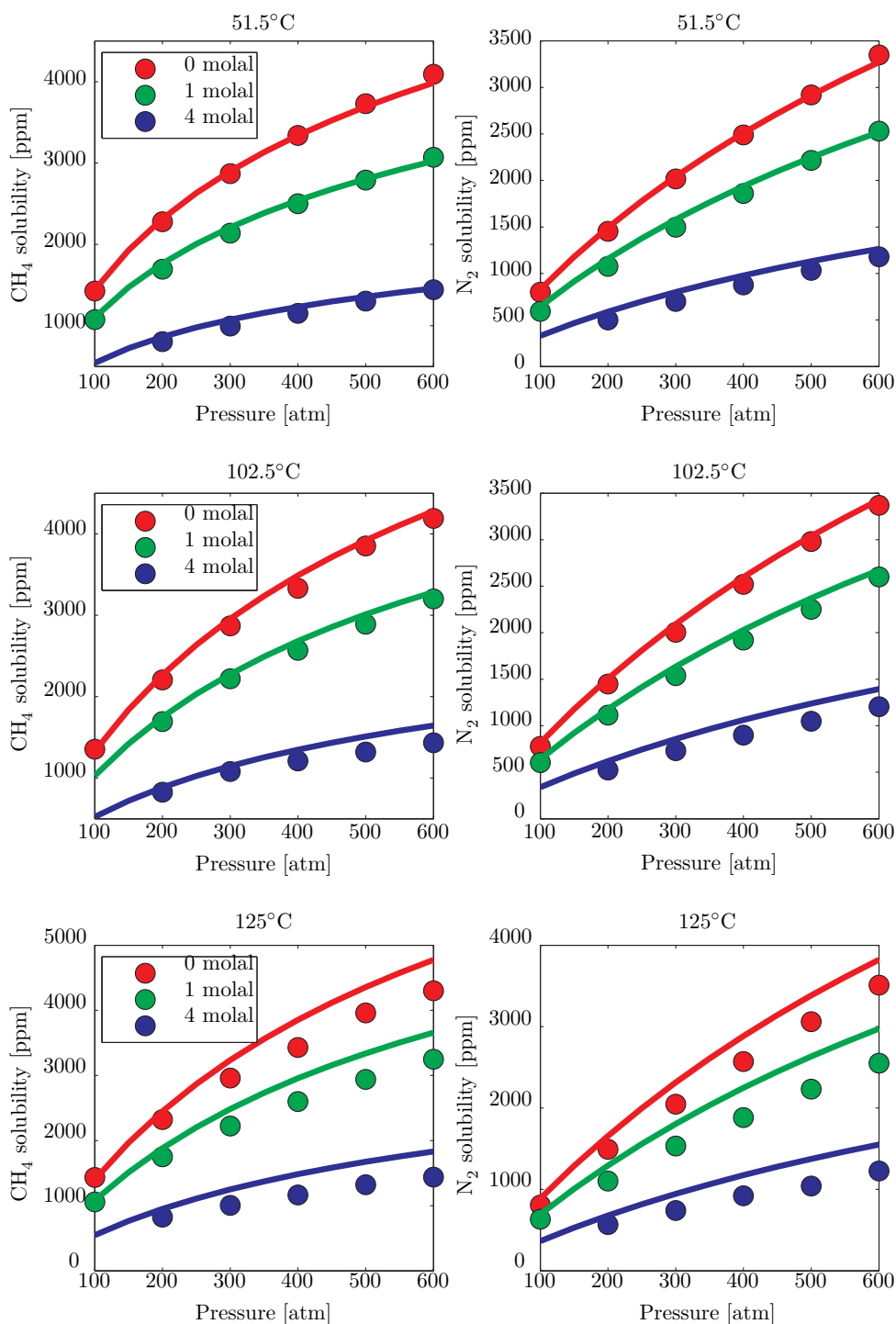
Figure 7.13: Solubility of methane and nitrogen in Water+NaCl at 51.5, 102.5, and 125°C and with 0, 1 and 4 mol/kg NaCl. Data from O'Sullivan and Smith (1970) [341].

7.3.1 Mixed Solvents

As shown in Chapter 5, the electrolyte CPA model coupled with the new model for the static permittivity provides an excellent representation of the static permittivity of mixtures, making it suitable for mixed-solvent electrolyte applications. When dealing with mixed solvents, there is limited data concerning mean molal activity coefficients or osmotic coefficients. The most common data available at elevated temperatures is in fact solid-liquid equilibrium. The solubility of the salt in the pure solvent is used to predict the salt-solvent interaction parameters. The solubility of NaCl and NaBr in methanol and ethanol are summarized in Table 7.3: The salt-

Solvent	Methanol		Ethanol	
	Solubility [wt%]	$\Delta U_{sa}/R$ [K]	Solubility [wt%]	$\Delta U_{sa}/R$ [K]
NaCl	1.375	-344.9	0.055	-167.1
NaBr	14.938	-706.6	2.496	-626.3

Table 7.3: Solubility of different salts in water, methanol, and ethanol at 25°C [342] and the calculated salt-alcohol interaction coefficient ΔU_{sa}. The aqueous standard state parameters for ions are shown in Table 4.4. The solid NaCl uses $\Delta_f G^o = -384.14$kJ/mol, $\Delta_f H^o = -411.15$ kJ/mol and $C_p = 50.5$ J/mol/K, and solid NaBr uses $\Delta_f G^o = -350.83$kJ/mol, $\Delta_f H^o = -362.51$ kJ/mol and $C_p = 51.4$ J/mol/K [13].

alcohol interaction coefficient is calculated using the solubility of the salt in the pure solvent, which provides quite satisfactory predictions of the solubility in the mixed solvent as shown in Figure 7.14 and 7.15. While the temperature dependence is reasonable for NaCl, the solubility of NaBr at 50°C in pure water or methanol is not predicted satisfactorily, which also affects the solubility in the mixed solvent. Figure 7.16 shows that the e-CPA model can also predict the solubility of NaCl and NaBr in the non-aqueous mixture of methanol and ethanol.
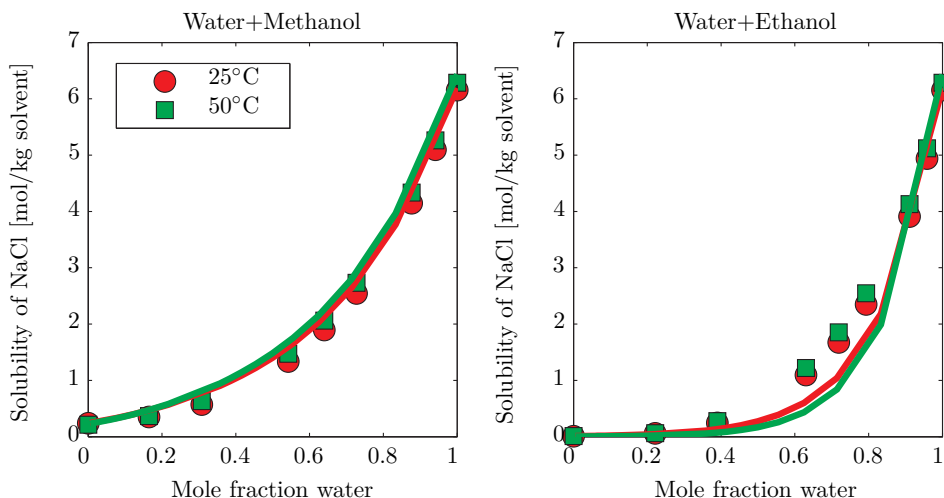
Figure 7.14: Solubility of NaCl in water with methanol and ethanol. The salt-alcohol interaction parameter was fitted to data for pure methanol/ethanol at 25°C and the solubility in the mixture is predicted by the model (see Table 7.3). Data from Pinho and Macedo (1996) [343].
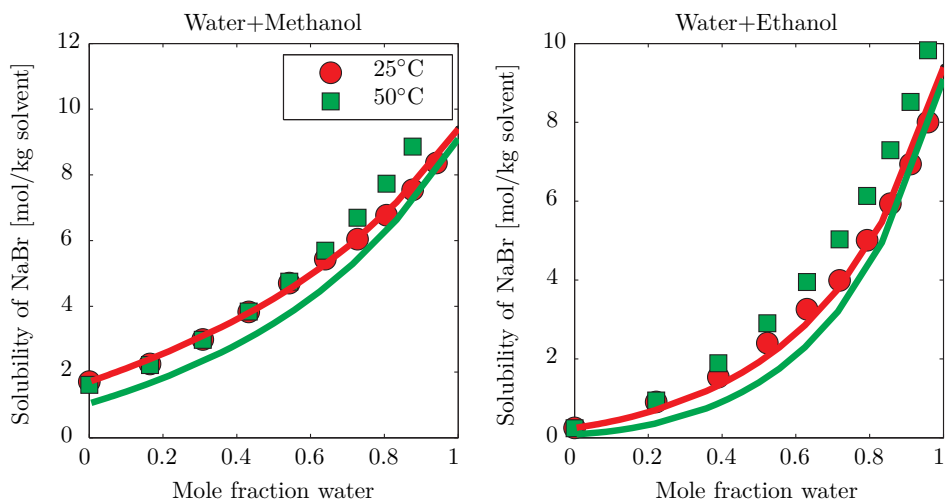
Figure 7.15: Solubility of NaBr in water with methanol and ethanol. The salt-alcohol interaction parameter was fitted to data for pure methanol/ethanol at 25°C and the solubility in the mixture is predicted by the model (see Table 7.3)l. Data from Pinho et al. (1996, 2005) [342, 343].
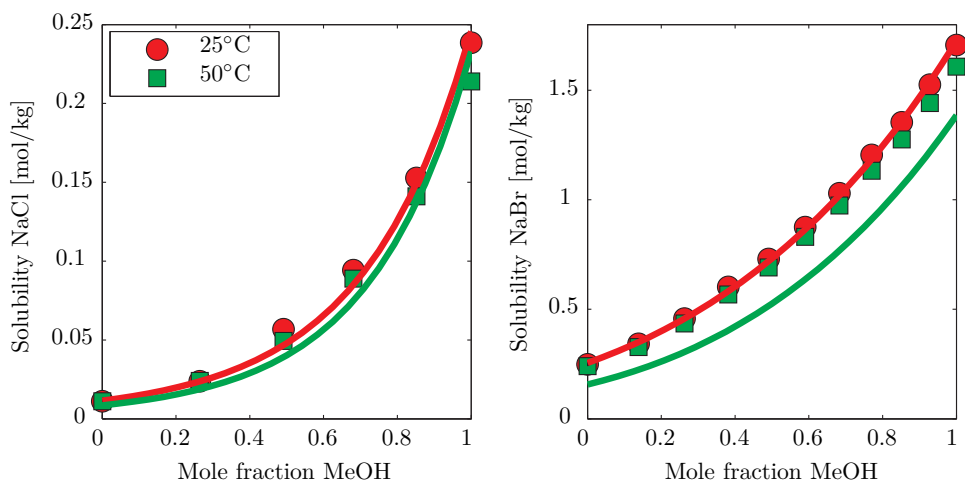
Figure 7.16: Solubility of NaCl and NaBr in (non-aqueous) mixtures of methanol and ethanol. The salt-alcohol interaction parameter was fitted to data for pure methanol/ethanol at 25°C and the solubility in the mixture is predicted by the model (see Table 7.3). Data from Pinho et al. [342].

7.3.2 Solubility of CO₂ in Water+Methanol

Once all interaction parameters have been established for NaCl-methanol, and NaCl-CO₂ it is possible to predict the solubility in a mixed solvent consisting of water + methanol. The results are summarized in Figure 7.17 showing that the model captures all trends within an acceptable accuracy for the gas solubility. However, it also appears that the mixtures containing significant parts of methanol and NaCl over-estimates the solubility of CO₂. While the situation could

possibly be improved through parameter optimization, it could also mean that a more detailed chemical treatment that includes the speciation of CO_2 and ion pairing of NaCl in the mixed solvent would be needed to provide satisfactory predictions. Further validation is also needed for the CO_2-water and CO_2-methanol interaction and cross-association parameters in order to eliminate errors in the representation of the solubility in the mixed solvent. Future investigations must also include the solubility in other mixed solvent solutions and with other gases and salts to see if this discrepancy is a general problem.

7.3.3 Gas Hydrate Formation Pressure

As a final application of the e-CPA model, this section presents calculations for the gas hydrate dissociation pressure with a structure I methane clathrate. The calculation procedure is identical to that of Folas [202], and will only be presented in brief. The hydrate phase is calculated from the van der Waals-Platteeuw model, in which the fugacity of water in the hydrate phase can be calculated using Eq. (7.3):

$$f_w^H = f_w^{EH} \exp\left(\frac{\mu_w^H - \mu_w^{EH}}{RT}\right) \tag{7.3}$$

The fugacity of water in the empty hydrate may be calculated from Eq. (7.4):

$$f_w^{EH} = P_w^{EH} \phi_w^{EH} \exp\left(\int_{P_w^{EH}}^{P} \frac{V_w^{EH}}{RT} dP\right) \tag{7.4}$$

In which P_w^{EH} is the vapor pressure of the empty structure I hydrate in [atm] is calculated from Eq. (7.5) from Sloan [345] and the volume of the structure I hydrate phase in [cm^3/mol] is calculated from Eq. (7.6) from Avlonitis (1994)[346]:

$$\ln P_w^{EH} = 17.44 - \frac{6003.9}{T} \tag{7.5}$$

$$V_w^{EH} = \quad 22.35 + 3.1075 \cdot 10^{-4} (T - 273.15) + 5.9537 \cdot 10^{-7} (T - 273.15)^2$$
$$+ 1.3707 \cdot 10^{-10} (T - 273.15)^3 \tag{7.6}$$

The change in chemical potential from the empty hydrate to the hydrate with CH_4 as a guest molecule is calculated from Eq. (7.7):

$$\frac{\mu_w^H - \mu_w^{EH}}{RT} = v_s \ln\left(1 - \Theta_{CH_4}^s\right) + v_l \ln\left(1 - \Theta_{CH_4}^l\right) \tag{7.7}$$

Where v_s and v_l are the number of cavities per water molecule ($v_s = 1/23$ and $v_l = 3/23$ for structure I hydrates). $\Theta_{CH_4}^s$ and $\Theta_{CH_4}^l$ denote the occupancy of the large and small cavities, and are in the case of a single gas calculated from the Langmuir-equation in Eq. (7.8).

$$\Theta_{CH_4} = \frac{C_{CH_4} f_{CH_4}}{1 + C_{CH_4} f_{CH_4}} \tag{7.8}$$

The Langmuir constant C_{CH_4} is calculated from the simplified method by Parrish and Prausnitz [347] that uses different parameters for the small and large cavities using the parameters from Karakatsani [348]:

$$C_{CH_4}^s = \frac{1}{T} \exp\left(\frac{1970}{T}\right) \qquad C_{CH_4}^l = \frac{0.316}{T} \exp\left(\frac{2048}{T}\right) \tag{7.9}$$

Calculations for the gas hydrate formation pressure with structure I methane clathrate were performed and they are summarized in Figure 7.18 showing excellent predictions of the gas hydrate formation pressure, even in a mixed solvent with water, methanol, and NaCl.
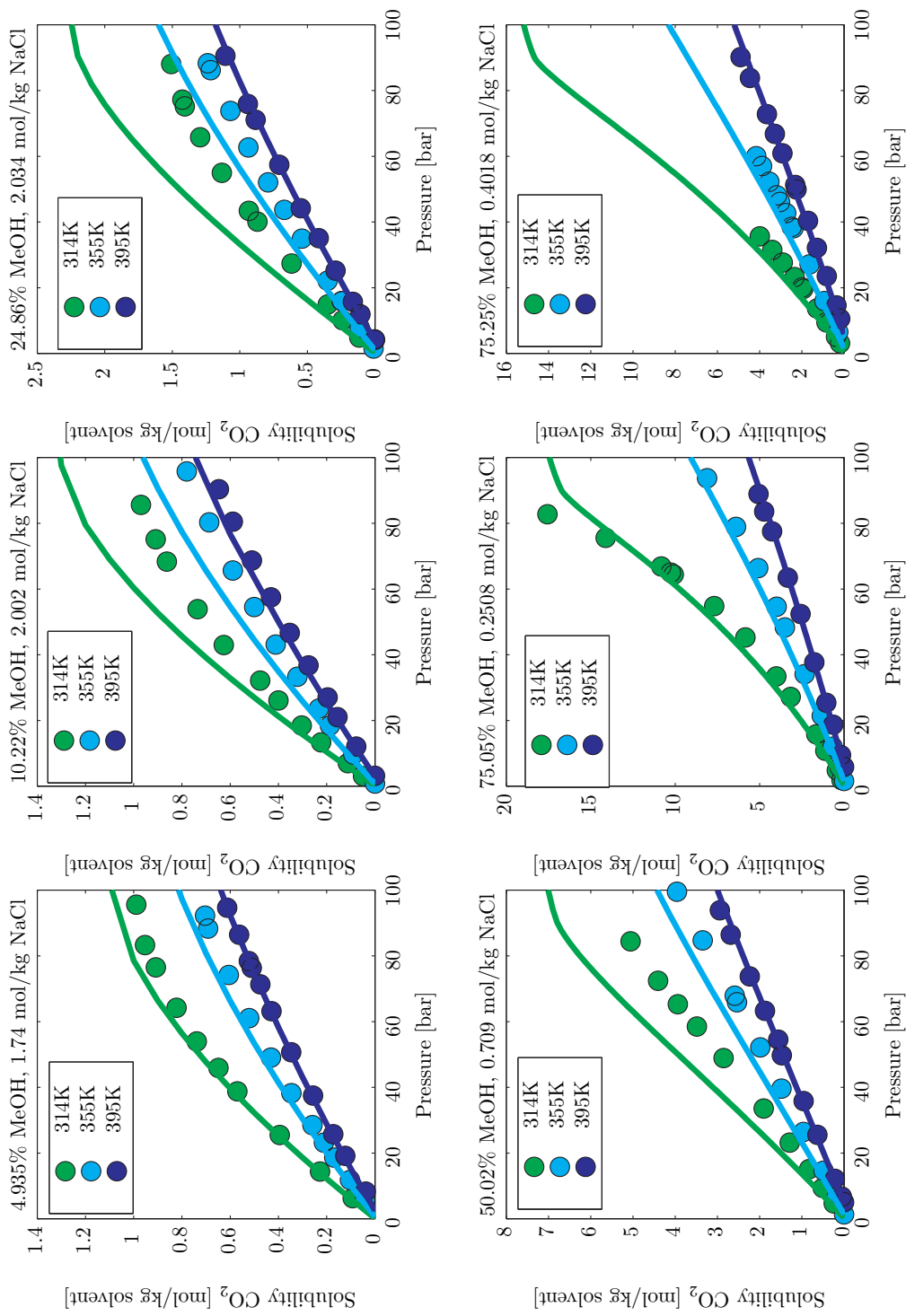
Figure 7.17: Predicted solubility of CO_2 in mixtures of NaCl, water, and methanol. Data from Pérez-Salado Kamps et al. [344].
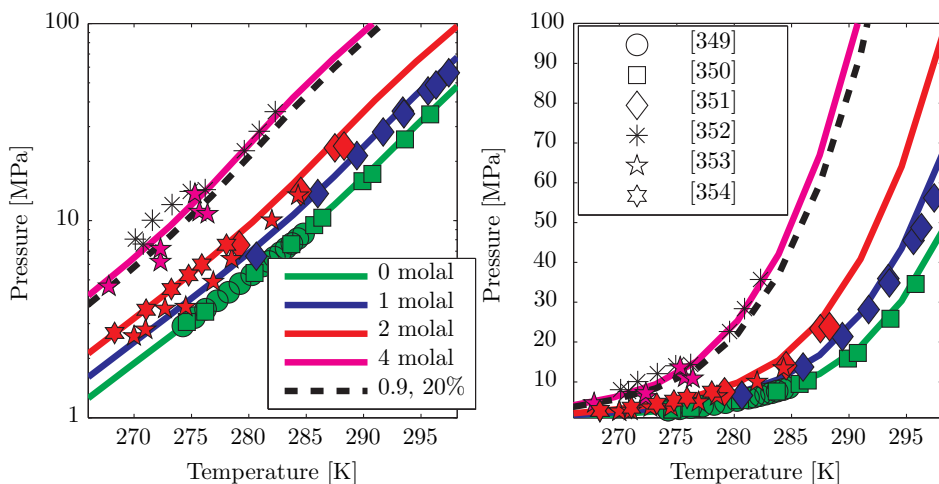
Figure 7.18: Effect of NaCl on CH_4 structure I gas hydrate formation pressure. The black line consists of 20wt% methanol with 0.9 mol/kg NaCl. Data was obtained from the NIST Hydrate Database [355].

7.4 Salt Effect on Liquid-Liquid Equilibrium

Salts may induce a two-phase liquid-liquid split in an otherwise miscible solution of water + alcohol. This peculiar effect was first reported by Timmermans [356] in 1907 and analyzed by Frankforter and Frary (1913) [357]. The e-CPA results with the system water+propan-1-ol+NaCl shown in Figure 7.19-7.20 using the salt-propanol interaction coefficient $\Delta U_{sp}/R = -86.28$K predicted from the solubility of NaCl in propanol (0.124 g/kg)
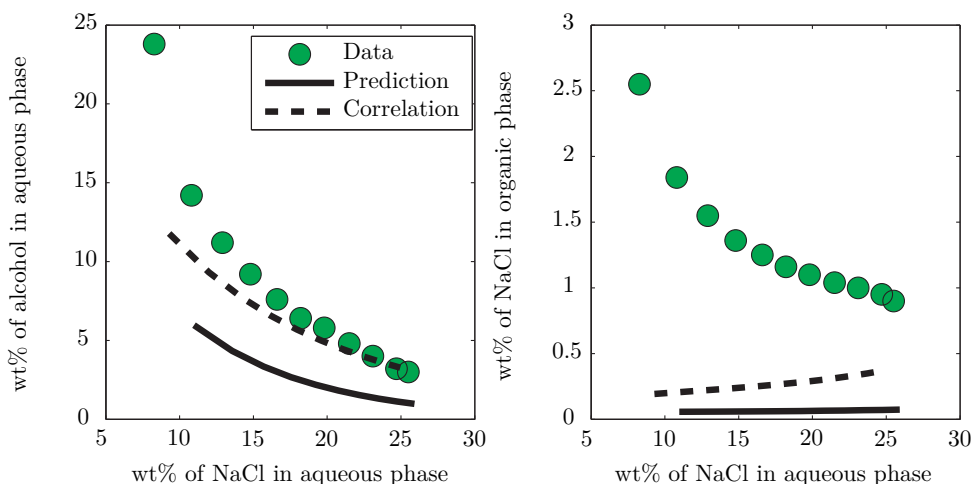
Figure 7.19: Distribution of NaCl and propanol in LLE at 25°C. Data from de Santis et al. (1976) [358].
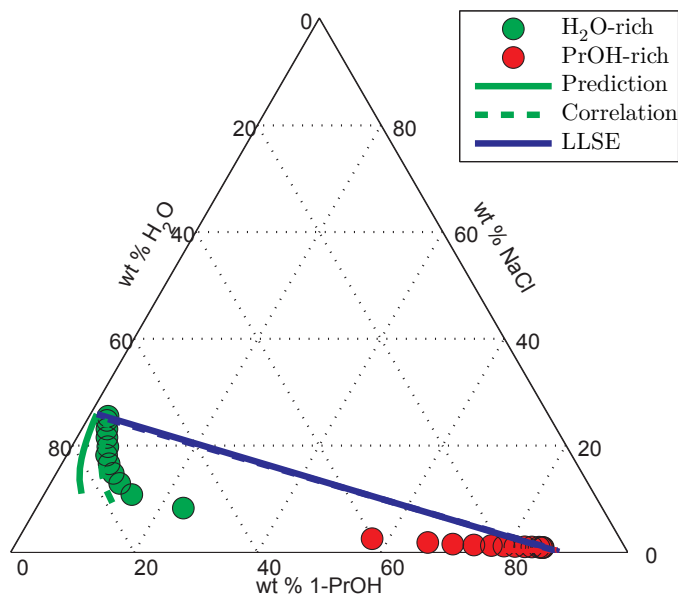
Figure 7.20: Salt-induced liquid-liquid equilibrium of water and propanol at 25°C. Data from de Santis et al. (1976) [358].

The situation may be alleviated by adjusting either the water-propanol interaction coefficient/association parameters to the liquid-liquid data, rather than the vapor-liquid data which was used to estimate the current value of the binary interaction parameter. In this case, the propanol-salt interaction coefficient was adjusted to give a better representation of the experimental data for the liquid-liquid equilibrum $\Delta U_{sp}/R = -450$K. Still, as evident from Figure 7.19, the model fails to obtain a good description of the solubility of salt in the polar phase, indicating that the model should be extended to include ion-ion association, which is expected be more prevalent in the propanol-rich phase than in the water-rich phase due to the lower static permittivity.

Salts may also cause the appearance and disappearance of phases in multicomponent mitxures. While the data is scarce, measurements of the water-propan-1-ol-NaCl-octane mixture was performed by Negahban et al. (1986) [359]. They mixed equal volumes of water, propanol, and octane at 25°C and added NaCl after which measurements of the distribution of chemicals was conducted. In order to model this system, the propanol-octane binary interaction coefficient k_{ij} was correlated to experimental data as shown in Figure 7.21.

Furthermore, the n-octane-NaCl Setschenow constant was estimated to be $k_s = 0.321$mol/kg by extrapolating the data for the C1-C6 alkanes, from which the salt-octane interaction coefficient $\Delta U_{os}/R = -451.5$K was obtained. Figure 7.22 shows the distribution of chemicals in the two- or three-phase equilibrium predicted by e-CPA. A relatively poor agreement with the solubility of propanol in the octane-rich phase is obtained if the k_{ij} for octane-propanol based on vapor-liquid equilibrium is used. If the k_{ij} is adjusted to -0.0065 good agreement with all phases can be obtained (this does not affect the VLE much in comparison to the pure prediction
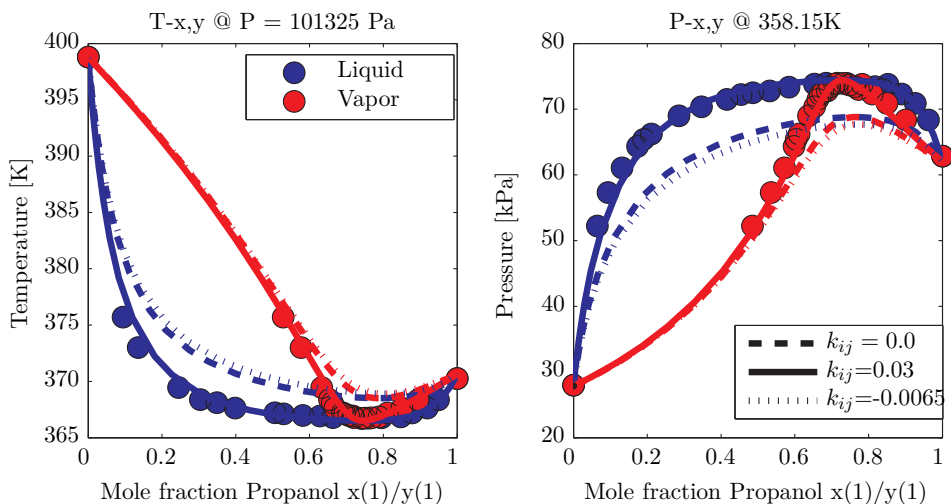
Figure 7.21: Correlation of Propanol-Octane Vapor-Liquid Equilibrium. Data from [360, 361].

$k_{ij} = 0$ as evident from Figure 7.21. It is not unusual that the k_{ij} from liquid-liquid equilibrium differs from the optimal vapor-liquid equilibrium k_{ij}, but it requires further investigations on the parameters for the salt-free mixtures in order to determine whether adjusting the k_{ij} can be justified. The result after adjusting the k_{ij} parameter is quite satisfactory with this type of data, as e-CPA can not only catch the three-liquid equilibrium, but also the range of salt concentrations where the three phases exist. Still, the amount of water in the octane-rich phase is greatly underestimated by e-CPA, which could be due to the k_{ij} of water-propanol being adopted from vapor-liquid equilibrium data. In order to shed further light on this complex system, it is suggested to perform a more detailed investigation of the distributions in water-alcohol-alkane liquid-liquid equilibrium systems in the absence of salts. While such investigations have been done extensively for water-methanol in the past, less work has been done targeting alcohols such as propanol and butanol.

7.5 Summary and Discussion

In this chapter, the electrolyte CPA approach was validated against data not included in the parameter estimation. The model investigated was the simplest formulation of an electrolyte CPA equation of state that was based on the Debye-Hückel and Born terms for electrostatics and using the new theory for the static permittivity and neglects ion-solvent association as well as ion-ion association. While the model has an approximate description of the physical interactions, the results show that the model is still capable of providing a good description for a variety of applications, especially for vapor-liquid equilibrium and gas hydrate formation pressures in mixed solvents.

As discussed in Chapter 1, Cobble and Murray (1981) suggested that structural effects will be dominating at low temperatures, where as the electrical field (and therefore the static permittivity) will provide the main contribution to the thermodynamic behavior of electrolyte solutions at high temperatures. In the intermediate region near room temperature both effects will play a role. The results in Figures 7.3-7.4 fits well in this picture as the model was shown to give a good description of the pressure-dependence of the activity coefficients, excess enthalpy and apparent molar volumes with increasing deviation at low temperatures where the struc-
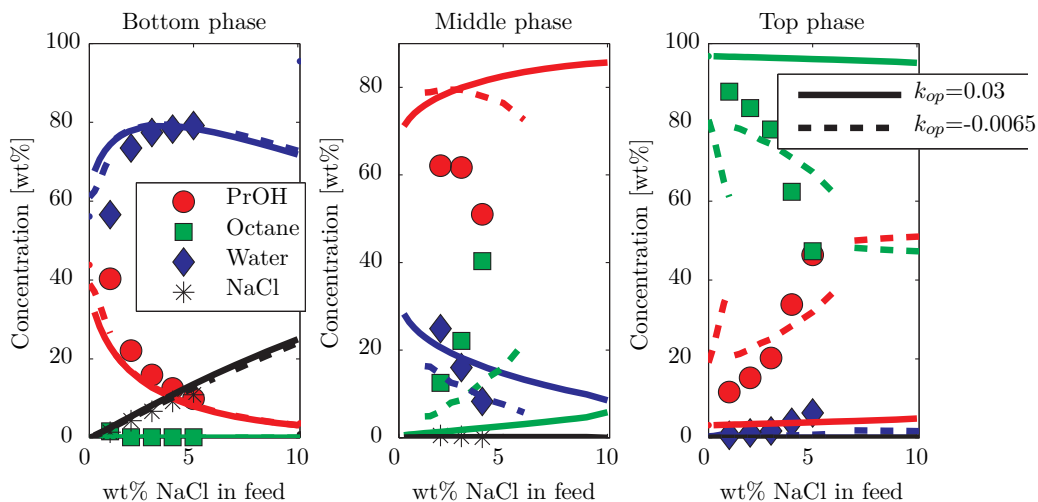
Figure 7.22: Distribution in three-liquid equilibrium with NaCl+propanol+water+octane to the calculated solubility limit of NaCl (ca. 10.5 wt%). Data from Negahban et al. (1986) [359].

ture of the fluid becomes dominating. Deviations were also higher in concentrated solutions, which may be related to the simplified description of the reduction in the static permittivity as discussed in Chapter 6. In order to justify the inclusion of ion-solvent association in a future version of the electrolyte CPA EoS, it must be shown to improve the pressure-dependent properties.

The ion-specific parameters developed in Chapter 6 were shown to work satisfactorily for mixed chloride salts in Figures 7.5-7.6 but failed to provide a good description of a mixture of NaCl-Na_2SO_4 (see Figure 7.8), despite a good description of the osmotic coefficients and activity coefficients of the pure salts (see Figure 7.7). However, it was shown that this is not a defect of the model but rather of the ion-specific parameters, since simple salt-specific parameters estimated solely from the solubility of the pure salts provided an excellent prediction of the mixed salt SLE. It is evident that more work is needed in order to improve the parameterization of the model, and it is recommended that future approaches would also include solid-liquid equilibrium of mixed salts.

The remaining modeling work was focused on validating the model for single-salt solutions and therefore utilized salt-dependent interaction parameters. A complete electrolyte CPA model should use ion-specific parameters and ion-specific interaction parameters with solute compounds, but in this work the focus was on validating the approach for many possible applications to identify other weaknesses in the presented model. The results were based on the ion-specific parameters, as these would still provide a good description in the absence of other salts.

It was shown that the Setschenow coefficients for salting out of non-electrolytes at 25°C, 1 bar provided an excellent basis for defining the salt-solute interaction coefficients, which could be used to predict the gas solubility up to high temperatures and pressures (see Figures 7.10-7.13). Excellent predictions are obtained (at least up to 4 molal solutions), but these may in the future also be improved by adjusting the salt-solute interaction coefficient to the experimental data, and possibly by defining temperature-dependent parameters.

By fixing the salt-alcohol interaction coefficient to the solubility of the salt in pure alcohol, the model is capable of predicting the solubility in the water-alcohol mixture or even a non-aqueous mixture of two alcohols as evident from Figures 7.14-7.16 without fitting additional parameters. The temperature dependence of the solubility in the mixed solvent could however not be predicted from the solubility at 25°C, and requires further parameterization. While other groups have succesfully correlated the salt solubility in mixed solvents, only Simon et al. (1991) [92] have shown a similar prediction without introducing additional solvent-dependent parameters.

Using the NaCl-CO$_2$ and NaCl-methanol interaction parameters estimated from Setschenow coefficients and salt solubility, respectively, it was possible to predict the solubility of CO$_2$ in a mixed solvent of water+methanol with NaCl as shown in Figure 7.17. While the model captures the trends of the system, the modeling results show some unsatisfactory deviations in the mixed solvent at high salt concentrations, and further work is needed to determine the source of this error. This defect could be related to the model parameters, experimental data, or be due to a more fundamental problem with the model that requires further improvements of the physics of the model.

In Figure 7.18, the e-CPA model was also used to calculate the gas hydrate formation pressure for the structure I methane hydrate. It was shown to give excellent predictions of the effect of salts and mixed solvents on the formation pressure of the hydrate. Generally, it seems that the model provides good predictions of vapor-liquid equilibrium and may also be applied to solid-liquid equilibrium. The temperature dependence of the model must however be improved/correlated in order to provide a satisfactory representation of solid-liquid equilibrium.

Activity coefficient models such as electrolyte NRTL, Extended UNIQUAC, and the OLI Mixed Solvent Electrolyte have all been applied to modeling of liquid-liquid equilibrium systems of water+alcohol, whereas only a few electrolyte EoS have been used for this type of application (e.g. Gmehling et al. (2006) [102], and Sadowski et al. (2013) [120]). In all cases, additional parameter estimation has been necessary to provide a good description of liquid-liquid equilibrium. The e-CPA model was shown to predict a liquid-liquid phase split of water-propanol-NaCl. The model was however shown to underpredict the amount of propanol in the aqueous phase, and also the amount of salt in the propanol-rich phase. The situatoin could be improved by modifying the propanol-NaCl interaction coefficient, but this did not significantly improve the distribution of salt between the water and alcohol phases. This problem indicates that ion pairing is required in order to properly predict the liquid-liquid equilibrium. The neutral ion pairs will be more prevalent in the propanol-rich solution as it has a lower static permittivity. The effect of ion pairing will increase the solubility of NaCl in the least polar phase.

Finally, the model was applied to a three liquid-phase equilibrium of water-propanol-octane-NaCl. The system is very sensitive to the interaction parameters, and it was shown that the k_{ij} for propanol-octane derived from vapor-liquid equilibrium data did not result in a satisfactory agreement with the solubility of propanol in the octane-rich phase. Furthermore, the solubility of H$_2$O in the octane phase was also under-estimated, indicating that the water-propanol k_{ij} may not be optimal for this system. Further work should investigate the mutual solubilities in salt-free ternary solutions of water-alcohol-alkane to validate the current CPA parameters for this type of phase equilibrium. The next step will then involve improving the distribution of salt in the liquid-liquid equilibrium for water-alcohol-salt mixtures; presumably by accounting for the effect of ion-ion association.

Chapter 8

Conclusion and Future Work

8.1 Conclusion

An electrolyte extension of the Cubic Plus Association equation of state has been developed during the course of this PhD project. A comprehensive literature review revealed that while the field of electrolyte equations of state had been investigated by many groups over the past thirty years, it had not yet reached a concensus on the approach needed to develop an electrolyte equation of state. A systematic research effort was therefore performed in order to harmonize the approach to modeling of electrolyte mixtures within an equation of state. During this work, it was shown that:

- Electrostatic interactions can be modeled through primitive and non-primitive electrolyte models. The full Debye-Hückel equation yields similar results as the implicit non-restricted mean spherical approximation [161]. A complete model should also take into account ion-ion association and the dipole-charge interactions between ion pairs and free ions.

- The static permittivity is the most important property for primitive electrolyte models. It should be seen as a shielding effect for the Coulombic interactions in the fluid, and is a property that depends on all components in the mixture. A simple correlation of the static permittivity may not provide the correct physical behavior, which can impact the performance of the EoS, and possibly introduce non-physical volume roots.

- Conversion from the McMillan-Mayer to the Lewis-Randall framework is not needed when a physical model is used for the static permittivity that takes into account all components in the mixture and thereby indirectly provides a description of the direct correlation functions of all molecules in the mixture.

- The EoS must include a model for the Gibbs energy of hydration, such as the Born model. This model provides the main driving force at infinite dilution for ions towards the most polar phase, and none of the other terms of the equation of state can provide a similar description of the fugacity coefficient at infinite dilution.

- Ion-solvent association is important for representing the partial molar volumes of electrolytes as well as the decrease in the static permittivity with the salt concentration. Ion-ion association is more prevalent in solutions with a low static permittivity and reduces the effective ionic strength of the mixture.

A new model was developed to predict the static permittivity as a function of temperature, pressure, and composition [162, 163]. In this work, the Onsager-Kirkwood-Fröhlich framework for the static permittivity was extended to handle associating compounds. When this new model is coupled with a modern equation of state that explicitly accounts for association and

hydrogen bonding, it provides an excellent basis for correlating the permittivity of pure compounds using 1-2 parameters. The static permittivity of binary and ternary mixtures was then predicted (without adjusting any parameters) over wide ranges of temperature, pressure, and composition. By accounting for ion-solvent association the model could also predict the decrease in the static permittivity caused by the presence of salts.

The simplest possible electrolyte extension to the CPA equation of state was parameterized for 16 ions and 55 salts. It was shown that volumetric data required a Peneloux volume translation term when the model neglects ion-solvent association. It was also shown that the Huron-Vidal/NRTL mixing rule could be used to enable the use of the model with either salt- or ion-specific parameters. The ion-specific parameters were shown to not always give good predictions for mixed anions, in spite of the model having good agreement with the experimental data for pure salts.

It was shown that Setschenow coefficients at 25°C and 1 bar could be used to determine salt-solute interaction parameters. When the interaction parameter had been determined, the simple model provided quite satisfactory predictions of the solubility of light gases, hydrocarbons, and aromatics as a function of temperature, pressure and salt concentration.

For mixed solvent applications, the alcohol-salt interaction parameter was fitted to the solubility of a salt in the pure alcohol at 25°C. Using this approach it was possible to predict the solubility in a mixture of water+alcohol or even the non-aqueous mixture of methanol+ethanol, but the temperature dependence was not accurately predicted by this approach requiring further investigations. Reasonable predictions were obtained when the model was used to calculate the CO_2 solubility in a mixture of water, methanol, and NaCl, but some discrepancy was observed in the more concentrated solutions. The model was also shown to give excellent predictions for the gas hydrate formation pressure for the methane structure I hydrate. All in all, the model shows good potential for applications to phase equilibrium and gas hydrate formation in relation to oil and gas production.

The model was also tested against liquid-liquid equilibrium in the system containing water, propan-1-ol, and NaCl. It was shown that while the model predicts the existence of the liquid-liquid equilibrium as well as the salt solubility in the mixture, it does not accurately determine the distribution of alcohol in the water-rich phase, or the amount of salt in the alcohol-rich phase. By adjusting the salt-propan-1-ol interaction coefficient it was possible to improve the correspondence for the distribution of alcohol, but not the salt. After improving the liquid-liquid equilibrium, the model was applied to the three-liquid phase equilibrium with water, propan-1-ol, octane, and NaCl. The model predicts the presence of three liquid phases when NaCl is added to equal volumes of water, propan-1-ol, and octane at 25°C, but does not properly account for the solubility of water or propan-1-ol in the octane-rich phase. If the propan-1-ol-octane binary interaction parameter was adjusted, the model provides a good description the distribution of chemicals in all phases, except for the amount of water in the octane-rich phase. These problems may in fact be related to the distribution of chemicals in the salt-free mixture and requires a systematic investigation of the distribution of chemicals in the water-alcohol-alkane system with the CPA EoS.

8.2   Future Work

The first step towards improving the e-CPA EoS will be to improve the parameterization and the ion-specific parameters by including solid-liquid equilibrium and mixed salt data. The optimal functional form for the temperature dependence of the ion-water interaction parameters

should also be determined.

Ion-specific interaction paramters with gas molecules must be determined in order to provide an ion-specific framework for predicting gas and hydrocarbon solubility in mixed solvents containing salts. This could be done using the Setschenow coefficients or through parameterization against the available experimental data for gas solubility in salts.

Ion-specific interaction parameters with alcohols and glycols should also be determined. The Electrolyte database must be extended to include more data for the solubility of salts in the non-aqueous solvents, and the model should be validated for SLE in mixed salts up to elevated temperatures.

The framework for the electrolyte CPA equation of state may furthermore be improved by accounting explicitly for ion-solvent and ion-ion association. However, in order to justify the additional complexity caused by the introduction of these terms these models must be compared to the results from the simplest possible e-CPA. It is therefore important to further develop the current e-CPA approach and apply it to a variety of industrially important systems.

Bibliography

[1]   GM Kontogeorgis and GK Folas. *Thermodynamic Models for Industrial Applications: From Classical and Advanced Mixing Rules to Association Theories*. Wiley, 2010. ISBN: 978-0-470-69726-9.

[2]   K Thomsen. Electrolyte Notes, Technical University of Denmark, Department of Chemical and Biochemical Engineering. In print, 2009.

[3]   E Hendriks, GM Kontogeorgis, R Dohrn, J-C de Hemptinne, IG Economou, LF Zilnik, and V Vesovic. Industrial requirements for thermodynamics and transport properties. *Industrial & Engineering Chemistry Research*, 49(22):11131–11141, 2010.

[4]   R Dohrn and O Pfohl. Thermophysical properties - Industrial directions. *Fluid phase equilibria*, 194:15–29, 2002.

[5]   JP O'Connell, R Gani, PM Mathias, G Maurer, JD Olson, and PA Crafts. Thermodynamic property modeling for chemical process and product engineering: some perspectives. *Industrial & Engineering Chemistry Research*, 48(10):4619–4637, 2009.

[6]   Sumnesh Gupta and James D Olson. Industrial needs in physical properties. *Industrial & engineering chemistry research*, 42(25):6359–6374, 2003.

[7]   PM Mathias. Applied thermodynamics in chemical technology: current practice and future challenges. *Fluid phase equilibria*, 228:49–57, 2005.

[8]   CC Chen and PM Mathias. Applied thermodynamics for process modeling. *AIChE Journal*, 48(2):194–200, 2002.

[9]   E Robertson. Low-Salinity Waterflooding to Improve Oil Recovery-Historical Field Evidence. In *SPE Annual Technical Conference and Exhibition*, 2007.

[10]   PL Fosbøl. *Carbon Dioxide Corrosion:: Modelling and Experimental Work Applied to Natural Gas Pipelines*. PhD thesis, Technical University of Denmark, 2007.

[11]   M Crabtree, D Eslinger, P Fletcher, M Miller, A Johnson, and G King. Fighting Scale-Removal and Prevention. *Oilfield Review*, 11(3):30–45, 1999.

[12]   E Mackay, M Jordan, N Feasey, D Shah, P Kumar, and S Ali. Integrated Risk Analysis for Scale Management in Deepwater Developments. *Old Production & Facilities*, 20(2):138–154, 2005.

[13]   K Thomsen. CERE Electrolyte Database. Online, 2014. `http://www.cere.dtu.dk/Expertise/Data_Bank/Search`.

[14]   YS Choi and CM Criss. Partial molal heat capacities and volumes of electrolytes in nonaqueous solvents and ion–solvent interactions. *Faraday Discussions of the Chemical Society*, 64:204–219, 1977.

[15] AJ Pasztor and CM Criss. Apparent molal volumes and heat capacities of some 1: 1 electrolytes in anhydrous methanol at 25Â° C. *Journal of Solution Chemistry*, 7(1):27–44, 1978.

[16] U Sen. Partial molal volumes of monovalent ions in ethylene glycol, formamide, and formic acid. *The Journal of Physical Chemistry*, 81(1):35–40, 1977.

[17] F Kawaizumi and R Zana. Partial molal volumes of irons in organic solvents from ultrasonic vibration potentials and density measurements. II. Ethanol and dimethylformamide. *The Journal of Physical Chemistry*, 78(11):1099–1105, 1974.

[18] R Zana, GA Lage, and CM Criss. Partial molal volumes of ions in organic solvents. IV. Ethylene glycol. *Journal of Solution Chemistry*, 9(9):667–682, 1980.

[19] JW Cobble, RC Murray, and U Sen. Field and structure behaviour of electrolytes. *Nature*, 291:566–568, 1981.

[20] KD Collins and MW Washabaugh. The Hofmeister effect and the behaviour of water at interfaces. *Quart. rev. of biophysics*, 18(4):1, 1985.

[21] Y Marcus. Effect of ions on the structure of water: structure making and breaking. *Chemical reviews*, 109(3):1346–1370, 2009.

[22] AP dos Santos, A Diehl, and Y Levin. Surface tensions, surface potentials, and the Hofmeister series of electrolyte solutions. *Langmuir*, 26(13):10778–10783, 2010.

[23] Springer Materials. Landolt Börnstein Database. Website, 2014. `http://www. springermaterials.com`.

[24] YY Akhadov. *Dielectric Properties of Binary Solutions: A Data Handbook*. Elsevier, 1980. ISBN: 978-0080236001.

[25] J Barthel, R Buchner, and M Münsterer. *Electrolyte Data Collection, Part 2: Dielectric Properties of Water and Aqueous Electrolyte Solutions*. Dechema, Frankfurt, 1995. ISBN: 3-926959-62-2.

[26] P Debye and E Hückel. Zur Theorie der Elektrolyte. *Physikalische Zeitschrift*, 24:179–207, 1923.

[27] E Hückel. Zur Theorie konzentrierter wässeriger Lösungen starker Elektrolyte. *Physikalische Zeitschrift*, 26:93–147, 1925.

[28] N Bjerrum. *Mat. -fys. Medd*, 7:9, 1926.

[29] FH Stillinger Jr and R Lovett. Ion-Pair Theory of Concentrated Electrolytes. I. Basic Concepts. *The Journal of Chemical Physics*, 48:3858, 1968.

[30] JV Walther and J Schott. The dielectric constant approach to speciation and ion pairing at high temperature and pressure. *Nature*, 332:635–638, 1988.

[31] H Weingärtner, VC Weiss, and W Schröer. Ion association and electrical conductance minimum in Debye–Hückel-based theories of the hard sphere ionic fluid. *The Journal of Chemical Physics*, 113:762, 2000.

[32] R Buchner and J Barthel. Dielectric relaxation in solutions. *Annual Reports Section" C"(Physical Chemistry)*, 97:349–382, 2001.

[33] R Buchner et al. What can be learnt from dielectric relaxation spectroscopy about ion solvation and association? *Pure and Applied Chemistry*, 80(6):1239–1252, 2008.

[34] RRA Robinson and RRH Stokes. *Electrolyte Solutions*. Dover Publications, 1970. ISBN: 0-486-42225-9.

[35] HP Meissner and JW Tester. Activity coefficients of strong electrolytes in aqueous solutions. *Industrial & Engineering Chemistry Process Design and Development*, 11(1):128–133, 1972.

[36] HP Meissner and CL Kusik. Activity coefficients of strong electrolytes in multicomponent aqueous solutions. *AIChE Journal*, 18(2):294–298, 1972.

[37] LA Bromley. Thermodynamic properties of strong electrolytes in aqueous solutions. *AIChE Journal*, 19(2):313–320, 1973.

[38] KS Pitzer. Thermodynamics of electrolytes. I. Theoretical basis and general equations. *The Journal of Physical Chemistry*, 77(2):268–277, 1973.

[39] P Wang, A Anderko, and RD Young. A speciation-based model for mixed-solvent electrolyte systems. *Fluid Phase Equilibria*, 203(1):141–176, 2002.

[40] P Wang, RD Springer, A Anderko, and RD Young. Modeling phase equilibria and speciation in mixed-solvent electrolyte systems. *Fluid phase equilibria*, 222:11–17, 2004.

[41] P Wang, A Anderko, RD Springer, and RD Young. Modeling phase equilibria and speciation in mixed-solvent electrolyte systems: II. Liquid–liquid equilibria and properties of associating electrolyte solutions. *Journal of molecular liquids*, 125(1):37–44, 2006.

[42] Peiming Wang, Jerzy J Kosinski, Malgorzata M Lencka, Andrzej Anderko, and Ronald D Springer. Thermodynamic modeling of boric acid and selected metal borate systems. *Pure & Applied Chemistry*, 85(11), 2013.

[43] AT Kan, G Fu, and MB Tomson. Effect of methanol and ethylene glycol on sulfates and halite scale formation. *Industrial & engineering chemistry research*, 42(11):2399–2408, 2003.

[44] DK Brenner, EW Anderson, S Lynn, and JM Prausnitz. Liquid-liquid equilibria for saturated aqueous solutions of sodium sulfate+ 1-propanol, 2-propanol, or 2-methylpropan-2-ol. *Journal of Chemical and Engineering Data*, 37(4):419–422, 1992.

[45] M Born. Volumen und hydratationswärme der ionen. *Zeitschrift für Physik A Hadrons and Nuclei*, 1(1):45–48, 1920.

[46] AA Kornyshev and AG Volkov. On the evaluation of standard Gibbs energies of ion transfer between two solvents. *Journal of electroanalytical chemistry and interfacial electrochemistry*, 180(1):363–381, 1984.

[47] L Blum. Mean spherical model for asymmetric electrolytes: I. Method of solution. *Molecular Physics*, 30(5):1529–1535, 1975.

[48] L Blum. Primitive electrolytes in the mean spherical approximation. *Theoretical Chemistry: Advances and Perspectives*, 5:1–66, 1980. ISBN: 9780126819052.

[49] L Blum and O Bernard. The general solution of the binding mean spherical approximation for pairing ions. *Journal of statistical physics*, 79(3-4):569–583, 1995.

[50] JP Simonin, O Bernard, and L Blum. Real ionic solutions in the mean spherical approximation. 3. Osmotic and activity coefficients for associating electrolytes in the primitive model. *The Journal of Physical Chemistry B*, 102(22):4411–4417, 1998.

[51] JP Simonin, O Bernard, and L Blum. Ionic solutions in the binding mean spherical approximation: Thermodynamic properties of mixtures of associating electrolytes. *The Journal of Physical Chemistry B*, 103(4):699–704, 1999.

[52] H Zhao, MC dos Ramos, and C McCabe. Development of an equation of state for electrolyte solutions by combining the statistical associating fluid theory and the mean spherical approximation for the nonprimitive model. *The Journal of chemical physics*, 126:244503, 2007.

[53] ME Fisher and Y Levin. Criticality in ionic fluids: Debye-Hückel theory, Bjerrum, and beyond. *Physical review letters*, 71(23):3826, 1993.

[54] DM Zuckerman, ME Fisher, and BP Lee. Critique of primitive model electrolyte theories. *Physical Review E*, 56(6):6569, 1997.

[55] JM Romero-Enrique, G Orkoulas, AZ Panagiotopoulos, and ME Fisher. Coexistence and criticality in size-asymmetric hard-core electrolytes. *Physical review letters*, 85(21):4558, 2000.

[56] J Jiang, L Blum, O Bernard, JM Prausnitz, and SI Sandler. Criticality and phase behavior in the restricted-primitive model electrolyte: Description of ion association. *The Journal of chemical physics*, 116:7977, 2002.

[57] JN Aqua, S Banerjee, and ME Fisher. Criticality in charge-asymmetric hard-sphere ionic fluids. *Physical Review E*, 72(4):041501, 2005.

[58] G Hura, D Russo, RM Glaeser, T Head-Gordon, M Krack, and M Parrinello. Water structure as a function of temperature from X-ray scattering experiments and ab initio molecular dynamics. *Physical Chemistry Chemical Physics*, 5(10):1981–1991, 2003.

[59] M Boström, FW Tavares, D Bratko, and BW Ninham. Specific ion effects in solutions of globular proteins: comparison between analytical models and simulation. *The Journal of Physical Chemistry B*, 109(51):24489–24494, 2005.

[60] I Kalcher and J Dzubiella. Structure-thermodynamics relation of electrolyte solutions. *The Journal of chemical physics*, 130:134507, 2009.

[61] S Rajamani, T Ghosh, and S Garde. Size dependent ion hydration, its asymmetry, and convergence to macroscopic behavior. *The Journal of chemical physics*, 120:4457, 2004.

[62] D Wei and L Blum. The mean spherical approximation for an arbitrary mixture of ions in a dipolar solvent: Approximate solution, pair correlation functions, and thermodynamics. *The Journal of chemical physics*, 87:2999, 1987.

[63] L Blum and DQ Wei. Analytical solution of the mean spherical approximation for an arbitrary mixture of ions in a dipolar solvent. *The Journal of chemical physics*, 87:555, 1987.

[64] L Blum, F Vericat, and WR Fawcett. Erratum: On the mean spherical approximation for hard ions and dipoles [J. Chem. Phys. 96, 3039 (1992)]. *The Journal of Chemical Physics*, 101(11):10197–10197, 1994.

[65] Z Liu, Y Li, and J Lu. Low-density expansion of the solution of mean spherical approximation for ion-dipole mixtures. *The Journal of Physical Chemistry B*, 106(20):5266–5274, 2002.

[66] MSt Wertheim. Exact solution of the mean spherical model for fluids of hard spheres with permanent electric dipole moments. *The Journal of Chemical Physics*, 55:4291, 1971.

[67] Z Liu, W Wang, and Y Li. An equation of state for electrolyte solutions by a combination of low-density expansion of non-primitive mean spherical approximation and statistical associating fluid theory. *Fluid phase equilibria*, 227(2):147–156, 2005.

[68] SA Adelman. The effective direct correlation function: An approach to the theory of liquid solutions. *The Journal of Chemical Physics*, 64:724, 1976.

[69] SA Adelman. The effective direct correlation function, an approach to the theory of liquid solutions: A new definition of the effective solute potential. *Chemical Physics Letters*, 38(3):567–570, 1976.

[70] Y Lin, A ten Kate, M Mooijer, J Delgado, PL Fosbøl, and K Thomsen. Comparison of activity coefficient models for electrolyte systems. *AIChE Journal*, 56(5):1334–1351, 2010.

[71] CC Chen and LB Evans. A local composition model for the excess Gibbs energy of aqueous electrolyte systems. *AIChE Journal*, 32(3):444–454, 1986.

[72] Y Song and CC Chen. Symmetric electrolyte nonrandom two-liquid activity coefficient model. *Industrial & Engineering Chemistry Research*, 48(16):7788–7797, 2009.

[73] A Anderko, P Wang, and M Rafal. Electrolyte solutions: from thermodynamic and transport property models to the simulation of industrial processes. *Fluid Phase Equilibria*, 194:123–142, 2002.

[74] K Thomsen, P Rasmussen, and R Gani. Correlation and prediction of thermal properties and phase behaviour for a class of aqueous electrolyte systems. *Chemical Engineering Science*, 51(14):3675–3683, 1996.

[75] K Thomsen and P Rasmussen. Modeling of vapor–liquid–solid equilibrium in gas–aqueous electrolyte systems. *Chemical Engineering Science*, 54(12):1787–1802, 1999.

[76] DS Abrams and JM Prausnitz. Statistical thermodynamics of liquid mixtures: a new expression for the excess Gibbs energy of partly or completely miscible systems. *AIChE Journal*, 21(1):116–128, 1975.

[77] KS Pitzer and JM Simonson. Thermodynamics of multicomponent, miscible, ionic systems: theory and equations. *The Journal of Physical Chemistry*, 90(13):3005–3009, 1986.

[78] K Thomsen. Thermodynamic Modeling of the Solubility of Alkali and Earth Alkali Borates. In *15th International Symposium on Solubility Phenomena and Related Equilibrium Processes*, 2012.

[79] WG Chapman, KE Gubbins, G Jackson, and M Radosz. New reference equation of state for associating liquids. *Industrial & Engineering Chemistry Research*, 29(8):1709–1721, 1990.

[80] MS Wertheim. Fluids with highly directional attractive forces. I. Statistical thermodynamics. *Journal of Statistical Physics*, 35(1-2):19–34, 1984.

[81] J Gross and G Sadowski. Perturbed-chain SAFT: An equation of state based on a perturbation theory for chain molecules. *Industrial & Engineering Chemistry Research*, 40(4):1244–1260, 2001.

[82] GM Kontogeorgis, EC Voutsas, IV Yakoumis, and DP Tassios. An equation of state for associating fluids. *Industrial & engineering chemistry research*, 35(11):4310–4318, 1996.

[83] GM Kontogeorgis. Association theories for complex thermodynamics. *Chemical Engineering Research and Design*, 91(10):1840–1858, 2013.

[84] W Raatschen, AH Harvey, and JM Prausnitz. Equation of state for solutions of electrolytes in mixed solvents. *Fluid Phase Equilibria*, 38(1):19–38, 1987.

[85] TW Copeman and FP Stein. A perturbed hard-sphere equation of state for solutions containing an electrolyte. *Fluid phase equilibria*, 35(1):165–187, 1987.

[86] G Jin and MD Donohue. An equation of state for electrolyte solutions. 1. Aqueous systems containing strong electrolytes. *Industrial & engineering chemistry research*, 27(6):1073–1084, 1988.

[87] G Jin and MD Donohue. An equation of state for electrolyte solutions. 2. Single volatile weak electrolytes in water. *Industrial & engineering chemistry research*, 27(9):1737–1743, 1988.

[88] G Jin and MD Donohue. An equation of state for electrolyte solutions. 3. Aqueous solutions containing multiple salts. *Industrial & Engineering Chemistry Research*, 30(1):240–248, 1991.

[89] AH Harvey and JM Prausnitz. Thermodynamics of high-pressure aqueous systems containing gases and salts. *AIChE journal*, 35(4):635–644, 1989.

[90] Y Liu, AH Harvey, and JM Prausnitz. Thermodynamics of concentrated electrolyte solutions. *Chemical Engineering Communications*, 77(1):43–66, 1989.

[91] YX Zuo and TM Guo. Extension of the Patel-Teja equation of state to the prediction of the solubility of natural gas in formation water. *Chemical engineering science*, 46(12):3251–3258, 1991.

[92] HG Simon, H Kistenmacher, JM Prausnitz, D Vortmeyer, et al. An equation of state for systems containing electrolytes and nonelectrolytes. *Chemical Engineering and Processing: Process Intensification*, 29(3):139–146, 1991.

[93] K Aasberg-Petersen, E Stenby, and A Fredenslund. Prediction of high-pressure gas solubilities in aqueous mixtures of electrolytes. *Industrial & engineering chemistry research*, 30(9):2180–2185, 1991.

[94] W Fürst and H Renon. Representation of excess properties of electrolyte solutions using a new equation of state. *AIChE Journal*, 39(2):335–343, 1993.

[95] VQ Vu, PD Suchaux, and W Fürst. Use of a predictive electrolyte equation of state for the calculation of the gas hydrate formation temperature in the case of systems with methanol and salts. *Fluid phase equilibria*, 194:361–370, 2002.

[96] J Li, HM Polka, and J Gmehling. A gE model for single and mixed solvent electrolyte systems: 1. Model and results for strong electrolytes. *Fluid Phase Equilibria*, 94:89–114, 1994.

[97] HM Polka, J Li, and J Gmehling. A gE model for single and mixed solvent electrolyte systems: 2. Results and comparison with other models. *Fluid phase equilibria*, 94:115–127, 1994.

[98] J Li, M Topphoff, K Fischer, and J Gmehling. Prediction of gas solubilities in aqueous electrolyte systems using the predictive Soave-Redlich-Kwong model. *Industrial & engineering chemistry research*, 40(16):3703–3710, 2001.

[99] J Kiepe, S Horstmann, K Fischer, and J Gmehling. Experimental determination and prediction of gas solubility data for CO2+ H2O mixtures containing NaCl or KCl at temperatures between 313 and 393 K and pressures up to 10 MPa. *Industrial & engineering chemistry research*, 41(17):4393–4398, 2002.

[100] J Kiepe, S Horstmann, K Fischer, and J Gmehling. Experimental determination and prediction of gas solubility data for methane+ water solutions containing different monovalent electrolytes. *Industrial & engineering chemistry research*, 42(21):5392–5398, 2003.

[101] J Kiepe, S Horstmann, K Fischer, and J Gmehling. Application of the PSRK model for systems containing strong electrolytes. *Industrial & engineering chemistry research*, 43(20):6607–6615, 2004.

[102] J Kiepe, O Noll, and J Gmehling. Modified LIQUAC and modified lifac a further development of electrolyte models for the reliable prediction of phase equilibria with strong electrolytes. *Industrial & engineering chemistry research*, 45(7):2361–2373, 2006.

[103] E Collinet and J Gmehling. Prediction of phase equilibria with strong electrolytes with the help of the volume translated Peng-Robinson group contribution equation of state (VTPR). *Fluid phase equilibria*, 246(1):111–118, 2006.

[104] J Huang, J Li, and J Gmehling. Prediction of solubilities of salts, osmotic coefficients and vapor–liquid equilibria for single and mixed solvent electrolyte systems using the LIQUAC model. *Fluid Phase Equilibria*, 275(1):8–20, 2009.

[105] M Li, D Constantinescu, L Wang, A Mohs, and J Gmehling. Solubilities of NaCl, KCl, LiCl, and LiBr in methanol, ethanol, acetone, and mixed solvents and correlation using the LIQUAC model. *Industrial & Engineering Chemistry Research*, 49(10):4981–4988, 2010.

[106] MY Li, LS Wang, B Jiang, and J Gmehling. Generalized LIQUAC model for the single- and mixed-solvent strong electrolyte systems. *AIChE Journal*, 57(9):2535–2546, 2011.

[107] MY Li, LS Wang, and J Gmehling. Thermodynamics of Phase Equilibria in Aqueous Strong Electrolyte Systems. *Industrial & Engineering Chemistry Research*, 50(6):3621–3631, 2011.

[108] MY Li, LS Wang, KP Wang, B Jiang, and J Gmehling. Experimental measurement and modeling of solubility of LiBr and LiNO$_3$ in methanol, ethanol, 1-propanol, 2-propanol and 1-butanol. *Fluid Phase Equilibria*, 307(1):104–109, 2011.

[109] J Wu and JM Prausnitz. Phase equilibria for systems containing hydrocarbons, water, and salt: An extended Peng-Robinson equation of state. *Industrial & engineering chemistry research*, 37(5):1634–1643, 1998.

[110] A Galindo, A Gil-Villegas, G Jackson, and AN Burgess. SAFT-VRE: Phase behavior of electrolyte solutions with the statistical associating fluid theory for potentials of variable range. *The Journal of Physical Chemistry B*, 103(46):10272–10281, 1999.

[111] P Paricaud, A Galindo, and G Jackson. Recent advances in the use of the SAFT approach in describing electrolytes, interfaces, liquid crystals and polymers. *Fluid phase equilibria*, 194:87–96, 2002.

[112] BH Patel, P Paricaud, A Galindo, and GC Maitland. Prediction of the salting-out effect of strong electrolytes on water+ alkane solutions. *Industrial & engineering chemistry research*, 42(16):3809–3823, 2003.

[113] WB Liu, YG Li, and JF Lu. A new equation of state for real aqueous ionic fluids based on electrolyte perturbation theory, mean spherical approximation and statistical associating fluid theory. *Fluid phase equilibria*, 158:595–606, 1999.

[114] JA Myers, SI Sandler, and RH Wood. An equation of state for electrolyte solutions covering wide ranges of temperature, pressure, and composition. *Industrial & engineering chemistry research*, 41(13):3282–3297, 2002.

[115] LF Cameretti, G Sadowski, and JM Mollerup. Modeling of aqueous electrolyte solutions with perturbed-chain statistical associated fluid theory. *Industrial & engineering chemistry research*, 44(9):3355–3362, 2005.

[116] C Held, LF Cameretti, and G Sadowski. Modeling aqueous electrolyte solutions: Part 1. Fully dissociated electrolytes. *Fluid Phase Equilibria*, 270(1):87–96, 2008.

[117] C Held and G Sadowski. Modeling aqueous electrolyte solutions. Part 2. Weak electrolytes. *Fluid Phase Equilibria*, 279(2):141–148, 2009.

[118] C Held, A Prinz, V Wallmeyer, and G Sadowski. Measuring and modeling alcohol/salt systems. *Chemical Engineering Science*, 68(1):328–339, 2012.

[119] C Held, G Sadowski, A Carneiro, O Rodríguez, and EA Macedo. Modeling thermodynamic properties of aqueous single-solute and multi-solute sugar solutions with PC-SAFT. *AIChE Journal*, 59(12):4794–4805, 2013.

[120] A Nann, C Held, and G Sadowski. Liquid-liquid equilibria of 1-butanol/water/IL systems. *Industrial & Engineering Chemistry Research*, 52:18472–18481, 2013.

[121] SP Tan, H Adidharma, and M Radosz. Statistical associating fluid theory coupled with restricted primitive model to represent aqueous strong electrolytes. *Industrial & engineering chemistry research*, 44(12):4442–4452, 2005.

[122] X Ji, SP Tan, H Adidharma, and M Radosz. Statistical associating fluid theory coupled with restricted primitive model to represent aqueous strong electrolytes: Multiple-salt solutions. *Industrial & engineering chemistry research*, 44(19):7584–7590, 2005.

[123] SP Tan, X Ji, H Adidharma, and M Radosz. Statistical associating fluid theory coupled with restrictive primitive model extended to bivalent ions. SAFT2: 1. single salt+ water solutions. *The Journal of Physical Chemistry B*, 110(33):16694–16699, 2006.

[124] X Ji, SP Tan, H Adidharma, and M Radosz. Statistical associating fluid theory coupled with restrictive primitive model extended to bivalent ions. SAFT2: 2. Brine/seawater properties predicted. *The Journal of Physical Chemistry B*, 110(33):16700–16706, 2006.

[125] X Ji and H Adidharma. Ion-based SAFT2 to represent aqueous single-and multiple-salt solutions at 298.15 K. *Industrial & engineering chemistry research*, 45(22):7719–7728, 2006.

[126] X Ji and H Adidharma. Ion-based statistical associating fluid theory (SAFT2) to represent aqueous single-salt solutions at temperatures and pressures up to 473.15 K and 1000 bar. *Industrial & engineering chemistry research*, 46(13):4667–4677, 2007.

[127] X Ji and H Adidharma. Ion-based SAFT2 to represent aqueous multiple-salt solutions at ambient and elevated temperatures and pressures. *Chemical Engineering Science*, 63(1):131–140, 2008.

[128] Y Lin, K Thomsen, and JC de Hemptinne. Multicomponent equations of state for electrolytes. *AIChE journal*, 53(4):989–1005, 2007.

[129] R Inchekel, J-C de Hemptinne, and W Fürst. The simultaneous representation of dielectric constant, volume and activity coefficients using an electrolyte equation of state. *Fluid Phase Equilibria*, 271(1):19–27, 2008.

[130] H Haghighi, A Chapoy, and B Tohidi. Freezing point depression of electrolyte solutions: experimental measurements and modeling using the cubic-plus-association equation of state. *Industrial & Engineering Chemistry Research*, 47(11):3983–3989, 2008.

[131] H Haghighi, A Chapoy, and B Tohidi. Methane and Water Phase Equilibria in the Presence of Single and Mixed Electrolyte Solutions Using the Cubic-Plus-Association Equation of State. *Oil & Gas Science and Technology-Revue de l'IFP*, 64(2):141–154, 2009.

[132] Y Liu, Z Li, J Mi, and C Zhong. Modeling of aqueous electrolyte solutions based on primitive and first-order mean spherical approximation. *Industrial & Engineering Chemistry Research*, 47(5):1695–1701, 2008.

[133] BS Lee and KC Kim. Modeling of aqueous electrolyte solutions based on perturbed-chain statistical associating fluid theory incorporated with primitive mean spherical approximation. *Korean journal of chemical engineering*, 26(6):1733–1747, 2009.

[134] S Seyfi, G Pazuki, SF Aghamiri, and M Beheshti. On the prediction of equilibrium phase behavior of amino acids in aqueous and aqueous-electrolyte solutions using SAFT equation of state. *Fluid Phase Equilibria*, 287(1):15–22, 2009.

[135] SG Doozandeh, G Pazuki, and A Asghar. Study of Protein Partitioning in Polymer-Salt Aqueous Two-Phase Systems Using Electrolyte-SAFT (E-SAFT) Equation of State. *Journal of Dispersion Science and Technology*, 33(5):756–762, 2012.

[136] A Haghtalab and SH Mazloumi. A square-well equation of state for aqueous strong electrolyte solutions. *Fluid Phase Equilibria*, 285(1):96–104, 2009.

[137] Ali Haghtalab and Seyed Hossein Mazloumi. Electrolyte Cubic Square-Well Equation of State for Computation of the Solubility CO2 and H2S in Aqueous MDEA Solutions. *Industrial & Engineering Chemistry Research*, 49(13):6221–6230, 2010.

[138] S Herzog, J Gross, and W Arlt. Equation of state for aqueous electrolyte systems based on the semirestricted non-primitive mean spherical approximation. *Fluid Phase Equilibria*, 297(1):23–33, 2010.

[139] J Rozmus, JC deHemptinne, A Galindo, D Simon, and P Mougin. Modelling of strong electrolytes with ePPC-SAFT up to high temperatures. *Industrial & Engineering Chemistry Research*, 52(29):9979–9994, 2013.

[140] A Zuber, RF Checoni, R Mathew, JPL Santos, FW Tavares, and M Castier. Thermodynamic Properties of 1: 1 Salt Aqueous Solutions with the Electrolattice Equation of State. *Oil & Gas Science and Technology - Revue d'IFP Energies nouvelles*, 68(2):255–270, 2013.

[141] A Zuber, RF Checoni, and M Castier. Thermodynamic properties of aqueous solutions of single and multiple salts using the Q-electrolattice equation of state. *Fluid Phase Equilibria*, 362:268–280, 2014.

[142] D Luedecke and JM Prausnitz. Phase equilibria for strongly nonideal mixtures from an equation of state with density-dependent mixing rules. *Fluid Phase Equilibria*, 22(1):1–19, 1985.

[143] A Haghtalab and SH Mazloumi. A new coordination number model for development of a square-well equation of state. *Fluid Phase Equilibria*, 280(1):1–8, 2009.

[144] P Paricaud. Modeling the dissociation conditions of salt hydrates and gas semiclathrate hydrates: application to lithium bromide, hydrogen iodide, and tetra-n-butylammonium bromide+ carbon dioxide systems. *The Journal of Physical Chemistry B*, 115(2):288–299, 2010.

[145] S Seyfi, GR Pazuki, SF Aghamiri, and M Beheshti. Application of Restrictive Primitive SAFT Coupled with Different Hard-Sphere Equations to Model Mean Ionic Activity Coefficients of Electrolyte Solutions. *Journal of Dispersion Science and Technology*, 31(4):536–550, 2010.

[146] A Haghtalab, M Zare, AN Ahmadi, and K Nazari. Prediction of hydrate equilibrium conditions using Electrolyte Cubic Square-Well Equation of State. *Fluid Phase Equilibria*, 2012.

[147] TJ Edwards, G Maurer, J Newman, and JM Prausnitz. Vapor-liquid equilibria in multicomponent aqueous solutions of volatile weak electrolytes. *AIChE Journal*, 24(6):966–976, 1978.

[148] C Avendaño and A Gil-Villegas. Monte Carlo simulations of primitive models for ionic systems using the Wolf method. *Molecular Physics*, 104(09):1475–1486, 2006.

[149] M Llano-Restrepo and WG Chapman. Monte Carlo simulation of the structural properties of concentrated aqueous alkali halide solutions at 25Â° C using a simple civilized model. *The Journal of chemical physics*, 100:8321, 1994.

[150] L Onsager. Electric moments of molecules in liquids. *Journal of the American Chemical Society*, 58(8):1486–1493, 1936.

[151] JG Kirkwood. The dielectric polarization of polar liquids. *The Journal of Chemical Physics*, 7:911, 1939.

[152] H Frölich. *Theory of dielectrics*. Oxford: Clarendon Press, 1949.

[153] AD Buckingham. A theory of the dielectric polarization of polar substances. *Proceedings of the Royal Society of London. Series A. Mathematical and Physical Sciences*, 238(1213):235–244, 1956.

[154] JB Hasted. Dielectric properties of water and of aqueous solutions. *Dielectric and Related Molecular Processes, Chemical Society, London*, 1:121–161, 1972.

[155] AH Harvey and JM Prausnitz. Dielectric constants of fluid mixtures over a wide range of temperature and density. *Journal of solution chemistry*, 16(10):857–869, 1987.

[156] SA Adelman and JM Deutch. The structure of polar fluids. *Advances in Chemical Physics: Non-Simple Liquids, Volume 31*, pages 103–153, 1975.

[157] G Stell, PN Patey, and JS Hø ye. Dielectric constants of fluid models: statistical mechanical theory and its quantitative implementation. *Advances in Chemical Physics*, 48:183, 1981.

[158] HL Friedman. Theory of the dielectric constant of solutions. *The Journal of Chemical Physics*, 76:1092, 1982.

[159] C Mavroyannis and MJ Stephen. Dispersion forces. *Molecular Physics*, 5(6):629–638, 1962.

[160] J Li, Y Lin, and J Gmehling. gE Model for Single-and Mixed-Solvent Electrolyte Systems. 3. Prediction of Salt Solubilities in Aqueous Electrolyte Systems. *Industrial & engineering chemistry research*, 44(5):1602–1609, 2005.

[161] B Maribo-Mogensen, GM Kontogeorgis, and K Thomsen. Comparison of the Debye-Hückel and the Mean Spherical Approximation Theories for Electrolyte Solutions. *Industrial & Engineering Chemistry Research*, 51(14):5353–5363, 2012.

[162] B Maribo-Mogensen, GM Kontogeorgis, and K Thomsen. Modeling of dielectric properties of complex fluids with an equation of state. *The Journal of Physical Chemistry B*, 117(12):3389–3397, 2013.

[163] B Maribo-Mogensen, GM Kontogeorgis, and K Thomsen. Modeling of Dielectric Properties of Aqueous Salt Solutions with an Equation of State. *The Journal of Physical Chemistry B*, 117(36):10523–10533, 2013.

[164] G Soave. Equilibrium constants from a modified Redlich-Kwong equation of state. *Chemical Engineering Science*, 27(6):1197–1203, 1972.

[165] DY Peng and DB Robinson. A new two-constant equation of state. *Industrial & Engineering Chemistry Fundamentals*, 15(1):59–64, 1976.

[166] MS Wertheim. Fluids with highly directional attractive forces. II. Thermodynamic perturbation theory and integral equations. *Journal of statistical physics*, 35(1-2):35–47, 1984.

[167] MS Wertheim. Fluids with highly directional attractive forces. III. Multiple attraction sites. *Journal of statistical physics*, 42(3-4):459–476, 1986.

[168] MS Wertheim. Fluids with highly directional attractive forces. IV. Equilibrium polymerization. *Journal of statistical physics*, 42(3-4):477–492, 1986.

[169] G Jackson, WG Chapman, and KE Gubbins. Phase equilibria of associating fluids: Spherical molecules with multiple bonding sites. *Molecular Physics*, 65(1):1–31, 1988.

[170] WG Chapman, G Jackson, and KE Gubbins. Phase equilibria of associating fluids: Chain molecules with multiple bonding sites. *Molecular Physics*, 65(5):1057–1079, 1988.

[171] WG Chapman, KE Gubbins, G Jackson, and M Radosz. SAFT: Equation-of-state solution model for associating fluids. *Fluid Phase Equilibria*, 52:31–38, 1989.

[172] N von Solms, ML Michelsen, CP Passos, SO Derawi, and GM Kontogeorgis. Investigating models for associating fluids using spectroscopy. *Industrial & engineering chemistry research*, 45(15):5368–5374, 2006.

[173] Martin P Breil, Georgios M Kontogeorgis, Paul K Behrens, and Michael L Michelsen. Modeling of the thermodynamics of the acetic acid- water mixture using the cubic-plus-association equation of state. *Industrial & Engineering Chemistry Research*, 50(9):5795–5805, 2011.

[174] MJ Huron and J Vidal. New mixing rules in simple equations of state for representing vapour-liquid equilibria of strongly non-ideal mixtures. *Fluid Phase Equilibria*, 3(4):255–271, 1979.

[175] SH Huang and M Radosz. Equation of state for small, large, polydisperse, and associating molecules. *Industrial & Engineering Chemistry Research*, 29(11):2284–2294, 1990.

[176] Design Institute for Physical Properties (DIPPR). DIPPR Project 801 Database. Application, 2014. `http://www.aiche.org/dippr`.

[177] SO Derawi, GM Kontogeorgis, ML Michelsen, and EH Stenby. Extension of the Cubic-Plus-Association Equation of State to Glycol-Water Cross-associating Systems. *Industrial & engineering chemistry research*, 42(7):1470–1477, 2003.

[178] J-Y Huot, E Battistel, R Lumry, G Villeneuve, J-F Lavallee, A Anusiem, and C Jolicoeur. A comprehensive thermodynamic investigation of water-ethylene glycol mixtures at 5, 25, and 45Â° C. *Journal of solution chemistry*, 17(7):601–636, 1988.

[179] GM Kontogeorgis, P Coutsikos, V I Harismiadis, A Fredenslund, and DP Tassios. A novel method for investigating the repulsive and attractive parts of cubic equations of state and the combining rules used with the vdW-1f theory. *Chemical engineering science*, 53(3):541–552, 1998.

[180] P Coutsikos, K Magoulas, and GM Kontogeorgis. Prediction of solid–gas equilibria with the Peng–Robinson equation of state. *The Journal of supercritical fluids*, 25(3):197–212, 2003.

[181] DA McQuarrie. *Statistical Mechanics*. University Science Books, 2000. ISBN: 978-1891389153.

[182] M Michelsen and J Mollerup. *Thermodynamic Models: Fundamentals & Computational Aspects*. Tie-Line Publications: Holte (Denmark), 2007. ISBN: 87-989961-3-4.

[183] P Attard. Asymptotic analysis of primitive model electrolytes and the electrical double layer. *Physical Review E*, 48(5):3604, 1993.

[184] JR Loehe and MD Donohue. Recent advances in modeling thermodynamic properties of aqueous strong electrolyte systems. *AIChE Journal*, 43(1):180–195, 1997.

[185] L Onsager. Theories of Concentrated Electrolytes. *Chemical Reviews*, 13(1):73–89, 1933.

[186] L Onsager. A Correction to the Poisson-Boltzmann Equation for Unsymmetrical Electrolytes. *Journal of the American Chemical Society*, 86(17):3421–3423, 1964.

[187] KS Pitzer. *Thermodynamics. 3rd*. New York: McGraw Hill, 1995.

[188] JS Høye and G Stell. Thermodynamics of the MSA for simple fluids. *The Journal of Chemical Physics*, 67:439, 1977.

[189] PV Giaquinta, M Parrinello, and MP Tosi. Hydrodynamic correlation functions for molten salts. *Physics and Chemistry of Liquids*, 5(4):305–324, 1976.

[190] P Vieillefosse. Fluctuations de charge et de masse dans un sel fondu binaire a la limite hydrodynamique. *Journal de Physique Lettres*, 38(2):43–46, 1977.

[191] Y Marcus. Ionic radii in aqueous solutions. *Chemical Reviews*, 88(8):1475–1498, 1988.

[192] JG Kirkwood. On the Theory of Strong Electrolyte Solutions. *Journal of Chemical Physics*, 2:767–781, 1934.

[193] M Holovko. Concept of ion association in the theory of electrolyte solutions. In *Ionic Soft Matter: Modern Trends in Theory and Applications*, pages 45–81. Springer, 2005.

[194] W Ebeling, S Hilbert, and H Krienke. On Bjerrum's mass action law for electrolytes and Onsager's bookkeeping rule. *Journal of molecular liquids*, 96:409–423, 2002.

[195] L Onsager and SW Provencher. Relaxation effects in associating electrolytes. *Journal of the American Chemical Society*, 90(12):3134–3140, 1968.

[196] G Stell. Criticality and phase transitions in ionic fluids. *Journal of statistical physics*, 78(1-2):197–238, 1995.

[197] W Schröer. Criticality of ionic liquids in solution. In *Ionic Soft Matter: Modern Trends in Theory and Applications*, pages 143–180. Springer, 2005.

[198] W Schröer. A Short History of Phase Transitions in Ionic Fluids. *Contributions to Plasma Physics*, 52(1):78–88, 2012.

[199] JG Kirkwood. Theoretical Studies upon Dipolar Ions. *Chemical Reviews*, 24(2):233–251, 1939.

[200] AZ Panagiotopoulos. Molecular simulation of phase equilibria: simple, ionic and polymeric fluids. *Fluid Phase Equilibria*, 76:97–112, 1992.

[201] I Kalcher. *Aqueous Electrolytes: Ion-Specific Structure and Thermodynamics*. PhD thesis, München, Technische Universität München, Diss., 2011, 2011.

[202] GK Folas, EW Froyna, J Lovland, GM Kontogeorgis, and E Solbraa. Data and prediction of water content of high pressure nitrogen, methane and natural gas. *Fluid phase equilibria*, 252(1):162–174, 2007.

[203] R Fernandez-Prini, AH Harvey, and DA Palmer. *Aqueous systems at elevated temperatures and pressures: Physical chemistry in water, steam and hydrothermal solutions*. Access Online via Elsevier, 2004.

[204] E Djamali and JW Cobble. A unified theory of the thermodynamic properties of aqueous electrolytes to extreme temperatures and pressures. *The Journal of Physical Chemistry B*, 113(8):2398–2403, 2009.

[205] E Djamali and JW Cobble. Thermodynamic Properties of Aqueous Polyatomic Ions at Extreme Temperatures and Pressures. *The Journal of Physical Chemistry B*, 114(11):3887–3893, 2010.

[206] CODATA. International Council for Science: Committee on Data for Science and Technology. Website, 2014. http://www.codata.org/resources/databases/key1.html.

[207] WM Haynes. CRC Handbook of Chemistry and Physics, 93rd ed. Website, 2014. http://www.hbcpnetbase.com.

[208] DD Wagman, WH Evans, VB Parker, RH Schlumm, I Halow, SM Bailey, KL Churney, and RL Nutall. The NBS Tables of Chemical Thermodynamic Properties, Supplement no. 2. *J. Phys. Chem. Ref. Data*, 1982.

[209] JW Johnson, EH Oelkers, and HC Helgeson. SUPCRT92: A software package for calculating the standard molal thermodynamic properties of minerals, gases, aqueous species, and reactions from 1 to 5000 bar and 0 to 1000 C. *Computers & Geosciences*, 18(7):899–947, 1992.

[210] J Sedlbauer, JP O'Connell, and RH Wood. A new equation of state for correlation and prediction of standard molal thermodynamic properties of aqueous species at high temperatures and pressures. *Chemical Geology*, 163(1):43–63, 2000.

[211] AV García, K Thomsen, and EH Stenby. Prediction of mineral scale formation in geothermal and oilfield operations using the extended UNIQUAC model: Part I. Sulfate scaling minerals. *Geothermics*, 34(1):61–97, 2005.

[212] AV García, K Thomsen, and EH Stenby. Prediction of mineral scale formation in geothermal and oilfield operations using the Extended UNIQUAC model: Part II. Carbonate-scaling minerals. *Geothermics*, 35(3):239–284, 2006.

[213] Aspentech. Aspentech Aspen Plus. Website, 2014. `https://www.aspentech.com/products/aspen-plus.aspx`.

[214] Y Marcus. *Ion Propierties*, volume 1. CRC Press, 1997. ISBN: 978-0824-00119.

[215] National Institute of Standards and Technology (NIST). NIST-JANAF Thermochemical Tables, 2014. `http://kinetics.nist.gov/janaf`.

[216] Y Marcus. Thermodynamics of solvation of ions. Part 5. Gibbs free energy of hydration at 298.15 K. *Journal of the Chemical Society, Faraday Transactions*, 87(18):2995–2999, 1991.

[217] Y Marcus. Thermodynamic Functions of Transfer of Single Ions from Water to Nonaqueous and Mixed Solvents. Part 4: Selection of Extrathermodynamic Assumptions. *Pure & Applied Chemistry*, 58(12):1721–1736, 1986.

[218] National Institute of Standards and Technology (NIST). Computational Chemistry Comparison and Benchmark Database, 2014. `http://cccbdb.nist.gov`.

[219] National Institute of Standards and Technology (NIST). NIST Gas-Phase Ion Thermochemistry, 2014. `http://webbook.nist.gov/chemistry/ion`.

[220] ML McKee. Computational Study of the Mono-and Dianions of SO2, SO3, SO4, S2O3, S2O4, S2O6, and S2O8. *The Journal of Physical Chemistry*, 100(9):3473–3481, 1996.

[221] JH Van't Hoff. Osmotic pressure and chemical equilibrium. *Nobel Lecture*, 13, 1901.

[222] Svante Arrhenius. *Theories of solutions*. Yale University Press, 1912.

[223] WG McMillan Jr and JE Mayer. The statistical mechanics of multicomponent solutions. *J. Chem. Phys*, 13:276, 1945.

[224] E Djamali, AT Kan, and MB Tomson. A Priori Prediction of Thermodynamic Properties of Electrolytes in Mixed Aqueous–Organic Solvents to Extreme Temperatures. *The Journal of Physical Chemistry B*, 116(30):9033–9042, 2012.

[225] E Djamali, H Lu, A Kan, and M Tomson. Effects of Hydrate Inhibitors on the Solubility of Barite and Halite in Produced Water. In *SPE International Conference on Oilfield Scale*, 2012.

[226] X Tang and J Gross. Modeling the phase equilibria of hydrogen sulfide and carbon dioxide in mixture with hydrocarbons and water using the PCP-SAFT equation of state. *Fluid Phase Equilibria*, 293(1):11–21, 2010.

[227] MP Breil and JM Mollerup. The McMillan–Mayer framework and the theory of electrolyte solutions. *Fluid phase equilibria*, 242(2):129–135, 2006.

[228] CA Haynes and J Newman. On converting from the McMillan-Mayer framework I. Single-solvent system. *Fluid phase equilibria*, 145(2):255–268, 1998.

[229] J Hunger, A Stoppa, S Schrödle, G Hefter, and R Buchner. Temperature dependence of the dielectric properties and dynamics of ionic liquids. *ChemPhysChem*, 10(4):723–733, 2009.

[230] U Kaatze. Bound water: Evidence from and implications for the dielectric properties of aqueous solutions. *Journal of Molecular Liquids*, 162(3):105–112, 2011.

[231] J Hubbard and L Onsager. Dielectric dispersion and dielectric friction in electrolyte solutions. I. *The Journal of Chemical Physics*, 67:4850, 1977.

[232] JB Hubbard, L Onsager, WM Van Beek, and M Mandel. Kinetic polarization deficiency in electrolyte solutions. *Proceedings of the National Academy of Sciences*, 74(2):401–404, 1977.

[233] JB Hubbard. Dielectric dispersion and dielectric friction in electrolyte solutions. II. *The Journal of Chemical Physics*, 68:1649, 1978.

[234] JB Hubbard, P Colonomos, and PG Wolynes. Molecular theory of solvated ion dynamics. III. The kinetic dielectric decrement. *The Journal of Chemical Physics*, 71:2652, 1979.

[235] Peter Josef William Debye. *Polar Molecules*, volume 172. Dover Publications, New York, 1929.

[236] B Bagchi and R Biswas. Polar and nonpolar solvation dynamics, ion diffusion, and vibrational relaxation: role of biphasic solvent response in chemical dynamics. *Adv. Chem. Phys*, 109:207–433, 1999.

[237] N Nandi, K Bhattacharyya, and B Bagchi. Dielectric relaxation and solvation dynamics of water in complex chemical and biological systems. *Chemical Reviews*, 100(6):2013–2046, 2000.

[238] DQM Craig. *Dielectric analysis of pharmaceutical systems*. Taylor & Francis London, 1995.

[239] G Smith, AP Duffy, J Shen, and CJ Olliff. Dielectric relaxation spectroscopy and some applications in the pharmaceutical sciences. *Journal of pharmaceutical sciences*, 84(9):1029–1044, 1995.

[240] BKP Scaife. *Principles of Dielectrics*. Oxford University Press, 1998. ISBN: 978-0-19-856557-4.

[241] GH Haggis, JB Hasted, and TJ Buchanan. The dielectric properties of water in solutions. *The Journal of Chemical Physics*, 20:1452, 1952.

[242] G Oster and JG Kirkwood. The influence of hindered molecular rotation on the dielectric constants of water, alcohols, and other polar liquids. *The Journal of Chemical Physics*, 11:175, 1943.

[243] AP Gregory and RN Clarke. Traceable measurements of the static permittivity of dielectric reference liquids over the temperature range 5–50 C. *Measurement Science and Technology*, 16(7):1506, 2005.

[244] SO Nelson. Dielectric spectroscopy in agriculture. *Journal of non-crystalline solids*, 351(33):2940–2944, 2005.

[245] BR Spies. Electrical and electromagnetic borehole measurements: A review. *Surveys in Geophysics*, 17(4):517–556, 1996.

[246] SJ Suresh and VM Naik. Hydrogen bond thermodynamic properties of water from dielectric constant data. *The Journal of Chemical Physics*, 113:9727, 2000.

[247] SJ Suresh and VM Naik. Theory of dielectric constant of aqueous solutions. *The Journal of chemical physics*, 116:4212, 2002.

[248] SJ Suresh. Detailed molecular model for dielectric constant of multicomponent, associating liquids. *The Journal of Physical Chemistry B*, 108(2):715–720, 2004.

[249] RJD Tilley. *Colour and the Optical Properties of Materials*. Wiley, 2000. ISBN: 0-471-85197-3.

[250] SA Korff and G Breit. Optical dispersion. *Reviews of Modern Physics*, 4(3):471, 1932.

[251] DS Reid. Traditional Indirect Methods for Estimation of Water Content: Measurement of° Brix. *Current Protocols in Food Analytical Chemistry, UNIT A1.4.*, 2004.

[252] M Fukuta, T Yanagisawa, S Miyamura, and Y Ogi. Concentration measurement of refrigerant/refrigeration oil mixture by refractive index. *International journal of refrigeration*, 27(4):346–352, 2004.

[253] MP Breil and JM Mollerup. Modelling of molecular light scattering. *Fluid Phase Equilibria*, 310(1):120–128, 2011.

[254] J Escobedo and GA Mansoori. Surface-tension prediction for liquid mixtures. *AIChE Journal*, 44(10):2324–2332, 1998.

[255] Mohammad R Riazi and Yousef A Roomi. Use of the refractive index in the estimation of thermophysical properties of hydrocarbons and petroleum mixtures. *Industrial & engineering chemistry research*, 40(8):1975–1984, 2001.

[256] G Foca, M Manfredini, D Manzini, A Marchetti, L Pigani, S Sighinolfi, L Tassi, and A Ulrici. Dielectric properties in ternary mixtures of ethane-1, 2-diol+ 1, 2-dimethoxyethane+ water. *International journal of thermophysics*, 25(3):839–855, 2004.

[257] U Kaatze. The dielectric properties of water in its different states of interaction. *Journal of solution chemistry*, 26(11):1049–1112, 1997.

[258] JZ Yang, DZ Lu, M Deng, J Lui, HC Li, and CJ Hou. Dielectric properties of urea-water mixed solvents and its effect on the second dissociation process of carbonic acid. *Zeitschrift für Physikalische Chemie*, 205(Part_2):199–209, 1998.

[259] J Hamelin, JB Mehl, and MR Moldover. The static dielectric constant of liquid water between 274 and 418 K near the saturated vapor pressure. *International journal of thermophysics*, 19(5):1359–1380, 1998.

[260] DP Fernandez, ARH Goodwin, and JMH Levelt Sengers. Measurements of the relative permittivity of liquid water at frequencies in the range of 0.1 to 10 kHz and at temperatures between 273.1 and 373.2 K at ambient pressure. *International journal of thermophysics*, 16(4):929–955, 1995.

[261] JM Lukashov. *Izv. Vyssh. Uchebn. Zaved. Energ.*, 20:89, 1976.

[262] M Nicolas, M Malineau, and R Reich. The Eyring significant structure theory applied to methanol-tetrahydrofuran mixtures. *Physics and Chemistry of Liquids an International Journal*, 10(1):11–22, 1980.

[263] F Travers and P Douzou. Dielectric constants of alcoholic-water mixtures at low temperature. *The Journal of Physical Chemistry*, 74(10):2243–2244, 1970.

[264] DW Davidson. The dielectric properties of Methanol and Methanol-d. *Canadian Journal of Chemistry*, 35(5):458–473, 1957.

[265] DJ Denney. Dielectric Properties of Some Liquid Alkyl Halides. *The Journal of Chemical Physics*, 27:259, 1957.

[266] GH Barbenza. Dielectric dispersion in pure methyl alcohol as a function of temperature. *J. Chim. Phys. Phys.-Chim. Biol*, 65:906, 1968.

[267] F Corradini, A Marchetti, M Tagliazucchi, L Tassi, and G Tosi. Associating Behavior of Mixed Liquids: Dielectric Properties of the Ethane-1, 2-Diol+ 1, 4-Dioxan Solvent System From-10 to+ 80 C. *Australian journal of chemistry*, 48(6):1193–1200, 1995.

[268] AP Krasnoperova, GD Juchno, and TI Lebedinez. *Vestn. Khark. Univ.*, 236:90, 1982.

[269] KK Kundu, PK Chattopadhyay, D Jana, and MN Das. Thermodynamics of self-ionization of ethylene and propylene glycols. *The Journal of Physical Chemistry*, 74(13):2633–2639, 1970.

[270] VV Levin and TL Podlovchenko. Dispersion of the Dielectric Permittivity of Ethylene Glycol. *Zh. Strukt. Khim.*, 11:766, 1970.

[271] AV Komandin and BD Shimit. Dielectric Properties of Polyatomic Alcohols in the Liquid State. *Zh. Fiz. Khim.*, 37:510, 1963.

[272] N Koizuim and T Hanai. Dielectric properties of lower-membered polyethylene glycols at low frequencies. *The Journal of Physical Chemistry*, 60(11):1496–1500, 1956.

[273] G Akerlof. Dielectric constants of some organic solvent-water mixtures at various temperatures. *Journal of the American Chemical Society*, 54(11):4125–4139, 1932.

[274] WAP Luck. A Model of Hydrogen-Bonded Liquids. *Angewandte Chemie International Edition in English*, 19(1):28–41, 1980.

[275] JC Hindman. Proton resonance shift of water in the gas and liquid states. *The Journal of Chemical Physics*, 44:4582, 1966.

[276] MM Hoffmann and MS Conradi. Are there hydrogen bonds in supercritical water? *Journal of the American Chemical Society*, 119(16):3811–3817, 1997.

[277] TF Lin, SD Christian, and HE Affsprung. Self-association and hydration of ketones in carbon tetrachloride. *The Journal of Physical Chemistry*, 71(4):968–973, 1967.

[278] B Ancian, B Tiffon, and J-E Dubois. Molecular interactions and reorientational motion of neat acetone in the liquid state.< sup> 17</sup> O NMR chemical shifts and linewidths at variable temperature. *Chemical Physics*, 74(2):171–177, 1983.

[279] RH Cole. Dielectric constants of aliphatic ketones. *The Journal of Chemical Physics*, 9:251, 1941.

[280] T Teutenberg, S Wiese, P Wagner, and J Gmehling. High-temperature liquid chromatography. Part III: determination of the static permittivities of pure solvents and binary solvent mixtures - implications for liquid chromatographic separations. *Journal of Chromatography A*, 1216(48):8480–8487, 2009.

[281] RL Smith Jr, SB Lee, H Komori, and K Arai. Relative permittivity and dielectric relaxation in aqueous alcohol solutions. *Fluid Phase Equilibria*, 144(1):315–322, 1998.

[282] T Sato and R Buchner. Dielectric relaxation processes in ethanol/water mixtures. *The Journal of Physical Chemistry A*, 108(23):5007–5015, 2004.

[283] RJ Sengwa, SS Madhvi, and S Sharma. Characterization of Heterogeneous Interaction Behavior in Ternary Mixtures by a Dielectric Analysis: Equi-Molar H-bonded Binary Polar Mixtures in Aqueous Solutions. *J. Solution Chem.*, 35:1037–1055, 2006.

[284] A Chmielewska, M Zurada, K Klimaszewski, and A Bald. Dielectric properties of methanol mixtures with ethanol, isomers of propanol, and butanol. *Journal of Chemical & Engineering Data*, 54(3):801–806, 2008.

[285] AV Gubskaya and PG Kusalik. Molecular dynamics simulation study of ethylene glycol, ethylenediamine, and 2-aminoethanol. 1. The local structure in pure liquids. *The Journal of Physical Chemistry A*, 108(35):7151–7164, 2004.

[286] AV Gubskaya and PG Kusalik. Molecular dynamics simulation study of ethylene glycol, ethylenediamine, and 2-aminoethanol. 2. Structure in aqueous solutions. *The Journal of Physical Chemistry A*, 108(35):7165–7178, 2004.

[287] F Corradini, L Marcheselli, A Marchetti, M Tagliazucchi, L Tassi, and G Tosi. A Non-Linear Correlation Model for the Relative Permittivity of Ternary Amphiprotic (Solvent) Mixtures. *Australian Journal of Chemistry*, 46(10):1545–1555, 1993.

[288] F Travers and P Douzou. Dielectric Constant of Mixed Solvents Used for a Low Temperature Biochemistry. *Biochimie*, 56:509–514, 1974.

[289] NG Tzierkezos and IE Molinou. Transport Properties of 2: 2 Symmetrical Electrolytes in (Water+ Ethylene Glycol) Binary Mixtures at T= 293.15 K . *J. Chem. Thermodynamics*, 38:1422–1431, 2006.

[290] G Douheret and A Pal. Dielectric Constants and Densities of Aqueous Mixtures of 2-Alkoxyethanols at 25. Degree. C. *J. Chem. Eng. Data*, 33:40–43, 1988.

[291] J George and NV Sastry. Partial Excess Molar Volumes, Partial Excess Isentropic Compressibilities and Relative Permittivities of Water + Ethane-1,2-diol Derivative and Water + 1,2-Dimethoxyethane at Different Temperatures. *Fluid Phase Equilibria*, 216:307–321, 2004.

[292] DK Kuila and SC Lahiri. Comparison of the Macroscopic Molecular Properties in Understanding the Structural Aspects of Mixed Aquo-Organic Binary Mixtures. *Z. Phys. Chem.*, 218:803–828, 2004.

[293] A Yurquina, ME Manzur, P Brito, R Manzo, and MAA Molina. Solubility and Dielectric Properties of Benzoic Acid in a Binary Solvent: Water-Ethylene Glycol . *J. Mol. Liq.*, 108:119–133, 2003.

[294] Y Uosaki, S Kitaura, and T Moriyoshi. Static Relative Permittivities of Water + Ethane-1,2-diol and Water + Propane-1,2,3-triol under Pressures up to 300 MPa at 298.15 K. *J. Chem. Eng. Data*, 51:423–429, 2006.

[295] A Chaudhari, GS Raju, A Das, H Chaudhari, NK Narain, and SC Mehrotra. Dielectric study of ethanol-ethylene glycol mixtures using time domain technique. *INDIAN JOURNAL OF PURE AND APPLIED PHYSICS*, 39(3):180–183, 2001.

[296] Ch Wohlfarth. Dielectric constant of the mixture (1) ethanol;(2) ethane-1, 2-diol. In *Supplement to IV/6*, pages 924–925. Springer, 2008.

[297] F Travers, P Douzou, T Pederson, and IC Gunsalus. Ternary Solvents to Investigate Proteins at Sub-zero Temperatures. *Biochimie*, 57:43–48, 1975.

[298] P Wang and A Anderko. Computation of dielectric constants of solvent mixtures and electrolyte solutions. *Fluid Phase Equilibria*, 186(1):103–122, 2001.

[299] HC Helgeson, DH Kirkham, and GC Flowers. Theoretical prediction of the thermodynamic behavior of aqueous electrolytes by high pressures and temperatures; IV, Calculation of activity coefficients, osmotic coefficients, and apparent molal and standard and relative partial molal properties to 600 degrees C and 5kb. *American Journal of Science*, 281(10):1249–1516, 1981.

[300] KA Dill, TM Truskett, V Vlachy, and B Hribar-Lee. Modeling water, the hydrophobic effect, and ion solvation. *Annu. Rev. Biophys. Biomol. Struct.*, 34:173–199, 2005.

[301] Y Marcus. Electrostriction, ion solvation, and solvent release on ion pairing. *The Journal of Physical Chemistry B*, 109(39):18541–18549, 2005.

[302] U Kaatze, D Adolph, D Gottlob, and R Pottel. Static permittivity and dielectric relaxation of solutions of ions in methanol. *Berichte der Bunsengesellschaft für physikalische Chemie*, 84(12):1198–1203, 1980.

[303] U Kaatze. Dielectric Effects in Aqueous Solutions of 1: 1, 2: 1, and 3: 1 valent Electrolytes: Kinetic Depolarization, Saturation, and Solvent Relaxation. *Zeitschrift für Physikalische Chemie*, 135(135):51–75, 1983.

[304] C Rønne, L Thrane, PO Åstrand, A Wallqvist, KV Mikkelsen, and SR Keiding. Investigation of the temperature dependence of dielectric relaxation in liquid water by THz reflection spectroscopy and molecular dynamics simulation. *The Journal of chemical physics*, 107:5319, 1997.

[305] F Booth. The dielectric constant of water and the saturation effect. *The Journal of Chemical Physics*, 19(4):391, 1951.

[306] F Booth. Dielectric constant of polar liquids at high field strengths. *The Journal of Chemical Physics*, 23:453, 1955.

[307] PJ Lenart, A Jusufi, and AZ Panagiotopoulos. Effective potentials for 1: 1 electrolyte solutions incorporating dielectric saturation and repulsive hydration. *The Journal of chemical physics*, 126:044509, 2007.

[308] K Giese, U Kaatze, and R Pottel. Permittivity and dielectric and proton magnetic relaxation of aqueous solutions of the alkali halides. *The Journal of Physical Chemistry*, 74(21):3718–3725, 1970.

[309] I Ruff. Theory of concentrated solutions of strong electrolytes. Part 1.- Some thermodynamic quantities of a lattice-like network of ions surrounded by a dielectric gradient. *J. Chem. Soc., Faraday Trans. 2*, 73(7):1858–1877, 1977.

[310] Y Marcus. Evaluation of the Static Permittivity of Aqueous Electrolytes. *Journal of Solution Chemistry*, 42(12):2354–2363, 2013.

[311] H Fricke. A mathematical treatment of the electric conductivity and capacity of disperse systems I. The electric conductivity of a suspension of homogeneous spheroids. *Physical Review*, 24(5):575, 1924.

[312] VC Weiss and W Schröer. Macroscopic theory for equilibrium properties of ionic-dipolar mixtures and application to an ionic model fluid. *The Journal of chemical physics*, 108:7747, 1998.

[313] A Levy, D Andelman, and H Orland. Dielectric constant of ionic solutions: A field-theory approach. *Physical Review Letters*, 108(22):227801, 2012.

[314] R Pottel. Dielectric Properties. In *Aqueous Solutions of Simple Electrolytes*, pages 401–431. Springer, 1973.

[315] J-P Simonin, L Blum, and P Turq. Real ionic solutions in the mean spherical approximation. 1. Simple salts in the primitive model. *The Journal of Physical Chemistry*, 100(18):7704–7709, 1996.

[316] JN Israelachvili. *Intermolecular and surface forces: revised third edition*. Academic press, 2011. ISBN: 978-0-12-391927-4.

[317] M Laliberte and WE Cooper. Model for calculating the density of aqueous electrolyte solutions. *Journal of Chemical & Engineering Data*, 49(5):1141–1151, 2004.

[318] M Laliberté. A model for calculating the heat capacity of aqueous solutions, with updated density and viscosity data. *Journal of Chemical & Engineering Data*, 54(6):1725–1760, 2009.

[319] P Novotny and O Sohnel. Densities of binary aqueous solutions of 306 inorganic substances. *Journal of Chemical and Engineering Data*, 33(1):49–55, 1988.

[320] R Pottel, E Asselborn, R Eck, and V Tresp. Dielectric relaxation rate and static dielectric permittivity of water and aqueous solutions at high pressures. *Berichte der Bunsengesellschaft für physikalische Chemie*, 93(6):676–681, 1989.

[321] ML Michelsen and EM Hendriks. Physical properties from association models. *Fluid phase equilibria*, 180(1):165–174, 2001.

[322] ML Michelsen. Robust and efficient solution procedures for association models. *Industrial & engineering chemistry research*, 45(25):8449–8453, 2006.

[323] WM Latimer, KS Pitzer, and CM Slansky. The free energy of hydration of gaseous ions, and the absolute potential of the normal calomel electrode. *The Journal of Chemical Physics*, 7:108, 1939.

[324] KS Pitzer, J C Peiper, and RH Busey. Thermodynamic properties of aqueous sodium chloride solutions. *Journal of Physical and Chemical Reference Data*, 13(1):1–102, 1984.

[325] D Saad, J Padova, and Y Marcus. Thermodynamics of mixed electrolyte solutions. VI. An isopiestic study of a pseudo-ternary system: NaCl- KCl- MgCl2- H2O at 25Â° C. *Journal of Solution Chemistry*, 4(12):983–993, 1975.

[326] HE Armstrong, JV Eyre, AV Hussey, and WP Paddison. Studies of the Processes Operative in Solutions. Parts II-V. *Proceedings of the Royal Society of London. Series A*, 79(534):564–597, 1907.

[327] Gösta Åkerlöf and Harlow E Turck. The Determination of the Activity Coefficient of Hydrochloric Acid at High Concentrations from Solubility Measurements. *Journal of the American Chemical Society*, 56(9):1875–1878, 1934.

[328] F Serowy and B Kassner. Special salting-out processes in saturated solution of mineral salts of organic origin. *Chem. Tech. Leipzig*, 9(1):27–38, 1957.

[329] JA Rard, SL Clegg, and RF Platford. Thermodynamics of {z NaCl+ (1- z) Na$_2$SO$_4$}(aq) from T= 278.15 K to T= 318.15 K, and representation with an extended ion-interaction (Pitzer) model. *The Journal of Chemical Thermodynamics*, 35(6):967–1008, 2003.

[330] CHIGP. Chemicals in Gas Processing, Joint Industry Project, Technical University of Denmark, Department of Chemical and Biochemical Engineering. Website, 2014. `http://www.chigp.dk/`.

[331] William L Masterton. Salting coefficients for gases in seawater from scaled-particle theory. *Journal of Solution Chemistry*, 4(6):523–534, 1975.

[332] Frank Millero. The activity coefficients of non-electrolytes in seawater. *Marine chemistry*, 70(1):5–22, 2000.

[333] WH Xie, WY Shiu, and D Mackay. A review of the effect of salts on the solubility of organic compounds in seawater. *Marine Environmental Research*, 44(4):429–444, 1997.

[334] N Ni and SH Yalkowsky. Prediction of Setschenow constants. *International journal of pharmaceutics*, 254(2):167–172, 2003.

[335] P Perez-Tejeda, A Maestre, P Delgado-Cobos, and J Burgess. Single-ion Setschenow coefficients for several hydrophobic non-electrolytes in aqueous electrolyte solutions. *Canadian Journal of Chemistry*, 68(2):243–246, 1990.

[336] A Yasunishi and F Yoshida. Solubility of carbon dioxide in aqueous electrolyte solutions. *Journal of Chemical and Engineering Data*, 24(1):11–14, 1979.

[337] B Rumpf, H Nicolaisen, C Öcal, and G Maurer. Solubility of carbon dioxide in aqueous solutions of sodium chloride: experimental results and correlation. *Journal of Solution Chemistry*, 23(3):431–448, 1994.

[338] CF Prutton and RL Savage. The Solubility of Carbon Dioxide in Calcium Chloride-Water Solutions at 75, 100, 120oC and High Pressures. *Journal of the American Chemical Society*, 67(9):1550–1554, 1945.

[339] R Wiebe and VL Gaddy. The solubility of carbon dioxide in water at various temperatures from 12 to 40 and at pressures to 500 atmospheres. critical phenomena*. *Journal of the American Chemical Society*, 62(4):815–817, 1940.

[340] LC Price. Aqueous solubility of petroleum as applied to its origin and primary migration. *AAPG Bulletin*, 60(2):213–244, 1976.

[341] TD O'Sullivan and NO Smith. Solubility and partial molar volume of nitrogen and methane in water and in aqueous sodium chloride from 50 to 125. deg. and 100 to 600 atm. *The Journal of Physical Chemistry*, 74(7):1460–1466, 1970.

[342] SP Pinho and EA Macedo. Solubility of NaCl, NaBr, and KCl in water, methanol, ethanol, and their mixed solvents. *Journal of Chemical & Engineering Data*, 50(1):29–32, 2005.

[343] SP Pinho and EA Macedo. Representation of salt solubility in mixed solvents: A comparison of thermodynamic models. *Fluid Phase Equilibria*, 116(1):209–216, 1996.

[344] A Pérez-Salado Kamps, M Jödecke, J Xia, M Vogt, and G Maurer. Influence of Salts on the Solubility of Carbon Dioxide in (Water+ Methanol). Part 1: Sodium Chloride. *Industrial & engineering chemistry research*, 45(4):1505–1515, 2006.

[345] ED Sloan and C Koh. *Clathrate hydrates of natural gases*. CRC press, 2007.

[346] D Avlonitis. The determination of Kihara potential parameters from gas hydrate data. *Chemical engineering science*, 49(8):1161–1173, 1994.

[347] WR Parrish and JM Prausnitz. Dissociation pressures of gas hydrates formed by gas mixtures. *Industrial & Engineering Chemistry Process Design and Development*, 11(1):26–35, 1972.

[348] EK Karakatsani and GM Kontogeorgis. Thermodynamic Modeling of Natural Gas Systems Containing Water. *Industrial & Engineering Chemistry Research*, 52(9):3499–3513, 2013.

[349] T Nakamura, T Makino, T Sugahara, and K Ohgaki. Stability boundaries of gas hydrates helped by methane - structure-H hydrates of methylcyclohexane and cis-1, 2-dimethylcyclohexane. *Chemical engineering science*, 58(2):269–273, 2003.

[350] AH Mohammadi, R Anderson, and B Tohidi. Carbon monoxide clathrate hydrates: equilibrium data and thermodynamic modeling. *AIChE journal*, 51(10):2825–2833, 2005.

[351] MD Jager and ED Sloan. The effect of pressure on methane hydration in pure water and sodium chloride solutions. *Fluid Phase Equilibria*, 185(1):89–99, 2001.

[352] MD Jager, CJ Peters, and ED Sloan. Experimental determination of methane hydrate stability in methanol and electrolyte solutions. *Fluid Phase Equilibria*, 193(1):17–28, 2002.

[353] R Kobayashi, HJ Withrow, GB Williams, and DL Katz. Gas hydrate formation with brine and ethanol solutions. In *Proceeding of the 30th Annual Convention, Natural Gasoline Association of America*, pages 27–31, 1951.

[354] JL De Roo, CJ Peters, RN Lichtenthaler, and GAM Diepen. Occurrence of methane hydrate in saturated and unsaturated solutions of sodium chloride and water in dependence of temperature and pressure. *AIChE Journal*, 29(4):651–657, 1983.

[355] National Institute of Standards and Technology (NIST). NIST Clathrate Hydrate Physical Property Database, 2014. http://gashydrates.nist.gov.

[356] J Timmermans. Critical solubility temperatures of ternary mixtures. *Z. Phys. Chem.*, 58:129–131, 1907.

[357] GB Frankforter and FC Frary. Equilibria in systems containing alcohol, salts and water, including a new method of alcohol analysis. *The Journal of Physical Chemistry*, 17(5):402–473, 1913.

[358] R De Santis, L Marrelli, and PN Muscetta. Liquid-liquid equilibria in water-aliphatic alcohol systems in the presence of sodium chloride. *The Chemical Engineering Journal*, 11(3):207–214, 1976.

[359] S Negahban, GP Willhite, SM Walas, and MJ Michnick. Three-liquid-phase equilibria of ternary and quaternary mixtures, water/n-decane/2-butyloxyethanol and water/n-octane/1-propanol/sodium chloride - experimental measurements and their correlation with the UNIQUAC model. *Fluid phase equilibria*, 32(1):49–61, 1986.

[360] T Hiaki, K Takahashi, T Tsuji, M Hongo, and K Kojima. Vapor-liquid equilibria of 1-propanol or 2-propanol with octane at 101.3 kPa. *Journal of Chemical and Engineering Data*, 40(1):274–276, 1995.

[361] Toshihiko Hiaki, Kenji Takahashi, Tomoya Tsuji, Masaru Hongo, and Kazuo Kojima. Vapor-Liquid Equilibria of Ethanol+ Octane at 343.15 K and 1-Propanol+ Octane at 358.15 K. *Journal of Chemical and Engineering Data*, 40(1):271–273, 1995.

[362] G Åkerlöf, JW Teare, and H Turck. The Variation of the Activity Coefficient of Hydrochloric Acid in Hydrochloric Acid-Sodium Chloride Solutions of Constant Total Ionic Strength from 0 to 50Â° and the Solubility of Sodium Chloride in Hydrochloric Acid Solutions at 25oC with Methyl Alcohol-Water Mixtures as Solvent. *Journal of the American Chemical Society*, 59(10):1916–1920, 1937.

[363] JA Barker and D Henderson. What is" liquid"? Understanding the states of matter. *Reviews of Modern Physics*, 48(4):587, 1976.

[364] JE Bartmess. Thermodynamics of the electron and the proton. *The Journal of Physical Chemistry*, 98(25):6420–6424, 1994.

[365] RH Boyd. Extension of Stokes' law for ionic motion to include the effect of dielectric relaxation. *The Journal of Chemical Physics*, 35:1281, 1961.

[366] MG Cacace, EM Landau, and JJ Ramsden. The Hofmeister series: salt and solvent effects on interfacial phenomena. *Quarterly reviews of biophysics*, 30(03):241–277, 1997.

[367] BE Conway. The evaluation and use of properties of individual ions in slution. *Journal of Solution Chemistry*, 7(10):721–770, 1978.

[368] COLaN. CAPE-OPEN Laboratories Network. Website, 2014. `http://www.co-lan.org`.

[369] CJ Cramer and DG Truhlar. A universal approach to solvation modeling. *Accounts of chemical research*, 41(6):760–768, 2008.

[370] W Dannhauser and LW Bahe. Dielectric constant of hydrogen bonded liquids. III. Superheated alcohols. *The Journal of Chemical Physics*, 40:3058, 1964.

[371] V Darde, B Maribo-Mogensen, WJM van Well, EH Stenby, and K Thomsen. Process simulation of CO2 capture with aqueous ammonia using the Extended UNIQUAC model. *International Journal of Greenhouse Gas Control*, 10:74–87, 2012.

[372] Z Duan and R Sun. An improved model calculating CO2 solubility in pure water and aqueous NaCl solutions from 273 to 533 K and from 0 to 2000 bar. *Chemical Geology*, 193(3):257–271, 2003.

[373] WMF Fabian. Accurate thermochemistry from quantum chemical calculations? *Monatshefte für Chemie-Chemical Monthly*, 139(4):309–318, 2008.

[374] WR Fawcett and AC Tikanen. Role of solvent permittivity in estimation of electrolyte activity coefficients on the basis of the mean spherical approximation. *The Journal of Physical Chemistry*, 100(10):4251–4255, 1996.

[375] RM Fuoss. Dependence of the walden product on dielectric constant. *Proceedings of the National Academy of Sciences of the United States of America*, 45(6):807, 1959.

[376] ME Harding, J Vázquez, B Ruscic, AK Wilson, J Gauss, and JF Stanton. High-accuracy extrapolated ab initio thermochemistry. III. Additional improvements and overview. *The Journal of chemical physics*, 128:114111, 2008.

[377] PJ Herslund, K Thomsen, J Abildskov, and N von Solms. Application of the cubic-plus-association (CPA) equation of state to model the fluid phase behaviour of binary mixtures of water and tetrahydrofuran. *Fluid Phase Equilibria*, 356:209–222, 2013.

[378] LL Lee. Thermodynamic consistency and reference scale conversion in multisolvent electrolyte solutions. *Journal of Molecular Liquids*, 87(2):129–147, 2000.

[379] AV Marenich, CJ Cramer, and DG Truhlar. Universal solvation model based on solute electron density and on a continuum model of the solvent defined by the bulk dielectric constant and atomic surface tensions. *The Journal of Physical Chemistry B*, 113(18):6378–6396, 2009.

[380] JL Martin, JL Gómez-Estévez, and M Canales. Simple statistical mechanics of electrolytes with a concentration dependent dielectric constant. Part 1. The pressure equation. *Journal of solution chemistry*, 16(2):87–104, 1987.

[381] B Maribo-Mogensen and GM Kontogeorgis. Development of a CAPE-OPEN Compatible Library for Thermodynamic Models and Unit Operations using .NET. . In *"8th ECCE (European Congress of Chemical Engineering), Berlin, Germany"*, 2011.

[382] B Maribo-Mogensen, K Thomsen, and MP Breil. Modelling Electrolyte Systems Using an Extended UNIQUAC User Model Implemented In Aspen Plus. In *"24th ESAT (European Symposium on Applied Thermodynamics), Santiago de Compostela, Spain"*, 2009.

[383] S Mattedi, FW Tavares, and M Castier. Group contribution equation of state based on the lattice fluid theory: Alkane-alkanol systems. *Fluid phase equilibria*, 142(1-2):33–54, 1998.

[384] J Mitroy, MS Safronova, and CW Clark. Theory and applications of atomic and ionic polarizabilities. *Journal of Physics B: Atomic, Molecular and Optical Physics*, 43(20):202001, 2010.

[385] G Nienhuis and JM Deutch. Comparison of Two Theories for the Two Particle Distribution Function of Polar Fluids. *The Journal of Chemical Physics*, 56:5511, 1972.

[386] PI Nagy, WJ Dunn III, G Alagona, and C Ghio. Theoretical calculations on 1, 2-ethanediol. Gauche-trans equilibrium in gas-phase and aqueous solution. *Journal of the American Chemical Society*, 113(18):6719–6729, 1991.

[387] BW Ninham and V Yaminsky. Ion binding and ion specificity: the Hofmeister effect and Onsager and Lifshitz theories. *Langmuir*, 13(7):2097–2108, 1997.

[388] BW Ninham. The present state of molecular forces. In *Smart Colloidal Materials*, pages 65–73. Springer, 2006.

[389] J Nocedal and SJ Wrigth. *Numerical Optimization*. Springer, 2006. ISBN: 0-387-30303-0.

[390] BA Pailthorpe, DJ Mitchell, and BW Ninham. Ion–solvent interactions and the activity coefficients of real electrolyte solutions. *J. Chem. Soc., Faraday Trans. 2*, 80(2):115–139, 1984.

[391] KA Peterson, D Feller, and DA Dixon. Chemical accuracy in ab initio thermochemistry and spectroscopy: current strategies and future challenges. *Theoretical Chemistry Accounts*, 131(1):1–20, 2012.

[392] A Peyman, C Gabriel, and EH Grant. Complex permittivity of sodium chloride solutions at microwave frequencies. *Bioelectromagnetics*, 28(4):264–274, 2007.

[393] T Rosenfeld and L Blum. Statistical mechanics of charged objects: General method and applications to simple systems. *The Journal of chemical physics*, 85:1556, 1986.

[394] B Ruscic, RE Pinzon, ML Morton, NK Srinivasan, MC Su, JW Sutherland, and JV Michael. Active thermochemical tables: Accurate enthalpy of formation of hydroperoxyl radical, HO2. *The Journal of Physical Chemistry A*, 110(21):6592–6601, 2006.

[395] L Saiz, JA Padro, and E Guardia. Structure of liquid ethylene glycol: A molecular dynamics simulation study with different force fields. *The Journal of Chemical Physics*, 114:3187, 2001.

[396] S Sastre, R Casasnovas, F Muñoz, and J Frau. Isodesmic reaction for pK a calculations of common organic molecules. *Theoretical Chemistry Accounts*, 132(2):1–8, 2013.

[397] BKP Scaife. Dipole Moment Fluctuations of a Dielectric Body. *Proceedings of the Physical Society. Section B*, 70(3):314, 1957.

[398] AK Soper. The radial distribution functions of water and ice from 220 to 673 K and at pressures up to 400 MPa. *Chemical Physics*, 258(2):121–137, 2000.

[399] JWH Sutherland, Gerard Nienhuis, and JM Deutch. Thermodynamics of pure and multicomponent dipolar hard-sphere fluids. *Molecular Physics*, 27(3):721–739, 1974.

[400] T Tripathy and BR De. Making Sense About Dipole Moments. *Journal of Physical Sciences*, 12:155–172, 2008.

[401] XB Wang, JB Nicholas, and LS Wang. Photoelectron spectroscopy and theoretical calculations of SO4-and HSO4-: Confirmation of high electron affinities of SO4 and HSO4. *The Journal of Physical Chemistry A*, 104(3):504–508, 2000.

[402] PK Weissenborn and RJ Pugh. Surface tension of aqueous solutions of electrolytes: relationship with ion hydration, oxygen solubility, and bubble coalescence. *Journal of colloid and interface science*, 184(2):550–563, 1996.

[403] PG Wolynes. Dynamics of electrolyte solutions. *Annual Review of Physical Chemistry*, 31(1):345–376, 1980.

[404] WD Yan, YJ Xu, and Han SJ. Activity Coefficients of Sodium Chloride in Methanol - Water Mixed Solvents at 298.15 K. *Hua Hsueh Hsueh Pao*, 52(1):937–946, 1993.

[405] R Zwanzig. Dielectric friction on a moving ion. II. Revised theory. *The Journal of Chemical Physics*, 52:3625, 1970.

Part IV

Appendices

Appendix A

Description of PhD Activities

A.1   Attended Conferences

Contributions at international conferences

- **2011**
  - 25th ESAT, St. Petersburg, Russia. Poster: An Electrolyte CPA Equation of State for Applications in the Oil- and Gas Industry. B Maribo-Mogensen, G M Kontogeorgis, K. Thomsen
  - 8th ECCE, Berlin, Germany. Oral: Development of a CAPE-OPEN Compatible Library for Thermodynamic Models and Unit Operations using .NET., B Maribo-Mogensen, G M Kontogeorgis, K Thomsen
  - SAFT2011, Pau, France. Poster: An Electrolyte CPA Equation of State for Applications in the Oil- and Gas Industry. B Maribo-Mogensen, G M Kontogeorgis, K Thomsen

- **2012**
  - NIST ThermoSymposium, Boulder, Colorado, USA. Oral: Recent Applications of the CPA Equation of State for the Petroleum and Chemical Industries, B Maribo-Mogensen, G M. Kontogeorgis, I Tsivintzelis, M Riaz, M Michelsen and Erling Stenby
  - NIST ThermoSymposium, Boulder, Colorado, USA. Oral: Comparison of Debye-Hückel and the Mean Spherical Approximation for Electrolyte Equations of State, B Maribo-Mogensen, G M Kontogeorgis and K Thomsen

- **2013**
  - PPEPPD 2013, Iguazu, Argentina. Poster: Modeling of Dielectric Properties with an Associating Equation of State. B. Maribo-Mogensen, G M Kontogeorgis, K Thomsen
  - Thermodynamics 2013, Manchester. UK. Oral: The Electrolyte CPA Equation of State, B. Maribo-Mogensen, G M Kontogeorgis, K Thomsen.
  - CAPE-OPEN Annual Meeting, Lyon. Dissemination of University Research Through CAPE-OPEN, B Maribo-Mogensen
  - AIChE 2013, San Francisco, USA. Oral: Dissemination of University Research Through CAPE-OPEN, B Maribo-Mogensen.
  - AIChE 2013, San Francisco, USA. Posters: Modeling of Thermodynamic, Volumetric, and Electrical Properties With the Electrolyte CPA Equation of State, and Modeling of Dielectric Properties of Complex Fluids With the Electrolyte CPA Equation of State, B Maribo-Mogensen, G Kontogeorgis and K Thomsen

A.2 List of Publications

Publications in internationally recognized journals as first or second author

- **2012**

    - Comparison of the Debye-Hückel and the Mean Spherical Approximation Theories for Electrolyte Solutions, B Maribo-Mogensen, G M Kontogeorgis, and K Thomsen, Ind. Eng. Chem. Res., 2012, 51 (14), pp 5353-5363

    - Process simulation of CO2 capture with aqueous ammonia using the Extended UNI-QUAC model, V Darde, B Maribo-Mogensen, W J M van Well, E H Stenby, K Thomsen, International Journal of Greenhouse Gas Control, Volume 10, September 2012, pp 74-87

    - Approach to Improve Speed of Sound Calculation within PC-SAFT Framework, X Liang, B Maribo-Mogensen, K Thomsen, W Yan, G M Kontogeorgis, Ind. Eng. Chem. Res., 2012, 51 (45), pp 14903-14914

- **2013**

    - Modeling of Dielectric Properties of Complex Fluids with an Equation of State, B Maribo- Mogensen, G M Kontogeorgis, K Thomsen, J. Phys. Chem. B (2013), 117 (2), pp 3389-3397

    - Modeling of Dielectric Properties of Aqueous Salt Solutions with an Equation of State, B Maribo-Mogensen, G M Kontogeorgis, K Thomsen, J. Phys. Chem. B, 117 (36), pp. 10523-10533

    - Solids Modelling and Capture Simulation of Piperazine in Potassium Solvents, P L Fosbøl, B Maribo-Mogensen, K Thomsen, GHGT-11, Kyoto. Energy Procedia (2013), 37, pp 844-859

- **Pending in 2014**

    - Process Design of Industrial Triethylene Glycol Processes using the Cubic Plus Assocation (CPA) Equation of State, A Arya, B Maribo-Mogensen, I Tsivintzelis, GM Kontogeorgis (submitted)

    - Development of an electrolyte CPA Equation of State for strong electrolytes, B. Maribo-Mogensen, GM Kontogeorgis, K Thomsen (to be finalized)

A.3 Attended Courses

- Optimization and Data Fitting (2010)

- Constrained Optimization (2010)

- Multivariate Statistics (2010)

- Statistical Thermodynamics for Chemical Engineering (2010)

- Thermodynamic Models , Fundamentals and Computational Aspects (2010)

- Knowledge-based entrepreneurship (2012)

- Exploring Quantum Physics (2013)

A.4   Teaching and Supervision

- Assistant teacher in Applied Colloid and Surface Chemistry (2010)

- Assistant teacher in Mathematical Models in Chemical Engineering (2011, 2012) + development of course material for Maple

- Assistant teacher in Thermodynamic Models - Fundamentals and Computational Aspects (2012, 2014) + development of course material and plugins for MATLAB

- Co-supervisor: Towards the development of a polar CPA equation of state, by MSc student Daniel K. Eriksen (2012)

- Supervision of research assistants and student helpers in relation to programming and process design with commercial simulators

Appendix B

Standard States for Electrolyte Models

B.1 Volumetric properties

If a pressure-dependent aqueous standard state is used, the volume-dependence of the equation of state becomes less important, as the main contribution to the apparent molar volume of electrolytes is from the transfer of the solute from the ideal gas (B.1).

$$\Delta_{hyd} V_i^{aq} = V_i^{aq} = \left(\frac{\partial \Delta_{hyd} G}{\partial P} \right) \tag{B.1}$$

Eq. (B.1) gives the apparent molar volume at infinite dilution. Figure B.1 shows a representative behaviour of the apparent molar volume of electrolytes at 25°C: Figure B.1 shows that the largest contribution to the apparent molar volume is from the standard state hydration free energy $\Delta_{\mathrm{hyd}} G^o$, and that linear or quadratic behavior is observed as a function of concentration.

The relationship between the pure solute (e.g. a solid) and the ideal gas reference state is given by Eq. (B.2)

$$\Delta_f G_i^{aq} (T, P) = \Delta_f G_i^{ig} (T, P_0) + \Delta_{hyd} G_i^{aq} = \Delta_f G_i^* (T, P) + \Delta_{sol} G_i \tag{B.2}$$

Ionic species are formed by dissociation from an original neutral molecule. The Gibbs energy of formation of that original molecule must be related through Eq. (B.3):

$$\Delta_f G_{A_v B_w}^{aq} = v \Delta_f G_{A^{w+}}^{aq} + w \Delta_f G_{B^{v-}}^{aq} \tag{B.3}$$

Thus it is not possible to determine the formation energies of the ionic species individually without making an extrathermodynamic assumption. The conventional approach is to define the aqueous standard state relative to the hydrogen ion. To distinguish between the true formation energy and the relative formation energy for the aqueous solids, the conventional standard state relative to hydrogen is denoted with the superscript ^{o} instead of $^{\mathrm{aq}}$ shown in Eq. (B.4) and (B.5):

$$\Delta_f H_{\mathrm{H^+}}^o (T_{ref}) \equiv 0 \qquad\qquad \Delta_f G_{\mathrm{H^+}}^o (T_{ref}) \equiv 0 \qquad\qquad \Delta S_{\mathrm{H^+}}^o (T_{ref}) \equiv 0 \tag{B.4}$$

$$C_{p,H^+}^o (T) \equiv 0 \qquad\qquad V_{H^+}^o (T) \equiv 0 \tag{B.5}$$

The conventional standard state provides the following relationship between the "true" aqueous properties of the ion M^z carrying charge z, and the properties relative to hydrogen as shown in Eq. (B.6) and Eq. (B.7):

$$\Delta_f X_{\mathrm{M}^z}^o (conv) = \left(X_{\mathrm{M}^z}^{aq} - \frac{1}{v} X_{\mathrm{M}_v}^{\bullet} \right) - z \left(X_{\mathrm{H^+}}^{aq} - \frac{1}{2} X_{\mathrm{H_2}}^{\bullet} \right) \qquad X = G, H, A \tag{B.6}$$
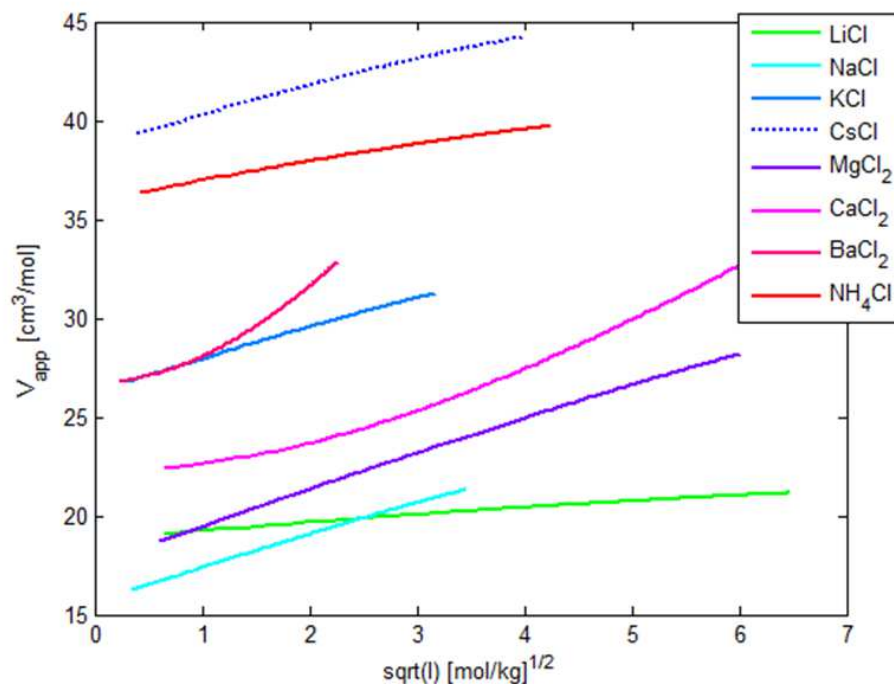
Figure B.1: Representative behaviour of the apparent molar volume as a function of square root of ionic strength.

$$X_{M^z}^o (conv) = X_{M^z}^{aq} - z X_{H^+}^{aq} \qquad X = S, C_p, V \tag{B.7}$$

Above applies to all physical properties shown in Eq. (B.5). The superscript ^{o} indicates neutral species. As long as the same convention is used and the system has an overall charge balance, the choice of the reference state does not matter as the contribution from the hydrogen ion will be balanced out when calculating the total energy/heat capacity. By the use of an extrathermodynamic conditions (i.e. that the Gibbs energy of hydration of tetraphenylarsonium and tetraphenylborate ions is set equal) one can derive a different reference state that attempts to incorporate the absolute hydration energy and entropy of the hydrogen ion[217]. While it is possible to obtain values, it is more sensitive to experimental errors and is impractical as these large ions will disintegrate at higher concentrations.

Standard state properties for the enthalpy of formation and the aqueous standard state entropy is available online in the CO-DATA collection [206], or in the CRC Handbook of Physics and Chemistry [207], where the values appear to be adopted from Marcus (1997) [214]. In the Extended UNIQUAC model, the formation energies were adopted from Wagman et al. (1982) [208]. A comparison of the values for selected ions is shown in Tables B.2-B.4. The standard state formation Gibbs energies can be measured using voltaic or galvanic cells. The electromotive force $\mathcal{E}$ may be measured at different concentrations and this may be related to the

$\Delta_f G^{\text{form}}$	Y. Marcus[214]	CRC [207]	K. Thomsen [2]
H^+	0	0	0
Li^+	-293.3	-293.3	-293.31
Na^+	-261.9	-261.9	-261.905
K^+	-283.3	-283.3	-283.27
Mg^{2+}	-454.8	-454.8	-454.8
Ca^{2+}	-553.6	-553.6	-553.58
F^-	-278.8	-278.8	-278.487
Cl^-	-131.2	-131.2	-131.228
SO_4^{2-}	-744.5	-744.5	-744.53
NO_3^-	-111.3	-111.3	-111.25
OH^-	-157.2	-157.2	-157.25

Table B.1: Standard state Gibbs free energy of formation in water at 25°C from different sources. Unit is kJ/mol. CODATA does not provide Gibbs energy of formation.

$\Delta_f H^{\text{form}}$	Y. Marcus [214]	CRC [207]	CODATA[206]	K. Thomsen[2]
H^+	0	0	0	0
Li^+	-278.5	-278.5	-278.47±±0.08	-278.49
Na^+	-240.1	-240.1	-240.34±0.06	-240.12
K^+	-252.4	-252.4	-252.14±0.08	-252.38
Mg^{2+}	-466.9	-466.9	-467.0±0.6	-466.85
Ca^{2+}	-542.8	-542.8	-543.0±1.0	-542.83
F^-	-332.6	-332.6	-335.35±0.65	-333.051
Cl^-	-167.2	-167.2	-167.080±0.1	-167.159
SO_4^{2-}	-909.3	-909.3	-909.34±0.4	-909.27
NO_3^-	-207.4	-207.4	-206.85±0.4	-207.36
OH^-	-157.2	-157.2	-230.02±0.04	-230.2

Table B.2: Standard state heat of formation in water at 25°C from different sources. Unit is kJ/mol.

standard state $\mathcal{E}_0$ by extrapolation to 0 molal as shown in Eq. B.8:

$$\mathcal{E} = \mathcal{E}_0 - \frac{RT}{v_e F} \ln \left(\prod_i a_i^{v_i} \right) \tag{B.8}$$

v_e	Stoichiometric coefficient of the electrons in the half-cell reactions
a_i	Activity of component i

By using the standard hydrogen cell electrode H/H^+ as the anode or cathode, the Gibbs energy of formation can be directly calculated from $\Delta_f G = -v_e F \mathcal{E}_0$. Care must be taken in the extrapolation towards 0 molal, as the activity coefficients are very non-linear [2].

For the standard state heat capacity (i.e. the temperature dependence of the standard state properties), the data is less reliable. Marcus e.g. cites ideal gas heat capacities for Mg^{++} and Ca^{++} and the values by K. Thomsen[2] differ for several of the other ions. However, the temperature dependence is of high importance and the optimal way of establishing this must be determined.

The approach used e.g. by K. Thomsen [2] in Extended UNIQUAC is to evaluate the aqueous heat capacity is correlated relative to the hydrogen ion. Extended UNIQUAC uses Eq. (B.9), which was suggested by Helgeson et al. [299]. This results in the non-monotonic behaviour for

S^o	Y. Marcus[214]	CRC[207]	CODATA[206]
H^+	0	0	0
Li^+	13.4	13.4	12.24±0.15
Na^+	59	59	58.45±0.15
K^+	102.5	102.5	101.2±0.2
Mg^{2+}	-138.1	-138.1	-137±4
Ca^{2+}	-53.1	-53.1	-56.2±1
F^-	-13.8	-13.8	-13.8±0.8
Cl^-	56.5	56.5	56.60±0.2
SO_4^{2-}	20.1	20.1	18.5±0.4
NO_3^-	146.4	146.4	146.7±0.4
OH^-	-10.8	-10.8	-10.9±0.2

Table B.3: Standard state entropy in water at 25°C from different sources.

C_p^o	Y. Marcus[214]	CRC[207]	K. Thomsen[75]
H^+	0	0	0
Li^+	68.6	68.6	68.6
Na^+	46.4	46.4	35.767
K^+	21.8	21.8	6.1055
Mg^{2+}	20.79	-	-18.635
Ca^{2+}	20.79	-	-32.809
F^-	-106.7	-106.7	-102.95
Cl^-	-136.4	-136.4	-126.17
SO_4^{2-}	-293	-293	-267.76
NO_3^-	-86.6	-86.6	-60.969
OH^-	-148.9	-148.5	-133.63

Table B.4: Standard state heat capacity in water at 25°C from different sources. CODATA does not provide heat capacities. Unit is J/mol/K.

different valency salts as shown in Figure B.2:

$$C_p = A + BT + \frac{C}{T - 200} \tag{B.9}$$

Note that the due to the standard state convention where H^+ has zero heat capacity, Eq. (B.9) includes the true heat capacity of the hydrogen ion as shown in Eq. (B.10). The T-dependent correlation shown in Eq. (B.9) must therefore capture the temperature and pressure dependence from the heat of hydration of the ion and that of H^+ as shown in Eq. (B.10):

$$C_{p,M^z}^{aq}(T) \approx C_{p,M^z}^{ig}(T, P_r) + \Delta_{\text{hyd}}C_{p,M^z}(T, P) - z \times \left(C_{p,H^+}^{ig}(T, P_r) + \Delta_{\text{hyd}}C_{p,H^+}(T, P) \right) \tag{B.10}$$

In order to correctly represent the heat capacity and apparent molar volume of the electrolytes over wider temperature and pressure ranges, a pressure-dependent standard state must be used - alternatively, the ideal gas standard state with an equation of state capable of representing the hydration free energy can be applied.

The geochemical community has developed several models available for the standard state properties of ions at wide ranges of temperature and pressure. Most famous is the Helgeson-Kirkham-Flowers, HKF [203]. The HKF package is implemented in the software SUPCRT92 [209]. Another similar model is the SOCW [210]. Common to these models are that they are build on correlations of measured apparent molar volume and heat capacities. The HKF and
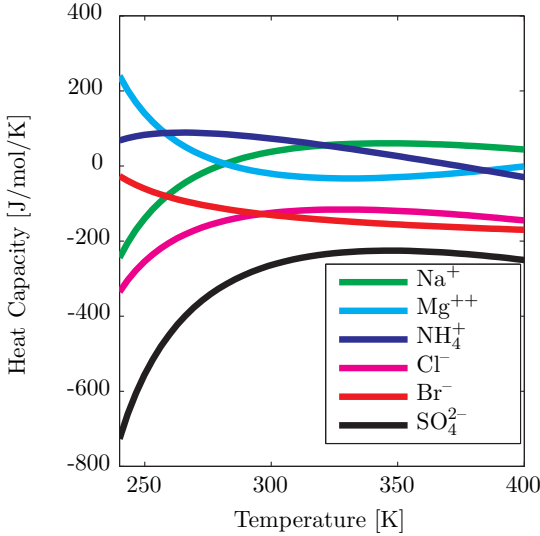
Figure B.2: Standard state heat capacities as calculated with Eq. (B.9).

SOCW model both have the limitation that they cannot be used at temperatures below -30 degrees due to a divergence of the heat capacity correlation. Furthermore, these approaches require determination of a large number of parameters and therefore require a large amount of high-quality data.

B.1.0.1 Unified Electrolyte Theory

In a recent approach by Djamali and Cobble [204, 205, 224, 225] called the Unified Electrolyte Theory (UET), the standard state properties of a set of electrolytes are described over wide ranges of temperatures and pressures using a simple approach that corrects the Born hydration energy by a non-Born hydration energy using only two parameters. They related the standard state Gibbs energy of hydration to effects due to Born and non-Born-type hydration effects, as well as changing the standard state from a hypothetically ideal gas to a liquid with density ρ^o as shown in Eq. (B.11):

$$\Delta_{\mathrm{hyd}}G = \Delta_{\mathrm{Born}}G + \Delta_{\mathrm{non-Born}}G + \Delta_{\mathrm{SS}}G \tag{B.11}$$

The Born contribution is given by Eq. (B.12):

$$\Delta_{\mathrm{Born}}G = -\frac{N_A e^2}{4\pi\varepsilon_0} \sum_i \frac{v_i z_i^2}{2R_{B,i}} \left(1 - \frac{1}{\varepsilon_r}\right) \tag{B.12}$$

The non-Born contributions are collected in an enthalpic term C_H and entropic term C_S using Eq. (B.13):

$$\Delta_{\mathrm{non-Born}}G = C_H - C_S T \tag{B.13}$$

And finally, the standard state term in Eq. (112) is from converting between an hypothetically ideal gas at $p^o = 1\mathrm{bar}$, to the hypothetically ideal $m^o = 1\mathrm{molal}$ aqueous solution with d^o as the density of the pure solvent in g/cm^3.

$$\Delta_{SS}G = vRT_{ref} \ln\left(\frac{m^o d^o R T_{ref}}{1000 p^o}\right) \tag{B.14}$$

Note that the above equation is equivalent to adding the natural logarithm of the compressibility factor. The total Gibbs energy of hydration is calculated using Eq. (B.15):

$$\Delta_{\text{hyd}}G\left(T,P\right) = \left(\Delta_{\text{hyd}}G\left(T_{\text{ref}},P_{\text{ref}}\right) - vRT_{ref}\ln\left(\frac{m^o d^o RT_{ref}}{1000p^o}\right) - C_H + T_{ref}C_S\right)F_1\left(D\right)$$
$$- C_S T + C_H + vRT\ln\left(\frac{m^o d^o RT}{1000p^o}\right)$$

$$(B.15)$$

Where the function $F(\varepsilon_r)$ is given as Eq. (B.16):

$$F_1\left(\varepsilon_r\right) = \frac{1 - \varepsilon_r\left(T,P\right)}{1 - \varepsilon_r\left(T_{\text{ref}},P_{\text{ref}}\right)}\frac{\varepsilon_r\left(T_{\text{ref}},P_{\text{ref}}\right)}{\varepsilon_r\left(T,P\right)} \qquad (B.16)$$

It is noted that by Djamali and Cobble use the Born radius as an effective radius that calculated from the Gibbs energy of hydration from Eq. (B.17):

$$\frac{1}{R_B} = \sum_i \frac{v_i z_i^2}{R_i} = \frac{8\pi\varepsilon_0}{N_A e^2}\frac{\Delta_{\text{hyd}}G\left(T_{ref},P_{ref}\right) - vRT_{ref}\ln\left(\frac{m^o d^o RT_{ref}}{1000p^o}\right) - C_H + T_{ref}C_S}{\frac{1}{\varepsilon_r\left(T_{ref},P_{ref}\right)} - 1} \quad (B.17)$$

It is evident that Eq. (B.17) can be used to rewrite Eq. (B.15) as shown in Eq. (B.18):

$$\Delta_{\text{hyd}}G\left(T,P\right) = \frac{1}{4\pi\varepsilon_0}\frac{N_A e^2}{2R_B}\left(\frac{1}{\varepsilon_r\left(T,P\right)} - 1\right) + C_H - C_S T + vRT\ln\left(\frac{m^o d^o RT}{1000p^o}\right) \quad (B.18)$$

Their approach is therefore equivalent to using the two parameters C_H and C_S to fix the temperature-dependence of the non-Born contributions to the hydration energy and subsequently calculate the Born radius from the standard state Gibbs energy at 25°C using Eq. (B.15). Their approach is quite successful for the following selection of salts over wide temperature ranges (up to above the critical temperature of water):

HCl, NaCl, CsCl, HReO$_4$, NaReO$_4$, NaOH, BaCl$_2$, CoCl$_2$, CuCl$_2$, GdCl$_3$, NaNO$_3$, NH$_4$Cl, NaB(OH)$_4$, Na(HCO$_3$), Na(HSO$_4$), Na(H$_2$PO$_4$), Na$_2$SO$_4$, Na$_2$CO$_3$, Na$_2$(HPO$_4$), Na$_3$PO$_4$

Djamali and Cobble use the Unified Electrolyte Theory from Eq. (B.11) to calculate the standard state Gibbs energy, the equilibrium constant for dissociation of water, sulfuric, phosphoric, carbonic, and boric acid. Furthermore, they calculate the temperature-dependence of the standard state volume (given the standard state molar volume at the reference conditions), entropy, and heat capacity (from the ideal gas heat capacity) with promising results again up to high temperatures and pressures.

The standard state properties from the Unified Electrolyte Theory are also suited for handling solid-liquid equilibrium mixed solvents as shown by Djamali et al. [224] when coupled with a simple correlation for the mean ionic activity coefficient of the salts. Djamali et al. [225] presented results for the solubility of BaSO4 with 1 molal NaCl in mixtures of water and ethylene glycol as well as water and methanol as a function of temperature and pressure. It is evident from Figure B.3 that the pressure can have a significant effect on not only pure component properties but also chemical equilibrium. The origin of the temperature/pressure-dependence captured by the UET is due to the Born term which depends on the behaviour of the dielectric constant, and a complete model should be able to take this into account. This is also relevant when dealing with mixed solvents or liquid-liquid equilibria of electrolytes, where the Born term provides the main driving force for the phase distribution.

The UET was also used to capture the temperature- and pressure dependence of the apparent
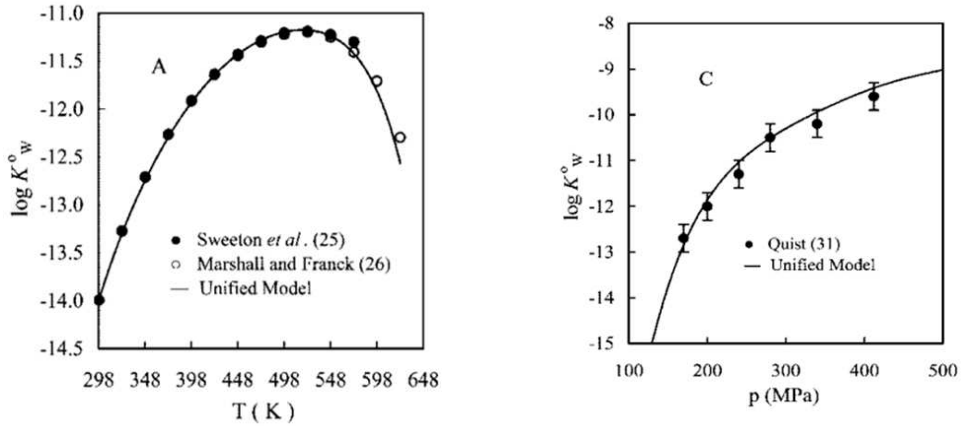
Figure B.3: Temperature dependence of the $H_2O_{<}\mathbin{=>}H^+ + OH^-$ dissociation reaction [204].
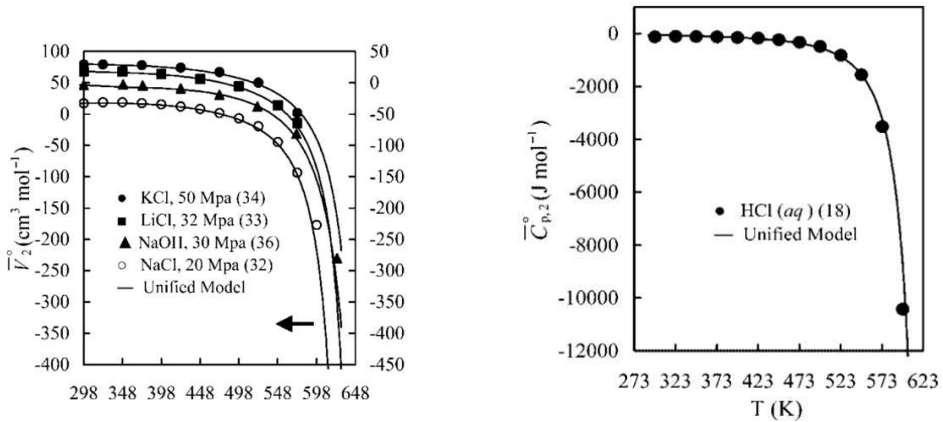
Figure B.4: Apparent molar volume and heat capacity of HCl [204].

molar volume and heat capacity as shown in Figure B.4: Finally, they used a semi-empirical model for calculation of the activity coefficients in mixed solvents and were able to predict the solubility of NaCl in mixed solvents at high temperatures as shown in Figure B.5. Figure B.5 indicates that if the dielectric constant can be modeled as a function of temperature, pressure, and composition, the standard state properties could be obtained using e.g. the UET, and the equation of state can then be used to determine the excess properties.

B.2 Conversion Between Standard States

There are many different standard states that define the chemical potential. The total chemical potential is given by Eq. (B.19):

$$\mu_i = \mu_i^\ominus + RT \ln a_i^\ominus \tag{B.19}$$

Where $\mu_i^\ominus$ and $a_i^\ominus$ are the standard state chemical potential and activity, respectively. The different reference states and the expression for the activity are summarized in Table B.5:
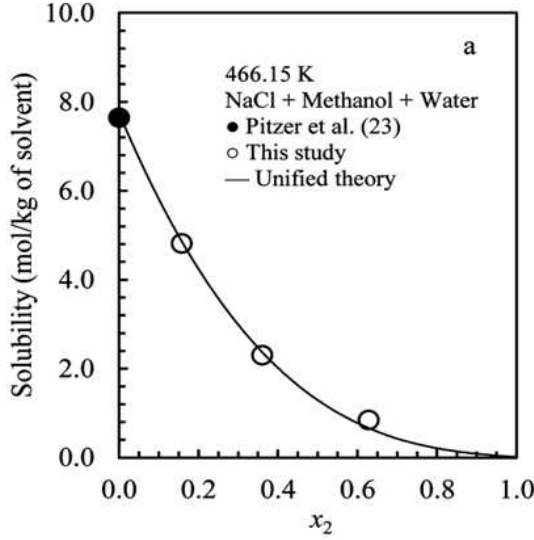
Figure B.5: Solubility of NaCl in mixtures of water (1) and methanol (2) [225].

Reference state	$\mu^{\ominus}$	$a^{\ominus}$	Symmetrical	Concentration basis
Ideal gas	μ^{ig}	$x_i \hat{\varphi}_i P$	Yes	Mole fraction
Symmetric rational	μ^{x}	$x_i \gamma_i$	Yes	Mole fraction
Asymmetric rational	$\mu^{\infty\text{x}}$	$x_i \gamma_i^*$	No	Mole fraction
Symmetric molal	μ^{m}	$m_i \gamma_i$	Yes	Molality
Asymmetric molal	$\mu^{\infty\text{m}}$	$m_i \gamma_i^*$	No	Molality
Symmetric concentration	μ^{c}	$c_i \gamma_i$	Yes	Concentration
Asymmetric concentration	$\mu^{\infty\text{c}}$	$c_i \gamma_i^*$	No	Concentration

Table B.5: Overview of reference states and concentration scales

Note that the activity and fugacity coefficient does not depend on the standard state for the concentration basis. The activity coefficient is defined in Eq. (B.20) [182]:

$$\gamma_i (T, P, \mathbf{n}) \equiv \frac{a_i}{x_i} = \frac{f_i (T, P, \mathbf{n})}{x_i f_i (T, P)} = \frac{\hat{\varphi}_i (T, P, \mathbf{n})}{\hat{\varphi}_i (T, P)} \tag{B.20}$$

Similarly, the infinite dilution activity coefficient is defined in Eq. (B.21):

$$\gamma_i^{\infty} (T, P, n_k) = \lim_{n_i=0} \gamma_i (T, P, \mathbf{n}) \tag{B.21}$$

The asymmetric activity coefficient γ_i^* is defined in Eq. (B.22):

$$\gamma_i^* = \frac{\gamma_i (T, P, \mathbf{n})}{\gamma_i^{\infty} (T, P, n_k)} = \frac{\hat{\varphi}_i (T, P, \mathbf{n})}{\hat{\varphi}_i^{\infty} (T, P, n_k)} \tag{B.22}$$

Where Eq. (B.23) defines the fugacity coefficient of component i at infinite dilution in single solvent k

$$\hat{\varphi}_i^{\infty} (T, P, n_k) = \lim_{n_i=0} \hat{\varphi}_i (T, P, \mathbf{n}) \tag{B.23}$$

There are a variety of methods to convert between the concentration basis using the following identities:

$$c_i = x_i c m_i = \frac{x_i m_0}{x_w} m_0 = \frac{1}{M_w} \tag{B.24}$$

It is found that the conversion between the standard states can be obtained using Eq. (B.25) and Eq. (B.26):

$$\mu_i^x = \mu_i^m + RT \ln m_0 - RT \ln x_w = \mu_i^c + RT \ln \rho \tag{B.25}$$

$$\mu_i^{\infty x} = \mu_i^{\infty m} + RT \ln m_0 = \mu_i^{\infty c} + RT \ln \rho_w \tag{B.26}$$

Furthermore, it is found that conversion to the ideal gas standard state can be done using Eq. (B.27) and Eq. (B.28):

$$\mu_i^{ig} = \mu_i^x - RT \underbrace{\ln\left(\varphi_i(T, P) \frac{P}{P_0}\right)}_{\text{Pure component fugacity}} \tag{B.27}$$

$$\mu_i^{ig} = \mu_i^{\infty x} - RT \underbrace{\ln\left(\hat{\varphi}_i^{\infty}(T, P, n_k) \frac{P}{P_0}\right)}_{\text{Fugacity at infinite dilution in solvent k}} \tag{B.28}$$

Following Eq. (B.25)-(B.28), the conversion can be performed explicitly provided that the model uses the mole-fraction or molality scale or asymmetric properties.

The reference state is typically selected at 298.15K and 1 bar. It is however important to realize that the different reference states are related through standard thermodynamic routes, and so the ideal gas Gibbs energy may be transformed into the aqueous state using the following steps:

$$\tfrac{1}{2}H_2(g) \rightleftharpoons H(g) \quad \Delta G = \Delta_{\text{form}} G^{ig} \tag{B.29}$$

$$H(g) \rightleftharpoons H^+(g) + e^- \quad \Delta G = IE \tag{B.30}$$

$$H^+(g) \rightleftharpoons H^+(aq) \quad \Delta G = \Delta_{\text{solvation}} G \tag{B.31}$$

The value of the solvation free energy may be calculated from the equation of state using Eq. (B.32):

$$\Delta_{\text{solvation}} G = -RT \underbrace{\ln\left(\hat{\varphi}_i^{\infty}(T_{ref}, P_{ref}, n_k) \frac{P}{P_0}\right)}_{\text{Fugacity of H}^+ \text{ at infinite dilution in solvent k}} \tag{B.32}$$

Resource on ion solvation models: [369]. Another resource using a continuum solvent model coupled with quantum chemical calculations [379].

Note that the total change in Gibbs energy by transferring a neutral molecule from the gas phase to the liquid phase is given by the Gibbs energy of hydration [114]:

$$\Delta_{H(g) \to H^+(aq)} G = IE + \Delta_{\text{solvation}} G = \Delta_{\text{hyd}} G \tag{B.33}$$

The relationship of Eq. (B.33) to to the Born model for ion hydration is obtained by setting the ion charging in vacuum equal to the ionization energy. This enables calculation of the equivalent
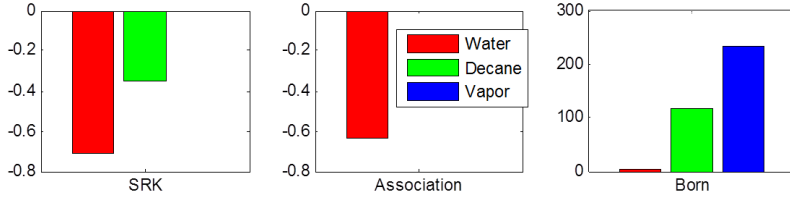
Figure B.6: Contributions to the chemical potential at infinite dilution from different terms.

Born radii, which was also done by Born in his original paper [45]. He noted that the energy of charging of a sphere in a medium with uniform dielectric constant ε_r is given by Eq. (B.34):

$$U_{\text{charging}} = \frac{1}{4\pi\varepsilon_r\varepsilon_0} \sum_i \frac{n_i z_i^2}{d_i} \tag{B.34}$$

Whereas the ionization energy is a constant and therefore takes on the same value in all phases, Eq. (B.32) shows that the equation of state must be able to quantify the Gibbs energy of solvation. To get a general idea on the values of this Gibbs energy of solvation, the contribution from ion charging in the liquid phase (with dielectric constant ε_r) can be calculated. Three cases are set up to evaluate the contributions at infinite dilution at 0°C from the different terms of the EoS:

- Vapor - volume from ideal gas equation, $\varepsilon_r = 1$

- Oil - modeled as liquid decane, $\varepsilon_r = 2$

- Water - $\varepsilon_r = 80$

Figure B.6 shows the individual contributions from different terms of the equation of state to the reduced chemical potential $\frac{\mu_i}{RT} = \left(\frac{\partial A^r/RT}{\partial n_i}\right)_{T,V,n_{j\neq i}}$ of the ions at infinite dilution. This demonstrates the importance of the solvation term in the equation of state, as it provides a significantly larger driving force towards the polar phase compared to the SRK term, which cannot provide a sufficiently large difference between the water and oil phases (at least not without fitting large binary interaction parameters).

B.3 Ideal Gas Reference State

The ideal gas reference state is well defined for many compounds and may either be measured or calculated. In order to calculate the ideal Gibbs energy of formation, there is a need to evaluate the enthalpy of formation and the absolute ideal gas entropy:

$$\Delta_{\text{form}}G^{ig}_{H+}(T_{ref}) = \Delta_{\text{form}}H^{ig}_{H+}(T_{ref}) - T_{ref}S^{ig}_{H+}(T_{ref}) \tag{B.35}$$

The ideal gas heat of formation at 298.15K is calculated through Eq. (B.36):

$$H^{ig}_{form}(T_{ref}) = H^{ig}_{form}(0K) + \int_0^{T_{ref}} C_p dT \tag{B.36}$$

The ideal gas heat of formation of ions in the gas phase is related to the adiabatic ionization energy (IE) for cations and the adiabatic electron affinity (EA) for anions:

$$\Delta_f H^{ig}_{H+} = \Delta_f H^{ig}_H + IE_{H+} - \Delta_f H^{ig}_{e-} \tag{B.37}$$

$$\Delta_f H^{ig}_{\text{OH}^-} = \Delta_f H^{ig}_{\text{OH}} - EA_{OH} + \Delta_f H^{ig}_{e^-} \tag{B.38}$$

The definition of the enthalpy of formation of the electron depends on the convention[219]. The ion convention (IC) adopts $\Delta_f H^{ig}_{e^-} = 0$ and is primarily used in mass spectroscopy and the ion physics/chemistry community, while the thermodynamic community typically use the electron convention (EC) uses $\Delta_f H^{ig}_{e^-} = \frac{5}{2} RT_{ref}$ [1]. Values may be reported using either convention, and it is therefore important to keep an eye on what convention is used by the given data source. The change in Gibbs energy/enthalpy due to a reaction is however independent of the convention when the reaction obeys the principle of charge neutrality and as long as the same convention for the pure component formation energies is used.

An overview of the different database for ion energetic and their convention is presented in NIST Webbook [219] and replicated in Table B.6: The conversion between the two conventions

Compilation	Convention	Is integration of Cp included (Eq. (B.36))?		Integrated Cp [kJ/mol]
		Molecules/Ions	Electrons	
JANAF Tables	Electron	Yes	Yes	6.197
Gurvich et al.	Electron	Yes	Yes	6.197
NBS Tables	Electron	No	Yes	6.197
Rosenstock et al.	Ion	Yes	-	-
GIANT	Ion	Yes	-	-
NIST Database 19A Version 1.09	Ion	Yes	-	-
NIST Database 19A Versions 2.0 / 3.05	Ion	No	-	-
NIST Database 19B	Ion	Yes	-	-
NIST Web-Book	Ion	Yes	-	-
NIST CC-CBDB	Ion	Yes	-	-

Table B.6: Sources for ionization energies and electron affinities and their respective conventions for the enthalpy of formation for the electron.

is obtained using Eq. (B.39) where z is the charge:

$$\Delta_f H^{\textbf{IC}}_{M^z} (T_{ref}) = \Delta_f H^{\textbf{EC}}_{M^z} (T_{ref}) - z \times 6.197 \frac{\text{kJ}}{\text{mol}} \tag{B.39}$$

CO-DATA [206] has published ideal gas formation energy/entropy for different compounds as shown in Table B.7: It may be possible to determine the entropy and ideal gas heat capacity

---

[1]In fact, the electron convention using $\Delta_f H^{ig}_{e^-} = \frac{5}{2} RT_{ref}$ arises from incorrect use of Boltzmann statistics to evaluate the integrated heat capacity; when using the Fermi-Dirac rather than Boltzmann statistics [364].

	$\Delta_f H^{\text{ig}}\ \left[\frac{\text{kJ}}{\text{mol}}\right]$ @ 0K	$\Delta_f H^{\text{ig}}\ \left[\frac{\text{kJ}}{\text{mol}}\right]$ @ 298.15K	$S^\circ\ \left[\frac{\text{J}}{\text{mol}\times\text{K}}\right]$ @ 298.15K	$C_p\ \left[\frac{\text{J}}{\text{mol}\times\text{K}}\right]$
H	211.8±0.006	217.998±0.006	114.717±0.002	20.785±0.0067
Li	153.1±1.0	159.3±1.0	138.782±0.010	20.785±0.0335
Na	101.3±0.7	107.5±0.7	153.718±0.003	20.785±0.01
K	82.803±0.8	89.0±0.8	160.341±0.003	20.785±0.01
Mg	140.90±0.8	147.1±0.8	148.648±0.003	20.785±0.01
Ca	171.6±0.8	177.8±0.8	154.887±0.004	20.785±0.01
F	72.862±0.3	79.38±0.3	158.751±0.004	21.861±0.0134
Cl	115.029±0.008	121.301±0.008	165.190±0.008	21.036±0.0134
SO4	-	-	-	-
NO3	-	-	-	-
OH	-	-	-	-

Table B.7: The ideal gas reference state for a selection of neutral molecules Data taken from CODATA (2013).

from statistical thermodynamics. By assuming independence of the translational, vibrational, rotational, and electronic to the molecular partition function, Eq. (B.40) is obtained:

$$Q = Q_{trans}Q_{rot}Q_{vib}Q_{elec} \tag{B.40}$$

Each of the contributions to Eq. (B.40) may be calculated separately, and from this it is possible to determine the reference state properties. For simple monatomic ions, there are no contributions from vibrational or rotational motion and this approach simply yields the contributions from translational energies:

$$C_p^{ig} = 5/2\ R = 20.785\text{J/mol}\cdot\text{K} \tag{B.41}$$

$$H_{\text{form}}^{ig}\left(T_{ref}\right) - H_{\text{form}}^{ig}\left(T=0\right) = \int_0^{T_{ref}} C_p^{ig}dT = 5/2\ RT_{ref} \tag{B.42}$$

$$S_{ref}^\circ = R\left(\frac{3}{2}\ln\left(\frac{2\pi mk_B T_{ref}}{h^2}\right) + \ln\frac{k_B T_{ref}}{P_{ref}} + \frac{5}{2}\right) \tag{B.43}$$

$$\Delta G_{form}^{ig} = \Delta H_{form}^{ig} - T_{ref}\Delta S^o \tag{B.44}$$

For polyatomic molecules the calculation becomes more complex as the vibrational, rotational, and possibly electronic contributions must be taken into account. Analytical solutions are possible for certain molecular configurations, but in general, the molecule geometry may be calculated with quantum chemical methods. There are several methods available for obtaining the ideal gas reference state for ions. One option is to calculate the reference state from the neutral molecule, and then use the principal ionization reactions in Eqs. (B.45)-(B.46) with literature values for the ionization energy (IE) or electron affinity (EA):

$$A \rightleftharpoons A^{n+} + ne^- \tag{B.45}$$

$$B + ne^- \rightleftharpoons B^{n-} \tag{B.46}$$

Recommended values for IE and EA are available for many ions in the NIST CCCBDB [218] and CRC Handbook of Chemistry and Physics [207]. Note that the 2nd ionization/electron affinity is always higher than the first. To calculate the enthalpy of formation, the ionization energy and the enthalpy of formation of the neutral species are needed. The data in Table B.8

	$\Delta_f H^{ig}$	S^{ig}	C_p^{ig}	IE / EA	Ion	$\Delta_f H_{ion}^{ig}$	Orig. Source
	$\left[\frac{\text{kJ}}{\text{mol}}\right]$	$\left[\frac{\text{J}}{\text{mol}\times\text{K}}\right]$	$\left[\frac{\text{J}}{\text{mol}\times\text{K}}\right]$	[eV]		$\left[\frac{\text{kJ}}{\text{mol}}\right]$	
H	218	114.7	20.79	13.6	H^+	1530.1	CODATA [206] / NIST [218]
Li	159.3±1	138.8	20.79	5.392	Li^+	679.55	CODATA [206] / NIST [218]
Na	107.5±0.7	153.7	20.79	5.139	Na^+	603.34	CODATA [206] / NIST [218]
K	89±0.8	160.2	20.79	4.341	K^+	507.85	CODATA [206] / NIST [218]
Mg	147.1±0.8	148.7	20.79	Mg/Mg+: 7.646	Mg^{++}	2336	CODATA [206] / NIST [218]
				Mg+/Mg++: 15.04			
Ca	177.8±0.8	154.9	20.79	Ca/Ca+: 6.113	Ca^{++}	1912.9	CODATA [206] / NIST [218]
				Ca+/Ca++: 11.87			
F	79.38±0.3	158.8	22.75	3.401	F^-	-248.87	CODATA [206] / NIST [218]
Cl	121.31±0.1	165.19	21.84	3.613	Cl^-	-227.29	CODATA [206] / NIST [218]
SO$_4$	-245.7±15	-	-	SO4/SO4-: 5.1±0.1	SO_4^-	-737.8±12	Wang et al. (2000) [401]
				SO4-/SO4–: -1.69*	$SO_4{}^{--}$	-574.7±18	McKee (1996) [220]
NO$_3$	73.7±1.4	252.62	46.93	3.937	NO_3^-	-306.16	NIST-JANAF [215]
OH	37.36±0.13	183.74	29.89	1.828	OH^-	-139.02	[394]

Table B.8: Ideal gas enthalpy of formation at 25°C for the neutral molecules from NIST CCCBDB and the resulting ideal gas of formation for the ions using the ion convention. For SO$_4$, the ideal gas energy of formation can be calculated backwards from the ideal gas enthalpy of formation of the SO_4^- radical and the electron affinity. The 2nd electron affinity for SO$_4$ was calculated with B3LYP/6-311+G(2d)+ZPC basis set, which calculates the first electron affinity to 5.28eV (ca. 1.8 kcal/mol from the experimental value within uncertainties - not completely satisfactory, but it's the best value available).

[J/mol/K]	C_p	$S°$	Ion	C_p	$S°$	ΔC_p	$\Delta S°$	Method
H	20.79	114.7	H+	20.79	108.95	0	5.75	Translation
Li	20.79	138.8	Li+	20.79	133	0	5.8	Translation
Na	20.79	153.7	Na+	20.79	148	0	5.7	Translation
K	20.79	160.2	K+	20.79	154.6	0	5.6	Translation
Mg	20.79	148.7	Mg++	20.79	148.7	0	0	Translation
Ca	20.79	154.9	Ca++	20.79	154.9	0	0	Translation
F	22.75	158.8	F-	20.79	145.6	(1.96)	13.2	Translation
Cl	21.84	165.19	Cl-	20.79	153.4	(1.05)	11.79	Translation
SO_4	66.27	267.55	SO4–	66.27	267.55	0	0	B3LYP (6-31G*)
NO_3	46.93	252.62	NO3-	-	261.5	-	-8.88	B3LYP (6-31G*)
				44.85	257.8	2.08	-5.18	LSDA (6-31G*)
OH	29.89	183.74	OH-	29.1	173.64	0.79	10.1	Translation + rotation

Table B.9: Ideal gas heat capacity and entropy from the NIST CCCBDB [218] at 298.15K. Note that the values for F^- and Cl^- ions are equal to the theoretical ideal gas monatomic heat capacity, and are therefore not believed calculated with the same method as for the uncharged species.

uses the ion convention: The ideal gas enthalpies in Table B.8 neglects changes in the heat capacity from the neutral molecule to the ion. Albeit a reasonable assumption for atomic ions, this may not always be the case for polyatomic ions. In such cases, insight can be provided by computational chemistry, where recently significant advances have been made in calculating thermophysical properties from ab initio methods. Table B.9 summarizes results obtained from these methods found in the NIST CCCBDB for different ions. Eq. B.47 may be used to correct the values in Table B.8 to include the change in heat capacity as calculated in Table B.9.

$$\Delta_f H_{M^+}^{ig} - \Delta_f H_M^{ig} = IE_{M^+} + \int_0^{T_{ref}} \Delta C_p dT \approx IE_{M^+} + \Delta C_p T_{ref} \tag{B.47}$$

It is unclear why there are some ions in Table B.9 that undergo a change in entropy and heat capacity, while some do not. Most likely this is not a physical effect and is simply due to calculations being done with different assumptions. Unfortunately, it makes it unreliable to take values directly from these tables, and it is therefore necessary to recalculate these values.

B.4   Accurate Thermochemistry from Ab Initio Methods

The aim of extrapolated ab initio methods is to yield heat of formation and ionization potentials within the chemical accuracy, which is defined as 1 kcal/mol in a 95% confidence interval. The variation should therefore be within 0.5 kcal/mol for thermochemical methods to give acceptable results. This remains a challenge for single quantum chemistry methods such as CCSD(T), but has been achieved by using e.g. the focal-point extrapolation methods, the Weizmann (Wn) family, and the high-accuracy extrapolated ab initio thermochemistry (HEAT) protocol. Such goal has been achieved for molecules consisting of light components from the first few rows of the periodic table [373, 376, 391].

The energy/entropy difference may be computed through the atomization scheme shown in Eq. (B.48), which builds up molecules from it's atomic constituents and then determine energy/entropy changes through its atomization reaction.

$$CH_4 \rightleftharpoons C + 4H \tag{B.48}$$

The HEAT paradigm [376] is based on the atomization scheme calculates the total ground state energy of atoms and molecules using:

$$\Delta E = \Delta E_{\text{HF}}^{\infty} + \Delta E_{\text{CCSD(T)}}^{\infty} + \Delta E_{\text{CCSDT}} + \Delta E_{\text{HLC}} + \Delta E_{\text{rel}} + \Delta E_{\text{SO}} + \Delta E_{\text{DBOC}} + \Delta E_{\text{ZPE}} \quad \text{(B.49)}$$

$\Delta E_{\text{HF}}^{\infty}$	Hartree-Fock limit energy (restricted HF for closed shells and unrestricted HF for open shells)
	Estimate for $CCSD(T)$ correlation energy.
$\Delta E_{\text{CCSD(T)}}^{\infty}$	
	account for deficiencies in electron correlations in the $CCSD(T)$
$\Delta E_{\text{CCSDT}}+$ ΔE_{HLC}	model
ΔE_{rel}	accounts for scalar relativistic effects via perturbation theory
ΔE_{SO}	accounts for differences in treatment of the ground-state energy and the weighted average of spin orbits
ΔE_{DBOC}	is the diagonal Born-Oppenheimer correction (includes the contribution of core effects)
ΔE_{ZPE}	accounts for the vibrational zero-point energy

One limitation of the protocols based on atomization reactions is that they become less accurate for larger molecules (>10 atoms) and the inaccuracies will increase with the number of atoms and it is deemed as unrealistic that an atomization scheme such as HEAT can calculate formation enthalpies of e.g. benzene within chemical accuracy [376]. Harding et al. (2008) [376] notes that abandoning or altering the separate treatment of the core and valence electrons (Born-Oppenheimer) is needed if the field is to progress towards larger molecules through atomization reactions.

Another approach is to use isodesmic reactions to achieve partial error cancellation [396]. This involves coming up with hypothetical reaction schemes where the bond hybridization are conserved in the reaction. This works favourably in terms of error cancellation and has been used since the 1970s to devise information of thermochemistry through simple models [396]. Homodesmic reaction schemes improve of the isodesmic approach by also ensuring that there is no change in the number of hydrogen joined to the carbon atoms. The latter comes with higher accuracy, but also longer computation times.

So far, all known work on electrolyte systems has used the aqueous reference state. This is mainly due to two reasons:

- The thermodynamic models employed have mainly been based on activity coefficients

- Using the ideal gas reference state requires accounting for the Gibbs energy of solvation

However, none of the above points are show-stoppers for using the ideal gas as the reference state in e-CPA, if the residual properties can be calculated to a reasonable accuracy. The most widely used model for ion solvation is attributed to Max Born (1920) [45]. The model was developed to estimate the Gibbs energy of solvation by transferring an ion from the vapour phase to the liquid phase. The electrical work required to charge a sphere and the electrical field is given by Eq. (B.50):

$$W = \int_0^{z_i e} \int_{r_i}^{\infty} E(r) \, dr \, dq \qquad E(r) = \frac{1}{4\pi\varepsilon_r\varepsilon_0} \frac{q_i}{r^2} \quad \text{(B.50)}$$

Evaluating the integral in Eq. (B.50) yields Eq. (B.51):

$$W_i = \frac{e^2}{8\pi\varepsilon_r\varepsilon_0} \frac{z_i^2}{R_i} \quad \text{(B.51)}$$

	IE / EA [eV]	Ion	r_{Born} [Å]	r_{Marcus} [Å]	$\frac{r_{\text{Born}}}{r_{\text{Marcus}}}$	$r_{\text{Born}} - r_{\text{Marcus}}$ [Å]
H	13.6	H^+	0.53	-	-	-
Li	5.392	Li^+	1.34	0.69	1.93	0.64
Na	5.139	Na^+	1.4	1.02	1.37	0.38
K	4.341	K^+	1.65	1.38	1.2	0.28
Mg	Mg=>Mg^+: 7.646	Mg^{++}	1.27	0.71	1.79	0.56
	Mg^+=>Mg^{++}: 15.04					
Ca	Ca=>Ca^+: 6.113	Ca^{++}	1.6	1	1.6	0.6
	Ca^+=>Ca^{++}: 11.87					
F	3.401	F^-	2.11	1.33	1.59	0.78
Cl	3.613	Cl^-	1.99	1.81	1.1	0.18
SO_4	5.1±0.1	SO_4^-	1.41	-	-	-
	5.1-1.69	$SO_4{}^{--}$	8.44	2.3	3.67	6.14
NO_3	3.937	NO_3^-	1.83	1.79	1.02	0.04
OH	1.828	OH^-	3.94	1.33	2.96	2.6

Table B.10: Ionic radii as calculated from Eq. (B.51) and measured ion diameters Marcus (1997)[214].

Born (1920) [45] estimated the solvation radius R_i by setting the work required to charge the ion in vacuum equal to the ionization energy or electron affinity of a range of molecules using Eq. (B.51) - note that this approach neglects change in the ideal gas entropy. Table B.10 presents the radii calculated from Eq. (B.51): The differences between the measured ion diameters and the calculated Born radius is often interpreted as being due to the inclusion of the solvation shell surrounding the molecules [216].

The Born term takes into account the effect of ion charging, but not the effect of reorientation of the solvent molecules in the vicinity of the ion. Israelichvili (2011) [316] derives the interaction energy between ion and dipoles for the first shell using (Eq. (B.52)):

$$w_1(r) = -\frac{(z_i e)\,\mu_j \cos\theta}{4\pi\varepsilon_0\varepsilon_r r^2} \tag{B.52}$$

Where $\cos\theta$ is obtained from the maximum attraction (i.e. $0°$ when the dipole is near a cation and $180°$ for anions). This gives Eq. (B.53) for the interaction energy:

$$w_1(r) = -\frac{e\,|z_i|\,\mu_j}{4\pi\varepsilon_0\varepsilon_r r^2} \tag{B.53}$$

The interaction energy with the subsequent shells are calculated from Eq. (B.54):

$$w_2(r) = -\frac{e^2 z_i^2 \mu_j^2}{6(4\pi\varepsilon_r\varepsilon_0)^2 k_B T r^4} = w_1(r)\left(\frac{e\,|z_i|\,\mu_j}{24\pi\varepsilon_r\varepsilon_0 k_B T r^2}\right) \tag{B.54}$$

Note that while Eq. (B.53) follows the same functional behaviour as the Born-term (inverse proportional to the dielectric constant), the 2nd term has a different behaviour and also depends on the temperature. However, as this is only included for the outer hydration shells and the energy decreases with the distance cubed, the dominating term may be assumed to be from the inner hydration shell. If this is the case, the total interaction energy may be calculated by including the first shell contributions from:

$$W = \sum_i n_i N_A \left(\frac{e^2}{8\pi\varepsilon_r\varepsilon_0}\frac{z_i^2}{r_i} - N_{ij}w_1(r_i + r_w)\right) \approx \sum_i \beta_i n_i N_A \left(\frac{e^2}{8\pi\varepsilon_r\varepsilon_0}\frac{z_i^2}{r_i}\right) \tag{B.55}$$

That is, if an empirical parameter in water is fitted, it may be possible to determine the hydration free energy. This parameter is expected to be between 0 and 1 (as the contribution from

hydration by the dipoles is negative). This is well in line with the observation that the hydration free energies calculated with the Born model are too large. Eq. (B.55) justifies fitting a Born radius to take into account the effect of ion solvation including the hydration shell. However, when the solvent is no longer water, the energy from the solvation shell could change.

There are also experimental sources available for the enthalpy of hydration. Marcus (1986) [217] reviewed different sources for the enthalpy of solvation of various ions, and showed that the en-

thalpy and entropy of hydration of the H$^+$ ion was given by: $\Delta_{hyd}H = \begin{cases} -1098 \pm 5 \\ -1091 \pm 10 \\ -1104 \pm 17 \\ -1103 \pm 7 \end{cases} \left[\frac{\text{kJ}}{\text{mol}}\right] \Delta_{hyd}S^o \approx$

$-131 \pm 1 \frac{\text{J}}{\text{molK}}$ The relatively similar standard hydration enthalpies were determined from extrapolation methods, measured via electrode potentials and from the so-called TATB extrathermodynamic assumption, where the enthalpy of hydration of three molecules of similar size and charge are defined as equal, enabling determination of other ions from the lattice enthalpy and heats of solution of salts with tetraphenyl ions and suitable counterions [217]:

$$\Delta_{hyd}H^o\left[(C_6H_5)_4As^+\right] = \Delta_{hyd}H^o\left[(C_6H_5)_4P^+\right] = \Delta_{hyd}H^o\left[B\left(C_6H_5\right)_4^-\right] \tag{B.56}$$

So, in order to convert between normal the aqueous standard state and the ideal gas standard state, it is necessary to apply the following correction at 25°C (where z is the charge of the ion:

$$\underbrace{\Delta_f H_{M^z}^{ig}}_{\substack{\text{Idealgas}}} + \underbrace{\Delta_{hyd} H_{M^z}^{aq}}_{\substack{\text{Truehyd.energy}}} = \underbrace{\Delta_f H_{M^z}^{aq}}_{\substack{\text{Conventional} \\ \text{AqueousS.S.}}} + z \times \underbrace{\Delta_f H_{H^+}^{aq}}_{\substack{\text{Trueformation} \\ \text{enthalpyofH}^+}} \tag{B.57}$$

When the true hydration energy is available, the conventional standard state formation enthalpy can be calculated as shown in Table B.11. Good agreement with the values presented by K. Thomsen for is observed all ions but sulphate. If the 2nd ionization energy is back-calculated from the conventional standard state, EA $\left(SO_4^- \to SO_4^{--}\right) = -0.1\text{eV}$ is obtained, and this value is significantly less than -1.6eV obtained from quantum chemical calculations [220]. By using the back-calculated value, a Born radius $r_{Born} = 5.76$Å can be calculated, and this is closer to the crystallographic radius. The aqueous standard state entropy of the different components was investigated by Marcus [217]. By using measured values for the absolute entropy of the hydrogen ion in the aqueous standard state, Marcus [217] recalculated the standard state using Eq. (B.58).

$$\underbrace{S_{M^z(g)}^o}_{\substack{\text{Idealgas}}} + \underbrace{\Delta_{\text{hyd}}S_{M^z}^o}_{\substack{\text{Hydration} \\ \text{entropy}}} = \underbrace{S_{M^z(aq)}^o}_{\substack{\text{Conventional} \\ \text{AqueousS.S.}}} + z \underbrace{S_{H^+(aq)}^o}_{\substack{\text{Absolute} \\ \text{entropyofH}^+}} \tag{B.58}$$

The absolute entropy of the hydrogen ion in water was calculated from various methods and the recommended value was set to $-22.2 \pm 1.2\frac{\text{J}}{\text{molK}}$. Using this value and the aqueous standard state entropies shown in Table B.3 Marcus [217] calculated the entropy of hydration.
The Gibbs energy of formation in the aqueous phase was analyzed by Marcus [216], who also used a Born-type model for calculation of the hydration free energy. The Gibbs energy of formations are related using Eq. (B.59):

$$\underbrace{\Delta_f G_{M^z}^{ig}}_{\substack{\text{Idealgas}}} + \underbrace{\Delta_{\text{hyd}}G_{M^z}}_{\substack{\text{Freeenergyof} \\ \text{hydration}}} = \underbrace{\Delta_f G_{M^z}^{aq}}_{\substack{\text{Conventional} \\ \text{AqueousS.S.}}} + z \underbrace{\Delta_f G_{H^+}^{aq}}_{\substack{\text{Absoluteformationfree} \\ \text{energyofH}^+(aq)}} \tag{B.59}$$

The Gibbs energy of hydration can be calculated from the e-CPA from the change in Gibbs energy at infinite dilution from Eq. (B.32). In order for the definition of the aqueous heat capacity

Ion	$\Delta_f H^{\mathrm{ig}}$ [kJ/mol]	$\Delta_{hyd} H^{\mathrm{ig}}$ [kJ/mol]	$\Delta_f H^{\mathrm{aq}}$ [kJ/mol]	$\Delta_f H^{\mathrm{aq,conv}}$ [kJ/mol]	$\Delta_f H^{\mathrm{aq,conv}}$ (K. Thomsen)
H+	1530.1	-1103	427.05	0	
Li+	679.55	-531	148.55	-278.5	-278.49
Na+	603.34	-416	187.34	-239.71	-240.12
K+	507.85	-334	173.84	-253.21	-252.38
Mg++	2336	-1949	386.97	-467.13	-466.85
Ca++	1912.9	-1602	310.9	-543.2	-542.83
F-	-248.87	-510	-758.77	-331.72	-333.051
Cl-	-227.29	-367	-594.3	-167.24	-167.159
SO4-	-737.8±12				
SO4--	-574.7±18	-1035	-1609.7	-755.64	-909.27
NO3-	-306.16	-325	-631.17	-204.11	-207.36
OH-	-139.02	-520	-659.01	-231.96	-230.243

Table B.11: Calculation of conventional standard state aqueous formation enthalpy from the ideal gas enthalpy and the heat of hydration. Ideal gas formation enthalpies were taken from Table B.10. Hydration energies were taken from Marcus [214]

of the hydrogen ion to be zero at all temperatures, the heat capacity must be compensated in a similar way. The aqueous state heat capacity may be calculated using:

$$\underbrace{C^{ig}_{p,M^z}}_{\text{Ideal gas}} + \underbrace{\Delta_{\mathrm{hyd}} C^{ig}_{p,M^z}}_{\substack{\text{Hydration heat} \\ \text{capacity}}} = \underbrace{C^{aq}_{p,M^z}}_{\substack{\text{Conventional} \\ \text{Aqueous S.S.}}} + z \underbrace{C^{aq}_{p,\mathrm{H^+}}}_{\substack{\text{Absolute heat} \\ \text{capacity of H}^+(aq)}} \tag{B.60}$$

Eq. (B.60) has several important implications for the heat capacities of aqueous electrolytes. By isolating the conventional heat capacity, it is evident that the aqueous standard state heat capacity is given by Eq. (B.61):

$$C^{aq}_{p,M^z} = C^{ig}_{p,M^z} + \Delta_{\mathrm{hyd}} C_{p,M^z} - z \times C^{aq}_{p,\mathrm{H^+}} \tag{B.61}$$

So when the heat capacity is correlated using the functional form given by Eq. (B.9), this includes all of the above contributions; the ideal gas contribution (which is fairly constant), the hydration contribution, as well as the contribution from the true heat capacity of the hydrogen ion (that is, ideal gas + hydration). While this is possible to do when data is available, it is very difficult to predict the values going into the correlation as it contains many different contributions of different signs, which was also evident from the behaviour shown in Figure B.2.

Appendix C

Computational Aspects

This chapter discusses the implementation of the e-CPA equation of state and includes details on the derivations and the computational aspects.

C.1 Unconstrained Minimization of Helmholtz Energy for the Implicit MSA

This work presents an alternative method based on an unconstrained minimization of the Helmholtz energy, as shown in (C.1):

$$\min_\Gamma Q = \frac{V\Gamma^3}{3\pi} - \frac{1}{k_B T}\frac{Ve^2}{4\pi\varepsilon_r\varepsilon_0}\sum_i^N \rho_i z_i \left[\frac{\Gamma z_i + \eta\sigma_i}{1+\sigma_i\Gamma}\right] \tag{C.1}$$

At the solution, the gradient of Eq. (C.1) is zero, meaning that Eq. (4.28) is fulfilled. This simultaneously fulfills the MSA closure equation given by Eq. (4.22). The initial estimate is generated based on assuming N_i in Eq. (4.22), and subsequently minimize Eq. (C.1) by converging the iterative Newton scheme shown in Eq. (C.2) within a specified absolute or relative tolerance on Γ.

$$\Gamma^{(k+1)} = \Gamma^{(k)} - \left(\frac{\partial Q}{\partial\Gamma}\right)_{V,T,\underline{n}}\left(\frac{\partial^2 Q}{\partial\Gamma^2}\right)_{V,T,\underline{n}}^{-1} \tag{C.2}$$

From the solution of Eq. (C.1) it is simple to obtain the first and second order derivatives of MSA against any variable a or b, as shown in Eqs. (C.3)-(C.4):

$$\frac{\partial}{\partial a}\left(\frac{A^{MSA}}{RT}\right)_{T,V,\underline{n}} = \frac{\partial}{\partial a}(Q)_{T,V,\underline{n},\Gamma} + \frac{\partial}{\partial\Gamma}(Q)_{T,V,\underline{n},\Gamma}\left(\frac{\partial\Gamma}{\partial a}\right)_{T,V,\underline{n}} = \frac{\partial}{\partial a}(Q)_{T,V,\underline{n},\Gamma} \tag{C.3}$$

$$\frac{\partial^2}{\partial a\partial b}\left(\frac{A^{MSA}}{RT}\right)_{T,V,\underline{n}} = \left(\frac{\partial^2 Q}{\partial a\partial b}\right)_{T,V,\underline{n},\Gamma} + \left(\frac{\partial^2 Q}{\partial\Gamma\partial a}\right)_{T,V,\underline{n},\Gamma}\left(\frac{\partial\Gamma}{\partial b}\right)_{T,V,\underline{n}} \tag{C.4}$$

The sensitivity of Γ wrt. b can be obtained using a linearization of the gradient at the solution as shown in Eq. (C.5):

$$\left(\frac{\partial Q}{\partial\Gamma}\right)_{V,T,\underline{n}} = \left(\frac{\partial Q}{\partial\Gamma}\right)_{V,T,\underline{n}} + \left(\frac{\partial^2 Q}{\partial\Gamma^2}\right)_{V,T,\underline{n}}\left(\frac{\partial\Gamma}{\partial b}\right) = 0 \tag{C.5}$$

The MSA equations are then solved using the following scheme:

- Calculate the initial estimate from assuming $N_i = 0$ in Eq. (4.22)

- Perform three damped successive substitution steps using Eq. (4.22)

- Set the maximum value of Γ from the relation $(2\Gamma)^2 \leq \kappa^2$

- Solve the iterative Newton scheme from Eq. (C.2) until a reasonable convergence is obtained

C.2   Derivation of the Multicomponent Onsager-Kirkwood Equation

The equation for the dielectric constant of multi-component mixtures with association (Eq. (5.4)) was presented by by Hasted (1972) [154]. In this section the equation will be derived following the procedure by Buckingham (1956) [153].

The investigated system consists of a large sphere of homogeneous isotropic material with the relative static permittivity ε_r that is exposed to an uniform electrical field $E_0\mathbf{e}$, where E_0 is a measure of the strength and $\mathbf{e}$ is a unit vector in the direction of the field. The static permittivity is calculated from Eq. (C.6):

$$\frac{\varepsilon_r - 1}{\varepsilon_r + 2} = \frac{1}{3\varepsilon_0 V}\left(\frac{\partial}{\partial E_0}\left\langle \mathbf{M}\cdot\mathbf{e}\right\rangle\right)_{E_0=0} \tag{C.6}$$

$\mathbf{M}$ constitutes the sum of the total molecular electrical moments given by Eq. (C.7)

$$\mathbf{M} = \sum_i \mathbf{m}_i \tag{C.7}$$

To avoid the effect of the electrical field on the derivative is taken at the limit where $E_0 = 0$. The property $\langle \mathbf{M}\cdot\mathbf{e}\rangle$ relates the mean moment of a small macroscopic sphere with volume V at the center of the large sample. The statistical mechanical average over all configurations τ indicated by the brackets is defined by Eq. (C.8):

$$\langle X\rangle = \frac{\int X \exp\left(-\beta U\left(\tau, E_0\right)\right)d\tau}{\int \exp\left(-\beta U\left(\tau, E_0\right)\right)d\tau} \tag{C.8}$$

Where $U\left(\tau, E_0\right)$ is the total potential energy of the system for configuration τ subject to the external field strength E_0. It is related through Eq. (C.9):

$$\frac{\partial U\left(\tau, E_0\right)}{\partial E_0} = -\mathcal{M}\left(\tau, E_0\right)\cdot\mathbf{e} \tag{C.9}$$

Where $\mathcal{M}$ is the electrical moment of the large sphere at the configurations τ. Insertion of Eq. (C.8) into Eq. (C.6) yields Eq. (C.10):

$$\frac{\varepsilon_r - 1}{\varepsilon_r + 2} = \frac{1}{3\varepsilon_0 V}\left[\left\langle\frac{\partial\mathbf{M}\cdot\mathbf{e}}{\partial E_0}\right\rangle + \frac{1}{3k_BT}\left\langle\mathbf{M}\cdot\mathcal{M}\right\rangle\right] \tag{C.10}$$

The term $\left\langle\frac{\partial\mathbf{M}\cdot\mathbf{e}}{\partial E_0}\right\rangle$ may be related to the mean polarizability of the inner sphere and can be related to the high-frequency dielectric constant, such that Eq. (C.10) may be rewritten as Eq. (C.11):

$$\frac{\varepsilon_r - 1}{\varepsilon_r + 2} - \frac{\varepsilon_\infty - 1}{\varepsilon_\infty + 2} = \frac{\langle\mathbf{M}\cdot\mathcal{M}\rangle}{9\varepsilon_0 k_BTV} \tag{C.11}$$

If the central sphere had been in a vacuum instead of in the interior of a larger sphere Eq. (C.11) may be written as Eq. (C.12):

$$\frac{\varepsilon_r - 1}{\varepsilon_r + 2} - \frac{\varepsilon_\infty - 1}{\varepsilon_\infty + 2} = \frac{\left\langle M^2\right\rangle_0}{9\varepsilon_0 k_BTV} \tag{C.12}$$

Eq. (C.12) was also obtained by [397]. It is possible to expand $\left\langle M^2\right\rangle_0$ into the powers of the molecular polarizabilities. If the total electrical moment is given by the sum of the gas moment

and the induced moment, it may be shown that $\mathbf{m}_i = \mu_{0i} + \mathbf{m}'_i$, yielding the expansion in Eq. (C.13):

$$
\left\langle M^2 \right\rangle_0 = \sum_i \left\langle (\mu_{0i} + \mathbf{m}'_i) \cdot \mathbf{M} \right\rangle_0
$$
$$
= \sum_i \left\langle \mu_{0i} \cdot \mathbf{M} \right\rangle_0 + \sum_i \sum_j \left\langle \mu_{0i} \cdot \mathbf{m}'_j \right\rangle_0 + \sum_i \sum_j \left\langle \mathbf{m}'_i \cdot \mathbf{m}'_j \right\rangle_0
$$
(C.13)

When all molecules are of the same kind, Eq. (C.13) can be transformed into Eq. (C.14):

$$
\left\langle M^2 \right\rangle_0 = N \langle \mu_{01} \cdot \mathbf{M} \rangle_0 + N \langle \mu_{01} \cdot \mathbf{M}' \rangle_0 + O\left(\alpha_0^2\right) \tag{C.14}
$$

Where the error is in the order of the square of the molecular polarizability. $\langle \mu_{01} \cdot \mathbf{M} \rangle_0$ evaluates as Eq. (C.15):

$$
\langle \mu_0 \cdot \mathbf{M} \rangle_0 = \frac{9\varepsilon_r}{(2\varepsilon_r + 1)(\varepsilon_r + 2)} \mu_0 \cdot \bar{\mathbf{m}} \tag{C.15}
$$

Where $\bar{\mathbf{m}}_1$ is the average molecular moment of molecule 1 at fixed positions/orientations. $\langle \mu_{01} \cdot \mathbf{M}' \rangle_0$ becomes Eq. (C.16):

$$
\langle \mu_0 \cdot \mathbf{M}' \rangle_0 = \frac{3(2\varepsilon_r + \varepsilon_\infty)}{(2\varepsilon_r + 1)(\varepsilon_\infty + 2)} \mu_0 \bar{\mathbf{m}} - \mu_0 \cdot \overline{\mu}_0 \tag{C.16}
$$

Inserting Eq. (C.16) into Eq. (C.12) yields Eq. (C.17):

$$
\frac{3(\varepsilon_r - \varepsilon_\infty)}{(\varepsilon_r + 2)(\varepsilon_\infty + 2)} = \frac{N}{9k_B TV} \left[\frac{1}{(2\varepsilon_r + 1)} \left[\frac{9\varepsilon_r}{(\varepsilon_r + 2)} + \frac{3(2\varepsilon_r + \varepsilon_\infty)}{(\varepsilon_\infty + 2)} \right] \mu_0 \cdot \bar{\mathbf{m}} - \mu_0 \cdot \overline{\mu}_0 \right] \tag{C.17}
$$

Buckingham [153] concludes that a rigorous description of the static permittivity of a polar fluid requires two interaction moments $\bar{\mathbf{m}}$ and $\overline{\mu}_0$. Onsager [150] assumes absence of short-range directional forces between molecules, and thus $\mu_0 \cdot \overline{\mu}_0 = \mu_0^2$, and furthermore determines the total moment from the relation in Eq. (C.18):

$$
\mathbf{m} = \frac{(2\varepsilon_r + 1)(\varepsilon_\infty + 2)}{3(2\varepsilon_r + \varepsilon_\infty)} \mu_0 \tag{C.18}
$$

Inserting Eq. (C.18) into Eq. (C.16) yields $\langle \mu_0 \cdot \mathbf{M}' \rangle_0 = 0$. Buckingham[153] notes that Eq. (C.18) is a good approximation for many liquids but is inaccurate in imperfect gases. Assuming that $\langle \mu_0 \cdot \mathbf{M}' \rangle_0 = 0$ is also true for a mixture, Eq. (C.14) can be simplified as:

$$
\left\langle M^2 \right\rangle_0 = \sum_i \langle \mu_{0i} \cdot \mathbf{M} \rangle_0 \tag{C.19}
$$

Using Eq. (C.16) Eq. (C.19) is expanded yielding Eq. (C.20):

$$
\left\langle M^2 \right\rangle_0 = \frac{9\varepsilon_r}{(2\varepsilon_r + 1)(\varepsilon_r + 2)} \sum_i N_i \sum_j \langle \mu_{0,i} \cdot \mathbf{m}_j \rangle \tag{C.20}
$$

Additionally, if Eq. (C.18) is introduced (whereby it is assumed that there is no local variation in ε_∞ near the central sphere compared to the medium) into Eq. (C.20), Eq. (C.21) is obtained:

$$
\left\langle M^2 \right\rangle_0 = \frac{3\varepsilon_r}{(2\varepsilon_r + \varepsilon_\infty)} \frac{(\varepsilon_\infty + 2)}{(\varepsilon_r + 2)} \sum_i N_i \sum_j \langle \mu_{0,i} \cdot \mu_{0,j} \rangle \tag{C.21}
$$

Introducing Eq. (C.21) into Eq. (C.12) yields a multi-component version of the Onsager equation:

$$\frac{(\varepsilon_r - \varepsilon_\infty)(2\varepsilon_r + \varepsilon_\infty)}{\varepsilon_r(\varepsilon_\infty + 2)^2} = \frac{1}{9\varepsilon_0 k_B T V} \sum_i N_i \sum_j \langle \mu_{0,i} \cdot \mu_{0,j} \rangle \tag{C.22}$$

Eq. (C.22) is equivalent to Eq.(C.23), where $\mu'_{0,j}$ is introduced as the concentration of all surrounding molecules:

$$\frac{(\varepsilon_r - \varepsilon_\infty)(2\varepsilon_r + \varepsilon_\infty)}{\varepsilon_r(\varepsilon_\infty + 2)^2} = \frac{1}{9\varepsilon_0 k_B T V} \sum_i N_i \left(\mu_{i,0}^2 + \sum_j \left\langle \mu_{0,i} \cdot \mu'_{0,j} \right\rangle \right) \tag{C.23}$$

From which it is trivial to deduce the g-factor shown in Eq. (5.11) p. (5.11).

C.3 Derivation of Dipolar Projections

While the problem of molecular geometry may be considered trivial, the number of different results for the same configuration found in literature suggests that it is important to show a detailed description of the procedure used to determine the bonding angles in this work. This section shows the general method used to determine the tetrahedral bonding angles in this work, and furthermore includes examples on how this is done in practice for different groups of molecules. The treatment builds on the work by Tripathy and De (2008)[400]. $\cos \gamma$ can be calculated from the projection of the dipole moment of a de-central molecule μ_D onto the central molecule μ_C using Eq. (C.24):

$$\langle \cos \gamma \rangle = \frac{\langle \mu_C \cdot \mu_D \rangle}{\mu_C \mu_D} \tag{C.24}$$

If free rotation is assumed around the hydrogen bond, Eq. (C.24) in terms of the dipole moment in the direction of the hydrogen-bond μ_H towards the other molecule:

$$\langle \cos \gamma \rangle = \frac{\mu_H \cdot \mu_D}{\mu_C \mu_D} \tag{C.25}$$

It becomes useful to define the dipole moment of the central molecule may be determined from the two-dimensional molecular geometry around a central oxygen atom using Eq. (C.26):

$$\mu_C = \mu_{OH} \delta_{OH} + \mu_R \delta_{OR} \tag{C.26}$$

In which $\delta_{OH} = (0, 1)$ and $\delta_{OR} = (\sin \varphi_C, \cos \varphi_C)$. The dipole moment of the central molecule (μ_C) is calculated from the identity shown in Eq. (C.27):

$$\mu_C^2 = \mu_{OH}^2 + \mu_{OR}^2 + 2\mu_{OH} \mu_{OR} \cos \varphi_C \tag{C.27}$$

The projected dipole moment in the direction of the hydrogen bond δ_H becomes $\mu_H = \mu_{OH} + \mu_{OR} \cos \varphi_C$. The dipole moment of the hydrogen bonded molecule can then be defined based on the three-dimensional geometry around a central oxygen atom from Eq. (C.28):

$$\mu_D = \mu_{OH} \delta_{OH} + \mu_{OR} \delta_{OR} \tag{C.28}$$

Where the unit vectors are given by $\delta_{OH} = (0, 0, 1)$ and $\delta_{OR} = (\sin \varphi_D, 0, \cos \varphi_D)$. Next, the direction of the hydrogen bond δ_H is defined as Eq. (C.29) in the case of tetrahedral hydrogen bonding, and Eq. (C.30) in the case of planar networks.

$$\delta_H = \left(-\frac{1}{2} \sin \theta, \sqrt{\frac{3}{4}} \sin \theta, \cos \theta \right) \tag{C.29}$$

$$\delta_H = (-\sin \theta, 0, \cos \theta) \tag{C.30}$$

Using Eq. (C.25) the expressions given by Eq. (C.31) and Eq. (C.32) for the tetrahedral and planar networks are obtained:

$$\langle \cos \gamma \rangle = -\frac{\mu_H}{\mu_C \mu_D} \left(\mu_{OH,D} \cos \theta + \mu_{OR,D} \left(\cos \theta \cos \varphi_D - \frac{1}{2} \sin \theta \sin \varphi_D \right) \right) \tag{C.31}$$

$$\langle \cos \gamma \rangle = -\frac{\mu_H}{\mu_C \mu_D} \left(\mu_{OH,D} \cos \theta + \mu_{OR,D} \left(\cos \theta \cos \varphi_D - \sin \theta \sin \varphi_D \right) \right) \tag{C.32}$$

Where $\mu_H = \mu_{OH,C} + \mu_{OR,C} \cos \varphi_C$. Eq. (C.33) and (C.34) may be used for pure components as well as mixtures, and are valid for angles between proton donors and proton acceptors, and

vice versa. For the tetrahedral network, the angle $\theta = 109.47°$ is used. For the planar network, the angle $\theta = 120°$ is used.

$$\langle \cos \gamma \rangle = -\frac{\mu_{OH} + \mu_{OR} \cos \varphi}{\mu_C \mu_D} \left(\mu_{OH} \cos \theta + \mu_{OR} \left(\cos \theta \cos \varphi - \frac{1}{2} \sin \theta \sin \varphi \right) \right) \tag{C.33}$$

$$\langle \cos \gamma \rangle = -\frac{\mu_{OH} + \mu_{OR} \cos \varphi}{\mu_C \mu_D} \left(\mu_{OH} \cos \theta + \mu_{OR} \left(\cos \theta \cos \varphi - \sin \theta \sin \varphi \right) \right) \tag{C.34}$$

C.4 Volume Root Solver

The task of the volume root solver is to determine a volume, where the pressure calculated from the equation of state equals the specified pressure. A simple algorithm is to set up the objective function shown in Eq. (C.60):

$$Q_1 = P(V) - P_{spec} = 0 \tag{C.35}$$

A Newton-Rhapson scheme may be used to find the root from Eq.(C.36)

$$V^{(k+1)} = V^{(k)} - Q_1/Q'_1 \tag{C.36}$$

Once the volume matches the pressure, the compressibility factor and the fugacity coefficients can be calculated. Unfortunately, the simple Newton scheme shown in Eq. (C.36) will be able to converge to either one of the three real roots that exists below the critical temperature as shown in Figure C.1 for an example solution near the critical point of methane. In order to
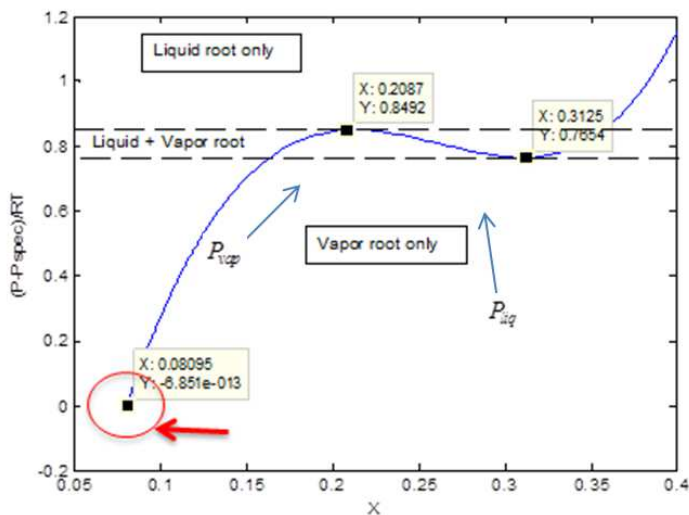

Figure C.1: Pressure as a function of the reduced density for methane at 190K with pressure specified at 4000Pa (in the region where a vapor phase exists). The maximum pressure where a vapor phase can exist is named P_{vap} and the minimum pressure where a liquid phase exists at is named P_{liq}.

provide reliable physical properties at all possible conditions to the process simulator, robust numerical methods and algorithms for solving for the site fractions and volume roots must be developed. However, the algorithms must also be computationally efficient, as they represent the innermost loop in the process flow-sheet simulation. At any given pressure the equation of state may return 1 or 3 volume roots (some EoS may yield even more (unphysical) volume roots, but here focus is on the CPA EoS). Above the critical point only a single volume root is present.

The volume root solver must be able to handle requests for the vapor and liquid root in all regions of the diagram. It is expected that the volume root solver to have the behavior summarized in Table C.1:

While v is the natural variable used for the volume root search, it may be advantageous to

Temperature	$T < T_c$	$T > T_c$
Pressure / Request	Possible roots	
$P > P_{vap}$	Liquid root	
$P_{vap} > P > P_{liq}$	Vapor, liquid, and unstable root	Supercritical vapor
$P < P_{liq}$	Vapor root	

Table C.1: Expected volume root solver behavior. MT = 0 will always return the volume root with minimum Gibbs energy.

use the variable $X = b/v$, as it limits the search space from 0 (gas) to 1 (liquid). Figure C.2 compares the convergence behavior using different objective functions (Eqs. (C.35)-(C.38)) in terms of average no. of iterations to find a root starting the search from the vapor or liquid side of ethane.

$$Q_2 = (1 - X)Q_1 = 0 \tag{C.37}$$

$$\min_X \frac{G}{RT} = \frac{A}{RT} + \frac{P^{spec}V}{RT} \Rightarrow Q_3 = \left(\frac{\partial G}{\partial X}\right) = -\frac{B}{X^2}\left(\frac{\partial G}{\partial V}\right) = -\frac{BQ_1}{X^2} = 0 \tag{C.38}$$

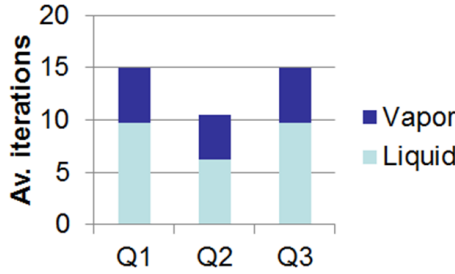The objective function Q_2 yields a less steep increase in the liquid side of the objective function

Figure C.2: Average no. of iterations from 100000 calculations for ethane from T= 10-1000K, P = 10Pa-100kbar

which improves the convergence behavior. The Newton directions taken with Eq. C.35 and Eq. (C.37) are shown in Eq. (C.39) and Eq. (C.40), respectively:

$$\Delta X_1 = -\frac{Q_1}{Q'_1} \tag{C.39}$$

$$\Delta X_2 = -\frac{(1 - X)Q_1}{(1 - X)Q'_1 - Q_1} \tag{C.40}$$

Note that the sign of the two directions are similar, except if $(1 - X)Q'_1 < Q_1$. In that case, the algorithm should revert to the original Newton step. In order to identify the vapor or a liquid phase, the path from the initial estimate being either a vapor or a liquid is used. The algorithm attempts to determine both roots when a liquid is requested, and if only one root can be identified, it is assumed to be the supercritical vapor. Additionally, it is checked whether $\frac{\partial P}{\partial V} > 0$ and if so, the bounds are updated accordingly ($X_{\max} = X$ for vapor search and $X_{\min} = X$ for liquid search). The calculated pressure for the vapor-side of a system containing ethane, ethylene glycol and water is shown in Figure C.4. The maximum pressure $P_{vap} = 10.99732307$ bar is slightly less than 11 bars, and this algorithm does indeed fail to find a vapor root when the pressure is 0.02 Pa higher than the specified pressure. This gives us confidence that the algorithm will return robust results.
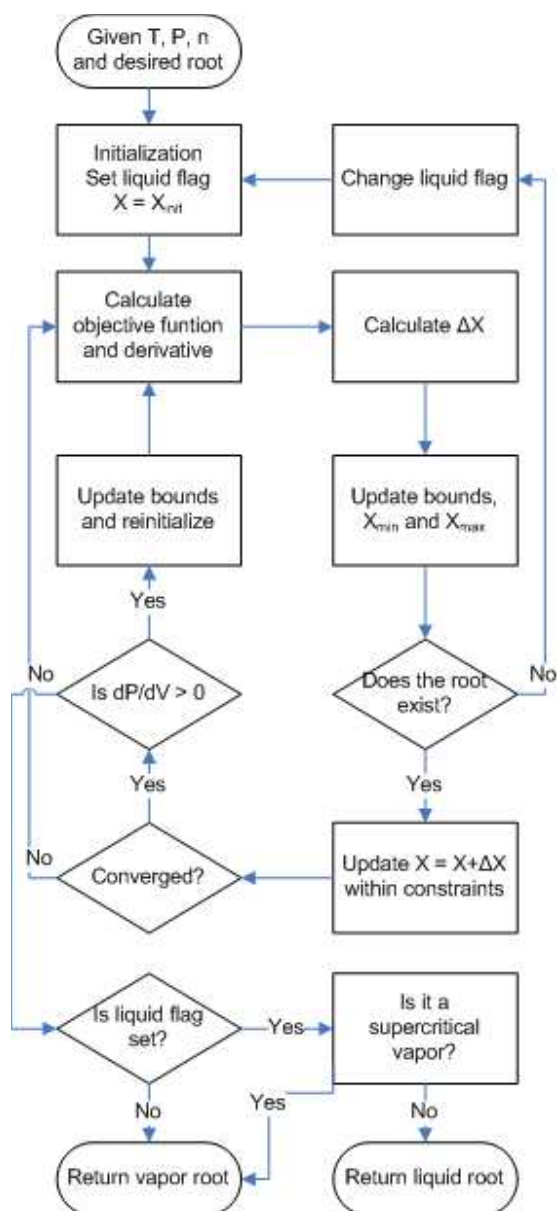
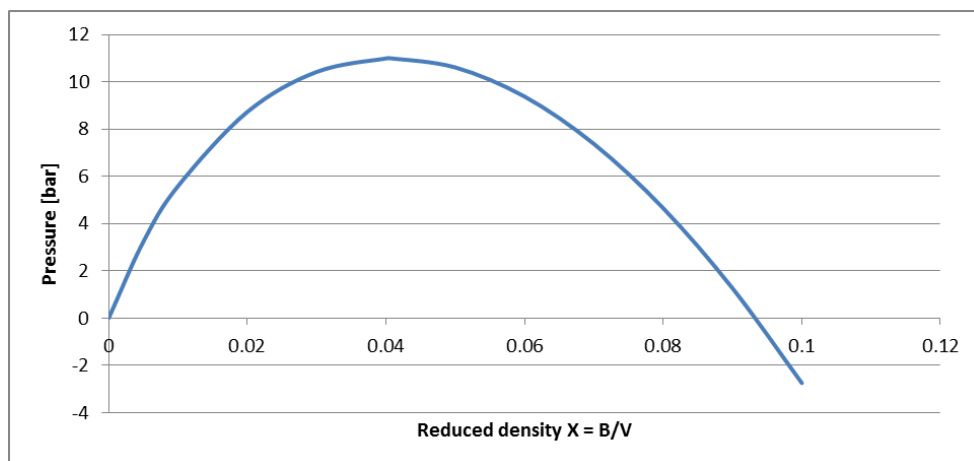**Figure C.3:** Overview of the volume root solver used in e-CPA

Figure C.4: Calculated pressure for an ethane (50%)-ethylene glycol(3.4%)-water(46.6%) system at 10°C

C.5   Apparent Components Approach

The Helmholtz free energy can be calculated at the true equilibrium composition **n** (ion-based) and the apparent composition **e** (salt-based) (C.41):

$$A\left(T, V, \mathbf{n}\right) = A\left(T, V, \mathbf{e}\right) \tag{C.41}$$

The chemical potential of apparent components are given by Eq. (C.42):

$$\mu_i^{app} = \left(\frac{\partial A}{\partial e_i}\right) = \sum_j \left(\frac{\partial n_j}{\partial e_i}\right)\left(\frac{\partial A}{\partial n_j}\right) = \sum_j v_{ij}\left(\frac{\partial A}{\partial n_j}\right) \tag{C.42}$$

Where v_{ij} is the stoichiometric composition of ion j in salt i. The chemical potential consists of the standard state chemical potential and the activity of the molecule as shown in Eq. (C.43):

$$\mu_i\left(T, P\right) = \left(\frac{\partial A}{\partial n_i}\right) = \mu_i\left(T, P_0\right) + RT \ln a_i \tag{C.43}$$

The standard state chemical potential of the fully dissociated apparent components is defined as Eq. C.44:

$$\mu_{i,app} \equiv \sum_j v_{ij}\mu_j \tag{C.44}$$

And thus, the apparent activity can be calculated from Eq. (C.45):

$$\ln a_{i,app} = \sum_j v_{ij} \ln a_j \tag{C.45}$$

It is evident that when using the ideal gas reference state, Eq. (C.46) can be used to calculate the fugacity coefficient:

$$\ln \hat{\varphi}_i^{\text{app}} = -\ln \frac{x_i^{\text{app}} P}{P_0} + \sum_j v_{ij} \ln \frac{x_j \hat{\varphi}_j P}{P_0} \tag{C.46}$$

The derivatives of Eq. (C.46) are calculated from the chain rule:

$$\left(\frac{\partial \ln \hat{\varphi}_i^{\text{app}}}{\partial P}\right) = -\frac{1}{P} + \sum_j \frac{v_{ij}}{P} + \sum_j v_{ij}\left(\frac{\partial \ln \hat{\varphi}_j}{\partial P}\right) \tag{C.47}$$

$$\left(\frac{\partial \ln \hat{\varphi}_i^{\text{app}}}{\partial T}\right) = \sum_j v_{ij}\left(\frac{\partial \ln \hat{\varphi}_j}{\partial T}\right) \tag{C.48}$$

$$\left(\frac{\partial \ln \hat{\varphi}_i^{\text{app}}}{\partial e_k}\right) = -\left(\frac{\partial \ln x_i^{\text{app}}}{\partial e_k}\right) + \sum_j v_{ij}\left(\frac{\partial \ln x_j}{\partial e_k}\right) + \sum_j v_{ij}\left(\frac{\partial \ln \hat{\varphi}_j}{\partial e_k}\right) \tag{C.49}$$

x_i^{app} Apparent mole fraction $x_i^{app} = e_i/e_T$

Where the derivative of the apparent composition is calculated from the total no. of moles $e_T = \sum_i e_i$ using Eq. (C.50):

$$\left(\frac{\partial \ln x_i^{\text{app}}}{\partial e_k}\right) = \frac{\delta_{ik}}{e_k} - \frac{1}{e_T} \tag{C.50}$$

The true composition is calculated as Eq. (C.51) from the stoichiometric factors v_{ij} and the total true composition $n_T = \sum_j \sum_i v_{ij} e_i$ and its derivative wrt. apparent composition is given by Eq. (C.52):

$$x_i = \frac{\sum_i v_{ij} e_i}{n_T} \tag{C.51}$$

$$\left(\frac{\partial \ln x_i}{\partial e_k}\right) = \sum_j \left(\frac{\partial n_j}{\partial e_k}\right)\left(\frac{\partial \ln x_i}{\partial n_j}\right) = \frac{v_{ki}}{n_i} - \frac{1}{n_T}\sum_j v_{kj} \tag{C.52}$$

And thus, the second order compositional derivatives of the fugacity coefficients are given by Eq. (C.53) :

$$\left(\frac{\partial \ln \hat{\varphi}_i^{\text{app}}}{\partial e_k}\right) = \frac{1}{e_T} - \frac{\delta_{ik}}{e_k} + \sum_j v_{ij}\left(\frac{\delta_{ik}}{e_k} - \frac{v_{kj}}{n_T}\right) + \sum_j \sum_l v_{ij} v_{kl}\left(\frac{\partial \ln \hat{\varphi}_j}{\partial n_l}\right) \tag{C.53}$$

C.6 Implementation of Generalized Cubic EoS

The Helmholtz energy for the general Cubic EoS may be written as:

$$\frac{A^{\text{Cubic}}}{RT} = -n_t \ln (1 - \beta) + \frac{D}{\varsigma_2 - \varsigma_1} \ln \left(\frac{1 + \varsigma_2 \beta}{1 + \varsigma_1 \beta} \right) \tag{C.54}$$

The function $\beta(V, \mathbf{n}) = B/V$ determines the reduced density whereas the function $D = D(T, \mathbf{n}) = Rn_T\Gamma$ is the attractive energy. The derivatives of *beta* are given by:

$$\beta = \frac{B}{V} \quad \beta_V = -\frac{\beta}{V} \quad \beta_{VV} = -\frac{2\beta_V}{V} \quad \beta_i = \frac{b_i}{V} \quad \beta_{iV} = -\frac{\beta_i}{V}$$

The Huron-Vidal/NRTL mixing rule is given by Eq. (C.55):

$$\frac{a}{b} = \sum_i x_i \frac{a_i}{b_i} - \frac{g^{E,\infty}}{h(1)} \tag{C.55}$$

Where $h(\beta)$ is given by Eq. (C.56):

$$h(\beta) = \frac{1}{\delta_2 - \delta_1} \ln \left(\frac{1 + \varsigma_2 \beta}{1 + \varsigma_1 \beta} \right) \tag{C.56}$$

From the Huron-Vidal/NRTL mixing rule Eq. (C.57) is used to calculate the excess Gibbs energy:

$$\frac{g^{E,\infty}}{RT} = \sum_i x_i \frac{\sum_j x_j v_j \exp \left(-\alpha_{ji} \frac{\Delta U_{ji}}{RT} \right) \frac{\Delta U_{ji}}{RT}}{\sum_j x_j v_j \exp \left(-\alpha_{ji} \frac{\Delta U_{ji}}{RT} \right)} \tag{C.57}$$

Where the volume of a molecule v_i is typically set equal to the co-volume parameter, b_i. Note that the classical mixing rule for a as shown in Eq. (C.58) are recovered if the following values for the parameters are used:

$$\alpha_{ji} = 0 \quad U_{ii} = \frac{a_i}{b_i} h(1) \quad U_{ji} = \left(\frac{2a_i}{b_i} - \frac{a_{ji}}{b_j} \right) h(1)$$

$$\Delta U_{ji} = U_{ji} - U_{ii} = \left(\frac{a_i}{b_i} - \frac{a_{ji}}{b_j} \right) h(1) \quad a_{ij} = \sqrt{a_i a_j} (1 - k_{ij})$$

$$\frac{a}{b} = \sum_i x_i \frac{a_i}{b_i} - \frac{1}{b} \sum_i x_i \left(\frac{a_i}{b_i} \right) \sum_j x_j b_j + \frac{1}{b} \sum_i x_i \sum_j x_j a_{ji} = \frac{1}{b} \sum_i x_i \sum_j x_j a_{ji} \tag{C.58}$$

Note that it is also possible to let $\alpha = \Delta U_{ij} = \Delta U_{ji} = 0$, in which case the so-called a/b mixing rule shown in Eq. (C.59) is obtained. This mixing rule which has been shown to work well for athermal mixtures [1]:

$$\frac{a}{b} = \sum_i x_i \frac{a_i}{b_i} \tag{C.59}$$

C.7 Site Fraction Solver

When the site mole count as $m_j = \phi_{ij} n_i$ is introduced (where ϕ_{ij} is the repeat factor of site j on component i), the association term may be written as a constrained optimization problem:

$$\min_{\Xi} \frac{A^r_{\text{assoc}}}{RT} = \sum_i m_i \left(\ln \Xi_i - \frac{1}{2} \Xi_i + \frac{1}{2} \right) \tag{C.60}$$

$$s.t. \frac{1}{\Xi_i} = 1 + \frac{1}{V} \sum_j M_j \Xi_j \Delta^{ij} \tag{C.61}$$

M_i	[mol]	Moles of the sites of type i
Ξ_i		Fraction of site i which is not bonded to any other sites
Δ^{ij}		Association strength between component i and j

The Michelsen Q-function [321, 322] may then be derived by using the Wolfe Dual transform [389, p. 347]:

$$\max_{\underline{\Xi}, \underline{\lambda}} \mathcal{L}\left(\underline{\Xi}, \underline{\lambda}\right) = f\left(\underline{\Xi}\right) - \underline{\lambda}^T \underline{c}\left(\underline{\Xi}\right)$$
$$s.t. \frac{\partial \mathcal{L}}{\partial \Xi_i} = 0, \lambda_i \geq 0 \tag{C.62}$$

Using Eq. (C.62) the Lagrangian for Eq. (C.60) and (C.61) in Eq. (C.63) is obtained:

$$\mathcal{L}\left(\underline{\Xi}, \underline{\lambda}\right) = \sum_i M_i \left(\ln \Xi_i - \left(\frac{1}{2} + \lambda \right) \Xi_i + \left(\frac{1}{2} + \lambda \right) \right) - \frac{\lambda}{V} \sum_i \sum_j M_i M_j \Xi_i \Xi_j \Delta^{ij} \tag{C.63}$$

The derivative of the Lagrangian wrt. site fractions Ξ_i is obtained in Eq. (C.64)

$$\frac{\partial \mathcal{L}}{\partial \Xi_i} = M_i \left(\frac{1}{\Xi_i} - \left(\frac{1}{2} + \lambda \right) \right) - \frac{2\lambda M_i}{V} \sum_j M_j \Xi_j \Delta^{ij} = 0 \tag{C.64}$$

Using the constraint in Eq. (C.61) leads to Eq. (C.65):

$$\left(\frac{\partial \mathcal{L}}{\partial \Xi_i} \right) = M_i \left(\frac{1 - 2\lambda}{\Xi_i} - \left(\frac{1}{2} + \lambda - 2\lambda \right) \right) = 0 \tag{C.65}$$

It is evident that above equation is satisfied when $\lambda = 1/2$. It is therefore possible to formulate the equivalent maximization problem as Eq. (C.66)

$$\max_{\underline{\Xi}} Q\left(\underline{\Xi}\right) = \mathcal{L}\left(\underline{\Xi}, \lambda = \frac{1}{2}\right) = \sum_i M_i \left(\ln \Xi_i - \Xi_i + 1 \right) - \frac{1}{2V} \sum_i \sum_j M_i M_j \Xi_i \Xi_j \Delta^{ij} \tag{C.66}$$

At the solution, Ξ satisfies Eq. (C.61), and Eq. (C.66) reduces to Eq. (C.60). In order to make a concice implementation in FORTRAN, it is noted that it is advantageous to define the function $h(V)$ as well as matrix K as shown in Eq. (C.67):

$$h\left(V, \mathbf{n}\right) = \frac{g\left(V, \mathbf{n}\right)}{V} K_{ij} = M_i M_j v_{ij} \left[\exp \left(\frac{\varepsilon_{ij}}{k_B T} \right) - 1 \right] \tag{C.67}$$

Note that the matrix K only changes when the temperature or the composition changes, while h changes when volume or compositon changes. Figure C.5 illustrates how the functions for the association term are evaluated in the fugacity calculation. The function $h(V, n)$ is recalculated During each iteration of the volume root solver, whereas K is calculated before entering the volume root solver. This minimizes the number of calculations required in comparison to the Δ^{ij} matrix, which would need to be recalculated upon every iteration. During the initial
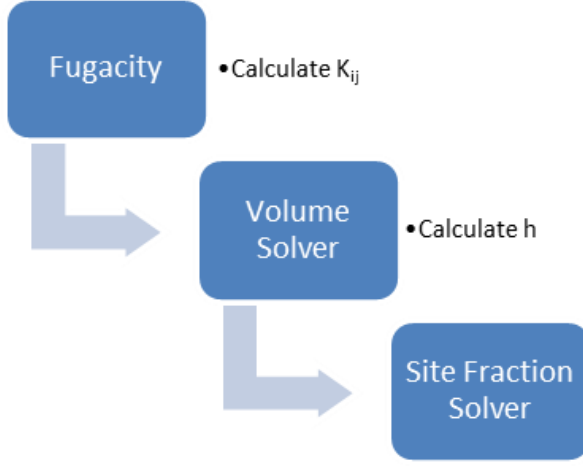
Figure C.5: Calculation of $\mathbf{K}(T, \mathbf{n})$ and $h(V, \mathbf{n})$ functions and solution of site fractions during fugacity calculation.

calculation for the volume root solver (where no solution to the site fractions Ξ_i is available), the solution procedure is initialized using five steps in a damped direct substitution method using the damping factor $\chi = 1/3$ [322]:

$$\Xi_i^{(k+1)} = \chi \Xi_i^{(k)} + (1 - \chi) \left(1 + \frac{h}{M_i} \sum_i \Xi_i^{(k)} K_{ij} \right)^{-1} \tag{C.68}$$

Subsequently the Newton scheme shown in Eq. (C.69) is used to solve for the site fractions:

$$\vec{\Xi}^{(k+1)} = \vec{\Xi}^{(k)} - \vec{H}^{-1} \vec{g} \tag{C.69}$$

The gradient $\vec{g}$ is given by:

$$g_i = \left(\frac{\partial}{\partial \Xi_i} \frac{A_{\text{assoc}}^r}{RT} \right) = M_i \left(\frac{1}{\Xi_i} - 1 \right) - h \Sigma_i \tag{C.70}$$

Note that Eq. (C.70) is zero at the solution. The Hessian $\vec{H}$ is given by Eq. (C.71):

$$H_{ij} = \left(\frac{\partial^2}{\partial \Xi_i \partial \Xi_j} \frac{A_{\text{assoc}}^r}{RT} \right) = -\frac{\delta_{ij} M_j}{\Xi_j^2} - h K_{ij} \tag{C.71}$$

Note that only the diagonal elements in Eq. (C.71) will change during the iterations. At the solution, Eq. (C.71) can be approximated as Eq. (C.72) using Eq. (C.61):

$$\tilde{H}_{ij} = \left(\frac{\partial^2}{\partial \Xi_i \partial \Xi_j} \frac{A_{\text{assoc}}^r}{RT} \right) = -\delta_{ij} \frac{1}{\Xi_j} (M_j + h \Sigma_i) - h K_{ij} \tag{C.72}$$

It is possible to show that Eq. (C.72) is negative definite [182] and therefore that the convergence of the Newton solver is guaranteed, regardless of the quality of the initial estimate for the site fractions. The matrix $\vec{A}$ in Eq. (C.73) is introduced to avoid updating off-diagonal elements:

$$\mathbf{H}^{-1} = (h \mathbf{A_{ij}})^{-1} \tag{C.73}$$

The diagonal elements of the A matrix are then $\vec{A}_{ii} = -\Xi_i^{-1} \left(h^{-1} M_i + \mathbf{\Sigma}_i \right)$. From here, the Newton step can be calculated from Eq. (C.74):

$$\Delta\vec{\mathbf{\Xi}} = -\vec{\vec{H}}^{-1} \vec{g} = \vec{A}^{-1}\vec{b} \tag{C.74}$$

In which $\vec{b} = h^-1\vec{g}$. The matrix $\vec{A}$ is inverted using LDL defactorization. The next step can be calculated using a simple line search to calculate the next step:

$$\vec{\Xi}^{(k+1)} = \vec{\Xi}^{(k)} + \alpha\Delta\vec{\Xi} \tag{C.75}$$

The full Newton step ($\alpha = 1$) is usually taken; otherwise the value of α that ensures that $\mathbf{\Xi}_i^{(k+1)} > 0.1\mathbf{\Xi}_i^{(k)}$ is used.

C.7.0.2 Sensitivity of Helmholtz Energy to Solution of Site Fractions

In order to evaluate the sensitivity of the Helmholtz energy and its derivatives to the solution of the site fractions $\mathbf{\Xi}$, four possible versions of the association term were implemented. It was noted that by assuming that the gradient $\mathbf{g} = 0$, some of the derivatives can be simplified, and these simplifications were introduced in case B and D.

- A) Derivatives based on Eq. (C.60)

- B) Derivatives based on Eq. (C.60) assuming zero gradient $\mathbf{g} = 0$

- C) Derivatives based on Eq. (C.66)

- D) Derivatives based on Eq. (C.66) assuming zero gradient $\mathbf{g} = 0$

The calculation is performed for 4 components with 10 sites at random conditions and determine a reference solution for the site fractions by using a very strict tolerance close to machine precision $|\Delta\mathbf{\Xi}| < 10^{-16}$. Subsequently, the tolerance was changed to $|\Delta\mathbf{\Xi}| < 1$, i.e. that only one Newton step will betaken after initializing with five successive substitutions and compare the differences in the Helmholtz energy and their derivatives. The results are summarized in Figure C.6-C.9 from which it is evident that model D is the optimal implementation, i.e. to use the Michelsen Q-function Eq. (C.66) and assume a gradient of 0. The reason for this is that the original (C.60) requires first order derivatives in site fractions (e.g. $\partial\Xi_i/\partial V$), which do not have a sufficiently high accuracy when the system is far from the solution - the Michelsen Q-function does not require this, and by furthermore assuming that the gradient is zero, it was observed that better correspondence with the derivatives of the true Helmholtz energy is obtained.
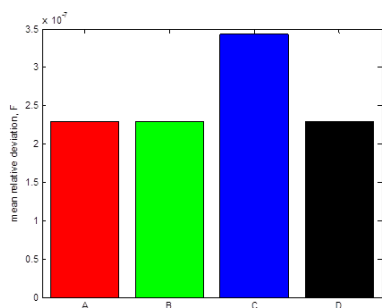
Figure C.6: Mean relative deviation in Helmholtz energy. Models are summarized on p. 229.
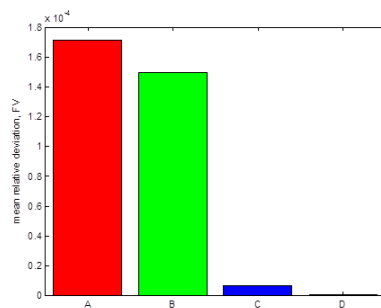

Figure C.7: Mean relative deviation in volume derivative of Helmholtz energy. Models are summarized on p. 229.
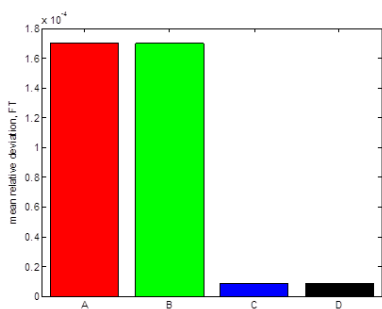

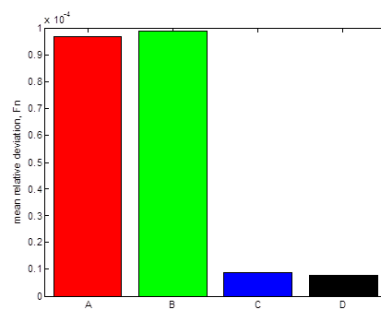**Figure C.8:** Mean relative deviation in temperature derivative of Helmholtz energy. Models are summarized on p. 229.

Figure C.9: Mean relative deviation in compositional derivative of Helmholtz energy. Models are summarized on p. 229.

C.8 Calculation of Dielectric Constant

The static permittivity is evaluated from the solution of Eq. (5.4) p. 82 which is a 2nd degree polynomial in ε_r. The root with $\varepsilon_r > 1$ is given by Eq. (C.76):

$$\varepsilon_r = \frac{1}{4}\left(\varepsilon_\infty + \Gamma + \sqrt{(\varepsilon_\infty + \Gamma)^2 + 8\varepsilon_\infty^2}\right) \tag{C.76}$$

Where the function Γ is a measure of the dipolar character of the fluid (shown in Eq. (C.77)):

$$\Gamma = \frac{1}{k_B T}\frac{N_A}{V\varepsilon_0}\left(\frac{\varepsilon_\infty + 2}{3}\right)^2 \sum_i^N n_i g_i \mu_{i,0}^2 \tag{C.77}$$

Note that in the absence of dipolar molecules, ε_r becomes ε_∞. In order to evaluate the derivatives of Γ, it is necessary to calculate the derivatives of the Kirkwood g-factor given by Eq. (5.47) p. 105. This involves evaluating the probability of association between each component (from Eq. (5.25)), which requires sensitivites of the solution to the site fractions with regards to temperature, volume, and composition up to second order. These are evaluated using Eq. (C.78) and Eq. (C.79):

$$\vec{H}\vec{\Xi}_a + \vec{g}_a = 0 \tag{C.78}$$

Where $\vec{\Xi}_a = \partial\vec{\Xi}/\partial a$ and $\vec{g}_a = \partial\vec{g}/\partial a$. Note that Eq. (C.78) can be calculated from the Hessian at the solution

$$\vec{g}_{ab} + \vec{H}_b\vec{\Xi}_a + \vec{H}_a\vec{\Xi}_b + \vec{\Xi}_a^T\vec{H}_\Xi\Xi_b + \vec{H}\vec{\Xi}_{ab} = 0 \tag{C.79}$$

Where the third order derivatives of the objective function, with regards to the site fractions is given by Eq. (C.80), which is only non-zero when $i = j = k$.

$$\left(\frac{\partial H_{ij}}{\partial \Xi_k}\right) = \frac{\delta_{ijk}2M_k}{\Xi_k^3} = D_k \tag{C.80}$$

Using Eq. (C.80), Eq. (C.79) can be simplified as shown in Eq. (C.81):

$$\mathbf{g}_{ab} + \mathbf{H}_b\mathbf{\Xi}_a + \mathbf{H}_a\mathbf{\Xi}_b + \mathbf{\Xi}_a \otimes \mathbf{D} \otimes \Xi_b + \mathbf{H}\mathbf{\Xi}_{ab} = 0 \tag{C.81}$$

Note that Eq. (C.81) requires calculation of the sensitivities Ξ.

The function Λ is defined in Eq. (C.82) to simplify the equations for obtaining the dielectric constant and it's derivatives:

$$\Lambda = \varepsilon_\infty + E\Gamma \tag{C.82}$$

In which Γ is given by Eq. (C.83)

$$\Gamma = \sum_i^N n_i g_i \mu_{i,0}^2 \tag{C.83}$$

And E is given by Eq. (C.84)

$$E = \frac{1}{k_B T}\frac{N_A}{V\varepsilon_0}\left(\frac{\varepsilon_\infty + 2}{3}\right)^2 \tag{C.84}$$

After which the static permittivity can be obtained from Eq. (C.85)

$$\varepsilon_r = \frac{1}{4}(\Lambda + Y) \tag{C.85}$$

In which the function Y is defined as Eq. (C.86):

$$Y = \sqrt{\Lambda^2 + 8\varepsilon_\infty^2} \tag{C.86}$$

The infinite frequency permittivity ε_∞ is calculated by isolating ϵ_∞ from the Clausius-Mossotti Eq. (C.87):

$$\varepsilon_\infty = \frac{2\sum\limits_{i} n_T a_0 + 3V\varepsilon_0}{3V\varepsilon_0 - \sum\limits_{i} n_T a_0} \tag{C.87}$$

Appendix D

Parameter Estimation

D.1 Results from Second Sequential Parameter Optimization

Table D.1 shows the fitted ion-specific parameters with the volume parameter ν and the ion-water interaction energy $\Delta_U iw/R = \Delta U_{wi}/R = u_{iw}^0$, and the predictions for other salts are shown in Table D.2.

Ion	Salt	σ	b_0	ν	u_{iw}^0	Peneloux	RAD $\gamma_{\pm}^*$ [%]	RAD Φ [%]	AAD V_{app} [%]
F$^-$	KF	2.63	22.94	3.95*	-7922*	23.0*	3.73	2.37	4.35
Cl$^-$	HCl	3.19	40.83	15.28*	-4490*	11.7*	2.19	1.18	5.38
Br$^-$	KBr	3.37	48.40	35.37*	-2693*	8.8*	0.54	0.29	0.60
I$^-$	KI	3.65	61.18	46.48*	-2296*	4.4*	0.88	0.24	1.23
NO$_3^-$	KNO$_3$	3.16	39.80	39.64*	-2055*	20.0*	0.27	0.65	0.38
SO$_4^{--}$	K$_2$SO$_4$	3.82	70.03	85.23*	-1967*	19.4*	1.14	0.93	7.05
Li$^+$	LiCl	2.08	11.35	11.35*	2319*	-51.2*	10.6	5.01	1.7
Na$^+$	NaCl	2.36	16.49	15.66*	3431*	-64.2*	1.34	0.88	1.7
K$^+$	KCl	2.78	27.62	27.62	2754*	-71.0*	0.83	0.49	1.0
Rb$^+$	RbCl	2.89	30.4	40.34*	2139*	-69.7*	0.51	0.45	0.9
Cs$^+$	CsCl	3.14	39.01	53.40*	1781*	-72.9*	1.97	2.54	1.7
Mg^{++}	MgCl$_2$	2.09	11.51	11.51*	4105*	-98.2*	10.7	6.18	3.9
Ca^{++}	CaCl$_2$	2.42	17.92	17.92*	4673*	-104.2*	9.65	6.59	6.2
Sr^{++}	SrCl$_2$	2.64	23.20	20.41*	5144*	-122.7 *	4.45	3.21	4.0
Ba^{++}	BaCl$_2$	3.00	34.05	34.13*	4652*	-134.4*	5.35	2.36	1.8
Average							3.61	2.22	2.8

Table D.1: Parameters fitted to data up to solubility limit at 25°C. Note that ν_0 for K$^+$ was set to b_0, as the correspondence with the data was already satisfactory without fitting ν_0.

Salt	RAD $\gamma_{\pm}^{*}$ [%]	RAD Φ [%]	AAD V_{app} [%]
LiBr	56.42	16.6	0.9
LiI	39.2	18.2	1.3
LiNO$_3$	122.5	18.8	2.6
Li$_2$SO$_4$	178.8	65.4	6.3
NaF	3.2	4.14	0.8
NaBr	4.34	3.27	1.8
NaI	8.08	5.06	0.3
NaNO$_3$	4.83	4.94	1.2
K$_2$SO$_4$	4.68	17.1	5.0
RbF	2.13	1.86	1.0
RbBr	3.32	1.55	0.2
RbI	9.3	4.48	0.3
RbNO$_3$	4.5	5.62	0.4
Rb$_2$SO$_4$	19.6	48.5	2.4
CsF	3.24	1.01	0.8
CsBr	2.79	2.32	-
CsI	8.52	4.78	-
CsNO$_3$	6.13	6.67	0.04
Cs$_2$SO$_4$	24.7	64.6	2.1
MgBr$_2$	96.6	20.2	2.0
MgI$_2$	129	25.6	2.5
Mg(NO$_3$)$_2$	20.6	12.4	2.2
MgSO$_4$	-	165	7.5
CaBr$_2$	40.7	17.5	5.1
CaI$_2$	37.7	19.7	0.9
Ca(NO$_3$)$_2$	-	44.4	4.0
CaSO$_4$	14.5	-	6.5
SrBr$_2$	15.4	10.5	1.7
SrI$_2$	15.6	10.3	1.2
Sr(NO$_3$)$_2$	-	36.0	3.9
BaBr$_2$	9.16	2.93	0.5
BaI$_2$	17.1	9.6	1.1
Ba(NO$_3$)$_2$	1.92	5.81	1.5
Average	30.2	21.1	2.2

Table D.2: Predictions using the parameters from Table D.1 at 25°C.

D.2 Temperature Dependent Results

The following section presents results for all ions investigated in Chapter 6 using the parameters from Table 6.11. Results are shown for each cation.
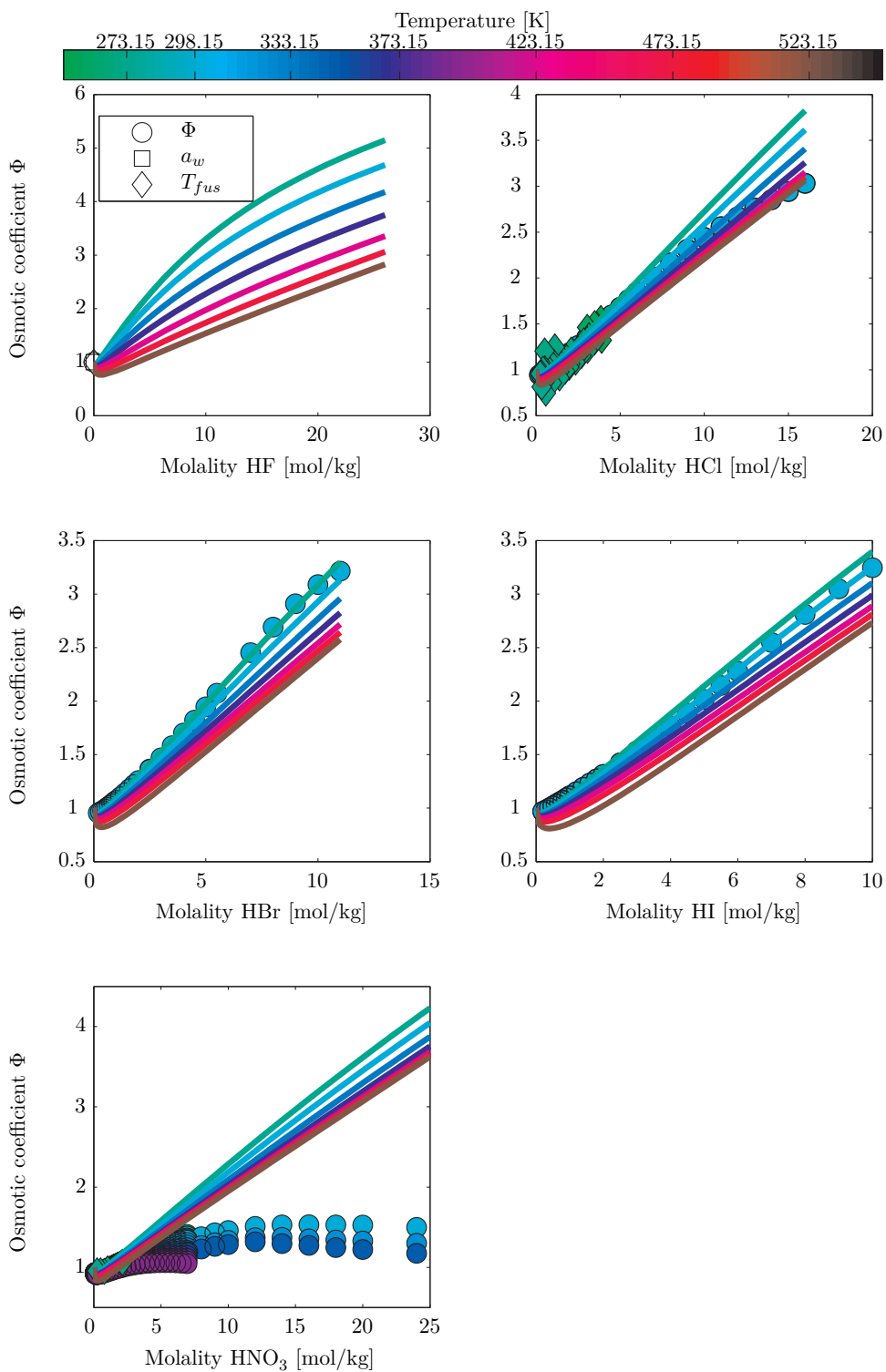
Figure D.1: Osmotic coefficients of salts containing Hydrogen. Note that HNO_3 was not included in the fit, as it cannot be assumed to be fully dissociated.
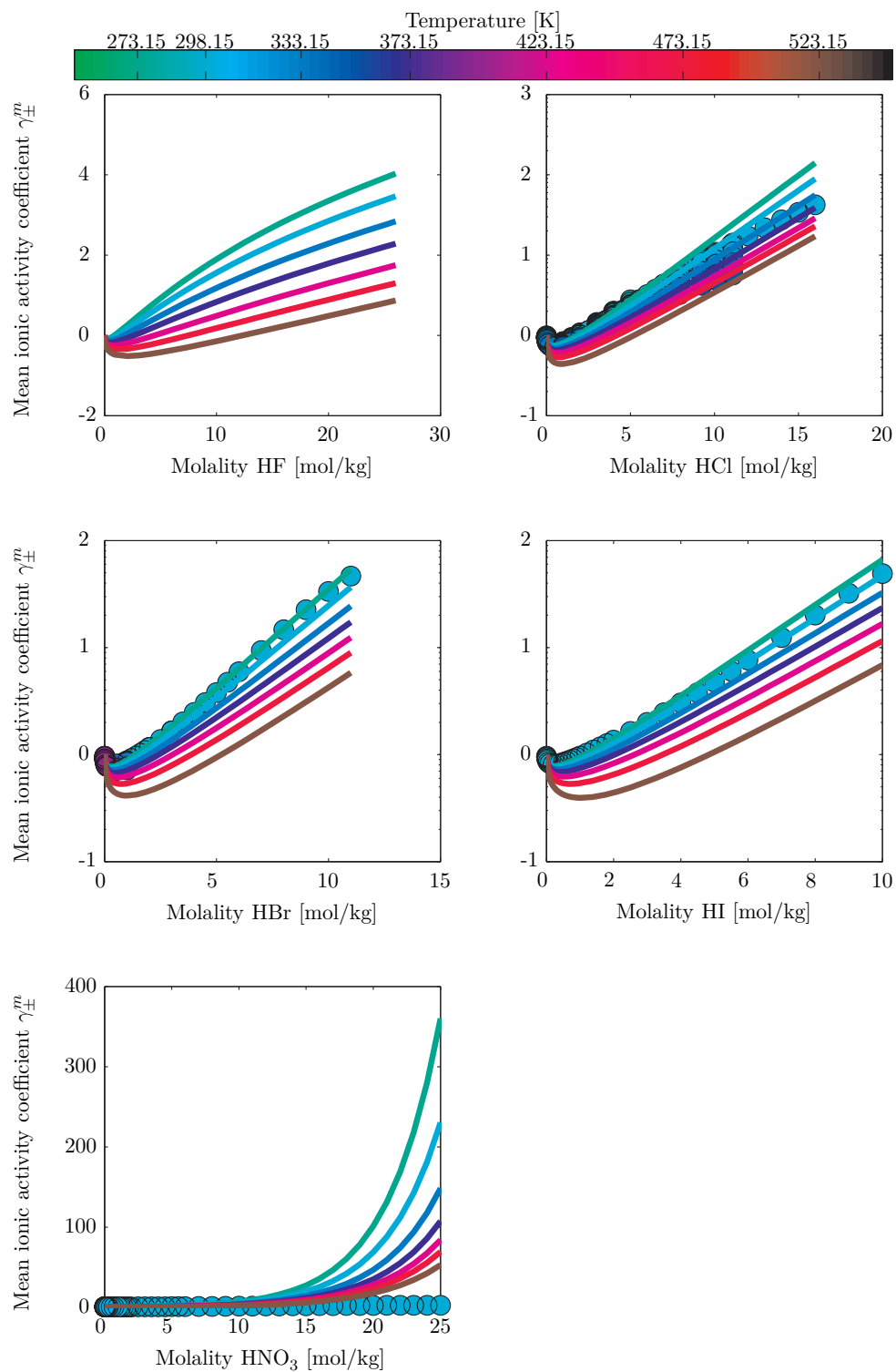
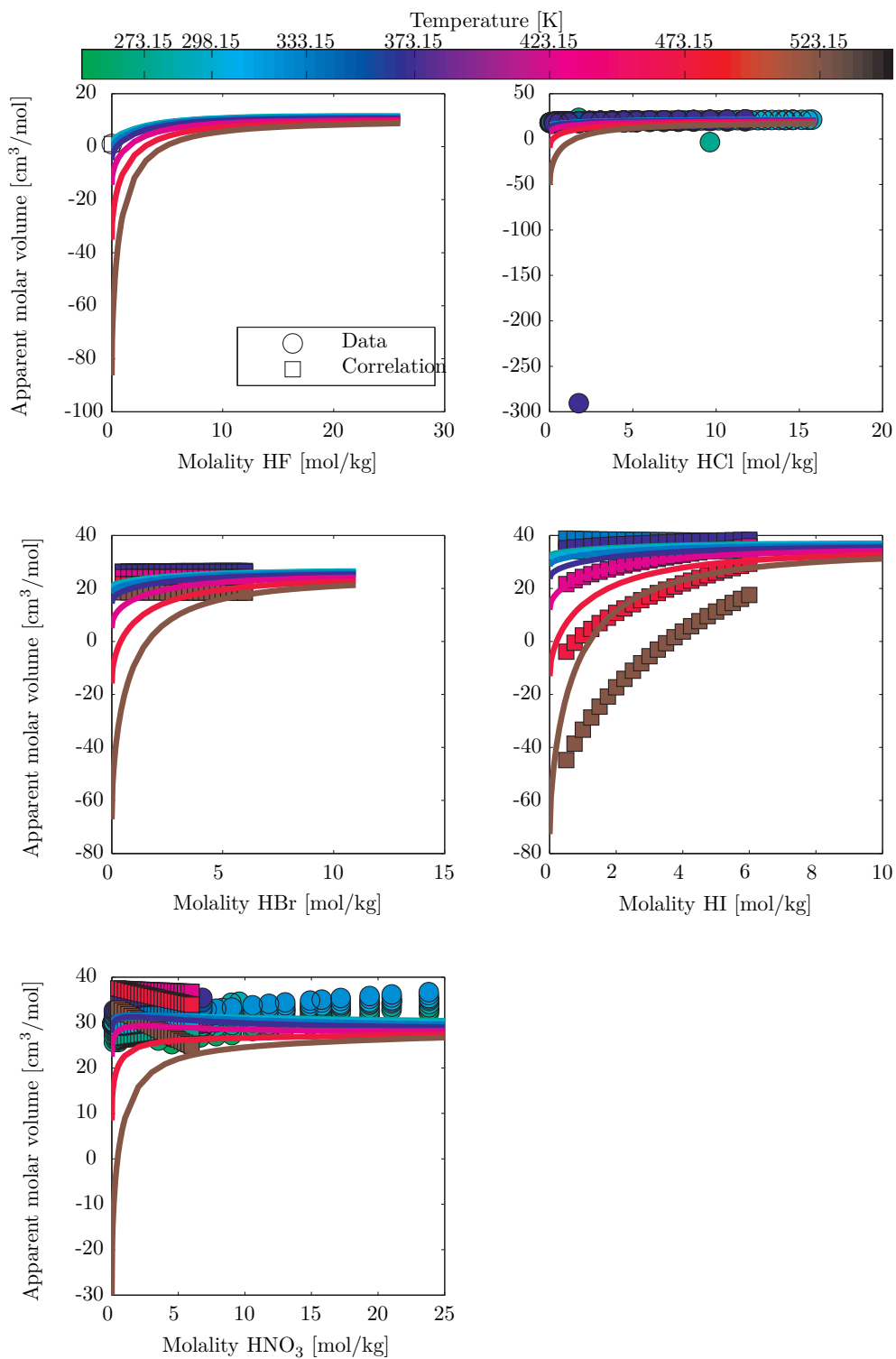**Figure D.2:** Mean ionic activity coefficients of salts containing Hydrogen.

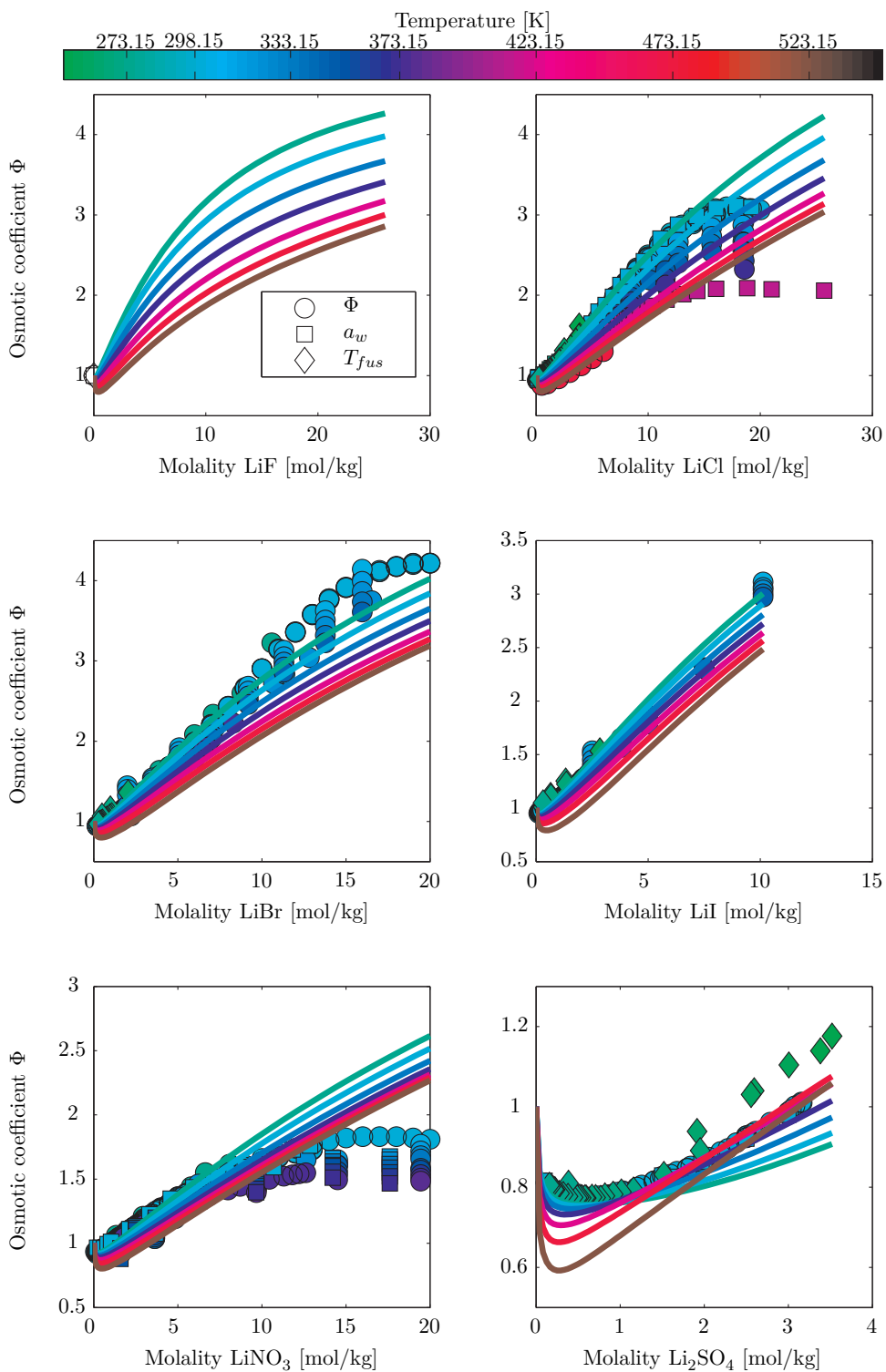**Figure D.3:** Apparent molar volume of salts containing Hydrogen.

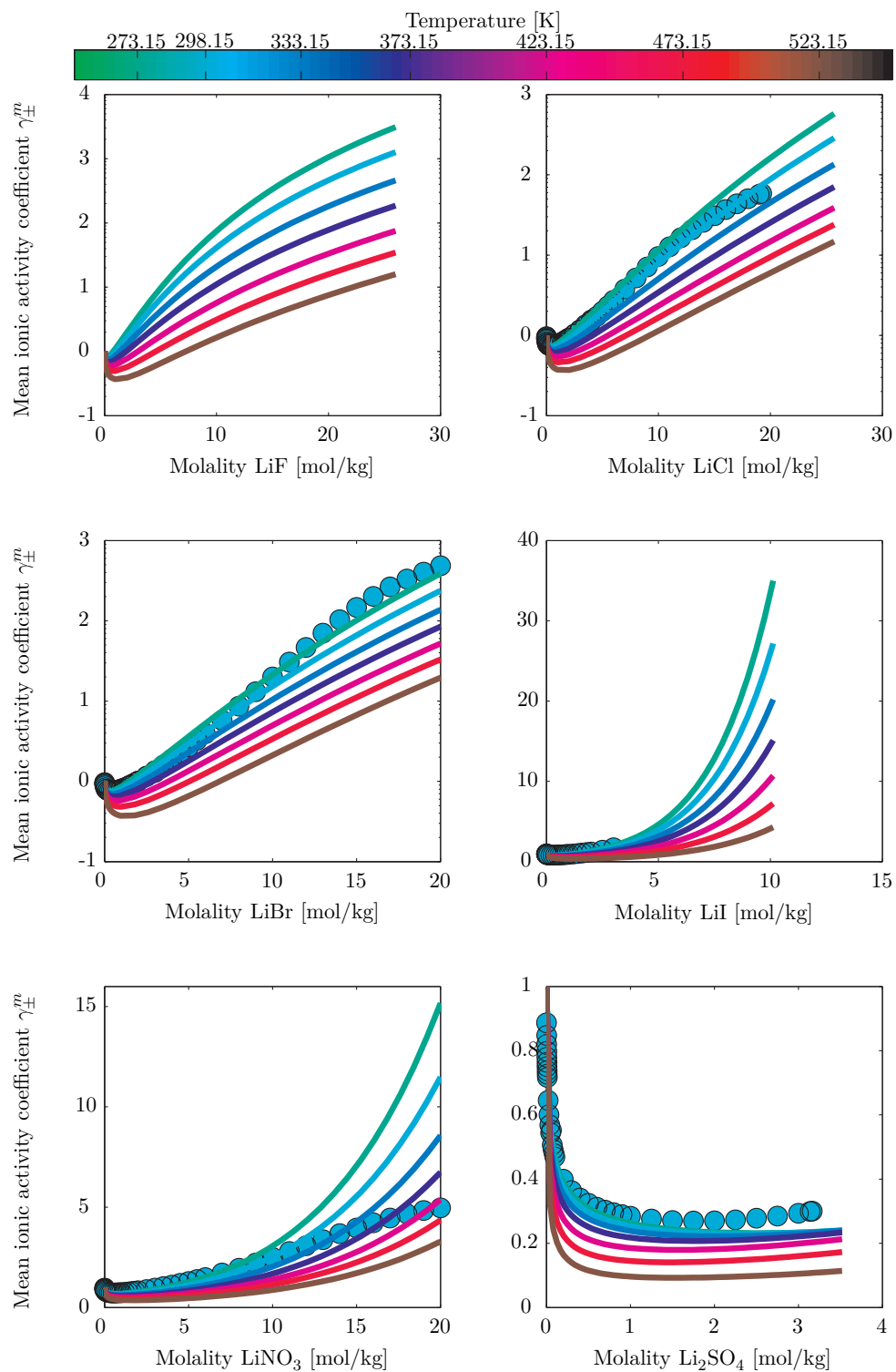**Figure D.4:** Osmotic coefficients of salts containing Lithium.

Figure D.5: Mean ionic activity coefficients of salts containing Lithium.
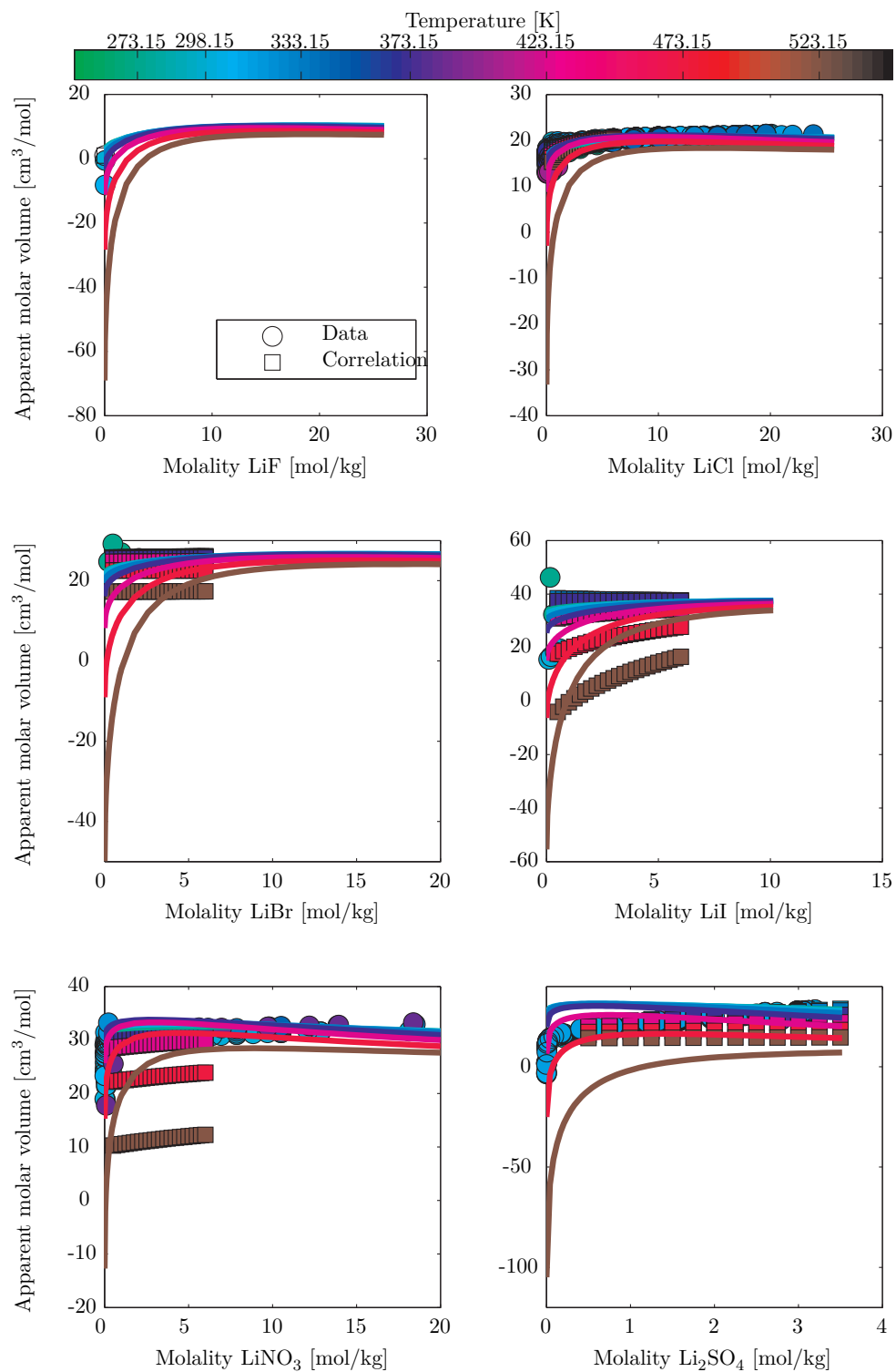
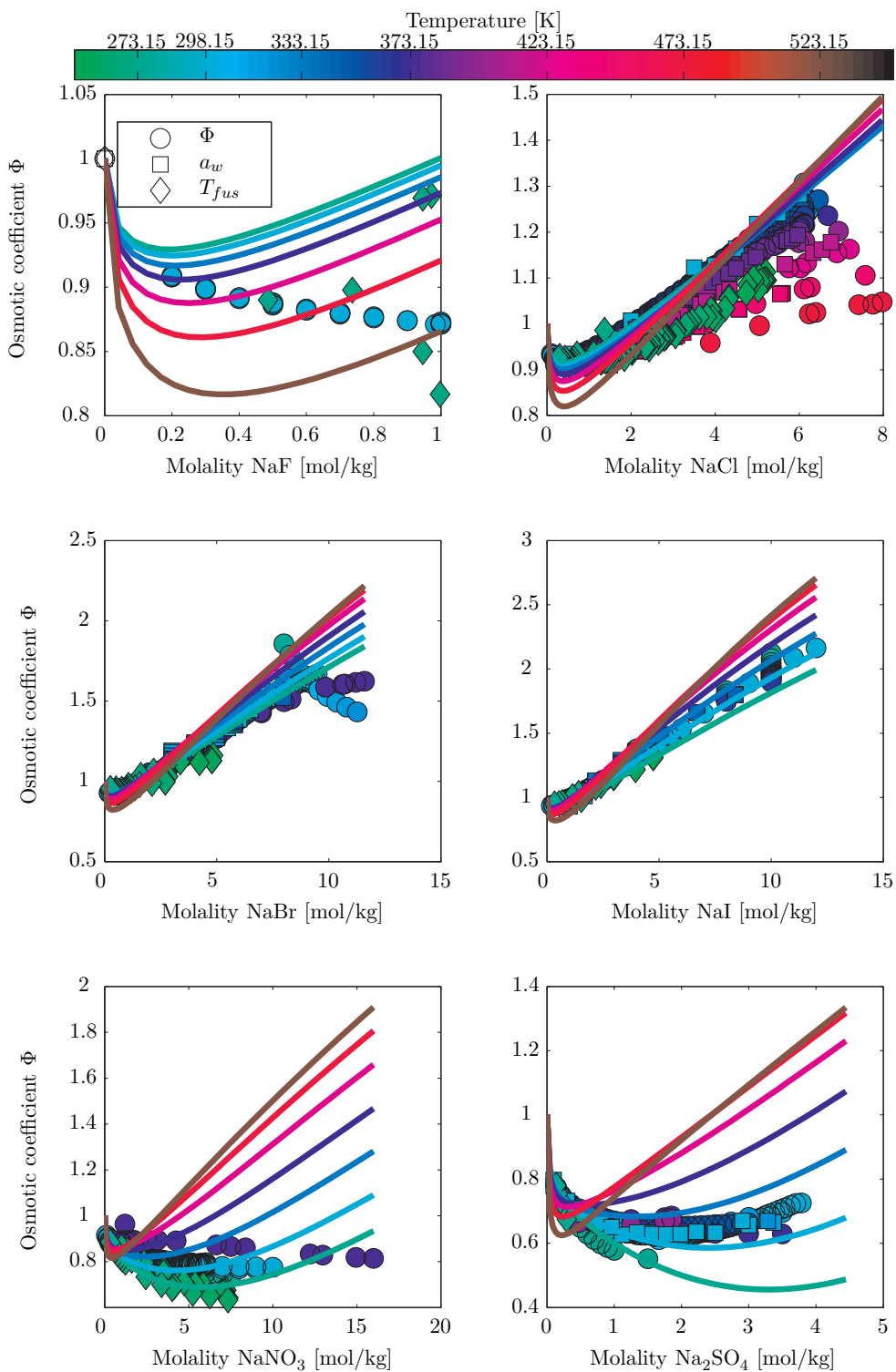**Figure D.6:** Apparent molar volume of salts containing Lithium.

Figure D.7: Osmotic coefficients of salts containing Sodium.

Figure D.8: Mean ionic activity coefficients of salts containing Sodium.

Figure D.9: Apparent molar volume of salts containing Sodium.

Figure D.10: Osmotic coefficients of salts containing Potassium.

Figure D.11: Mean ionic activity coefficients of salts containing Potassium.

Figure D.12: Apparent molar volume of salts containing Potassium.

Figure D.13: Osmotic coefficients of salts containing Rubidium.

Figure D.14: Mean ionic activity coefficients of salts containing Rubidium.

Figure D.15: Apparent molar volume of salts containing Rubidium.

Figure D.16: Osmotic coefficients of salts containing Cesium.
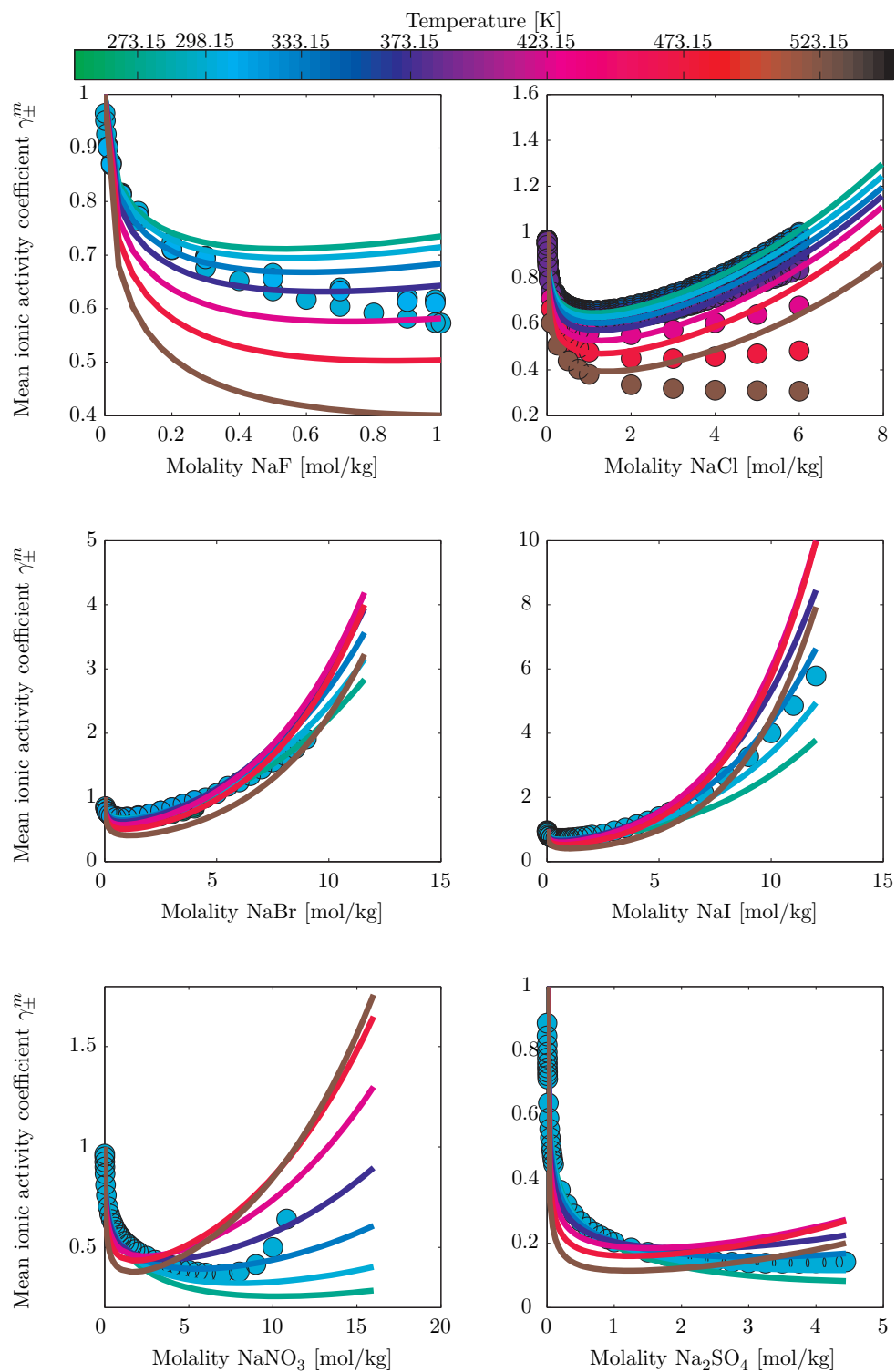
Figure D.17: Mean ionic activity coefficients of salts containing Cesium.

Figure D.18: Apparent molar volume of salts containing Cesium.

Figure D.19: Osmotic coefficients of salts containing Magnesium.

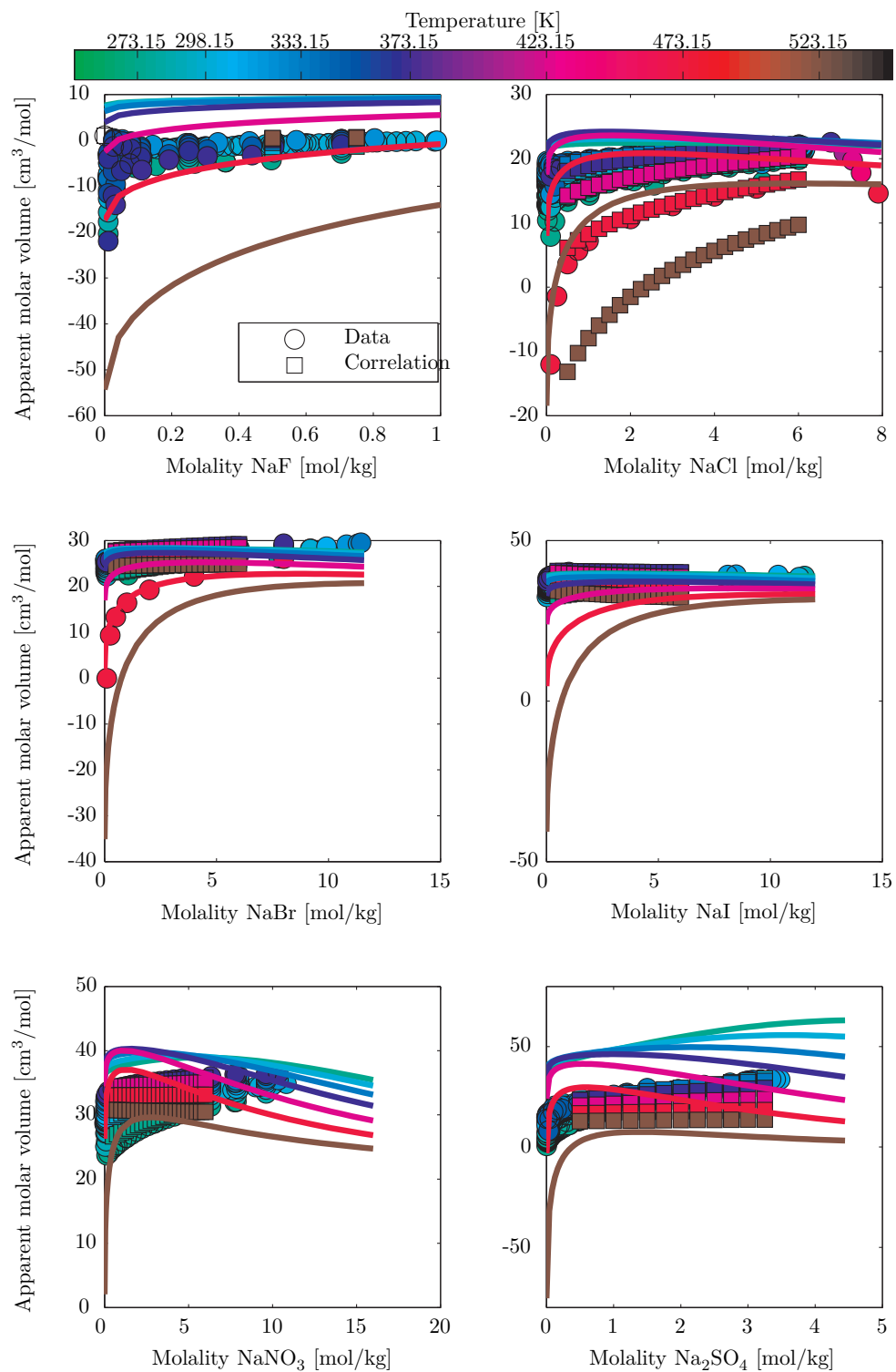**Figure D.20:** Mean ionic activity coefficients of salts containing Magnesium.

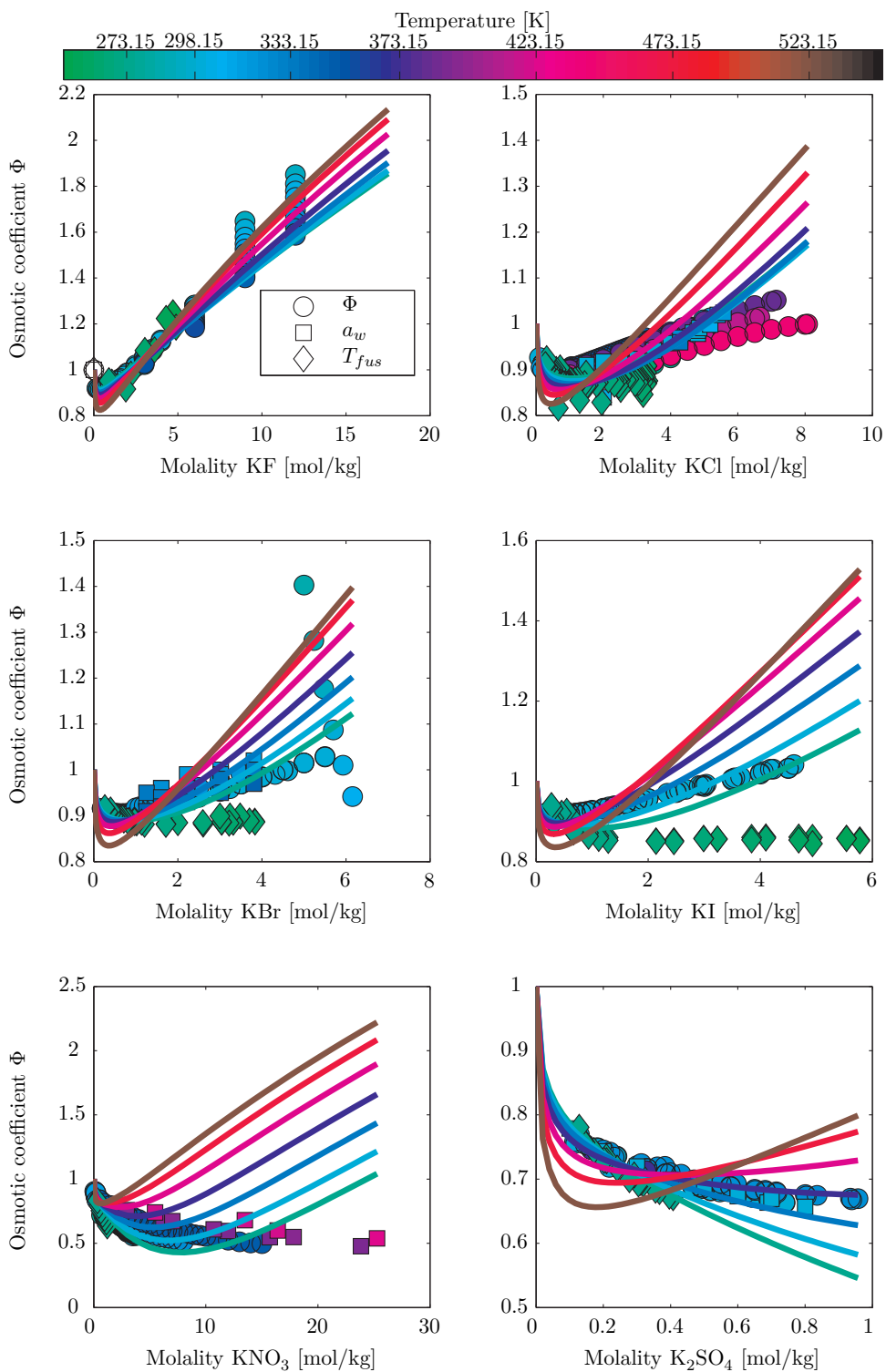**Figure D.21:** Apparent molar volume of salts containing Magnesium.
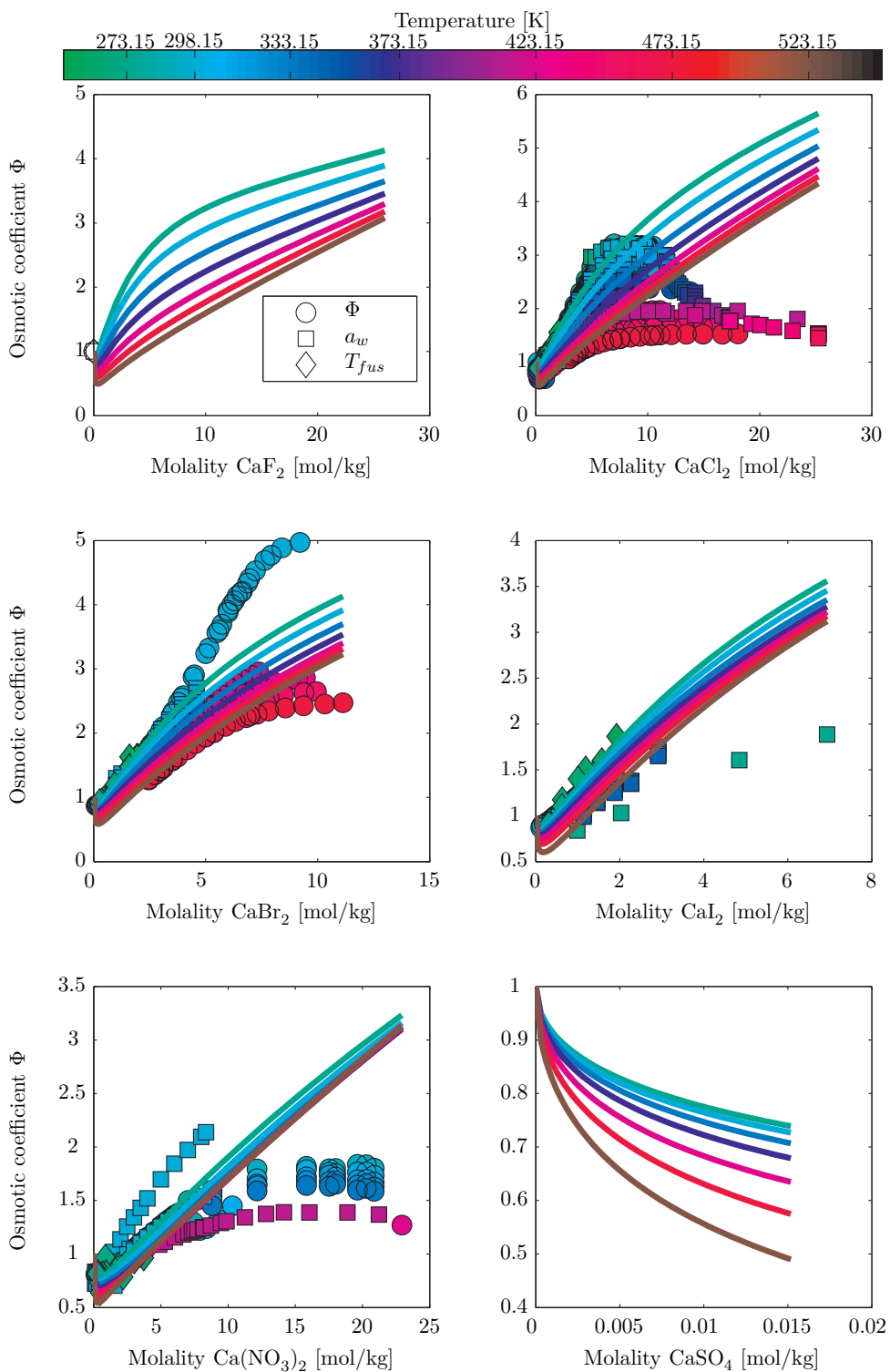
Figure D.22: Osmotic coefficients of salts containing Calcium.
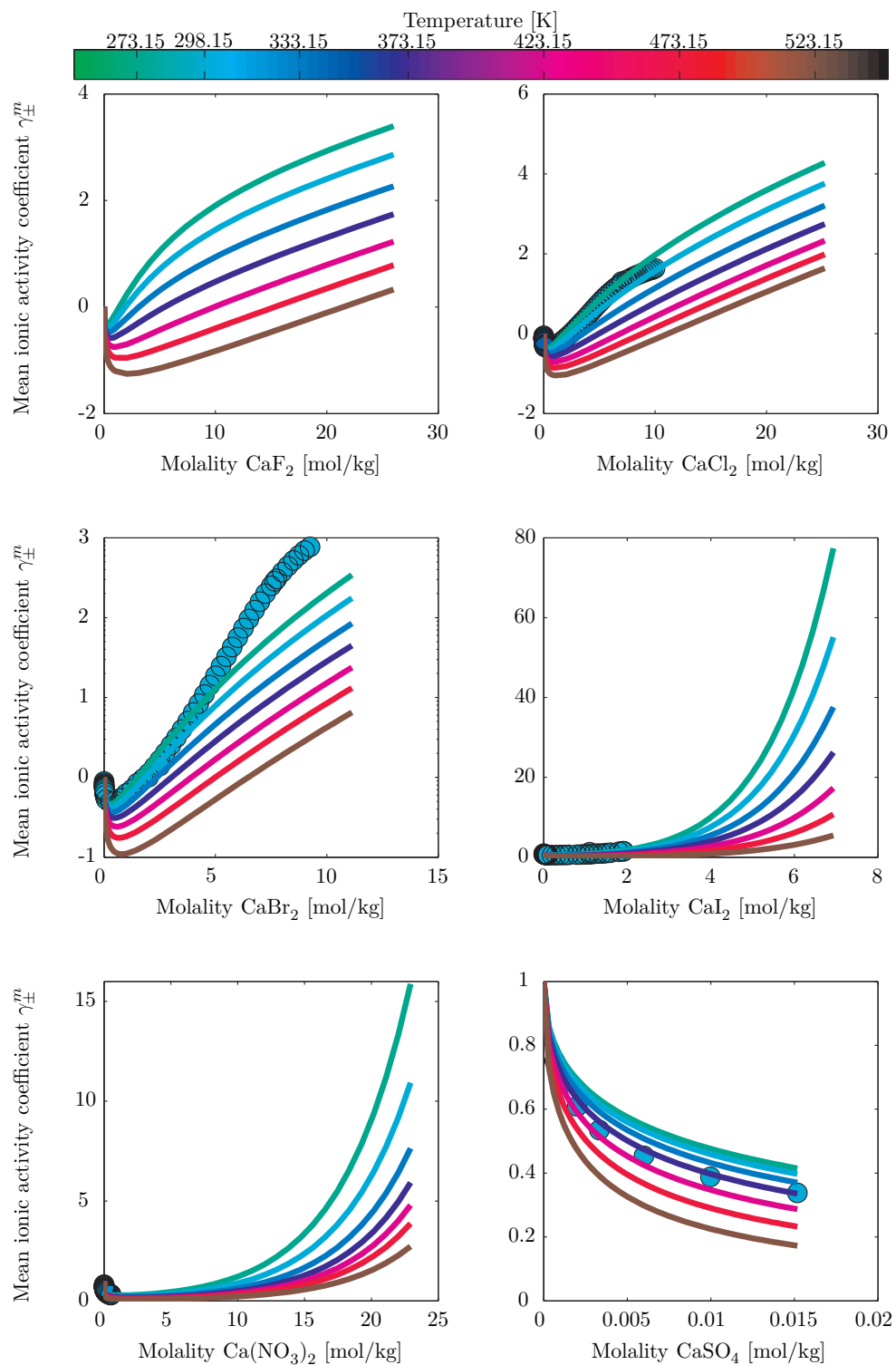
Figure D.23: Mean ionic activity coefficients of salts containing Calcium.
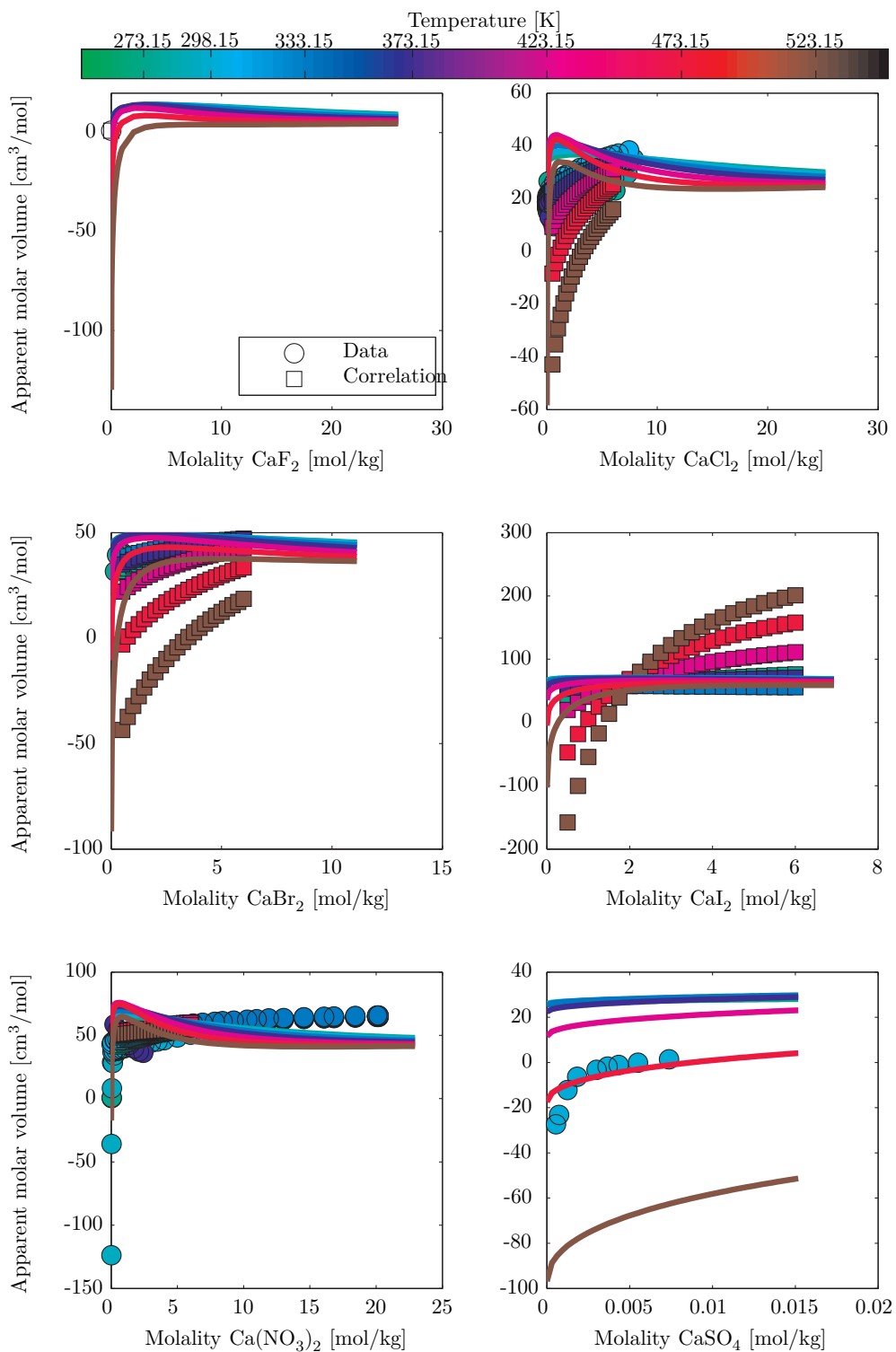
Figure D.24: Mean ionic activity coefficients of salts containing Calcium.
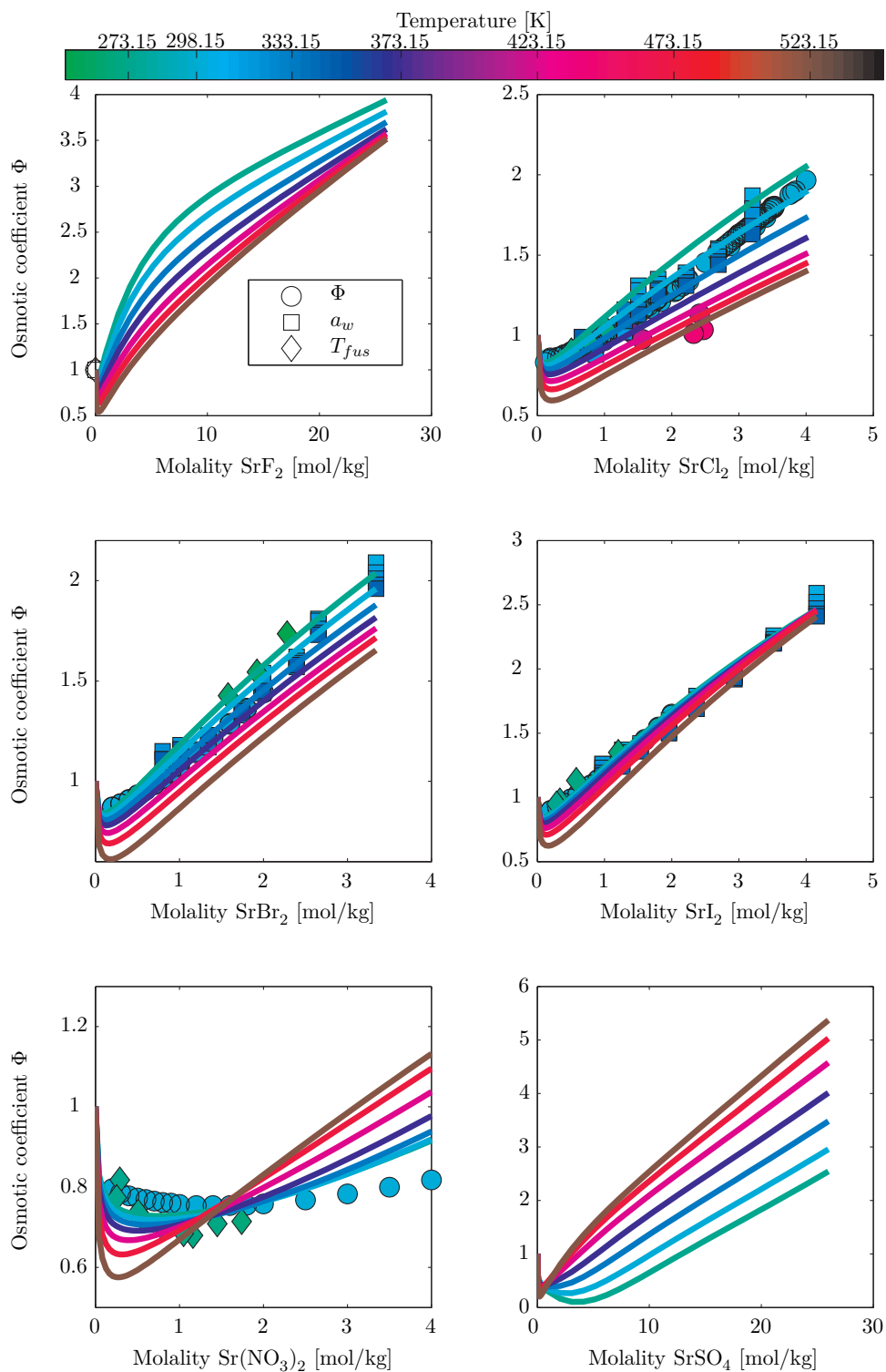
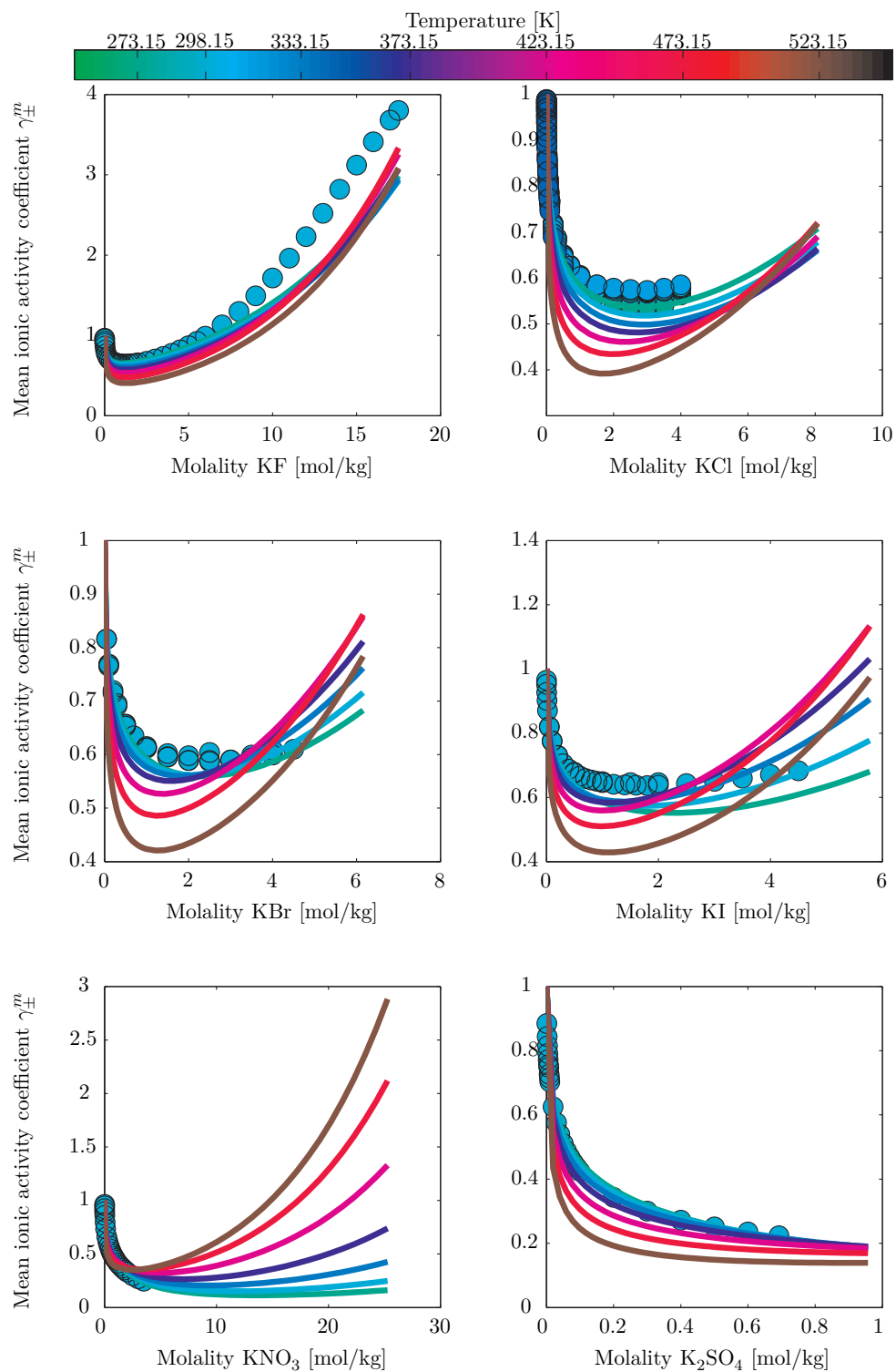**Figure D.25:** Osmotic coefficients of salts containing Strontium.
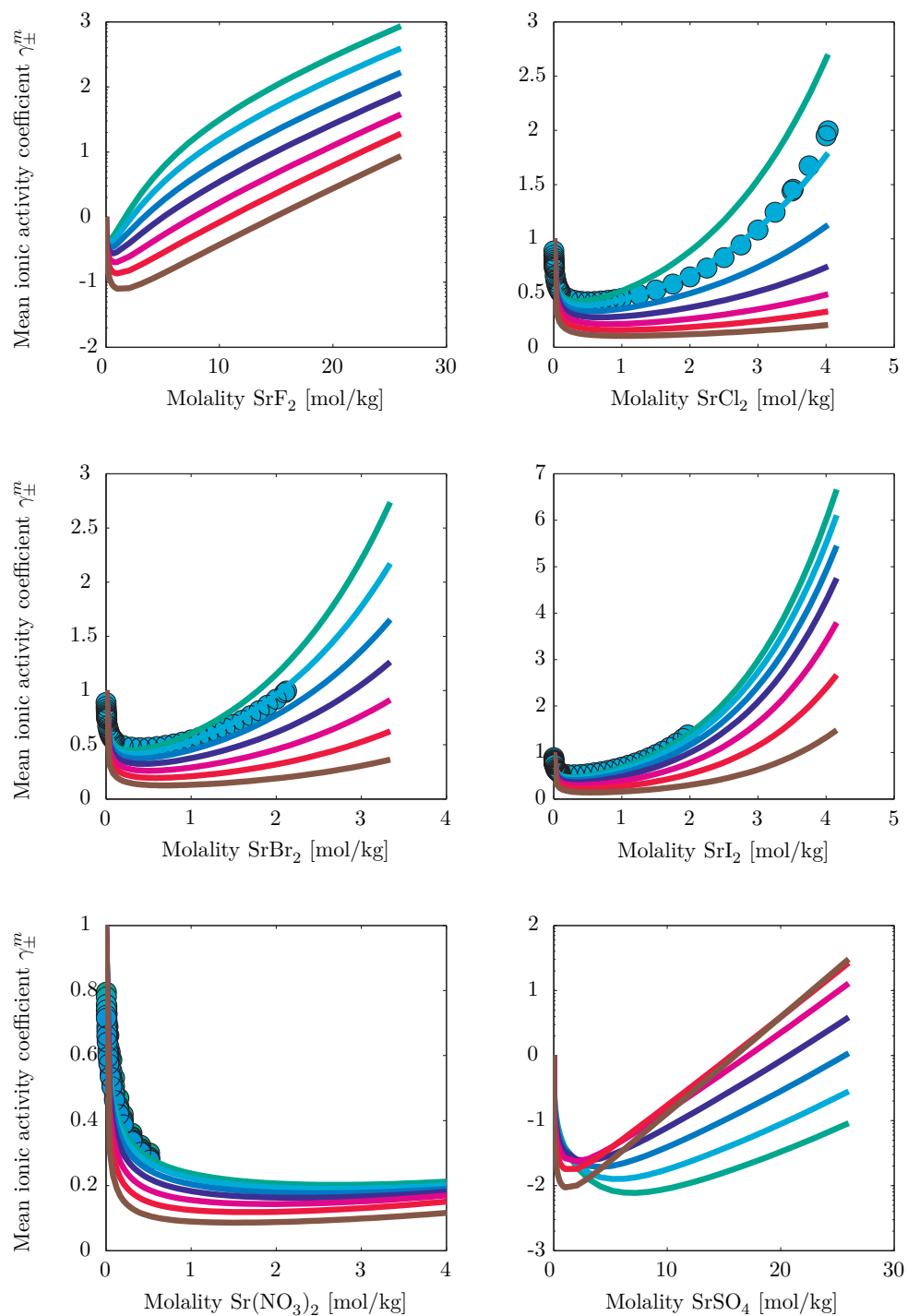
Figure D.26: Mean ionic activity coefficients of salts containing Strontium.
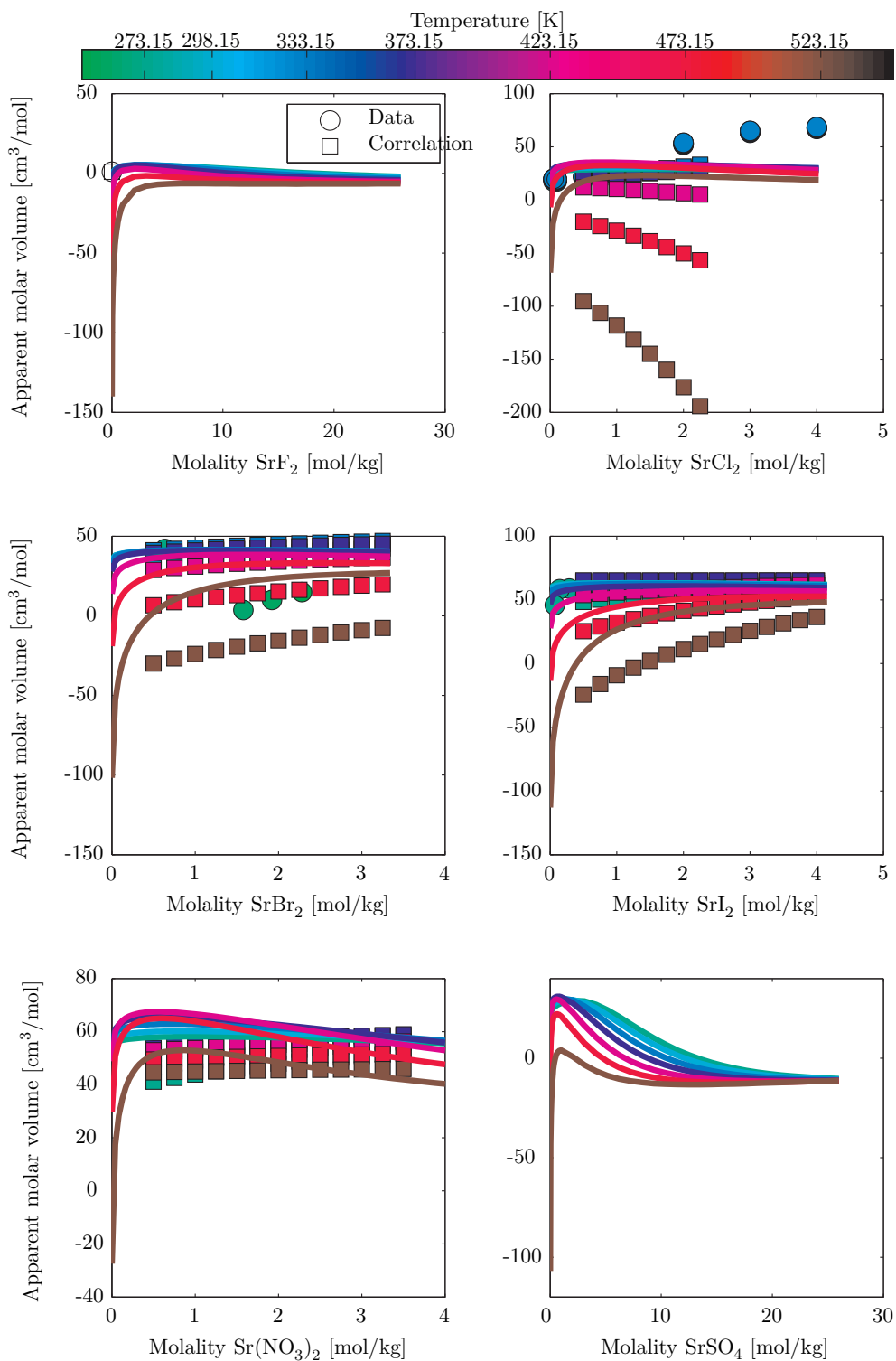
Figure D.27: Apparent molar volume of salts containing Strontium.
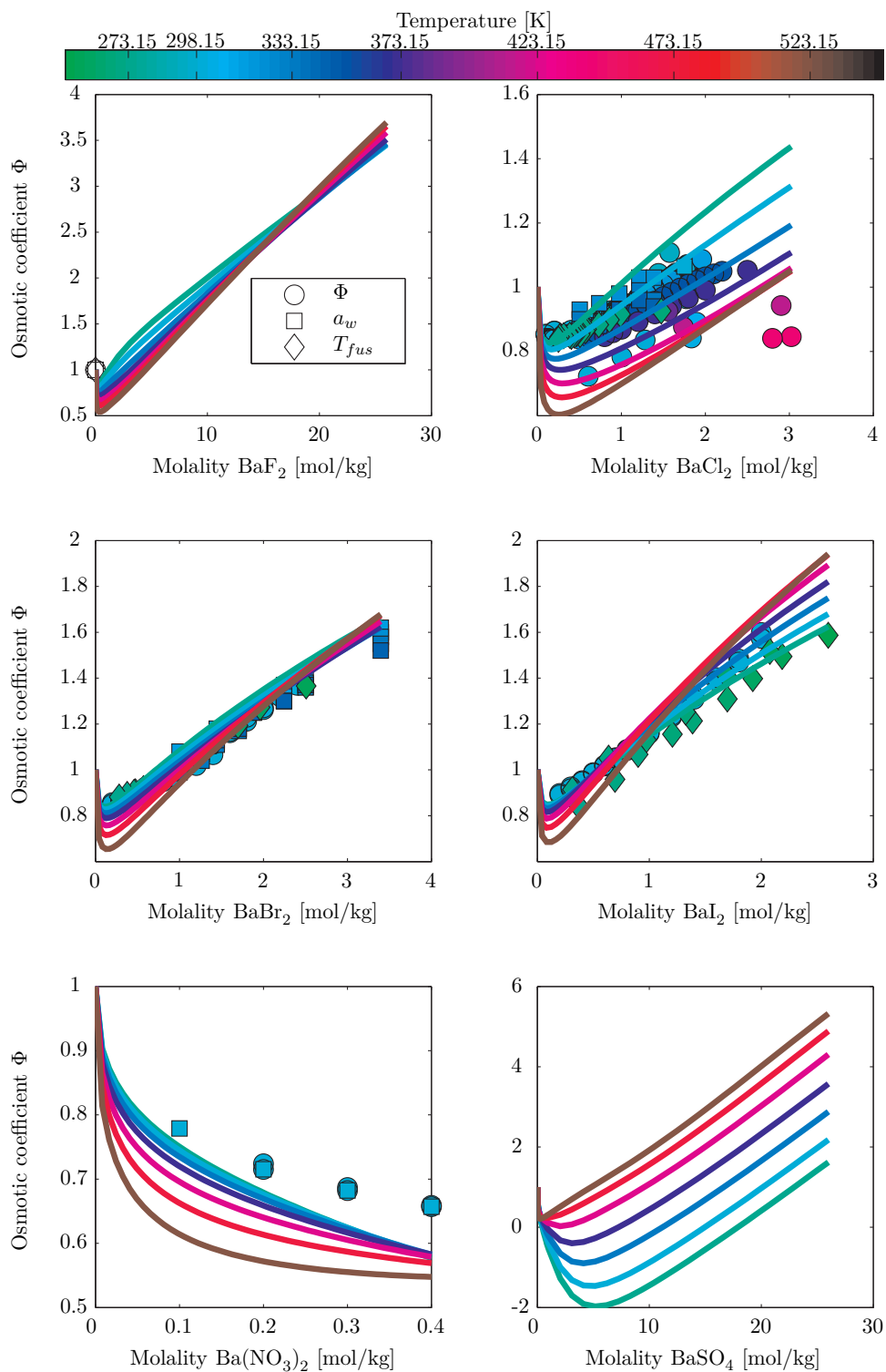
Figure D.28: Osmotic coefficients of salts containing Barium.
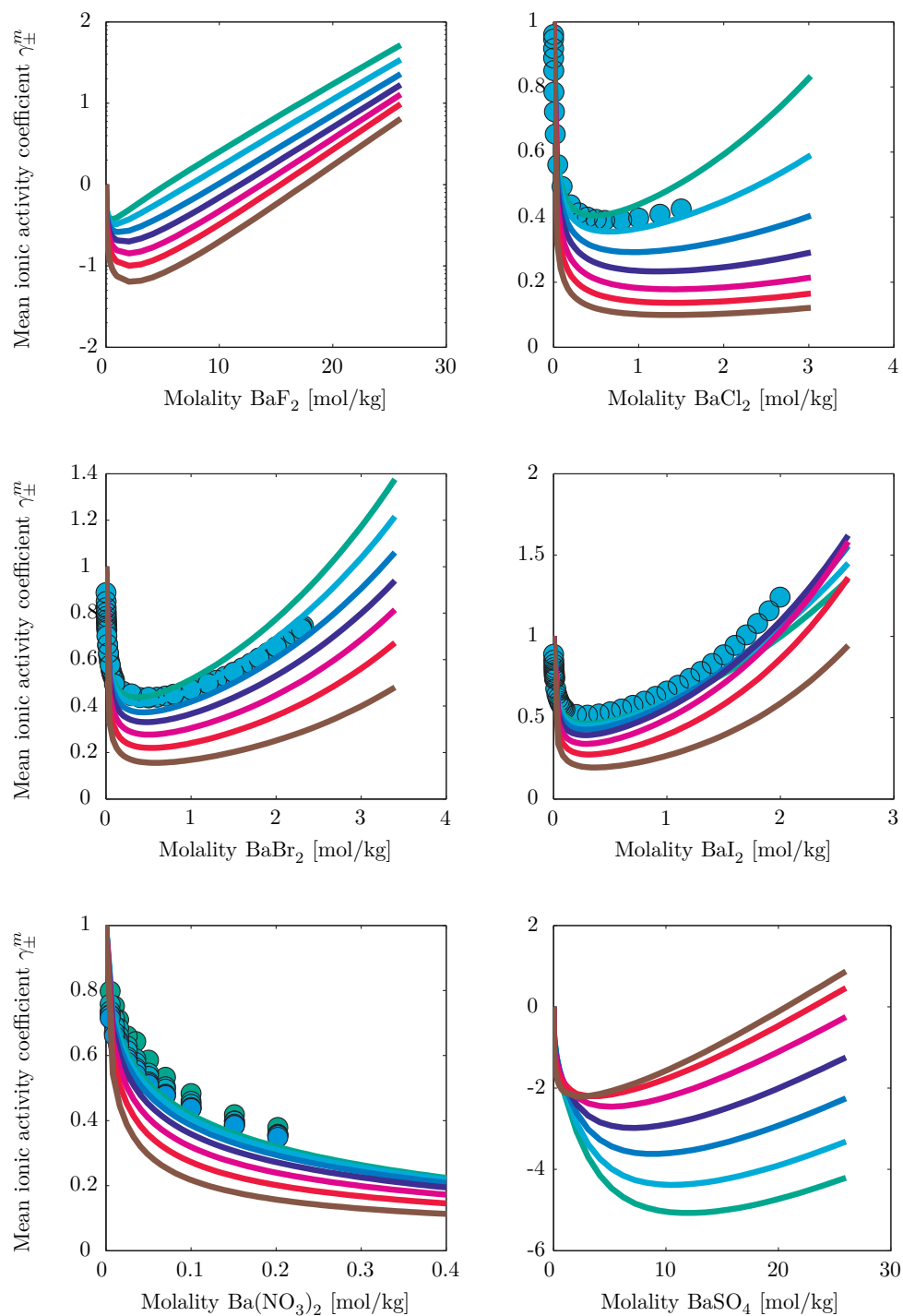
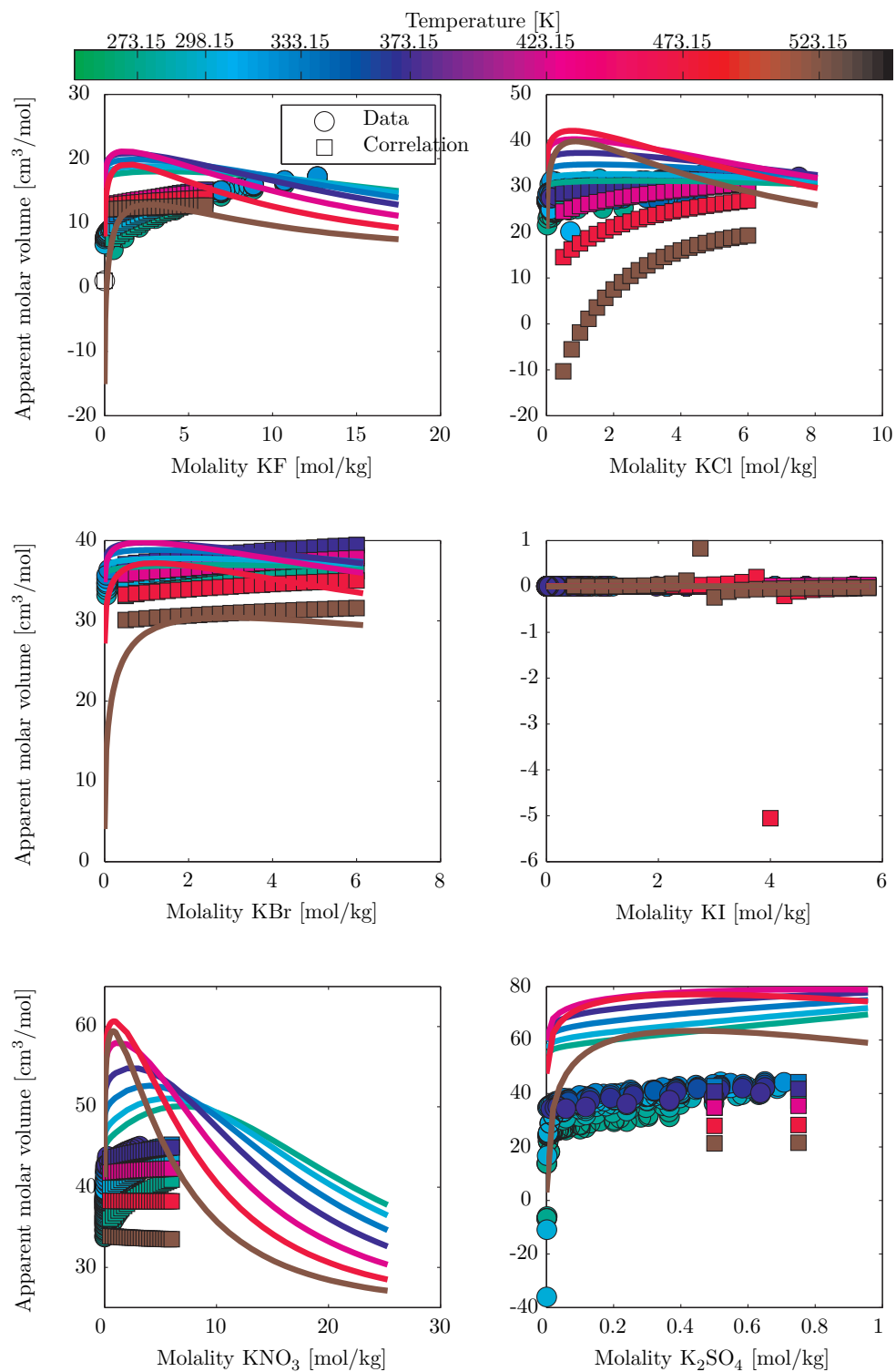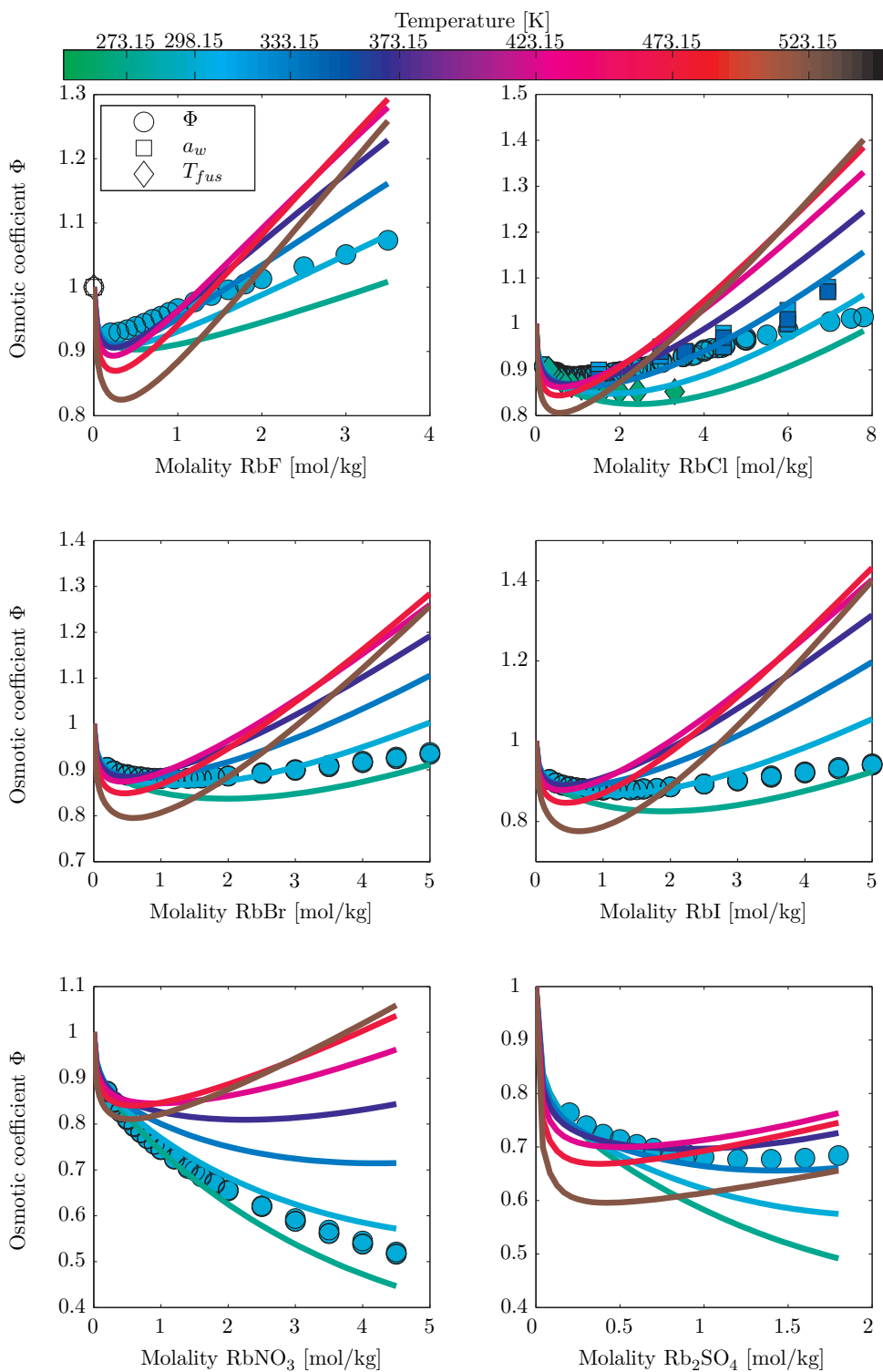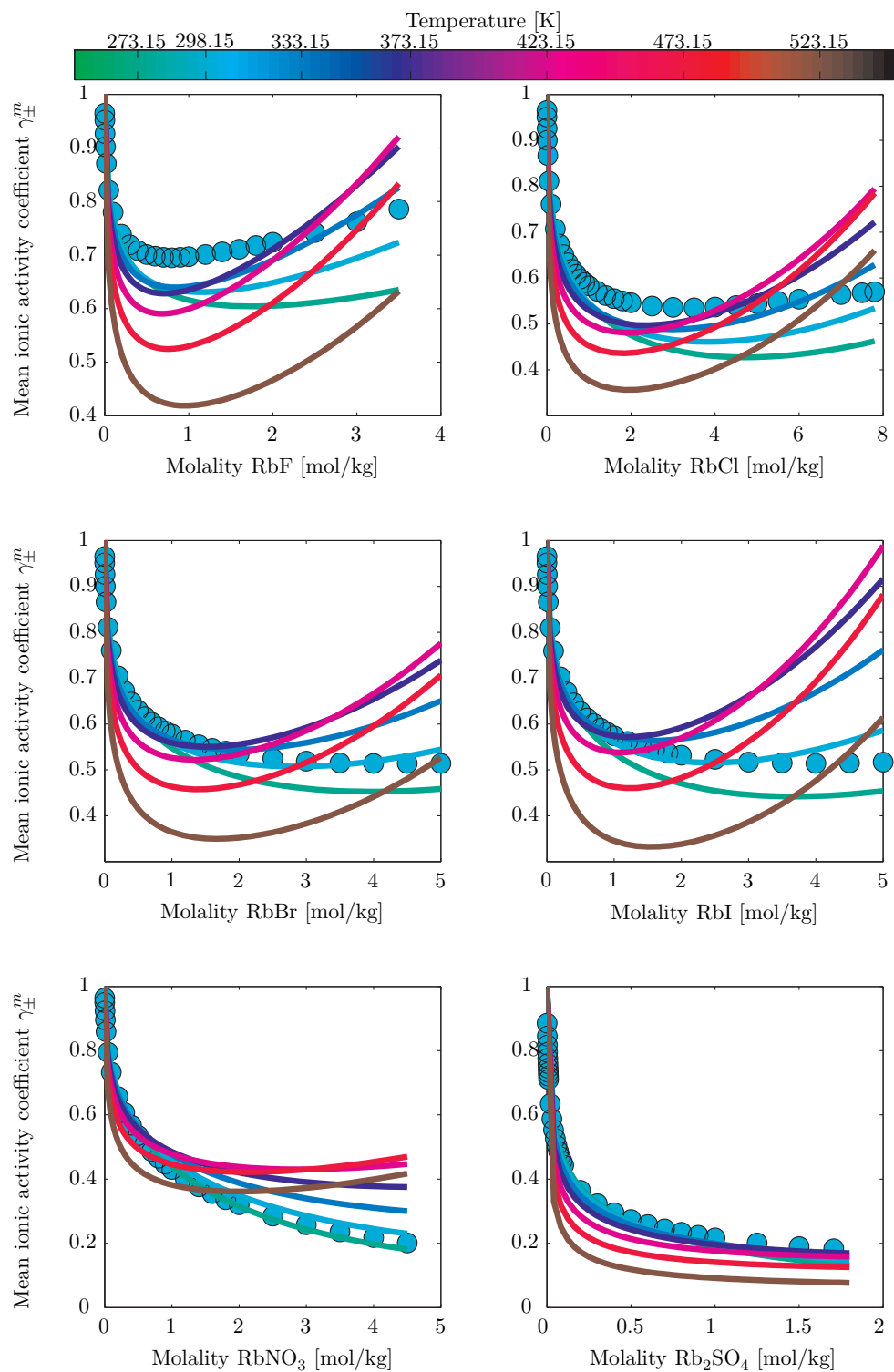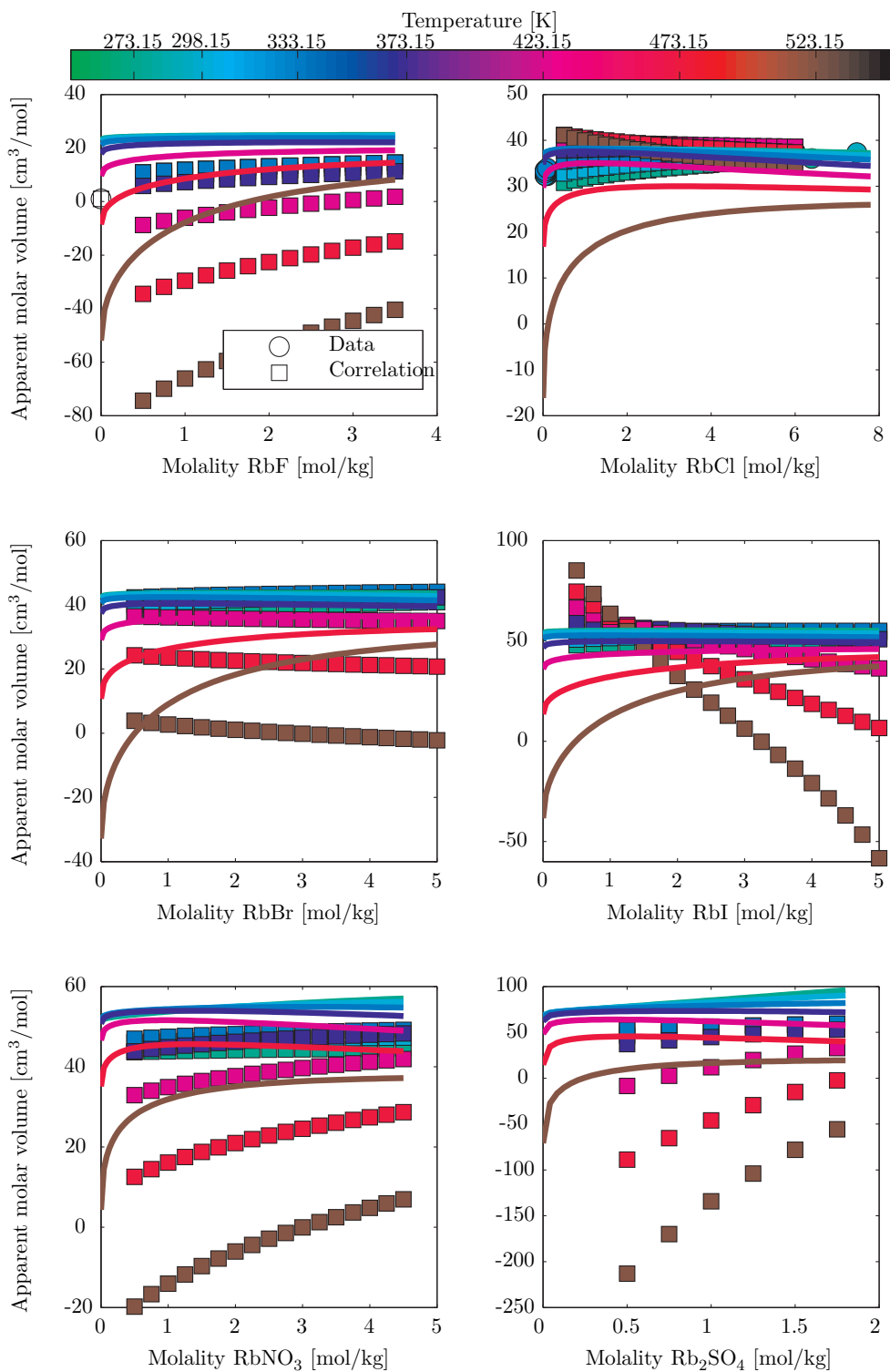**Figure D.29:** Mean ionic activity coefficients of salts containing Barium.
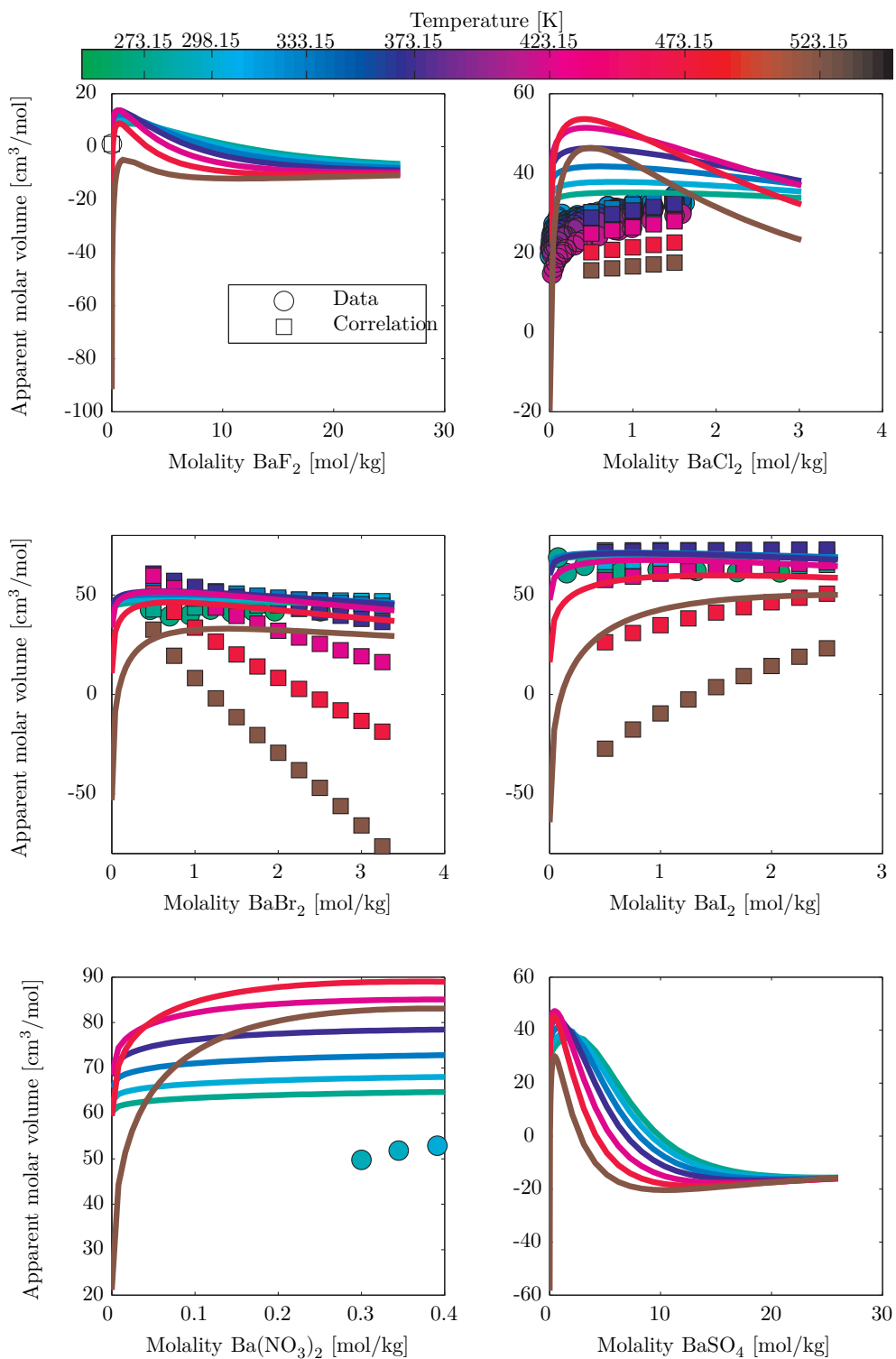
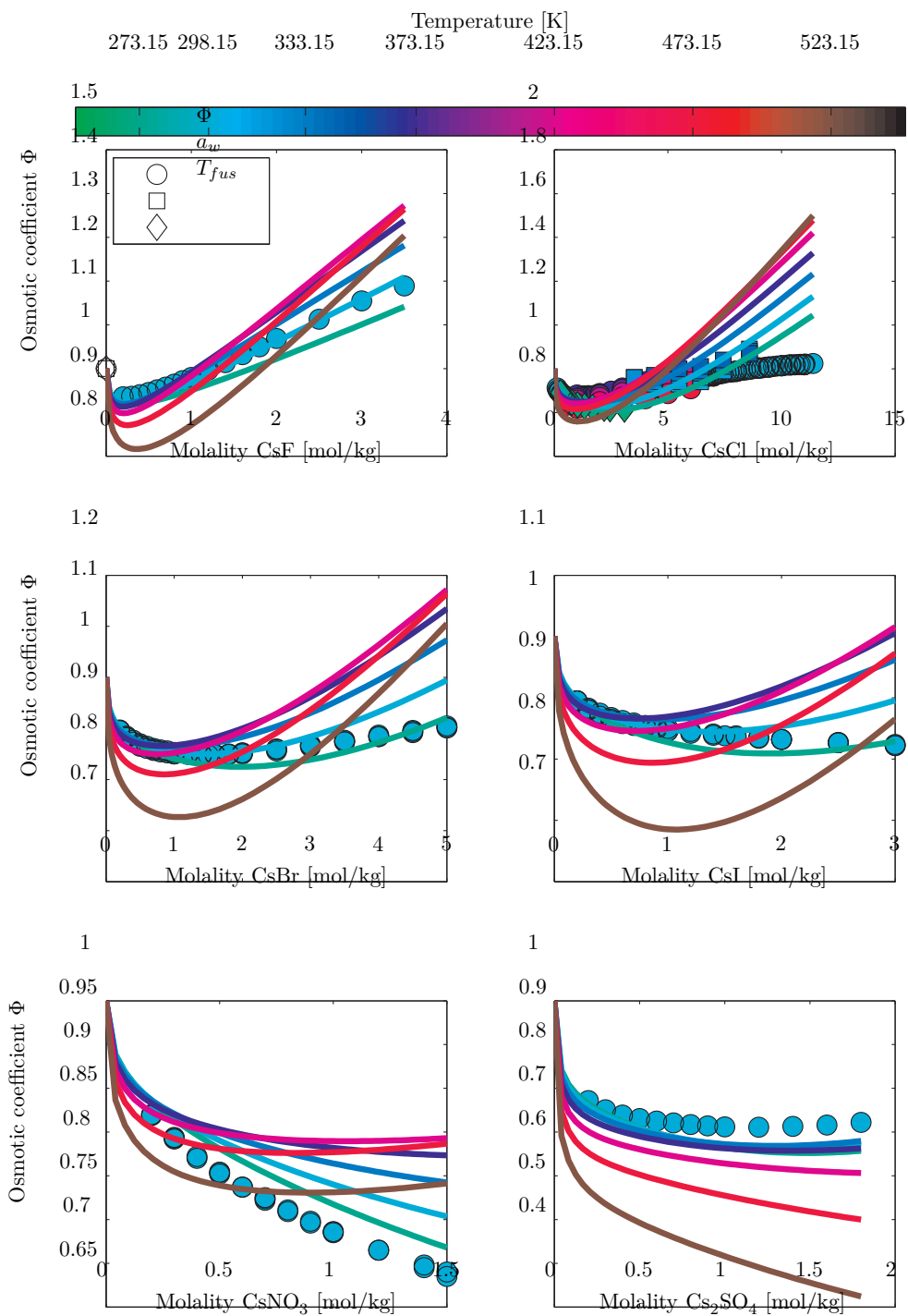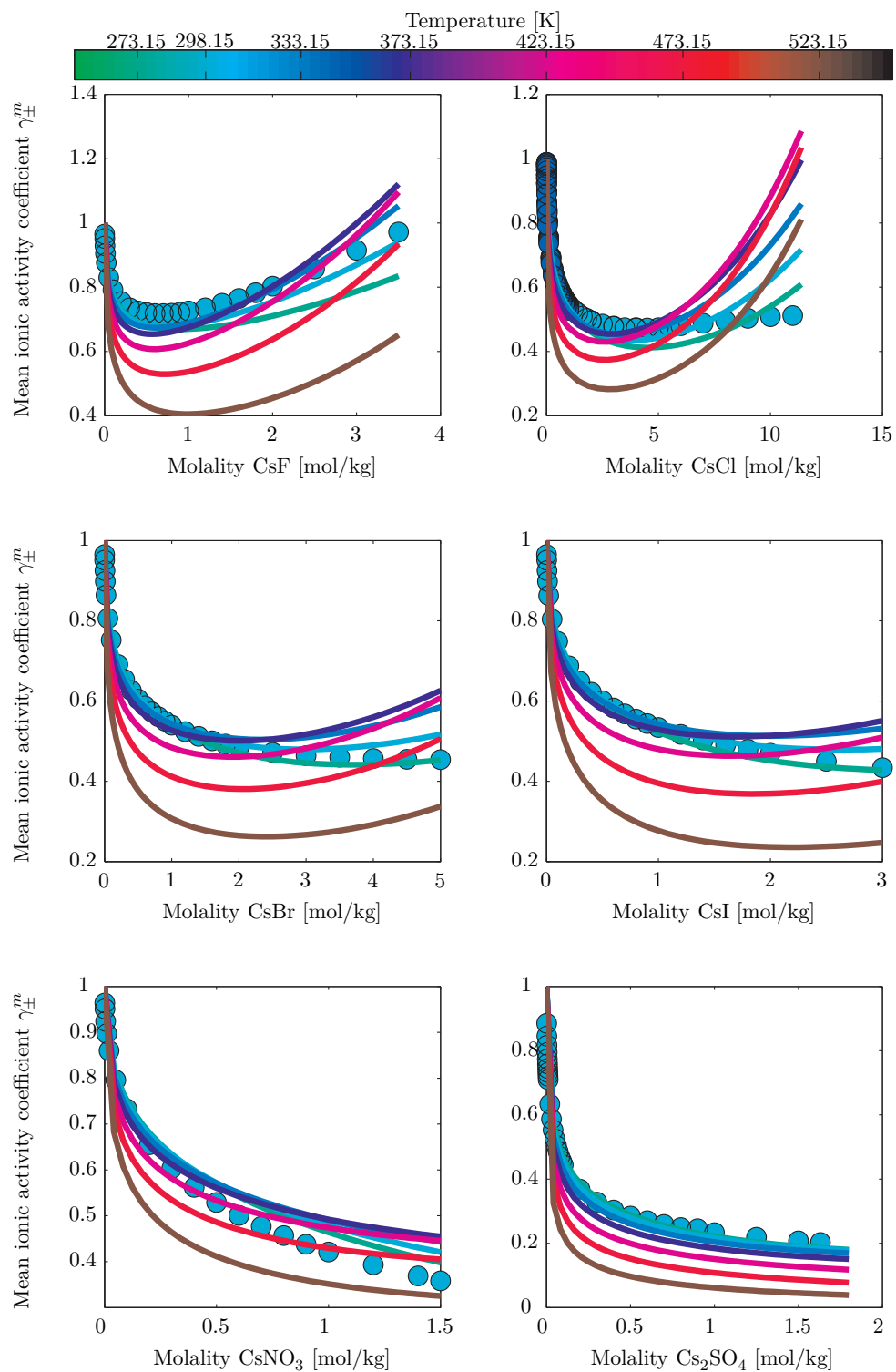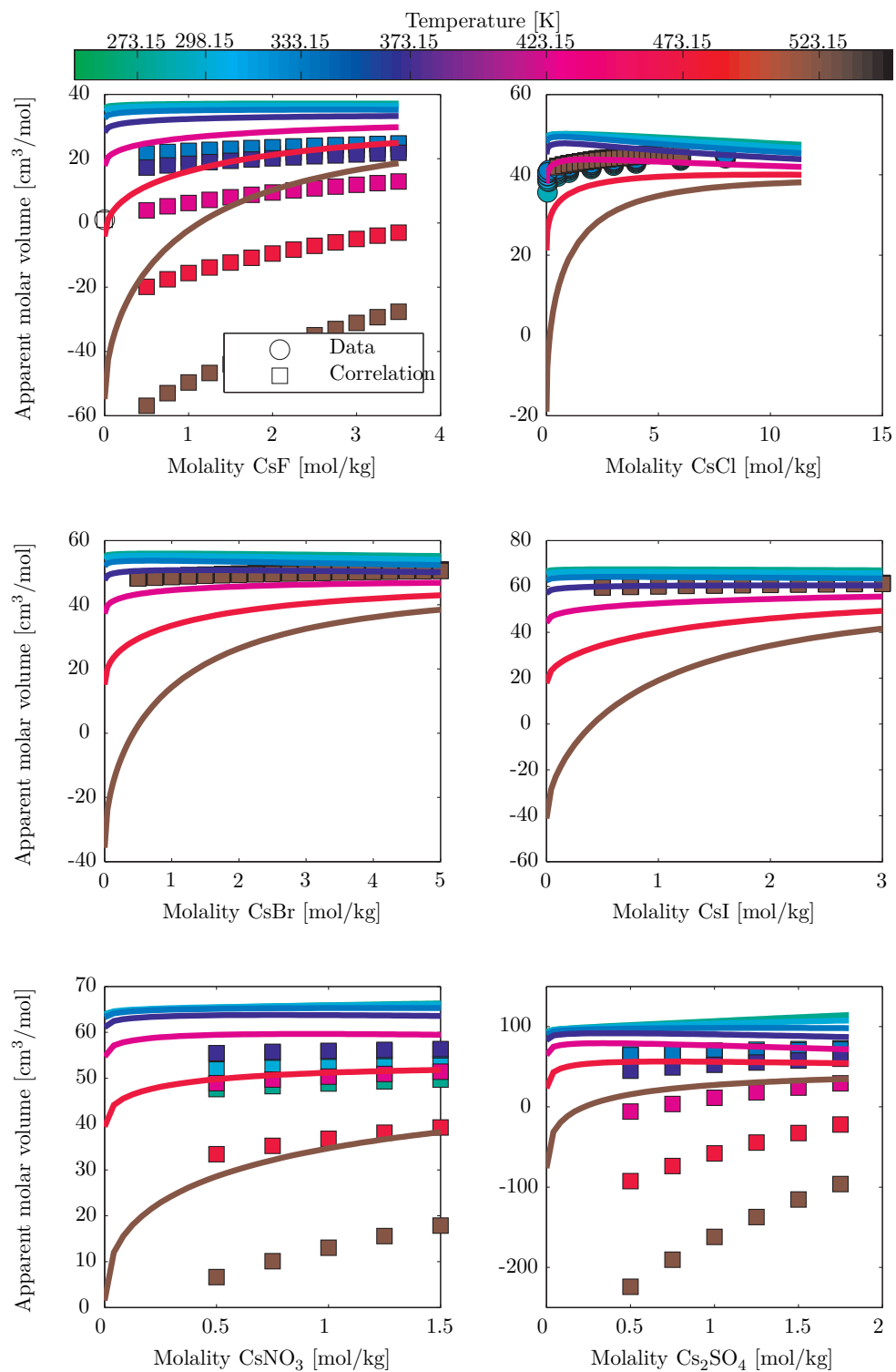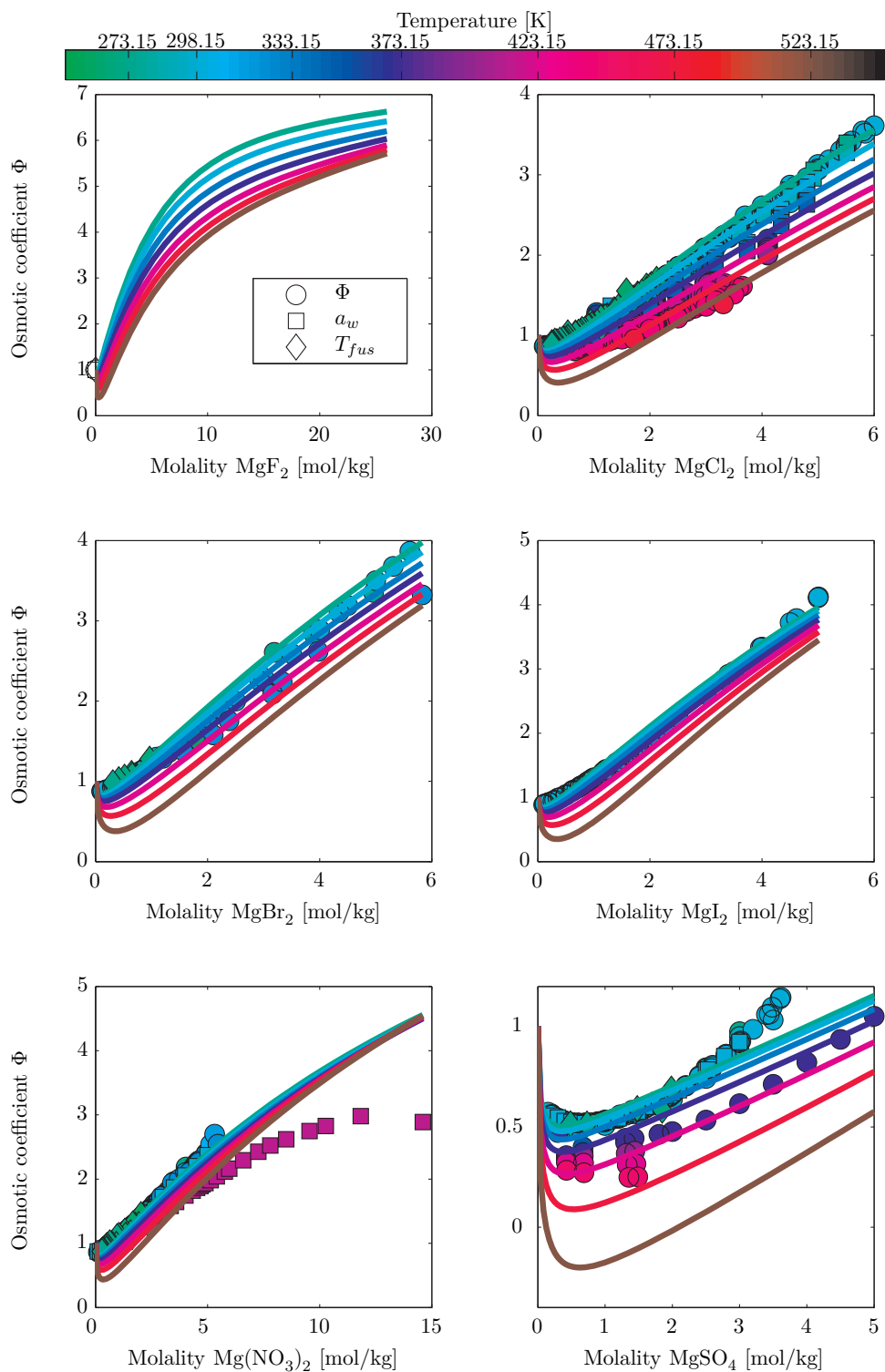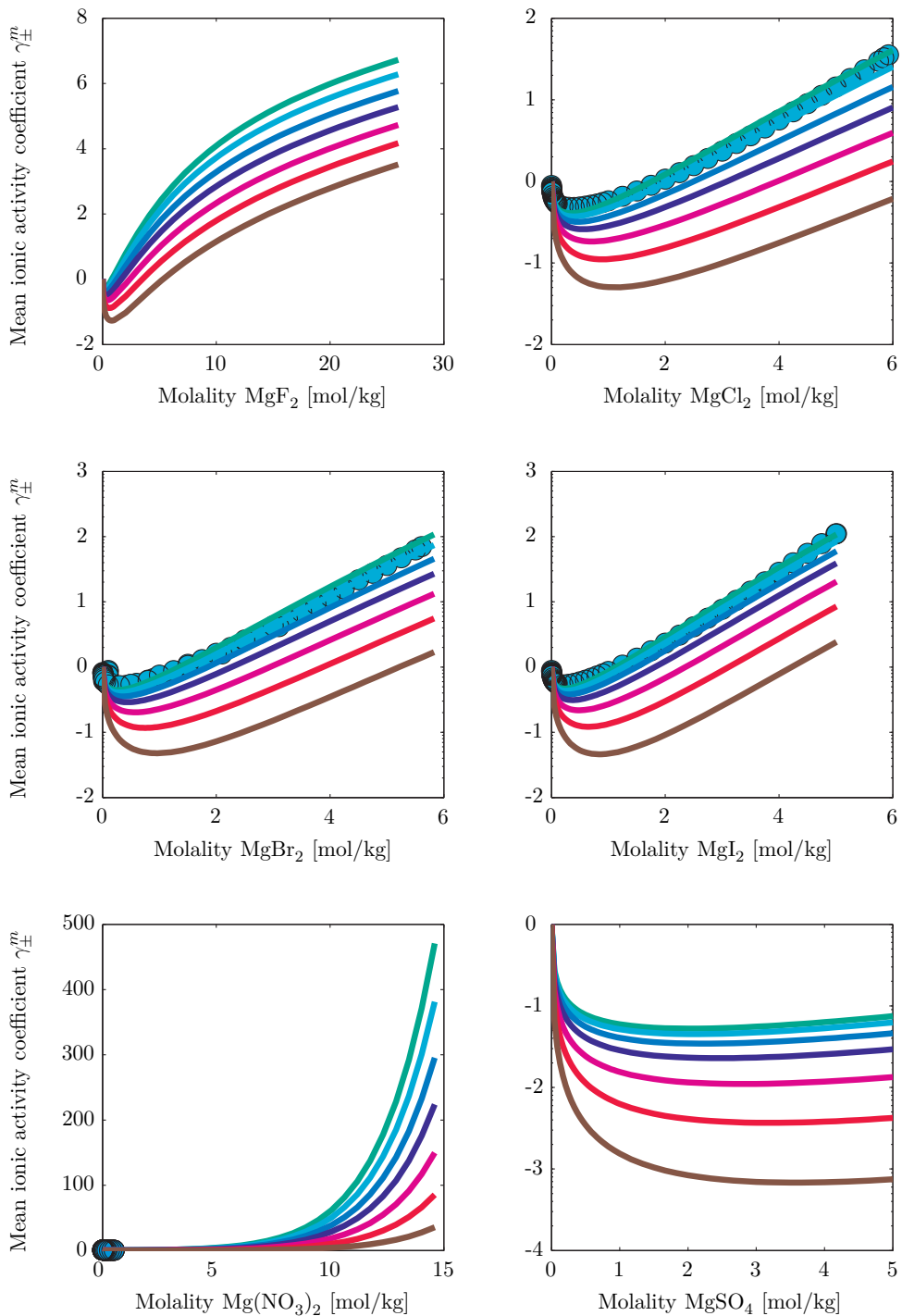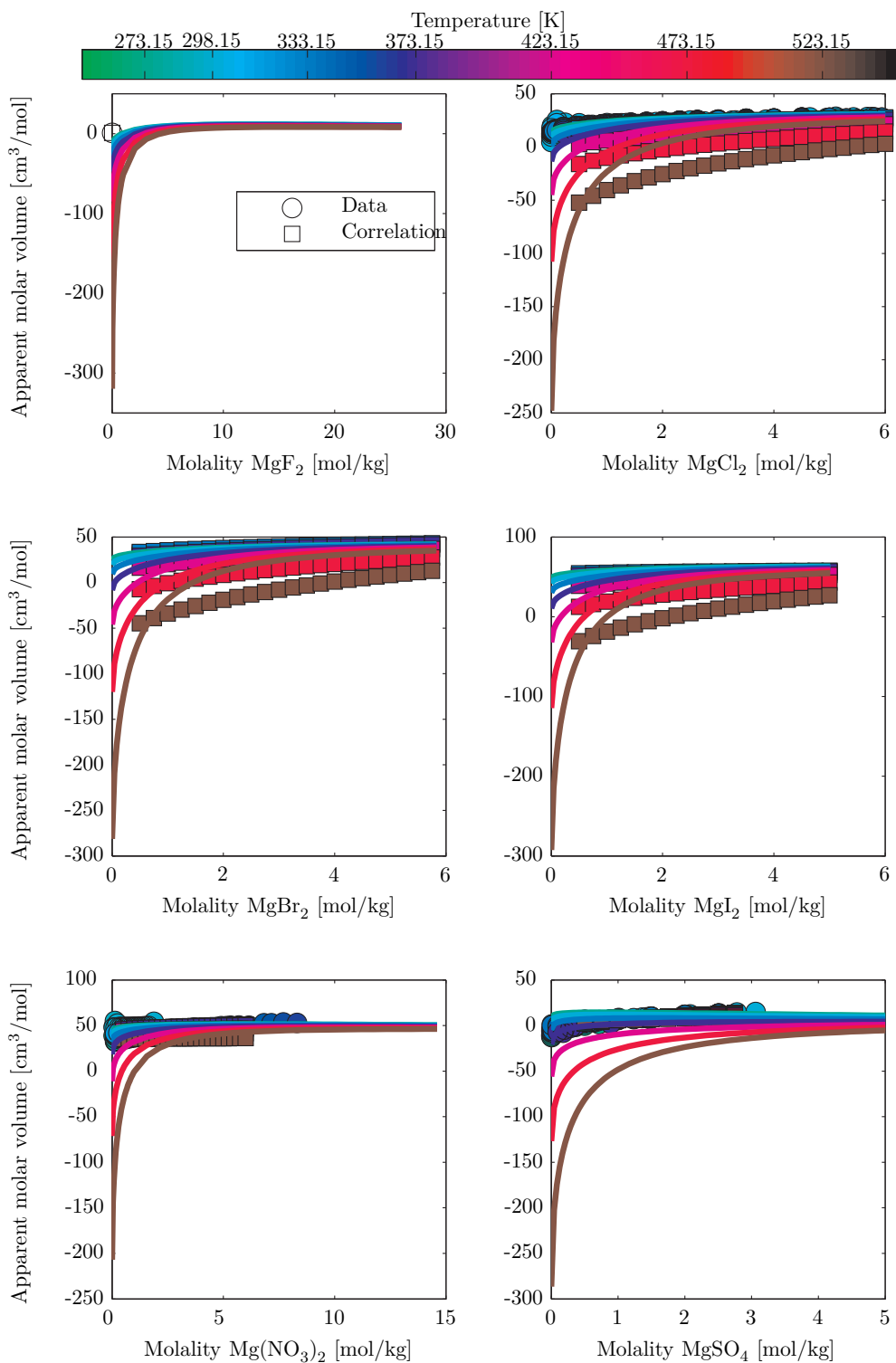**Figure D.30:** Apparent molar volume of salts containing Barium.

D.3 On Using the Ion Diameter in the Parameterization

In order to reduce the solution space and obtain reasonable physical trends in the ion diameters the cation diameters are kept fixed in the first round. In the next round, the anion diameters are kept fixed. In the final round, all diameters are adjusted simultaneously. We use Eq. (6.9) to calculate b_0 from the fitted ion diameter. σ. Optimal parameters are shown in Table D.3 and the results are summarized in Table D.4.

Ion	σ [Å]	b_0 [cm^3/mol]	ν [cm^3/mol]	u_{iw} [K]	Peneloux [cm^3/mol]	$(\nu_w + \nu_i)\,\Delta U_{iw}/R/298.15$ [cm^3/mol]
H$^+$	5.885*	0.0	-5.138*	-1899*	-0.1*	-7.182
Li$^+$	2.323*	15.81	3.781*	-3695*	-21.4*	-27.27
Na$^+$	1.721*	6.432	3.068*	-1979*	-14.8*	-14.03
K$^+$	1.911*	8.808	3.803*	-733.4*	-11.3*	-5.420
Rb$^+$	3.040*	35.44	4.470*	-488.5*	-38.0*	-3.741
Cs$^+$	2.938*	31.98	9.160*	-37.03 *	-25.1*	-0.3537
Mg^{++}	3.462*	52.32	-11.78*	-47124*	-67.6*	-52.08
Ca^{++}	3.302*	45.42	4.850*	-3022*	-57.9*	-23.61
Sr^{++}	2.990*	33.70	12.668*	-1759*	-57.6*	-19.29
Ba^{++}	2.924*	31.54	51.376*	80.60*	-63.0*	2.142
F$^-$	2.332*	15.99	7.142*	-3673*	-0.4*	-32.09
Cl$^-$	3.165*	40.00	14.959*	-719.8*	-20.2*	-8.558
Br$^-$	3.633*	60.47	16.234*	-1128*	-35.9*	-14.00
I$^-$	3.867*	72.92	20.656*	-1363*	-40.5*	-19.33
NO$_3^-$	2.544*	20.77	23.200*	490.8*	8.1*	7.467
SO$_4{-}^-$	5.044*	161.9	-7.439*	-11798*	-130.9*	-33.68

Table D.3: e-CPA parameters for different ions when all parameters were optimized simultaneously. Final column shows that there is still a reasonable physical trend in the effective energy parameter. The volume parameter increases with decreasing hydration. The diameters for H$^+$ and Li$^+$ may indicate strongly bonded water or just reflect the fact that these ions are typically very soluble and gets a slightly unphysical value to improve correspondence over the entire interval.

D.4 Temperature Dependence

Salt	RAD $\gamma_{\pm}^*$ [%]	Np. $\gamma_{\pm}^*$	RAD Φ [%]	Np. Φ	AAD V_{app} [cm^3/mol]	Np. V_{app}	m_{max}
NaF	2.28	27	2.69	24	4.1	2	1.0
KF	3.25	41	1.62	29	1.3	48	17.5
RbF	5.78	24	2.82	17	6.4	13	3.5
CsF	5.20	24	1.53	17	6.2	13	3.5
HCl	4.76	88	2.10	64	3.3	118	16
LiCl	4.40	59	2.65	161	1.0	75	20
NaCl	1.94	53	1.53	231	1.6	23	6.2
KCl	3.13	63	1.75	114	1.3	19	5.0
RbCl	5.04	32	3.31	88	2.0	30	7.8
CsCl	2.50	63	3.87	217	3.9	44	11.4
MgCl$_2$	4.38	49	2.80	166	6.7	23	6.0
CaCl$_2$	4.09	71	3.83	339	11.5	41	10.5
SrCl$_2$	3.63	42	3.04	92	7.4	8	4.0
BaCl$_2$	5.59	19	2.29	108	4.4	5	1.8
HBr	3.82	51	2.10	27	3.8	32	11
LiBr	5.21	45	4.30	107	1.5	79	20
NaBr	3.99	60	0.77	110	2.1	36	9.5
KBr	3.13	32	1.75	48	1.3	21	5.7
RbBr	3.46	27	2.92	53	3.4	19	5.0
CsBr	0.86	27	1.16	53	5.9	19	5.0
MgBr$_2$	9.65	60	2.63	47	5.1	21	5.6
CaBr$_2$	7.03	61	4.65	69	9.8	35	9.2
SrBr$_2$	4.66	40	3.66	28	7.8	7	2.1
BaBr$_2$	5.08	55	4.90	30	0.9	8	2.4
HI	2.41	33	1.03	42	1.4	39	10
LiI	3.33	33	2.59	64	1.2	11	3.2
NaI	3.49	39	1.27	47	0.7	44	12
KI	3.85	7	2.72	54	1.1	17	4.6
RbI	3.32	27	3.80	53	1.7	19	5.0
CsI	3.92	23	3.17	41	4.3	11	3.0
MgI$_2$	5.61	41	2.10	52	6.5	19	5.0
CaI$_2$	6.55	38	2.46	37	21.3	7	2.0
SrI$_2$	7.26	38	2.09	28	7.8	7	2.0
BaI$_2$	7.91	38	1.31	28	1.2	7	2.0
LiNO$_3$	6.36	43	1.54	128	0.9	79	20
NaNO$_3$	3.11	34	3.03	122	0.5	42	8.3
KNO$_3$	1.04	24	1.98	122	1.1	14	3.8
RbNO$_3$	1.54	26	2.87	50	3.3	17	4.5
CsNO$_3$	2.95	19	3.10	29	6.4	5	1.5
Mg(NO$_3$)$_2$	6.00	13	3.74	146	6.2	19	5.1
Ca(NO$_3$)$_2$	6.16	13	3.11	55	9.1	32	8.4
Sr(NO$_3$)$_2$	6.37	13	3.62	18	3.7	13	4.0
Ba(NO$_3$)$_2$	6.91	10	11.14	6	2.0	1	0.4
Li$_2$SO$_4$	3.18	38	4.40	51	10.4	11	3.2
Na$_2$SO$_4$	1.58	43	0.60	133	8.1	12	4.4
K$_2$SO$_4$	4.44	25	1.02	51	19.0	2	0.8
Rb$_2$SO$_4$	3.34	31	6.01	13	12.1	6	1.8
Cs$_2$SO$_4$	2.89	31	3.98	13	19.5	6	1.8
MgSO$_4$	-	-	5.16	70	13.4	10	3.6
CaSO$_4$	17.05	7	-	-	49.0	10	0.0152
Average	4.40		2.75	-	5.9		

Table D.4:]
Deviations from experimental data with parameters from Table D.3.

Ion	σ [Å]	b_0 [cm^3/mol]	ν [cm^3/mol]	u_{iw}^0 [K]	u_{iw}^T	Peneloux [cm^3/mol]
H$^+$	5.885	0.0	-5.138	-1899	82.90*	-0.1
Li$^+$	2.323	15.81	3.781	-3695	5.952*	-21.4
Na$^+$	1.721	6.432	3.068	-1979	-23.14*	-14.8
K$^+$	1.911	8.808	3.803	-733.4	-10.46*	-11.3
Rb$^+$	3.040	35.44	4.470	-488.48	-13.69*	-38.0
Cs$^+$	2.938	31.98	9.160	-37.03	-8.178*	-25.1
Mg^{++}	3.462	52.32	-11.78	-47124	-472.4*	-67.6
Ca^{++}	3.302	45.42	4.850	-3022	96.81*	-57.9
Sr^{++}	2.990	33.70	12.67	-1759	11.62*	-57.6
Ba^{++}	2.924	31.54	51.38	80.60	-0.7562*	-63.0
F$^-$	2.332	15.99	7.142	-3673	4.802*	-0.4
Cl$^-$	3.165	40.00	14.96	-719.8	6.172*	-20.2
Br$^-$	3.633	60.47	16.23	-1128	4.989*	-35.9
I$^-$	3.867	72.92	20.66	-1363	1.400*	-40.5
NO$_3^-$	2.544	20.77	23.20	490.8	-1.263*	8.1
SO$_4$--$^-$	5.044	161.9	-7.439	-11798	34.51*	-130.9

Table D.5: Temperature dependence of the e-CPA water-ion interaction parameter. σ, ν, and u_{iw}^0 were all optimized at 298.15K and only u_{iw}^T was optimized to the temperature dependence.

Ion	σ [Å]	b_0 [cm^3/mol]	ν [cm^3/mol]	u_{iw}^0 [K]	u_{iw}^T	Peneloux [cm^3/mol]
H$^+$	9.160*	0.0	-0.6883*	-6492*	-12.62*	18.3*
Li$^+$	2.768*	26.76	5.775*	-2880*	1.277*	-16.4*
Na$^+$	2.237*	14.11	2.849*	-1283*	-15.00*	-4.8*
K$^+$	2.482*	19.29	1.923*	-23.02*	-18.18*	-4.0*
Rb$^+$	3.236*	42.74	1.222*	-248.4*	-28.26*	-25.3*
Cs$^+$	3.070*	36.48	1.203*	84.77*	-22.47*	-9.1*
Mg^{++}	3.040*	35.42	4.863*	-7567*	-2.728*	-18.0*
Ca^{++}	3.374*	48.44	9.947*	-2518*	25.00*	-28.1*
Sr^{++}	3.701*	63.94	10.52*	-792.4*	19.21*	-56.5*
Ba^{++}	3.843*	71.57	24.79*	1107*	-3.447*	-69.9*
F$^-$	1.971*	9.662	12.12*	-2750*	9.924*	-13.8*
Cl$^-$	2.583*	21.74	11.36*	-1689*	8.328*	-16.9*
Br$^-$	3.202*	41.42	11.27*	-2435*	10.51*	-31.6*
I$^-$	3.476*	52.99	12.52*	-3406*	2.255*	-32.5*
NO$_3^-$	2.022*	10.42	20.80*	224.5*	1.431*	2.3*
SO$_4$--$^-$	3.273*	44.22	-5.175*	-290.7*	-49.06*	-47.8*

Table D.6: e-CPA parameters for different ions when all parameters were optimized simultaneously to data at all temperatures and we use the published ion diameters. Results are summarized in Table D.8.

Ion	σ [Å]	b_0 [cm^3/mol]	$\tilde{v}_i$ [cm^3/mol]	$\tilde{u}_{iw}^0$ [K]	$\tilde{u}_{iw}^T$	Peneloux [cm^3/mol]
H$^+$	14.18*	0.0	-1.892*	-9676*	-42.99*	25.3*
Li$^+$	2.805*	27.84	2.833*	-4386*	2.185*	-12.1*
Na$^+$	2.866*	29.70	-0.4768*	-2344*	-7.00*	-16.1*
K$^+$	2.332*	16.00	0.1235*	-472.8*	-16.55*	6.2*
Rb$^+$	3.440*	51.35	1.478*	-583.4*	-20.02*	-30.6*
Cs$^+$	3.557*	56.77	5.433*	18.44*	-5.00*	-29.7*
Mg^{++}	3.560*	56.92	-1.210 *	-12396*	-20.37*	-29.8*
Ca^{++}	2.650*	23.46	11.69*	-3882*	-0.9025 *	7.7*
Sr^{++}	4.178*	91.98	12.91*	-779.3*	9.177*	-80.1*
Ba^{++}	3.902*	74.94	41.15*	434.8*	1.360*	-62.6*
F$^-$	2.164*	12.78	8.987*	-4277*	2.819*	-21.4*
Cl$^-$	1.725*	6.477	15.17*	-1219*	1.931*	-5.7*
Br$^-$	2.758*	26.46	15.14*	-1481*	-2.283*	-21.6*
I$^-$	3.048*	35.78	16.76*	-1892*	-9.481*	-20.8*
NO$_3^-$	1.991*	9.958	16.54*	523.4*	-0.4297 *	-1.7*
SO$_4{}^{--}$	3.493*	53.77	0.2823*	-6372*	-13.40*	-58.8*

Table D.7: e-CPA parameters for different ions when all parameters were optimized simultaneously to data at all temperatures. Results are summarized in Table D.8.

Salt	RAD [%] $\gamma_\pm^*$		Np.	RAD [%] Φ		Np	RAD [%] a_w		Np.	m_{max}	T-range
Table	D.5	6.11	$\gamma_\pm^*$	D.5	6.11		D.5	6.11			
NaF	2.38 (2.40)	3.67	47	2.69 (2.69)	5.82	24	0.15 (0.15)	0.20	8	1.0	269-308
KF	3.25 (3.25)	2.99	41	2.14 (2.15)	2.74	77	0.74 (0.92)	0.97	9	17.5	251-357
RbF	5.78 (5.78)	6.38	24	2.82 (2.82)	2.93	17	-	-	-	3.5	298.15
CsF	5.20 (5.20)	12.42	24	1.53 (1.53)	6.56	17	-	-	-	3.5	298.15
HCl	4.35 (7.98)	2.36	229	2.11 (2.11)	1.14	58	2.85 (2.08)	2.16	64	16.0	204-353
LiCl	4.40 (4.40)	4.86	59	2.65 (3.59)	2.69	385	3.30 (4.07)	3.07	106	25.7	207-473
NaCl	3.82 (8.40)	4.18	697	2.53 (2.77)	2.46	891	7.96 (0.80)	0.68	183	8.0	252-473
KCl	2.34 (2.34)	2.15	216	3.18 (3.29)	2.24	282	0.30 (0.31)	0.27	103	8.1	262-445
RbCl	5.04 (5.04)	4.27	32	3.31 (3.31)	2.47	88	0.31 (0.36)	0.24	37	7.8	263-343
CsCl	1.30 (1.32)	0.61	151	4.07 (4.08)	2.28	267	0.92 (0.98)	0.65	36	11.4	264-473
MgCl$_2$	4.38 (4.38)	8.38	49	12.22 (12.92)	4.61	306	1.66 (1.18)	1.66	131	6.0	240-473
CaCl$_2$	14.27 (14.02)	8.09	109	13.07 (24.27)	9.34	253	21.57 (21.25)	17.1	770	25.2	222-473
SrCl$_2$	3.63 (3.63)	3.09	42	2.97 (4.07)	2.74	97	0.91 (3.98)	1.00	41	4.03	267-444
BaCl$_2$	5.59 (5.59)	4.46	19	3.66 (3.89)	3.16	165	0.31 (0.15)	0.21	31	3.02	266-444
HBr	3.03 (3.31)	2.49	78	2.10 (2.10)	1.55	27	-	-	27	11.0	298-398
LiBr	5.22 (5.22)	5.13	45	5.33 (4.46)	5.30	182	1.14 (0.40)	1.25	21	20.0	201-373
NaBr	3.93 (4.81)	4.32	156	2.13 (2.71)	1.98	202	0.47 (0.89)	0.54	80	11.6	246-374
KBr	4.13 (4.13)	3.07	32	3.13 (3.15)	3.09	63	0.45 (6.16)	0.49	64	6.2	261-343
RbBr	3.46 (3.46)	2.84	27	2.92 (2.92)	2.29	53	-	-	-	5.0	298.15
CsBr	0.86 (0.86)	1.28	27	1.16 (1.16)	1.01	53	-	-	-	5.0	298.15
MgBr$_2$	9.66 (9.66)	9.63	60	4.44 (4.40)	4.89	62	0.90 (0.72)	2.89	13	5.8	230-323
CaBr$_2$	7.04 (7.04)	8.29	61	10.20 (29.2)	7.65	176	4.11 (1.75)	2.11	67	11.1	221-473
SrBr$_2$	4.67 (4.67)	4.10	40	3.66 (3.66)	3.33	28	0.82 (0.36)	0.96	41	3.3	251-343
BaBr$_2$	5.08 (5.08)	4.04	55	5.27 (5.27)	3.77	30	0.59 (0.84)	0.75	48	3.4	254-343
HI	2.41 (2.41)	3.65	33	1.03 (1.03)	1.37	42	-	-	-	10.0	298.15
LiI	3.33 (3.33)	4.44	23	2.92 (2.92)	2.52	94	3.55 (2.08)	3.07	13	10.1	204-343
NaI	3.49 (3.49)	4.31	49	2.12 (2.69)	2.56	96	0.34 (1.59)	0.60	64	12.0	242-363
KI	3.85 (3.86)	3.84	33	2.72 (2.72)	3.31	54	2.24 (2.74)	2.48	35	5.8	255-298
RbI	3.32 (3.32)	3.16	53	3.80 (3.80)	3.56	-	-	-	-	5.0	298.15
CsI	3.92 (3.92)	4.01	23	3.18 (3.18)	3.43	-	-	-	-	3.0	298.15
MgI$_2$	5.61 (5.61)	8.46	41	2.10 (2.10)	2.67	52	5.33 (4.16)	4.31	5	5.0	226-298
CaI$_2$	6.55 (6.55)	6.43	38	2.41 (2.43)	3.73	38	8.30 (5.73)	7.07	45	6.9	208-343
SrI$_2$	7.26 (7.26)	7.34	38	2.09 (2.09)	1.64	28	0.41 (0.85)	0.64	44	4.2	264-343
BaI$_2$	7.91 (7.91)	6.61	38	1.31 (1.31)	1.52	28	2.01 (1.79)	2.50	19	3.3	240-298
LiNO$_3$	6.36 (6.36)	6.46	43	3.08 (3.31)	3.18	221	2.23 (2.75)	2.21	71	20	273-378
NaNO$_3$	5.46 (5.46)	7.89	34	3.47 (4.12)	2.33	144	1.75 (2.46)	2.36	33	10.8	255-373
KNO$_3$	1.04 (1.04)	0.63	24	2.50 (4.73)	1.37	172	5.06 (5.63)	4.59	21	25.3	270-424
RbNO$_3$	1.54 (1.54)	2.03	26	2.87 (2.87)	1.39	50	-	-	-	4.5	298.15
CsNO$_3$	2.95 (2.95)	0.87	19	3.10 (3.10)	0.87	29	-	-	-	1.5	298.15
Mg(NO$_3$)$_2$	6.60 (6.51)	7.79	78	4.31 (4.11)	4.33	174	11.2 (4.11)	5.33	75	14.6	241-413
Ca(NO$_3$)$_2$	7.66 (7.19)	7.28	78	16.59 (21.64)	9.65	114	17.00 (7.78)	6.50	99	22.9	243-424
Sr(NO$_3$)$_2$	7.50 (7.58)	6.16	78	3.62 (3.62)	3.81	18	0.33 (0.17)	0.49	9	4.0	266-318
Ba(NO$_3$)$_2$	8.24 (8.19)	6.03	60	11.15 (11.14)	7.32	6	0.10 (0.10)	0.07	4	0.4	273-318
Li$_2$SO$_4$	3.51 (3.51)	2.69	38	4.73 (4.72)	2.09	57	0.58 (0.42)	3.52	58	3.52	250-298
Na$_2$SO$_4$	3.26 (3.26)	3.03	43	2.75 (3.82)	5.16	216	0.17 (0.20)	0.22	44	4.44	272-398
K$_2$SO$_4$	4.54 (4.53)	1.39	25	1.13 (1.09)	1.15	83	0.03 (0.03)	0.96	30	0.96	272-373
Rb$_2$SO$_4$	3.34 (3.34)	3.52	31	6.01 (6.01)	7.02	13	-	-	-	1.80	298.15
Cs$_2$SO$_4$	2.89 (2.89)	6.18	31	3.98 (3.98)	11.43	13	-	-	-	1.80	298.15
MgSO$_4$	-	-	-	6.57 (38.6)	6.76	131	0.21 (0.30)	0.22	26	5.0	268.1-448
CaSO$_4$	17.06 (17.06)	14.52	7	-	-	-	-	-	-	0.015	298.15
Average	4.95 (5.12)	4.93	3268	4.05 (5.59)	3.68	6293	2.51 (2.51)	2.78 (2.17)	2.16	2025	

Table D.8: Deviations from experimental data with parameters from Table 6.11.